Initiators for the production of PLA and terpene derived bioplastics

Quilter, Helena

Award date:
2018

Awarding institution:
University of Bath

Initiators for the production of PLA and terpene derived bioplastics

Quilter, Helena

Award date:
2018

Awarding institution:
University of Bath

Initiators for the production of PLA and terpene derived bioplastics

Helena C. Quilter

A thesis submitted for the degree of Doctor of Philosophy

Department of Chemistry

University of Bath

May 2018

Contents

Acknowledgements

Firstly, I would like to thank my supervisor, Dr. Matthew Jones. I am extremely grateful for his supervision and guidance throughout my PhD, as well as his enthusiasm, knowledge, and encouragement. I also thank him for his assistance with crystallography. I would also like to thank the CSCT for providing me with the opportunity to carry out this project, and the EPSRC for the funding which made it possible. I also acknowledge my co-supervisors, Prof. Matthew Davidson and Prof. Davide Mattia for helpful discussions.

My time in Bath has been invaluable, and I would like to thank the many members of the Jones group, past and present, who have made this experience so enjoyable, particularly Paul McKeown, Sarah Kirk, Heather Parker, James Beament, Tomos Clarke, and visiting students Fernando Peleias Junior, Simoní da Ros and Angi Metz. Thank you for making the lab such a fun environment, for guidance and support, and for Floyd Fridays. I have been fortunate to work with some excellent MChem students, and I acknowledge Rachel Drewitt for her contributions to Chapter 2. My thanks also to the wider 5W SusChemLab, particularly Dr Antoine Buchard for DFT calculations and many useful discussions. I also thank the staff of CCAF: Dr. John Lowe, Dr. Tim Woodman and Dr. Catherine Lyall for their expertise in all things NMR. Dr. Anneke Lubben and Dr. Shaun Reeksting for help with MS and Dr. Rémi Castaing for GPC. I also acknowledge Dr. Mary Mahon and Dr. Gabriele Kociok-Köhn for X-ray crystallography assistance. I have been fortunate to be a member to the wider *Terpene-based manufacturing group* at Bath. My thanks to Bill Cunningham and Dr. Marc Hutchby for their help with synthesis and keeping an eye on my ozonolysis reactions while I'm on the other side of campus. Sincere thanks to Dr. Rob Chapman for his help with chemoselective BVO. I would also like to thank Dr. Ceri Hammond and Keiko Yakabi at Cardiff University for providing me with a sample of the Sn-β catalyst used in Chapter 4.

I was incredibly fortunate to spend three months in Minneapolis under the supervision of Prof. Marc Hillymer at the University of Minnesota during my PhD. My sincere thanks to him, and all the members of his group for hosting me during my internship. It was an invaluable learning experience. Special thanks to Annabelle Watts and Dr. Mike Larsen for excellent discussions over coffee and teaching me the ways of the Hillmyer lab. A million thanks to Ceci Hall for spontaneous trips, water bears, and making my whole internship so enjoyable (no, *you're* the best).

The best part of being in a DTC has been being a part of Cohort ’13. You’re all wonderful and I’m proud to be a part of the group. Thank you all for all the laughs, games nights and wonderful memories. Jemma and Emma – thanks for taking the mess out of my Northern faffing, asking *“what’s the significance?”* and for that story involving spiders that led to a car full of conkers. You guys have kept me going and I can always rely on you for a laugh or a shoulder to cry on – thank you!

My thanks to the University of Bath Counselling Service, particularly Moe, for helping me to help myself through the harder times. I feel incredibly fortunate to have had access to such a wonderful service and I hope it remains in place for many years to come. I would also like to thank Sheila Apps, without whom I wouldn’t have made it past my first year in Bath.

I would like to thank all my friends and family, particularly my parents and John, who have always supported me in all my endeavours. Finally, my utmost appreciation to my partner, Dom, for supporting me in all that I do, for the endless love and encouragement. I’m excited for the next chapter.

Abstract

As we experience the detrimental effects of plastics on the environment, preparing new bio-derived alternatives has become an important challenge in both academia and industry. Bio-derived polylactide (PLA) is a promising candidate, being biodegradable and biocompatible, although challenges include the synthesis of isotactically enriched PLA from racemic monomer feeds through utilisation of stereoselective initiators, and copolymerisation with other bio-derived monomers to prepare fully bio-based copolymers. In Chapter 1 the synthesis of PLA and current research into stereoselective initiators for the polymerisation of *rac*-lactide (LA) are discussed, with a focus on lithium, magnesium, zinc, aluminium and zirconium complexes. Routes to novel substituted ε-caprolactone and ε-caprolactam monomers from abundant terpene feedstocks are also introduced, in the context of preparing fully bio-based copolymers.

In Chapter 2, the synthesis and characterisation of multinuclear zirconium, lithium, magnesium and zinc complexes with amine bis(phenolate) ligands is discussed. These complexes were applied as initiators in the ring-opening polymerisation (ROP) of r*ac*-LA. Most initiators resulted in atactic PLA, although in some cases PLA with a slight heterotactic bias (P_r <0.58) was obtained. Two different lithium tetrametallic structures were characterised by X-ray crystallography. Dimeric magnesium complexes were active for ROP under solvent-free and solution conditions, with undesirable transesterification occurring and atactic PLA produced in all cases. Magnesium complexes were also trialled for ring-opening copolymerisation of epoxides and anhydrides. Interesting tri- and tetranuclear species were observed with zinc, which exhibited different levels of aggregation in solution. Finally, attempts to prepare a new bis(phenolate) ligand with a bi-isoindolene backbone are reported.

In Chapter 3, the synthesis of salen ligands and their complexation to aluminium to prepare mononuclear and dinuclear complexes is discussed. Complexes were characterised in the solid-state and in solution. A dinuclear complex with a 1,8-naphthalene backbone was found to be highly active for ROP of *rac*-LA even at room temperature, producing isotactically enriched PLA (P_m <0.82). This is a rare example of a LAlMe_2 complex imparting stereoselectivity to this process. DFT calculations support potential cooperativity occurring between metal centres, and results are compared with analogous mononuclear and dinuclear complexes where cooperativity is not possible. The preparation of aluminium and

lithium complexes bearing imidazolidine bis(phenolate) ligands is also reported, with some interesting structures isolated and characterised.

In Chapter 4 the preparation of a substituted ε-caprolactone monomer from a terpene feedstock, β-pinene, and its polymerisation to a novel, low $T_{g,}$ aliphatic polyester is reported. The copolymerisation of this monomer with lactide is discussed. The preparation of a substituted ε-caprolactam from β-pinene is also described. Chemoselective synthetic routes to novel unsaturated substituted ε-caprolactone monomers are discussed, and the synthesis of a polyester bearing pendant isopropenyl moieties is reported. Initial attempts at post-polymerisation modification of unsaturated polymers highlights their potential for post-polymerisation modification in the development of new functional materials.

Synthetic procedures and characterisation for ligands, complexes, monomers and polymers are given in Chapter 6, along with details of general experimental methodologies and techniques.

Abbreviations

4^{i}PrCL	4-isopropylcaprolactone
BDI	β-diketaminate
BnOH	benzyl alcohol
BVO	Baeyer-Villiger oxidation
CEM	chain end mechanism
CHO	cyclohexene oxide
ε-CL	ε-caprolactone
CST	crude sulfate turpentine
D	diffusion coefficient
$Đ$	dispersity (M_w/M_n)
DFT	density functional theory
DOSY	diffusion ordered spectroscopy
DSC	differential scanning calorimetry
ESI	electron spray ionisation
eq.	equivalents
FTIR	Fourier-transform infrared spectroscopy
GC	gas chromatography
GPC	gel permeation chromatography
k_{app}	apparent rate constant
k_{init}	rate constant of initiation
k_{prop}	rate constant of propagation
LA	lactide
[M]:[I]	monomer-to-initiator ratio
mp	melting point
M_n	number-average molecular weight
M_w	weight-average molecular weight
MALDI	matrix assisted laser desorption ionisation
mCPBA	*meta*-chloroperoxybenzoic acid
MS	mass spectrometry
NMR	nuclear magnetic resonance
P_m	probability of isotactic enchainment
P_r	probability of heterotactic enchainment
PCL	poly(ε-caprolactone)
PCM	poly(carvomenthide)
PD	poly(dihydrocarvomenthide)
PEF	poly(ethylene furanoate)
PET	poly(ethylene terephthalate)
PLA	polylactide
PM	polymenthide
PO	propylene oxide
ppm	parts per million
PPM	post-polymerisation modification
PS	polystyrene
r_H	hydrodynamic radius
RI	refractive index
ROCOP	ring-opening copolymerisation
ROP	ring opening polymerisation
RT	room temperature
SA	succinic anhydride
SBP	square based pyramidal
SCM	site-controlled mechanism
τ_4	degree of tetrahedrality
τ_5	degree of trigonality
T_g	glass transition temperature
T_m	melting temperature
TLC	thin layer chromatography
ToF	time of flight

Publications

Kirk, SM, Quilter, HC, Buchard, A, Thomas, LH, Kociok-Kohn, G & Jones, MD 2016, 'Monomeric and dimeric Al(III) complexes for the production of polylactide', Dalton Transactions , vol. 45, no. 35, pp. 13846-13852. https://doi.org/10.1039/C6DT02861F

Polymer Chemistry

COMMUNICATION

View Article Online
View Journal | View Issue

CrossMark click for updates

Cite this: Polym. Chem., 2017, 8, 833

Received 21st November 2016,
Accepted 20th December 2016

DOI: 10.1039/c6py02033j

rsc.li/polymers

Polymerisation of a terpene-derived lactone: a bio-based alternative to ε-caprolactone†

Helena C. Quilter,[a,b] Marc Hutchby,[b] Matthew G. Davidson[b] and Matthew D. Jones*[b]

A high-yielding 4-step process for converting a naturally occurring terpene, β-pinene, into a substituted ε-caprolactone is herein reported. Investigations into the ring-opening polymerisation and copolymerisation of this monomer are also described.

Dwindling fossil fuel supply and growing environmental concerns have increased demand for new renewable, biodegradable plastics.[1–4] One such plastic is poly(lactide) (PLA), an aliphatic polyester derived from starchy biomass *via* ring-opening polymerisation (ROP) of the cyclic monomer lactide (LA).[5–8] The physical properties (*e.g.* rate of degradation, gas permeability) of PLA can be altered by copolymerisation with other cyclic esters, such as petrochemically-derived ε-caprolactone (CL).[9] This is an essential method as it widens the usage of PLA in biomedical and engineering applications.[10,11] For example, poly(lactide-*co*-caprolactone) has improved mechanical properties (impact and elongation strengths), and biodegrades more rapidly than PLA alone.[12] Renewable routes to ε-caprolactone such as Heeres' route from HMF (which can be derived from D-fructose)[13] or, alternatively, novel bio-derived substituted caprolactones are highly desirable. Caprolactone is an important industrial chemical and is produced on multi-tonne scale *via* oxidation of cyclohexane.[14]

A growing source of bio-derived monomers are terpenes and terpenoids.[15–17] These naturally occurring molecules are widely utilised in the flavourings and fragrance industries and are the principle component of essential oils in many plants.[18] Some of the most commonly occurring terpenes are the cyclic monoterpenes α- and β-pinene (from gum turpentine, crude sulphate turpentine) and D-limonene (from citrus waste), as well as the simplest terpene : isoprene.[15–17,19,20] The abundance of double bonds in terpenes allows for cationic and radical polymerisation, as well as epoxidation as a route to biodegradable oxygenated polymers, as reported for limonene oxide[21,22] and α-pinene oxide.[23]

While few examples of terpenoid monomers suitable for ROP are available, Hillmyer and co-workers have reported the use of substituted monomers derived from oxidised menthol[24] and carvone[25] for the production of functional polyesters and elastomers *via* block copolymerisation with LA. Building on this work, Winnacker and co-workers reported a method for producing oligoamides from menthone following a similar concept to the synthesis of poly(caprolactam) (nylon 6) from petrochemically-derived cyclohexanone.[26] Bio-based polyamide monomers are also highly desirable, with the current scope being somewhat limited, particularly for functionalised polyamides.[27]

While menthol has shown potential in this area, its annual production of around 19 000 tonnes[28] is somewhat limiting for development of commodity materials. The production of turpentine, however, is estimated at 350 000 tonnes per annum, of which up to almost a third may be β-pinene.[29] The work reported herein aims to widen the library of bio-based monomers for ROP available from terpene feedstocks by developing a process of converting abundant, naturally occurring β-pinene into 4-isopropylcaprolactone (4-^{i}PrCL) and its subsequent polymerisation. An intermediate in this process, 4-isopropylcyclohexanone, could also be converted to a lactam *via* Beckmann rearrangement to prepare a bio-based monomer for functionalised polyamides, similar to nylon. While 4-^{i}PrCL has been previously synthesised as a product in enantioselective Baeyer–Villiger oxidation reactions,[30,31] to the best of our knowledge its polymerisation has not been reported nor has it been prepared form a naturally occurring starting material. We herein report the preparation of 4-^{i}PrCL from β-pinene in 4 high yielding steps (see Fig. 1), overall yield 64%.

Ozonolysis of β-pinene afforded the terpenoid (+)-nopinone (**1**) on a 30 g scale, with characterisation matching literature data.[32] Lewis acid promoted isomerisation of **1**[33] was found to cleave the strained *cis*-cyclobutane ring to produce exclusively the monocyclic product (±)-cryptone (**2**) in high yield. No

[a]Doctoral Training Centre in Sustainable Chemical Technologies, University of Bath, Bath BA2 7AY, UK
[b]Department of Chemistry, University of Bath, Bath, BA2 7AY, UK.
E-mail: mj205@bath.ac.uk

† Electronic supplementary information (ESI) available: Full characterisation of monomer and polymer. See DOI: 10.1039/c6py02033j

Quilter, H, Drewitt, R, Mahon, M, Kociok-Kohn, G & Jones, M 2017, 'Synthesis of Li(I), Zn(II) and Mg(II) complexes of amine bis(phenolates) and their exploitation for the ring opening polymerisation of rac-lactide', Journal of Organometallic Chemistry, vol. 848, pp. 325-331. https://doi.org/10.1016/j.jorganchem.2017.08.014

1 Introduction

1.1. Biorenewable and biodegradable polymers

Polymers are ubiquitous in global society. The annual production of plastics has grown rapidly over the last 50 years from 15 million tonnes in 1964 to 311 million tonnes in 2004, and this amount is expected to double again in the next 20 years.[1] The polymer industry relies heavily on the use of petrochemical feedstocks and the generation of nondegradable products, contributing around 7% of total worldwide oil and gas consumption.[2] While many plastic materials can be efficiently recycled, or utilised in energy recovery, estimates suggest that 40% of plastic packaging ends up in landfill, and most plastic packaging is almost exclusively single-use.[1] Concerns surrounding the persistence of plastics in the environment, dwindling fossil fuel reserves and the effects of climate change have led to a shift towards the derivation of plastics from renewable sources, and implementation of green chemistry principles in polymer research.[3,4]

Most commodity plastics (Figure 1.1) such as polyethylene (PE), polypropylene (PP) and polystyrene (PS) contain hydrocarbon chains and are impervious to degradation. The widely used polyesters poly(ethylene terephthalate) (PET) and bisphenol A polycarbonate (BPAPC) are also very resilient to degradation. Most commercial plastics are thermoplastics, which become molten upon heating over a glass transition temperature (T_g) and therefore can be reformed and recycled. However, this requires intensive energy consumption and mixing of waste streams readily leads to contamination.

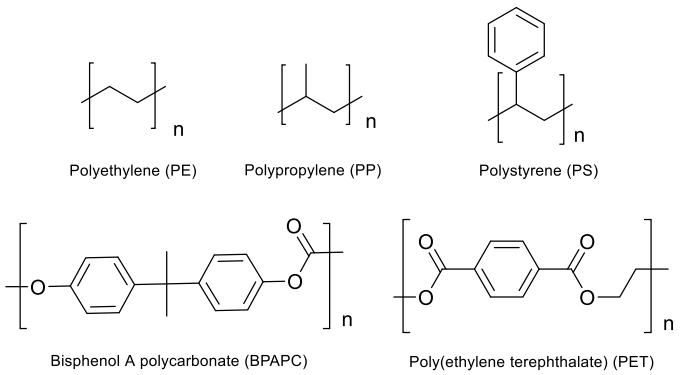

Figure 1.1. Structures of widely used petrochemically-derived plastics.

There are currently very few commercial plastics derived from renewable feedstocks available, and introduction is hampered by the elevated production cost compared to traditional petrochemical materials.[5,6] The plastic economy is built on many years of infrastructure designed for petrochemical feedstocks, allowing for cheap plastic production

(threatened slightly by fluctuations in global oil prices).[5] By contrast, production of renewable plastics requires alternative technologies, to deal with variation in feedstocks, and new processes.[6]

In recent years, considerable research has been focussed on the development of renewable monomers from plant biomass.[2,6–13] Various multi-disciplinary approaches are being considered, including fermentation,[14] enzymatic processes,[15] chemical transformations of naturally occurring polymers (e.g. cellulose[16]) and metabolic engineering to increase the production of molecular biomass such as terpenes.[17] Naturally occurring molecular biomass can be roughly categorised into three types: oxygen-rich biomass (having a carbon-oxygen ratio less than 5.0), hydrocarbon-rich biomass (C:O > 5.0) and hydrocarbon biomass, in addition to non-hydrocarbon biomass (CO_2/CO), as summarised in Figure 1.2.[2]

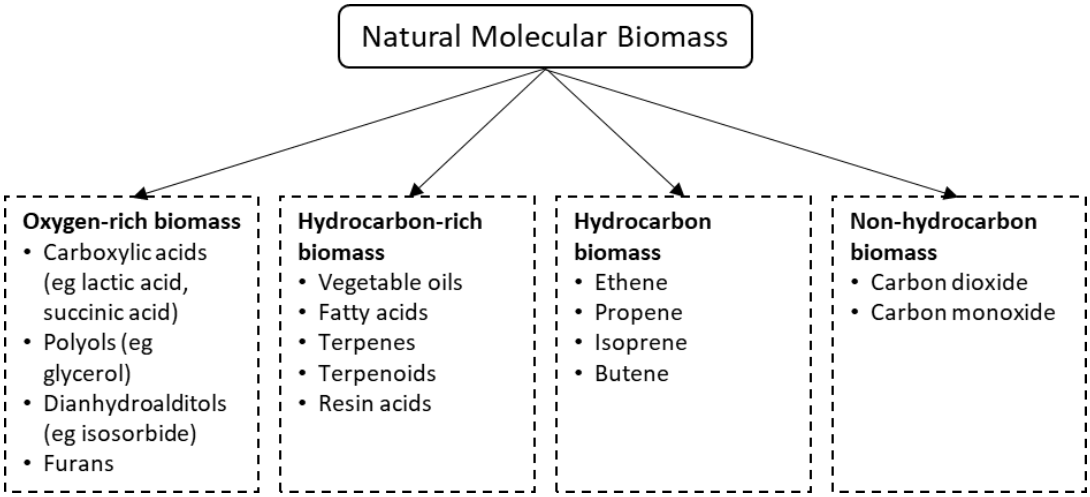

Figure 1.2. Classification of major natural molecular biomass[2]

When designing biomaterials, it is important to consider both the synthesis and end-of life opportunities to determine if they are more sustainable than existing plastics. Materials that are designed to be chemically recyclable or environmentally biodegradable are ideal candidates for materials for the circular economy, and represent the preferred end-of-life option for sustainable polymers.[6] Ideally, depolymerization and purification of recovered feedstocks would be possible.

It is possible to derive “drop-in” replacements for current plastics from renewable resources, although this does not address the persistence of the plastic in the environment. An excellent example of this is the drive to prepare PET from bio-based monomers. Conventionally, PET is prepared *via* polycondensation of oil-based monomers: ethylene glycol and terephthalic acid. However, ethylene glycol can be derived from biomass

through fermentation of sugars. Coca-Cola® have commercialised the partially renewable plantbottle™, made from PET containing bio-ethylene glycol.[18] Coca-Cola® have also unveiled a fully biomass-derived PET bottle,[19] and the derivation of terephthalic acid from various biomass sources such as limonene and furfural is actively pursued.[20]

Poly(ethylene furanoate) (PEF, Figure 1.3) is an analogue of PET prepared from ethylene glycol and bio-based 2,5-furandicarboxylic acid (FDCA). Compared to PET, PEF has superior gas barrier properties (3-fold improvement for CO_2 for PEF *vs* PET), which can be difficult to achieve in bio-based materials. PEF also has improved mechanical and thermal properties compared to PET, with PEF having a tensile modulus 1.6 times that of PET, and higher glass transition temperature (T_g) (88 °C for PEF *vs* 80 °C for PET).[20] FDCA is amenable to current PET production infrastructure, but lower greenhouse gas (GHG) emissions are produced during manufacture, with a cradle-to grave assessment proposing a 45-55% reduction in GHG production for PEF *vs* PET.[21] This is an example of a bio-based alternative having comparable properties, rather than a "drop-in" replacement.

Figure 1.3. The structures of poly(ethylene terephthalate) (PET) and fully renewable analogue poly(ethylene furanoate) (PEF)

At present, few biopolymers have the potential to replace petroleum-based products. Synthetic, biodegradable, and biorenewable polymers such as, poly(hydroxylalkanoates) (PHAs), poly(butylene succinate) (PBS), and polylactide (PLA) (Figure 1.4) are becoming more attractive for use in industrial applications. PLA is probably the most recognised synthetic biopolymer at present and will be covered in greater detail in section 1.1.1. PHAs, such as poly(3-hydroxybutyrate) (PHB), are a diverse class of polyesters produced naturally by various microbial organisms *via* fermentation, some of which have been reported to have comparable properties to polypropylene,[22] and have been used for various biomedical applications.[23] PBS is biodegradable under industrial conditions (EN13432) and has good levels of flexibility and heat resistance (up to 100 °C).[24] Industrially, PBS is prepared *via* polycondensation of oil-derived 1,4-butane diol and succinic acid. Succinic acid was one of the US Department of Energy's top 12 platform chemical targets from biomass,[25] and bio-PBS has gained interest recently due to the potential availability of bio succinic acid.[23] A summary of some current commercial plastics is given in Table 1.1.

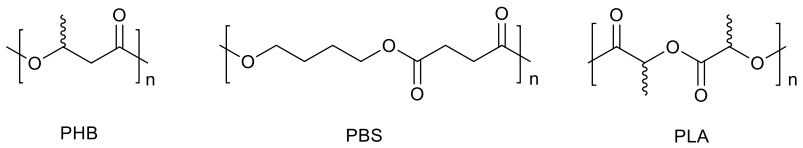

Figure 1.4. Structures of bio-based polymers: PHB, PBS and PLA

Table 1.1.Classification of some common plastics[26]

	Bio-based plastics (renewable resources)	Oil-based plastics (non-renewable resources)
Biodegradable plastics	polylactide (PLA)	poly(ε-caprolactone) (PCL)
	Poly(hydroxylalkanoate) (PHA)	poly(butylene succinate) (PBS)
	bio-poly(butylene succinate) (bio-PBS)	
Non-biodegradable plastics	bio-polyethylene (bio-PE)	polyethylene (PE)
	bio-poly(ethylene 2,5-furandicarboxylate)	polypropylene (PP)
	bio-poly(ethylene terephthalate) (bio-PET)	polystyrene (PS)
		poly(ethylene terephthalate) (PET)

1.1.1 Polylactide/poly(lactic acid) (PLA)

Probably the most extensively researched synthetic plant-derived polymer to date is polylactide (PLA), an aliphatic polyester typically derived from corn starch or sugarcane. PLA is biodegradable, biocompatible, and has US Food and Drug Administration (FDA) approval for use in food packaging[27,28] and biomedical applications.[29] PLA can be hydrolysed to lower molecular weight PLA and then further degraded (*via* the Krebs cycle) to produce CO_2, H_2O and humus.[30] PLA will gradually degrade if composted but the process is very slow unless elevated temperatures are used.[31]

Typically, the starch is broken down to glucose, which in turn is fermented to produce an α-hydroxyacid: lactic acid (Scheme 1.1). This can be polymerised *via* direct condensation to poly(lactic acid), yielding low molecular weight polymers due to the hydrolysis equilibrium arising from the production of one equivalent of water per condensation step. While polycondensation allows for a broad range of monomers to be used and therefore a much larger range of polymer properties, polycondensations require driving conditions to remove water and drive the reaction towards completion. Stoichiometric quantities of monomers are also required to provide high molecular weight polymers. The presence of water causes chain-transfer, hence the low molecular weight of the products.[30]

An alternative approach is to convert lactic acid to a cyclic diester, lactide (3,6-dimethyl-1,4-dioxan-2,5-dione). This is achieved industrially in a two-step process by

polycondensation of lactic acid to low molecular weight oligomers, followed by depolymerisation. Approaches of preparing lactide directly from lactic acid have been recently reviewed.[32] Lactide can undergo ring-opening polymerisation (ROP), which is thermodynamically favourable due to the relief of ring strain,[33] preparing high quality, high molecular weight PLA.

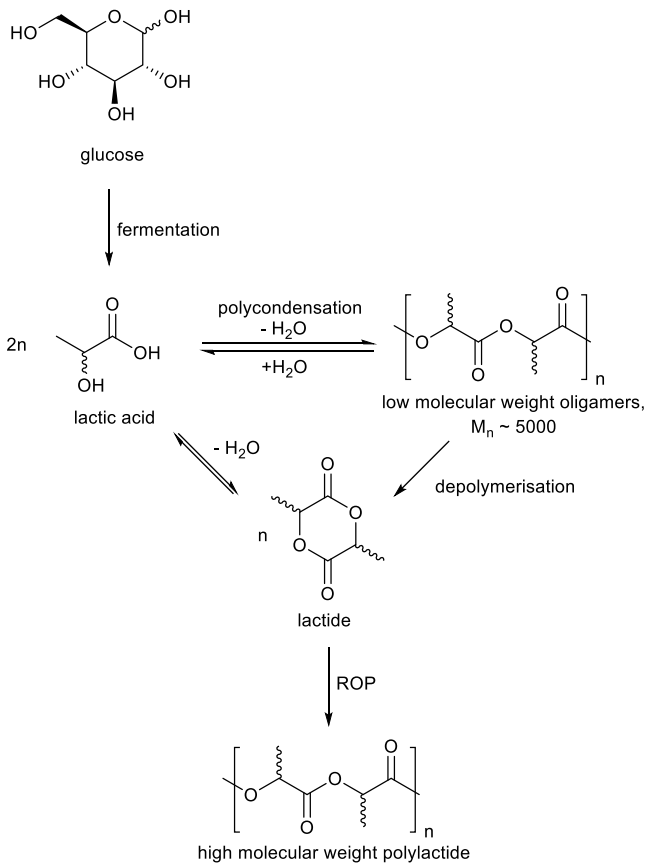

Scheme 1.1. Industrial prodution of PLA[30]

There are several companies now producing PLA on a global scale. The largest producer of PLA is NatureWorks LLC, producing on a scale of 150 kT p a,[28] and Corbion intend to open a 75 kTpa scale production plant towards the latter half of 2018.[34] Industrially the ROP of lactide is catalysed by tin(II) 2-ethylhexanoate, $Sn(Oct)_2$,[30] although development of alternative catalysts, organocatalysts and enzymatic ROP processes are all being investigated.

PLA is seen as one of the most promising bio-based alternatives to low and high-density polyethylene (LDPE and HDPE), PET, and PS. Its mechanical properties and its permeability to O_2 and H_2O allow it to replace these traditional polymers for commodity food packaging and short shelf life products such as food containers, drinks cups and plastic wrappers. The limited performance of PLA (including low T_g, brittleness and low impact strength) restrict

its applications where these things are an important factor.[30] For example, the thermal properties of commercially available PLA, particularly a melting point (T_m) below the boiling point of water has limited its use for hot food and beverage containers, although recent developments have led to PLA withstanding temperatures up to 120 °C, allowing for higher temperature applications.[35,36]

The results of a cradle-to-gate life cycle analysis (LCA) of the production of PLA *vs* PET bottles are summarised in Table 1.2. This study showed that the production of PLA bottles had benefits over PET in producing lower carbon emissions (17.2 kg of CO_2 for PLA *vs* 38.2 kg of CO_2 for PET per 1000 bottles).[33] However, this study did highlight the shortcomings of PLA in terms of land usage and eutrophication through the use of pesticides and consumption of water to attain raw materials. For PLA to be truly sustainable, it is important to use biomass supplies which do not compete with food sources.

Table 1.2. Values for the main impact categories for the overall process of making PET and PLA bottles[33]

Impact categories / 1000 bottles	PLA total	PET total
Global warming $kgCO_{2eq}$	17.20	38.19
Non-renewable energy MJ_{eq}	924.88	1319.43
Renewable energy MJ_{eq}	389.67	92.23
Acidification gSO_{2eq}	171.04	150.79
Eutrophication $gPO_4^{3-}{}_{eq}$	95.40	38.80

1.1.1.1 PLA stereochemistry

The thermal properties of PLA are determined by the polymer architecture. As lactic acid exists in two optically isomeric forms, *L*- and *D*, the lactide dimer contains two chiral centres. This leads to two possible enantiomers structures, known as *D*-lactide, *L*-lactide, and a diasteroisomer: *D,L*- or *meso*-lactide (Figure 1.5). The industrial two-step production of lactide produces a racemic mixture of *D*- and *L*- lactide (*rac*-LA). The ROP of these different lactide units can lead to varied stereochemistry in the PLA product. Poly(*L*-lactide) (PLLA) and poly(*D*-lactide) (PDLA) are both (semi)crystalline, while poly(*D,L*-lactide) is a brittle, amorphous polymer.

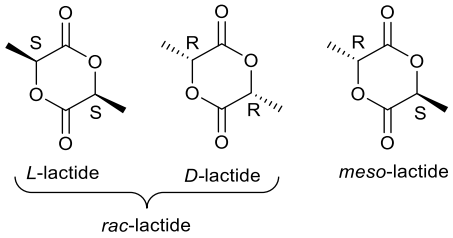

Figure 1.5. Possible stereoisomers of lactide

The ROP of *rac*-LA can afford different PLA microstructures, and the choice of initiator employed can have significant effects on the outcome. The microstructure of the polymer chain influences the thermal and mechanical properties of the polymer. Properties can be further tuned by additional processing steps (adding additional components). Possible PLA microstructures (also known as *tacticities*) are shown in Figure 1.6. By using a single monomer feed of *L*-LA or *D*-LA, isotactic PLLA or PDLA can be produced. *Meso*-LA can be polymerised to syndiotactic, heterotactic or atactic PLA. Atactic PLA is prepared from a feed of *rac*-LA when the initiator employed exhibits no selectivity (such as industrially used $Sn(Oct)_2$). There is much interest in developing new initiators which will selectively produce hetero- or isotactic PLA from *rac*-LA. When ROP is performed with a heteroselective initiator, heterotactic PLA is produced. Here the initiator preferentially coordinates to the alternate monomer than the previously enchained monomer, producing a perfectly alternating chain of *D*- and *L*-lactide monomers. Isotactic PLA can be produced from a feed of *rac*-LA with an isoselective initiator. This is particularly advantageous as it may lead to the formation of stereoblock isotactic PLA with superior thermal properties.

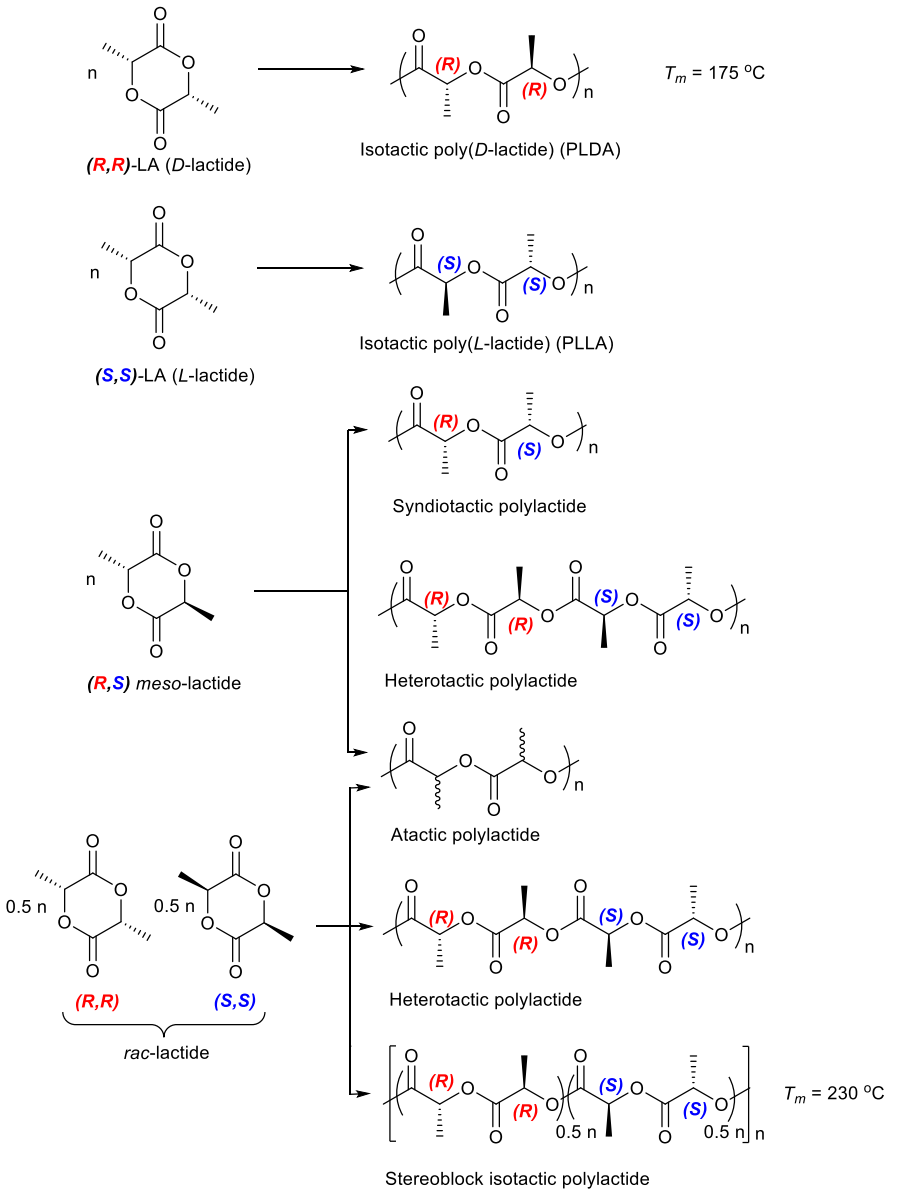

Figure 1.6. PLA microstructures possible from the polymerisation of different lactides. Adapted from Ovitt and Coates[37]

There are two key thermal parameters for polymers: the glass transition temperature (T_g) and the melting temperature (T_m). The T_g is the temperature at which a polymer stops being hard and brittle and becomes rubbery. Thermoplastic materials are rubbery at $T > T_g$, while thermoset materials become brittle when heated above the T_g, which may also be describes as a curing temperature for irreversible transitions. T_m is the point at which a polymer becomes liquid.

Isotactically pure PLA exhibits a high degree of crystallinity, manifested by a high melt temperature of 170-190 °C, whereas heterotactic PLA is amorphous and has a T_m of *ca.* 130 °C.[38] In addition to the PLA microstructures, the thermal stability of PLA can be enhanced

by stereocomplexation of complementary enantiomerically pure chains of PLLA and PDLA to form a highly regular material with increased crystallinity and heightened T_m up to 230 °C.[29,39] Sterecomplexed isotactic PLA is also tougher and more elastic than PLA with other tacticities. The properties of different polylactides are summarised in Table 1.3.

Table 1.3. Physical properties of polylactides[40]

Physical properties	Stereocomplexed PLA	PLLA	PDLLA (atactic)	Syndiotactic PLA
T_m (°C)	220-230	170-190	130	151
T_g (°C)	65-72	50-65	50-60	34
Density (gcm^{-3})	-	1.25-1.29	1.27	-
Tensile strength (GPa)	0.88[a]	0.12-2.3[a]	0.04-0.05[b]	-
Young's modulus (GPa)	8.6[a]	7-10[a]	1.5-1.9[b]	-
Elongation at break (%)	30[a]	12-26[a]	5-10[b]	-

a) Oriented fibre, b) non-oriented films

1.1.2 Ring-opening polymerisation (ROP) mechanisms

The polymerisation of lactide is typically achieved through ring-opening polymerisation (ROP). This is a form of chain-growth polymerisation, where the end of the growing polymer chain acts as the propagating centre to attack the next monomer. This method offers a route to polyesters and polycarbonates (*via* cyclic carbonates) with unrivalled control in terms of molecular weights, dispersities and end group functionality.[38] There are different mechanisms available: coordination-insertion, anionic, cationic, activated monomer, organocatalytic and enzymatic.

The majority of ROP initiators are metal alkoxide complexes which proceed *via* a coordination-insertion mechanism (Figure 1.7).[31] Firstly, the metal centre coordinates to the carbonyl oxygen of a lactide molecule, followed by attack of the alkoxide on the carbonyl carbon. Ring-opening occurs by cleavage of the acyl-oxygen bond. Propagation occurs through the metal centre coordinating to the next monomer in the same fashion.

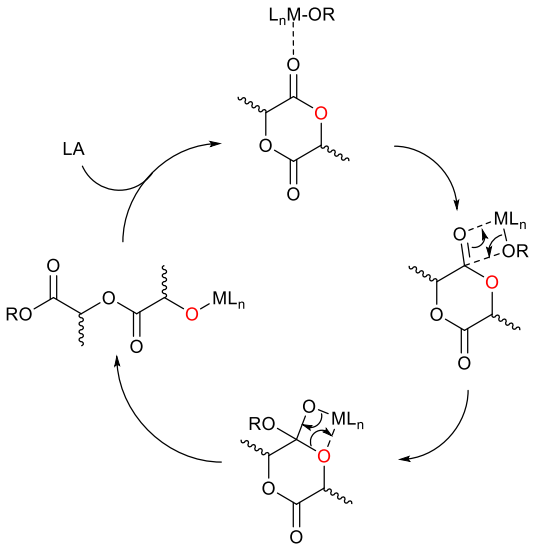

Figure 1.7. Coordination-insertion mechanism for ROP of lactide

The tacticity of the polymer product is highly dependent on the initiator employed in the coordination-insertion mechanism. Typically, the stereochemistry is determined by one of two mechanisms: chain end control (CEM) or enantiomorphic site control (SCM) (Figure 1.8). The term "chain end control" is used to describe generic interactions between the polymer chain and the incoming monomer, resulting in stereoregular insertion.[41] This is often the mechanism for stereocontrol for an achiral initiator.[42] In this mechanism, the last inserted monomer defines the stereochemistry of the subsequent ring-opening step. For example, with an isoselective initiator, if *L*-lactide was the most recently added monomer to the chain, the next monomer to be added would also be *L*-lactide.[43] So-called "*misinsertion*" of the opposite enantiomer would lead to a change in stereochemistry of the polymer product by changing the preference of the initiator, forming multiblock stereopolymers (PLLA-PDLA).[42]

For an enantiomorphic site control mechanism (SCM), the structure of the initiator, particularly chirality, determines the stereochemistry of monomer insertions. Generally, this occurs when an initiator has an initial chiral preference for an incoming monomer unit. This is observed as a faster polymerisation rate for *D*- or *L*- lactide, and preferential consumption of one monomer. The extent of this preference (or difference in rate) can limit lactide consumption to 50%, and mis-insertions may cause a dramatic drop-off in polymerisation rate and form tapered stereoblock microstructures.[37]

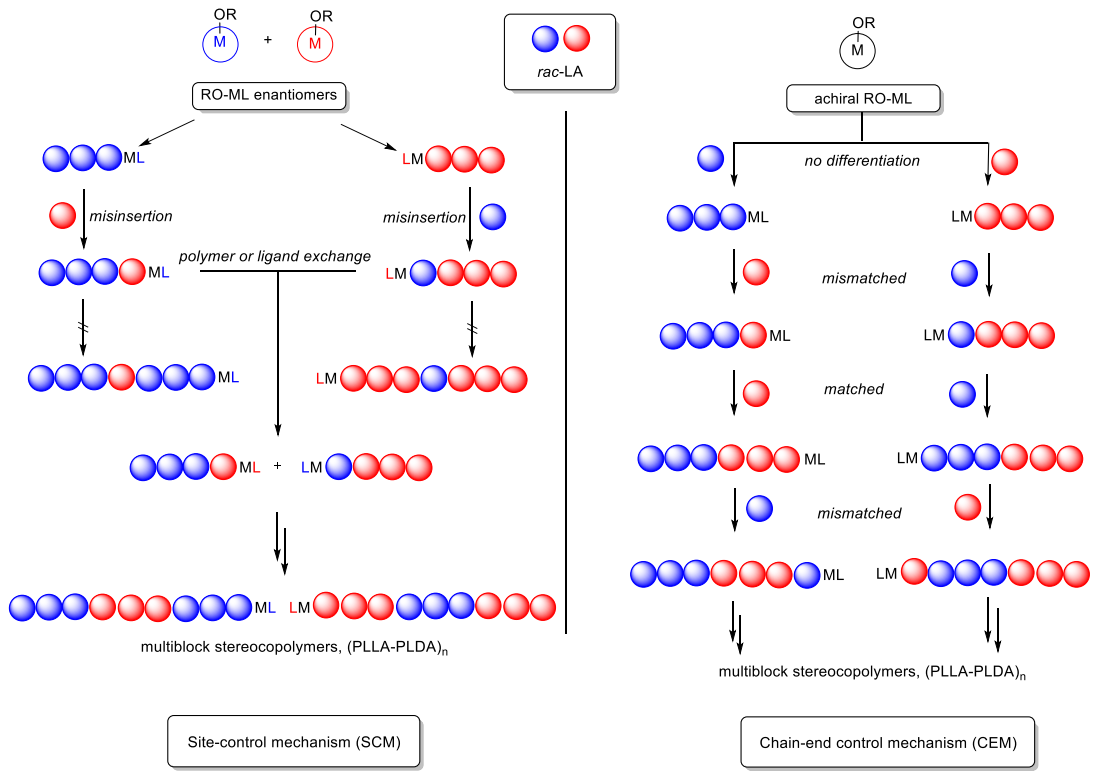

Figure 1.8. Synthesis of isotactic PLA via SCM or CEM. Adapted from Nomura *et al.*[42]

Polymerisation may also occur through an activated monomer mechanism. This is slightly different to the coordination-insertion mechanism in that the role of the metal is simply to activate the monomer by coordination, and ring-opening occurs by attack of a co-initiator rather than formation of a metal-alkoxide bond (Figure 1.9). This mechanism usually occurs when the complex is coordinatively saturated , having no labile ligands, or inert groups such as chloride ligands.[44]

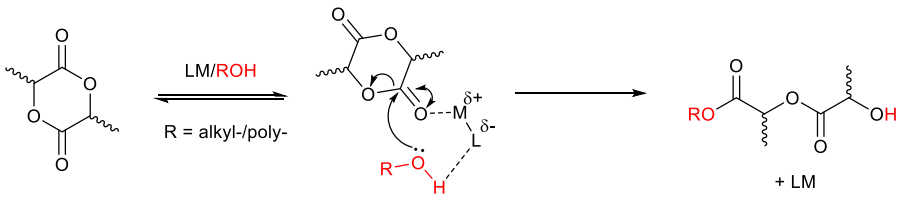

Figure 1.9. Activated monomer mechanism for ROP[32]

ROP with charged initiators follows either an anionic or cationic mechanism. For anionic ROP, nucleophilic attack on the carbonyl, resulting in acyl bond cleavage is the initiating step, producing an alkoxide functionalised polymer chain that can perform further nucleophilic attack (Figure 1.10). Generally, low temperatures are required to achieve a level of control in anionic ROP, and to limit epimerisation or transesterification.[32] In the less-studied cationic mechanism, initiation occurs through activation of a lactide monomer

via protonation, making the monomer susceptible to attack by an acid counterion at an sp^3 carbon centre, leading to alkyl-oxygen bond cleavage.

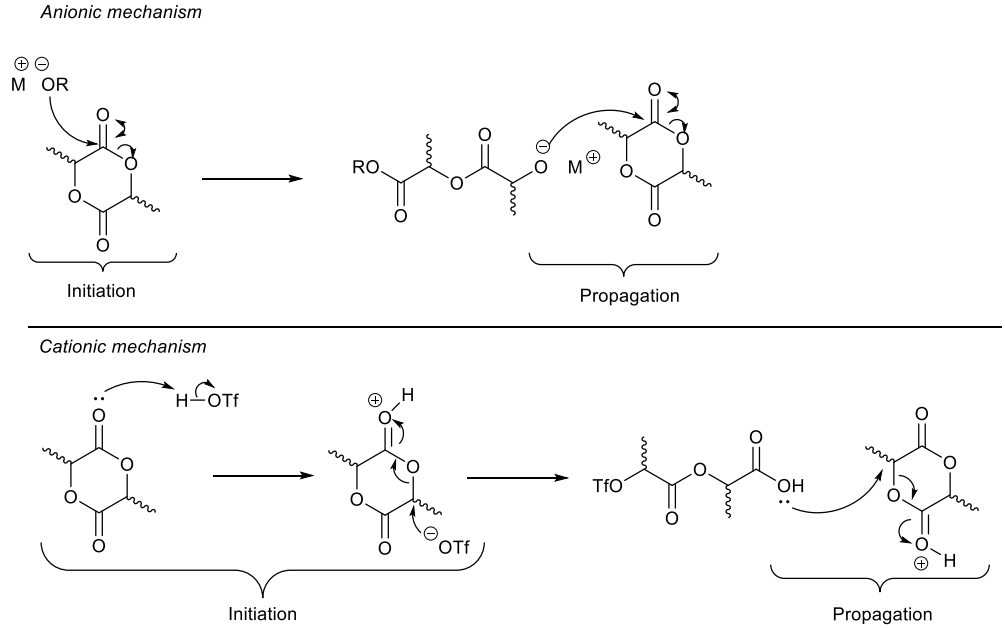

Figure 1.10. Anionic and cationic mechanisms for ROP of lactide

Organocatalytic routes are popular as the organocatalysts are generally active at room temperature and produce PLA containing no residual metal from the initiator, as generally a neutral organic molecule is used. Traditionally, organocatalytic ROP results in poor stereocontrol during the process.[38] Common organocatalysts include *N*-heterocyclic carbenes, guanidines (e.g. triazabicyclodecene, TBD), amidines (e.g. 1,8-Diazabicyclo[5.4.0]undec-7-ene, DBU) and substituted thioureas.[45]

Polymerisation is classed as "living" when the rate of initiation is much faster than that of propagation ($k_{init} >> k_{prop}$). This leads to the linear growth of polymer chains with a relatively small distribution of molecular weights, which can be predicted by variation of the monomer to initiator ratio. Addition of further monomer units would facilitate continued polymerisation of the polymer chain. There is no termination step in this process, but termination can be induced through quenching by addition of an alcohol or by cyclisation of the growing polymer chain.

By contrast, "immortal" ROP is not terminated by alcohol addition or the presence of excess alcohol. Instead, the alcohol acts as a chain transfer agent *via* alkoxide exchange at the metal and increases the number of growing polymer chains. In this scenario, monomer-to-alcohol ratio is generally a good predictor of molecular weight.[32]

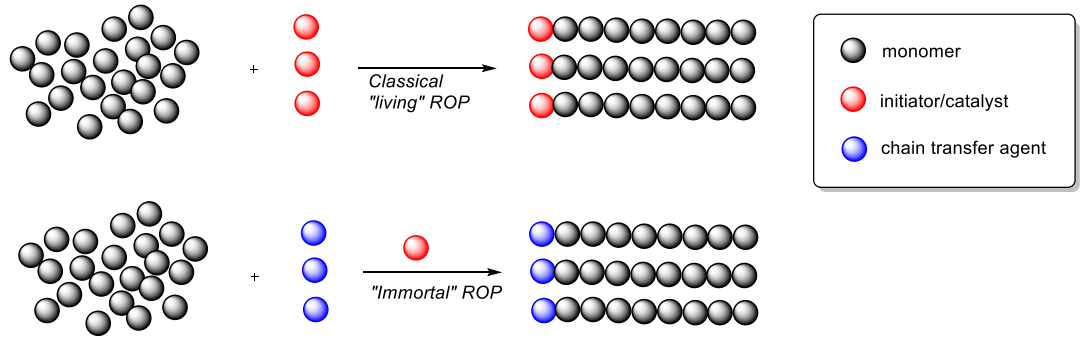

Figure 1.11. Illustration of "living" and "immortal" ROP processes.[46]

Transesterification is a common side-reaction during the ROP of lactide by any mechanism. This can occur between polymer chains in an intermolecular chain transfer, or *via* intramolecular 'backbiting' into the same polymer chain (Figure 1.12). These side-reactions are undesirable as they can lead to larger dispersity of molecular weights and a loss of stereocontrol over the polymer architecture. Transesterification tends to happen at high temperatures, so it is important that initiators can work at high temperatures without being susceptible to these undesirable side-reactions.

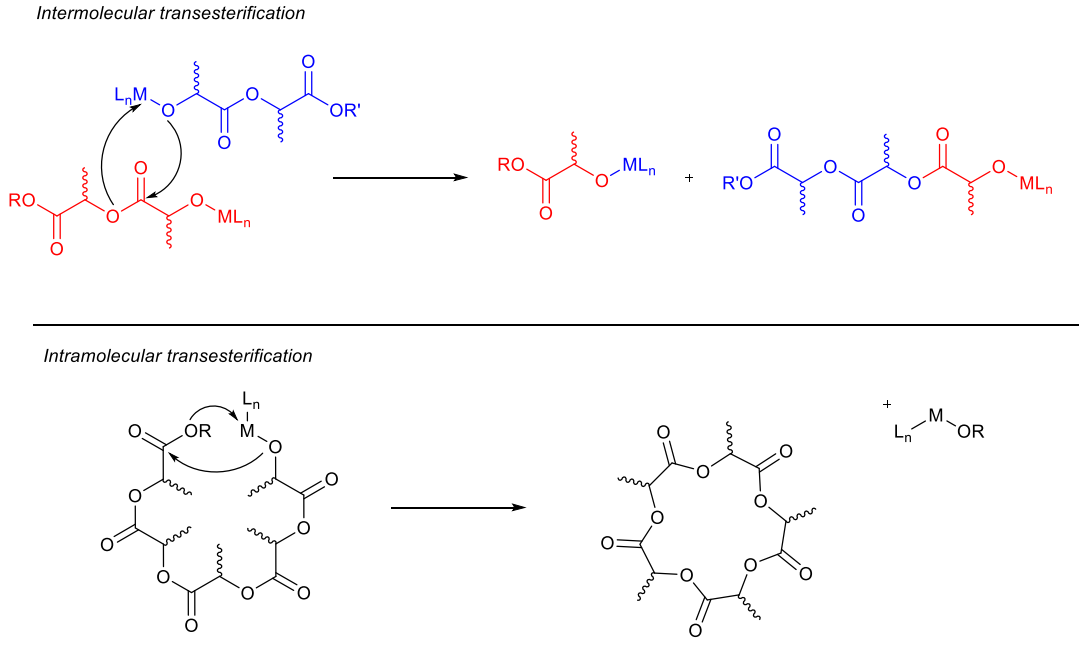

Figure 1.12. Inter- and intramolecular transesterification reactions in lactide polymerisation

1.1.3 Ring-opening copolymerisation (ROCOP)

An alternative route to polyesters, which was first reported in the 1960s but which has gained more interest in recent years, is the ring-opening copolymerisation (ROCOP) of epoxides with cyclic anhydrides.[47,48] This method allows for a large range of potential monomers to be incorporated into the polymer product, including introducing aromatic

regions into the chain which could modify the glass transition temperature, and can be desirable to increase the mechanical strength of the polymer.[49] ROP requires entirely new monomers or co-monomers to introduce different structures into the polymer backbone, which may not polymerise under the same conditions thus limiting the number of potential accessiblenmaterials.[48] ROCOP has the advantage that many different epoxide or anhydride monomers can be substituted under the same polymerisation conditions, changing the structure of the product. Ideally the anhydrides or epoxides would be from renewable sources: there is great interest in developing organic acids from biomass fermentation (e.g. succinic, levulinic, and adipic acids), which provide a route to renewably sources anhydrides.[50] Terpolymerisation with CO_2 is also a possibility to produce poly(ester–carbonate)s,[48] as is combining ROP and ROCOP methodologies with a single initiator, as many initiators applied for ROP are also investigated for ROCOP.[51]

There have been many reported initiators for ROCOP for epoxides with anhydrides or CO_2, which can generally be applied to both methods. Initiators are often MLX-type, where M is the metal centre, L is a ligand and X is the initiating group, where propagation occurs (Figure 1.13). Once initiation has occurred, the epoxide and anhydride monomers will add sequentially to form the polyester, although competing epoxide homopolymerisation can lead to the formation of ether linkages.[48]

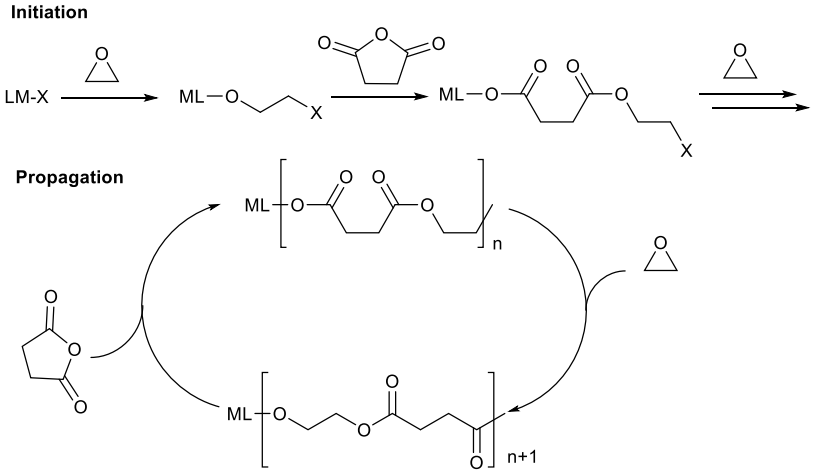

Figure 1.13. ROCOP initiation and propagation mechanisms.[48]

A further possibility with epoxide ROCOP is the formation of polycarbonates by copolymerisation with carbon dioxide, a highly desirable monomer for the plastics industry as it is abundant, has low toxicity, cheap and is a waste product in many chemical processes. This type of copolymerisation has been fairly extensively reviewed, including different monomers, initiators and computational investigations.[52–56]

1.1.4 Polymer characterisation

1.1.4.1 Gel permeation chromatography (GPC)

Gel permeation chromatography (GPC) is a technique used to determine polymer molecular weight. From GPC it is possible to probe the number average molecular weight (M_n) and the weight average molecular weight (M_w), directly related to the chain lengths within the polymer. M_n is a measure of the total molecular mass divided by the total number of molecules, while the fact that larger molecules have a larger contribution to the average molecular mass is considered by M_w.

The polymer sample is dissolved in an appropriate solvent (typically THF for PLA), passed through a column of porous beads and the eluent is detected at the end of the column by UV absorption or refractive index (RI) detectors. GPC is a form of size-exclusion chromatography: the smaller polymer chains can permeate the beads, while the larger chains flow around them. The larger chains therefore elute more quickly, having a faster retention time, while smaller chains take longer to pass through the column and have an increased retention time. Molecular weight and dispersity may be determined for each peak in the GPC chromatograph by comparison to a calibration curve.

Dispersity ($Đ$), a measure of polymer weight distribution, may be determined from the relationship of M_w/M_n. The equations required to calculate these are given in Equation 1.1 where M_i and N_i values are obtained from the GPC trace. For a perfectly uniform sample, $Đ$ would equal 1, with the number increasing as the range of polymer chain molecular weights become more varied. Narrow dispersity is indicative of a well-controlled polymerisation, while a large $Đ$ could be a sign of competing reactions, such as transesterification of polymer chains, or indicative of similar rates of initiation and propagation ($k_{init} \approx k_{prop}$) where chains are initiated over a period of time whilst propagating at the same rate. Under these circumstances the chains initiated first will have a larger molecular weight than those initiated later, resulting in a broad molecular weight distribution. [57] Referencing against internal standards, usually polystyrene, allow for correlation of M_w to retention times, although this can lead to overestimation of molecular weights for samples with a different hydrodynamic volume (the volume of the polymer in solution) to PS. For PLA, a correction factor of 0.58 is frequently applied.[58]

Equation 1.1. Equations relating to polymer chain length (M_n, M_w) and distribution ($Đ$)

$$M_w = \frac{\Sigma {M_i}^2 N_i}{\Sigma M_i N_i};\ M_n = \frac{\Sigma M_i N_i}{\Sigma M_i}\quad Đ = \frac{M_w}{M_n}$$

Other GPC detection methods available include viscometry and light scattering. For single detection viscometry measurements, the intrinsic viscosity and concentration of the polymer sample is measured and compared to a calibrant. For light scattering, the size of the molecule is equated to the angle of light diffraction by the sample. The three methods can be combined in a triple detection instrument, giving more accurate estimates of the polymer molecular weights.[59]

1.1.4.2 MALDI-TOF mass spectrometry

Matrix-assisted laser desorption ionisation time-of-flight (MALDI-ToF) is a mass spectrometry technique, used to determine polymer repeat units and end groups. In MALDI-ToF, a soft ionisation technique is used to prevent fragmentation of the polymer molecule. The analyte is prepared by solution mixing with a suitable matrix and ion source which assist the ionisation and charging of the sample. The matrix is usually acidic and acts as a proton source during ionisation. Generally, it is important to match the matrix polarity with the polymer under investigation. The mass and the distribution of the chain lengths can be determined from the time taken for the ions to reach the detector. The high resolution in MALDI-ToF allows for individual polymer chain masses to be quantified.

The spacing between the peaks on a MALDI chromatograph give information on the mass of the polymer repeat unit. For PLA this is particularly useful – a spacing of 72 $gmol^{-1}$ indicates transesterification has occurred during the polymerisation process (for PLA the spacing should be 144 $gmol^{-1}$, the mass of a ring-opened lactide monomer). The chain end groups may also be identified, allowing elucidation of polymerisation mechanism and the extent of side reactions.[60,61]

There are some limitations in polymer characterisation by MALDI-ToF spectrometry. Ionisation of the polymer chains is required, and these ions need to be susceptible to an electric field. This can lead to discrepancies between molecular weight values calculated by MALDI-ToF and GPC, and samples are limited to maximum molecular weights around 10 $kgmol^{-1}$. Generally, accurate molecular weight values may not be accurately determined by MALDI-ToF for disperse samples ($Đ > 1.2$).[62]

1.1.4.3 Nuclear magnetic resonance (NMR) spectroscopy

Nuclear magnetic resonance (NMR) spectroscopy is a very powerful tool in polymer chemistry. From a simple ^{1}H NMR spectrum of a crude polymer sample, the conversion from monomer to polymer can be readily obtained from the integrals of relative resonances. NMR spectroscopy is particularly useful for characterising PLA. Homonuclear decoupled (HND) NMR spectroscopy can be utilised to elucidate the tacticity of the material produced from *rac*-LA by decoupling the resonances of the methine protons (δ ~ 5 ppm in $CDCl_3$). This resolves the methine region into five distinct resonances, which correspond to different tetrads in the polymer chain (Figure 1.14). These arise from the linkages between four lactic acid units, where the linkage can be an isotactic linkage, *i* (*R,R* or *S,S*) or a syndiotactic linkage, *s*, (*R,S* or *S,R*). It therefore follows that a purely isotactic sample of PLA would show a tetrad of [*iii*], where all chiral centres are in the same configuration. The relationship between these tetrad resonances can be related to the overall tacticity of the sample based on Bernoullian statistics (Table 1.4).[63] This analysis affords P_r, the probability of heterotactic enchainment, and P_m, the probability of isotactic enchainment, with the sum of these probabilities equalling 1. P_r is readily calculated from the normalised intensity of the [*sis*] tetrad using Equation 1.2.

Table 1.4: Tetrad probabilities based on Bernoullian statistics for *rac*-lactide[63]

Tetrad	*rac*-LA
[*iii*]	$P_m^2 + P_r P_m /2$
[*iis*]	$P_r P_m /2$
[*sii*]	$P_r P_m /2$
[*sis*]	$P_r^2/2$
[*isi*]	$(P_r^2 + P_r P_m)/2$

Equation 1.2. Calculation of P_r

$$P_r = \sqrt{2 \times [sis]}$$

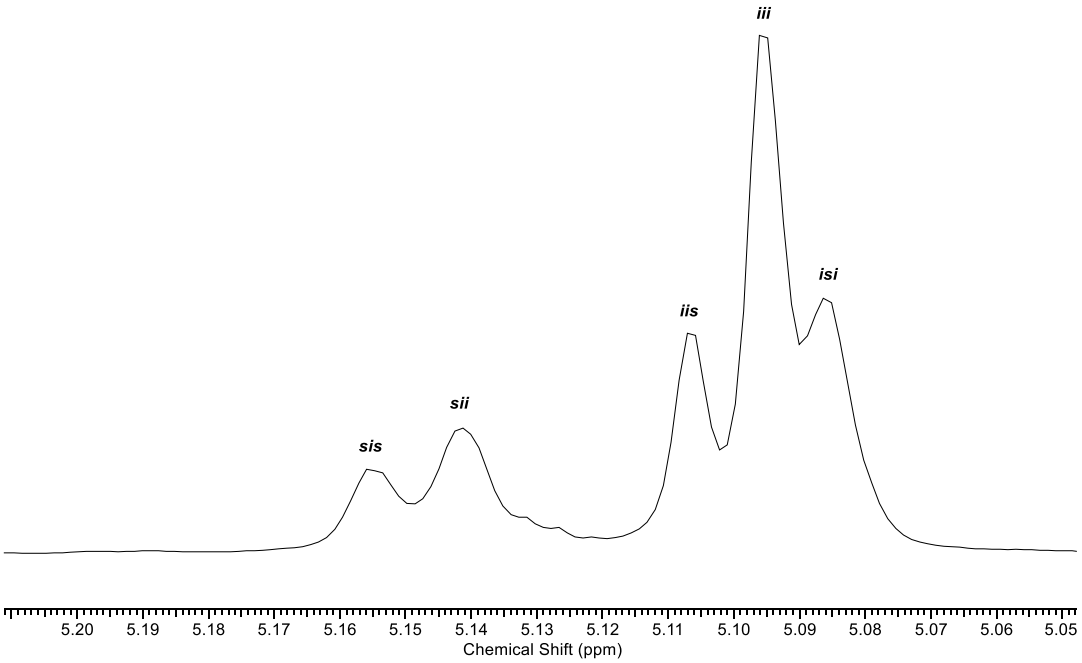

Figure 1.14. Representative homonuclear decoupled ^{1}H NMR spectrum, showing the five resonances corresponding to five possible tetrads in PLA chains prepared from polymerisation of *rac*-LA.

When the calculated P_r value is below 0.5, the polymer has some isotactic microstructure. When the [*isi*] tetrad and [*sis*] tetrads are the major resonances, the polymer will have heterotactic character, with a P_r value greater than 0.5 enchainment (Table 1.5). Perfectly isotactic PLA would have a P_r of 0.0 while perfectly heterotactic PLA would have a P_r value of 1.0. A P_r value of 0.5 is indicative of atactic PLA.

Table 1.5. Assignment of PLA microstructures based on values of P_r and P_m for polymerisation of *rac*-LA

P_r	P_m	PLA microstructure
$0.5 < P_r \leq 1$	$0 \leq P_m < 0.5$	Heterotactic
$0 \leq P_r < 0.5$	$0.5 < P_m \leq 1$	Isotactic
0.5	0.5	Atactic

1.1.4.4 Differential scanning calorimetry (DSC)

Differential scanning calorimetry (DSC) provides information about a material's thermal properties and can identify thermal events such as glass transition (T_g), melting (T_m) and crystallisation temperatures (T_c). These phase changes are accompanied by a change in heat capacity, which can be measured by the heat required to heat a solid sample against a blank reference at the same heating rate to maintain a constant temperature. The difference in heat flux is plotted against temperature. At phase changes, there will be a greater or lesser amount of heat required, which will be observed as a peak or trough in

the DSC trace. Another method which may afford this information is dynamic mechanical analysis (DMA), which can also be useful for studying the viscoelastic properties of a material such as stress and strain.

1.2 Stereoselective initiators for ROP

Research into the derivation of stereoselective initiators for ROP is extensive. Tin octanoate $Sn(Oct)_2$ (Figure 1.15) is the industrially preferred initiator as it is robust, cheap and facilitates immortal ROP, allowing for the preparation of high molecular weight PLA (10^5-10^6 kDa) in the presence of alcohol under industrial conditions (180-210 °C, [LA]:[Sn]:[BnOH] = 1000:1:10).[64] However, its lack of stereoselectivity over ROP of *rac*-LA and potential toxicity concerns (particularly where PLA is used for biomedical applications) have led to alternatives being sought.

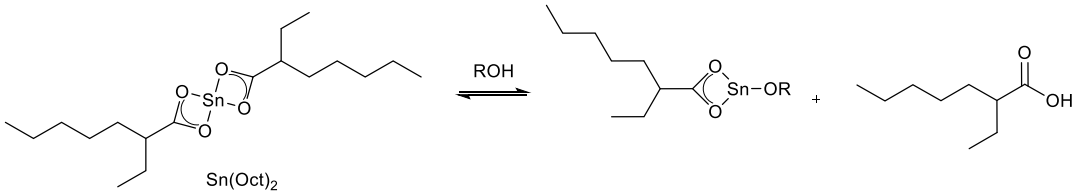

Figure 1.15. Generation of the active Sn-alkoxide species for ROP with $Sn(Oct)_2$/ROH

Due to the large and varied literature available on the ROP of lactide, the focus on this introduction will be on lithium, magnesium aluminium, zinc and zirconium with emphasis on complexes bearing bis(phenolate) ligands, as these are of relevance to this project. Commonly used ligands include Schiff bases such as salan, salen, salalen ligands and alkoxy-amino phenolate ligands. All of these have been studied for widespread applications in inorganic catalysis thanks to ease of ligand preparation, structural modification and high affinity of the ligand with a wide variety of metal ions in different oxidation states.[65,66]

1.2.1 Li(I) initiators

Group I metals such as Li(I) and K(I) are attractive as initiators for the polymerisation of *rac*-lactide due to their biocompatibility and abundance. Generally, group I initiators are cited as highly active but lacking stereocontrol and low temperatures may be required.[67] Complexes tend to be multinuclear, although monomeric species as initiators for ROP have also been reported.[68] An early example using lithium tert-butoxide (LiO^tBu) as an initiator was reported by Kasperczyk, who reported the preparation of heterotactic PLA in 1 hour at 20 °C.[69] By lowering the reaction temperature to -20 °C, high molecular weight heterotactic PLA was achieved in 5 minutes (P_r = 0.94, M_n = 35,000). The increased stereoselectivity was

attributed to a reduction in transesterification reactions. Potassium *tert*-butoxide has also demonstrated moderate catalytic activity for ROP.

Metal complexes bearing phenolate ligands have attracted a great deal of interest as initiators/catalysts in the ROP of PLA due to their ease of preparation and potential for structural variation. Initiators with numerous lithium centres have been reported with a wide variety of structural motifs including cubes, ladders, lattices, pinwheels and dimers.[67]

A series of lithium aggregate compounds supported by a 2,2-ethylidene-bis(4,6-di-tert-butylphenol) ligand, with coordinated benzyl alcohol or 2-ethoxyethanol, were synthesised by Ko and Lin (Figure 1.16, **1**-**3**).[70] No ROP activity was reported with complex **1**, but complexes **2** and **3** were applied for ROP of *L*-LA, with the authors finding controlled polymerisation to PLA with narrow dispersity (*Đ* = 1.06-1.43), with near-quantitative conversion in 1 hr at RT or 6 h at 0 °C, and good agreement between predicted and observed M_n values. In a later publication, complexes **2** and **3** were further modified in THF to yield pentalithium lattice-like structures **4** and **5** respectively.[71] The ROP of *L*-LA with **5** was systematically examined in CH_2Cl_2, with high conversions (< 96%) observed within 3 hours at 0 °C, with polymers having narrow dispersities (*Đ* = 1.06-1.07) and no observable epimerisation by ^{1}H NMR. A linear relationship between the number-average molecular weight (M_n) and the monomer-to-initiator ratio was observed. End group analysis suggested insertion of an -OCH_2CH_2OEt moiety from the complex was the initiation process, suggesting a coordination-insertion mechanism. This contrasts to the proposed mechanism for complex **2**, which the authors suggest proceeds by an activated monomer mechanism.

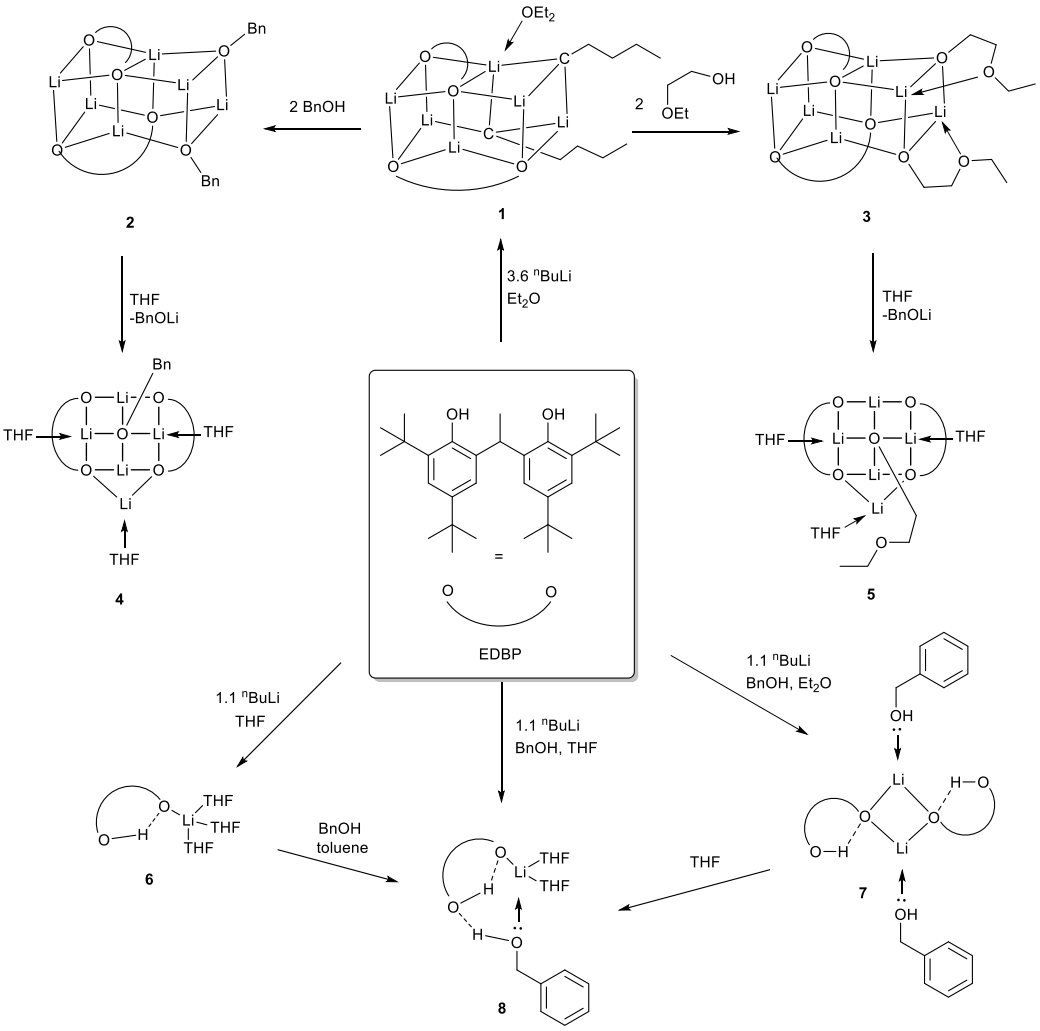

Figure 1.16. Lithium complexes of the 2,2-ethylidene-bis(4,6-di-tert-butylphenol) ligand reported for ROP[70–72]

Furthering this work, Hsueh *et al.* prepared monomeric and dimeric lithium complexes from the same ligand (Figure 1.16, complexes **6**-**8**).[72] **7** and **8** were both shown to be effective initiators for ROP of *L*-lactide, yielding polymers with very narrow dispersity in a wide range of monomer-to-initiator ratios. Block copolymer polystyrene-b-poly(*L*-lactide), was also prepared from the ROP of *L*-latide catalysed by **8** using hydroxy-functionalised polystyrene as a macroinitiator. The polymerisation with BnOH as a chain transfer agent was investigated, with 32 eq. of BnOH added, with the resultant M_n and $Đ$ values supporting immortal polymerisation. The authors propose a coordination-insertion mechanism *via* a monomeric intermediate (Figure 1.17). The reaction was much slower with **8** than **7**, and the authors suggest that coordination of LA to lithium centres is hindered by competition with THF molecules. A similar effect was observed by Lu *et al.*, who reported that by changing coordination number of the ligands from 3 to 2, the activity

dramatically increased. This was justified by competition between the third coordination atom with *L*-lactide.[73]

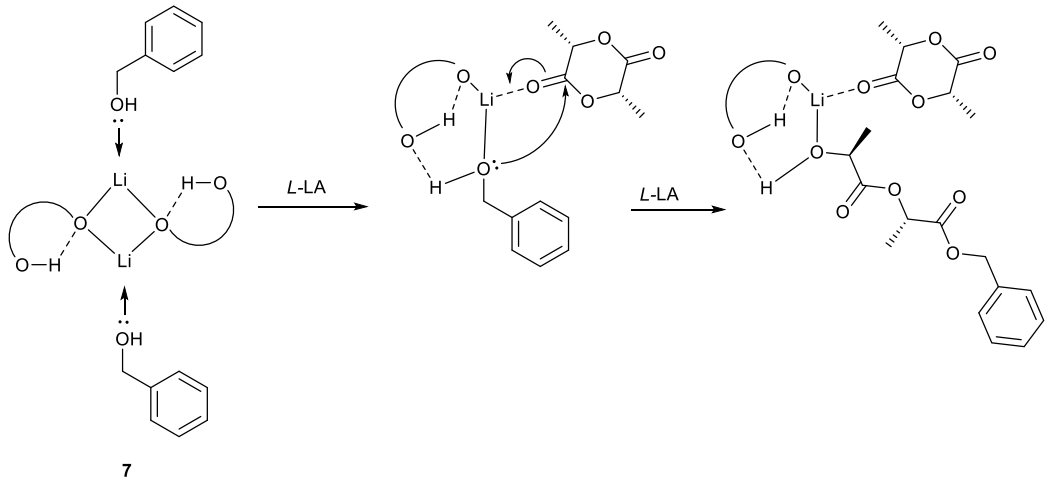

Figure 1.17. Proposed Mechanism for ring-opening polymerization of *L*-Lactide Initiated by complex **7**[72]

Lithium bis(phenolate) complexes were reported by Chisolm *et al*, who reported the unusual "n-butyllithium trap" lithium aggregate, **9**, comprising two ligands and eight lithium centres (Figure 1.18).[74] This octo-lithium complex was easily converted into an alkoxy-containing structure, **10**, with a dramatic skeleton change. This structure was investigated as an intermediate in the synthesis of zinc, aluminium and titanium structures, although some polymerisation studies were performed with the lithium alkoxide itself. The authors found it was active for ROP of *rac*-LA at ambient temperature (1 hr), and at 0 °C (4 hr), yielding atactic PLA with broad dispersity in both cases (*Đ* = 1.70-1.72).

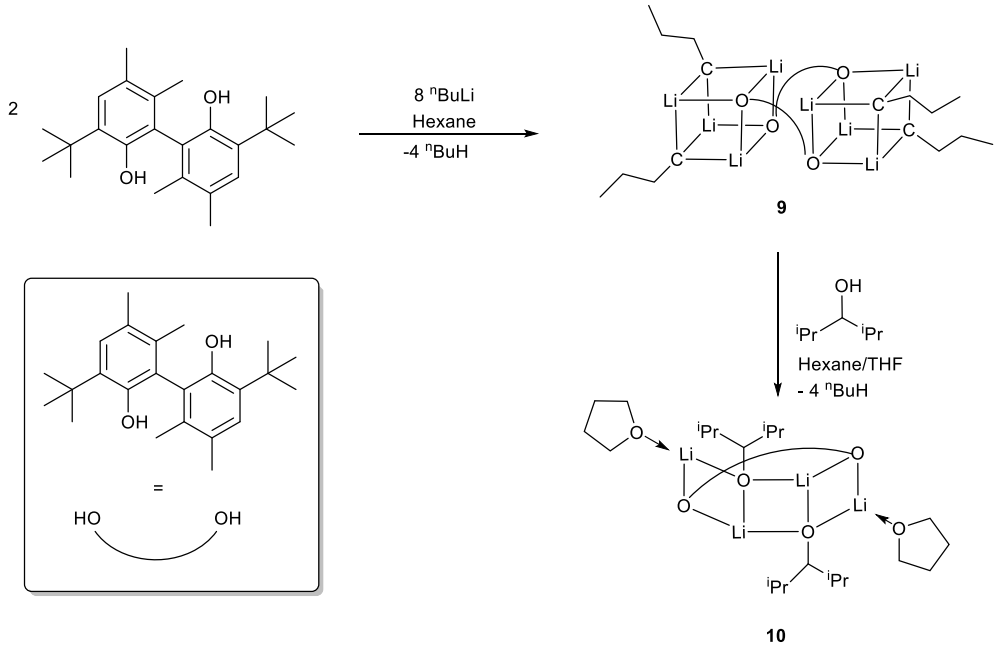

Figure 1.18. Lithium structures **9** and **10** observed by Chisholm *et al.* and studied for ROP of *rac*-LA[74]

Another study investigated lithium and sodium complexes of a tridentate analogue of this ligand.[75] Complexes **11**-**13** were obtained and characterised in the solid-state, with a wide range of structural motifs observed (Figure 1.19). Most of these dinuclear and tetranuclear alkali-metal complexes were active toward the ROP of *L*-lactide in the presence of BnOH. A comparison of the ROP activity of the tetranuclear and dinuclear initiators was reported, with tetranuclear lithium and sodium complexes being more active in the ROP of *L*-lactide than in the ROP for dinuclear complexes. The polymerisation processes appear to possess "immortal" character by a faster reaction using 2 equivalents of BnOH with half of the molecular weight of the polymer found in the reactions compared with those when 1 equivalent of BnOH was used.

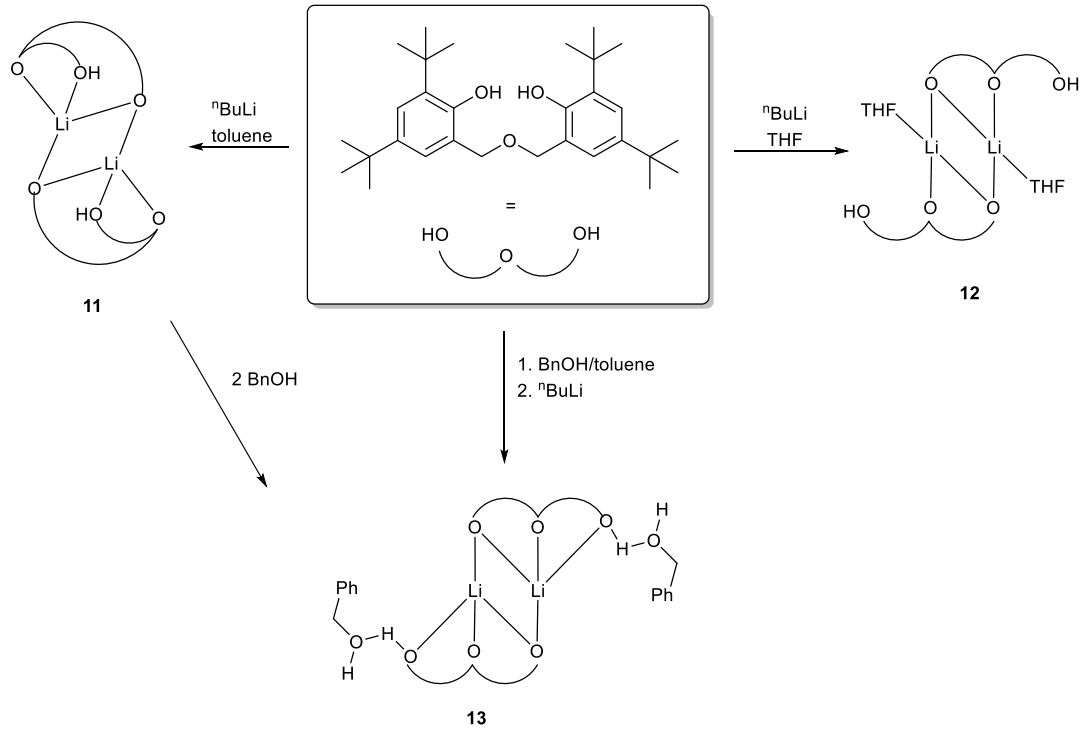

Figure 1.19. Preparation of lithium complexes of tridentate ligand, **11**-**13**[75]

Another study investigated sodium, lithium and potassium complexes of tetra(phenolate) ligands **14** and **15** (Figure 1.20), finding that polymerisation with complexes of the *meta*-substituted ligand **15** had inferior control over the polymerisation compared to complexes of the *para*-substituted ligand **14**, and suggest that the presence of asymmetric active metal centres in these complexes give rise to different initiation and propagation rates for ROP of lactide.[76]

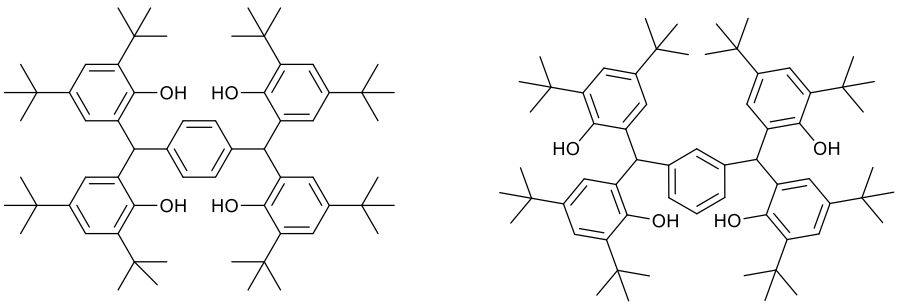

14 **15**

Figure 1.20. Tetra(phenolate) ligands **14** and **15** employed by Zhang *et al.* [76]

Some other recent examples of lithium aggregates for ROP of lactide are shown in Figure 1.21, showing the wide range of structural diversity available with phenolate ligands, such as cisoidal ladders (**16**, **17**), cubane-like structures (**18**-**23**), pinwheels (**24**, **25**) and tetranuclear aggregates (**26**, **27**). Strategies such as increasing steric bulk around the imine moiety of a ligand have been shown to increase kinetic activity of the complex to initiate ROP in a controlled manner.[73,77,78]

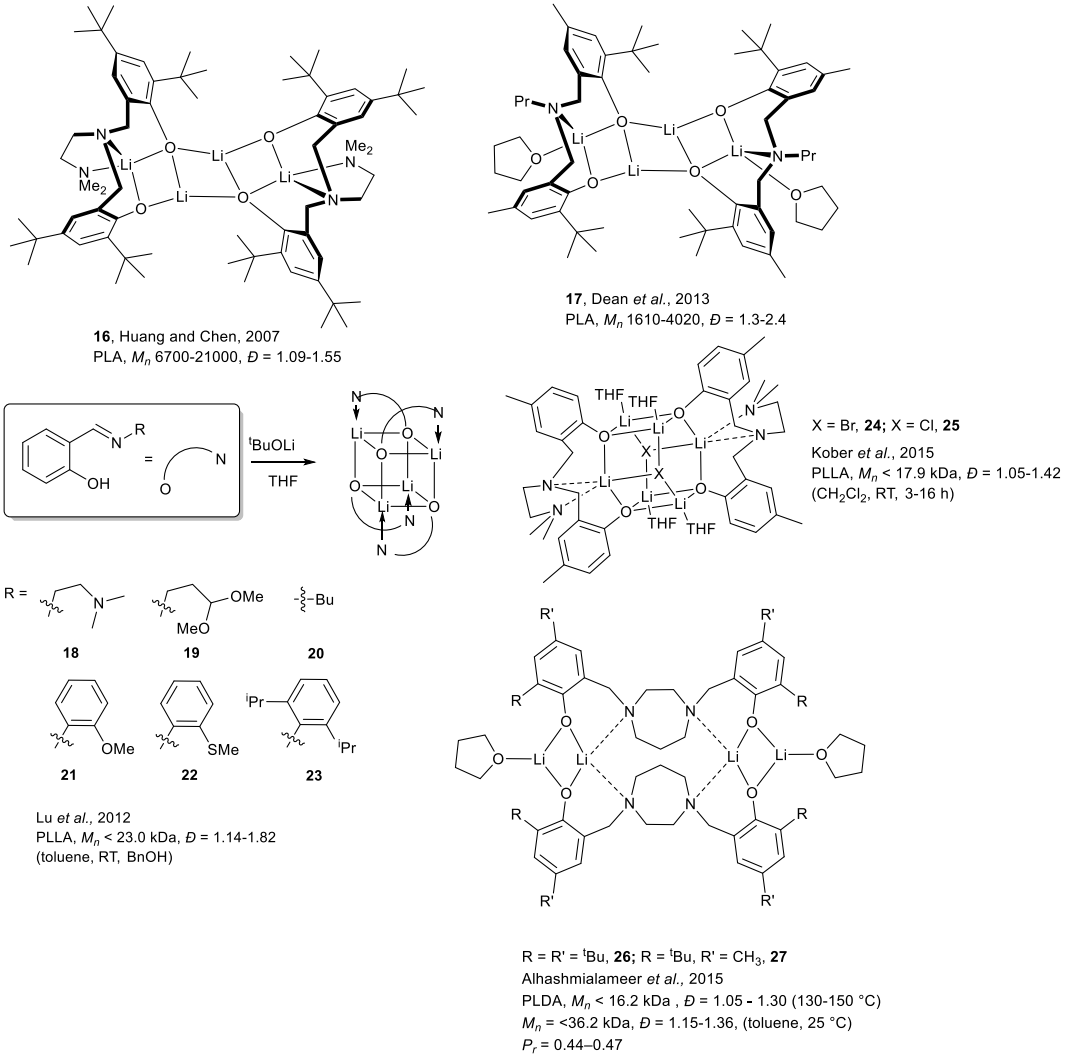

Figure 1.21. Lithium aggregates reported for ROP of lactide[73,77–80]

Generally, polymerisations are well controlled in terms of molecular weight and dispersity but there have been few examples of polymerisations performed with *rac*-LA and initiators imparting stereocontrol over the process. One example which reported the synthesis of heterotactic PLA from *rac*-LA was reported by Char *et al.* in 2016, in which a series of Li(I) complexes of amine bis(phenolate) ligands were prepared *in situ*, with P_r values observed up to 0.86, although the authors were unable to isolate or characterise active organometallic species.[81]

1.2.2 Zn(II) and Mg(II) Initiators

Group II initiators are attractive in PLA synthesis due to their biocompatibility and suitability for biomedical applications.[82] They are also readily available and cheap. Group II metal-based initiators often exhibit high activity towards the ROP of LA, which is typically related to their high Lewis acidity. The majority of reports describe Mg(II)

initiators, although examples with selective Ca(II) initiators have also been reported.[83] Zn(II) is often reported and contrasted with Group II metals, having similar charge and valency, and is often coordinated to similar ligands.[82] Zn(II) enjoys much interest due to its high activity, abundance and biocompatibility.[84]

Coates and co-workers developed a number of zinc β-diketiminate (BDI) initiators for selective production of heterotactic PLA (P_r < 0.94 when R = ^{i}Pr) in CH_2Cl_2 at 20 °C (**28**-**30**, Figure 1.22).[85,86] The magnesium analogue, **31**, did not exhibit the same selectivity, producing atactic PLA. The effect of backbone substitution on the production of PLA have since been further investigated by Chisolm *et al.*.[87] Increasing steric bulk in the backbone was found to have a reduction in heterotacticity, producing mostly atactic PLA. Polymerisation was highly controlled (*Đ* = 1.1). Chisolm also reported monomeric Zn(II) and Mg(II) alkoxide complexes with BDI ligands with a bulky O^{t}Bu alkoxide ligand (**32** and **33** respectively). The Zn(II) complex was found to be selective for heterotactic PLA, while the selectivity of the Mg(II) complex could be tuned by using different solvents for polymerisation: in THF heterotactic PLA was produced (P_r = 0.90), while in CH_2Cl_2 the product was atactic PLA.[88] The difference in selectivity is attributed to the coordination of a THF molecule to the Mg(II) centre, leading to more sterically hindered active site. The stereoselectivity of some Group II initiators drastically changing in different solvents has been reported previously.[89,90]

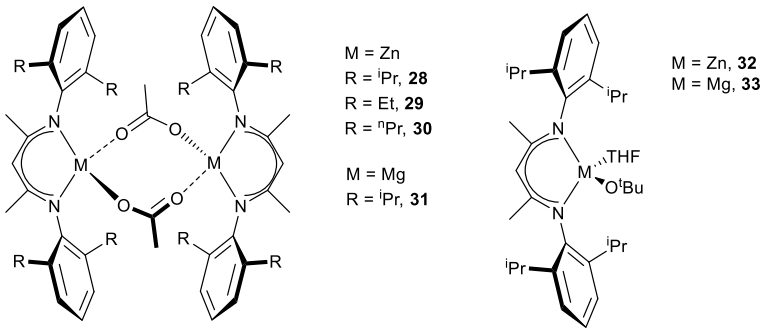

Figure 1.22. Zinc BDI initiators for heterotactic ROP of *rac*-LA reported by Coates *et al*.[85,86] and monomeric complexes reported by Chisolm *et al*.[88]

Tolman and co-workers reported a highly active zinc alkoxide initiator, **34**, with a tridentate alkoxide ligand (Figure 1.23).[84] Considerable effort was taken to determine the structure of the complex, which appeared to exist in a rapidly equilibrating mixture of the monomeric and dimeric species, **35**. The dimeric species was found to be highly active for ROP, achieving high molecular weights (up to 130 kgmol^{-1}) in good conversion in short reaction times (5 minutes). Molecular weights were somewhat lower than predicted, and

dispersities of roughly $Đ$ = 1.4 could suggest the presence of impurities causing chain transfer. This initiator was also later applied for the polymerisation of a menthone-derived lactone monomer.[91]

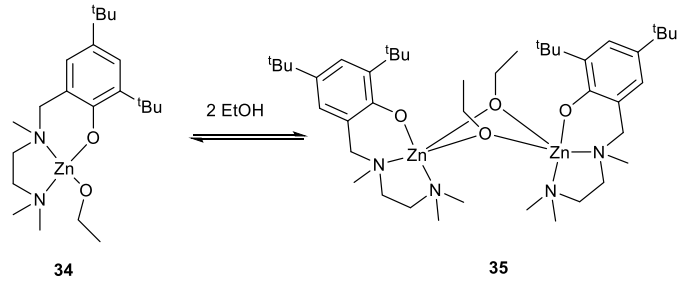

Figure 1.23. Zinc alkoxide initiator reported by Hillmyer, Tolman and co-workers[84]

Peng *et al.* also developed zinc initiators that form dimeric species, **36**, upon addition of a co-initiator (Figure 1.24), and showed their activity for the ROP of cyclic esters including lactide, ε-caprolactone, β-butyrolactone and δ-valerolactone.[92] The complex was found to dissociate upon heating above 30 °C, with the resulting monomeric species, **37**, not exhibiting any activity for ROP. The dimeric species exhibited no stereoselectivity in ROP of *rac*-LA.

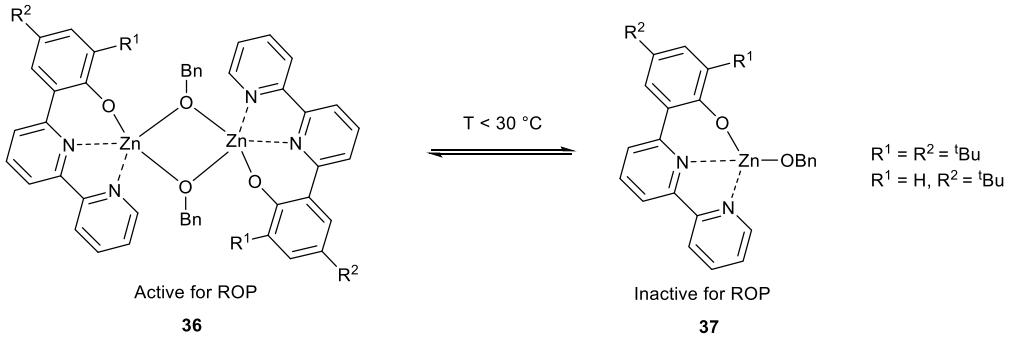

Figure 1.24. Equilibrium between monomeric and dimeric Zn(II) complexes with bipyridine ligands[92]

Mg(II) has also been used to produce almost perfectly heterotactic PLA in THF at 0 °C (P_r = 0.98) by Cui *et al.,* who employed phosphinimino-amine ligands with varying steric bulk.[93]

Racemic monophenolate ligands complexed to Mg(II) and Zn(II) have been shown to exhibit immortal polymerisation characteristics with good activity in both solvent and melt conditions (Figure 1.25). The diastereotopic complexes, **38**-**42**, showed modest heterotactic bias (P_r < 0.66), while good control was evidenced by predictable molecular weights and narrow dispersities. Zn(II) complexes **40** and **41** also showed immortal behaviour. Analogous Ti(IV) complexes did not display control during ROP.

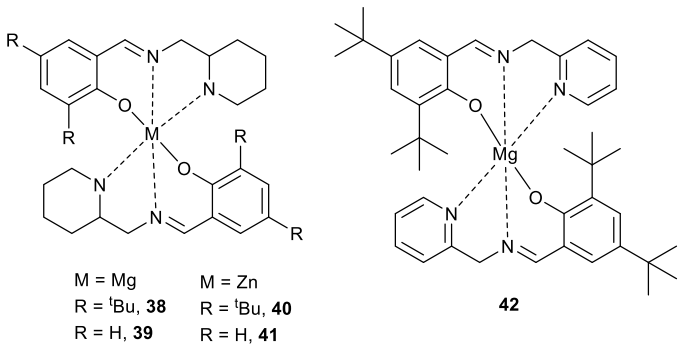

Figure 1.25. Piperidine-based Zn(II)) and Mg(II) complexes prepared by Jones *et al.*[94]

Kol and co-workers have prepared Mg(II) and Zn(II) complexes based on a chiral *R,R'*-bipyrrolidine ligand (Figure 1.26).[44,95] All complexes, **43**-**45**, are monomeric and pentacoordinate. The zinc bipyrrolidine system (**44**) achieved high conversion within 15 minutes (CH_2Cl_2, RT), producing PLA with a slight isotactic bias (P_m = 0.71).[95] The more flexible initiator system, **45**, was shown to have an induction period before polymerisation, being attributed to the formation of the active alkoxide complex. Polymerisation was rapid after this induction period, and higher isotactic bias was observed with the bulkier benzyl substituted ligand (R = Bn, P_m = 0.81).

High activity was reported with the analogous Mg(II) bipyrrolidine system, **43**, with full consumption of thousands of equivalents of *L*-LA within 6 minutes in a living fashion to give polymers with predictable molecular weights (M_n < 266 kDa) and narrow dispersity ($Đ$ = 1.04-1.07).[44] Sequential addition of *L*-LA and *D*-LA allowed for formation of precise block copolymers with up to eight segments. Thermal characterisation revealed stereocomplex formation, with high T_m values and melting enthalpies compare to homopolymers (T_m < 211 °C, ΔH_m = 65 J/g, 1:1 *L*-LA/*D*-LA diblock polymer).

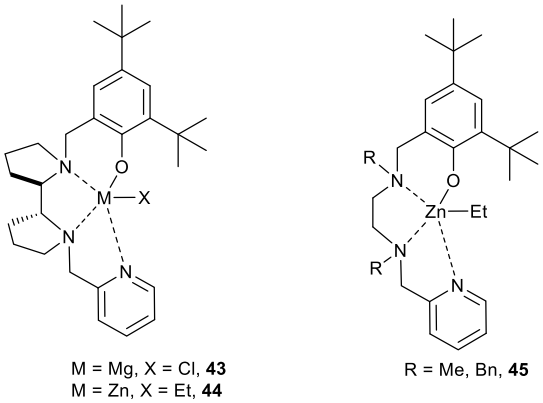

Figure 1.26. *R,R'*-bipyrrolidine and more flexible ethylenediamine complexes prepared by Kol *et al*.[44,95]

The highest isotacticity in a Zn(II) complex reported to date was by Abbina and Du, who employed chiral amido-oxazolinate ligands.[93] The authors reported P_m values up to 0.86 and high conversions of *rac*-LA in 30 minutes at 50 °C. At cooler temperatures this isoselectivity was enhanced, albeit at a slower rate (23 °C, P_m = 0.91). Isotacticity was somewhat maintained under melt conditions (P_m = 0.77) was, and the authors suggest a combination of SCM and CEM mechanisms occur, giving the stereoselectivity.

A series of dimeric Mg(II) complexes was prepared by Kozak *et al.* by complexation of tetradentate amine bis(phenolate) ligands to di(*n*-butyl)magnesium ($^nBu_2Mg$) (Figure 1.27).[96] This was the first example of magnesium complexes of amino(phenolate) ligands showing good lactide ROP activity in both melt and solvent conditions to yield largely atactic PLA. High conversion was observed with **46**, although M_n values were not consistent with calculated and dispersities were somewhat broad. In solution the polymerisation is much more rapid with the addition of BnOH co-initiator, with the authors suggesting an initiation period is due to formation of the alkoxide species *in situ.* Mechanisms for ROP with and without BnOH were proposed, with the dimers splitting into monomeric species in both cases. Analogous magnesium complexes have also shown to be active for ROP of ε-caprolactone by Bochmann *et al.*[97]

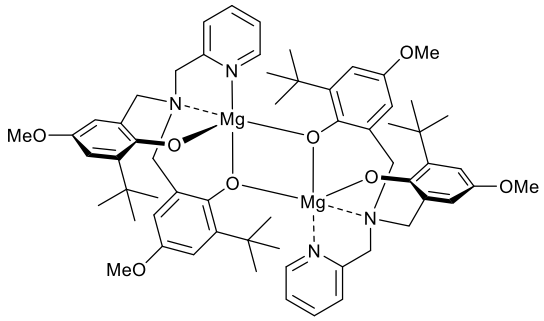

46

Figure 1.27. Dimagnesium complex prepared by Kozak *et al.*[96]

A series of Mg(II) complexes suppoorted by amine bis(phenolate) ligands **47**-**49** (Figure 1.28) were reported by Ghosh *et al.*[98] Here, the authors synthesied complexes that varied in amine alky chain length and phenol ring subsitutent to determine if any change in steric bulk or ligand rigidty could impose greater stereocontrol in the ROP of *rac*-lactide.

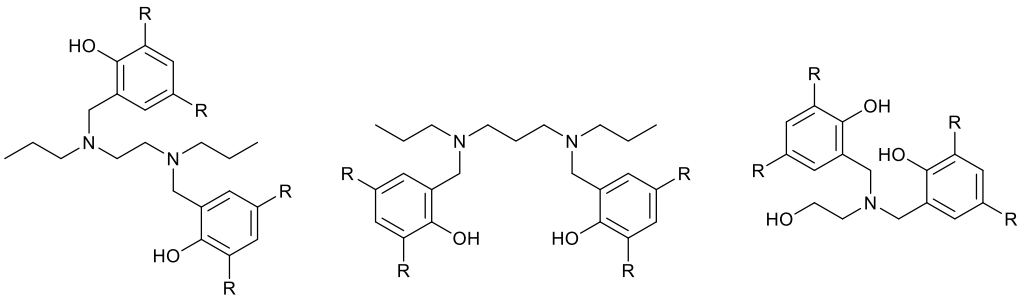

Figure 1.28. Salan ligands for complexation to Mg(II) reported by Ghosh and co-workers.[98]

In all cases dinuclear or trinuclear species were isolated, and these were trialled for the polymerisation of both *L*- and *rac*-lactide, exhibiting high activity with > 90 % conversion in 1 hour at 140 °C. When R = Me, the initiators were shown to be more active than those with R = ^{t}Bu. The authors proposed that the bulkier substituents hindered the approach of lactide to the Mg centres. A heterotactic bias was exerted with all initiators, P_r = 0.70-0.78, with or without the addition of benzyl alcohol at 140 °C. Improved control was observed with the addition of BnOH, with *Đ* decreasing marginally from 1.2 to 1.1. Linear correlation was observed between increasing molecular weight and lactide concentration. No solution-based studies were reported in this instance.

Dinuclear magnesium complexes have been previously shown to be active in the ROCOP of cyclohexane oxide (CHO) and CO_2.[99,100] The complexes reported by Ghosh were trialled for the ROCOP of CHO and CO_2 showing good catalytic activity, with conversion of > 78 % and high M_n. Being active in both ROP and ROCOP processes increases the appeal in large scale industrial applications of Mg(II) for the synthesis of polyesters and polycarbonates.

1.2.3 Group IV

Titanium, zirconium and hafnium complexes have gained interest as initiators for ROP of *rac*-lactide over the last decade. This area is considerably less studied than initiators with metals such as tin, zinc and rare earths, and there is further investigation into new ligand scaffolds required.[101] Zirconium initiators are attractive due to their similar coordination chemistry to tin whilst being considerably more benign. They have been reported to be particularly robust and capable of maintaining well-controlled polymerisation in the presence of water in solution polymerisations and with monomers with impurities for melt polymerisations.[102]

Davidson *et al.* reported a series of Zr(IV) and Ti(IV) initiators (**50**-**55**) with bidentate ligands (Figure 1.29). The titanium initiators **50** and **51** exhibited no activity in solvent

polymerisation conditions and melt polymerisation yielded only atactic PLA. However, the Zr(IV) complexes all yielded heterotactically enriched PLA under both conditions.[102]

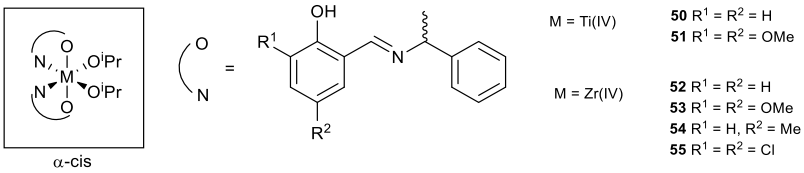

Figure 1.29. Bidentate group IV initiators for the ROP of *rac*-lactide[102]

In 2008 Davidson *et al.* also reported a C_3-symmetric amine tris(phenolate) ligand with group IV metals which were active under melt and solution polymerisation conditions (Figure 1.30). The zirconium tris(phenolate) complex, **57**, showed excellent activity for lactide melt polymerisation, with 78% conversion in 0.1 h to produce PLA of moderate molecular weight (32,300 g mol^{-1}), narrow dispersity ($Đ$ = 1.20) and strong heterotactic bias (P_r = 0.96). Hafnium complex **58** also gave moderate tacticity (P_r = 0.88). Again, the titanium complex, **56**, yielded atactic PLA.[103]

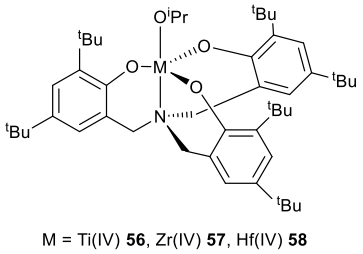

Figure 1.30. Group IV amine tris(phenolate) complexes applied for lactide polymerisation[103]

Several group IV complexes with tetradentate bis(phenolate) -ONNO- type ligands (Figure 1.31) have also been reported as initiators for ROP. These are simply prepared *via* a modified Mannich reaction with a diamine and appropriate 2,4-substituted phenol with excess paraformaldehyde in methanol. Zirconium complexes with A or B type ligands were generally found to yield isotactically-enriched PLA,[104] while zirconium complexes with homopiperazine or piperazine ligands (C and D) give very slight isotacticity with good control, with predictable molecular weights.

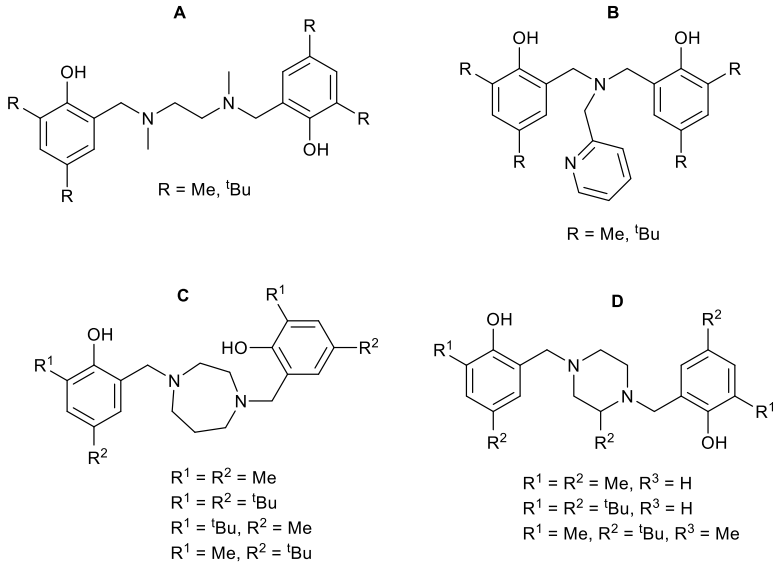

Figure 1.31. Tetradentate bis(phenolate) -ONNO-ligands developed for ROP initiators[104,105]

Recently reported work in the Jones group has investigated hetero- and isoselectivity for *rac*-lactide with a series of bis(phenolate) 2,2'-bipyrrolidine salan ligands with zirconium, hafnium, titanium and also aluminium (Figure 1.32).[106,107] The zirconium initiator *meso*-**59** yielded highly isotactically enriched PLA (P_m = 0.84).[106] The hafnium initiators (**60**) were selective for highly isotactic PLA, while aluminium (**63**) yielded heterotactic. Again, titanium complex **61** yielded atactic PLA. This example is unique in the literature as an example of an initiator which can be tuned for selectivity by modifying the metal centre to give either isotactic, heterotactic or atactic PLA.[107]

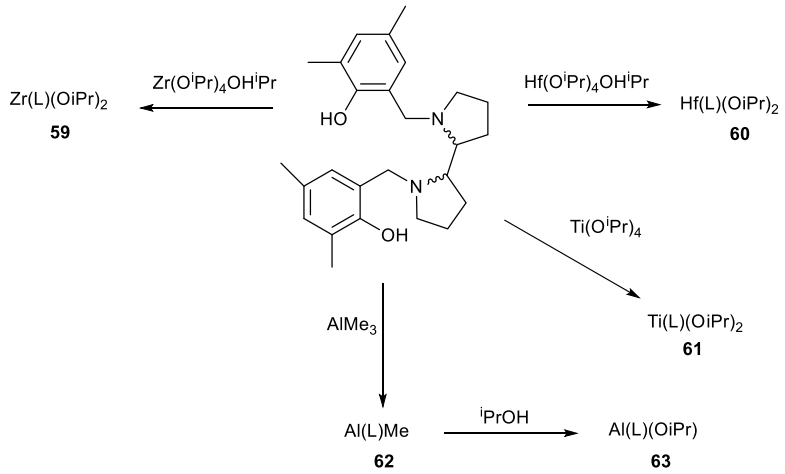

Figure 1.32. Initiators utilising bipyrrolidine ligands which have been reported by Jones *et al*.[106,107]

1.2.4 Al(III) initiators

Aluminium initiators have been extensively studied for isotactic selective ROP of *rac*-LA. It has been shown that ligands with greater coordination and steric bulk are preferable to achieve a degree of tacticity.

A notable early example of stereocontrol achieved with an Al(III) initiator was reported by Spassky *et al.* (complex **64**, Figure 1.33).[108] This selectivity arises from an enantiomorphic site control mechanism, with the imitator showing a slight preference for *D*-LA over *L*-LA, especially at low conversion. Feijen's initiator, **65**, based on a chiral Jacobsen's ligand was found to show high isotactic bias, producing PLA with P_m = 0.93, although long reaction times up to 12 days were required in toluene at 70 °C.[109] The mechanism here is also enantiomorphic site control, whereby both enantiomers of the initiator show a preference for one enantiomer of LA. A racemic initiator can therefore produce stereoblock PLA from *rac*-LA. A similar approach was reported by Sarazin, who reported enantiopure ligands based on a chiral (1,2)-diphenylethylene backbone complexed to Al(III), Ga(III) and In(III).[110] The authors achieved isotactic PLA with monomeric Al(III) initiators (P_m = 0.80-0.90), with evidence suggesting polymerisation occurred by a chain-end mechanism. With bulky ligand substituents and larger metals dinuclear species were isolated.

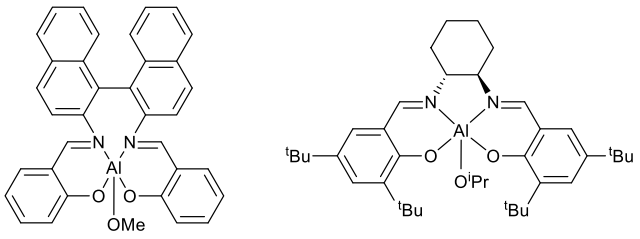

64, Spassky **65**, Feijen

Figure 1.33. Aluminium isotactic initiators reported by Spassky (**64**) and Feijen (**65**)[108,109]

Salen ligands have enjoyed much interest as initiators for ROP of cyclic esters. Investigations into modifying steric bulk of phenyl substituents and backbone substitution are common approaches to modifying complexes to achieve selectivity. Examples are shown in Figure 1.34. The simplest example, **66a**, was investigated by Spassky, who reported the ligand prepared from condensation of salicylaldehyde and ethylenediamine, and its complexation to Al(III) to give an initiator which exhibited mild isoselectivity (CH_2Cl_2, 70 °C) over *rac*-LA via a chain end controlled mechanism.[98] Conversion was kept below 70% to minimise transesterification side-reactions, and polymers had narrow dispersities ($Đ$ = 1.10-1.20).

This work was further explored by Nomura *et al.*, who investigated the relationship between selectivity and the backbone linkage between the salen groups,[42] and also varying the steric bulk of the phenyl substituents at the 2 position (Figure 1.34, **66b.**).[111] All initiators exhibited some degree of isotactic bias, and best results were seen with increasing steric bulk of the phenyl substituents in the *ortho*-position and increasing length

of the backbone. Lin and co-workers also investigated modifying the backbone of the initiator (**66c**.).[112] Isoselectivity (P_m = 0.94-0.97) and well-controlled polymerisation was observed in all cases, but little difference between the structures was observed, and polymerisations were slow, taking 12-14 h at 70 ° in toluene.

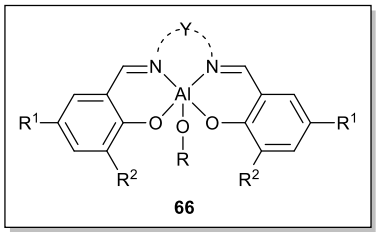

66

	Y	R^1	R^2	Reference
a.	$-CH_2CH_2-$	H	H	Spassky *et al*
b.	$-CH_2CH_2-$	H	Ph	Nomura *et al*
		^{t}Bu	^{t}Bu	
		H	^{t}BuMe$_2$Si	
c.		Cumyl	Cumyl	Lin *et al*

Figure 1.34. Achiral salen Al(III) complexes investigated by Spassky *et al.*,[98] Nomura *et al.*, [42,111] and Lin *et al.* [112]

The effects of varying backbone were further probed by Gibson *et al*, who studied a large range of different salen ligands for complexation to Al(III), including flexible alkyl backbones and more rigid backbones containing aromatic moieties (Figure 1.35, complexes **67**-**69**).[113] In most cases, bulky ^{t}Bu *ortho*- substituents (**69**) were preferred, as reported by Nomura.

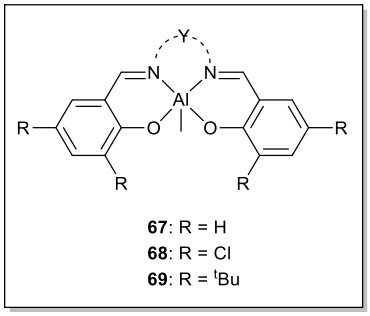

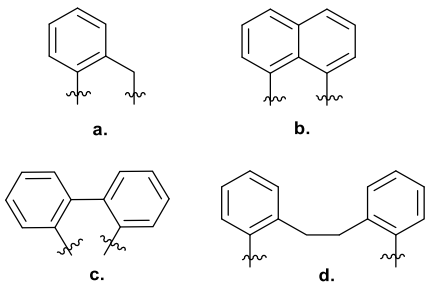

Figure 1.35. Al(III) salen complexes with aromatic backbones investigated by Gibson *et al.*[113]

Aluminium complexes with salan[107,114–116] and salalen[117–120] ligands have also been shown to be active and stereoselective for ROP. Recently, Jones *et al.* reported a salalen ligand comprising an *ortho*-phenylene backbone which is isoselective when complexed to Zr(IV) (P_m < 0.85) but only atactic PLA was produced by the Al(III) analogue.[121]

Recently, initiators comprising multiple Al(III)centres have gained increasing attention. Yu and Wang prepared a series of dinuclear salen and salan complexes (Figure 1.36, complexes **70**-**72**) which exhibited significantly higher turnover frequencies compared to

their monomeric counterparts (e.g. 3.10 h^{-1} for dinuclear h^{-1} *vs* 0.91 h^{-1} for monomeric).[122] X-ray crystallography showed that the aluminium centres were orientated on opposing sides of the complex, facilitated by free rotation about the methylene bridge. The authors suggest a cooperative effect between aluminium centres is possible during polymerisation, but further proof was needed to discount substituent effects.

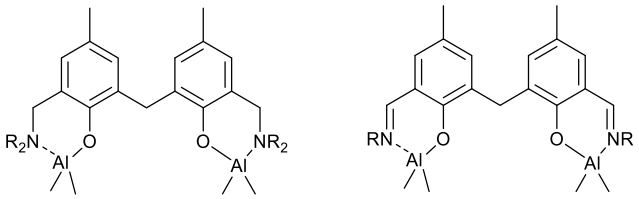

70: R = Me

71: R = 2,6-$^{i}Pr_2C_6H_3$
72: R = ^{t}Bu

Figure 1.36. Dinuclear aluminium complexes reported by Yu and Wang[122]

Higher activities for dinuclear complexes over monomeric counterparts were also observed by Normand *et al.*, who reported a 5-fold increase in rate for the dinuclear complex, **74**, over the monomeric complex, **73**, although presumably the polymer products were atactic as tacticities were not reported.[123] This rate increase was believed to be due to the fact that in these examples the aluminium centres could potentially come close enough to act cooperatively through rotation about the phenyl-phenyl bond (within 3.0 Å), potentially facilitating a dual activation mechanism. In a similar study, Chen *et al.* prepared monomeric (**75**) and dimeric (**76**) Al-alkyl complexes with piperazine ligands, observing a 2-8-fold increase in rate activity for **76** over **75** for ROP of ε-CL.[124]

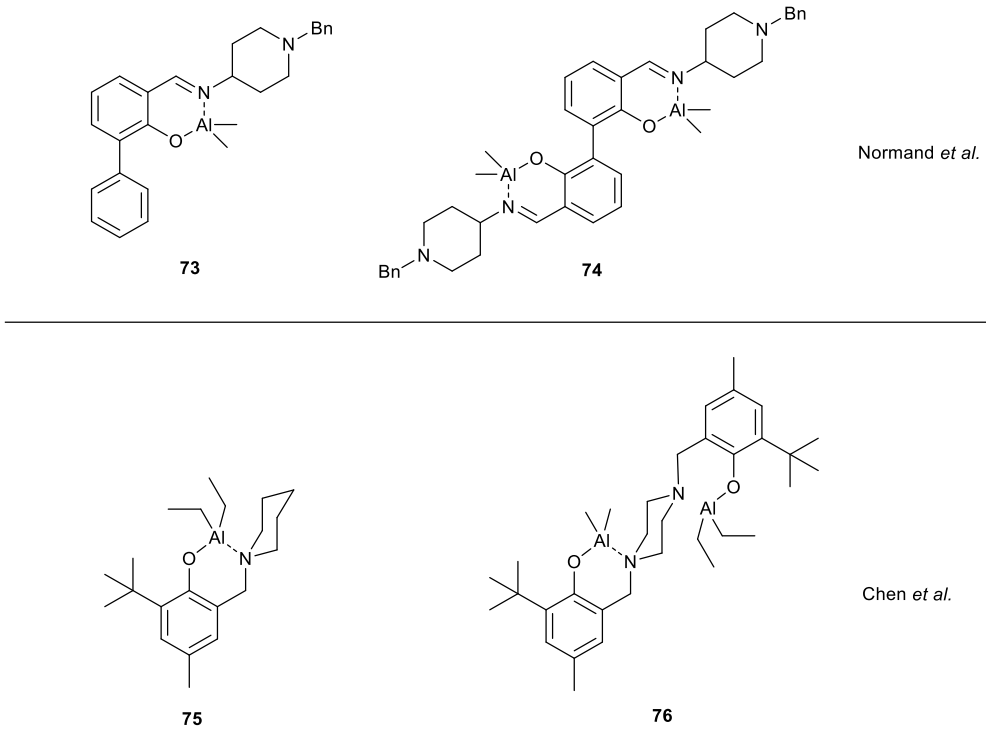

Figure 1.37. Mononuclear and dinuclear aluminium complexes reported by Normand *et al*[123] and Chen *et al*[124]

A study by Jones *et al.* described the synthesis of a series of mononuclear (**77**-**79**) and dinuclear Al(III) complexes (**80**-**82**) supported by naphthalene ligands (Figure 1.38).[125] The complexes were reasonably active for ROP of *rac*-LA, achieving high conversions in 2 hours in toluene at 80 °C. Little difference in rate of polymerisation of *rac*-lactide between the monometallic and bimetallic complexes, with the Al(III) centres existing effectively in identical electronic and steric environments and the rigid backbone disallowing rotation to facilitate approach of the Al centres. The polymerisation was well controlled, with predictable molecular weights and narrow dispersities, but no stereoselectivity was observed.

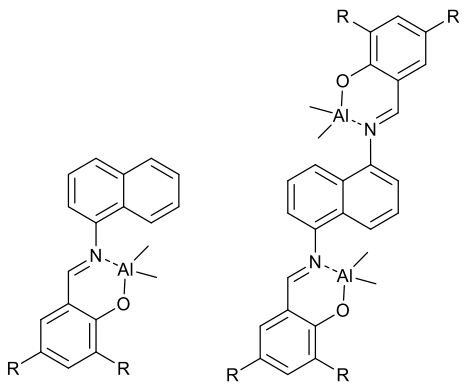

77: R = H
78: R = ^{t}Bu
79: R = Cl

80: R = H
81: R = ^{t}Bu
82: R = Cl

Figure 1.38. Mononuclear and dinuclear complexes investigated by Jones *et al.*[125]

While increases in activity have been documented, few examples of dinuclear complexes with stereoselectivity have been reported, with the exception of complexes **83**-**85**, reported by Chen *et al*, who were able to achieve a high degree of isotacticity (P_m = 0.91) and well-controlled polymerisation (Figure 1.39).[126] In this case the Al(III) centres are too far apart for any cooperativity to occur, and the selectivity is attributed to substitution around the ancillary ligands. The group have also investigated other ligands based on various tetraamine bridging moieties.[127]

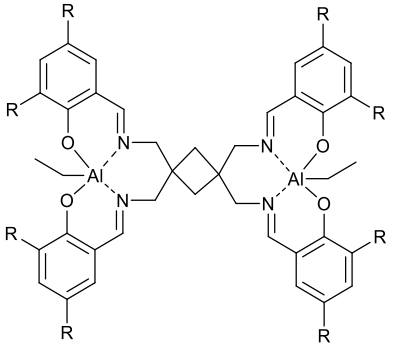

83: R = Cl
84: R = Me
85: R = ^{t}Bu

Figure 1.39. Dinuclear aluminium complexes as synthesised by Pang *et al*[126]

Redshaw and co-workers synthesised a series of macrocyclic ligands and prepared multinuclear Al(III) complexes from them for initiators for ROP of ε-CL.[128] This study found cooperative effects were present, with a favourable Al···Al distance of *ca.* 6.0 Å, while aluminoxane linkages [Al-O-Al] were found to be detrimental to any cooperativity effects. Mazzeo has also highlighted the importance of cooperativity in the polymerisation of *rac*-LA initiated with Al(III) salen complexes with Al···Al distance being the key parameter.[129] They propose that this is due to synergic interactions during the alcoholysis and polymer growth steps. Wang and Ma have also investigated the application of a dinuclear Al(III)

salan complex with a flexible alkyl backbone for the copolymerisation of L-LA and ε-CL.[130] The application of Al(III) complexes for controlled statistical LA/ε-CL copolymerisation has been recently reviewed.[131]

While the current literature on aluminium-based systems for ROP is extensive, there is scope to develop dinuclear complexes with beneficial cooperativity between metal centres and enhancement of catalytic properties. The enhancement in activity is highly beneficial, as traditionally Al(III) initiators can be highly stereoselective but very slow.

1.3 PLA copolymers

1.3.1 Caprolactone/butyrolactone/glycolide

Copolymerisation of lactide with other monomers to improve properties of PLA is an essential route to widening its use in biomedical and engineering applications. The copolymerisation of PLA with other cyclic esters such as ε-caprolactone δ-valerolactone, glycolide and β-butyrolactone (Figure 1.40) provides an effective way of combining the properties of the homopolymers, widening the usage of PLA in biomedical and engineering applications.[132–134]

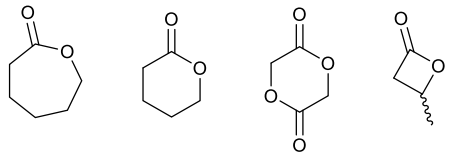

Figure 1.40. Structures of ε-caprolactone δ-vaerolactone, glycolide and β-butyrolactone

For example, PLA has a relatively low barrier to water vapour and CO_2, limiting its use for long term food packaging applications.[135] CO_2 atmospheres are introduced in packaging to keep products fresher for longer. The gas permeability properties of PLA can be improved by copolymerising with a monomer such as ε-caprolactone to introduce aliphatic regions into the polymer chain, which can increase the barrier properties to gases and produce thermally stable plastics up to 200 °C.[135]

ε-Caprolactone (ε-CL) is one of the most extensively researched comonomers for PLA. Polycaprolactone (PCL) is a biodegradable aliphatic polyester which has rubbery characteristics, low T_g (-60 °C) and is presently used in medical applications such as drug-delivery systems and tissue scaffolds.[136] Poly(lactide-co-ε-caprolactone) has improved mechanical properties (impact and elongation strengths), and biodegrades more rapidly than PLA alone.[30] Caprolactone is an important industrial chemical for the production of

polyesters and polyamides and is currently produced on multi-tonne scale *via* oxidation of non-renewable cyclohexane.[137] Renewable routes to ε-caprolactone such as Heeres' route from 5-hydroxymethylfurfural (HMF) (Scheme 1.2), which can be derived from *D*-fructose.[138] Alternatively, novel bioderived substituted caprolactones are highly desirable as the current scope for functionalised bio-polyamides is somewhat limited.[139]

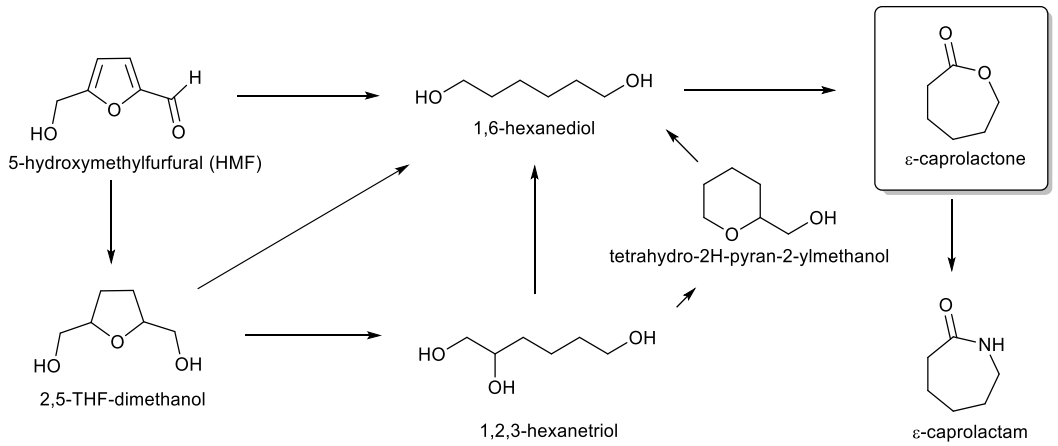

Scheme 1.2. Synthetic routes for the conversion of biomass-derived HMF into caprolactone and caprolactam[138]

1.3.2 Terpenes and terpenoids

Terpenes are a huge, diverse class of naturally occurring organic compounds derived from C5 isoprene units. There are some 30000 naturally occurring terpene compounds reported in the literature, containing many functional groups such as alkenes, ketones and alcohol moieties. Terpenes are classified by the number of isoprene units which are required to build the structure – including hemiterpenes (one isoprene unit), monoterpenes (two), and sesquiterpenes (three), although many more are possible. A terpene is strictly a hydrocarbon, while a compound containing heteroatoms is classified as a terpenoid (or isoprenoid). Terpenes and terpenoids enjoy widespread use in the flavourings and fragrance industries and are the principle component of essential oils in many plants.[140]

Terpenes and terpenoids represent a vast range of molecules which have great potential as a source of monomers in polymer science, and have been the subject of several reviews in the last five years.[7,10,141] Their abundance, structural diversity (Figure 1.41) and potential for functionalisation make them incredibly attractive as sources of renewable platform chemicals. Produced biosynthetically by many classes of plants and trees, terpenes provide a source of monomers which do not directly compete with food sources.[8]

Some of most commonly occurring terpenes and therefore best candidates for renewable monomers are the monoterpenes α- and β-pinene, *D*-limonene and *L*-menthol. The

synthesis, modification and functionalization of terpenes has become a hot topic, particularly for catalytic or enzymatic transformations.[141,142] The structural diversity of terpenes allows for various possible transformations to potential monomers, but only pinene, limonene and myrcene have been studied comprehensively to date in polymer science.[7]

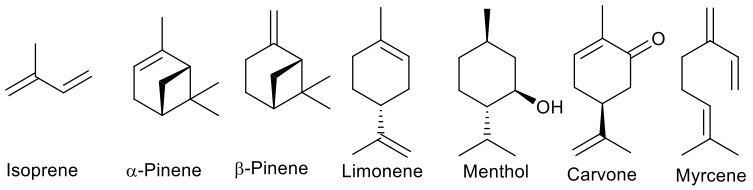

Figure 1.41. Structure of isoprene and some common terpene and terpenoids

By far the largest source of terpenes available is from turpentine, produced on some 350000 tonnes per year from gum resin or crude sulphate turpentine: a by-product in the Kraft process.[8] The major components of turpentine are α-pinene (45–97%) and β-pinene (0.5–28%), with smaller amounts of other monoterpenes. *D*-limonene is a by-product of the citrus industry, with an annual worldwide production of 70000 tonnes. Terpenoid menthol has an annual worldwide production of 19000 tonnes,[143] from natural sources (peppermint oil) or *via* commercial synthetic processes such as the Haarmann-Reimer (Symrise) process from *m*-cresol.[144] Both limonene and menthol are extensively used in flavourings and fragrances, somewhat limiting their availability as commodity platform chemicals.

Access to other valuable terpenes such as limonene is also possible *via* the isomerisation of α- and β-pinenes. Currently the isomerisation of pinene is performed on industrial scales over TiO_2 at elevated temperatures (> 100 °C).[140] The major products for this process are camphene and *p*-cymene, although other products are possible, such as limonene, or α-/γ-terpinenes (Figure 1.42). Camphene is used in the production of camphor, which is widely used in insect repellents, as a plasticiser for nitrocellulose in explosives and in medicinal products such as decongestants. More recently solid acids such as zeolites and modified clays have been investigated for the isomerisation of α- and β-pinenes to other valuable products. The upgrading potential of crude turpentine (from the paper pulping industry, for example) with heterogeneous catalysts has been recently thoroughly reviewed.[142]

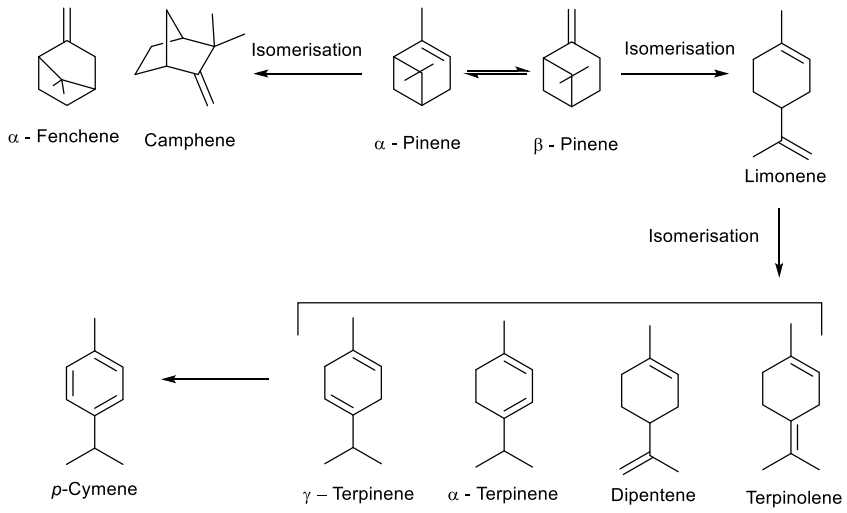

Figure 1.42. Possible isomerisation products from α- and γ-pinene.[140]

1.3.3 Direct polymerisation of terpenes

Due to the abundance of carbon-carbon double bonds in terpenes, much research has focussed upon polymerisation of these *via* radical or cationic methods. The homopolymerisation of α- and β-pinene and limonene with Friedel-Crafts type catalysts was first reported in 1950 by Roberts and Day.[145] The most viable terpene for this is β-pinene, owing to the accessibility of the endocyclic alkene bond.[8] The polymerisation with aluminium chloride ($AlCl_3$) is rapid and highly exothermic, driven by the high reactivity of the exomethylene double bond and cleavage of the highly strained cyclobutane ring. In the mechanism (Scheme 1.3), Lewis Acidic $AlCl_3$ reacts with water to give a strong proton donor which protonates the alkene to yield a carbenium ion. This readily isomerises to the more stable *para*-menthene type carbenium ion, which may undergo propagation.

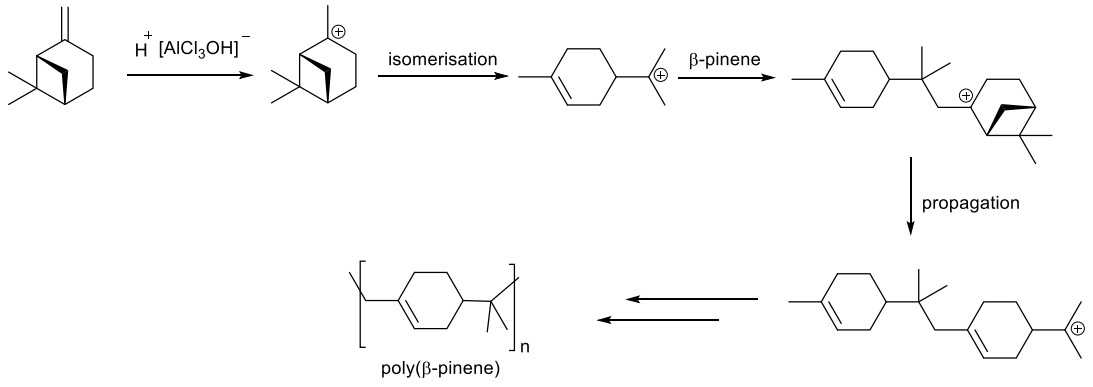

Scheme 1.3. Cationic polymerisation of β-pinene[145]

The majority of poly(β-pinene)s are low molecular weight ($M_n \leq 4000$ gmol^{-1}) hydrocarbon-like polymers, finding limited application as commercial adhesive components.[144] To achieve higher molecular weights, cryogenic temperature polymerisations have been

investigated, but little improvement was observed, and such low temperatures are not amenable to scale-up processes. Polymerisation of β-pinene giving relatively high molecular weights (M_n = 9000–14000 g mol^{-1}) has been achieved using a modified $AlCl_3$ etherate catalyst at room temperature. The poly(β-pinene)s produced had good thermal properties (T_g = 82-87 °C) and contained low catalyst content.[146] Examples utilising nickel Schiff base catalysts have also shown promise with the addition of methylaluminoxane required as an activator.[147] Copolymers have been produced with styrene and methacrylates, producing partially renewable, non-biodegradable polymers.[7]

α-Pinene is the most abundant naturally occurring terpene, being the principle component of turpentine. The endocyclic double bond in this structure is much less amenable to polymerisation, owing to the large steric hindrance around the trisubstituted C=C bond. Attempts at cationic polymerisation with Lewis Acids generally yield low molecular weight oligomers with poor conversion. Some improvement has been observed with the addition of antimony trichloride ($SbCl_3$) as an activator, but have also resulted in oligomers (M_n ≈ 1000 gmol^{-1}), with the authors reporting some difficulty in classifying the mechanism of polymerisation.[148–150]

The polymerisation of α-pinene in ionic liquids (ILs) had also been attempted, giving *ca* 52% conversion to oligomeric products. 1-(1-ethyl acetate-yl)-3-methylimidazolium chloroaluminate ([EtOCOCH$_2$-mim]Cl-$AlCl_3$), with molar fraction of $AlCl_3$ x = 0.67, showed good catalytic performance for the polymerization of α-pinene, with good recyclability possible for the IL.[151] Here the authors proposed two mechanisms for the polymerisation of α-pinene (Scheme 1.4).

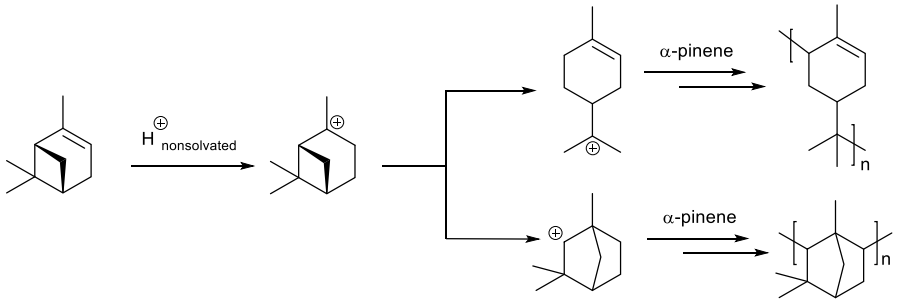

Scheme 1.4. Polymerisation of α-pinene in ionic liquid[151]

At present, polylimonene prepared *via* cationic methods has only been able to yield low molecular weight polymers, with poor conversions of monomer. It has been suggested that the low conversions are due to chain termination through β-elimination. Limonene has also

been investigated as a polymerisation solvent, and shown to act as a chain transfer agent, greatly influencing rate and polymer molecular weight.[152,153]

Linear terpene myrcene can be obtained from plants in small quantities,[154] or the pyrolysis of α-pinene.[155] The three double bonds in myrcene allow for radical or cationic polymerisation at three sites, leading to different possible polymer microstructures. Polymyrcene has been prepared by benign emulsion polymerisation techniques[156] and controlled reversible addition-fragmentation chain-transfer (RAFT) polymerisation in bulk, where the authors report low disperisties ($Đ$ = 1.1-1.4) and selectivity for up to 96% 1,4-polymyrcene content.[157]

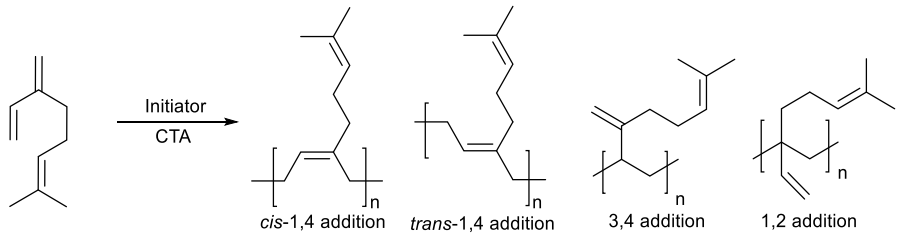

Scheme 1.5. Possible polymer microstructures from reversible addition-fragmentation chain-transfer polymerisation of myrcene[109]

Most of the research into the polymerisation of terpenes has given polymer products which lack desirable properties to make them competitive with current commercial polymers. Research has recently moved towards the derivation of functionalised monomers from terpenes as an alternative strategy, suitable for more controlled polymerisation methods such as ROP.

An elegant two-step process of preparing to semi-crystalline polymers from myrcene was described by Hillmyer, by initial ring-closing metathesis of myrcene using a second-generation Grubbs catalyst to the cyclic diene 3-methylenecyclopentene (Scheme 1.6).[158] Cationic polymerisation of this yielded high molecular weight regiopure polymers (M_n < 22 kDa, $Đ$ = 1.15-1.25). The by-product of this reaction is isobutene, which is the main component in butyl rubber production, adding value to this process. This was further expanded by an end-functionalisation reaction *via* reaction with maleic anhydride, opening the possibility for block copolymers.

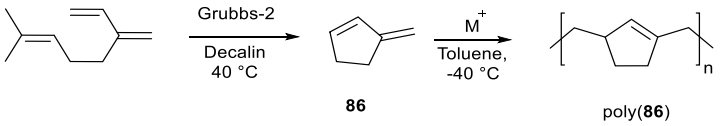

86 poly(**86**)

Scheme 1.6. Ring-closing metathesis of myrcene and cationic polymerization of 3-methylenecyclopentene, **86**.[158]

Recently, Miyaji *et al*. published an innovative method of preparing polyketones from α-pinene, providing a route to novel terpene-derived polymers which would be difficult to achieve from petrochemical sources.[159] In this process, α-pinene is first quantitatively converted into (+)-pinocarvone (**87**) under visible-light photoxidation (Scheme 1.7a). Pinocarvone possesses a reactive exo-methylene group, which can undergo cationic or radical polymerisation. Under bulk conditions, with 4,4'-azobis(isobutyronitrile) (AIBN) as a radical initiator at 60 °C, a mixed polymer was produced comprising a 68:32 ratio of units based on the bicyclic framework of pinocarvone from normal radical addition polymerisation, and a second unit comprising an unsaturated six-membered ring in the main chain, arising from radical addition followed by ring-opening of the four-membered ring. This bicyclic vinyl ketone was selectively polymerised *via* photo-radical methods in hexafluoroisopropanol (HFIP) to yield a unique six-membered ring polyketone polymer structure with conjugated ketone functionality which could undergo post-polymerisation modification (Scheme 1.7b). Polymerisations were trialled in a range of solvents, with faster polymerisation observed in fluorinated alcohols than toluene or DMF. The ratio of bicyclic and ring-opened units could also be varied in different solvents, with T_g values of polymers increasing with percentage of ring-opened units (T_g = 162 °C at 96% allyl ketone content).

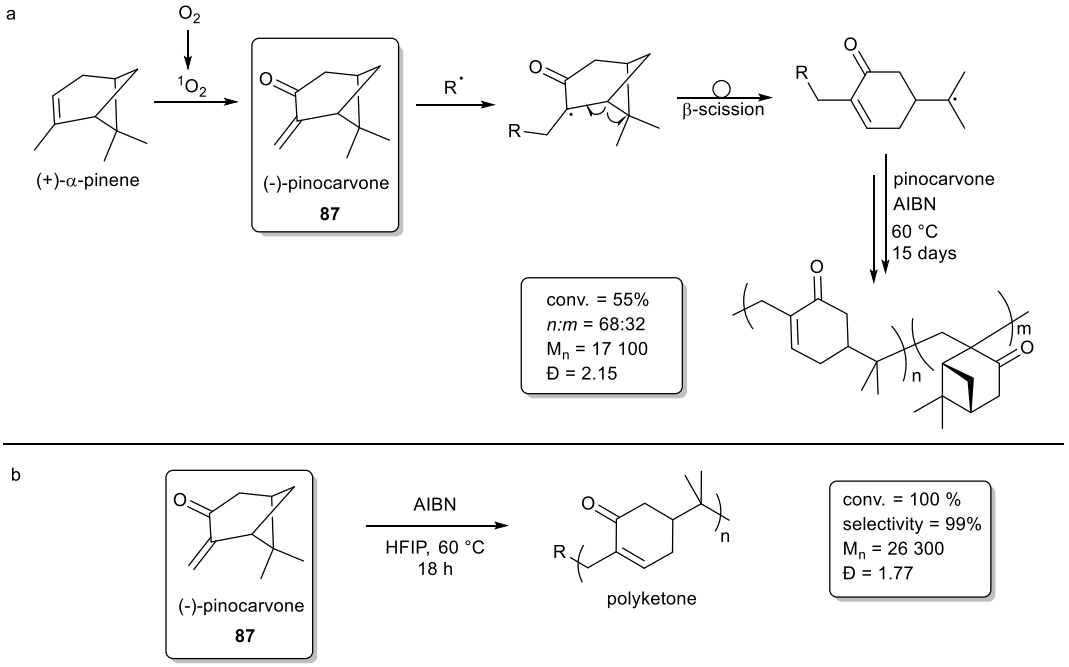

Scheme 1.7. Preparation of polypinocarvone from α-pinene *via* O_2 irradiation and radical polymerisation.[159]

Furthermore, the authors prepared both (-)-pinocarvone from naturally occurring (+)-α-pinene and (+)-pinocarvone from (-)-α-pinene. These polymerised at the same rate, allowing for copolymerisation yielding polymers with tuneable optical properties. Finally, the authors developed new block copolymers through controlled reversible addition-fragmentation chain transfer (RAFT) polymerisation of various acrylates followed by polymerisation with pinocarvone, enabling the synthesis of novel thermoplastic elastomers.

1.3.4 Terpene-derived monomers for ROP

1.3.4.1 Terpene epoxides

Limonene, particularly in the oxidised 1,2-limonene oxide (1,2-LO) form, has attracted much interest as a monomer for ROCOP, drawing on its structural similarity to cyclohexene oxide (CHO). The best-known polymer produced from 1,2-LO is poly(limonene carbonate) (PLC), produced by ROCOP of 1,2-LO and CO_2. This polymer was first introduced by Coates in 2004, who reported perfectly alternating polycarbonates (99% polycarbonate linkages) at 100 psi CO_2 and 25 °C using a Zn(II) BDI complex.[160] PLC has properties similar to polystyrene and is biodegradable. Recent work on this polymer has yielded an exciting example of macromolecule co-crystallisation as a stereocomplex, described by the authors as a *"steric zipper"*. By mixing enantiomerically pure amorphous PLC chains in a 1:1 ratio in

n-hexane, a semi-crystalline product formed which was characterised by PXRD and X-ray structures (Figure 1.43).[161,162]

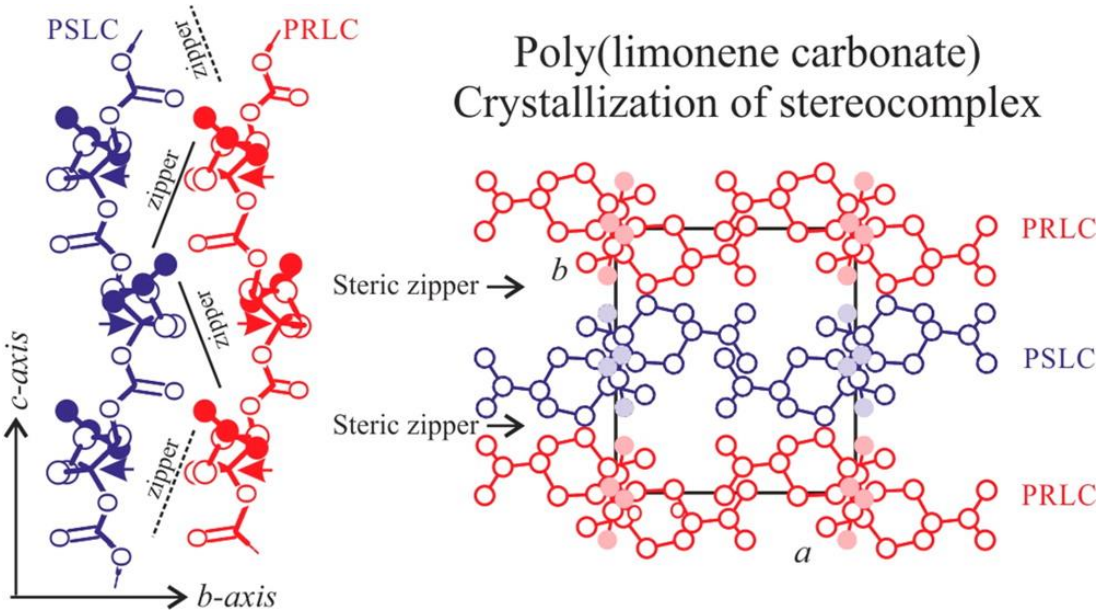

Figure 1.43. Crystal structure of PLC stereocomplex. Image reproduced with permission from Auriemma *et al.*[162] Copyright (2015) American Chemical Society.

CO_2 has also been added to limonene dioxide *via* catalytic carbonation to give limonene dicarbonate. This was then amine cured and used in the production of novel non-isocyanate polyurethanes. Limonene dicarbonate was prepared using limonene dioxide, CO_2 (30 bar) in the presence of a halide catalyst (tetrabutylammonium bromide, TBAB, or silica supported 4-pyrrolidino-pyridinium iodide) at 120-140 °C.[163]

In 2007, Coates and co-workers built on their success with poly(limonene carbonate) and reported the copolymerisation of 1,2-LO (amongst other epoxides) with maleic and diglycolic anhydrides, as well as reporting a zinc BDI complex as the first highly active catalyst for this type of polymerisation. Copolymers had molecular weights 12k-36k $gmol^{-1}$ and glass transition temperatures in the range 50-65 °C.[47]

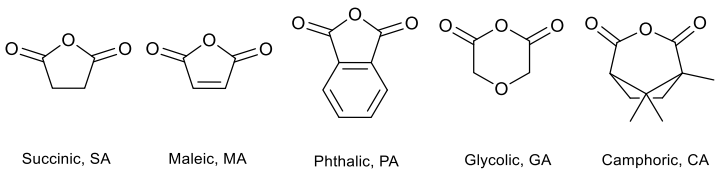

Figure 1.44. Anhydrides investigated for ROCOP with 1,2-LO[47]

More recently the copolymerisation of 1,2-LO with phthalic anhydride was reported using chromium, aluminium, cobalt and manganese ^{t}Bu-salophen complexes and a range of chain

transfer agents.[164] Kleij and co-workers have also recently reported the copolymerisation of several terpene oxides (limonene oxide, carene oxide, limonene dioxide, and menthene oxide) with aromatic anhydrides.[165] The authors report ranging glass transition temperatures from 59 to 243 °C depending on terpene substrate used, and excellent selectivity toward perfectly alternating polyesters (≥98% ester bonds). These new materials could potentially be useful toward the development of new coating and thermoset materials. Polyesters derived from propylene and terpene-derived anhydrides with Cr, Co or Al salophen ligands has also been reported by Coates *et al.*[166] The bicyclic anhydrides, **88**-**91**, were synthesised from terpenes with a diene functionality (α-phellandrene or α-terpinene) which could undergo Diels-Alder addition with maleic anhydride.

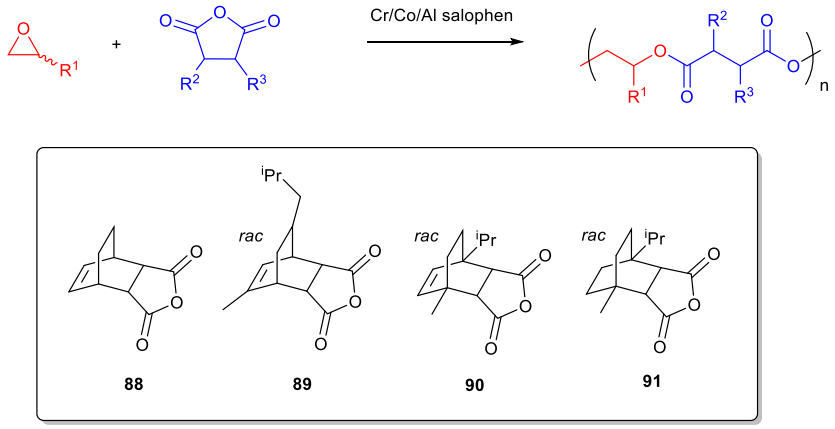

Figure 1.45. Terpene based anhydride monomers **88**-**91** developed by Coates *et al* for ROP catalysed by Cr/Co/Al salophen complexes.[166]

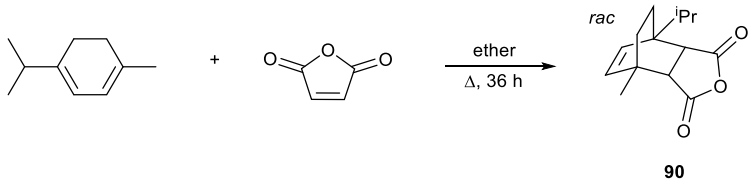

Scheme 1.8. Preparation of a terpene-derived racemic anhydride, **90**, from α-phellandrene[166]

A development to this method was reported in 2011, when Thomas *et al*. reported a tandem synthesis involving the cyclisation of commercially available dicarboxylic acids to corresponding anhydrides and subsequent ROCOP with epoxides (Scheme 1.9).[167] 1,2-LO was one of the epoxides investigated here, and polymers produced had narrow dispersities (*Đ* = 1.10-1.30) and predictable molecular weights. The authors also reported other terpenoids (camphoric acid and pinene oxide) as monomers.

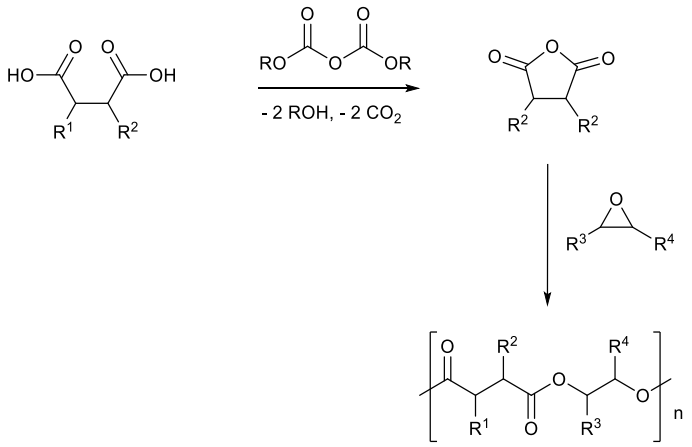

Scheme 1.9. Tandem synthesis of polyesters from epoxides and dicarboxylic acids.[167]

Other polymers have been produced from limonene *via* thiol-ene additions,[168] cationic and radical mechanisms[141] but are not covered here as these methods are beyond the scope of this work.

1.3.4.2 Terpene-derived lactones

The polymerisability of lactones has been a significant research topic as the size of the lactone, position of substituent, and size of substituent affect the thermodynamics and kinetics of polymerization.[169] A recent in-depth study demonstrated that the size of the lactone largely affects the thermodynamics of polymerization, while the position and nature of the substituent largely affects the kinetics of polymerization.[170] The thermodynamic favourability to form polyesters from ε-caprolactones provides a synthetic advantage over δ-valerolactones. It is possible to envisage numerous lactones from the oxidation of terpenes bearing six-membered rings, and therefore prepare new substituted caprolactone monomers.

At present, only a limited number of examples of such terpenoid monomers suitable for ROP have been investigated. This area of research was galvanised by Hillmyer and co-workers, who explored the Baeyer-Villiger oxidation (BVO) of menthone and carvone to produce substituted ε-caprolactone monomers.[91,171]

Menthone was among the earliest substrates reported by Baeyer and Villiger, who also described the BVO of camphor and dihydrocarvcone with peroxymonosulfuric acid (Caro's acid) to prepare the corresponding lactones.[172] An early report of the polymerisation of the lactone from menthone using Na to yield a *"thick white hygr. gel"* after 2 h at 170 °C was reported in 1958 by Hall and Schneider,[173] but was not further investigated until Zhang et al in 2005.[91] Here, menthone was readily oxidised into the corresponding lactone, menthide,

92, by addition of *meta*-chloroperoxybenzoic acid (mCPBA) (Scheme 1.10). Complete polymerisation of menthide was achieved in 8.5 hours in toluene at room temperature, with varying monomer-to-catalyst ratios ([M]:[Zn] = 10 – 400) allowing for a range of different molecular weight polymenthides to be prepared (M_n = 3.3 – 91.0 kDa, $Đ$ = 1.10-1.60).[91] The catalyst employed for ROP was a highly active, structurally defined zinc alkoxide which had been developed in the group as an initiator for PLA.[84]

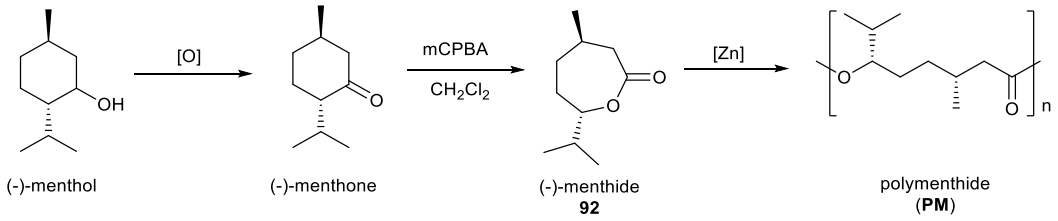

Scheme 1.10. Synthesis of menthide by Baeyer-Villiger oxidation of menthone and zinc catalysed ROP to give polymethide.[91]

The block copolymerisation of menthide with lactide was investigated for the preparation of new thermoplastic elastomers, having glassy midblock segments of PLA and rubbery regions of polymenthide (PM). Firstly, the PM midsection was prepared by ROP of menthide with diethylzinc and diethylene glycol as a di-functional initiator. Termination with water afforded a dihydroxy functionalised PM which could then be utilised as a macroinitiator for controlled polymerisation of lactide with trimethylaluminium to yield poly(lactide)-b-poly(menthide)-b-poly(lactide) triblock copolymers. Molecular weights and compositions could be readily controlled by varying the monomer-to-initiator ratios and the authors claim these biodegradable elastomers might be suitable for biomedical applications.[174,175]

Furthering this work, Lowe reported a similar approach using carvone as the starting material.[171] Carvone is a naturally occurring terpenoid, found in two enantiomeric forms as *L*-carvone in *Mentha spicata* (spearmint) and *D*-carvone in *Carum carvi* (caraway) oils. The combined annual production is in the scale of 10^4 metric tons annually, although the majority of carvone is currently used in flavourings and fragrances, antimicrobial agents, and as a potato sprouting inhibitor.[176] In this work, two lactones were prepared from the terpenoid carvone *via* the hydrogenation of dihydrocarvone, **93**, (may be derived from carvone) to carvomenthone, **94** (Scheme 1.11). Baeyer-Villiger oxidation of dihydrocarvone with Oxone® yielded an unsaturated lactone, **95,** with minimal epoxidation of the pendant alkene. BVO of carvomenthone to carvomenthide, **96**, was achieved on a 15 g scale with

mCPBA, yielding only the normal oxidation product with no apparent insertion of the oxygen between the carbonyl and the methylene 6 position.

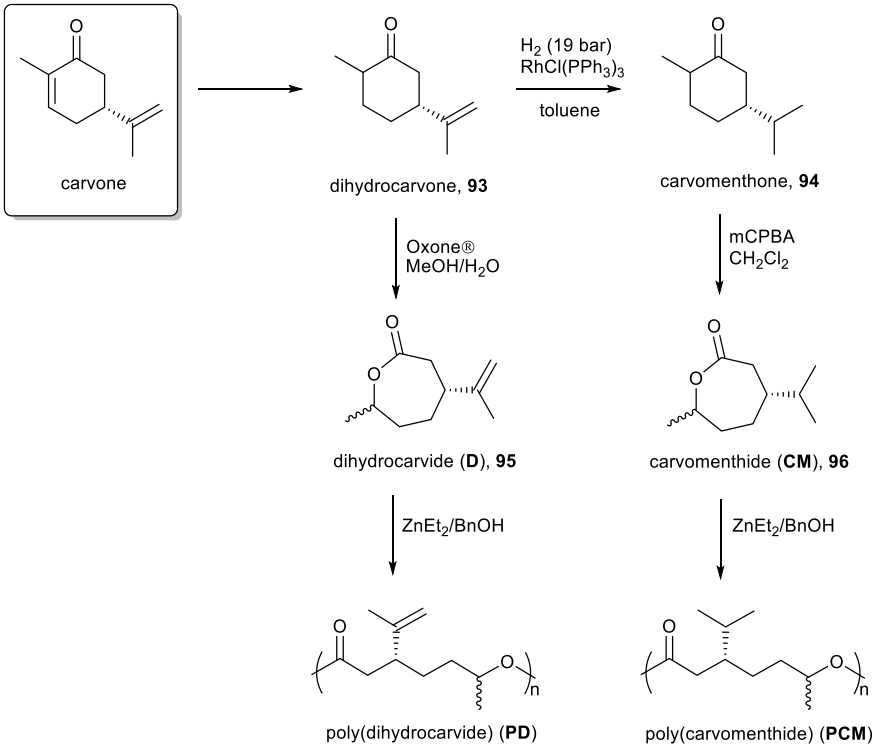

Scheme 1.11. Transformation of carvone into lactones **95/96** and their subsequent ring-opening polymerisation[171]

Ring-opening polymerisation of these monomers was performed in bulk at 100 °C with diethylzinc as a catalyst and benzyl alcohol as an initiator. Control of polymer molecular weights was achieved by varying monomer-to-initiator ratios (up to M_n = 10.5 kDa for PD, and M_n = 62.3 kDa for PCM) with good control maintained, as indicated by dispersities between 1.10-1.31 in all cases. Disparity between predicted and actual molecular weights for PD was rationalised as being due to trace amounts of epoxide impurity in the monomer feed. The glass transition temperature (T_g) of both polymers was observed to be very similar, and comparable to that of polymenthide. (T_g = -20 °C). The lack of crystallinity in PCM and PD was attributed both to mixed configuration of the methyl substituent and the presence of the bulky isopropyl substituent, as in PM. By comparison, polycaprolactone (PCL) has a T_g of -60 °C and is crystalline at room temperature.[177] Copolymerisation of the two carvone-derived monomers with varying feed ratios allowed the authors to prepare random copolymers exhibiting a single T_g which could be tuned depending on the composition.

Table 1.6. Glass transition temperatures of polymers prepared *via* ROP of terpene-derived monomers, and CL for comparison.[171,177]

	PM	PD	PCM	PCL
T_g / °C	-26	-20	-27	-60

The presence of the terminal alkene functionality was also exploited for post-polymerisation modification reactions including epoxidation and cross-linking with a dithiol and radical initiator. For a PCM-co-PD sample containing 10% dihydrocarvide units, little cross-linking was observed on analysis of the gel fraction. The authors suggested that repeated additions of radical initiator are needed to allow further crosslinking due to the low concentration of alkene moieties, or primary cyclisation *via* crosslinking between moieties in the same chain occurs.[169]

Oberleitner *et al.* recently reported a 4-step biocatalytic cascade process to prepare dihydrocarvide from limonene from waste orange peels, combining two established biotransformation pathways (Figure 1.46).[178] This approach could make the synthesis of functional monomers from terpene feedstocks on scale a more feasible reality.

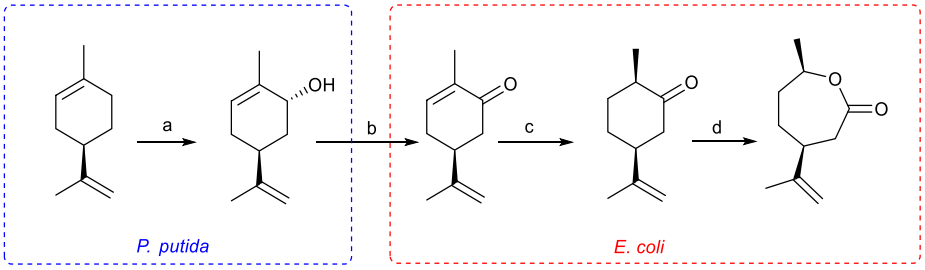

Figure 1.46. Cascade from limonene to dihydrocarvone., consisting of cumene dioxygenase (a), an alcohol dehydrogenase (b), an enolate reductase (c) and a Baeyer-Villiger monooxygenase (c) in a mixed culture set-up. Reproduced from Oberleitner *et al.* [178]

Lowe also reported a third monomer, from oxidised carvone for ROP.[179] In this study, dihydrocarvone was oxidised with mCPBA to form a 3:1 mixture of the "normal" (**97**) and "abnormal" (**97a**) epoxylactones (both existing as a pair of diastereoisomers) (Scheme 1.12). Homopolymerization using diethylzinc and $Sn(Oct)_2$ yielded only low molecular weight oligomers (apparent M_n < 2.5 kDa). Ring-opening of both lactone and epoxide groups was observed by ^{1}H NMR spectroscopy, yielding a branched polymer structure.

Copolymerisations of ε-caprolactone were performed with 0.3-50% of **97** with $Sn(Oct)_2$ as the catalyst. No cross-linking was observed on analysis of the product by solvent extraction. When $ZnEt_2$ was used as the catalyst and benzyl alcohol as initiator at 60 °C, flexible cross-

linked materials were obtained on a multigram scale in a one-pot reaction (Scheme 1.12). These cross-linked copolymers exhibited excellent shape memory properties even after many deformations.

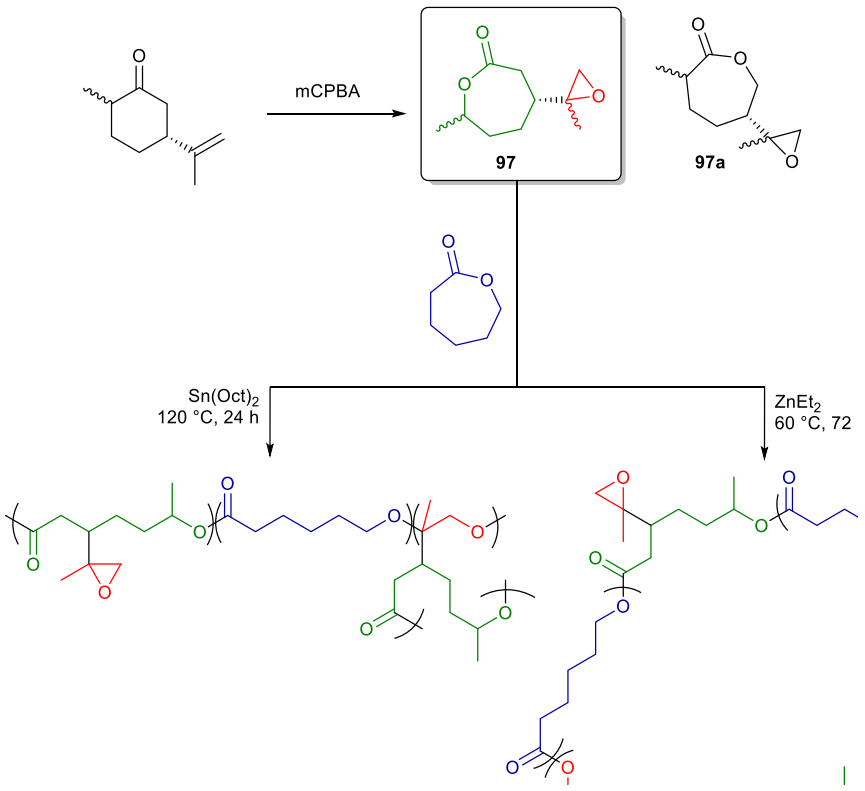

Scheme 1.12. Copolymerisation of ε-CL and an oxidised carvone monomer under different conditions[179]

Building on the work on carvone and menthone from the Hillymer group, Winnacker and co-workers reported a method of producing chiral oligoamides from menthone and carvone following a similar concept to the synthesis of polycaprolactam from petrochemically-derived cyclohexanone. Here menthone is converted first into an oxime by reaction with hydroxylamine-*O*-sulphonic acid (HOSA), which then can undergo a Beckmann rearrangement to a seven-membered lactam, **98**, which would polymerise under anionic or acid-catalysed conditions to give low molecular weight oligoamides (M_n < 2400 gmol^{-1}).[180,181] Methods to improve the synthesis of polyamides from menthone lactams by using either NaH or KO^{t}Bu as catalyst with a benzolyated lactam as a co-initiator in bulk at 200 °C (vacuum) have also been developed.[182] This revised "enhanced anionic" methodology has allowed the authors to access higher molecular weights (M_n < 5600) but dispersities remain broad ($Đ$ = 2.0-3.0). DSC analysis of these polyamides showed melting points (T_m) around 300 °C, significantly higher than that of polycaprolactam (T_m = 220 °C).

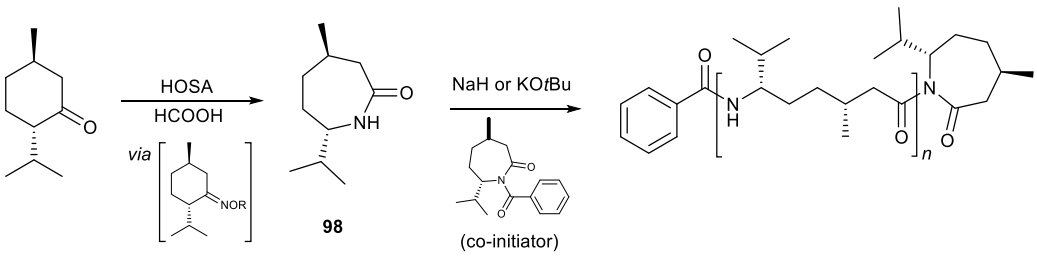

Scheme 1.13. Enhanced polymerisation of menthone-derived lactam developed by Winnacker.[182]

Very recently, the group has focussed on preparing lactams from a more abundant terpene: β-pinene.[183,184] Firstly, β-pinene was oxidised to nopinone, followed by conversion to the *N*-oxime (**99**) and subsequent Beckmann rearrangement to give two lactam products **100a**/**b** in a 5:1 ratio in favour of the "normal" product whereby the nitrogen inserts into the more sterically hindered side. Initially, the group focussed on utilising the cationic conditions using common acids such as H_3PO_4, HCl and aminocaproic acid at 250 °C to prepare polyamides. The polymers have interesting structures with chiral four-membered ring moieties in the polymer chain, arising from ring-opening of the caprolactone ring whilst leaving the cis-butane ring untouched, retaining some of the terpene functionality (Scheme 1.14).[183] By investigating a range of monomer-to-initiator loadings and varied reaction times, they were able to prepare polyamides with molecular weights up to 7700 $gmol^{-1}$ in 48 hours (H_3PO_4, $Đ$ = 2.6, 69% yield, [M]:[I] = 50). The melt temperature of the polyamide prepared from the "normal" lactam exhibited a melt temperature of 322 °C, and a slight glass transition at ≈ 160 °C. Decomposition was observed around 400 °C, and the proximity of this to the melt temperature could lead to some limitations in the polymer processability for future applications. The authors state that they are now investigating polyamides prepared from terpenoids pulegone and dihydrocarvone.

Under anionic conditions at 200 or 250 °C, polyamides with M_n < 3200 with $Đ$ = 1.7-2.8 were prepared from **100a**/**b** at a range of monomer-to-initiator loadings within 4 hours, although monomer conversions ranged from 9-81%, and control over the system is somewhat lacking.[184]

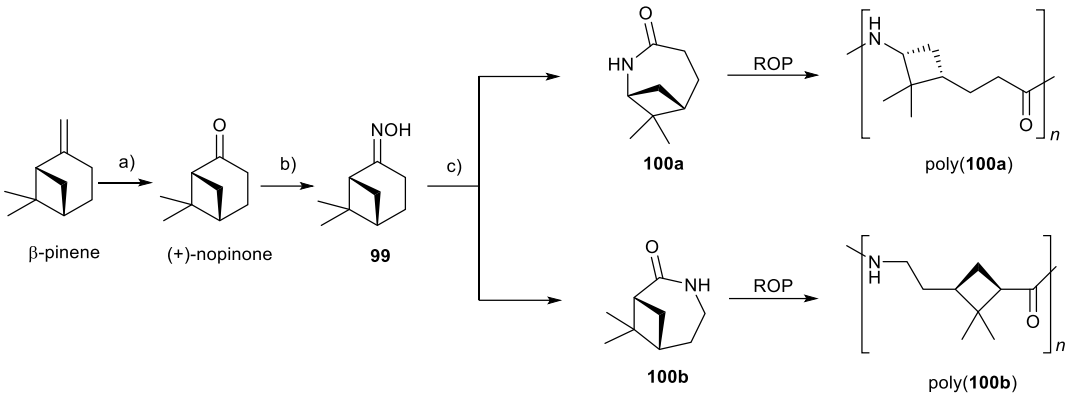

Scheme 1.14. Polymerisation of polyamides from β-pinene. Conditions: a) $KMnO_4$, Al_2O_3, H_2O/CH_2Cl_2, 63%. b) $NH_4OH•HCl$, $NaHCO_3$, $MeOH/H_2O$, 98%; ratio a/b ≈ 5:1. c) Polyphosphoric acid (73%)[183]

The BVO of (+)-nopinone with mCPBA is also known, yielding a mixture of bicyclic lactone products.[185] However, long reaction times (3 weeks) are required to give reasonable conversion to lactone product, and the separation of the abnormal and normal lactone products is non-trivial. The ring-opening of these lactones has been reported by refluxing in methanol,[186] but at present no polymers have been successfully reported. Likewise, the lactone of camphor is known but little polymerisation has been reported.[40,172] Recently, the biocatalytic lactone production from (+)-puleogone was reported using a Baeyer-Villiger monooxygenase (BVMO) enzyme, but no polymer formation was observed from ROP attempts, with the authors suggesting that steric hindrance due to the orientation of the isobutene moiety of the monomer is detrimental.[15]

Recently, Watts *et al.* published a study preparing sustainable aliphatic polyester elastomers from lactide and γ-methyl-ε-caprolactone (γMCL).[187] In this study, the authors proposed a retrosynthetic route to prepare γMCL from α-pinene (Scheme 1.15), although commercial 4-methylcyclohexanone was used in this study. This is a nice exemplar of how terpene feedstocks may be transformed into useful monomers for sustainable polymers.

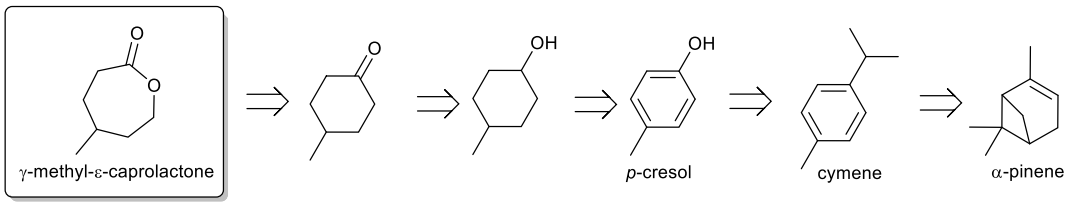

Scheme 1.15. Retrosynthetic approach to the synthesis of γ-methyl-ε-caprolactone from α-pinene[187]

1.4 Project aims

1. Prepare multinuclear complexes based on known salan ligands and investigate these for ROP of *rac*-LA, concentrating on abundant, cheap and biocompatible metals such as zinc, magnesium and lithium.
2. Develop new ligands based on salen and related structures to investigate structure-activity relationships in Al(III) complexes, with the aim to prepare isotactic PLA from *rac*-LA.
3. Develop novel substituted ε-caprolactone monomers from renewable biomass sources, concentrating on abundant terpene feedstocks (α/β-pinene).
4. Investigate the polymerisation of new lactone monomers with various catalytic systems and characterise new polymeric materials.
5. Investigate the copolymerisation of new lactone monomers with lactide and investigate the properties of these new copolymers.

1.5 References

1 Ellen MacArthur Foundation, *The New Plastics Economy: Rethinking the future of plastics*, 2016.
2 K. Yao and C. Tang, *Macromolecules*, 2013, **46**, 1689–1712.
3 P. T. Anastas and J. B. Zimmerman, *Environ. Sci. Technol.*, 2003, **37**, 94A–101A.
4 M. A. Dubé and S. Salehpour, *Macromol. React. Eng.*, 2014, **8**, 7–28.
5 A. J. Ragauskas, C. K. Williams, B. H. Davison, G. Britovsek, J. Cairney, C. A. Eckert, W. J. Frederick, J. P. Hallett, D. J. Leak, C. L. Liotta, J. R. Mielenz, R. Murphy, R. Templer and T. Tschaplinski, *Science*, 2006, **311**, 484–9.
6 X. Zhang, M. Fevre, G. O. Jones and R. M. Waymouth, *Chem. Rev.*, 2018, **118**, 839–885.
7 P. A. Wilbon, F. Chu and C. Tang, *Macromol. Rapid Commun.*, 2013, **34**, 8–37.
8 A. Gandini and T. M. Lacerda, *Prog. Polym. Sci.*, 2015, **48**, 1–39.
9 A. Llevot, P.-K. Dannecker, M. von Czapiewski, L. C. Over, Z. Söyler and M. A. R. Meier, *Chem. Eur. J.*, 2016, **22**, 11510–11521.
10 M. R. Thomsett, T. E. Storr, O. R. Monaghan, R. A. Stockman and S. M. Howdle, *Green Mater.*, 2016, **4**, 115–134.
11 G. L. Gregory, E. M. López-Vidal and A. Buchard, *Chem. Commun.*, 2017, **53**, 2198–2217.
12 Y. Zhu, C. Romain and C. K. Williams, *Nature*, 2016, **540**, 354–362.
13 D. K. Schneiderman and M. A. Hillmyer, *Macromolecules*, 2017, **50**, 3733–3749.
14 H. Kawaguchi and C. Ogino, *Bioresour. Technol.*, 2017, **245**, 1664–1673.
15 H. L. Messiha, S. T. Ahmed, V. Karuppiah, R. Suardíaz, G. A. Ascue Avalos, N. Fey, S. Yeates, H. S. Toogood, A. J. Mulholland and N. S. Scrutton, *Biochemistry*, 2018, **57**, 1997–2008.
16 J. Courtenay, R. Sharma and J. Scott, *Molecules*, 2018, **23**, 654.
17 M. Q. Styles, E. A. Nesbitt, S. Marr, M. Hutchby and D. J. Leak, *FEBS J.*, 2017, **284**, 1700–1711.

18 Coca-Cola, PlantBottle, http://www.coca-colacompany.com/our-company/plantbottle, (accessed 16 April 2018).
19 Coca-Cola, PlantBottle 2.0, http://www.coca-colacompany.com/press-center/press-releases/coca-cola-produces-worlds-first-pet-bottle-made-entirely-from-plants, (accessed 16 April 2018).
20 D. I. Collias, A. M. Harris, V. Nagpal, I. W. Cottrell and M. W. Schultheis, *Ind. Biotechnol.*, 2014, **10**, 91–105.
21 A. J. J. E. Eerhart, A. P. C. Faaij and M. K. Patel, *Energy Environ. Sci.*, 2012, **5**, 6407.
22 R. A. Gross and B. Kalra, *Science*, 2002, **297**, 803–7.
23 J. Lu, R. C. Tappel and C. T. Nomura, *Polym. Rev.*, 2009, **49**, 226–248.
24 Mitsubishi Chemical Company, BioPBS, http://www.mcpp-global.com/en/asia/products/brand/biopbstm/, (accessed 17 April 2018).
25 P. G. Werpy T., *Top value added chemicals from biomass: Results of screening for potential candidates from sugars and synthesis gas.*, Department of Energy Washington DC, 2004, vol. 1.
26 T. Iwata, *Angew. Chem. Int. Ed.*, 2015, **54**, 3210–3215.
27 V. Siracusa, I. Blanco, S. Romani, U. Tylewicz, P. Rocculi and M. D. Rosa, *J. Appl. Polym. Sci.*, 2012, **125**, 390–401.
28 E. Castro-Aguirre, F. Iñiguez-Franco, H. Samsudin, X. Fang and R. Auras, *Adv. Drug Deliv. Rev.*, 2016, **107**, 333–366.
29 H. Tsuji, *Macromol. Biosci.*, 2005, **5**, 569–97.
30 J. M. Becker and A. P. Dove, in *Green Polymerization Methods*, Wiley-VCH Verlag GmbH & Co. KGaA, 2011, pp. 201–220.
31 C. K. Williams and M. A. Hillmyer, *Polym. Rev.*, 2008, **48**, 1–10.
32 P. Van Wouwe, M. Dusselier, E. Vanleeuw and B. Sels, *ChemSusChem*, 2016, **9**, 907–921.
33 F. Gironi and V. Piemonte, *Environ. Prog. Sustain. Energy*, 2011, **30**, 459–468.
34 Corbion, Corbion launches PLA portfolio of neat bioplastic resins for the North American market, http://www.corbion.com/media/press-releases?newsId=2013684, (accessed 17 April 2018).
35 N. Peelman, P. Ragaert, K. Ragaert, B. De Meulenaer, F. Devlieghere and L. Cardon, *J. Appl. Polym. Sci.*, 2015, **132**, 42305.
36 Total and Corbion, PLA Performance, http://www.corbion.com/bioplastics/about-bioplastics/performance, (accessed 16 February 2016).
37 T. M. Ovitt and G. W. Coates, *J. Am. Chem. Soc.*, 2002, **124**, 1316–1326.
38 M. J. Stanford and A. P. Dove, *Chem. Soc. Rev.*, 2010, **39**, 486–494.
39 K. Fukushima and Y. Kimura, *Polym. Int.*, 2006, **55**, 626–642.
40 M. Zárraga, V. Salas, A. Miranda, P. Arroyo and C. Paz, *Tetrahedron: Asymmetry*, 2008, **19**, 79, 796-799
41 G. W. Coates, *Chem. Rev.*, 2000, **100**, 1223–1252.
42 N. Nomura, R. Ishii, Y. Yamamoto and T. Kondo, *Chem. Eur. J.*, 2007, **13**, 4433–4451.
43 A. P. Dove, H. Li, R. C. Pratt, B. G. G. Lohmeijer, D. A. Culkin, R. M. Waymouth and J. L. Hedrick, *Chem. Commun.*, 2006, **0**, 2881.
44 T. Rosen, I. Goldberg, V. Venditto and M. Kol, *J. Am. Chem. Soc.*, 2016, **138**, 12041–12044.
45 N. E. Kamber, W. Jeong, R. M. Waymouth, R. C. Pratt, B. G. G. Lohmeijer and J. L. Hedrick, *Chem. Rev.*, 2007, **107**, 5813–5840.
46 N. Ajellal, J.-F. Carpentier, C. Guillaume, S. M. Guillaume, M. Helou, V. Poirier, Y. Sarazin and A. Trifonov, *Dalt. Trans.*, 2010, **39**, 8363–8376.
47 R. C. Jeske, A. M. DiCiccio and G. W. Coates, *J. Am. Chem. Soc.*, 2007, **129**, 11330–11331.

48 S. Paul, Y. Zhu, C. Romain, R. Brooks, P. K. Saini and C. K. Williams, *Chem. Commun.*, 2015, **51**, 6459–6479.
49 E. Mahmoud, D. A. Watson and R. F. Lobo, *Green Chem.*, 2014, **16**, 167–175.
50 R. A. Sheldon, *Green Chem.*, 2014, **16**, 950–963.
51 P. K. Saini, C. Romain, Y. Zhu and C. K. Williams, *Polym. Chem.*, 2014, **5**, 6068–6075.
52 G. W. Coates and D. R. Moore, *Angew. Chem. Int. Ed.*, 2004, **43**, 6618–6639.
53 M. I. Childers, J. M. Longo, N. J. Van Zee, A. M. Lapointe and G. W. Coates, *Chem. Rev.*, 2014, **114**, 8129–8152.
54 S. Klaus, M. W. Lehenmeier, C. E. Anderson and B. Rieger, *Coord. Chem. Rev.*, 2011, **255**, 1460–1479.
55 D. J. Darensbourg and A. D. Yeung, *Polym. Chem.*, 2014, **5**, 3949–3962.
56 M. R. Kember, A. Buchard and C. K. Williams, *Chem. Commun. (Camb).*, 2011, **47**, 141–163.
57 M. Möller, F. Nederberg, L. S. Lim, R. Kånge, C. J. Hawker, J. L. Hedrick, Y. Gu, R. Shah and N. L. Abbott, *J. Polym. Sci. Part A Polym. Chem.*, 2001, **39**, 3529–3538.
58 T. Biela, A. Duda and S. Penczek, *Macromol. Symp.*, 2002, **183**, 1–10.
59 A. C. Ouano and W. Kaye, *J. Polym. Sci. Polym. Chem. Ed.*, 1974, **12**, 1151–1162.
60 M. W. F. Nielen, *Mass Spectrom. Rev.*, 1999, **18**, 309–344.
61 G. Montaudo, M. S. Montaudo, C. Puglisi, F. Samperi, N. Spassky, A. LeBorgne and M. Wisniewski, *Macromolecules*, 1996, **29**, 6461–6465.
62 K. J. Wu and R. W. Odom, *Anal. Chem.*, 1998, **70**, 456A–461A.
63 B. M. Chamberlain, M. Cheng, D. R. Moore, T. M. Ovitt, E. B. Lobkovsky and G. W. Coates, *J. Am. Chem. Soc.*, 2001, **123**, 3229–3238.
64 O. Dechy-Cabaret, B. Martin-Vaca and D. Bourissou, *Chem. Rev.*, 2004, **104**, 6147–6176.
65 K. Matsumoto, B. Saito and T. Katsuki, *Chem. Commun. (Camb).*, 2007, 3619–27.
66 P. G. Cozzi, *Chem. Soc. Rev.*, 2004, **33**, 410–421.
67 A. K. Sutar, T. Maharana, S. Dutta, C.-T. Chen and C.-C. Lin, *Chem. Soc. Rev.*, 2010, **39**, 1724–1746.
68 C. Alonso-Moreno, A. Garcés, L. F. Sánchez-Barba, M. Fajardo, J. Fernández-Baeza, A. Otero, A. Lara-Sánchez, A. Antiñolo, L. Broomfield, M. I. López-Solera and A. M. Rodríguez, *Organometallics*, 2008, **27**, 1310–1321.
69 J. E. Kasperczyk, *Macromolecules*, 1995, **28**, 3937–3939.
70 B. T. Ko and C. C. Lin, *J. Am. Chem. Soc.*, 2001, **123**, 7973–7977.
71 B. H. Huang, B. T. Ko, T. Athar and C. C. Lin, *Inorg. Chem.*, 2006, **45**, 7348–7356.
72 M.-L. Hsueh, B.-H. Huang, J. Wu and C.-C. Lin, *Macromolecules*, 2005, **38**, 9482–9487.
73 W.-Y. Lu, M.-W. Hsiao, S. C. N. Hsu, W.-T. Peng, Y.-J. Chang, Y.-C. Tsou, T.-Y. Wu, Y.-C. Lai, Y. Chen and H.-Y. Chen, *Dalt. Trans.*, 2012, **41**, 3659–3667.
74 M. H. Chisholm, C.-C. Lin, J. C. Gallucci and B.-T. Ko, *Dalt. Trans.*, 2003, **0**, 406–412.
75 Y. Huang, Y.-H. Tsai, W.-C. Hung, C.-S. Lin, W. Wang, J.-H. Huang, S. Dutta and C.-C. Lin, *Inorg. Chem.*, 2010, **49**, 9416–9425.
76 J. Zhang, C. Jian, Y. Gao, L. Wang, N. Tang and J. Wu, *Inorg. Chem.*, 2012, **51**, 13380–13389.
77 C.-A. Huang and C.-T. Chen, *Dalt. Trans.*, 2007, **0**, 5561–5566.
78 R. K. Dean, A. M. Reckling, H. Chen, L. N. Dawe, C. M. Schneider and C. M. Kozak, *Dalt. Trans.*, 2013, **42**, 3504–3520.
79 D. Alhashmialameer, N. Ikpo, J. Collins, L. N. Dawe, K. Hattenhauer and F. M. Kerton, *Dalt. Trans.*, 2015, **44**, 20216–20231.
80 E. Kober, R. Petrus, P. Kocięcka, Z. Janas and P. Sobota, *Polyhedron*, 2015, **85**, 814–823.

81 J. Char, O. G. Kulyk, E. Brulé, F. de Montigny, V. Guérineau, T. Roisnel, M. J.-L. Tschan and C. M. Thomas, *Comptes Rendus Chim.*, 2016, **19**, 167–172.
82 R. H. Platel, L. M. Hodgson and C. K. Williams, *Polym. Rev.*, 2008, **48**, 11–63.
83 M. H. Chisholm, J. C. Gallucci and K. Phomphrai, *Inorg. Chem.*, 2004, **43**, 6717–6725.
84 C. K. Williams, L. E. Breyfogle, S. K. Choi, W. Nam, V. G. Young, M. A. Hillmyer and W. B. Tolman, *J. Am. Chem. Soc.*, 2003, **125**, 11350–11359.
85 M. Cheng, D. R. Moore, J. J. Reczek, B. M. Chamberlain, E. B. Lobkovsky and G. W. Coates, *J. Am. Chem. Soc.*, 2001, **123**, 8738–8749.
86 M. Cheng, A. B. Attygalle, E. B. Lobkovsky and G. W. Coates, *J. Am. Chem. Soc.*, 1999, **121**, 11583–11584.
87 C. N. Ayala, M. H. Chisholm, J. C. Gallucci and C. Krempner, *Dalt. Trans.*, 2009, 9237–9245.
88 M. H. Chisholm, J. Gallucci and K. Phomphrai, *Inorg. Chem.*, 2002, **41**, 2785–2794.
89 S. Song, H. Ma and Y. Yang, *Dalt. Trans.*, 2013, **42**, 14200.
90 M. J. Walton, S. J. Lancaster and C. Redshaw, *ChemCatChem*, 2014, **6**, 1892–1898.
91 D. Zhang, M. A. Hillmyer and W. B. Tolman, *Biomacromolecules*, 2005, **6**, 2091–2095.
92 Y. L. Hsieh, Y. C. Lin, G. H. Lee and C. H. Peng, *Polym. (United Kingdom)*, 2015, **56**, 237–244.
93 H. Xie, Z. Mou, B. Liu, P. Li, W. Rong, S. Li and D. Cui, *Organometallics*, 2014, **33**, 722–730.
94 P. McKeown, J. Brown-Humes, M. G. Davidson, M. F. Mahon, T. J. Woodman and M. D. Jones, *Dalt. Trans.*, 2017, **46**, 5048–5057.
95 T. Rosen, Y. Popowski, I. Goldberg and M. Kol, *Chem. Eur. J.*, 2016, **22**, 11533–11536.
96 K. Devaine-Pressing, J. H. Lehr, M. E. Pratt, L. N. Dawe, A. A. Sarjeant and C. M. Kozak, *Dalt. Trans.*, 2015, **44**, 12365–12375.
97 Y. Sarazin, R. H. Howard, D. L. Hughes, S. M. Humphrey and M. Bochmann, *Dalt. Trans.*, 2006, **0**, 340–350.
98 S. Ghosh, P. K. S. Antharjanam and D. Chakraborty, *Polym. (United Kingdom)*, 2015, **70**, 38–51.
99 Youli Xiao, A. Zheng Wang and K. Ding, *Macromolecules*, 2006, **39**, 128–137.
100 P. K. Saini, C. Romain and C. K. Williams, *Chem. Commun. (Camb).*, 2014, **50**, 4164–7.
101 A. Sauer, A. Kapelski, C. Fliedel, S. Dagorne, M. Kol and J. Okuda, *Dalt. Trans.*, 2013, **42**, 9007–9023.
102 A. J. Chmura, D. M. Cousins, M. G. Davidson, M. D. Jones, M. D. Lunn and M. F. Mahon, *Dalt. Trans.*, 2008, 1437–1443.
103 A. J. Chmura, M. G. Davidson, C. J. Frankis, M. D. Jones and M. D. Lunn, *Chem. Commun.*, 2008, 1293–1295.
104 A. J. Chmura, M. G. Davidson, M. D. Jones, M. D. Lunn, M. F. Mahon, A. F. Johnson, P. Khunkamchoo, S. L. Roberts and S. S. F. Wong, *Macromolecules*, 2006, **39**, 7250–7257.
105 S. L. Hancock, M. F. Mahon, G. Kociok-Kőhn and M. D. Jones, *Eur. J. Inorg. Chem.*, 2011, **2011**, 4596–4602.
106 M. D. Jones, S. L. Hancock, P. McKeown, P. M. Schäfer, A. Buchard, L. H. Thomas, M. F. Mahon and J. P. Lowe, *Chem. Commun.*, 2014, **50**, 15967–15970.
107 M. D. Jones, L. Brady, P. McKeown, A. Buchard, P. M. Schäfer, L. H. Thomas, M. F. Mahon, T. J. Woodman and J. P. Lowe, *Chem. Sci.*, 2015, **6**, 5034–5039.
108 N. Spassky, M. Wisniewski, C. Pluta and A. Le Borgne, *Macromol. Chem. Phys.*, 1996, **197**, 2627–2637.
109 Z. Zhong, P. J. Dijkstra and J. Feijen, *Angew. Chem. Int. ed*, 2002, **41**, 4510–4513.
110 N. Maudoux, T. Roisnel, V. Dorcet, J.-F. Carpentier and Y. Sarazin, *Chem. Eur. J.*,

2014, **20**, 6131–6147.
111 N. Nomura, R. Ishii, M. Akakura and K. Aoi, *J. Am. Chem. Soc.*, 2002, **124**, 5938–5939.
112 H.-L. Chen, S. Dutta, P.-Y. Huang and C.-C. Lin, *Organometallics*, 2012, **31**, 2016–2025.
113 P. Hormnirun, E. L. Marshall, V. C. Gibson, R. I. Pugh and A. J. P. White, *Proc. Natl. Acad. Sci.*, 2006, **103**, 15343–15348.
114 P. Hormnirun, E. L. Marshall, V. C. Gibson, A. J. P. White and D. J. Williams, *J. Am. Chem. Soc.*, 2004, **126**, 2688–2689.
115 E. D. Cross, L. E. N. Allan, A. Decken and M. P. Shaver, *J. Polym. Sci. Part A Polym. Chem.*, 2013, **51**, 1137–1146.
116 P. McKeown, M. G. Davidson, G. Kociok-Köhn and M. D. Jones, *Chem. Commun.*, 2016, **52**, 10431–10434.
117 M. D. Jones, G. Loraine, M. F. Mahon and E. L. Whitelaw, *Dalt. Trans.*, 2011, **40**, 11469–11473.
118 S. L. Hancock, M. F. Mahon and M. D. Jones, *Dalt. Trans.*, 2013, **42**, 9279–9285.
119 A. Pilone, K. Press, I. Goldberg, M. Kol, M. Mazzeo and M. Lamberti, *J. Am. Chem. Soc.*, 2014, **136**, 2940–2943.
120 S. M. Kirk, P. McKeown, M. F. Mahon, G. Kociok-Köhn, T. J. Woodman and M. D. Jones, *Eur. J. Inorg. Chem.*, 2017, **45**, 5417–5426.
121 S. M. Kirk, G. Kociok-Köhn and M. D. Jones, *Organometallics*, 2016, **35**, 3837–3843.
122 X.-F. Yu and Z.-X. Wang, *Dalt. Trans.*, 2013, **42**, 3860–3868.
123 M. Normand, T. Roisnel, J.-F. Carpentier and E. Kirillov, *Chem. Commun.*, 2013, **49**, 11692–11694.
124 L. Chen, W. Li, D. Yuan, Y. Zhang, Q. Shen and Y. Yao, *Inorg. Chem.*, 2015, **54**, 4699–4708.
125 S. M. Kirk, H. C. Quilter, A. Buchard, L. H. Thomas, G. Kociok-Kohn and M. D. Jones, *Dalt. Trans.*, 2016, **4**, 835–864.
126 X. Pang, R. Duan, X. Li and X. Chen, *Polym. Chem.*, 2014, **5**, 3894–3900.
127 Z. Sun, R. Duan, J. Yang, H. Zhang, S. Li, X. Pang, W. Chen and X. Chen, *RSC Adv.*, 2016, **6**, 17531–17538.
128 A. Arbaoui, C. Redshaw and D. L. Hughes, *Chem. Commun.*, 2008, 4717–4719.
129 F. Isnard, M. Lamberti, L. Lettieri, I. D'auria, K. Press, R. Troiano, M. Mazzeo, X. Chen and M. Lamberti, *Dalt. Trans.*, 2016, **45**, 16001–16010.
130 Y. Wang and H. Ma, *Chem. Commun. Chem. Commun*, 2012, **48**, 6729–6731.
131 E. Stirling, Y. Champouret and M. Visseaux, *Polym. Chem.*, 2018, Advance Article.
132 M. Hiljanen-Vainio, T. Karjalainen and J. Seppälä, *J. Appl. Polym. Sci.*, 1996, **59**, 1281–1288.
133 R. M. Rasal, A. V. Janorkar and D. E. Hirt, *Prog. Polym. Sci.*, 2010, **35**, 338–356.
134 L. Wang, Z. Zhang, H. Chen, S. Zhang and C. Xiong, *J. Polym. Res.*, 2010, **17**, 77–82.
135 V. Siracusa, P. Rocculi, S. Romani and M. D. Rosa, *Trends Food Sci. Technol.*, 2008, **19**, 634–643.
136 M. A. Woodruff and D. W. Hutmacher, *Prog. Polym. Sci.*, 2010, **35**, 1217–1256.
137 S. Schmidt, C. Scherkus, J. Muschiol, U. Menyes, T. Winkler, W. Hummel, H. Gröger, A. Liese, H.-G. Herz and U. T. Bornscheuer, *Angew. Chem. Int. Ed. Engl.*, 2015, **54**, 2784–2787.
138 T. Buntara, S. Noel, P. H. Phua, I. Melián-Cabrera, J. G. de Vries and H. J. Heeres, *Angew. Chem. Int. Ed.*, 2011, **50**, 7083–7087.
139 M. Winnacker and B. Rieger, *Macromol. Rapid Commun.*, 2016, **37**, 1391–1413.
140 A. Corma, S. Iborra and A. Velty, *Chem. Rev.*, 2007, **107**, 2411–2502.
141 M. Winnacker and B. Rieger, *ChemSusChem*, 2015, **8**, 2455–2471.
142 M. Golets, S. Ajaikumar and J.-P. Mikkola, *Chem. Rev.*, 2015, **115**, 3141–3169.

143 J.-G. Yin, G.-C. Xu, G.-W. Zheng and J.-H. Xu, *Appl. Biochem. Biotechnol.*, 2015, **176**, 1102–1113.
144 J. Fleischer, K. Bauer and R. Hopp, US Patent, US3943181A, 1974.
145 W. J. Roberts and A. R. Day, *J. Am. Chem. Soc.*, 1950, **72**, 1226–1230.
146 N. A. Kukhta, I. V. Vasilenko and S. V. Kostjuk, *Green Chem.*, 2011, **13**, 2362.
147 P. Yu, A.-L. Li, H. Liang and J. Lu, *J. Polym. Sci. Part A Polym. Chem.*, 2007, **45**, 3739–3746.
148 T. Higashimura, J. Lu, M. Kamigaito, M. Sawamoto and Y.-X. Deng, *Die Makromol. Chemie*, 1992, **193**, 2311–2321.
149 T. Higashimura, J. Lu, M. Kamigaito, M. Sawamoto and Y.-X. Deng, *Die Makromol. Chemie*, 1993, **194**, 3441–3453.
150 T. Higashimura, J. Lu, M. Kamigaito, M. Sawamoto and Y.-X. Deng, *Die Makromol. Chemie*, 1993, **194**, 3455–3465.
151 S. Liu, L. Zhou, S. Yu, C. Xie, F. Liu and Z. Song, *Biomass and Bioenergy*, 2013, **57**, 238–242.
152 S. Ren, L. Zhang and M. A. Dubé, *J. Appl. Polym. Sci.*, 2015, **132**, 42821.
153 R. T. Mathers, K. C. McMahon, K. Damodaran, C. J. Retarides and D. J. Kelley, *Macromolecules*, 2006, **39**, 8982–8986.
154 M. das G. B. Zoghbi, E. H. A. Andrade, M. H. L. da Silva, L. M. M. Carreira and J. G. S. Maia, *Flavour Fragr. J.*, 2003, **18**, 421–424.
155 R. L. Burwell, *J. Am. Chem. Soc.*, 1951, **73**, 4461–4462.
156 P. Sarkar and A. K. Bhowmick, *RSC Adv.*, 2014, **4**, 61343–61354.
157 N. Bauer, J. Brunke and G. Kali, *ACS Sustain. Chem. Eng.*, 2017, **5**, 10084–10092.
158 S. Kobayashi, C. Lu, T. R. Hoye and M. A. Hillmyer, *J. Am. Chem. Soc.*, 2009, **131**, 7960–7961.
159 H. Miyaji, K. Satoh and M. Kamigaito, *Angew. Chem. Int. Ed.*, 2016, **55**, 1372–1376.
160 C. M. Byrne, S. D. Allen, E. B. Lobkovsky and G. W. Coates, *J. Am. Chem. Soc.*, 2004, **126**, 11404–11405.
161 F. Auriemma, C. De Rosa, M. R. Di Caprio, R. Di Girolamo, W. C. Ellis and G. W. Coates, *Angew. Chem. Int. Ed. Engl.*, 2015, **54**, 1215–1218.
162 F. Auriemma, C. De Rosa, M. R. Di Caprio, R. Di Girolamo and G. W. Coates, *Macromolecules*, 2015, **48**, 2534–2550.
163 M. Bähr, A. Bitto and R. Mülhaupt, *Green Chem.*, 2012, **14**, 1447–1454.
164 E. H. Nejad, A. Paoniasari, C. G. W. van Melis, C. E. Koning and R. Duchateau, *Macromolecules*, 2013, **46**, 631–637.
165 L. Peña Carrodeguas, C. Martín and A. W. Kleij, *Macromolecules*, 2017, **50**, 5337–5345.
166 N. J. Van Zee and G. W. Coates, *Angew. Chem. Int. Ed.*, 2015, **54**, 2665–2668.
167 C. Robert, F. De Montigny and C. M. Thomas, *Nat. Commun.*, 2011, **2**, 586.
168 M. Firdaus, L. Montero de Espinosa and M. A. R. Meier, *Macromolecules*, 2011, **44**, 7253–7262.
169 J. W. Peeters, O. Van Leeuwen, A. R. A. Palmans and E. W. Meijer, *Macromolecules*, 2005, **38**, 5587–5592.
170 D. K. Schneiderman and M. A. Hillmyer, *Macromolecules*, 2016, **49**, 2419–2428.
171 J. R. Lowe, M. T. Martello, W. B. Tolman and M. A. Hillmyer, *Polym. Chem.*, 2011, **2**, 702–708.
172 A. Baeyer and V. Villiger, *Berichte der Dtsch. Chem. Gesellschaft*, 1899, **32**, 3625–3633.
173 H. K. Hall and A. K. Schneider, *J. Am. Chem. Soc.*, 1958, **80**, 6409–6412.
174 C. L. Wanamaker, L. E. O'Leary, N. A. Lynd, M. A. Hillmeyer and W. B. Tolman, *Biomacromolecules*, 2007, **8**, 3634–3640.

175 M. A. Hillmyer and W. B. Tolman, *Acc. Chem. Res.*, 2014, **47**, 2390–2396.
176 C. C. C. R. de Carvalho and M. M. R. da Fonseca, *Food Chem.*, 2006, **95**, 413–422.
177 M. Labet and W. Thielemans, *Chem. Soc. Rev.*, 2009, **38**, 3484–3504.
178 N. Oberleitner, A. K. Ressmann, K. Bica, P. Gärtner, M. W. Fraaije, U. T. Bornscheuer, F. Rudroff and M. D. Mihovilovic, *Green Chem.*, 2017, **19**, 367–371.
179 J. R. Lowe, W. B. Tolman and M. A. Hillmyer, *Biomacromolecules*, 2009, **10**, 2003–2008.
180 M. Winnacker, S. Vagin, V. Auer and B. Rieger, *Macromol. Chem. Phys.*, 2014, **215**, 1654–1660.
181 M. Winnacker, A. Tischner, M. Neumeier and B. Rieger, *RSC Adv.*, 2015, **5**, 77699–77705.
182 M. Winnacker, M. Neumeier, X. Zhang, C. M. Papadakis and B. Rieger, *Macromol. Rapid Commun.*, 2016, **37**, 851–857.
183 M. Winnacker, J. Sag, A. Tischner and B. Rieger, *Macromol. Rapid Commun.*, 2017, **38**, 1600787–1600794.
184 M. Winnacker and J. Sag, *Chem. Commun.*, 2018, **54**, 841–844.
185 A. F. Thomas and F. Rey, *Tetrahedron*, 1992, **48**, 1927–1942.
186 A. F. Thomas and F. Rey, *Chim. Int. J. Chem.*, 1991, **45**, 164–164.
187 A. Watts, N. Kurokawa and M. A. Hillmyer, *Biomacromolecules*, 2017, **18**, 1845–1854.

2 Chapter 2. Multinuclear Zr(IV), Li(I), Mg(II) and Zn(II) amine bis(phenolate) complexes for the polymerisation of *rac*-LA

2.1 Preamble

Single-site metal complexes comprising tetradentate amine bis(phenolate) ligands have been extensively researched for the stereoselective ROP of lactide, due to ease of their preparation and potential for structural variation.[1–6] The choice of ligand has been shown to be highly significant in ROP in tuning the electronic and steric properties of the metal centre, thus influencing the stereochemistry of the architecture of the PLA product.[31] Judicial choice of Lewis acidic metal has also been shown to be an important factor in controlling stereoselectivity.[7] For example, the use of a *meso*-bipyrrolidine ligand has been reported with group 4 metals to produce either isotactic PLA (with zirconium or hafnium) or atactic PLA (titanium).[8] However, complexes of group 13 metals with this ligand have been shown to produce PLA with a heterotactic bias.[9,10]

Multinuclear complexes have recently received great interest as they can impart selectivity, or activity, which is not achievable with monomeric species,[11–14] and may be utilised in combining ROP and ROCOP polymerisation techniques.[15–18] The aim in this work was to synthesise new multinuclear initiators for ROP with cheap, abundant biocompatible metals (Zr(IV), Li(I), Mg(II) and Zn(II)) bearing amine bis(phenolate) ligands with varying backbone rigidity, and to apply these for the stereoselective ROP of *rac*-LA.

2.2 Synthesis of amine bis(phenolate) ligands

Ligands **1**-**6**H_2 (Figure 2.1) were prepared following previously reported methods.[4,8,19] An example of ligand synthesis *via* modified Mannich reaction is shown in Scheme 2.1. Generally, the reaction is a simple, one-pot procedure where the ligands precipitate and so are readily obtained in good yields by simple filtration and washing with cold methanol or recrystallisation to remove residual starting materials. Rigid salan ligand **7**H_2 was prepared by a slightly modified method reported by Maudoux *et al*., who reported both a one-pot and two-step procedure for preparing substituted hydropyrimidine ligands.[20] In this case, refluxing 2,2-dimethyl-1,3-propanediamine and 2,4-dimethylphenol (2 eq.) with paraformaldehyde (4 eq.) for 72 h yielded **7**H_2 as a white precipitate in 33% yield. All ligands isolated were fully characterised by ^{1}H and $^{13}C\{^{1}H\}$ NMR spectroscopy, and high

resolution ESI-TOF mass spectrometry, with values matching those reported in literature for published species.[4,8,19]

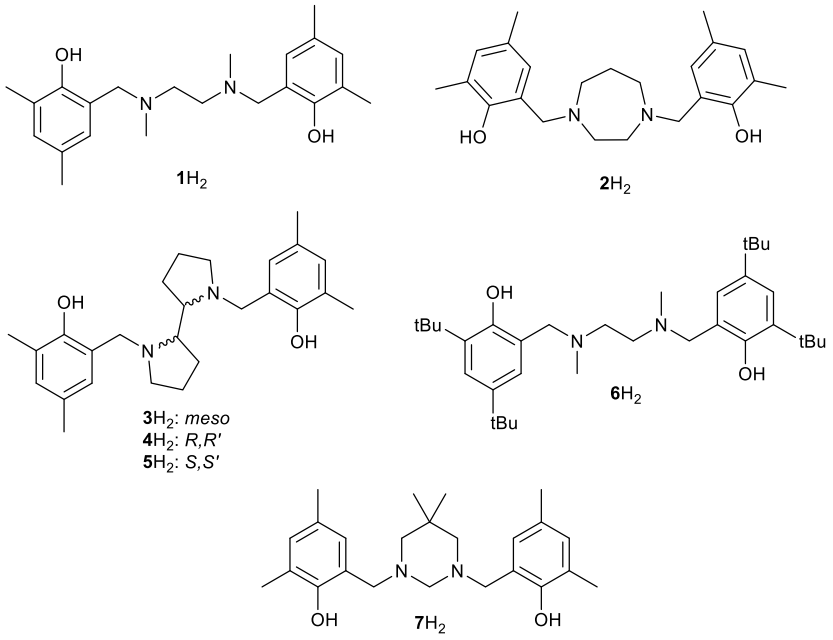

Figure 2.1. Tetradentate amine bis(phenolate) ligands of interest in this study

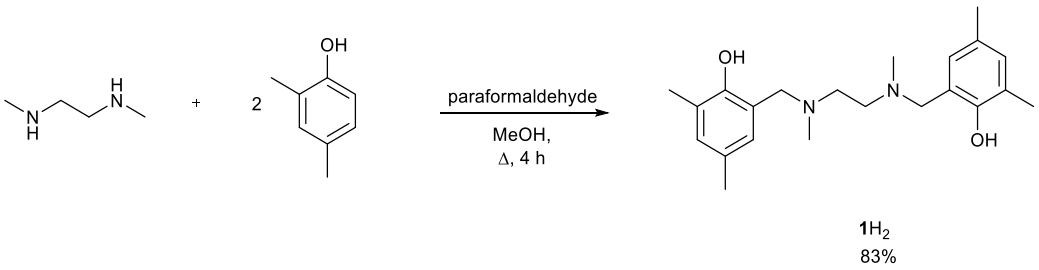

Scheme 2.1. Synthesis of **1**H_2 *via* modified Mannich reaction

2.3 Synthesis of dinuclear zirconium complexes

There are numerous examples of Zr(IV) salan complexes described in the literature, which have been employed for the ring-opening polymerisation (ROP) of lactide and other related lactones.[1,8,19,21–25] Recently there has been interest in preparing dinuclear species, such as the series of μ-oxo-bridged dinuclear group IV species reported by Su *et al.*, which were found to be active for both ROP of lactide and copolymerisation of cyclohexene oxide with CO_2.[17] Examples of Zr(IV) initiators for epoxide ring-opening copolymerisation (ROCOP) with either CO_2 or anhydrides are somewhat rare, and could be utilised for terpolymerisation of different types of monomers to widen the library of available materials from bio-based feedstocks.[15]

Both ligands **1**H_2 & **2**H_2 were prepared following modified Mannich conditions as previously reported.[4,19] The ligands were reacted with Zr(O^iPr)$_4$(^{i}PrOH) in a 1:1 molar ratio in toluene with stirring at room temperature. Removal of solvent after 2-4 h and recrystallisation from hexane or hexane/toluene yielded the monomeric species Zr(**1**)(O^iPr)$_2$ and Zr(**2**)(O^iPr)$_2$ in 32 and 33 % yield respectively, with ^{1}H NMR spectra matching those previously reported.[4,19]

Initial attempts to form μ-oxo-bridged species following the procedure used by Su,[17] by slowly adding 1 eq. of H_2O (1.0 M in THF) to Zr(**1**)(O^iPr)$_2$ in toluene, were unsuccessful. Analysis of the product by ^{1}H NMR spectroscopy showed no resonances corresponding to the isopropoxide ligand, indicating that the isolated structure had no labile initiating group. It was unclear from the ^{1}H NMR spectrum whether the species was a single zirconium centre with two coordinated ligands or if it was a dinuclear species where the isopropoxide ligands on the Zr(IV) centres had been replaced by a bridging μ-oxo. A solid-state structure was obtained, which showed the structure to be a 2:1 ligand/Zr complex, Zr(**1**)$_2$ (Figure 2.2). Bond lengths and angles were in good agreement with published values for this structure.[25] When trialled for the ROP of *rac*-LA under melt conditions with and without the addition of exogeneous alcohol, no polymerisation was observed. Thus, as expected, this complex is inactive for ROP.

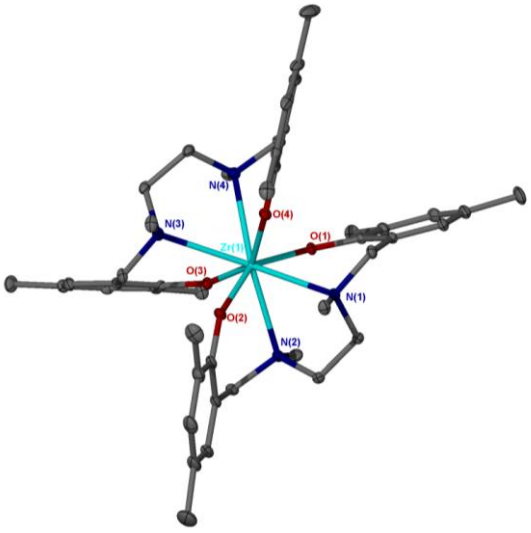

Figure 2.2: Solid state structure obtained in attempting to isolate crystals of Zr(**1**)$_2$. Ellipsoids are shown at the 30% probability level. All hydrogen atoms and a molecule of CH_2Cl_2 have been removed for clarity. Selected bond lengths (Å) and angles (°): Zr(1)-O(1) 2.0517(18), Zr(1)-O(2) 2.0491(18), Zr(1)-N(1) 2.597(2), Zr(1)-N(2) 2.597(2), O(2)-Zr(1)-O(1) 147.35(8), O(2)-Zr(1)-O(4) 89.73(8), O(1)-Zr(1)-O(4) 99.38(7), O(2)-Zr(1)-O(3) 99.15(7), O(1)-Zr(1)-O(3) 90.32(7), O(4)-Zr(1)-O(3) 146.64(7), O(2)-Zr(1)-N(2) 73.05(8), O(1)-Zr(1)-N(2) 79.88(7), O(4)-Zr(1)-N(2) 139.19(8), O(3)-Zr(1)-N(2) 73.82(7), O(2)-Zr(1)-N(1) 81.25(7), O(1)-Zr(1)-N(1) 71.65(7), O(4)-Zr(1)-N(1) 73.44(7), O(3)-Zr(1)-N(1)139.54(7), N(2)-Zr(1)-N(1) 67.62(7), O(2)-Zr(1)-N(4) 137.91(8), O(1)-Zr(1)-N(4) 74.26(7), O(4)-Zr(1)-N(4) 71.12(7), O(3)-Zr(1)-N(4) 81.17(7), N(2)-Zr(1)-N(4) 143.67(7), N(1)-Zr(1)-N(4) 125.00(7), O(2)-Zr(1)-N(3) 72.92(8), O(1)-Zr(1)-N(3) 139.38(7), O(4)-Zr(1)-N(3) 80.26(7), O(3)-Zr(1)-N(3) 71.95(7), N(2)-Zr(1)-N(3) 126.19(7), N(1)-Zr(1)-N(3) 142.98(7), N(4)-Zr(1)-N(3) 67.20(7).

Dissolving monomeric Zr(**1**)(O^iPr)$_2$ in anhydrous CH_2Cl_2, stirring for 1 h at room temperature, then exposing to moist air for 24 hours provided a route to a dinuclear complex, where a single isopropoxide ligand was retained per Zr(IV) centre. Zirconium complexes with ligands **1**H_2 and **2**H_2 were prepared in this manner and characterised by ^1H and $^{13}C\{^1H\}$ NMR spectroscopy and elemental analysis.

Complex {(Zr(**1**)(O^iPr)$_2$)$_2$μ-O} was isolated as a white solid in 61% yield from the monomeric species. The ^1H NMR spectrum of complex {(Zr(**1**)(OiPr)$_2$)$_2$μ-O} with predicted structure is shown in Figure 2.3, with the ^1H NMR spectrum for monomeric complex Zr(**1**)(O^iPr)$_2$ for comparison.

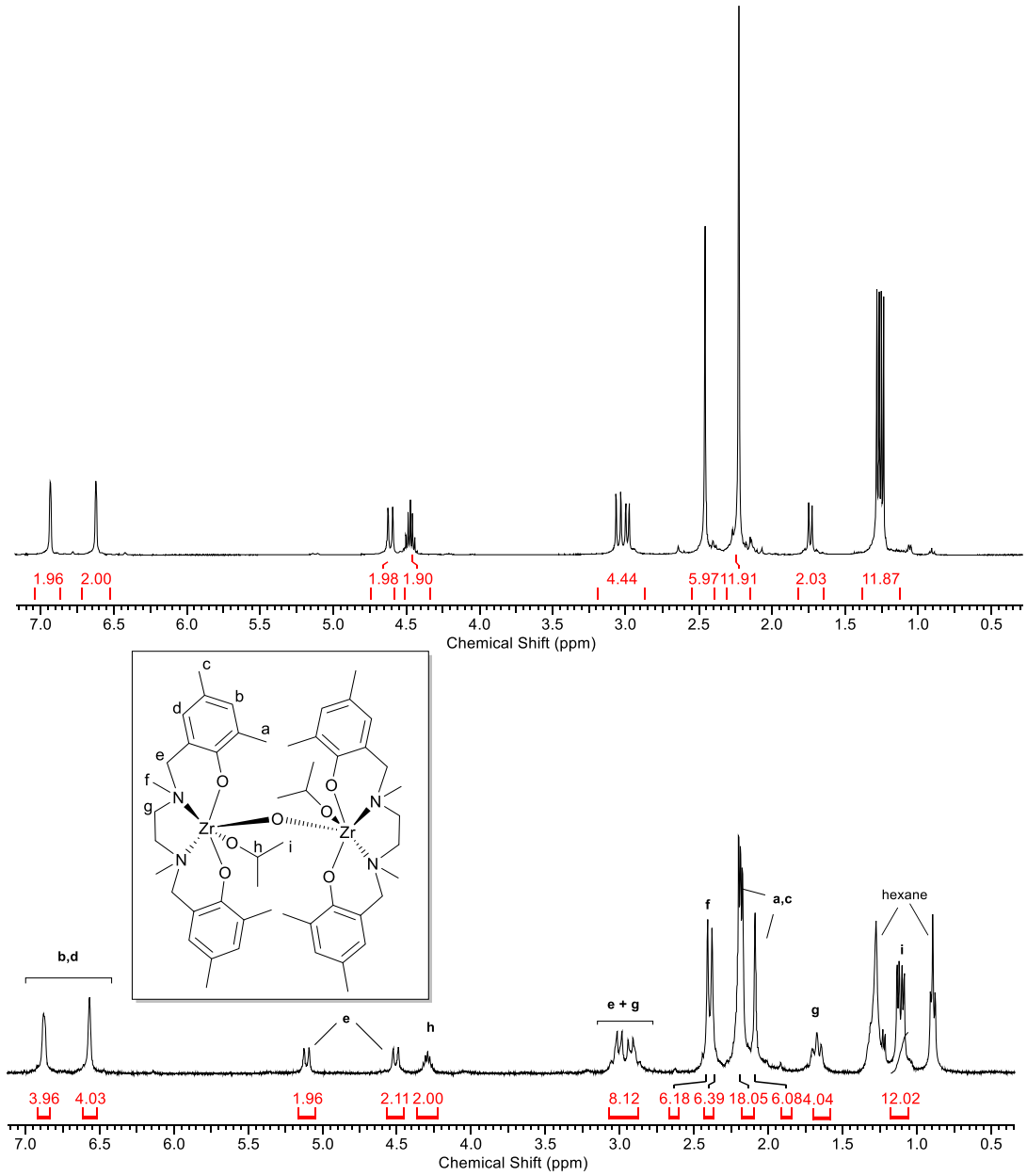

Figure 2.3. ^1H NMR spectra (400 MHz, $CDCl_3$) of complex Zr(**1**)(O^iPr)$_2$ (above) and predicted μ-oxo-bridged dimeric complex {(Zr(**1**)(O^iPr)$_2$)$_2$μ-O} (below).

The septet at 4.31 ppm corresponds to the two methine protons of the isopropoxide ligands. Without a crystal structure, it is difficult to tell if these ligands are terminal or bridging isopropoxides, although the resonance is similar to reported values for terminal isopropoxide ligands.[17] The two sets of doublets at 1.11 ppm, which integrate to 6 protons, correspond to the methyl groups of the isopropoxide ligand, which are chemically inequivalent due to restricted rotation. The N-C**H**$_2$-Ar resonances now appear as multiple resonances, suggesting that the methylene protons are locked in conformation as in Zr(**1**)(O^{i}Pr)$_2$, while in the free ligand (**1**H$_2$) these protons appear as a singlet resonance and exist in an equivalent environment. The resonances corresponding to the amine-methyl peaks, which appeared as a singlet in the monomeric complex spectrum, are now resolved into 2 singlets, meaning they are inequivalent. Despite drying under reduced pressure, it was not possible to remove traces of hexane, the solvent used in preparation and purification.

No crystals suitable for X-ray analysis were isolated for this structure, and it remains uncharacterised in the solid-state. The uncontrolled nature of preparation led to difficulties in preparing it in predictable yields for thorough investigation. Further work is required to fully understand the solution and solid-state behaviour of the μ-oxo-bridged complex. Some initial polymerisation data for {(Zr(**1**)(O^{i}Pr)$_2$)$_2$μ-O} will be discussed in section 2.7.1.

Dissolution of Zr(**2**)(O^{i}Pr)$_2$ in anhydrous CH_2Cl_2 and exposure to air for 24 h, followed by removal of solvent, yielded a white residue. Complex {(Zr(**2**)(O^{i}Pr)$_2$)$_2$μ-O} was isolated as a white solid in 21% yield *via* crystallisation from toluene and characterised by ^{1}H and ^{13}C{^{1}H} NMR spectroscopy. The ^{1}H NMR spectra of the isolated complex is shown in Figure 2.4 at 298 K (above) and 233 K (below). At 298 K two broad aromatic resonances were evident for the phenyl protons. The spectrum showed very broad resonances for the methylene protons, making it difficult to fully elucidate structural information.

Hancock *et al*. reported the ^{1}H NMR spectrum for the 1:1 species, Zr(**2**)(O^{i}Pr)$_2$, with broad resonances for the methylene -CH_2- moieties.[4] The authors reported that that variable temperature ^{1}H NMR spectroscopy was necessary to discern useful information, and a sharpened spectrum with clearly defined methylene resonances was observed at 233 K. Two isopropoxide groups were also seen, with one shifted significantly upfield from typical Zr/Hf-O^{i}Pr resonances.

Upon cooling {(Zr(**2**)(O^{i}Pr)$_2$)$_2$μ-O} to 233 K, four sharp resonances were observed in the ^{1}H NMR spectrum, corresponding to the eight aromatic protons, showing that each aromatic

proton exists in a different environment. In the 1:1 complex only two aromatic resonances are seen in the ^{1}H NMR spectrum.[4] The methylene protons of the homopiperazine backbone become visible, and sharp doublets for the N-CH_2-Ar protons are seen, showing that they are locked in conformation. Two resonances are now observed for the CH protons of the isopropoxide groups at 3.05 and 3.76 ppm. The CH_3 isopropoxide protons resolve into two doublets, appearing at 0.30 and 0.48 ppm. This shows the difference in environments for the two isopropoxide ligands, as reported for the monomeric complex.[4]

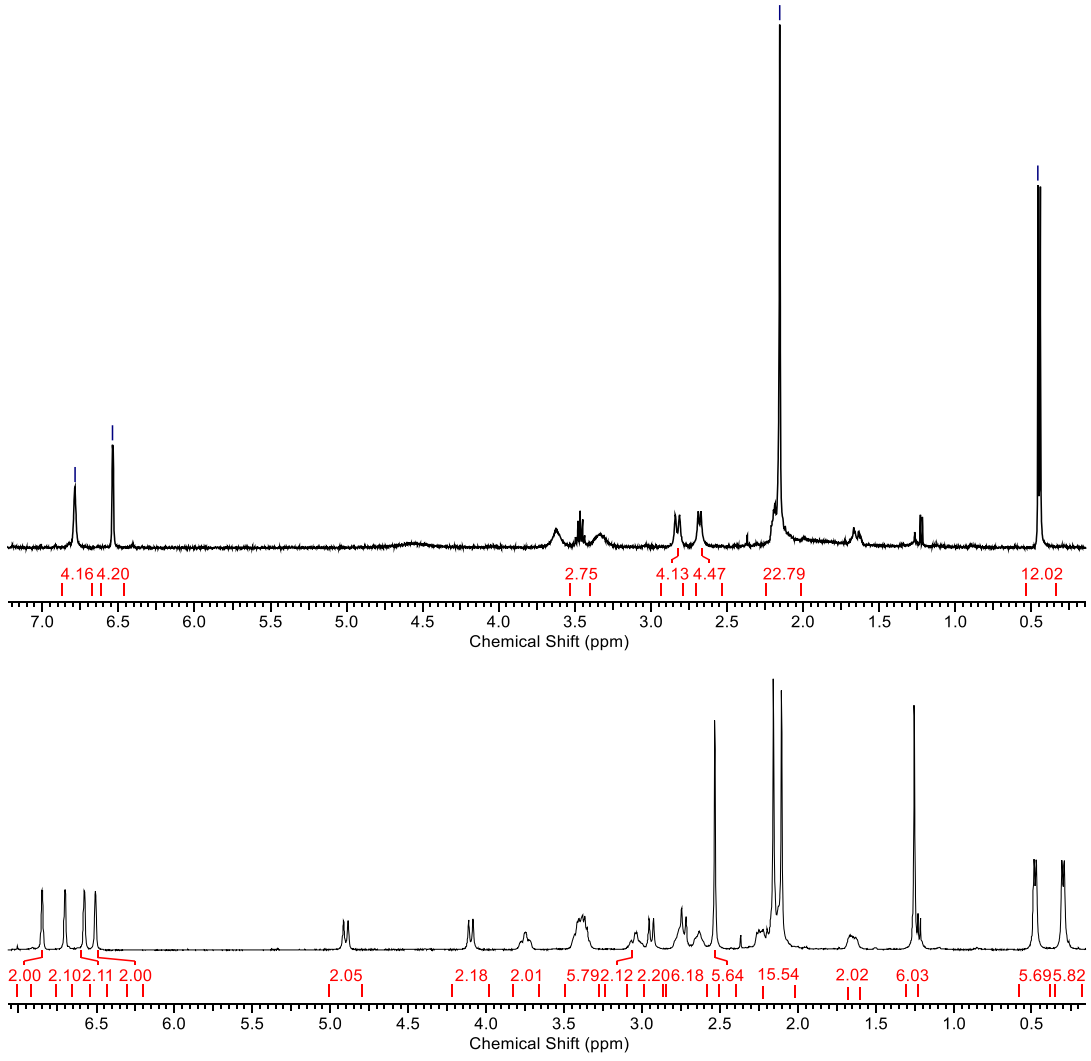

Figure 2.4: ^{1}H NMR spectra (400 MHz, $CDCl_3$) for {(Zr(**2**)($O^{i}Pr$)$_2$)$_2$μ-O} at 298 K (top) and 233 K (bottom)

Crystals suitable for single crystal X-ray diffraction studies were grown from toluene and a solid-state structure for the complex was obtained (Figure 2.5). The complex crystallises in the monoclinic space group *C*2/*c*. Both zirconium centres are 7-coordinate, with a phenolate from each ligand bridging both centres in addition to a single μ-oxo bridging

ligand. Both zirconium centres retain a labile isopropoxide ligand, crucial for ROP *via* a coordination-insertion mechanism.

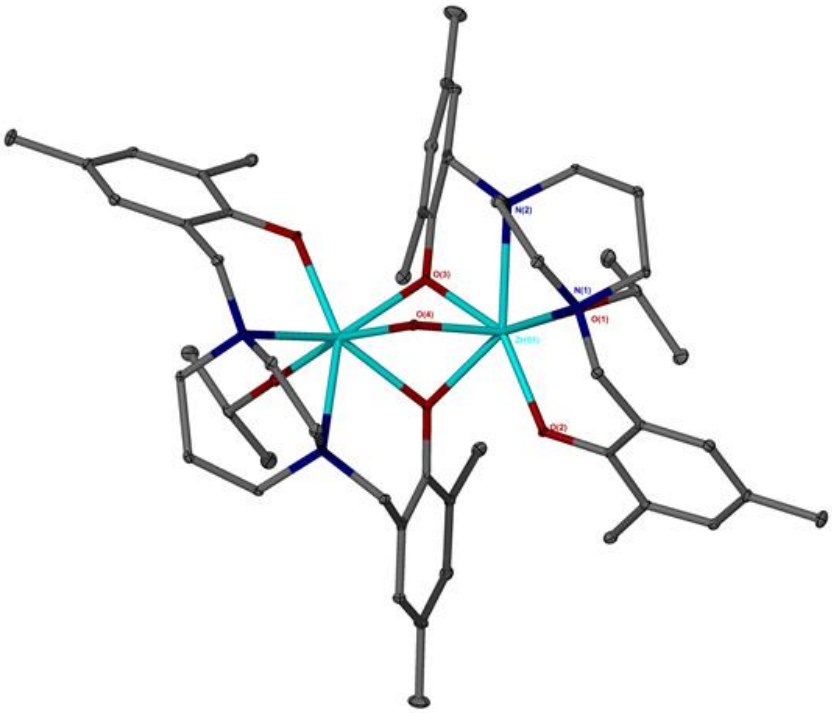

Figure 2.5. Solid-state structure of μ-oxo-bridged complex {(Zr(**2**)(O^iPr)$_2$)$_2$μ-O}. Ellipsoids are shown at the 30% probability level. All hydrogen atoms have been removed for clarity. Three molecules of CH_2Cl_2 are also present in the asymmetric unit and these are not shown. Symmetry-related atoms were generated by the symmetry transformation (-x+1, y, -z+3/2).

Selected bond angles and lengths for the complex are given in Table 2.1, alongside data for a previously reported complex, {(Zr(**A**)(O^iPr)$_2$)$_2$μ-O} for comparison. The pentadentate ligand **A**H_2 is shown in Figure 2.6. The structures differ in the nature of the coordination of phenolate groups. In {(Zr(**2**)(O^iPr)$_2$)$_2$μ-O}, one of the phenolate moieties of each ligand bridges between Zr centres, giving a dimeric structure where three Zr-O-Zr linkages are present. By contrast, {(Zr(**A**)(O^iPr)$_2$)$_2$μ-O} has a dimeric structure where a single μ-oxo linkage exists between Zr centres, which are both in octahedral environments. This is presumably due to rigidity of the ligand, which also has a less acute bite angle between phenolate groups.

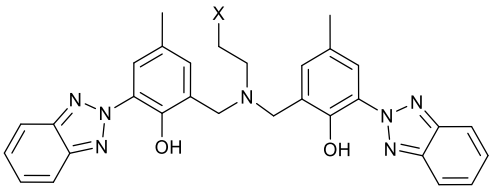

Figure 2.6. Ligand **A**H_2, investigated by Su.[17]

Table 2.1. Selected bond angles (°) and lengths (Å) for μ-oxo bridged Zr(IV) complexes {(Zr(**2**)(O^iPr)$_2$)$_2$μ-O} and with comparison {(Zr(**A**)(O^iPr)$_2$)$_2$μ-O} reported by Su.[17]

	{(Zr(**2**)(O^iPr)$_2$)$_2$μ-O}	{(Zr(**A**)(O^iPr)$_2$)$_2$μ-O}[17]
Zr(1)-N(1)	2.454(3)	2.4765(19)
Zr(1)-N(2)	2.516(3)	2.550(2)
Zr(1)-O(1)	1.964(2)	2.0646(15)
Zr(1)-O(2)	2.075(2)	2.0428(15)
Zr(1)-O(3)	2.242(2)	1.9128(16)
Zr(1)-O(3)#1	2.259(2)	-
Zr(1)-O(4)	2.010(2)	1.9552(16)
Zr(1)-Zr(1)#1	3.0926(6)	
Zr(1)-O(3)-Zr(1)#	86.81(7) (phenolate)	-
Zr(1)-O(4)-Zr(1)#1	100.56(13) (μ-oxo)	166.25(9)

#1 generated by the following symmetry transformation: (-x+1, y, -z+3/2)

In {(Zr(**2**)(O^iPr)$_2$)$_2$μ-O}, the bond length from zirconium centre Zr(1) to the isopropoxide ligand O(1) is the shortest of the Zr-O bonds. The distance from the amine groups to the zirconium centre in 2.454(3) Å, and to the phenolate is 2.075(2) Å. The distance between the bridging phenolate and zirconium centre is 2.242(2) Å, while the distance to the bridging oxo ligand is shorter, at 2.010(2) Å. In {(Zr(**A**)(O^iPr)$_2$)$_2$μ-O}, the μ-oxo linkage is close to linear (166.25(9)°), while in {(Zr(**2**)(O^iPr)$_2$)$_2$μ-O}, this bond is more acute, with Zr(1)-O(4)-Zr(1)#1 =100.56(13)°.

Polymerisation data will be discussed in section 2.7.1. While these structures are interesting and novel, irreproducibility due to the uncontrolled nature of the synthesis of these complexes led to attempts to synthesise multinuclear complexes with these ligands with alternative metals.

2.4 Synthesis of lithium complexes

Lithium complexes were prepared by reacting the bis(phenolate) ligands with 2 equivalents of an alkyllithium reagent (^{n}BuLi) in THF at -78 °C, as shown in Scheme 2.2. Li complexes with ligands **1**H_2 and **3**H_2 were initially prepared by Rachel Drewitt (MChem student 2016-2017). The solutions were stirred for 1 hour while slowly warming to room temperature, over which time the solutions were observed to turn yellow. The solvent was removed, and

the off-white residues were recrystallised in hexanes to yield products as colourless crystals in good yields.

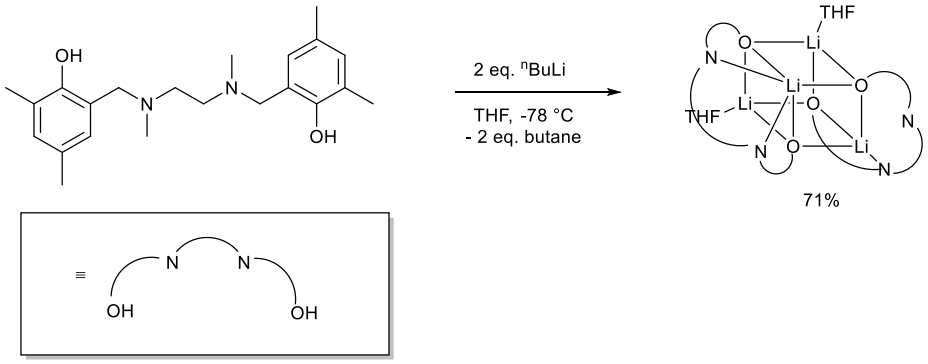

Scheme 2.2. Preparation of lithium complex $Li_4(\mathbf{1})_2(THF)_2$

The solid-state structure of $Li_4(\mathbf{1})_2(THF)_2$ is shown in Figure 2.7. The complex forms with a central Li_4O_4 cubic structure. This cube motif is prevalent in the literature, and the metric data are consistent with similar structures.[11,26,27] While many structures of this type have been reported, few have been thoroughly characterised in the solution-state. In this structure, three of the lithium centres Li(1-3) are four coordinate, while one lithium centre Li(4) is five coordinate. The coordination sphere is completed with N(3) and N(4) from one of the coordinated phenolate ligands. Li(1 and 3) both coordinate a molecule of THF. The phenolate oxygen centres are all μ_3 coordinated with an average Li-O distance of 1.993 Å, with the range being 2.098(4) – 1.945(4) Å, O-Li-O angles of 89.29(15) – 97.54(17)° and Li-O-Li 82.60(16) – 87.68(16)°. In this structure one of the nitrogen atoms in one phenolate ligand, N(1), does not coordinate to Li(2), with the distance of 2.897 Å being too long to be considered a formal bonding interaction. This complex differs from a complex reported using the ^{t}Bu analogue of the ligand, where a cisoidal "ladder" motif was observed.[26] This structural difference is presumably related to the reduced steric demand of the methyl groups on the phenolate ring over the bulkier ^{t}Bu substituents. The authors also reported a "monomeric" (dinuclear) structure with the Me analogue solvated with one molecule of tetramethylethylenediamine, rather than the cubane structure reported here.

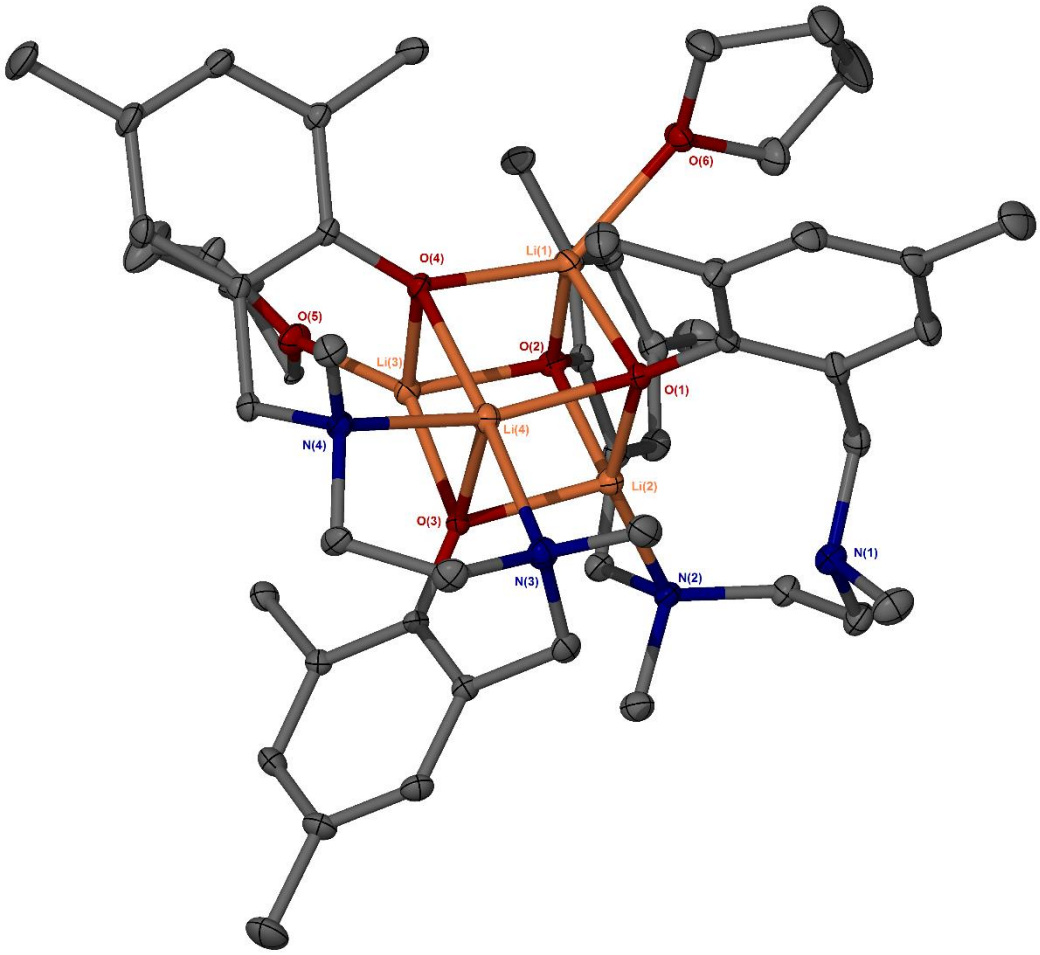

Figure 2.7. Solid-state structure of $Li_4(\mathbf{1})_2(THF)_2$, ellipsoids are shown at the 30% probability level and all hydrogen atoms have been removed for clarity.

The solution structure was probed by NMR spectroscopy in a range of solvents, with d^5-pyridine giving the most well-defined spectra. No resonances for the methylene proton environments could be discerned at room temperature (Figure 2.8), but when the solution was cooled resonances for the $-CH_2-$ functionality were observed. This spectrum is indicative of a highly fluxional system, which may be related to the lability and exchange of the amine moieties.

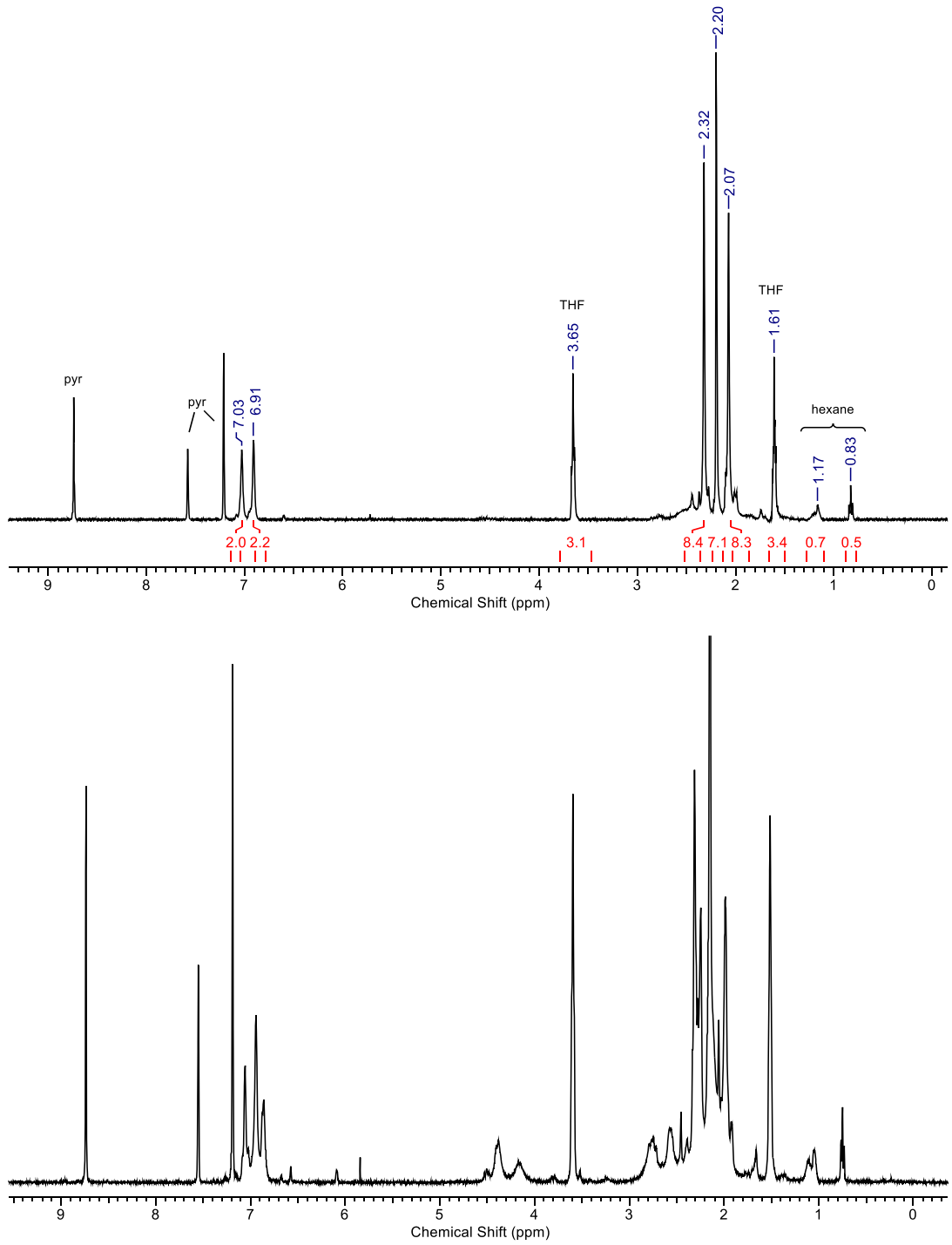

Figure 2.8. ^{1}H NMR spectrum (400 MHz, pyridine-d^{5}) of $Li_4(\mathbf{1})_2(THF)_2$ at 298 K (top) and 258 K (bottom).

DOSY has been utilised as a tool for monitoring levels of aggregation in organolithium species and correlating ^{1}H NMR spectra of solvated organometallic compounds with solid-state crystal structures by Williard and co-workers.[13] DOSY NMR (Figure 2.9) confirmed the complex exists as a single species in solution, with a single diffusion constant, D = 3.8 x10^{-10} m^{2}s^{-1} (400 MHz, pyridine-d^{5}, 298 K), while solvent signals correspond to a faster diffusion

rate (*ca.* 13.8 x10^{-10} m^2s^{-1}), suggesting competing binding of pyridine solvent displacing the THF molecules.

The diffusion coefficient can be equated to the hydrodynamic radius (r_H) of the diffusing molecule using the Stokes-Einstein equation (Equation 2.1), where k_B is the Boltzmann constant, T is the temperature of the experiment, f is a shape correction factor (for a perfect sphere f = 1) and η is the viscosity of the solvent.[28] A convenient tool for predicting molecular weights of organometallics has been developed by Morris and co-workers.[28,29] Using this, it was possible to calculate a hydrodynamic radius for Li_4(**1**)$_2$(THF)$_2$: r_H = 8.7 x 10^{-10} m (8.7 Å). This equates to a sphere of volume, V = 2.79 x 10^{-27} m^3 (2790 $Å^3$), although the complex deviates from the ideal spherical shape assumed by the Stokes-Einstein equation. From this, a calculated molecular weight of 1038.9 $gmol^{-1}$ was obtained, which is a slight overestimation of the actual value, M_n = 924.01 $gmol^{-1}$. This is a simple estimate of molecular weight as the Stokes-Einstein equation assumes the solute to exist as a hard sphere in solution, and for smaller molecules (<1 kDa) may lead to underestimation of molecular weight. The identity of the complex was also confirmed by elemental analysis.

Equation 2.1. Stokes-Einstein equation

$$D = \frac{k_B T}{6\pi f \eta r_H}$$

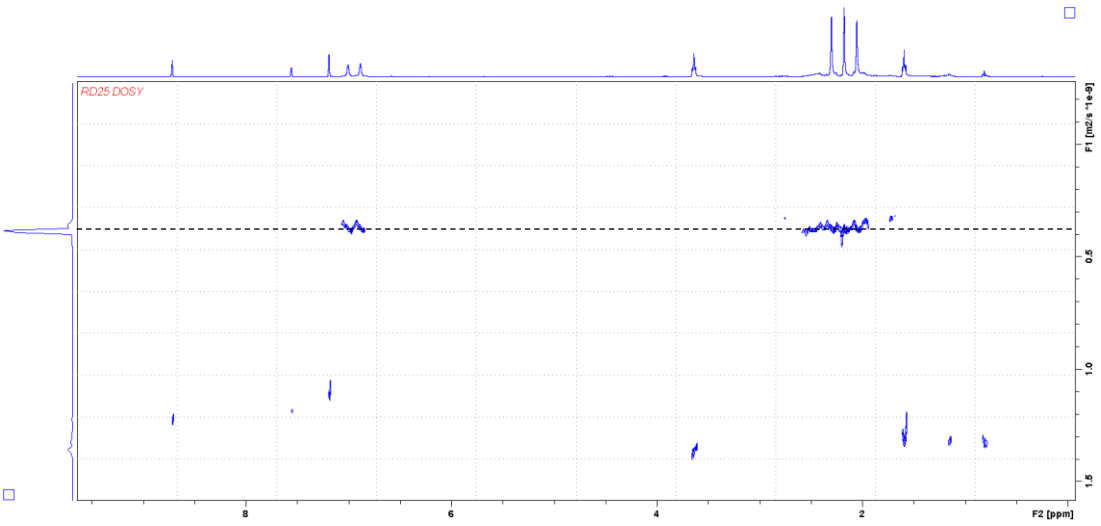

Figure 2.9. DOSY NMR (400 MHz, pyridine-d^5) of Li_4(**1**)$_2$(THF)$_2$ showing diffusion coefficient of 3.8 x 10^{-10} m^2s^{-1}

Li_4(**3**)$_2$(THF) was prepared in 59 % yield by reaction of ligand **3**H_2 with 2 eq. of ^{n}BuLi in THF. The solid-state structure for Li_4(**3**)$_2$(THF) is shown in Figure 2.10, which is slightly more complex than the structure of Li_4(**1**)$_2$(THF)$_2$. Bond lengths and angles are shown in Table

2.2. The Li_4O_4 core comprises three tetradentate and one pentadentate Li centres, which is similar to a Li complex with a tripodal ligand reported by Janas *et al.,* which also comprised two 5-coordinate Li atoms and two 4-coordinate.[11]

Here, each lithium centre is coordinated to three phenolate oxygen centres; Li(2/3) are coordinated to two nitrogen atoms; Li(4) is coordinated to a THF molecule; Li(1) has a weak η^1-Ph interaction with C(27) and an agostic interaction with a methyl group {H-Li = 2.338 Å, C-Li 2.749 Å and Li-H-C = 100.1°}. Again, the phenolate oxygen centres are all μ_3 coordinated with an average Li-O distance of 1.988 Å and the range being 2.224(4) – 1.890(5) Å, O-Li-O angles of 83.77(18) – 103.4(2)° and Li-O-Li 78.76(19) – 88.50(19)°. The Li-O_{THF} distance (1.970(5) Å) is within the normal range reported for tetrahedral lithium compounds in the literature.

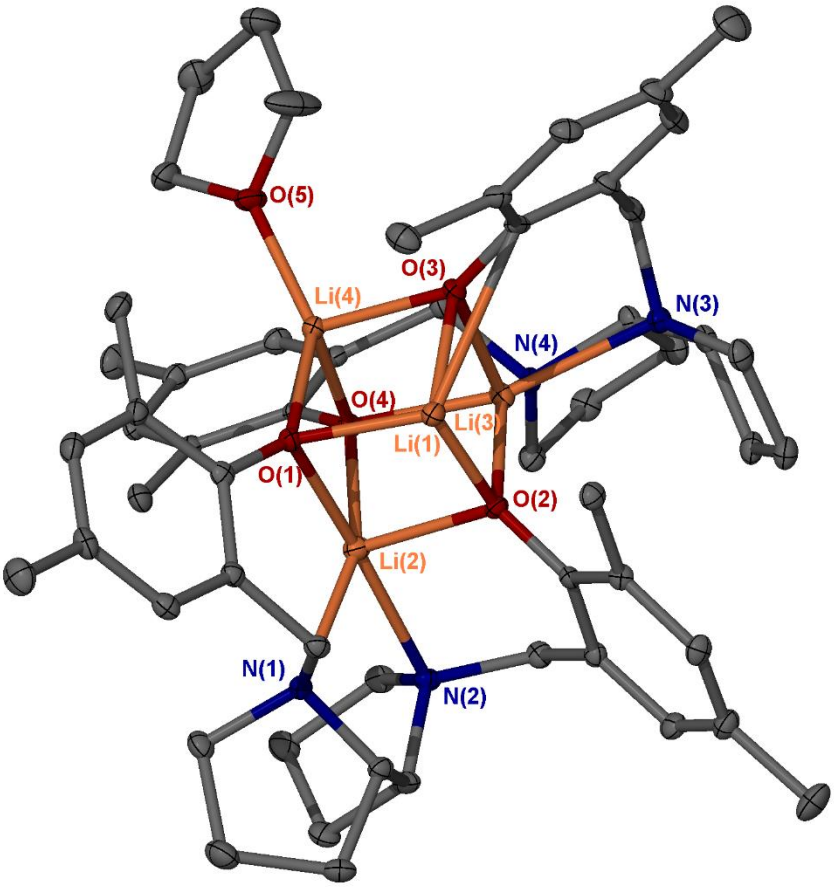

Figure 2.10. Solid-state structure of Li_4(**3**)$_2$(THF). Ellipsoids are shown at the 30% probability level. Hydrogen atoms and one and a half hexane molecules have been omitted for clarity.

Table 2.2. Selected bond lengths and angles for $Li_4(\mathbf{1})_4(THF)_2$ and $Li_4(\mathbf{3})_4(THF)$

$Li_4(\mathbf{1})_4(THF)_2$		$Li_4(\mathbf{3})_4(THF)$	
Li – O Central Cube			
O(1)-Li(1)	1.965(4)	O(1)-Li(1)	1.890(5)
O(2)-Li(3)	1.950(4)	O(2)-Li(3)	2.006(5)
Li(1)-O(2)	1.977(4)	Li(1)-O(2)	1.841(5)
O(3)-Li(3)	1.987(4)	O(3)-Li(3)	2.120(5)
O(4)-Li(1)	1.956(4)	Li(1)-O(3)	1.903(5)
O(4)-Li(3)	1.967(4)	Li(3)-O(4)	2.044(5)
O(1)-Li(2)	1.945(4)	O(1)-Li(2)	2.224(5)
O(1)-Li(4)	2.031(4)	O(1)-Li(4)	1.956(5)
O(2)-Li(2)	2.029(4)	O(2)-Li(2)	1.976(5)
O(3)-Li(4)	2.048(4)	O(3)-Li(4)	1.953(4)
O(3)-Li(2)	1.978(4)	Li(2)-O(4)	2.000(5)
O(4)-Li(4)	2.098(4)	O(4)-Li(4)	1.946(5)
Li-N bonds			
N(2)-Li(2)	2.111(4)	N(1)-Li(2)	2.231(5)
N(3)-Li(4)	2.271(4)	N(2)-Li(2)	2.293(5)
N(4)-Li(4)	2.195(4)	N(3)-Li(3)	2.243(5)
		Li(3)-N(4)	2.397(5)
Li -THF bonds			
Li(1)-O(6)	2.040(4)	Li(4)-O(5)	1.970(5)
Li(3)-O(5)	2.011(4)		
Central Cube angles			
O(4)-Li(1)-O(1)	95.46(17)	O(1)-Li(1)-O(2)	103.4(2)
O(2)-Li(3)-O(4)	97.54(17)	O(2)-Li(1)-O(3)	99.1(2)
O(4)-Li(1)-O(2)	97.00(17)	O(1)-Li(1)-O(3)	102.4(2)
O(2)-Li(3)-O(3)	94.00(16)	O(1)-Li(2)-O(2)	88.19(18)
O(1)-Li(1)-O(2)	93.79(16)	O(1)-Li(2)-O(4)	83.77(18)
O(4)-Li(3)-O(3)	96.83(17)	O(2)-Li(2)-O(4)	91.2(2)
O(1)-Li(2)-O(3)	97.78(17)	O(2)-Li(3)-O(3)	87.31(19)
O(1)-Li(4)-O(3)	92.86(16)	O(2)-Li(3)-O(4)	89.04(19)
O(1)-Li(2)-O(2)	92.79(16)	O(3)-Li(3)-O(4)	90.03(19)
O(1)-Li(4)-O(4)	89.29(15)	O(1)-Li(4)-O(3)	98.3(2)
O(3)-Li(2)-O(2)	91.87(16)	O(1)-Li(4)-O(4)	92.8(2)
O(3)-Li(4)-O(4)	91.00(15)	O(3)-Li(4)-O(4)	98.1(2)
M-L angles			
O(1)-Li(4)-N(4)	159.9(2)	O(1)-Li(2)-N(1)	92.23(19)
O(1)-Li(2)-N(2)	150.2(2)	O(2)-Li(2)-N(1)	110.3(2)
O(3)-Li(4)-N(4)	107.23(17)	O(4)-Li(2)-N(1)	158.1(2)
O(3)-Li(2)-N(2)	109.09(18)	O(1)-Li(2)-N(2)	170.5(2)
O(4)-Li(4)-N(4)	91.41(15)	O(2)-Li(2)-N(2)	90.67(19)
O(2)-Li(2)-N(2)	98.72(17)	O(4)-Li(2)-N(2)	105.6(2)
O(1)-Li(4)-N(3)	96.92(16)	N(1)-Li(2)-N(2)	79.36(17)
O(3)-Li(4)-N(3)	94.74(16)	O(2)-Li(3)-N(3)	111.3(2)
N(4)-Li(4)-N(3)	80.67(14)	O(3)-Li(3)-N(3)	90.27(18)
O(4)-Li(4)-N(3)	171.3(2)	O(4)-Li(3)-N(3)	159.6(3)
		O(2)-Li(3)-N(4)	138.4(2)
		O(3)-Li(3)-N(4)	134.1(2)
		O(4)-Li(3)-N(4)	87.01(17)
		N(3)-Li(3)-N(4)	78.22(16)

The ^{1}H NMR spectrum (pyridine-d^{5}), shown in Figure 2.10, is significantly clearer than the spectrum for Li_4(**1**)$_2$(THF)$_2$. Doublets can clearly be observed for the methylene protons at 4.61 and 2.98 ppm respectively. Furthermore, the ^{7}Li NMR spectra are comparable between the two structures, with resonances around 1 – 2 ppm being observed, similar to literature values for $Li_4L_2(THF)_x$ complexes.[30] DOSY NMR spectroscopy (400 MHz, 298 K, pyridine-d^{5}) indicated that a single species was present with a diffusion constant of 3.9 $\times$ 10^{-10} m^{2}s^{-1}, which is a similar to the diffusion coefficient determined for Li_4(**1**)$_2$(THF)$_2$. This equates to r_H = 8.56 Å, V = 2630 Å^3, and M_n = 979.4 gmol^{-1}, slightly underestimated compared to the actual molecular weight, 1042.23 gmol^{-1}.

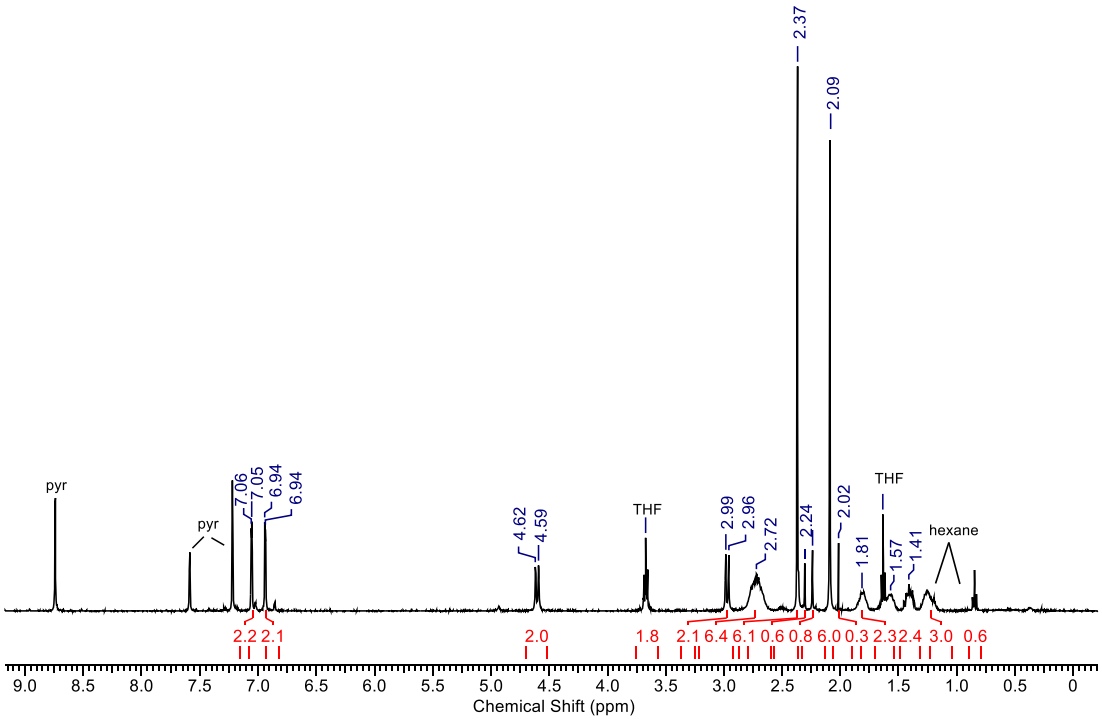

Figure 2.11. ^{1}H NMR (400 MHz, pyridine-d^{5}) spectrum of Li_4(**2**)$_2$(THF)

When the chiral ligands (**4**/**5**H$_2$) were reacted with 2 eq. of ^{n}BuLi, no crystalline material was isolated. This is possibly due to the high solubility of the resultant product in common organic solvents or subtle differences in the steric demands of the chiral backbone. It was also not possible to isolate complexes with the more rigid homopiperazine ligand, **2**H$_2$, although tetrametallic lithium complexes comprising homopiperazine ligands have also been reported previously.[31] Many examples of Li complexes with ^{t}Bu substituted ligands have been reported in the literature, generally existing as ladder-type structures to accommodate the bulky substituents. However, it was not possible to isolate complexes with the analogous ^{t}Bu substituted ligand, **6**H$_2$, despite following a published literature method.[26]

Ligands with a hexahydropyrimidine backbone were investigated in a study reported by Sarazin and co-workers.[20] In this study, crystals of an intermediate lithium complex were fortuitously obtained and characterised in the solid-state. The structure here exhibits a "back to back" arrangement rather than the Li_4O_4 cubic motif. Presumably the Li_4O_4 motif is difficult to achieve with more rigid ligands such as **2**H_2 as the backbone needs to be flexible enough to wrap around the central cube. While Sarazin reported the crystal structure of this complex, it was not investigated for ROP, with the authors preferring to prepare Li complexes as intermediates in the synthesis of triel metal complexes. A dimethyl analogue of this ligand, **7**H_2 was therefore prepared and treated with 2 eq. of ^{n}BuLi in THF, as with the previous lithium complexes (Scheme 2.3), with the aim to compare the ROP behaviour of complexes with two different structural motifs. Unlike the complexation with ligands **1**H_2 and **3**H_2, this solution became very turbid. On addition of toluene (6 mL) and gentle heating, the solid dissolved, and the yellow solution was left to cool. A crop of colourless crystals was obtained (72 %), which were suitable for X-ray crystallography. The solid-state structure of this complex is shown in Figure 2.12, and relevant bond angles and lengths are given in Table 2.3.

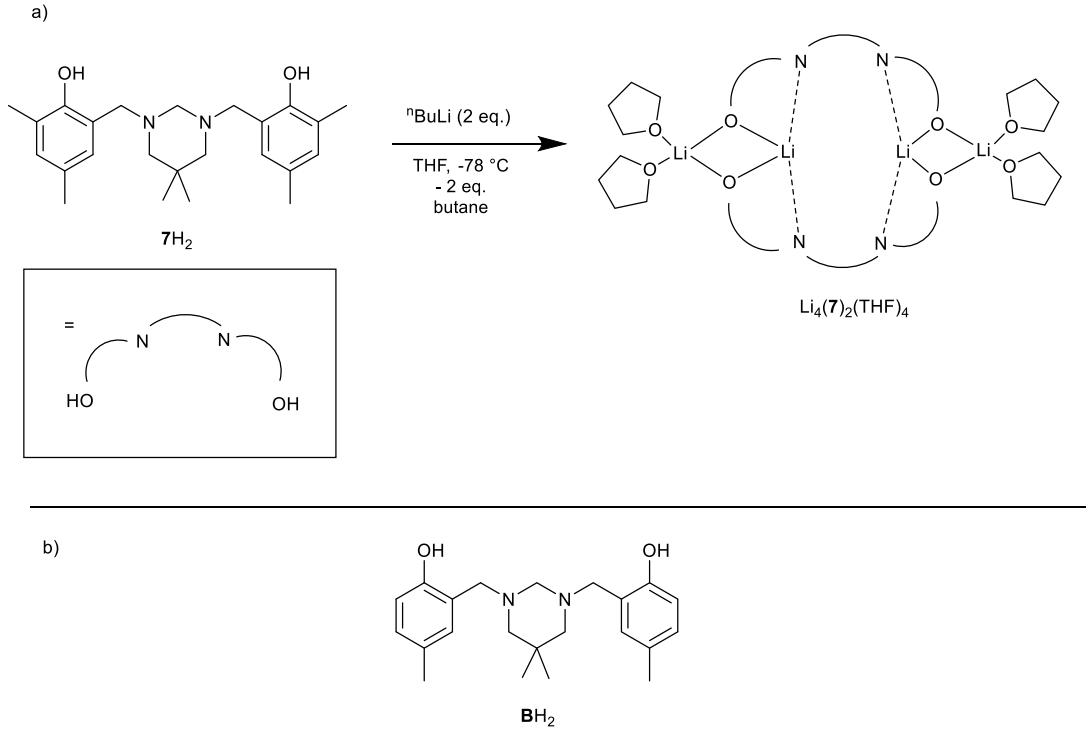

Scheme 2.3. a) Synthesis of Li_4(**7**)$_2$(THF)$_4$, b) ligand **B**H_2 reported by Sarazin and co-workers.[20]

Solid-state data for the cresol analogue is included in for comparison as $Li_4(\mathbf{B})_2(THF)_4$ in Table 2.3, with values closely matching the values for $Li_2(\mathbf{7})_2(THF)_4$.

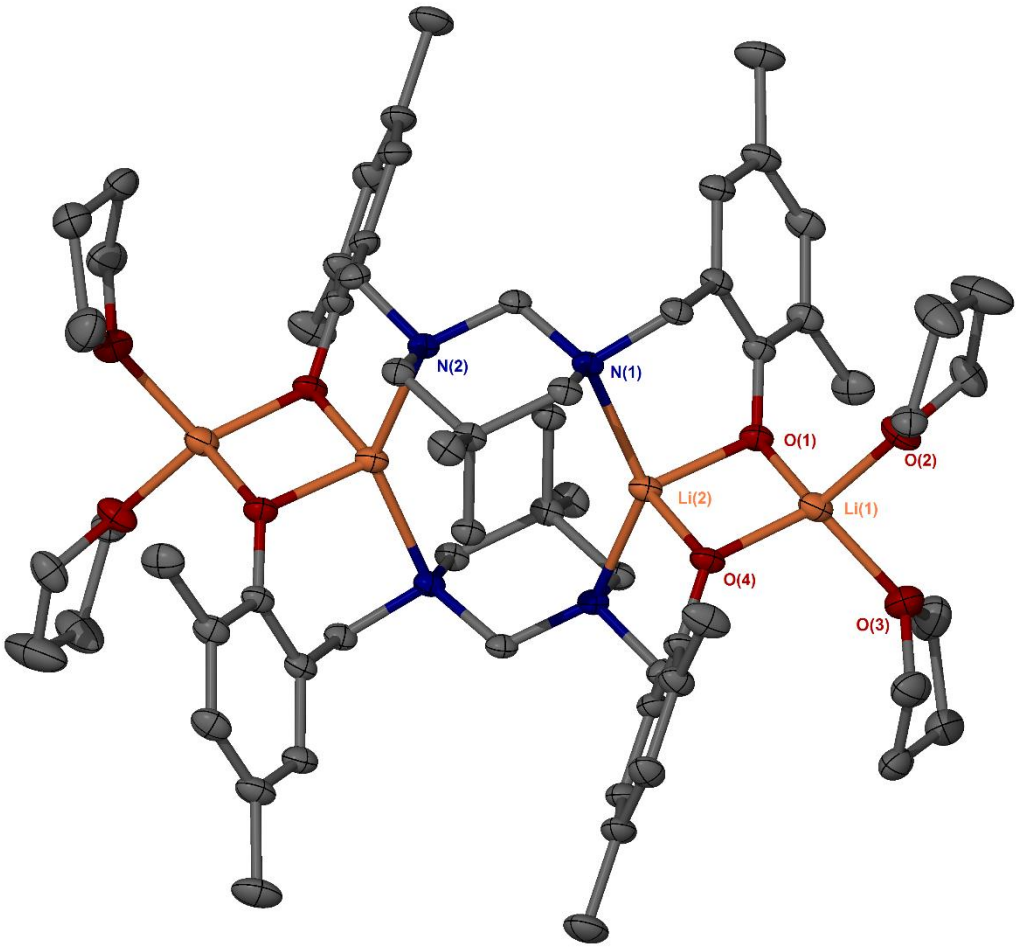

Figure 2.12. Solid-state structure of $Li_4(\mathbf{7})_2(THF)_4$ complex synthesised, similar to complex reported by Sarazin. Ellipsoids are shown at the 30% probability level and hydrogen atoms have been removed for clarity. Both coordinated THF molecules are disordered over two sites in approximately 55:45 (O2 – all atoms of THF disordered) and 65:35 (O3 only $-CH_2CH_2-$ modelled) ratio. There is also one molecule of THF solvent of crystallisation.

Table 2.3 Bond lengths (Å) for $Li_4(\mathbf{7})_2(THF)_4$ and literature comparison $Li_4(\mathbf{B})_2(THF)_4$[20]

	$Li_4(\mathbf{7})_2(THF)_4$	$Li_4(\mathbf{B})_2(THF)_4$
N(1)-Li(2)	2.214(3)	2.206(3)
O(4)-Li(1)	1.890(3)	1.899(3)
O(4)-Li(2)	1.915(3)	1.933(3)
O(2)-Li(1)	1.924(11)	1.978(3)
O(3)-Li(1)	1.966(3)	1.975(3)
Li(2)-O(1)	1.915(3)	1.938(3)
Li(2)-N(1)	2.232(3)	2.228(3)
Li(1)-O(1)	1.890(3)	1.896(3)

While the Li_4O_4 cube reported in this chapter is very common, there are limited examples of discrete bimetallic cubes where one of the vertices has been replaced. Heterometallic lithium-magnesium complexes have been shown to produce PLA with a heterotactic bias (P_r < 0.88).[32,33] Given the ease of crystallisation of **1**H_2 with ^{n}BuLi, attempts were made to prepare a mixed lithium magnesiate complex. Upon reaction of **1**H_2 with 1 eq. ^{n}BuLi followed by 1 eq. of ^{n}Bu_2Mg, a small crop of crystals was isolated after a period of 2 weeks. The solid-state structure of this complex is shown in Figure 2.13.

In this case, a novel $Li_3Mg_1O_4$ cube was identified, which has not been previously observed in the literature. However, the yield for this reaction was very low (*ca*. 10%), and the reaction was not reproducible, which did not allow for studies into the activity of this mixed metal complex for ROP. However, it is proof that the preparation of such mixed metallic cubic structures is possible.

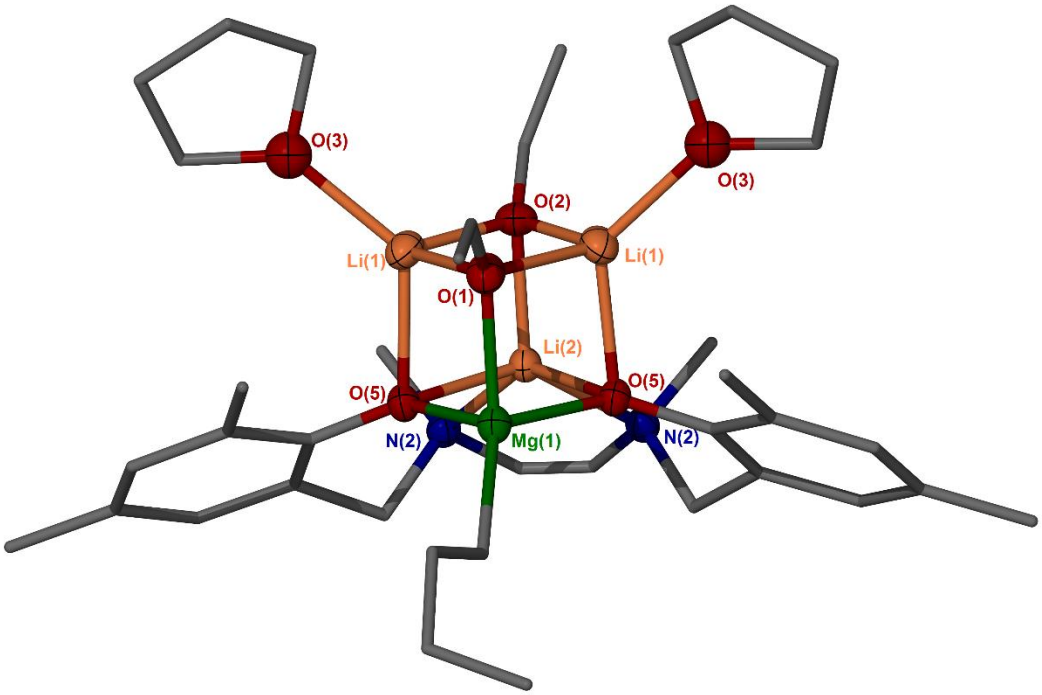

Figure 2.13. Solid-state structure obtained for Li_3(**1**)Mg(^{n}Bu)$(THF)_2(OCH{=}CH_2)_2$, ellipsoids (for O, Li, N, Mg) are shown at the 30% probability level and all hydrogen atoms have been removed for clarity. Mg(1)-O(5) 1.9909(16), Mg(1)-O(1) 2.012(3), Mg(1)- C(1) 2.138(4), O(1)-Li(1) 1.988(5), O(2)-Li(1) 1.891(5), O(2)-Li(2) 1.958(5), O(5)-Li(1) 2.018(4), O(5)-Li(2) 2.101(4), O(3)-Li(1)-1.97(2). O(5)-Mg(1)-O(5) 89.80(9), O(5)- Mg(1)-O(1) 89.16(7), O(5)-Mg(1)-O(1) 89.16(8), O(5)-Mg(1)-C(1) 123.41(8), O(5)- Mg(1)-C(1) 123.41(8), O(5)-Mg(1)-Li(1) 45.09(10), O(5)-Mg(1)-Li(1) 86.23(11), O(1)- Mg(1)-Li(1) 44.23(10), C(1)-Mg(1)-Li(1) 150.13(10).

This complex showed a significant degree of disorder, in both the coordinated THF molecules and in the ligand, with both the ethylene backbones being modelled over two sites in a 55:45 ratio. In this case two enolate moieties {O(1)} and {O(2)} were also

observed. Enolate formation is a common side reaction in these systems, caused by ether cleavage of THF, as observed previously by Henderson *et al.* and others.[34,35]

The ^{1}H NMR of the complex is shown in Figure 2.14 (400 MHz, toluene-d^{8}). Signals for the aromatic protons are observed as two doublets at 6.67 and 6.64 ppm. The doublet of doublets at 7.45 ppm (J = 5.0 Hz, 13.5 Hz) is similar to literature values for LiOC<u>H</u>=CH$_2$, while the doublet at 3.90 ppm (J = 5.0 Hz) is similar to reported values for the terminal alkene protons, LiOCH=C<u>H</u>$_2$.[35] The doublet at 4.04 ppm is also in a similar range to reported values for LiOCH=C<u>H</u>$_2$,[34] and has a large coupling constant, J = 13.5 Hz, due to vicinal coupling. The methylene protons of the ligand are seen as doublets at 4.35 and 2.76 (J = 12.0 Hz), and 2.49 and 1.42 (J = 9.0 Hz). Three singlets are observed for the Ar-CH$_3$ (1.98, 1.83 ppm) and N-CH$_3$ (2.18 ppm) protons. Resonances for the ^{n}Bu moiety are also seen in the alkyl region of the spectrum, while some hexane is also still present from crystallisation, which makes it difficult to distinguish between these.

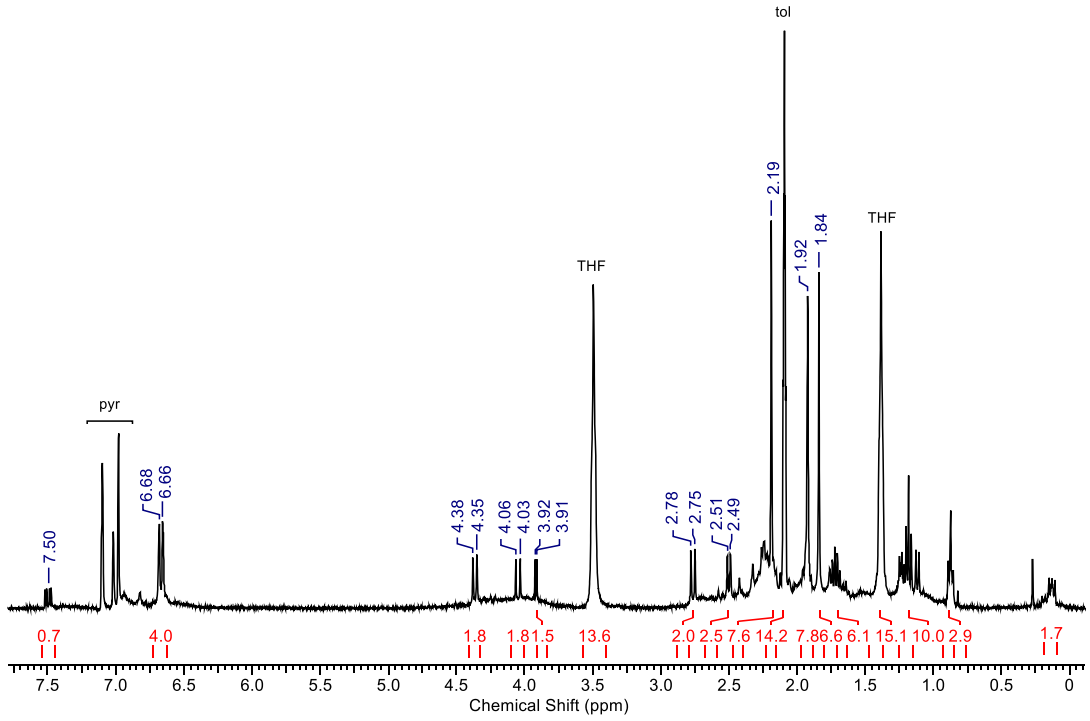

Figure 2.14 ^{1}H NMR (400 MHz, toluene-d^{8}) of Li$_3$(**1**)Mg(^{n}Bu)(THF)$_2$(OCH=CH$_2$)$_2$.

DOSY analysis suggested that one complex was present (Figure 2.15), with a diffusion coefficient, D = 5.2 x 10^{-10} m^{2}s^{-1} , which corresponds to a hydrodynamic radius, r_H = 9.35 Å. The molecular weight is estimated from the diffusion coefficient to be M_n = 1278.2 gmol^{-1}, almost twice the actual value of 687.04 gmol^{-1}. It is possible that dimerization of the structure occurs in solution. However, as stated previously, the prediction is not accurate

for molecular weights lower than *ca.* 1 kDa, although actual values for Li_4(**1**)$_4$(THF)$_2$ and Li_4(**3**)$_4$(THF) were in reasonable agreement with values predicted by DOSY. This is possibly indicative of aggregation of Li_3(**1**)Mg(^{n}Bu)(THF)$_2$(OCH=CH$_2$)$_2$ in solution.

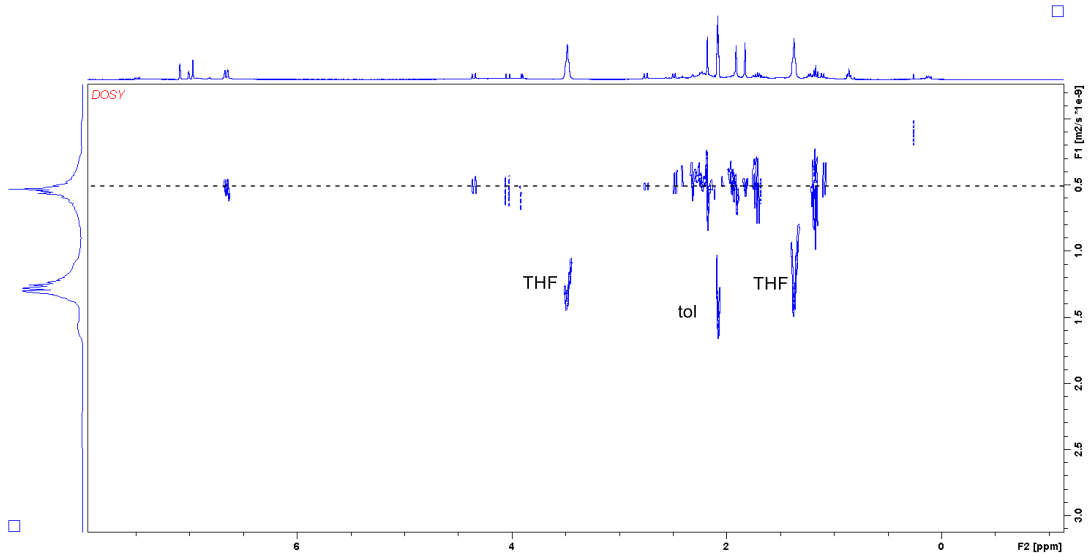

Figure 2.15. ^{1}H DOSY NMR of Li_3(**1**)Mg(^{n}Bu)(THF)$_2$(OCH=CH$_2$)$_2$ (400 MHz, d^8 toluene, 298 K)

2.5 Synthesis of dinuclear magnesium complexes

Magnesium complexes were prepared by simple deprotonation of the bis(phenolate) ligands with equimolar quantities of alkylmagnesium precursor ^{n}Bu$_2$Mg in toluene at room temperature with stirring (Scheme 2.4). After 2 hours the solvent was removed under pressure and the off-white residues were recrystallised from hexane/toluene to yield products as colourless crystals in good yields.

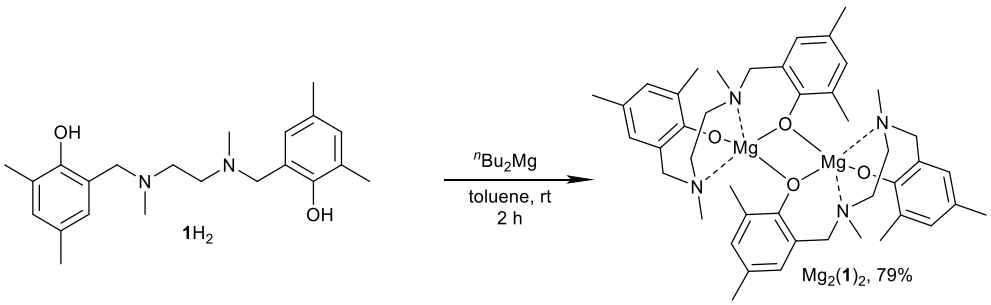

Scheme 2.4. Synthesis of dinuclear magnesium species, Mg$_2$(**1**)$_2$.

In all cases, dimeric species were observed, with the phenoxide moieties bridging between magnesium centres. This produced dimagnesiate complexes with 5-coordinate metal centres, analogous to complexes previously reported in the literature.[18,36,37] The solid-state structures for Mg$_2$(**1, 2, 4**)$_2$ are shown in Figure 2.16, while selected bond lengths and

angles are shown in Table 2.4. Mg_2(**5**)$_2$ was initially prepared by Rachel Drewitt (MChem student 2016-2017).

For complex Mg_2(**2**)$_2$, only enough material was isolated for analysis and it was not possible to prepare the complex on reasonable scale to allow for polymerisation studies. Possibly the rigidity of ligand hinders formation of the dinuclear species. Crystals for X-ray analysis were obtained but attempts to purify the crude residue through recrystallisation were unsuccessful. The ^{1}H NMR spectrum of the crude product showed some evidence of coordination but mostly free ligand. Attempts to complex the *meso*-bipyrrolidine ligand **3**H_2 to magnesium were also unsuccessful, despite evidence supporting complexation in the ^{1}H NMR spectrum. Attempts at recrystallisation yielded no purified material due to its high solubility in organic solvents. Magnesium complexes with enantiopure ligands crystallised readily from solutions and were isolated in reasonable yields (60 % for Mg_2(**4**)$_2$ and 28 % for Mg_2(**5**)$_2$), allowing for polymerisation studies to be performed. For ligand **3**H_2, the meso conformation forces the bipyrrolidine rings onto the same face, making it difficult to create a crystalline dimeric complex similar to that of Mg(**4**/**5**)$_2$. Finally, a ^{t}Bu substituted ligand, **6**H_2 was complexed to magnesium.

The geometry of 5-coordinate complexes may be determined by the degree of trigonality, τ_5, which can be calculated using the two largest bond angles (α and β) in the 5-coordinate complex, as reported by Addison *et al.*.[38] A perfectly trigonal bipyramidal coordination would have τ_5 = 1, while a square based pyramidal coordination would have τ_5 = 0. The equation to derive this angular structural parameter is given in Equation 2.2. In all cases, magnesium centres exist in distorted square based pyramidal geometry (τ_5 = 0.10-0.33) These values are also summarised in Table 2.4 for each complex. The chiral bipyrrolidine complexes have significantly lower τ_5 values, presumably due to steric constraints of the ligand. Data for a literature compound (Figure 2.17) have been included for comparison.

Equation 2.2. Degree of trigonality[38]

$$\tau_5 = \frac{\beta - \alpha}{60}$$

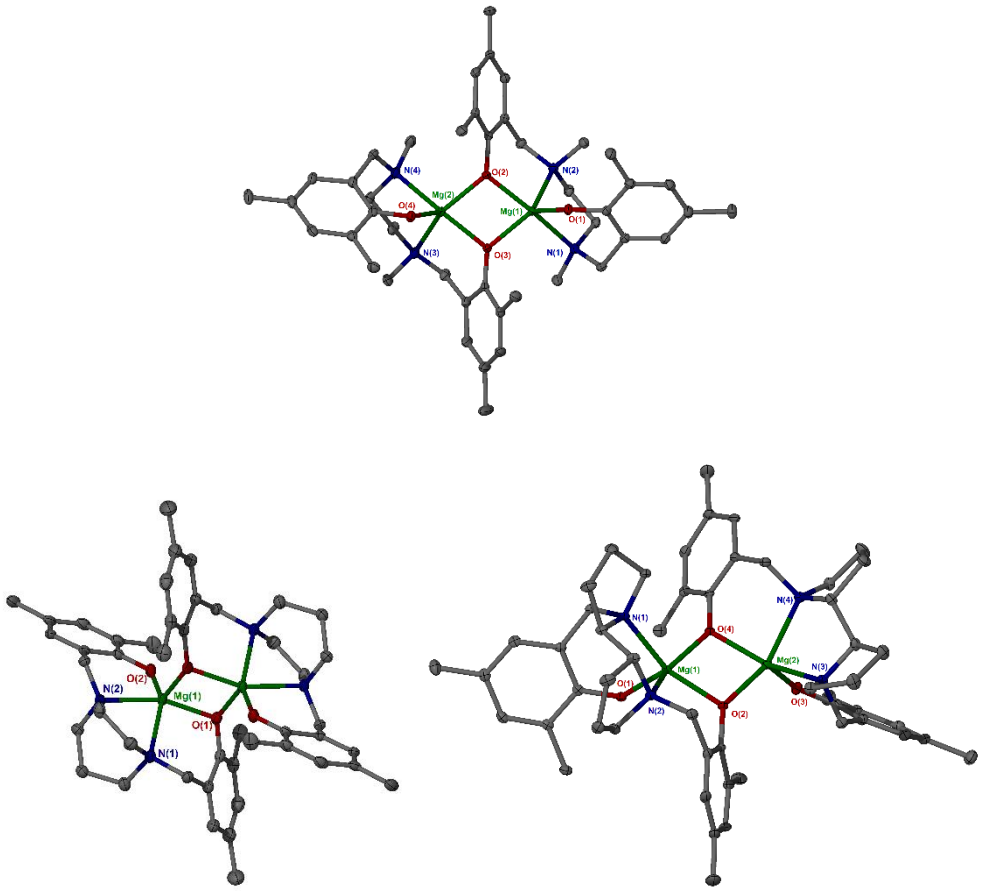

Figure 2.16. Solid state structures of Mg_2(**1**)$_2$, Mg_2(**2**)$_2$ and Mg_2(**4**)$_2$; ellipsoids are shown at the 30% probability level and all hydrogen atoms and solvent of recrystallisation are removed for clarity.

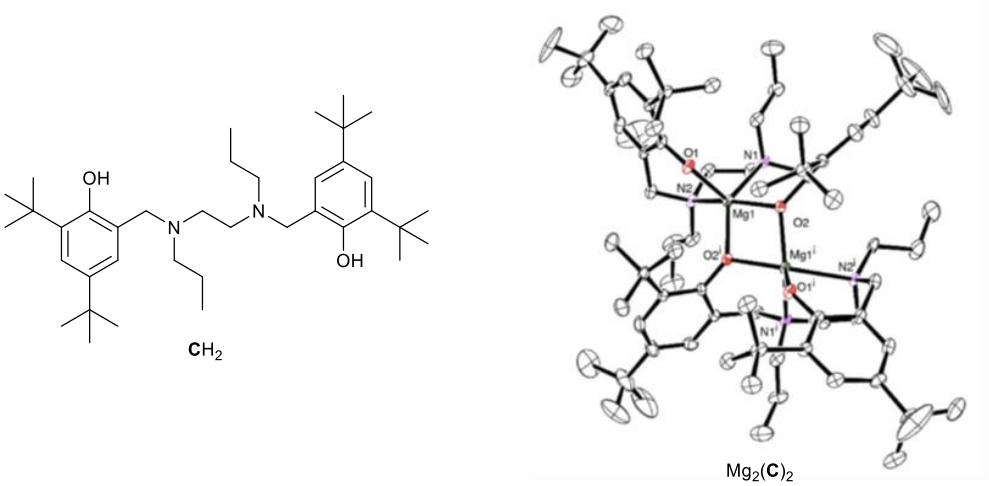

Figure 2.17. Ligand **C**H_2 and complex Mg_2(**C**)$_2$ reported by Ghosh and co-workers.[18] Reproduced with permission, Elseiver (2015).

Table 2.4. Selected bond angles (°) and lengths (Å) for magnesium complexes Mg_2(**1**,**2**,**4**-**6**)$_2$ and literature complex Mg_2(**C**)$_2$ for comparison.[18]

	Mg_2(**1**)$_2$	Mg_2(**2**)$_2$	Mg_2(**4**)$_2$	Mg_2(**5**)$_2$	Mg_2(**6**)$_2$	Mg_2(**C**)$_2$
Mg(1)-O(1)	1.9205(14)	1.9045(17)	1.911(3)	1.898(2)	1.9226(17)	1.905(3)
Mg(1)-O(3)	2.0121(14)	2.0036(19)	2.002(3)	2.019(2)	2.0173(16)	2.008(3)
Mg(1)-O(2)	2.0327(13)	2.0097(17)	2.009(3)	2.007(2)	2.0404(18)	2.053(3)
Mg(2)-O(2)	2.0018(15)	2.0036(19)	2.022(3)	2.005(2)	2.0263(15)	2.008(3)
Mg(2)-O(3)	2.0251(13)		2.007(3)	2.008(2)	2.0252(19)	
Mg(2)-O(4)	1.9032(15)		1.896(3)	1.905(2)	1.9138(18)	
Mg(1)-N(2)	2.2373(18)	2.169(2)	2.271(3)	2.269(3)	2.263(2)	2.358(4)
Mg(1)- N(1)	2.3178(16)	2.232(2)	2.203(3)	2.204(3)	2.298(2)	2.261(4)
Mg(2)- N(3)	2.2843(19)		2.201(3)	2.210(3)	2.274(2)	
Mg(2)- N(4)	2.2887(17)		2.272(3)	2.265(3)	2.321(2)	
O(1)-Mg(1)-O(3)	118.28(6)	113.95(8)	114.26(13)	115.98(10)	116.91(8)	116.21(14)
O(1)-Mg(1)-O(2)	112.76(6)	100.85(7)	118.16(12)	114.16(10)	117.00(8)	114.70(13)
O(3)-Mg(1)-O(2)	77.44(5)	85.04(8)	78.43(10)	78.23(8)	76.27(7)	
O(1)-Mg(1)-N(2)	106.21(7)	102.88(8)	103.84(12)	101.17(10)	106.18(7)	116.21(14)
O(3)-Mg(1)-N(2)	135.50(7)	142.47(9)	141.72(13)	142.85(10)	136.91(7)	137.68(14)
O(2)-Mg(1)-N(2)	86.68(6)	88.89(7)	87.15(12)	87.12(9)	84.25(7)	85.64(13)
O(1)-Mg(1)-N(1)	90.69(6)	89.64(7)	93.32(13)	94.46(10)	89.26(8)	89.03(14)
O(3)-Mg(1)-N(1)	99.26(6)	105.67(8)	95.66(12)	97.97(9)	101.66(7)	
O(2)-Mg(1)-N(1)	155.13(7)	160.62(8)	147.75(13)	149.96(10)	151.90(8)	154.05(14)
N(2)-Mg(1)-N(1)	78.53(6)	73.15(7)	78.05(12)	78.13(10)	78.53(8)	77.32(14)
Mg(1)-O(2)-Mg(2)	102.08(6)	94.96(8)	101.06(11)	101.58(9)	102.10(7)	
Mg(1)-O(3)-Mg(2)	101.98(6)		101.82(12)	101.02(9)	102.95(7)	
τ_5	0.33	0.30	0.10	0.11	0.25	0.27

The solution-state of the complex was determined by ^{1}H NMR spectroscopy to be in agreement with the solid-state structures, indicating that the dimer remains in solution. The ^{1}H NMR spectrum of Mg_2(**1**)$_2$ in $CDCl_3$ is shown in Figure 2.18. The dimeric nature of the complex is evidenced by the four aromatic proton resonances arising from the phenolate rings occupying inequivalent coordination sites around the magnesium centres. Additionally, all the methyl groups are chemically distinct, unlike in the ^{1}H NMR spectrum of the ligand, where one resonance is seen for each the *ortho*- and *para*- methyl substituents. The methylene protons, which are a singlet in the ligand spectrum, now exist

as four diastereotopic doublets. This is due to asymmetry arising from the bridging nature of the phenolates, where one phenolate from each ligand occupies the bridging position between Mg centres. The ^{1}H NMR spectrum differs from that reported by Ghosh for $Mg_2(\mathbf{C})_2$, where only two aromatic resonances are observed, and the methylene protons of the diamine backbone are observed as a singlet. The spectra reported by Ghosh in this study are almost identical to that of the uncoordinated ligands.[18]

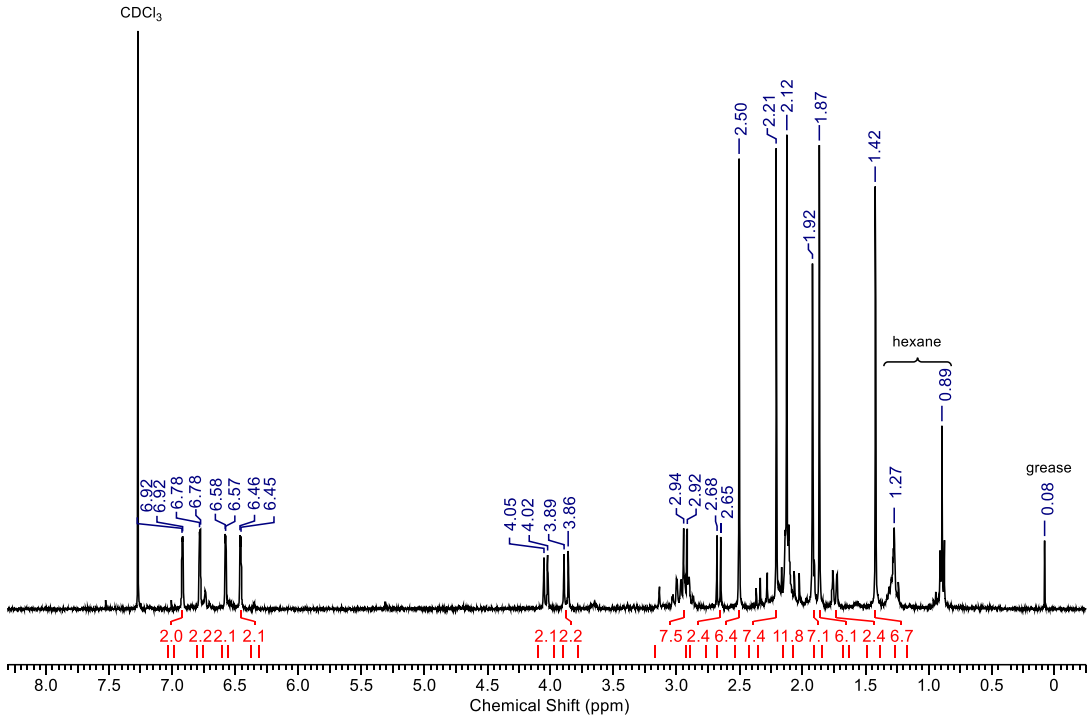

Figure 2.18. ^{1}H NMR spectrum of $Mg_2(\mathbf{1})_2$ (400 MHz, $CDCl_3$).

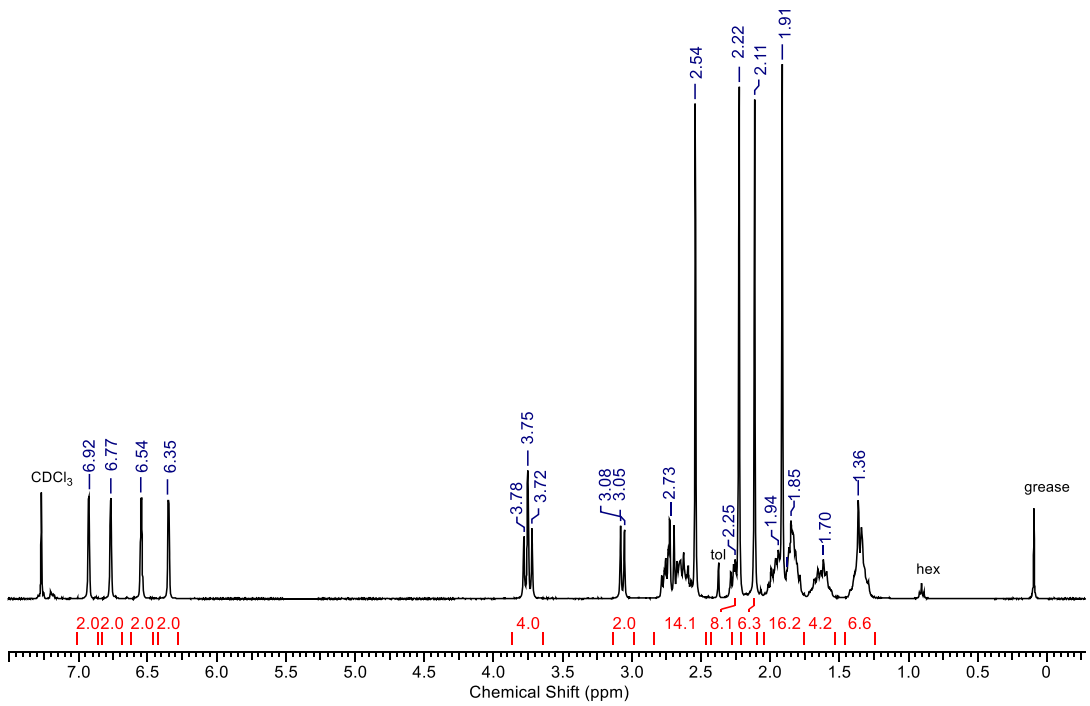

Figure 2.19. ^{1}H NMR spectrum of Mg_2(**3**)$_2$ (400 MHz, $CDCl_3$).

2.6 Synthesis of zinc complexes

Ligand **1**H_2 was treated with two equivalents of $ZnMe_2$ in toluene in an attempt to generate a monomeric Zn-Me complex. Instead, a trimetallic species, Zn_3(**1**)$_2$(Me)$_2$ was isolated in the solid state. The crystal structure is shown in Figure 2.20. In this structure, Zn(1) and Zn(3) are five-coordinate, while Zn(2) is four-coordinate. Both Zn(1) and Zn(3) are in highly distorted trigonal bipyramidal geometries with O(1)-Zn(1)-N(1) = 144.11(6)° and C(1)-Zn(1)-O(2) = 125.62(9)°, distorted away from the ideal 120°. Both terminal Zn centres are ligated by two nitrogen and oxygen centres from the amine bis(phenolate) ligand, with the coordination sphere being completed by a methyl group. Zn(2) is coordinated to four phenoxide oxygen moieties. The N-CH_2 groups are located in a cisoid fashion, and have an acute bite angle, N(1)-Zn(1)-N(2) = 79.92(7)°, as reported with other metal complexes of this ligand.[10] This complex was also prepared using 3:2 stoichiometric quantities of ligand and alkyl zinc reagent, with a slightly increased yield of 24%.

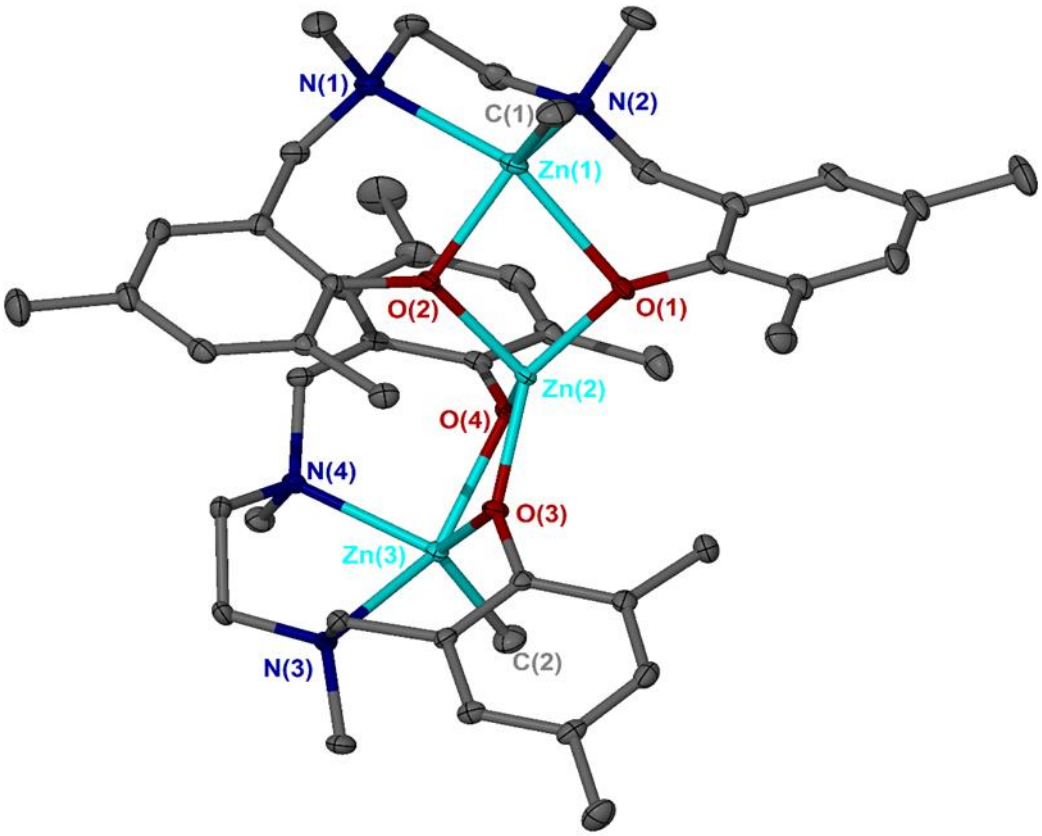

Figure 2.20. Solid-state structure of $Zn_3(\mathbf{1})_2(Me)_2$. Ellipsoids are shown at the 30% probability level and all hydrogen atoms and solvent of recrystallisation are removed for clarity. Selected bond lengths (Å) and angles (°): $Zn_3(\mathbf{1})_2(Me)_2$ Zn(1)-C(1) 1.980(2), Zn(1)-O(1) 2.2887(14), Zn(1)-O(2) 2.0228(13), Zn(1)-N(1) 2.3827(19), Zn(1)-N(2) 2.1804(17), Zn(2)-O(1) 1.9187(13), Zn(2)-O(2) 1.9757(13), Zn(2)-O(3) 1.9471(13), Zn(2)-O(4) 1.9561(14), Zn(3)-O(3) 2.0684(14), Zn(3)-O(4), Zn(3)-N(3) 2.3457(16), Zn(3)-N(4) 2.1799(17), Zn(3)-C(2) 1.979(2). C(1)-Zn(1)-O(2) 125.62(9), C(1)-Zn(1)-N(2) 119.76(9), O(1)-Zn(2)-O(3) 135.40(6), O(1)-Zn(2)-O(4) 126.70(6), O(3)-Zn(2)-O(4) 81.78(6), C(2)-Zn(3)-O(3) 122.28(9), C(2)-Zn(3)-N(4) 123.67(9), O(3)-Zn(3)-N(4) 113.94(6), O(2)-Zn(1)-N(2) 114.04(6).

The identity of the complex in solution is somewhat more complicated. A ^{1}H NMR spectrum was obtained in C_6D_6 (Figure 2.21), containing five different resonances for the Zn-Me moieties. There are also several doublets clearly observed for the methylene protons. Analysis by DOSY NMR spectroscopy in C_6D_6 (400 MHz, 298 K, Figure 2.22) indicates there are several species present, with diffusion constants of *ca*. 5.3 x 10^{-10}, 6.0 x 10^{-10} and 7.0 x 10^{-10} m^2s^{-1}. Using these values to predict molecular weights gives M_n = 1128.8 $gmol^{-1}$ for D = 5.3 x 10^{-10} m^2s^{-1}, M_n = 852.2 $gmol^{-1}$ for D = 6.0 x 10^{-10} m^2s^{-1} and M_n = 606.1 $gmol^{-1}$ for D =7.0 x 10^{-10} m^2 s^{-1}. The actual molecular weight of $Zn_3(\mathbf{1})_2(Me)_2$ is 935.1980 $gmol^{-1}$ which possibly corresponds to D = 6.0 x 10^{-10} m^2s^{-1}, while the other species presumably correspond to species existing in different levels of aggregation, such as dinuclear or tetranuclear species. Elemental analysis was in good agreement with predicted values for the structure determined by X-ray crystallography.

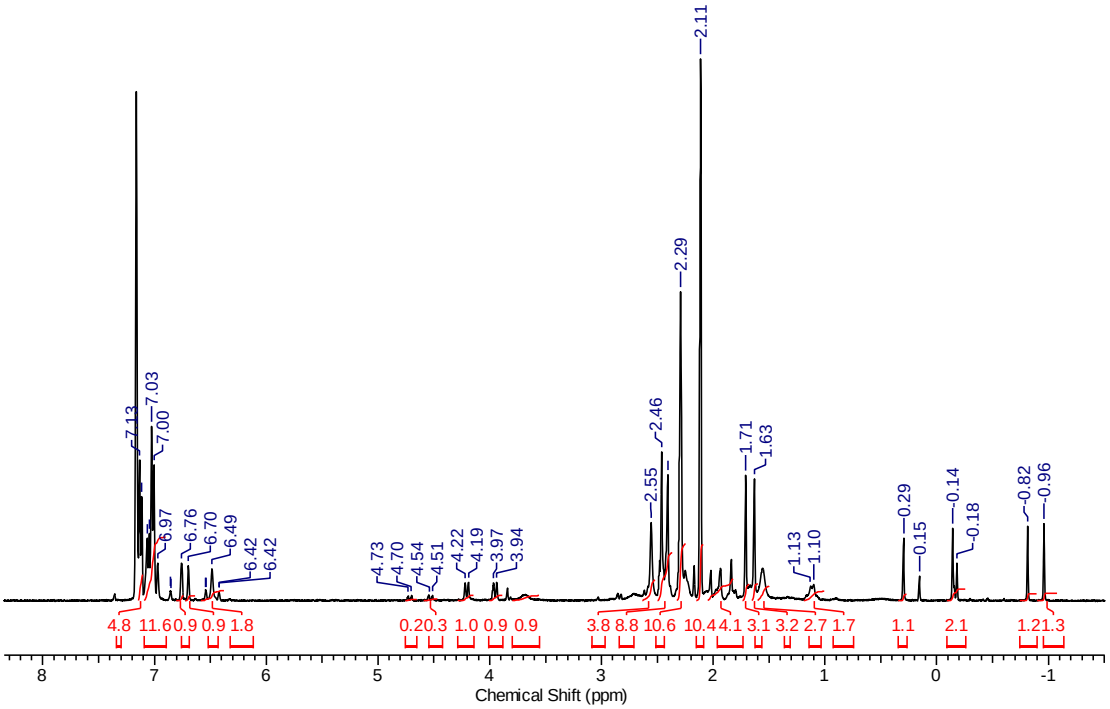

Figure 2.21. ^{1}H NMR (400 MHz, C_6D_6) spectrum of $Zn_3(\mathbf{1})_2(Me)_2$

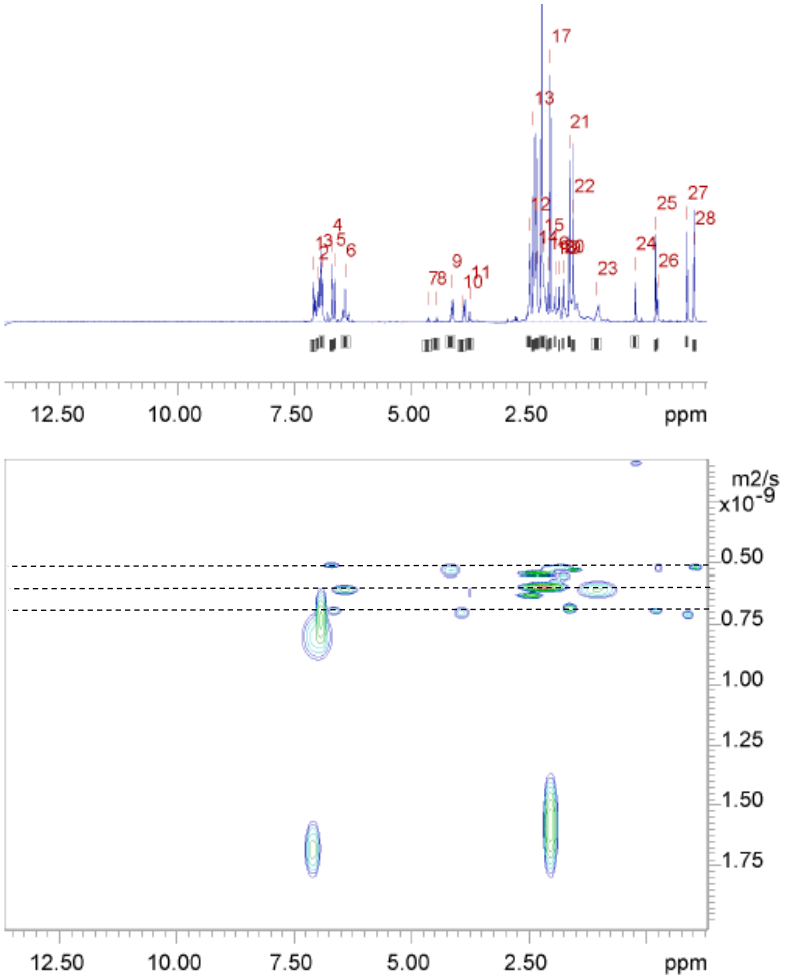

Figure 2.22. DOSY NMR (C_6D_6) spectrum of $Zn_3(\mathbf{1})_2(Me)_2$

Deprotonation of ligand **3**H_2 with two equivalents of dimethylzinc in toluene yielded a white precipitate, which was gently warmed until it dissolved back into solution. Upon cooling, a crop of crystals was obtained (17%), which were suitable for analysis by X-ray crystallography. The crystal structure of this complex is shown in Figure 2.23. The crystal structure corresponds to Zn_4(**3**)$_2$(Me)$_2$(OMe)$_2$, having two ligands and four zinc centres. Two zinc centres Zn(1) and Zn(4) are 5-coordinate and retain a methyl ligand, with τ_5 = 0.21 indicating a distorted square based bipyramidal geometry. The other two Zn centres are 4-coordinate, with bridging methoxy ligands, presumably arising from advantageous oxygen, present in the solvent or possibly residual from ligand synthesis, inserting into the Zn-C bond. This oxygen insertion has been previously reported in the literature.[39,40] Under rigorous Schlenk conditions, the same complex was isolated, in a *ca*. 33% yield. It is possible that this complex crystallises more readily from solution and preferentially precipitates from solution and attempts to isolate -OMe free complexes were unsuccessful. However, the presence of the methoxy ligands could be advantageous for the ROP of cyclic esters, which typically requires the addition of an alcohol co-initiator to prepare the metal alkoxide *in situ*, required for polymerisation *via* a coordination-insertion mechanism. All attempts to prepare complexes with the homochiral ligands were unsuccessful, as were attempts with the ^{t}Bu ligand, **6**H_2.

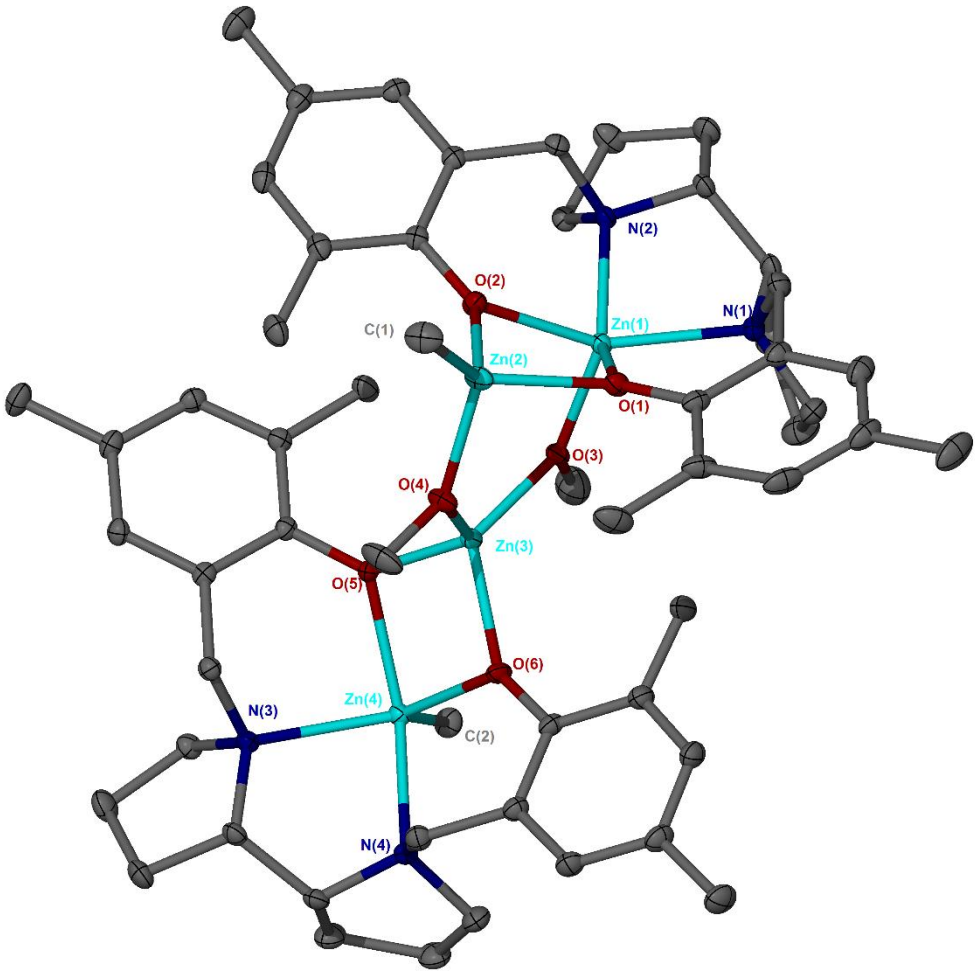

Figure 2.23. Solid-state structure of $Zn_4(\mathbf{2})_2(Me)_2(OMe)_2$. Ellipsoids are shown at the 30% probability level and all hydrogen atoms and solvent of recrystallisation are removed for clarity. Selected bond lengths (Å) and angles (°): Zn(1)-O(3) 1.9539(13), Zn(1)-O(1) 2.0328(13), Zn(1)-O(2) 2.0803(14), Zn(1)-N(2) 2.1424(16), Zn(1)-N(1) 2.2109(17), O(1)-Zn(2) 2.0698(15), Zn(3)-O(4) 1.9111(15), Zn(3)-O(3) 1.9508(13), Zn(3)-O(5) 1.9673(13), Zn(3)-O(6) 1.9803(14), N(3)-Zn(4) 2.2536(16), Zn(4)-O(5) 2.1657(13), Zn(4)-O(6) 2.1698(14), Zn(4)-N(4) 2.2553(16), O(3)-Zn(1)-O(1) 104.88(6), O(3)-Zn(1)-O(2) 97.54(6), O(1)-Zn(1)-O(2) 78.53(6), O(3)-Zn(1)-N(2) 117.10(6), O(1)-Zn(1)-N(2) 137.53(6), C(1)-Zn(2)-O(4) 119.95(9), C(1)-Zn(2)-O(2) 124.62(9), O(4)-Zn(2)-O(2) 97.06(6), C(1)-Zn(2)-O(1) 130.00(9), O(4)-Zn(2)-O(1) 95.62(6), O(4)-Zn(3)-O(3) 112.34(6), O(4)-Zn(3)-O(5) 118.58(6), O(3)-Zn(3)-O(5) 110.54(6), O(4)-Zn(3)-O(6) 112.64(6), C(2)-Zn(4)-O(5) 108.58(8), C(2)-Zn(4)-O(6) 115.85(8), O(5)-Zn(4)-O(6) 74.33(5), C(2)-Zn(4)-N(3) 118.60(8), O(5)-Zn(4)-N(3) 86.07(5).

The ^{1}H NMR spectrum of this complex is shown in Figure 2.24. Again, multiple resonances are observed for the Zn-Me protons, and several diasterotopic doublets are observed. DOSY analysis showed two species in solution with diffusion coefficients of *ca*. 4.9 and 5.3 x 10^{-10} m^2s^{-1}, corresponding to species with molecular weights, M_n = 1352.9 $gmol^{-1}$ and 1128.8 $gmol^{-1}$ respectively. The species identified by X-ray crystallography, $Zn_4(\mathbf{2})_2(Me)_2(OMe)$ has a molecular weight of 1166.7980 $gmol^{-1}$. Again, it is possible that different levels of aggregation are possible in solution which are not observed in the solid-state, or the solid-

state structure is not indicative of the bulk sample. However, the values obtained from elemental analysis of the solid were in good agreement with calculated values for Zn_4(**2**)$_2$(Me)$_2$(OMe).

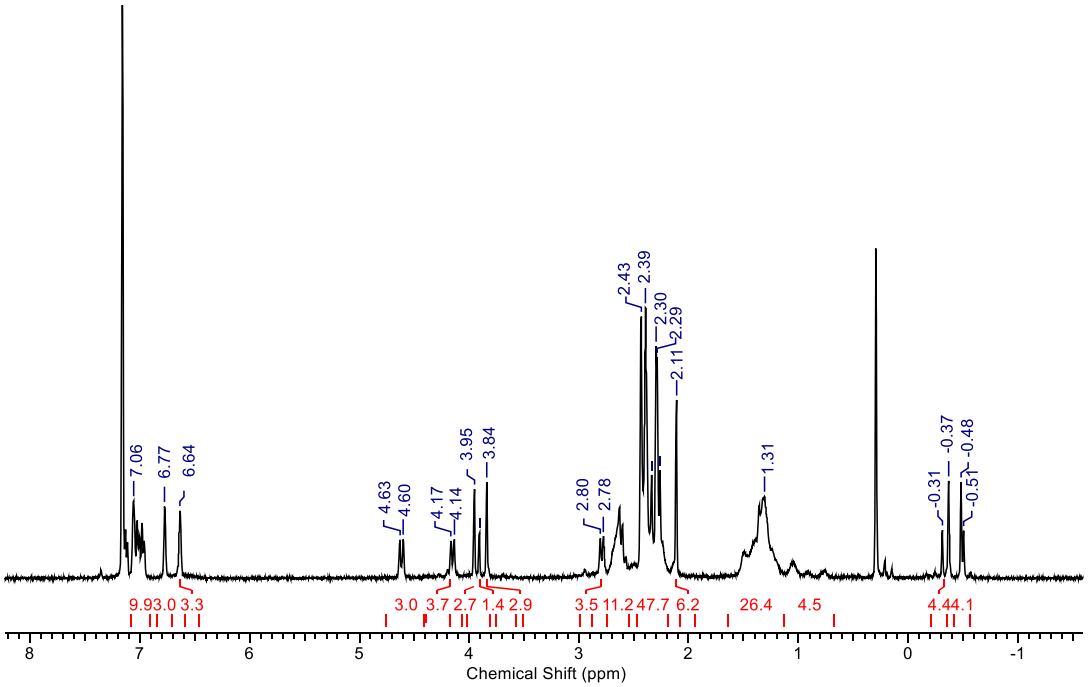

Figure 2.24. ^{1}H NMR (400 MHz, C_6D_6) spectrum of Zn_4(**3**)$_2$(Me)$_2$(OMe)$_2$

2.7 Polymerisation data

2.7.1 Oxo-bridged Zr complexes as initiators for *rac*-LA ROP

Both oxo-bridges complexes were trialled for ROP with *rac*-LA under solvent-free conditions (130 °C). Both complexes were active for the bulk polymerisation of *rac*-LA, showing high conversion in 2 hours (Table 2.5). Similar selectivity was observed to that of the literature compounds Zr(**1**)(O^{i}Pr)$_2$ and Zr(**2**)(O^{i}Pr)$_2$.[4,22] The ethylenediamine backboned complex {(Zr(**1**)(O^{i}Pr)$_2$)$_2$μ-O} induces some isotactic character in the polymer product (P_r = 0.32), which is similar the monomeric species (P_r = 0.30).[22] However, the polymerisation is poorly controlled, having a much lower molecular weight than predicted, and broad dispersity common in melt polymerisation ($Đ$ = 1.65). The homopiperazine complex {(Zr(**2**)(O^{i}Pr)$_2$)$_2$μ-O} produces PLA of mostly atactic character (having a P_r value of 0.44), compared to 0.38 for Zr(**2**)(O^{i}Pr)$_2$,[1] while the molecular weight is in close agreement with the predicted value.

Table 2.5. Polymerisation data for *rac*-LA with dimeric zirconium complexes

	Initiator	[LA]/[Zr]	Time / h	Conv. / %[a]	M_n calc.	M_n[b]	M_n corr.[c]	$Đ$[b]	P_r[d]
1	{(Zr(**1**)(O^{i}Pr)$_2$)$_2$μ-O}	300*	2	86	37200	12700	7400	1.65	0.32
2	{(Zr(**2**)(O^{i}Pr)$_2$)$_2$μ-O}	300*	2	87	37650	58900	34200	1.30	0.44

[a] Conversion calculated from ^{1}H NMR spectra. [b] Molecular weight and dispersity determined by GPC (THF) analysis. [c]Correction factor of 0.58 applied. [d] P_r calculated from HND ^{1}H NMR spectra. Theoretical molecular weight calculated from conversion {100 × (Conv. × 144.13) + 108.14} (rounded to the nearest 50). *Equivalents calculated per Zr(IV) centre.

Further polymerisation studies were not possible due to difficulty in reproducing the complex, thus other systems were investigated.

2.7.2 Polymerisation of *rac*-LA with Li(I) complexes

The polymerisation of *rac*-LA with the lithium complexes Li$_4$(**1**)$_2$(THF)$_2$, Li$_4$(**3**)$_2$(THF) and Li$_4$(**7**)$_2$(THF)$_4$ was carried out in toluene at room temperature with benzyl alcohol added as a co-initiator at a [LA]:[I]:[BnOH] ratio of 100:1:1 (Table 2.6). Addition of BnOH is commonly described in the scientific literature with Li(I) complexes.[41–43] Li$_4$(**1**)$_2$(THF)$_2$ and Li$_4$(**3**)$_2$(THF) were found to readily facilitate ROP of *rac*-LA, with good conversion observed in 2 hours at room temperature. Generally, polymerisations were stopped when the solutions became clear, and no visibly undissolved lactide remained. Data for literature compound Li$_4$(**C**)$_2$(THF)$_4$ is included for comparison (Figure 2.26).[31] Li$_4$(**1**)$_2$(THF)$_2$ and Li$_4$(**3**)$_2$(THF) were both also trialled for ROP of ε-CL, but no conversion was achieved under these conditions.

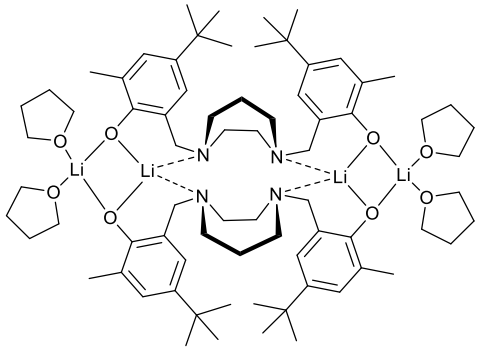

Figure 2.25. Literature complex Li$_4$(**C**)$_2$(THF)$_4$[31]

Table 2.6. Solution polymerisation data for *rac*-LA with Li(I) complexes $Li_4(\mathbf{1})_2(THF)_2$, $Li_4(\mathbf{3})_2(THF)$, $Li_4(\mathbf{7})_2(THF)_4$ and literature complex, $Li_4(\mathbf{C})_2(THF)_4$[31]

Entry	Initiator	[LA]:[I]	BnOH eq.	Time / h	Temp. / °C	Con. [a] / % LA	M_n calc	M_n [b]	Đ [b]	P_r [c]
1	$Li_4(\mathbf{1})_2(THF)$	50	1	2	RT	99	4240	4300	1.20	0.45
2	$Li_4(\mathbf{1})_2(THF)_2$	100	1	2	RT	99	14400	11200	1.10	0.55
3	$Li_4(\mathbf{1})_2(THF)$	100	0	2	RT	3	540	-	-	-
4	$Li_4(\mathbf{1})_2(THF)_2$	100	1	0.25	RT	26	3700	1600	1.01	0.56
5	$Li_4(\mathbf{1})_2(THF)_2$	100	1	0.5	RT	62	9050	11300	1.10	0.52
6[d]	$Li_4(\mathbf{1})_2(THF)_2$	100	1	2	RT	7	1100	8700	1.57	0.53
7[d]	$Li_4(\mathbf{1})_2(THF)_2$	100	1	24	RT	97	14100	2100	1.41	0.58
8	$Li_4(\mathbf{1})_2(THF)_2$	300	1	2	RT	50	21700	10500	1.12	0.56
9	$Li_4(\mathbf{1})_2(THF)_2$	400	1	2	RT	70	40400	24500	1.21	0.55
10	$Li_4(\mathbf{1})_2(THF)_2$	600	1	2	RT	27	23400	26800	1.02	0.55
11	$Li_4(\mathbf{1})_2(THF)_2$	600	6	2	RT	92	13300	9900	1.60	0.51
12	$Li_4(\mathbf{3})_2(THF)$	100	1	2	RT	98	14250	-	-	-
13[e]	$Li_4(\mathbf{3})_2(THF)$	100	1	2	RT	98	14250	-	-	-
14[f]	$Li_4(\mathbf{3})_2(THF)$	100	1	2	RT	87	12650	16200	1.12	0.49
15[f]	$Li_4(\mathbf{3})_2(THF)$	600	1	2	RT	98	84850	30700	1.48	0.44
16	$Li_4(\mathbf{7})_2(THF)_4$	100	1	2	RT	98	14250	8300	2.02	0.45
17[g]	$Li_4(\mathbf{C})_2(THF)_4$	250	1	2	RT	93	33600	n/a[$]	n/a[$]	0.44–0.47

Polymerisation in toluene unless otherwise stated. [a] Conversion calculated from ^{1}H NMR spectra. [b] Molecular weight and dispersity determined by GPC (THF) analysis. [c] P_r calculated from HND ^{1}H NMR spectra. [d] Polymerisations trialled in THF. [e] quenched in air and washed with MeOH, [f] no MeOH used. [g] CH_2Cl_2. Theoretical molecular weight calculated from conversion {100 × (Conv. × 144.13) + 108.14} (rounded to the nearest 50). [$] Not reported, reported as oligomers.

For $Li_4(\mathbf{1})(THF)_2$, the addition of 1 equivalent of BnOH allowed for well controlled polymerisation in toluene, with narrow molecular weight distributions observed in all cases ($Đ$ = 1.02-1.21). A very slight heterotactic bias was observed in most cases, P_r values < 0.58. A representative HND spectrum is shown in Figure 2.26. Polymerisation does not proceed without addition of BnOH (Table 2.6, entry 3). To examine the controlled nature of the polymerisation with $Li_4(\mathbf{1})(THF)_2$, polymerisations were run for regular time intervals over 2 hours. The linear relationship between conversion and molecular weight of PLA products is shown in Figure 2.27. The gradient of the line is ≈ 144 $gmol^{-1}$, which indicates that one PLA chain grows per metal centre. The dispersity remained constant while conversion increased, indicating a well-controlled process.

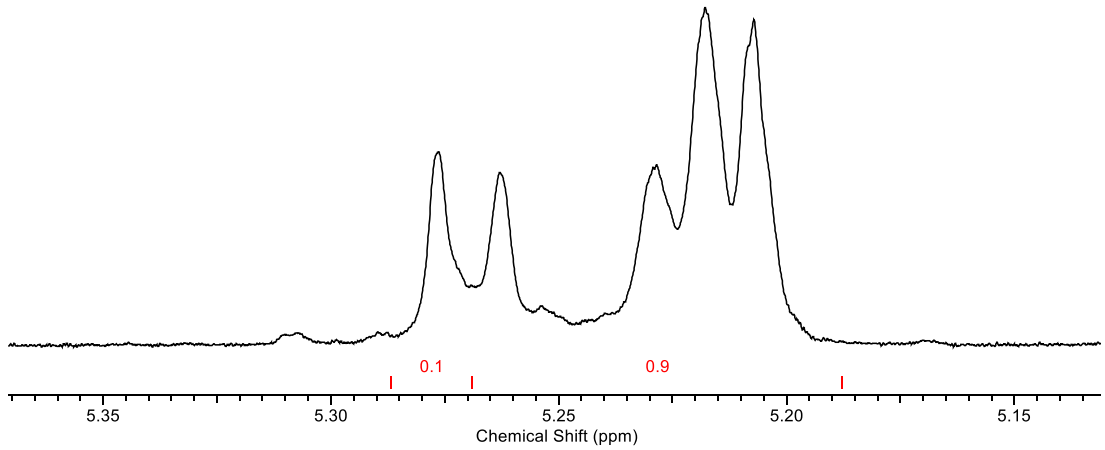

Figure 2.26. HND spectrum of the methine region of PLA produced from Table 2.6, entry 1

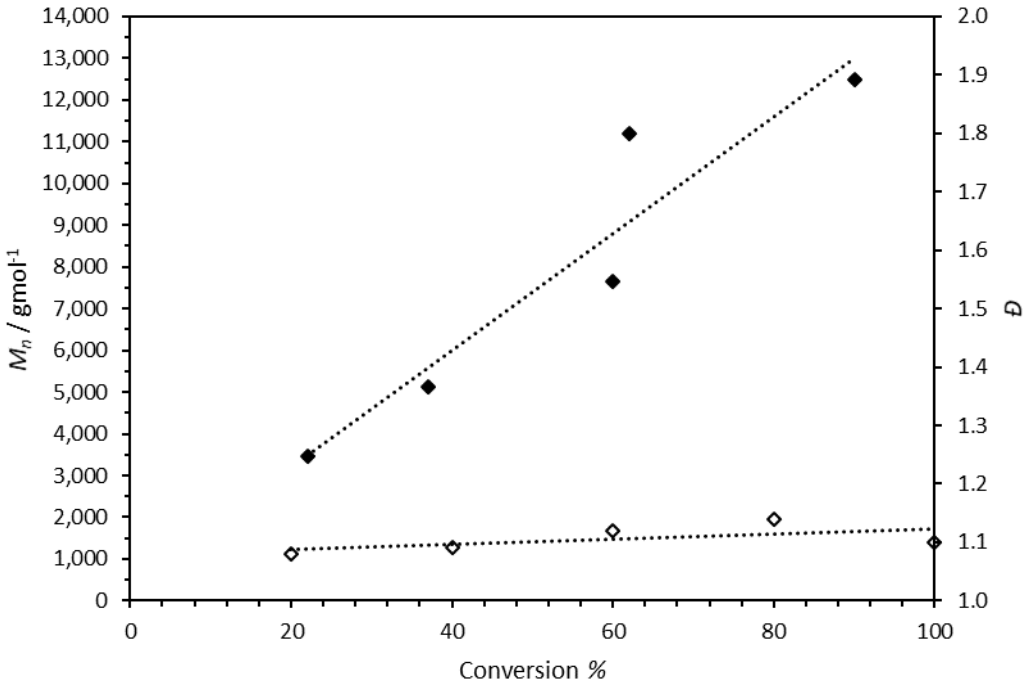

Figure 2.27. Graph showing the relationship between conversion and M_n (◆, left axis) and $Đ$ (◇, right axis) for ROP of *rac*-LA with Li_4(**1**)$(THF)_2$ determined by GPC (RI) relative to polystyrene standards with THF eluent. Polymerisations run in toluene at 25 °C for desired time periods with [LA]:[I]:[BnOH] = 100:1:1

Polymerisation in THF was trialled for Li_4(**1**)$(THF)_2$, to determine the effect of using a coordinating solvent. In these experiments, only oligomeric PLA was isolated (Table 2.6, entries 2 and 3). The polymerisation was much slower than in toluene, with only 7% conversion observed after 2 hours at RT (compared to near-quantitative conversion for the same initiator in toluene). This is possibly due to the coordinating nature of the THF solvent competing with lactide monomers for binding at lithium centres, giving a slower rate of polymerisation. At longer reaction times (entry 7), higher conversion was observed but the molecular weight of polymer produced was significantly lower than the predicted value.

Broad dispersities (*Đ* = 1.41, 1.57) could be indicative of undesirable side reactions such as transesterification.

Polymerisations with varying monomer-to-initiator ratios were run to investigate the living character of the polymerisation (Table 2.6, entries 8-10). The molecular weights of polymer products did not appear to increase relative to the [LA]:[I]:[BnOH] loading, with the M_n also being roughly half of the predicted molecular weight (Table 2.6, entries 8 and 9). At higher loadings ([LA]:[I]:[BnOH] = 600, entry 10), only 27% conversion was observed. This system appears to be very well controlled at lower monomer-to-initiator ratios but broadening of polymer dispersity and low molecular weights were observed with increasing concentration of lactide.

With $Li_4(\mathbf{3})_2(THF)$, no polymer was isolated when polymerisation was quenched, or polymer was washed with MeOH (Table 2.6, entry 12). High conversion of *rac*-LA was achieved when polymerisation was quenched by exposure to water in air (entry 13), as analysed by ^{1}H NMR spectroscopy upon removal of toluene solvent. However, washing with methanol to remove residual LA monomer, as often reported in scientific literature, again led to no polymeric product, and methyl lactate was observed in the ^{1}H NMR spectrum. Presumably the addition of methanol led to chain scission and degradation of the polymer. This has previously been observed in the group with Zr(IV) salalen complexes and Zn(II) piperidine complexes, with the degradation reported as a potential route for catalytic recycling of PLA.[6,44] Without any MeOH added, atactic PLA was produced within 2 hours (entry 14), in high yield (87%) with molecular weight in good agreement with the predicted value and narrow dispersity (*Đ* = 1.12). In this system near complete conversion was achieved in 2 hours at higher monomer loadings [LA]:[I]:[BnOH] = 600, although the polymer produced was of lower molecular weight than predicted. $Li_4(\mathbf{3})_2(THF)$ may be a good depolymerisation catalyst for PLA and could be investigated as such in the future.

A sample of PLA sample where polymerisation was quenched with 1 drop of MeOH was analysed by MALDI-ToF (Figure 2.28). A high degree of transesterification can be determined from the spectrum, with regular spacing between peaks of 72 gmol^{-1}. End group analysis of -OMe/-H suggests that transesterification may have occurred on addition of the MeOH.

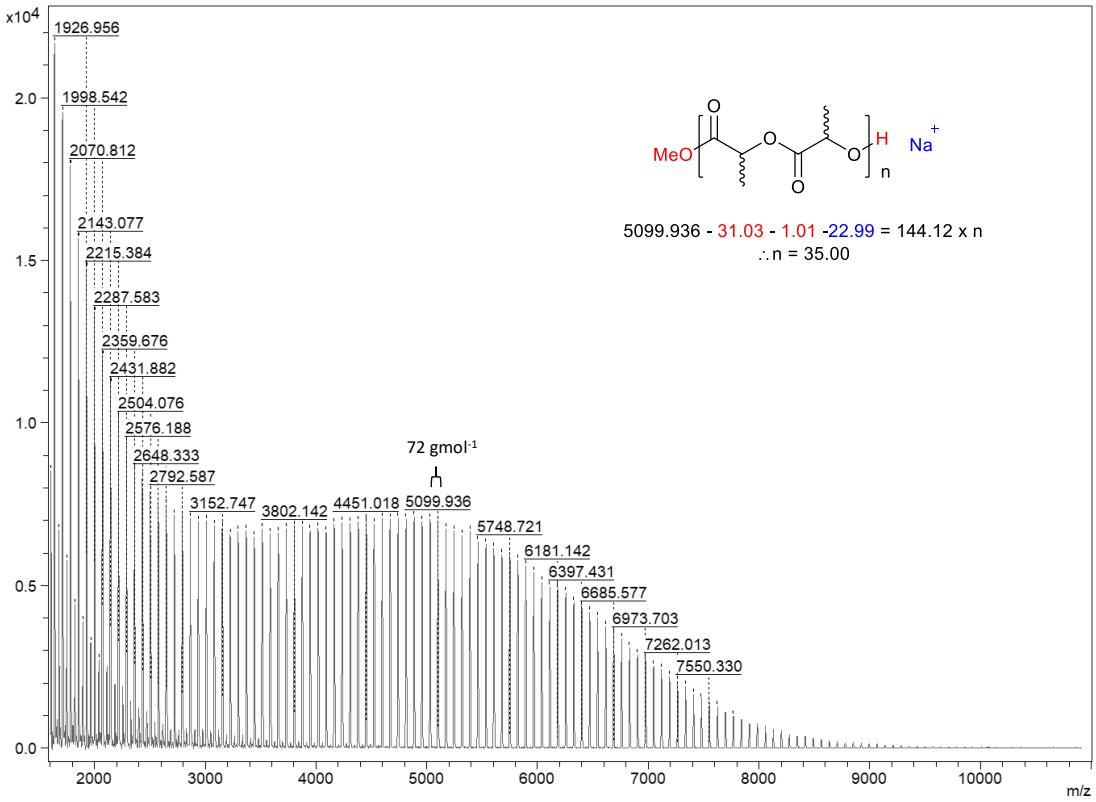

Figure 2.28.MALDI-ToF spectrum for polymer produced with Li_4(**3**)$_2$(THF).

The polymerisation was poorly controlled with Li_4(**7**)$_2$(THF)$_4$ (Table 2.6, entry 17), with the molecular weight being roughly half of the predicted molecular weight, and with a broad dispersity ($Đ$ = 2.02). A literature example with similar structure, Li_4(**C**)$_2$(THF)$_4$ (Figure 2.25) only achieved oligomeric PLA in solution (CH_2Cl_2, RT, [LA]:[I]:[BnOH] = 250:1:1).[31] This system was not further pursued, as it showed little promise compared to the structures comprising a Li_4O_4 motif.

2.7.3 Polymerisation of *rac*-LA with Mg(II) complexes

The ROP of *rac*-LA catalysed by magnesium complexes was initially performed in the absence and the presence of BnOH as a co-initiator at 130 °C under solvent free conditions, similar to conditions reported by Ghosh for similar initiators.[18] All three initiators were active for ROP in the bulk (Table 2.7), with polymerisations quenched when the molten lactide solidified and stirring was no longer possible.

Table 2.7. Polymerisation data with Mg complexes

Entry	Initiator	[LA]:[I]	Temp. / °C	BnOH eq.	Time / h	Con. [a] / % LA	$M_{n\ calc}$	M_n [b]	$Đ$ [b]	P_r [c]
1	Mg_2(**1**)$_2$	300	130	0	0.25	63	27200	20290	1.64	0.51
2	Mg_2(**1**)$_2$	300	130	1	0.33	82	35400	11170	1.78	0.52
3	Mg_2(**1**)$_2$	100	RT	0	24	-	-	-	-	-
4	Mg_2(**1**)$_2$	100	RT	1	24	43	6200	13550	1.08	0.54
5	Mg_2(**1**)$_2$	50	RT	1	24	61	4503	7400	1.04	0.55
7	Mg_2(**1**)$_2$	100	80	1	24	99	14400	3000	2.66	0.50
8	Mg_2(**1**)$_2$	100	80	2	24	99	7250	2300	2.31	0.51
9[d]	Mg_2(**1**)$_2$	100	RT	1	24	-	-	-	-	-
10	Mg_2(**4**)$_2$	300	130	0	0.25	65	28100	19400	1.80	0.52
11	Mg_2(**4**)$_2$	300	130	1	0.5	78	33200	11240	1.78	0.52
12	Mg_2(**4**)$_2$	100	RT	0	24	-	-	-	-	-
13	Mg_2(**4**)$_2$	100	RT	1	24	45	6600	12850	1.06	0.56
14	Mg_2(**4**)$_2$	100	80	1	24	99	7250	2550	2.31	0.51
15	Mg_2(**5**)$_2$	100	RT	1	2	-	-	-	-	-
16	Mg_2(**5**)$_2$	100	RT	1	24	18	2700	-	-	-
17	Mg_2(**5**)$_2$	100	RT	1	48	28	4150	8350	1.10	0.46
18	Mg_2(**5**)$_2$	300	130	0	0.3	63	12100	23280	1.55	0.54
19	Mg_2(**5**)$_2$	100	80	1	24	94	13600	3184	1.71	0.46
20	Mg_2(**5**)$_2$	100	50	1	24	60	6100	11100	1.36	0.45
21	Mg_2(**6**)$_2$	100	25	1	24	12	1850	-	-	-
22	Mg_2(**6**)$_2$	100	80	1	24	96	13900	8250	1.65	0.51

[a] Conversion calculated from ^{1}H NMR spectra. [b] Molecular weight and dispersity determined by GPC (THF) analysis. [c] P_r calculated from HND ^{1}H NMR spectra. Theoretical molecular weight calculated from conversion {100 × (Conv. × 144.13) + 108.14} (rounded to the nearest 50). Conversion factor of 0.58 has been applied. Monomer-to-initiator ratio calculated per Mg centre. [d] Polymerisation trialled in CH_2Cl_2.

The Mg(II) complexes were shown to be active for the polymerisation with atactic PLA being isolated, even when chiral ligands were employed. With Mg_2(**1**)$_2$, the addition of 1 equivalent of benzyl alcohol at room temperature it appears that the complex only initiates one growing PLA chain with the molecular weight almost twice that of the calculated M_n (Table 2.7, entries 4 & 5). The same was observed with Mg_2(**4**)$_2$ (entry 13) and Mg_2(**5**)$_2$ (entry 17). Magnesium complexes have been previously reported to undergo ROP *via* different mechanisms at different temperatures.[45] The polymerisation at room temperature is well-controlled, producing PLA with narrow disperity ($Đ \approx 1.10$), but slow,

with conversions < 50% in 24 h. With $Mg_2(\mathbf{5})_2$ only 18% conversion was achieved in 24 hours compared with the *R,R'*- enantiomer, $Mg_2(\mathbf{4})_2$, (45%). Increased reaction time to 48 h only increased the conversion to 28%, which could suggest a preference for one enantiomer of lactide over the other. By increasing the temperature to 50 °C (entry 20) it was possible to achieve 60% conversion in 24 h. Again, the molecular weight was almost twice that of the calculated M_n, suggesting a single polymer chain growing per complex. No polymerisation was observed in solution without the addition of BnOH (Table 2.7, entries 3 & 12), and polymerisation did not occur when CH_2Cl_2 was trialled as polymerisation solvent (entry 9). The ^{t}Bu complex, $Mg_2(\mathbf{6})_2$, achieved poor conversion in solution at room temperature, but atactic PLA with M_n = 8250, $Đ$ = 1.65 was achieved at 80 °C (entry 22). This directly contradicts previous reports of this complex being inactive for ROP by Davidson and co-workers.[46] This difference could be due to differences in the synthesis of the complex, where solvents of synthesis and purification may have been more stringently dried in this study, or possibly the purity of the lactide monomer,

In a study reported by Ghosh, oligomeric PLA samples were prepared and analysed by MALDI to gain insight into the polymerisation pathway.[18] In Ghosh's study they determined that one of the polymer end groups was the ligand and suggested that the ligand itself was the active initiating group in the system, despite the addition of BnOH. However, samples analysed by MALDI from this current study did not show the same result. A MALDI-ToF spectrum obtained for an oligomeric sample of PLA produced with $Mg_2(\mathbf{1})_2$ under bulk conditions ([LA]:[Mg]:[BnOH] = 50) is shown in Figure 2.29. This sample is cyclic, having no end groups as determined by MALDI. Cyclisation at high temperatures is relatively common, and this does not help elucidate the mechanism of polymerisation. Transesterification is also observed in this sample, with spacings between peaks of 72 $gmol^{-1}$. Cyclic polymer was also found to be the product in the MALDI-ToF of the polymer produced from Table 2.7, entry 7.

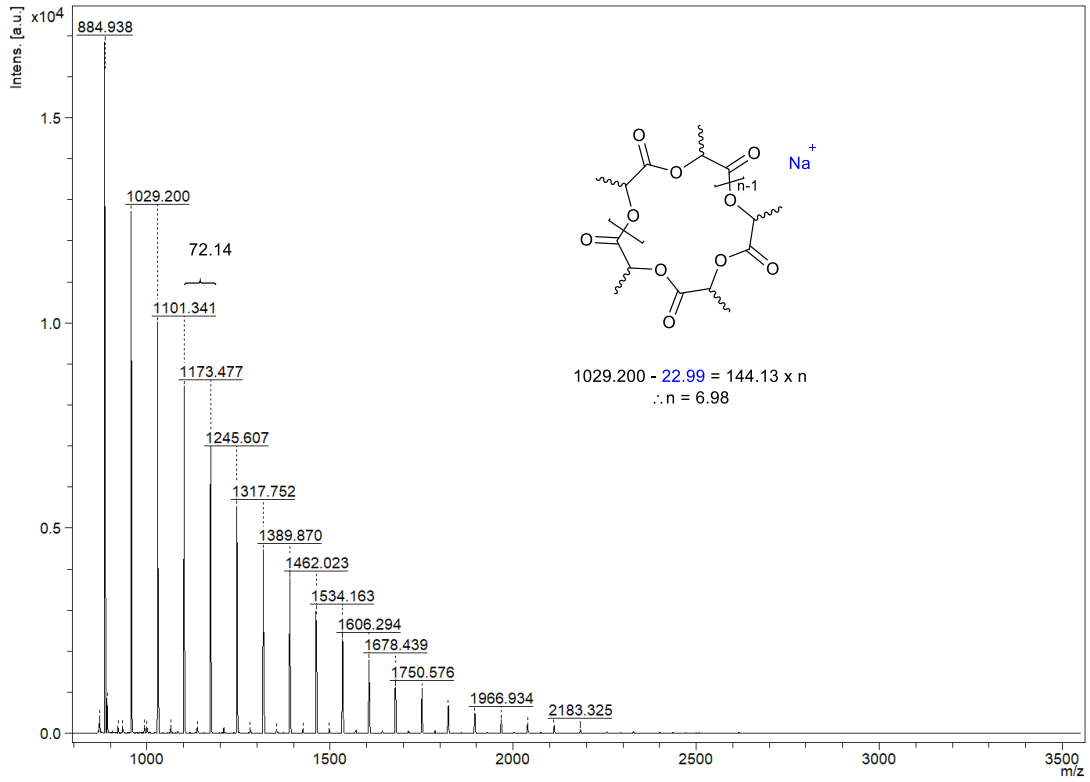

Figure 2.29. MALDI-ToF spectrum of cyclic PLA prepared with Mg_2(**1**)$_2$ ([LA]:[I]:[BnOH] = 50:1:1, T = 130 °C, solvent free, t = 5 minutes).

Dinuclear Mg(II) complexes have been recently reported for the copolymerisation of CO_2 and epoxides[18,47] and also for ROCOP of epoxides with anhydrides.[48] As the emphasis of this project is routes to sustainable polyesters, the magnesium complexes described in this chapter were investigated for ROCOP of propylene oxide (PO) or cyclohexene oxide (CHO) with succinic anhydride (SA) (Table 2.8). A large excess of epoxide (800 eq.) was used as polymerisation solvent, as reported for another dinuclear system.[48]

Table 2.8. Attempted polymerisation of propylene oxide (PO) or cyclohexene oxide (CHO) with succinic anhydride (SA) using magnesium complexes

Entry	Initiator	Epoxide (E)	[E]:[SA]:[I]	T / °C	Time / h	SA Conv. % [a]	M_n [b]	$Đ$ [b]
1	Mg_2(**1**)$_2$	PO	800:100:1	50	24	91	2500	1.25
2	Mg_2(**4**)$_2$	PO	800:100:1	50	24	-	-	-
3	Mg_2(**5**)$_2$	PO	800:100:1	50	24	27	350	1.33
4	Mg_2(**1**)$_2$	CHO	800:100:1	50	24	-	-	-
5	Mg_2(**4**)$_2$	CHO	800:100:1	50	24	-	-	-

[a] Determined from ^{1}H NMR spectra by integrating the resonances for SA (3.00 ppm) and the methylene signals in the polymer product (2.5-2.7 ppm). [b] Molecular weight and dispersity determined by GPC (THF) analysis.

With Mg_2(**1**)$_2$, 91% conversion of succinic anhydride was determined from comparing the integrations of the resonances for unreacted SA (3.00 ppm) and the methylene protons

arising from SA in the product in the NMR spectrum (Figure 2.30). PO is readily removed from the reaction mixture by applying a gentle vacuum. Good selectivity was achieved for polyester formation, determined by ^{1}H NMR spectroscopy of the polymer product, poly(propylene succinate). If ether formation had occurred (i.e. through epoxide homopolymerisation), resonances would be expected in the ether region of the spectrum (*ca.* 3.2-3.6 ppm),[48] which are not observed here. GPC analysis showed only low molecular weight oligomers with reasonably narrow dispersity (M_n = 2500 gmol^{-1}, $Đ$ = 1.25) (Table 2.8, entry 1). When the same polymerisation was attempted with bipyrrolidine complexes, Mg_2(**4**)$_2$ and Mg_2(**5**)$_2$, no conversion was observed with the *R,R'*- enantiomer and 27% conversion of SA with Mg_2(**5**)$_2$, although GPC showed the product in this case to have M_n = 350. With cyclohexene oxide (CHO), no conversion of SA was observed in the NMR spectrum of the product from attempts with either Mg_2(**1**)$_2$ or Mg_2(**4**)$_2$ (entries 4 & 5). Further investigations into ROCOP with initiators of this type should be performed in future experiments but were not pursued in this project. ROCOP as a method to product polyesters is reportedly capricious, with different activities observed with different epoxides leading to a tendency for publications to report ROCOP of a single epoxide.[15,16,49,50]

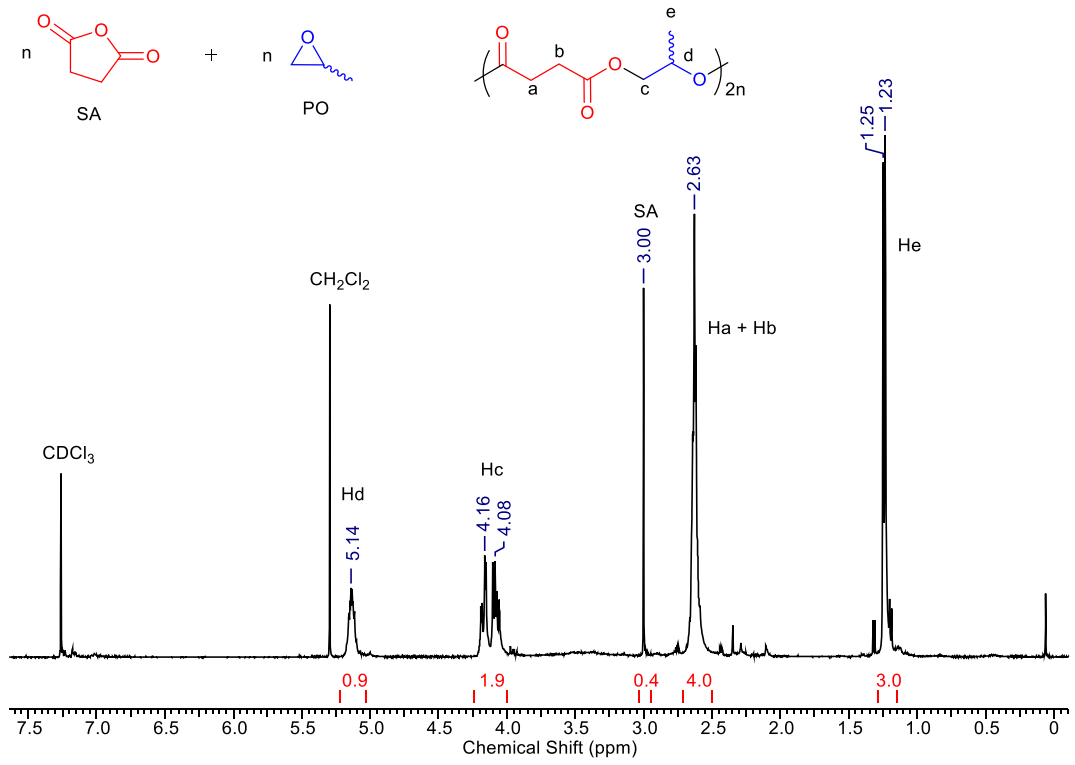

Figure 2.30. ^{1}H NMR spectrum (400 MHz, $CDCl_3$) of poly(propylene succinate) obtained from Table 2.8, entry 1.

2.7.4 Polymerisation of *rac*-LA with Zn(II) complexes

Both $Zn_3(\mathbf{1})_2(Me)_2$ and $Zn_4(\mathbf{3})_2(Me)_2(OMe)_2$ were trialled for the ROP of *rac*-LA (Table 2.9). $Zn_3(\mathbf{1})_2(Me)_2$ was found to be active with the addition of 1 equivalent of benzyl alcohol, with modest conversions being achieved after 24 h at room temperature with narrow molecular weight atactic PLA isolated. $Zn_4(\mathbf{3})_2(Me)_2(OMe)_2$ was attempted under the industrially relevant melt conditions (entry 2) and in solvent with and without the addition of exogenous alcohol as co-initiator due to the presence of methoxide ligands (entries 3-7). At 130 °C high conversion was achieved (98% in 2 h), although the molecular weight distribution was very broad ($Đ$ = 1.91). In toluene the polymerisation proceeded rapidly with high conversions achieved at room temperature in 2 hours, with polymerisations being stopped when the solutions became clear. There was little correlation between the calculated and observed molecular weight, with the observed molecular weight being far higher than expected. However, the dispersity of the polymer was very narrow. This is potentially because fewer polymer chains growing than expected, due to a much faster rate of propagation compared to initiation or aggregation, as observed in the DOSY spectra, could be reducing the number of active initiators. However, with the addition of benzyl alcohol (entry 3) a predictable molecular weight could be achieved.

Table 2.9. Polymerisation data for Zn complexes with *rac*-LA.

	Initiator	[LA]:[**I**]	BnOH eq.	Time / h	Temp / °C	Con. [a] / % LA	$M_{n\,calc}$	M_n [b]	$Đ$ [b]	P_r [c]
1	$Zn_3(\mathbf{1})_2(Me)_2$	100	1	2	RT	98	7050	7400	1.04	0.53
2[d]	$Zn_4(\mathbf{3})_2(Me)_2(OMe)_2$	300	0	2	130	98	42300	14900	1.91	0.51
3	$Zn_4(\mathbf{3})_2(Me)_2(OMe)_2$	100	1	2	RT	97	6950	7400	1.04	0.52
4	$Zn_4(\mathbf{3})_2(Me)_2(OMe)_2$	50	0	2	RT	89	6400	42600	1.05	0.53
5	$Zn_4(\mathbf{3})_2(Me)_2(OMe)_2$	100	0	2.5	RT	66	9500	84170	1.08	0.58
6	$Zn_4(\mathbf{3})_2(Me)_2(OMe)_2$	200	0	3	RT	67	19300	149200	1.06	0.57
7	$Zn_4(\mathbf{3})_2(Me)_2(OMe)_2$	800	0	4	RT	52	60000	239900	1.08	-

[a] Conversion calculated from ^{1}H NMR spectra. [b] Molecular weight and dispersity determined by GPC (THF) analysis. Conversion factor of 0.58 has been applied. [c] *Pr* calculated from HND ^{1}H NMR spectra. [d] Solvent-free.

Data obtained from MALDI-ToF analysis of polymer produced from Table 2.9, entry 3 was consistent with end groups of -OBn and -H, as expected from a coordination-insertion mechanism of polymerisation (Figure 2.31). Due to the poor molecular weight control without the addition of BnOH, no samples were attained that were suitable for analysis *via*

MALDI to ascertain the end groups and determine if the mechanism proceeds by classical co-ordination insertion, with LA inserting into the Zn-OMe bond, or an alternative mechanism such as activated monomer.

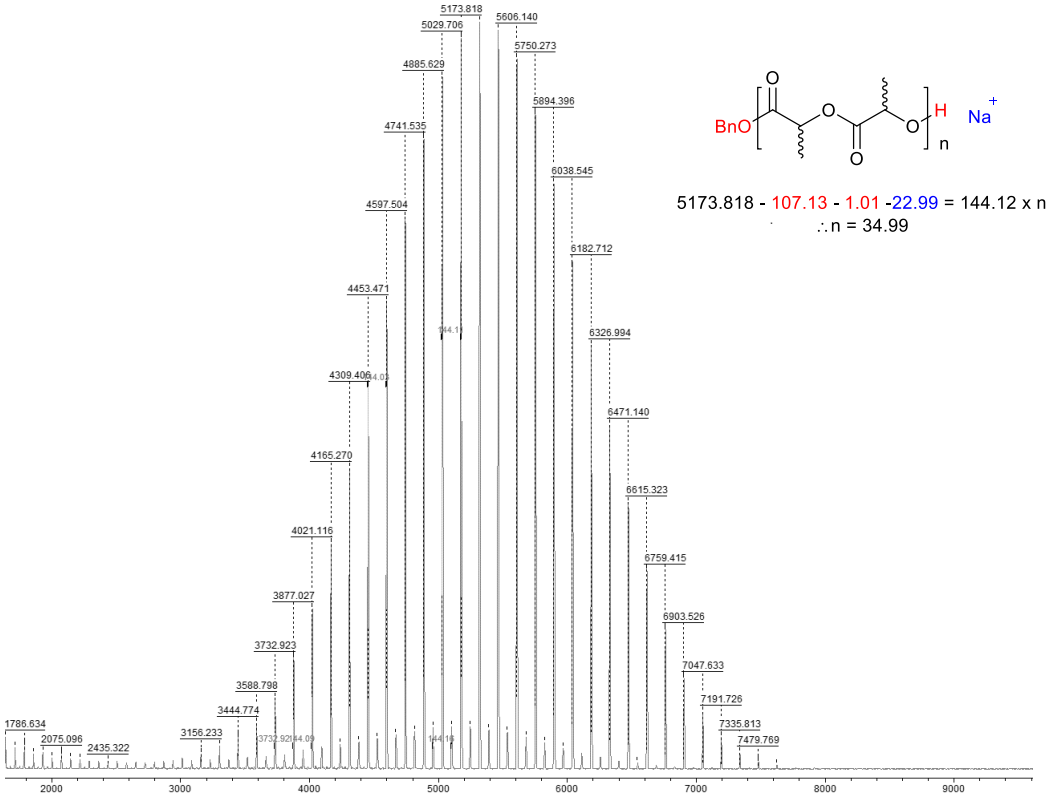

Figure 2.31. MALDI-TOF spectrum of polymer produced with $Zn_4(\mathbf{3})_2(Me)_2(OMe)_2$ from Table 2.9, entry 3. Conditions = [LA]:[I]:[BnOH] = 100:1:1,2 h, RT.

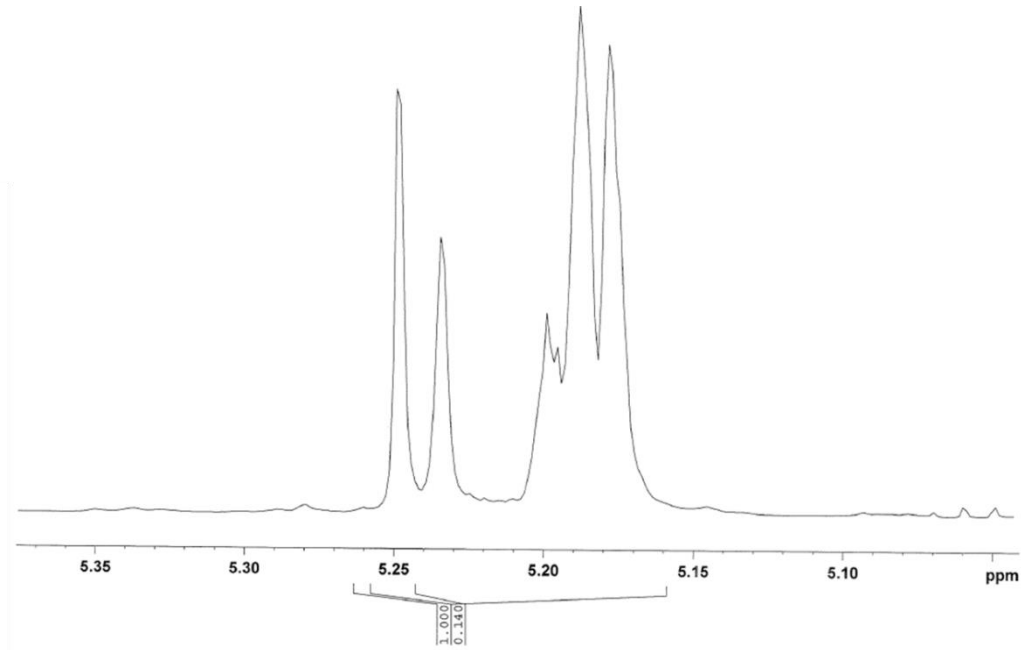

Figure 2.32. Representative ^{1}H HND NMR spectrum in the methine region for PLA produced with $Zn_3(\mathbf{1})_2(Me)_2$ from Table 2.9, entry 1. Conditions = [LA]:[I]:[BnOH] = 100:1:1, 2 h, RT.

Experiments with varying [M]:[I] loading were performed to investigate the "living" characteristics of the polymerisation. The molecular weight was seen to increase in a roughly linear fashion with monomer conversion. The solution polymerisation kinetics for $Zn(\mathbf{3})_2(Me)_2(OMe)_2$ at 100:1 in solution were investigated *via* NMR spectroscopy. The polymerisation found to be first order with respect to monomer and a pseudo first order rate constant was determined, k_{app} = 0.043 mins^{-1} (Figure 2.33), which is comparable with some of the fastest reported dinuclear zinc initiators in the literature (e.g. dinuclear species reported by Williams *et al*, k_{app} = 0.048 min^{-1} in CH_2Cl_2 at 25 °C).[51]

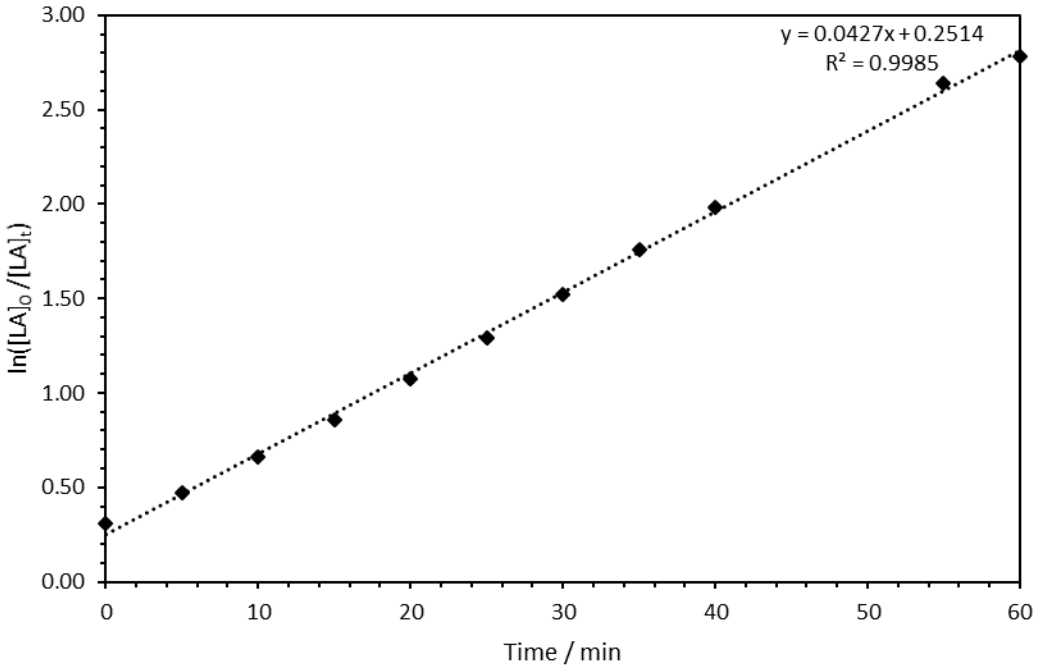

Figure 2.33. Semi-logarithmic plot for the solution polymerisation of *rac*-LA with Zn_4(**3**)$_2$$(Me)_2$$(OMe)_2$, (400 MHz, $CDCl_3$, 298 K, [LA]:[Zn-OMe] = 100:1).

2.8 Attempted synthesis of new bis(phenolate) ligands

A synthetic route to a rigid, chiral bi-isoindolene ligand was reported in 2009, *via* reaction between a chiral diamine: 1,2-bis(2-hydroxylphenyl)-1,2-diaminoethane, and methyl 2-formylbenzoate followed by a diaza-Cope rearrangement.[52] The chiral bi-isoindolene ligands were coordinated to Ni(II) in this study and applied as catalysts for the enantioselective Michael addition of malonates to conjugated nitroalkenes. The authors report two possible ligands from an imine intermediate *via* two synthetic routes: bi-isoindoline (A) or and hexahydrodibenzo[c,h]-[1,5]naphthyridine (B) (Figure 2.34).

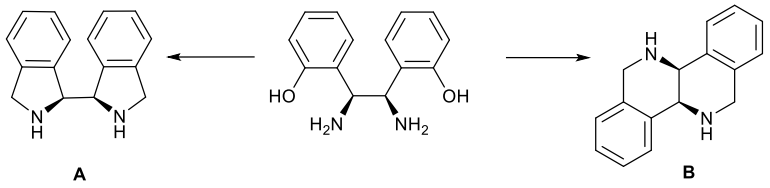

Figure 2.34. Ligands investigated by Zhu et al.[52]

Previously reported complexes bearing tetradentate bis(phenolate) ligands with a *meso*-2,2'- bipyrrolidine backbone have been shown to be excellent stereoselective initiators for ROP, which could be tuned depending on the metal deployed, yielding either isotactic, heterotactic or atactic PLA by simply changing the metal centre (Ti(IV), Zr(IV), Al(III) etc).[8–10] Preparation of tetradentate bis(phenolate) ligands based upon the bi-isoindolene ligand

reported by Zhu *et al.* followed to complexation to Zr(IV), for example may show enhanced isoselectivity compared to the 2,2'-bipyrrolidine analogue (P_m < 0.86). Changing the rigidity of the backbone may lead to a stronger preference for one enantiomer over another, and thus a more selective initiator. A modified Mannich condensation from the diamine with a disubstituted phenol and paraformaldehyde as utilised for ligand synthesis in this chapter should provide access to new tetradentate ligands (Figure 2.35).

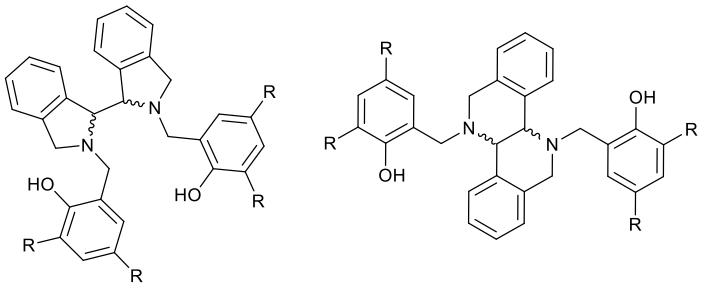

Figure 2.35. Structures of proposed bis(phenolate) ligands from rigidified diamines.

2.8.1 Diamine preparation

The *meso*-1,2-bis(2-hydroxylphenyl)-1,2-diaminoethane **11** was prepared in several steps (Scheme 2.5) from benzil and salicylaldehyde with aqueous ammonia, following a slightly modified literature method.[53] Interestingly, this method is also cited by Zhu *et. al*, but here the diamine is reported in the chiral form, whereas the original paper reports the preparation of a diamine with *meso* geometry.

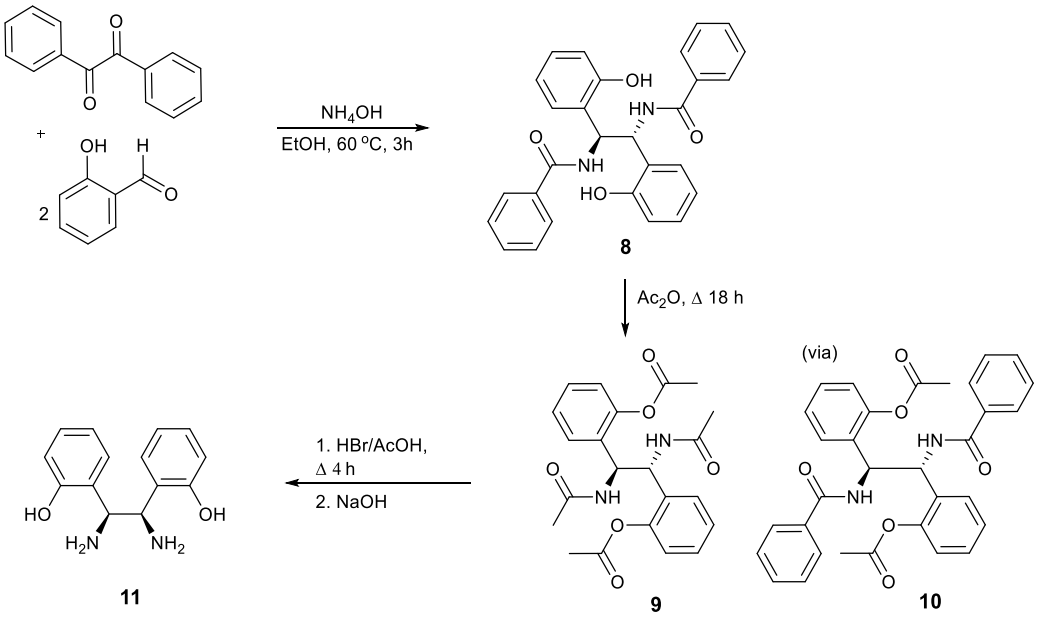

Scheme 2.5. Preparation of diamine **11** over three steps from benzil and salicylaldehyde.

Benzil, two equivalents of salicylaldehyde and large excess (10 eq.) of NH_4OH were heated to 60 °C in EtOH for 4 h, giving **8** in 76% yield as a bright yellow solid, which was easily isolated by filtration and washed with copious hot ethanol. The mechanism proceeds *via* a diaza[3,3]sigmatropic rearrangement (Diaza-Cope rearrangement, Figure 2.36).[53,54] Characterisation by ^{1}H and $^{13}C\{^{1}H\}$ NMR spectroscopy and mass spectrometry showed the product to require no further purification and it was used as is in the next step.

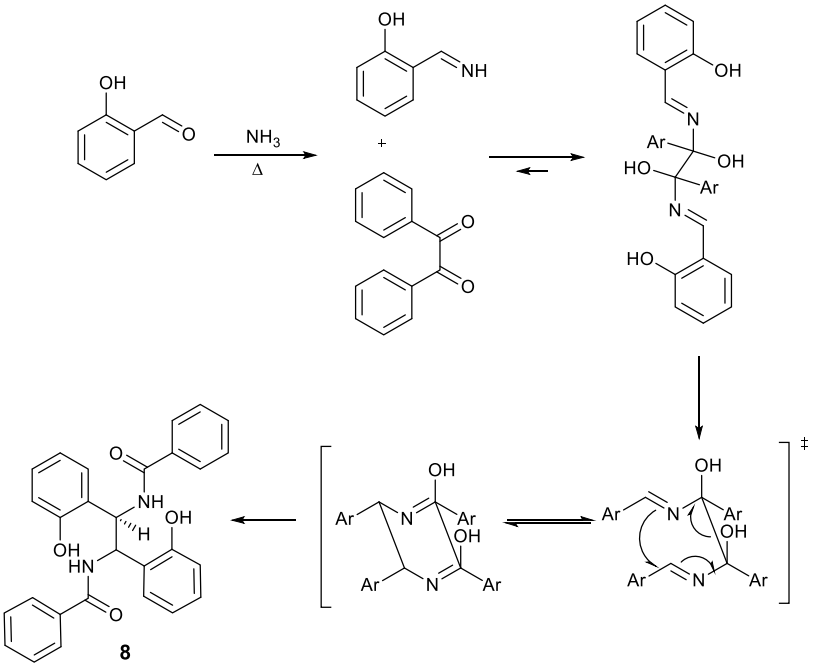

Figure 2.36. Diaza-Cope rearrangement to prepare compound **8**[54]

Refluxing **8** in acetic anhydride yielded the fully acetylated compound **9** in 67% yield. During the reaction, a white precipitate rapidly formed, which was characterised by ^{1}H NMR spectroscopy to be an intermediate species where only the phenol groups are acetylated and the benzamide groups remain intact. Crystals suitable for single crystal X-ray diffraction studies were grown from the NMR sample and a crystal structure for the intermediate was obtained (Figure 2.37). This structure confirms the *meso* geometry about the C-N bonds. It is clear to see the nitrogen atoms are arranged on opposite sides of the C-C bond, and the two chiral centres are arranged in a *meso* configuration.

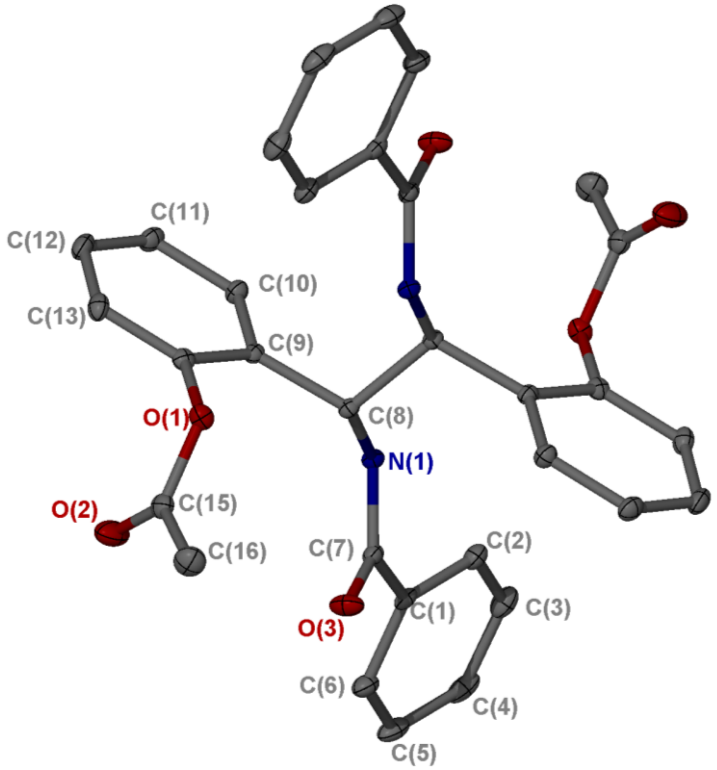

Figure 2.37. X-ray structure of intermediate species **10** showing *meso* geometry. Ellipsoids are shown at the 30% probability level. Two molecules of DMSO are present in the asymmetric unit which together with H-atoms has been removed for clarity.

On refluxing overnight, the intermediate dissolved and the solution turned a very deep brown. The fully acetylated compound **9** slowly precipitated from solution upon cooling to room temperature and was collected by filtration and washed until a white solid was observed with no brown discolouration, and the filtrate became clear. Analysis by ^{1}H NMR spectroscopy and mass spectrometry confirmed the desired product.

Finally, the acetyl groups were cleaved *via* reflux for 4 h in a 1:1 mixture of "superacid" HBr/AcOH. The resulting solid was collected by filtration, taken up in hot water and neutralised with 20 % NaOH. A solid precipitated from solution which was again collected by filtration and recrystallised from MeCN to give the desired *meso*-diamine **11** in 36% yield; with an overall process yield of 18% from salicylaldehyde and benzil.

Diamine **11** was characterised by ^{1}H NMR (Figure 2.38) and ^{13}C{^{1}H} NMR spectroscopy, and mass spectrometry. The literature values were obtained in $CDCl_3$, but this sample was found to be insoluble in chloroform and spectra were recorded in DMSO-d^{6}.

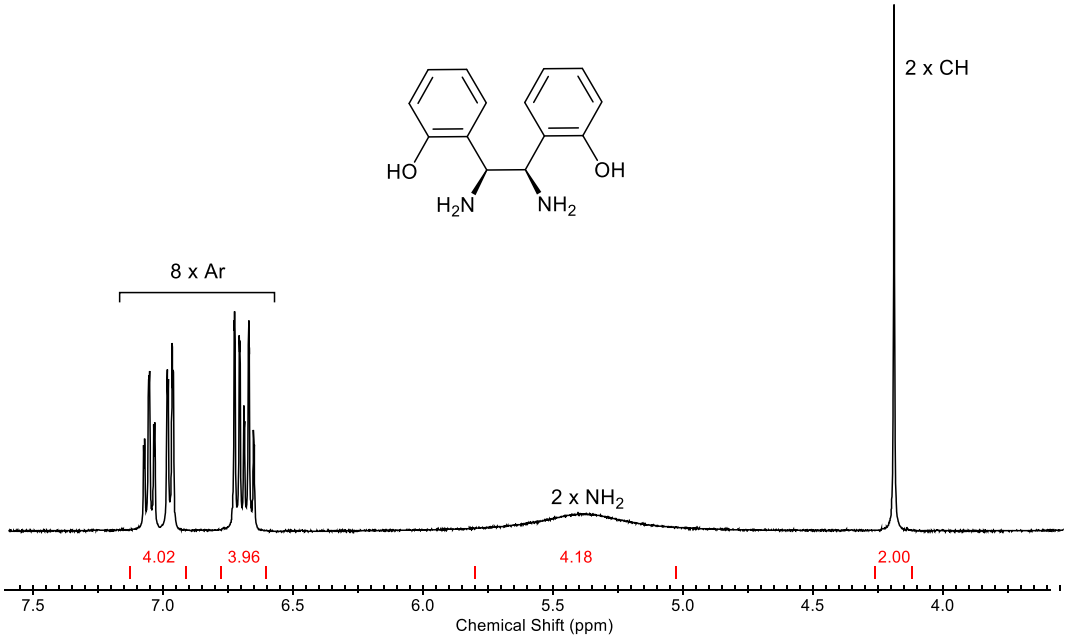

Figure 2.38. ^{1}H NMR spectrum of **11** (400 MHz, DMSO-d^{6}).

2.8.2 Preparation of bi-isoindolene ligand

Methyl 2-formylbenzoate was prepared in 72% yield following literature methods, *via* refluxing 2-carboxybenzaldehyde and iodomethane in acetone.[55] Imine **12** was afforded in 95% yield by refluxing diamine **11** and methyl 2-formylbenzoate in EtOH for 18 hours (Scheme 2.6). Zhu *et. al* report the imine condensation to occur with the chiral analogue of the parent diamine at room temperature in 2 hours.[52] However more forcing conditions were required here to form the imine, possibly due to the diamine being in *meso* geometry, and therefore having different solution chemistry than the chiral version.

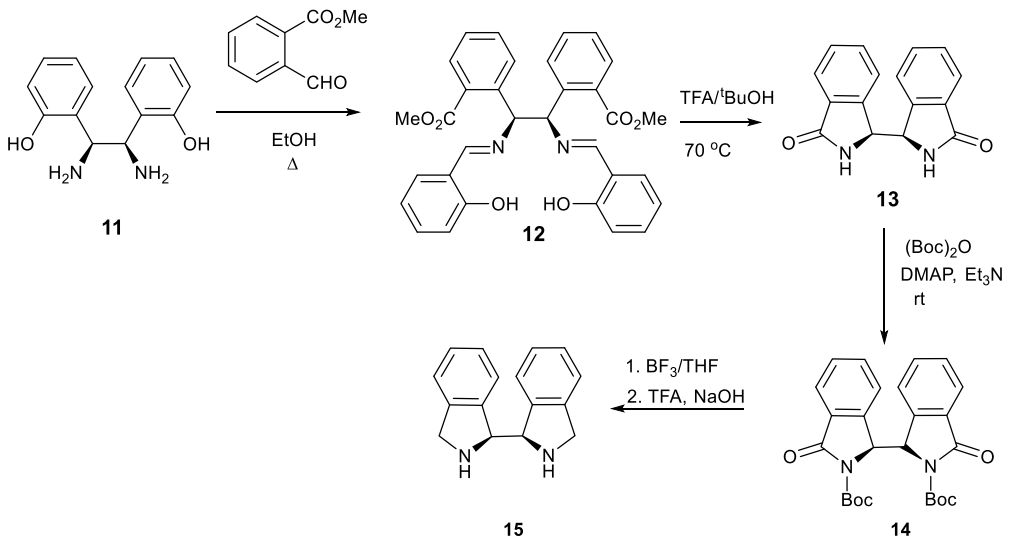

Scheme 2.6. Synthesis of bi-isoindolene **15** in 4 steps from diamine **11**.[52]

The formation of **12** was accompanied by a characteristic yellow colour change of the solution and formation of a yellow precipitate which could be easily isolated by vacuum filtration and characterised by ^{1}H and $^{13}C\{^{1}H\}$ NMR spectroscopy, and mass spectrometry. The ^{1}H NMR spectrum of **12** is shown in Figure 2.39, where characteristic resonances for the two imine protons at 8.39 ppm and for the two methoxy groups at 3.78 ppm are observed, confirming the formation of the desired product.

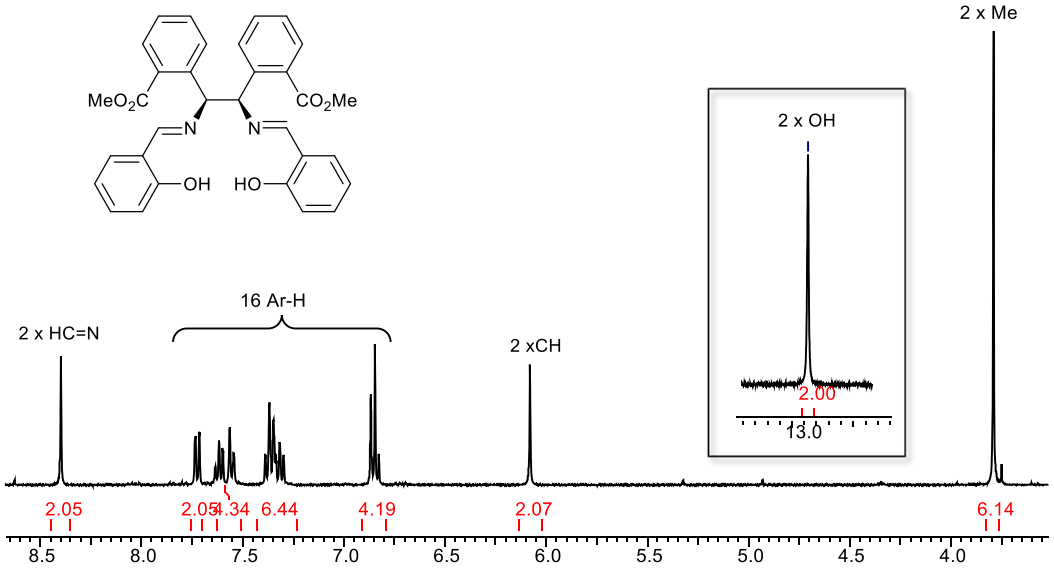

Figure 2.39. ^{1}H NMR spectrum of **12** (400 MHz, DMSO-d^{6}).

The double ring closing of the imine **12** to form *meso*-1,1'-bi-isoindoline-3,3'–dione (**13**) proceeded as reported, with 2 eq. of trifluoroacetic acid (TFA) in a 1:1 mixture of $^{t}BuOH/H_2O$. Stirring this mixture at 70 °C for two hours resulted in a loss of yellow colour.

Removal of the TFA under reduced pressure resulted in a white residue, which was suspended in EtOAc and collected by vacuum filtration and washed with further EtOAc. The product was deemed sufficiently pure from analysis *via* ^{1}H NMR and mass spectrometry.

Attempts to reduce the di-Boc protected compound **14** by refluxing with borane in THF following the literature procedure were unsuccessful. Several other methods were attempted but no diamine was isolated. As an alternative method, an S_N2 reaction with 2-(bromomethyl)-4,6-di-tert-butylphenol and triethylamine in THF was also attempted. The solution turned bright yellow and on work-up a bright yellow solid was isolated, which was recrystallised from MeOH to give fine, bright yellow needles. The ^{1}H NMR spectrum of this solid was not in agreement with the expected product, showing 4 distinct environments for the ^{t}Bu substituents rather than the expected 2 for the desired species (Figure 2.40). The identity of **16** was determined by X-ray crystallography (Figure 2.41).

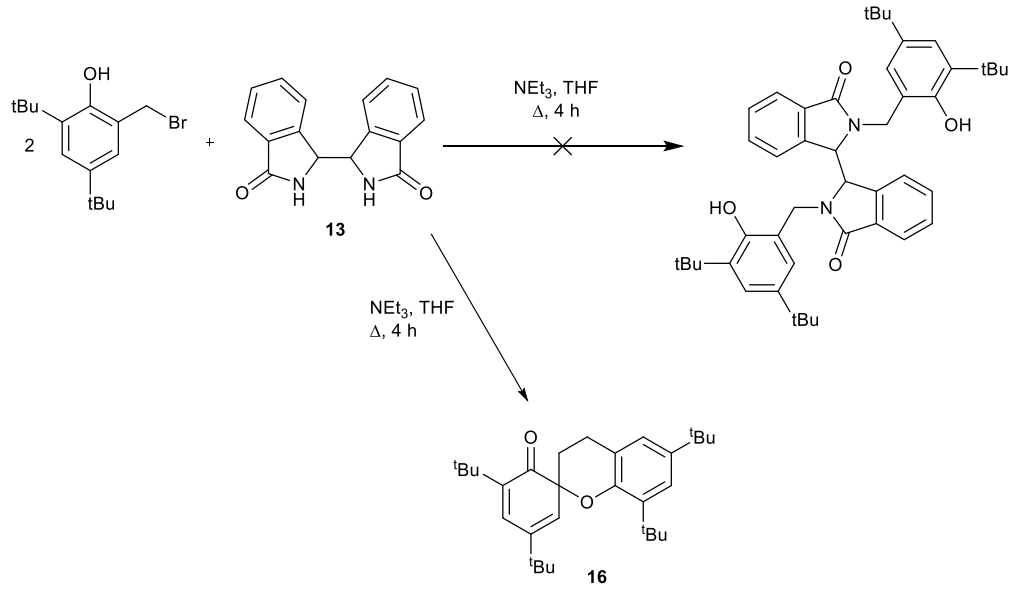

Scheme 2.7. Formation of compound **16**.

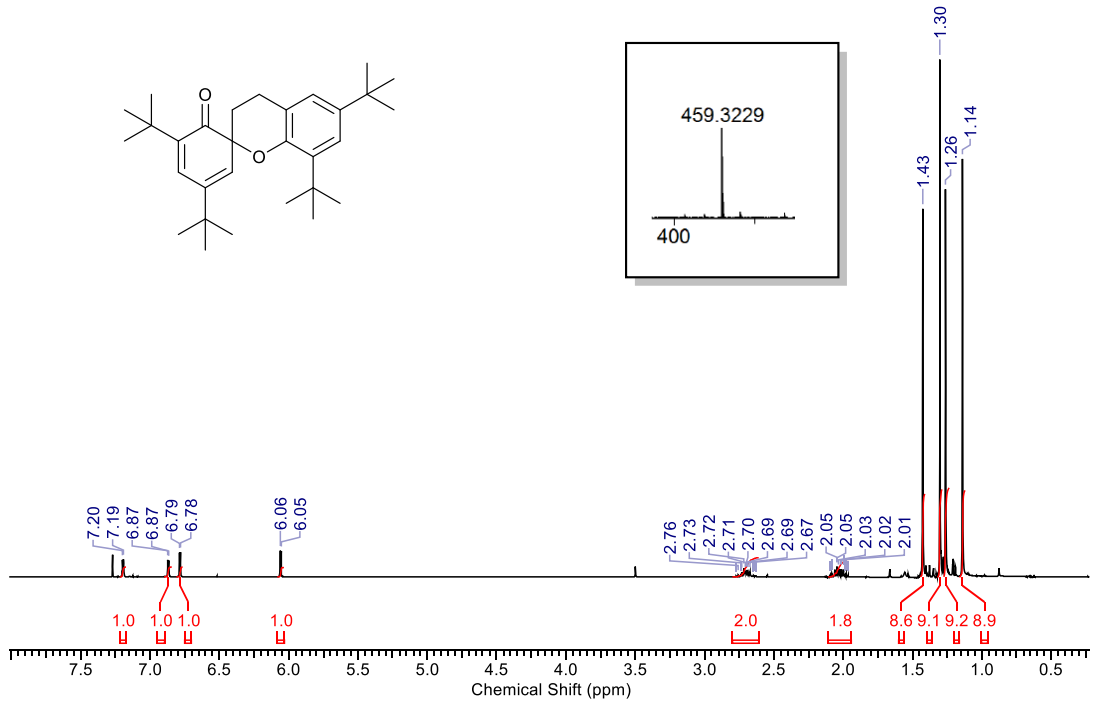

Figure 2.40. ^{1}H NMR spectrum (400 MHz, $CDCl_3$) of **16**, with MS (insert) showing the sodiated ion.

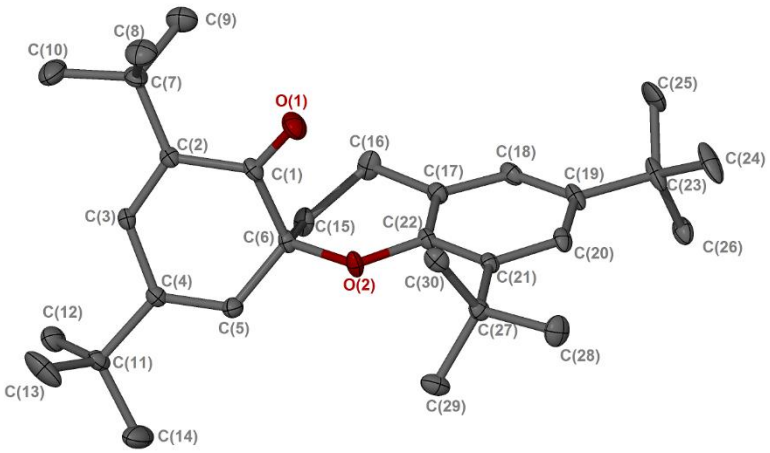

Figure 2.41. Crystal structure of unexpected product, **16**. Ellipsoids are shown at the 30% probability level. All hydrogen atoms are omitted for clarity. One set of Me groups of a ^{t}Bu moiety is disordered in a 60:40 ratio – only the major form is shown.

Attempts were also made to complex **12** to Al(III) and Zr(IV) but no products were isolated. This was attributed to the poor solubility of the Schiff base in organic solvents commonly utilised in metal complexations. This did, however, lead to interest in preparing Schiff base ligands with a *meso*-diphenylethylene backbone, which will be discussed in the next chapter.

2.9 Conclusions and future work

In this chapter, multinuclear complexes of known amine bis(phenolate) ligands with Zr(IV) Li(I), Mg(II) and Zn(II) have been prepared and investigated for the ROP of *rac*-LA.

Initial research into the preparation of Zr(IV) μ-oxo complexes yielded an interesting structure, {(Zr(**2**)O^{i}Pr)$_2$)$_2$μ-O}, characterised by X-ray crystallography and NMR spectroscopy as having a bridging μ-oxo and labile O^{i}Pr ligands to facilitate ROP. Polymerisation outcomes showed no improvement over published results for monomeric complex, Zr(**1**)(O^{i}Pr)$_2$, and the synthesis was difficult to reproduce.

Li(I) complexes comprising a central Li_4O_4 cubic core were prepared with two amine bis(phenolate) ligands, Li_4(**1**)$_2$(THF)$_2$ and Li_4(**3**)$_2$(THF). These complexes were characterised in the solid-state and in solution, observing subtle differences in the coordination modes of the ligands which presumably arise due to steric confines of the ligands used. A complex was also prepared with a more rigid backbone, Li_4(**7**)$_2$(THF)$_4$, which exhibited very different coordination. These complexes were all investigated as initiators for ROP of *rac*-LA, with near-complete conversion observed in 2 hours at RT in toluene for both Li_4(**1**)$_2$(THF)$_2$ and Li_4(**3**)$_2$(THF) with the addition of BnOH as a co-initiator. For Li_4(**1**)$_2$(THF)$_2$, polymerisation was well controlled at lower monomer concentrations, yielding PLA with a slight heterotactic bias (P_r < 0.58), while at higher loadings molecular weights were unpredictable. A linear relationship between conversion and molecular weight was observed, suggesting one chain growing per metal centre. For Li_4(**3**)$_2$(THF), addition of MeOH during work-up appeared to cause chain scission and depolymerisation of the polymer product. This complex could be taken further in future experiments as a catalyst for the depolymerisation (and recycling of PLA). Neither complex was active for the polymerisation of ε-caprolactone under these conditions. Li_4(**7**)$_2$(THF)$_4$ was also active for ROP but exhibited poor control over the polymerisation. An unusual heterometallic structure comprising a Li_3MgO_4 core was also isolated in the solid-state, which is believed to be the first structure of this type in the literature. Only a few crystals were isolated, so this was not pursued for polymerisation studies.

Dinuclear magnesium complexes were prepared with amine bis(phenolate) ligands. In some cases, attempts to prepare complexes were unsuccessful despite evidence of coordination in ^{1}H NMR spectra. Mg_2(**1**/**4**/**5**/**6**)$_2$, were all found to be active for ROP, yielding atactic PLA regardless of stereochemistry of ligand employed or phenyl

substitution. At room temperature, only one polymer chain was observed to grow per complex, which could imply different mechanisms for ROP occurring at different temperatures. At elevated temperatures (130°C, solvent free and 80° in toluene), MALDI-ToF analysis showed transesterification occurred in the polymer product.

Mg(II) complexes were also trialled for the ROCOP of epoxides with succinic anhydride, with $Mg_2(\mathbf{1})_2$ showing some promise in producing poly(propylene succinate) but was inactive with cyclohexene oxide. Future experiments should study this further, investigate the scope of bio-based substrates for the polymerisation and control conditions to improve molecular weights of products. Copolymerisation with CO_2 could also be investigated.

Tri-and tetranuclear Zn(II) complexes were also prepared with ligands $\mathbf{1}H_2$ and $\mathbf{3}H_2$ respectively. Both were characterised by X-ray crystallography. In both cases, ^{1}H NMR spectra suggested more than one species present, and DOSY ^{1}H NMR showed different levels of aggregation in solution. Both complexes were found to facilitate the ROP of lactide in a controlled manner with the addition of BnOH ($Đ$ < 1.10). $Zn_4(\mathbf{3})_2(Me)_2(OMe)_2$ was also found to facilitate ROP without the addition of BnOH but molecular weights were much higher than predicted, which is potentially due to a much faster rate of propagation compared to initiation or aggregation, as observed in the DOSY spectra, reducing the number of active initiators.

Significant attempts to prepare a novel amine bis(phenolate) ligand with a bi-isoindolene backbone were attempted, but ultimately these attempts were not successful. Alternative synthetic routes for the reduction of lactam intermediate might provide more success, although it is hard to predict how the phenyl rings might affect the activity of complexes of these ligands, and further attempts are possibly not worthwhile for minute improvements in activity or selectivity.

2.10 Chapter 2 References

1 A. Sauer, A. Kapelski, C. Fliedel, S. Dagorne, M. Kol and J. Okuda, *Dalt. Trans.*, 2013, **42**, 9007–9023.
2 M. J. Stanford and A. P. Dove, *Chem. Soc. Rev.*, 2010, **39**, 486–494.
3 X. Zhang, M. Fevre, G. O. Jones and R. M. Waymouth, *Chem. Rev.*, 2018, **118**, 839–885.
4 S. L. Hancock, M. F. Mahon, G. Kociok-Kőhn and M. D. Jones, *Eur. J. Inorg. Chem.*, 2011, **2011**, 4596–4602.
5 P. McKeown, M. G. Davidson, G. Kociok-Köhn and M. D. Jones, *Chem. Commun.*, 2016, **52**, 10431–10434.
6 P. McKeown, J. Brown-Humes, M. G. Davidson, M. F. Mahon, T. J. Woodman and M. D. Jones, *Dalt. Trans.*, 2017, **46**, 5048–5057.
7 C. Bakewell, A. J. P. White, N. J. Long and C. K. Williams, *Angew. Chem. Int. Ed.*, 2014, **53**, 9226–9230.
8 M. D. Jones, S. L. Hancock, P. McKeown, P. M. Schäfer, A. Buchard, L. H. Thomas, M. F. Mahon and J. P. Lowe, *Chem. Commun.*, 2014, **50**, 15967–15970.
9 M. D. Jones, L. Brady, P. McKeown, A. Buchard, P. M. Schäfer, L. H. Thomas, M. F. Mahon, T. J. Woodman and J. P. Lowe, *Chem. Sci.*, 2015, **6**, 5034–5039.
10 J. Beament, M. F. Mahon, A. Buchard and M. D. Jones, *New J. Chem.*, 2017, **41**, 2198–2203.
11 Z. Janas, T. Nerkowski, E. Kober, L. B. Jerzykiewicz and T. Lis, *Dalt. Trans.*, 2012, **41**, 442–447.
12 W.-L. Kong and Z.-X. Wang, *Dalt. Trans.*, 2014, **43**, 9126-9135.
13 W. Li, W. Wu, Y. Wang, Y. Yao, Y. Zhang and Q. Shen, *Dalt. Trans.*, 2011, **40**, 11378.
14 A. Thevenon, C. Romain, M. S. Bennington, A. J. P. White, H. J. Davidson, S. Brooker and C. K. Williams, *Angew. Chem. Int. Ed.*, 2016, **55**, 8680–8685.
15 S. Paul, Y. Zhu, C. Romain, R. Brooks, P. K. Saini and C. K. Williams, *Chem. Commun.*, 2015, **51**, 6459–6479.
16 C. Romain, Y. Zhu, P. Dingwall, S. Paul, H. S. Rzepa, A. Buchard and C. K. Williams, *J. Am. Chem. Soc.*, 2016, **138**, 4120–4131.
17 C. K. Su, H. J. Chuang, C. Y. Li, C. Y. Yu, B. T. Ko, J. Der Chen and M. J. Chen, *Organometallics*, 2014, **33**, 7091–7100.
18 S. Ghosh, P. K. S. Antharjanam and D. Chakraborty, *Polym.*, 2015, **70**, 38–51.
19 M. D. Jones, M. G. Davidson and G. Kociok-Kohn, *Polyhedron*, 2010, **29**, 697–700.
20 N. Maudoux, J. Fang, T. Roisnel, V. Dorcet, L. Maron, J.-F. Carpentier and Y. Sarazin, *Chem. Eur. J.*, 2014, **20**, 7706–7717.
21 A. J. Chmura, D. M. Cousins, M. G. Davidson, M. D. Jones, M. D. Lunn and M. F. Mahon, *Dalt. Trans.*, 2008, 1437–1443.
22 A. J. Chmura, M. G. Davidson, M. D. Jones, M. D. Lunn, M. F. Mahon, A. F. Johnson, P. Khunkamchoo, S. L. Roberts and S. S. F. Wong, *Macromolecules*, 2006, **39**, 7250–7257.
23 C.-Y. Tsai, H.-C. Du, J.-C. Chang, B.-H. Huang, B.-T. Ko and C.-C. Lin, *RSC Adv.*, 2014, **4**, 14527–14537.
24 J.-C. Buffet and J. Okuda, *Chem. Commun.*, 2011, **47**, 4796–4798.
25 S. Gendler, S. Segal, I. Goldberg, Z. Goldschmidt and M. Kol, *Inorg. Chem.*, 2006, **45**, 4783–4790.
26 W. Clegg, M. G. Davidson, D. V. Graham, G. Griffen, M. D. Jones, A. R. Kennedy, C. T. O'Hara, L. Russo and C. M. Thomson, *Dalt. Trans.*, 2008, **10**, 1295-1301.
27 J. J. Morris, D. J. MacDougall, B. C. Noll and K. W. Henderson, *Dalt. Trans.*, 2008, **0**, 3429.
28 R. Evans, Z. Deng, A. K. Rogerson, A. S. McLachlan, J. J. Richards, M. Nilsson and G. A. Morris, *Angew. Chem. Int. Ed.*, 2013, **52**, 3199–3202.

29 R. Evans, G. Dal Poggetto, M. Nilsson and G. A. Morris, *Anal. Chem.*, 2018, **90**, 3987–3994.
30 M. W. Drover, J. N. Murphy, J. C. Flogeras, C. M. Schneider, L. N. Dawe and F. M. Kerton, *Polyhedron*, 2015, **102**, 60–68.
31 D. Alhashmialameer, N. Ikpo, J. Collins, L. N. Dawe, K. Hattenhauer and F. M. Kerton, *Dalt. Trans.*, 2015, **44**, 20216–20231.
32 C. Gallegos, V. Tabernero, F. M. García-Valle, M. E. G. Mosquera, T. Cuenca and J. Cano, *Organometallics*, 2013, **32**, 6624–6627.
33 J. Char, E. Brulé, P. C. Gros, M.-N. Rager, V. Guérineau and C. M. Thomas, *J. Organomet. Chem.*, 2015, **796**, 47–52.
34 J. Randazzo, J. Jacob Morris, J. A. Rood, B. C. Noll and K. W. Henderson, *Inorg. Chem. Commun.*, 2008, **11**, 1270–1272.
35 B. Walfort, D. Stalke and S. K. Pandey, *Chem. Commun.*, 2001, **0**, 1640–1641.
36 E. Kober, Z. Janas, T. Nerkowski and L. B. Jerzykiewicz, *Dalt. Trans.*, 2013, **42**, 10847.
37 K. Devaine-Pressing, J. H. Lehr, M. E. Pratt, L. N. Dawe, A. A. Sarjeant and C. M. Kozak, *Dalt. Trans.*, 2015, **44**, 12365–12375.
38 A. W. Addison, T. N. Rao, J. Reedijk, J. van Rijn and G. C. Verschoor, *J. Chem. Soc., Dalt. Trans.*, 1984, **0**, 1349–1356.
39 J. Lewiński, W. Śliwiński, M. Dranka, I. Justyniak and J. Lipkowski, *Angew. Chem.*, 2006, **118**, 4944–4947.
40 C. Di Iulio, M. D. Jones, M. F. Mahon and D. C. Apperley, *Inorg. Chem.*, 2010, **49**, 10232–10234.
41 E. Kober, R. Petrus, P. Kocięcka, Z. Janas and P. Sobota, *Polyhedron*, 2015, **85**, 814–823.
42 M.-L. Hsueh, B.-H. Huang, J. Wu and C.-C. Lin, *Macromolecules*, 2005, **38**, 9482–9487.
43 C.-A. Huang and C.-T. Chen, *Dalt. Trans.*, 2007, **0**, 5561–5566.
44 E. L. Whitelaw, M. G. Davidson and M. D. Jones, *Chem. Commun.*, 2011, **47**, 10004–10006.
45 Y. Sun, Y. Cui, J. Xiong, Z. Dai, N. Tang and J. Wu, *Dalt. Trans.*, 2015, **44**, 16383–16391.
46 M. G. Davidson, M. D. Jones, D. Meng and C. T. O'Hara, in *Main Group Chemistry*, IOS Press, 2006, vol. 5, pp. 3–12.
47 M. R. Kember and C. K. Williams, *J. Am. Chem. Soc.*, 2012, **134**, 15676–15679.
48 P. K. Saini, C. Romain, Y. Zhu and C. K. Williams, *Polym. Chem.*, 2014, **5**, 6068–6075.
49 K. Bester, A. Bukowska, B. Myśliwiec, K. Hus, D. Tomczyk, P. Urbaniak and W. Bukowski, *Polym. Chem.*, 2018, **9**, 2147–2156.
50 N. J. Van Zee and G. W. Coates, *Angew. Chem. Int. Ed.*, 2015, **54**, 2665–2668.
51 C. K. Williams, L. E. Breyfogle, S. K. Choi, W. Nam, V. G. Young, M. A. Hillmyer and W. B. Tolman, *J. Am. Chem. Soc.*, 2003, **125**, 11350–11359.
52 Q. Zhu, H. Huang, D. Shi, Z. Shen and C. Xia, *Org. Lett.*, 2009, **11**, 4536–4539.
53 F. Vögtle and E. Goldschmitt, *Chem. Ber.*, 1976, **109**, 1–40.
54 R. Bohlmann, J. M. Brown, H. Brunner, A. P. Davis, M. El-Khawaga, H. Frauenrath, B. Giese, M. Gottwald, D. Hasselmann, G. Helmchen, H. M. R. Hoffmann, S. Hünig, J. L. Kallmerten, U. Kazmaier, K. Krohn, H. G. Leuenberger, J. Martens, P. K. Matzinger, M. M. Midland, Morell, A. Pfaltz, J. M. Takacs and M. Zaidlewicz, *Houben-Weyl Methods of Organic Chemistry Vol. E 21d, 4th Edition Supplement: Stereoselective Synthesis: C-C Bond Formation by Sigmatropic Rearrangements, Electrocyclic Reactions, C-H, C-Hal Bond Formation*, Georg Thieme Verlag, 2014.
55 Y. He, C. Cheng, B. Chen, K. Duan, Y. Zhuang, B. Yuan, M. Zhang, Y. Zhou, Z. Zhou, Y.-J. Su, R. Cao and L. Qiu, *Org. Lett.*, 2014, **16**, 6366–6369.

3 Chapter 3. Schiff base complexes and related ligands

3.1 Preamble

Salen ligands are among the most widely studied class of ligands in inorganic chemistry, finding wide ranging applications in catalysis, medicinal chemistry, dyes, and energy materials.[1–5] These rigid ligands complexed to aluminium have reported to be isoselective in ROP of *rac*-LA and active for ROP of other cyclic esters such as ε-CL and β-butyrolactone.[6–13] A large degree of ligand structural variation is possible by judicial selection of amine and salicylaldehyde starting materials, leading to many potential ligands for single site catalysts or more extensive salen frameworks.[14]

As discussed in section 1.2.4, some recent publications have suggested that higher activity in production of PLA can be achieved with dinuclear complexes over their monomeric counterparts.[8,15–18] Some examples of dinuclear aluminium initiators reported in the literature are shown in Figure 3.1. Recently reported dinuclear aluminium Schiff base complexes include the example shown in which was reported by Normand and co-workers, who observed a large increase in activity for the ROP of lactide with this complex over its monomeric counterpart.[15] The authors report five-fold increases in apparent rate constant, $k_{app,}$ from *ca.* 2.5 x 10^{-3} s^{-1} for the mononuclear complex to 12.2 x 10^{-3} s^{-1} for the dinuclear under comparable conditions. Kinetic studies demonstrated that the dialuminum complex provided a more favourable reaction pathway in terms of activation free energy than that of the monomeric systems. They suggested that this increased activity results from synergy between aluminium centres, facilitated by free rotation in the ligand backbone. In the solid-state the Al···Al bond length was observed to be *ca*. 8.0 Å but rotation about the phenyl-phenyl bond could permit the Al centres to come as close as 2.8 Å: within the range for cooperative effects. While the authors report increased activity, no PLA tacticity is reported and it is assumed that the polymer products were atactic.

In 2016, Mazzeo highlighted the importance of cooperativity in the polymerisation of *rac*-LA initiated with Al(III) salen complexes by varying the backbone of the ligand, finding the Al···Al distance being the key parameter.[19] The authors propose that this is due to synergistic interactions during the alcoholysis and polymer growth steps.

Chen has also extensively shown that dinuclear aluminium complexes of piperidine salan ligands have improved catalytic activity over mononuclear analogues, reporting 2-8-fold

increases in activity over a range of temperatures for the ROP of ε-caprolactone (e.g. $k_{app\ mono}$ = (1.51 ± 0.16) × 10^{-4} s^{-1} *vs* $k_{app\ di}$ = (4.68 ± 0.11) × 10^{-5} s^{-1} at 80 °C).[16]

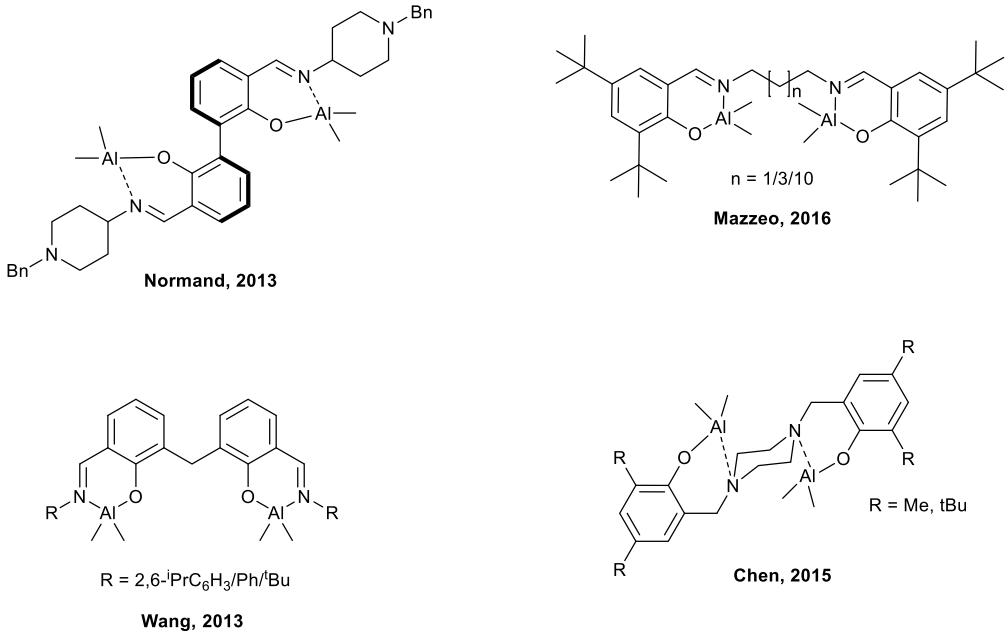

Figure 3.1. Dinuclear aluminium complexes reported in the literature[15,16,18,19]

The purpose of this research was to widen the library of possible ligands capable of forming dinuclear species. Further, in this work the research aimed to develop systems which would selectively produce isotactic PLA from *rac*-LA, and to further investigating potential cooperativity effects.

3.2 Synthesis of *meso*-1,2-diphenylethane-1,2-diamine complexes

3.2.1 Synthesis of ligands

In the previous chapter, attempts to prepare a bi-isoindoline ligand were described. A Schiff base intermediate in the process (Figure 3.2) was also trialled as a ligand in the synthesis of new initiators *via* complexation to Al(III) and Zr(IV). No complexes were isolated with either metal, regardless of reaction stoichiometry or conditions. This was attributed to poor solubility of the ligand in a range of organic solvents used for complexation. It was therefore decided to try the same complexations with simplified ligands containing a *meso*-1,2-diphenylethane backbone without -CO_2Me substituents, which could be prepared from commercially available starting materials.

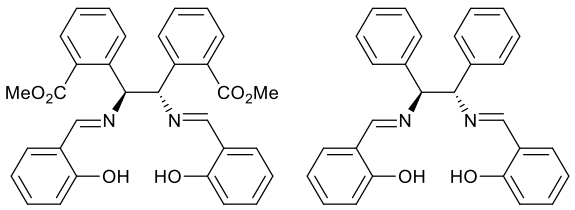

Figure 3.2. Schiff base intermediate prepared in Chapter 2 and unsubstituted analogue.

Schiff-base ligands, **1**-**3**H_2, were prepared by condensation of *meso*-1,2-diphenylethane-1,2-diamine with the required salicylaldehyde as shown in Scheme 3.1. 2-Hydroxy-3,5-dimethylbenzaldehyde was prepared in high yields (*ca.* 90%) following a previously reported method.[20] These ligands are also of interest as they are isomeric to ligands reported by Carpentier, who showed complexes of chiral analogues with aluminium, gallium and indium being active for ROP of *rac*-LA, yielding isotactially enriched PLA with values of P_m in the range 0.80–0.90.[8]

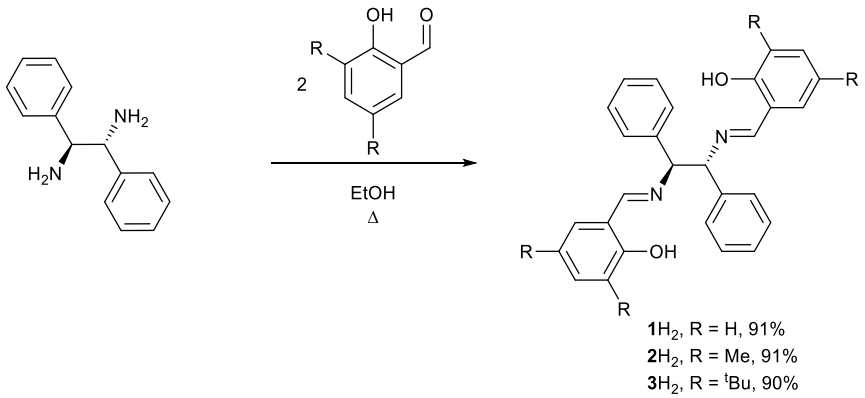

Scheme 3.1. Preparation of *meso*-diphenylethane-1,2-diamine ligands **1**-**3**H_2

A solid-state structure for **3**H_2 was obtained via crystallisation from toluene (Figure 3.3). Selected bond angles and lengths for this structure can be found in Table 3.1. Formation of the expected compound is confirmed in the solid-state, evidenced by the shorter imine bond (N(1)-C(14), 1.275(3) Å) compared to the amine (N(1)-C(15), 1.463(3) Å) and a C-N=C bond angle close to 120° (119.07°), as expected for a sp^2 hybridised nitrogen.

The solid-state structure differs slightly from the enantiopure analogue reported by Carpentier, where the molecule is twisted so that the phenyl rings are in the same plane (Figure 3.3). However, in **3**H_2 the phenyl rings are orientated on opposing sides of the molecule's backbone, as expected due to minimising steric repulsions and hydrogen bonding between phenol and amine moieties.

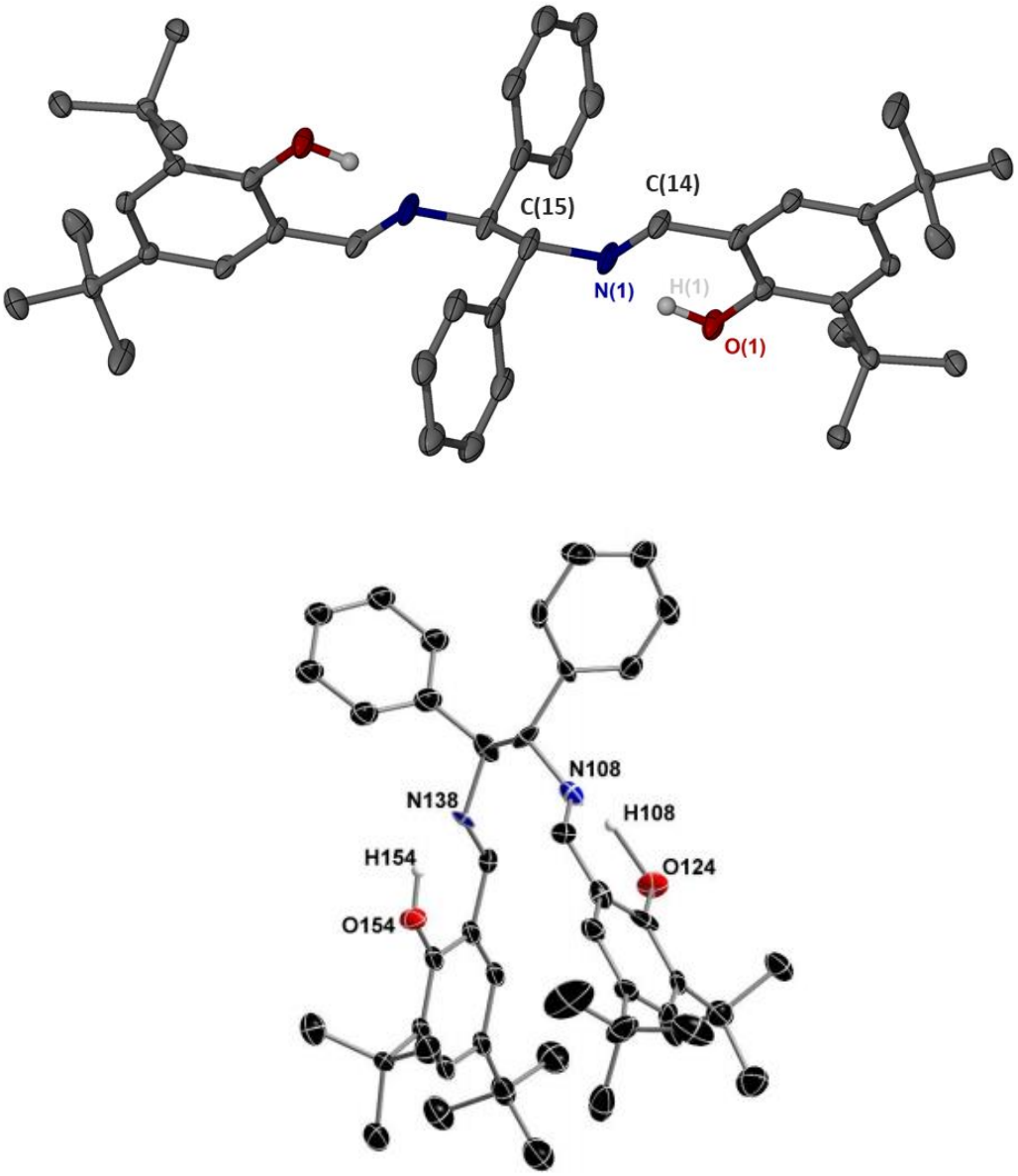

Figure 3.3. Solid-state structure of **3**H_2. Ellipsoids are shown at the 30 % probability level; hydrogen atoms have been removed for clarity. Also shown is the crystal structure of the *R,R'*- enantiomer, reproduced from Maudoux *et al*. with permission, copyright John Wiley and Sons (2014). [8]

Table 3.1. Selected bond lengths (Å) and angles (°) for **3**H_2

	3H_2
N(1)-C(14)	1.275(3)
N(1)-C(15)	1.463(3)
O(1)-C(1)	1.356(2)
N(1)-C(14)-C(5)	123.06(19)
C(14)-N(1)-C(15)	119.07(19)

The structure was confirmed in solution by the ^{1}H NMR spectrum of **3**H_2, shown in Figure 3.4. As expected, the ligand is highly symmetrical. Two intense resonances at 1.27 ppm and 1.46 ppm correspond to the tertiary butyl groups on the phenol rings and a singlet at 4.80 ppm corresponds to the two CH protons of the diphenylethane backbone. Formation of the Schiff base is confirmed by the presence of a singlet resonance in the ^{1}H NMR spectrum at 8.24 ppm, typical of an imine moiety.

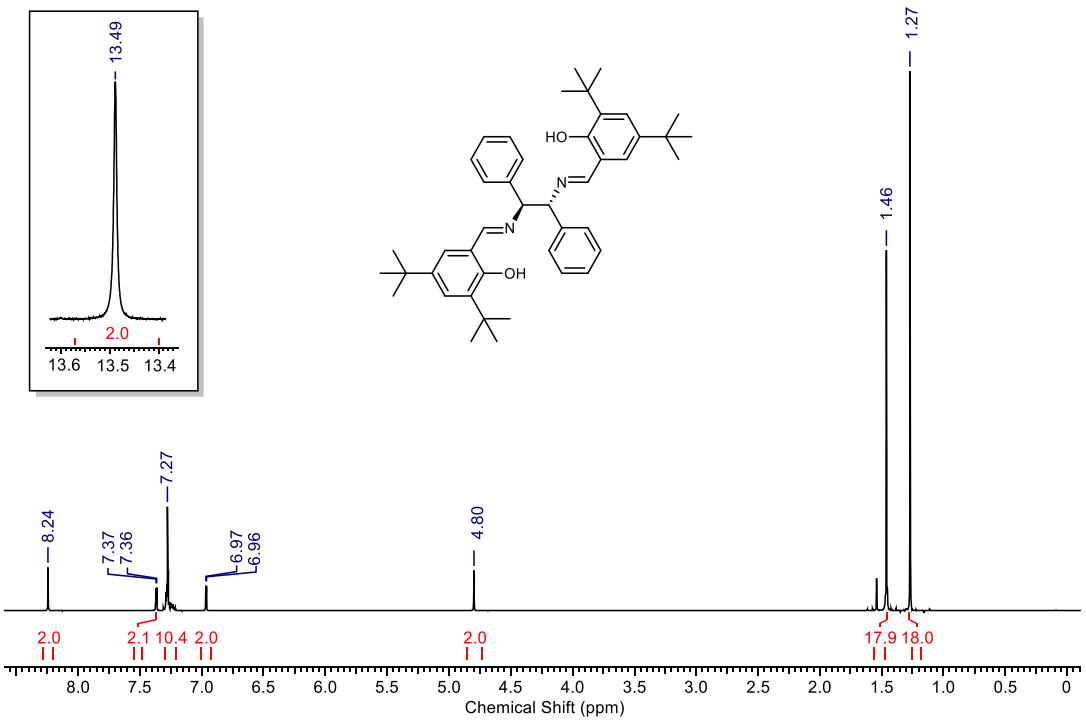

Figure 3.4. ^{1}H NMR spectrum (400 MHz, $CDCl_3$) of **3**H_2

3.2.2 Complexation to aluminium

The complexation of the ^{t}Bu and very similar *p*-cresol methyl substituted chiral ligands with trimethylaluminium has been previously reported by Carpentier.[8,21] Here both the mono- and disubstituted complexes were reported for the ^{t}Bu analogue, although the authors

acknowledge a large preference for formation of the dinuclear complex over the mononuclear complex, for it is structurally more demanding to wrap the ligand around the metal centre. The mononuclear complex could be accessed *via* the use of $Al(O^iPr)_3$ or $AlMe_2Cl$ rather than an alkylaluminium reagent. The monomeric isopropoxide species showed good control over the polymerisation of *rac*-LA, giving isotactically enriched PLA (P_m = 0.90) with a predictable molecular weight and narrow dispersity. The polymerisation proceeds relatively slowly, giving 38% conversion in 144 hours at 90 °C. The authors report that the enantiopure dinuclear species is active for ROP but, disappointingly, affords no stereocontrol over the polymerisation (P_m ≈ 0.50). However, this species does show a rate enhancement, with conversion of 87% in 25 h in toluene at 70 °C.

As previous research in the Jones group has shown subtle differences in chirality can have a marked effect on polymerisation outcome,[22] changing the chirality of the ligand from enantiopure to *meso* form was investigated. This could influence the coordination environment or polymerisation characteristics.

Complexation of ligands **1**H_2 and **2**H_2 to trimethylaluminium yielded monomeric species as yellow powders in reasonable yields (38% and 37% respectively). Crystals suitable for X-ray crystallography were obtained for Al(**2**)Me. The solid-state structure is shown in Figure 3.5, and bond angles (°) and lengths (Å) are given in Table 3.2. No solid-state structure was obtained for the unsubstituted complex, which was identified as Al(**1**)Me by ^{1}H NMR spectroscopy.

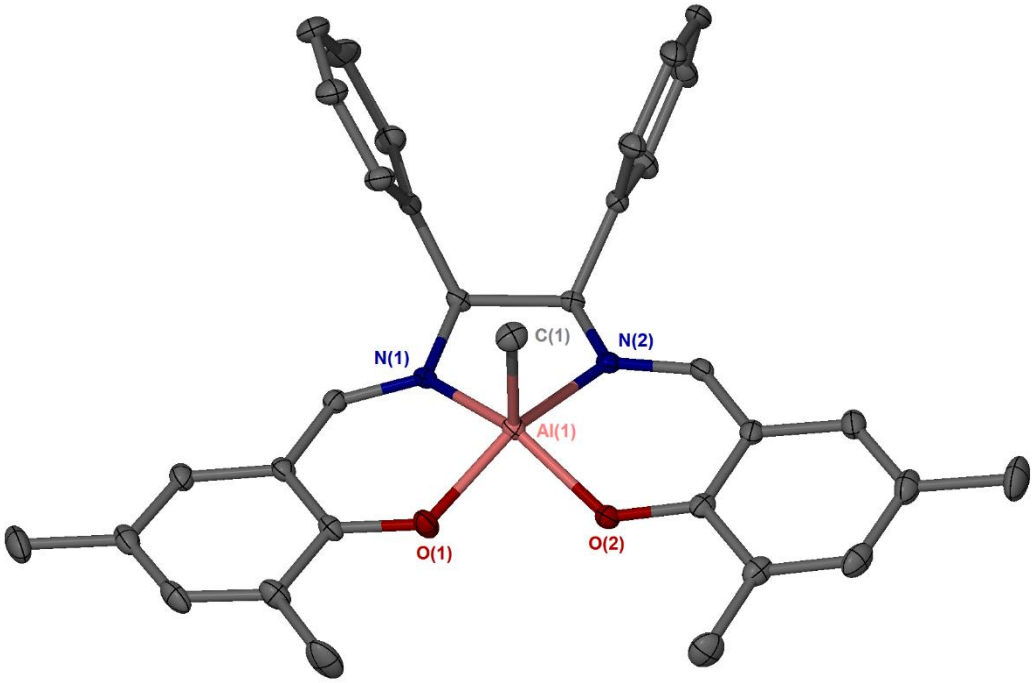

Figure 3.5. Solid-state structure for Al(**2**)Me. Ellipsoids are shown at the 30% probability level. Hydrogen atoms have been removed for clarity. Half a molecule of toluene was also present in the asymmetric unit which has been removed for clarity.

Complexation of the ^{t}Bu ligand, **3**H_2, to one equivalent of trimethylaluminium was also performed, and recrystallisation from toluene yielded a small amount of crystalline material which was suitable for X-ray diffraction. The solid-state structure is shown in Figure 3.6, and bond angles (°) and lengths (Å) are given in Table 3.2. The crystal structure of the dimeric species reported by Carpentier and co-workers is shown in Figure 3.7 or comparison.

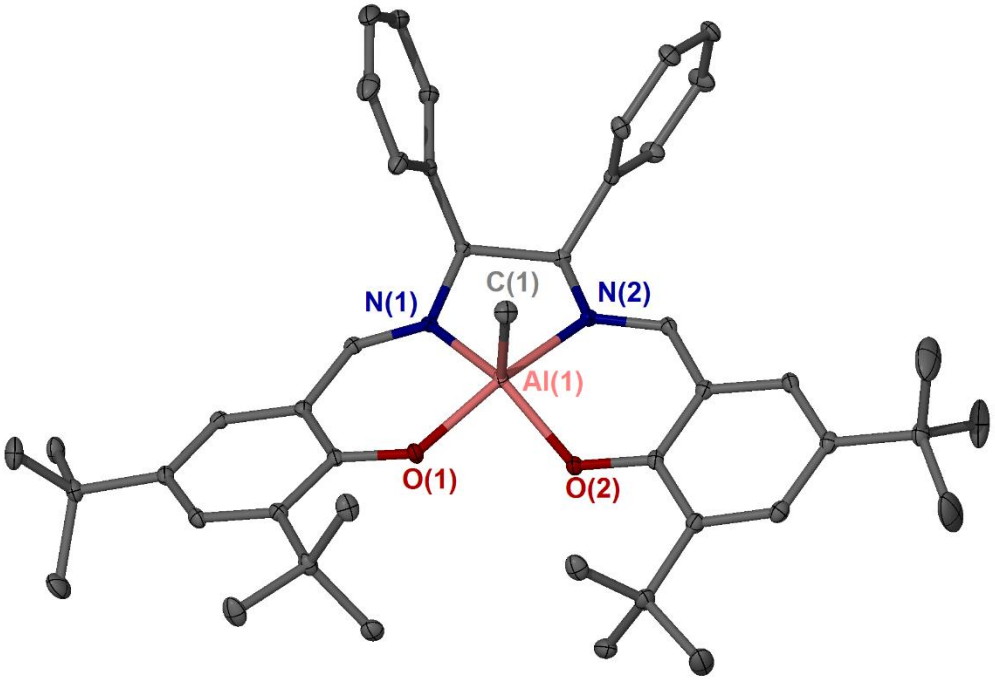

Figure 3.6. Solid-state structure of Al(**3**)Me. Ellipsoids are shown at the 30% probability level. Hydrogen atoms have been removed for clarity. Twinning (46%) is taken into account by virtue of 180 degrees about 1 0 0 (rec).

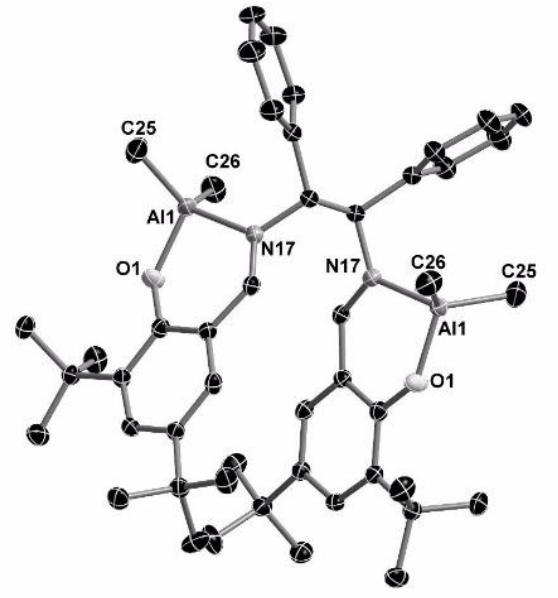

Figure 3.7. X-ray structure of dinuclear species reproduced from Maudoux *et al*. with permission, copyright John Wiley and Sons (2014).[8] Hydrogen atoms are omitted for clarity. Ellipsoids drawn at the 50% probability level.

The monomeric complex Al(**2**)Me was found to crystallise in the monoclinic space group $P2_1/n$ while Al(**3**)Me crystallised in the triclinic space group *P*-1. The bond lengths in both complexes are very similar, but there are subtle differences in coordination seen in the bond angles.

In 5-coordinate complexes a degree of trigonality, τ_5, may be calculated, as reported by Addison *et al.* using the two largest bond angles (α and β) in the 5-coordinate complex.[23] A perfectly trigonal bipyramidal complex would have $\tau_5 = 1$, while a square based pyramidal structure would have $\tau_5 = 0$. The equation to derive this angular structural parameter is given in Equation 2.2.

Equation 3.1. Degree of trigonality[23]

$$\tau_5 = \frac{\beta - \alpha}{60}$$

τ_5 values were calculated for Al(**2**)Me and Al(**3**)Me systems to be $\tau_5 = 0.09$ and 0.32 respectively. Both have distorted square based pyramidal (SBP) structures, with the Me analogue having almost perfect SBP geometry. For the ^{t}Bu analogue there appears to be more distortion about the diaminoethane backbone, presumably to minimise steric clashing between bulky substituents. The literature example **I** (Figure 3.7) is also close to perfect SBP geometry, having $\tau_5 = 0.12$.[8] This would be expected from coordination with a planar salen ligand with a flexible backbone, and bonding geometries and lengths are in good agreement with literature values for Al-salen complexes.[11] The main difference in these structures is the twisting of the backbone observed in the literature structure due to the chirality.[8]

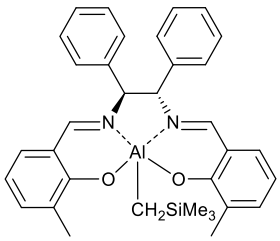

I

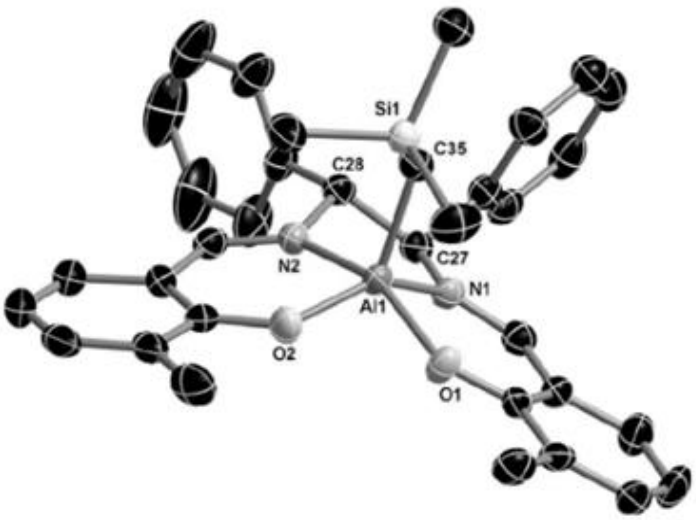

Figure 3.8. Literature complex, **I**, for comparison. Image reproduced from Maudoux *et al*. with permission, copyright John Wiley and Sons (2014).[8]

Table 3.2. Selected bond lengths (Å) and angles (°) for Al(**2**)Me and Al(**3**)Me, with values for a literature complex, **I**, for comparison.

	Al(**2**)Me	Al(**3**)Me	**I** [8]
Al(1)-O(1)	1.8179(14)	1.8245(15)	1.802(2)
Al(1)-O(2)	1.8158(14)	1.8063(16)	1.810(2)
Al(1)-N(1)	2.0169(17)	2.0102(18)	2.040(2)
Al(1)-N(2)	2.0372(17)	2.0317(19)	2.022(3)
Al(1)-C(1)	1.970(2)	1.964(2)	1.976(3)
O(1)-Al(1)-O(2)	87.24(7)	88.82(7)	87.91(10),
O(2)-Al(1)-C(1)	106.85(8)	110.75(9)	113.50(12)
O(1)-Al(1)-C(1)	108.90(9)	103.99(9)	108.60(12)
O(2)-Al(1)-N(1)	143.59(7)	135.88(8)	142.62(11)
O(1)-Al(1)-N(1)	88.24(6)	88.48(7)	88.21(10)
C(1)-Al(1)-N(1)	108.78(8)	112.61(9)	102.94(11)
O(2)-Al(1)-N(2)	87.98(7)	86.62(7)	88.02(10)
O(1)-Al(1)-N(2)	149.02(7)	155.18(7)	150.54(11)
C(1)-Al(1)-N(2)	101.78(8)	100.43(9)	99.76(12)
N(1)-Al(1)-N(2)	77.77(7)	78.06(7)	77.63(10)
τ_5	0.09	0.32	0.12

The ^{1}H NMR spectrum of Al(**2**)Me in C_6D_6 is given in Figure 3.9. The solid-state structure is confirmed in solution, evidenced by a single Al-Me resonance integrating to three protons observed at -0.12 ppm. Some small resonances are evident in the NMR spectrum, which could correspond to a dinuclear complex (highlighted in Figure 3.9). Attempts to selectively prepare a dinuclear complex by reaction with 2 equivalents of trimethylaluminium were unsuccessful.

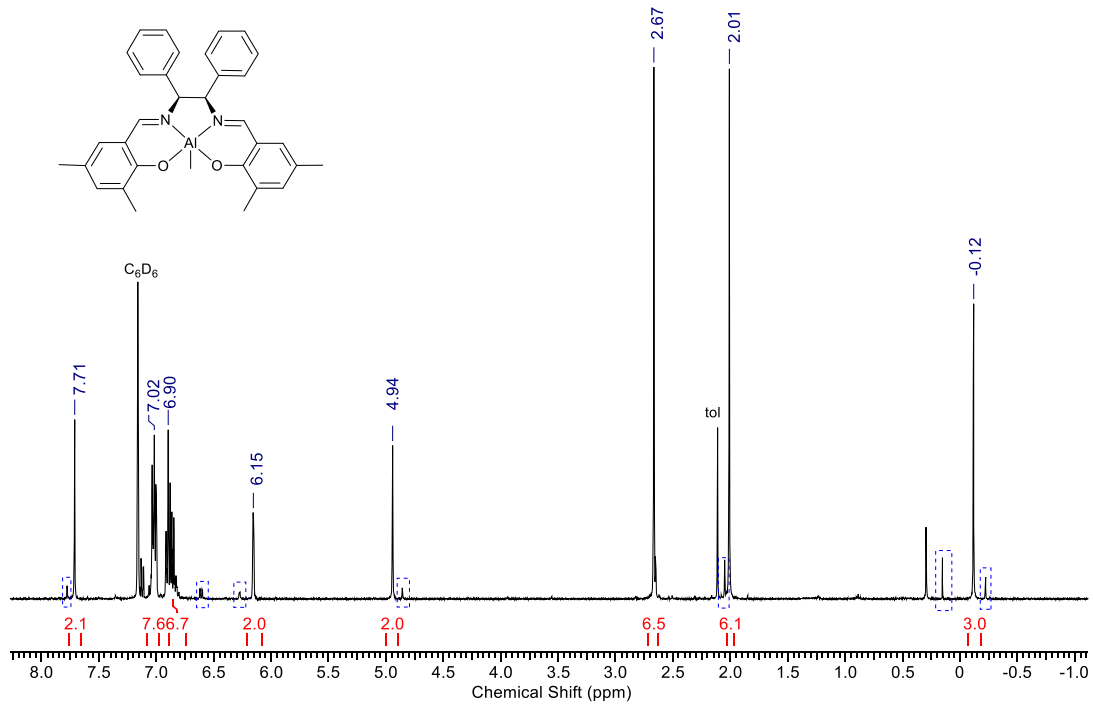

Figure 3.9. ^{1}H NMR spectrum of Al(**2**)Me (400 MHz, C_6D_6). Smaller resonances highlighted presumably arise from Al_2(**2**)Me_4.

The ^{1}H NMR spectrum of Al(**3**)Me in C_6D_6 is given in Figure 3.10, showing the solid-state structure is not representative of the bulk isolated product. The CH protons of the backbone appear as a characteristic singlet at 5.27 ppm. There are two distinct Al-Me resonances observed at -0.61 ppm and -0.38, each integrating to 6 protons, indicative of two inequivalent methyl ligands per aluminium centre. This suggests that in solution the dinuclear form, Al_2(**3**)Me_2 is favoured. The chemical inequivalence of the aluminium-methyl bonds indicates that the structure is "locked" in place. CHN analysis also confirmed the structure to be the dinuclear species. Despite attempts to selectively reproduce the 1:1 complex by stoichiometric reaction with trimethylaluminium, no isolated solid gave an NMR spectrum indicative of the monomeric complex. Reaction of ligand **3**H_2 with 2 equivalents of $AlMe_3$ gave only the dinuclear species in 72% yield, as determined by ^{1}H NMR spectroscopy. A crystal structure of the dinuclear complex was not attained. Presumably, the isolation of monomeric crystals was a minor component of < 5%, while formation of the dinuclear complex is favoured, as previously reported for the chiral ligands.[8]

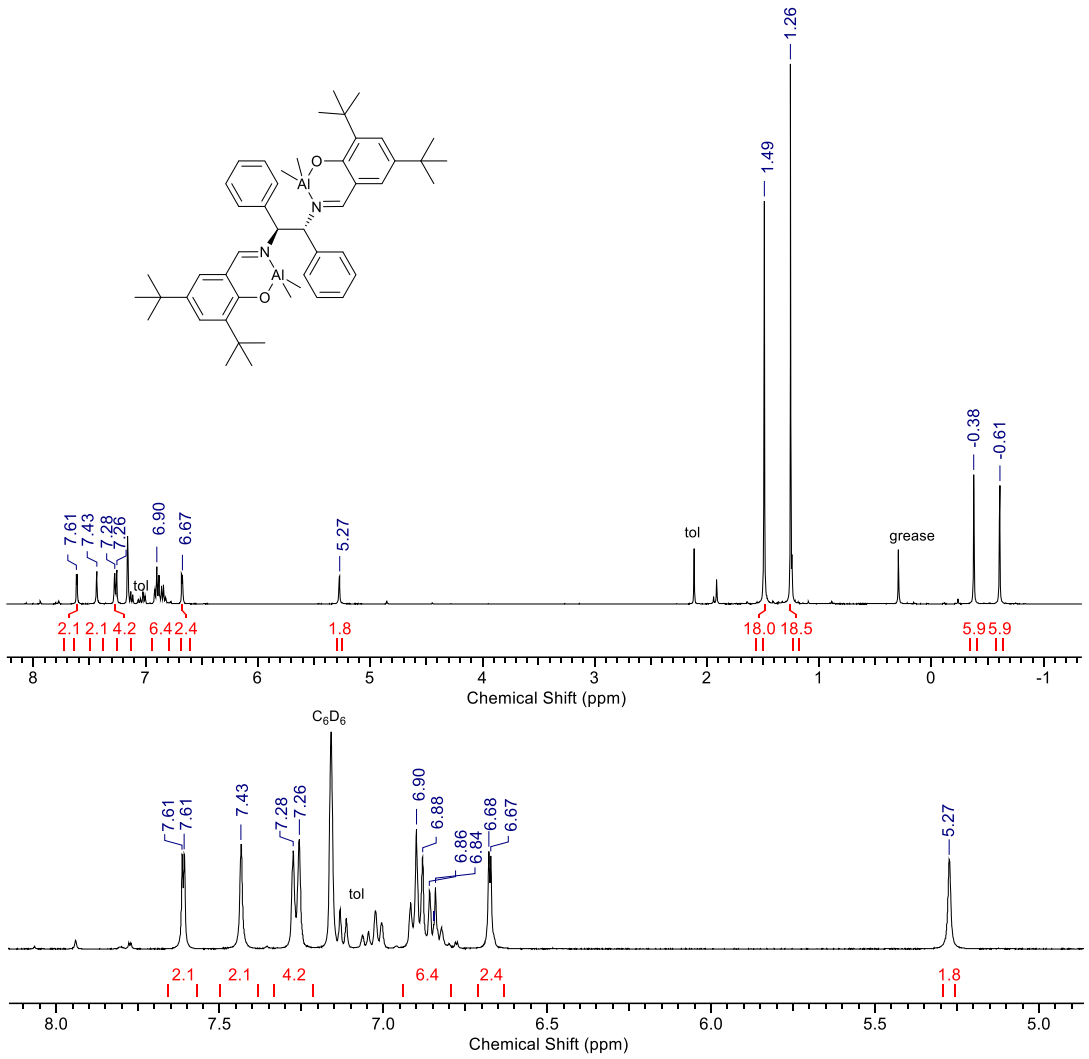

Figure 3.10. ^{1}H NMR of Al_2(**3**)Me_2 (400 MHz, C_6D_6) with expanded aromatic region

3.2.3 Polymerisation results

For complexes with Al-Me moieties, polymerisations were carried out in toluene at 80 °C, with benzyl alcohol (BnOH) added as a co-initiator to generate the alkoxide *in situ*. Initial polymerisations were carried out with a ratio of [LA]:[I]:[BnOH] = 100:1:1 (or 100:1:2 for complexes with two Al centres) for 24 hours, with a lactide concentration of 0.5M (Table 3.3). Polymerisations were attempted using *rac*-lactide to demonstrate any stereocontrol initiators impart on the polymer. Unless otherwise stated, the lactide used was recrystallised from toluene to align with industrial processes. It is frequently reported in the scientific literature to twice sublime lactide prior to use to remove trace impurities (lactic acid and water) to reduce side reactions and protect moisture sensitive initiators.[11,24,25] However, this energy intensive process, being carried out at high vacuum and temperature (for *rac*-lactide, *ca.* 110 °C), makes it impractical on larger scales. Initiators which exhibit high activity while tolerating these impurities would be desirable.

As in the previous chapter, an expected value for the number average molecular weight (M_n) may be calculated using the molecular mass of lactide (144 gmol^{-1}) and the molecular mass of benzyl alcohol (108 gmol^{-1}), as shown in Equation 3.2, where *I* is the ratio of [LA]:[I]:[BnOH]. Benzyl alcohol is expected to be present as the end group of the polymer if the reaction proceeds *via* a coordination-insertion mechanism, thus important to determine the mechanism of polymerisation.

Equation 3.2. Prediction of number average molecular weight.

$$M_n = (conversion \times 144 \times I) + 108$$

The term "initiator" is frequently used to describe the active metal species involved in a living polymerisation and this usage is widely supported by the scientific literature.[26–30] However, it is important to note that this term does not fully encapsulate the role of the active species during polymerisation, which also facilitates propagation. For immortal polymerisations, the term pre-catalyst may be used to recognise the reduction of active species concentration. The addition of BnOH as a co-initiator is included to generate the necessary alkoxide initiator *in situ*, as the alkoxide is more efficient at insertion into the carbonyl bond of the lactide than an aluminium-alkyl, as frequently reported in scientific literature.[8,11,13,31]

Table 3.3. Polymerisation data for *rac*-LA with aluminium complexes in toluene at 80 °C.

Entry	Initiator	[LA]:[I]:[BnOH]	Time (h)	Conv. (%)[a]	$M_{n\ theo}$ (gmol^{-1})	M_n (gmol^{-1})[b]	$Đ$ [b]	P_r[c]
1	Al(**1**)Me	100:1:1	24	93	13350	5450	1.74	0.49
2		200:1:1	24	88	25450	7250	1.85	0.51
3	Al(**2**)Me	100:1:1	2	12	1850	-	-	0.52
4		100:1:1	24	92	13350	8500	1.79	0.53
5		200:1:1	24	90	26000	17550	1.65	0.50
6	Al_2(**3**)Me_2	100:1:2	2	20	1450	-	-	-
7		100:1:2	24	97	7000	9150	1.14	0.52
8		100:1:1	24	95	13700	11050	1.33	0.59
9		200:1:2	24	86	12400	4750	1.18	0.53
10		400:1:2	24	11	3150	1000	1.18	0.54

[a] As determined *via* ^{1}H NMR, [b] Determined from GPC (in THF) referenced to polystyrene standards. It is noted that a Mark-Houwink correction is not required as triple detection was used; [c] P_r is the probability of heterotactic enchainment, determined *via* homonuclear decoupled ^{1}H NMR. Theoretical molecular weight calculated from conversion {[M]:[I]} × (Conv. × 144.13) + 108.14 (rounded to the nearest 50).

None of the initiators trialled in Table 3.3 imparted any stereoselectivity on polymer products. In all cases, atactic PLA was produced, with P_r values between 0.49 and 0.59. GPC

analysis showed some control over the polymerisation, with reasonably narrow dispersities when Al_2(**3**)Me_2 was used as the initiator with 2 eq. of BnOH added to the polymerisation. At a 200:1:2 loading (entry 9), a much lower molecular weight was observed by GPC than predicted, although *Đ* remained narrow (1.18). With 1 eq. (entry 8), a slightly broader dispersity was observed (*Đ* = 1.33) and a much lower molecular weight than predicted. The -Me and -H complexes achieved poor control over molecular weight and dispersity, with much lower weights than anticipated, and broad *Đ* (1.65-1.85).

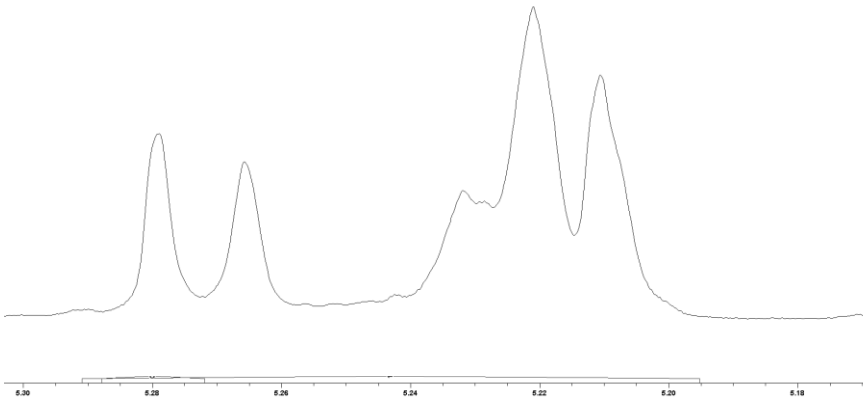

Figure 3.11. Homonuclear decoupled NMR spectrum ($CDCl_3$, 400 MHz) showing the methine region of PLA produced with Al(**2**)Me from Table 3.3, entry 4 ([LA]:[I]:[BnOH] = 100:1:1, 80 °C, toluene, 24 h).

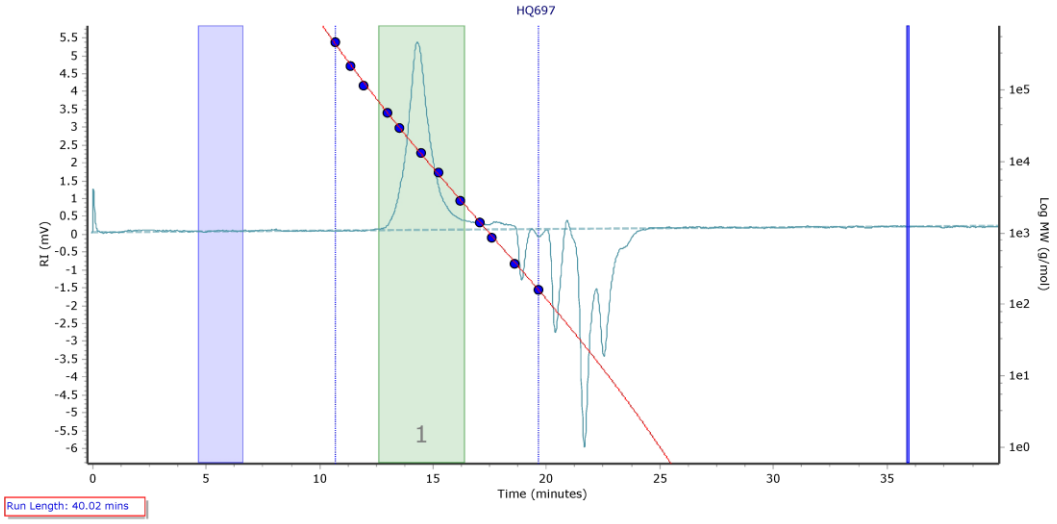

Figure 3.12. GPC chromatograph for polymer sample produced using Al_2(**3**)Me_4 from entry 8, Table 3.3 ([LA]:[I]:[BnOH] = 100:1:1, 80 °C, toluene, 24 h).

The MALDI-ToF spectrum of polymer produced from Table 3.3 entry 9 is given in Figure 3.13. There is a single, symmetrical series with repeat unit between major peaks of 144.1 $gmol^{-1}$, confirming no transesterification has occurred during polymerisation. There is good agreement between the molecular weight value obtained *via* GPC and from MALDI-ToF. The peak at 4714.5 m/z corresponds to the mass of a polymer chain featuring 32 lactide

units with -H and -OBn end groups. This indicates that the polymerisation proceeds *via* the expected coordination-insertion mechanism.

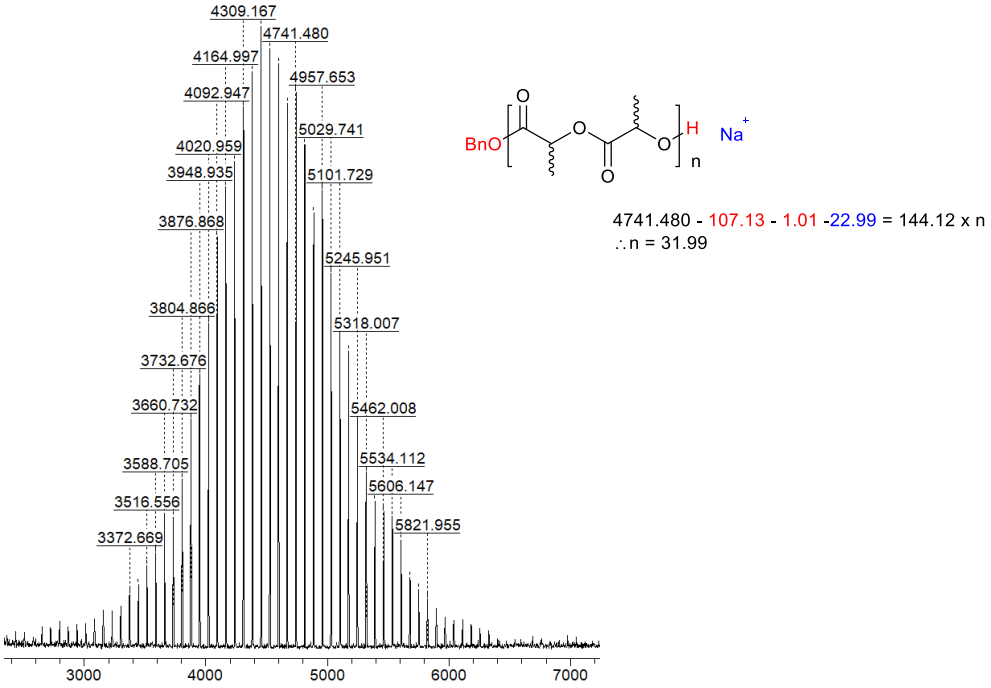

Figure 3.13. MALDI-ToF spectrum of PLA produced using Al_2(**3**)Me_2 ([LA]:[I]:[BnOH] = 200:1:2, 80 °C, toluene, Table 3.3, entry 9).

Little evidence for cooperative behaviour between aluminium centres in Al_2(**3**)Me_2 complex was observed, and 24 h was required for good conversion of monomer in toluene at 80 °C, as per the monomeric species. It was therefore decided to investigate other ligands which could potentially facilitate the synthesis of dinuclear aluminium complexes.

3.3 Synthesis of 1,8-diaminonaphthalene ligands and complexes

In work previously carried out by Jones *et al.,* salen ligands with 1,5-naphthalene backbones were complexed to two equivalents of aluminium to form dinuclear complexes, which were then trialled for the ring-opening polymerisation of lactide (Figure 3.14).[32] These initiators exhibited no stereoselectivity for this process, but were highly active, with near full conversion reached in 2 hours at 80 °C in toluene, producing polymers of predictable molecular weights and narrow dispersities. In a comparative study, the monomeric species were also prepared and investigated for ROP of *rac*-LA. These complexes have the same steric and electronic effects around the aluminium centres as the dinuclear complexes, facilitating an investigation into possible cooperativity between aluminium centres. Due to the high rigidity of the naphthalene backbone, any cooperativity would be intramolecular in nature due to the separation between the 1 and 5 positions.

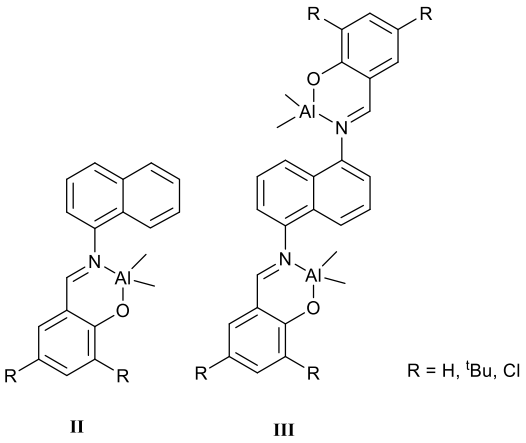

Figure 3.14. Mononuclear and dinuclear aluminium complexes previously prepared by Jones *et al.*[32]

This work attempted to prepare similar aluminium Schiff-base complexes with a 1,8-substituted naphthalene backbone. Only the ^{t}Bu ligand, **4**H_2, was successfully prepared *via* an imine condensation between 1,8-diaminonaphthalene and a substituted salicylaldehyde with a few drops of catalytic formic acid as reported by Clarkson *et al*. (Scheme 3.2).[33] Formation of the ligand (36 % yield) was confirmed by ^{1}H and ^{13}C{^{1}H} NMR spectroscopy. Attempts to prepare the unsubstituted analogue were fruitless, despite following literature procedures.[34] The methyl analogue remains unreported.

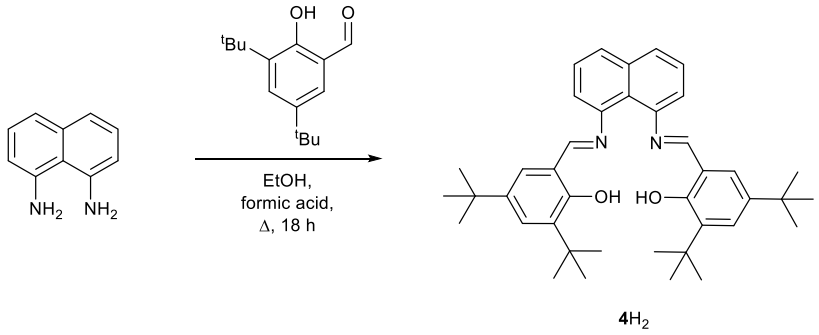

Scheme 3.2. Synthesis of Schiff base ligand **4**H_2, containing a 1,8-naphthalene backbone

An attempted complexation of this ligand with Zr(O^{i}Pr)$_4$(HO^{i}Pr) in toluene yielded square yellow crystals suitable for X-ray crystallography. These were not the expected Zr(IV) complex but uncoordinated ligand, as shown in Figure 3.15 and bond lengths and angles are given in Table 3.4. No complex with zirconium was successfully isolated with this ligand. It is possible that the binding cavity is not large enough to facilitate binding to second row transition metals.

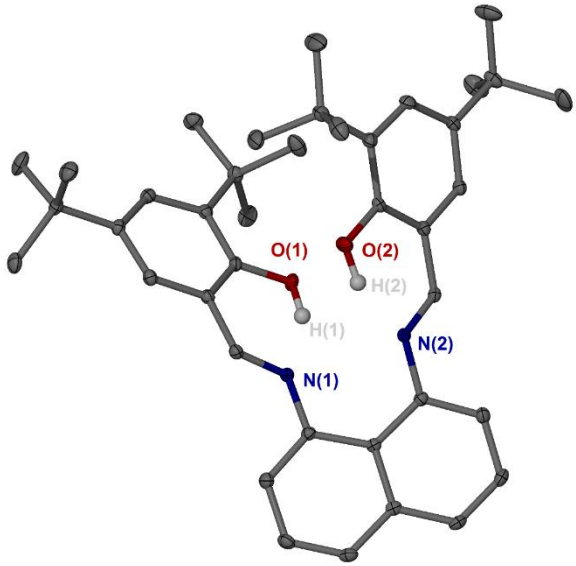

Figure 3.15.Solid-state structure of **4**H_2. Ellipsoids are shown at the 30% probability level. Two molecules of toluene and hydrogen atoms have been removed for clarity. The methyl groups of one ^{t}Bu are disordered over two positions – only one is shown.

Complexation of this ligand to aluminium by reaction with equimolar quantities of trimethyaluminium in toluene resulted in a bright yellow precipitate which was gently heated back into solution and allowed to recrystallise. The product here was not the anticipated 1:1 complex but a dinuclear complex, where two aluminium centres coordinate to one ligand. Al_2(**4**)Me_2 was isolated in 45 % yield. The solid-state structure of Al_2(**4**)Me_2 is given in Figure 3.16, and selected bond angles (°) and lengths (Å) are given in Table 3.4.

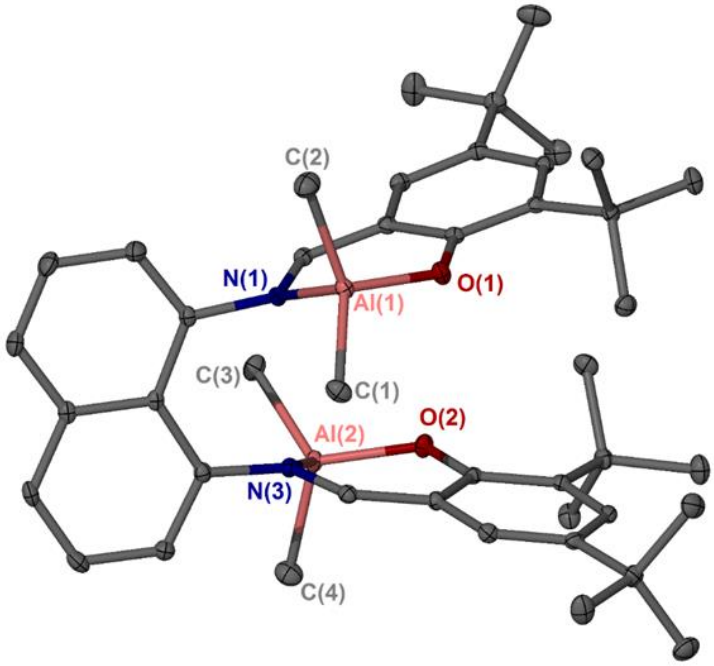

Figure 3.16. Solid-state crystal structure for Al_2(**4**)Me_2. Ellipsoids are shown at the 30% probability level. Hydrogen atoms have been omitted for clarity. The crystal was twinned about the 1 -1 0 lattice direction at *ca*. 43%.

An interesting feature of this structure is that the two aluminium centres orient themselves on either side of the aromatic naphthyl plane, giving an Al(1)-Al(2) distance of roughly 5.4 Å. This is presumably necessary to minimise steric clashes between the bulky ^{t}Bu substituents. A dinuclear complex has been previously reported by Jones *et al.,* **III**, which has a different substitution of the naphthalene backbone and has been included here for comparison (Figure 3.17). In this dinuclear example the Al(1)···Al(2) distance is *ca.* 9.0 Å.

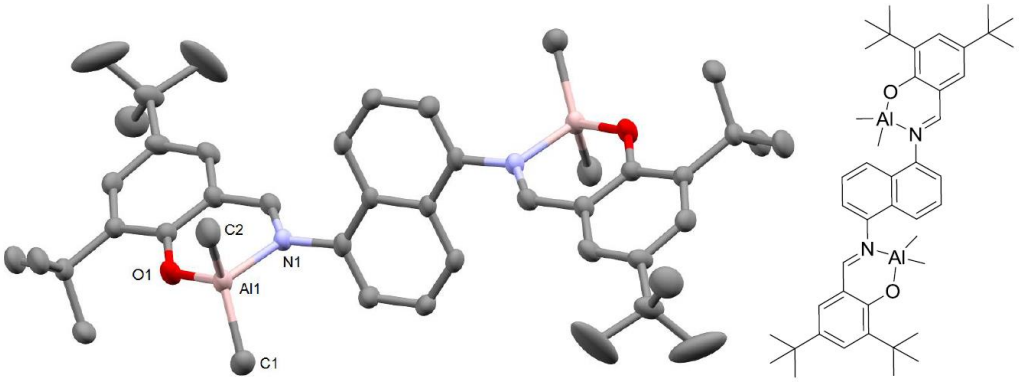

III

Figure 3.17. Solid-state structure for 1,5-diaminonaphthalene aluminium complex, **III**. Reproduced with permission, copyright University of Bath (2017).[35]

Tau values (τ_4 for four-coordinate structures) were calculated using Equation 3.3, as derived by Yang *et al*., where α and β are the two largest coordination angles.[36] For a perfectly tetrahedral geometry, τ_4 = 1, while τ_4 = 0 corresponds to a square planar geometry.

Equation 3.3. Degree of tetrahedrality[36]

$$\tau_4 = \frac{360 - (\alpha + \beta)}{141}$$

In both structures the aluminium has slightly distorted tetrahedral geometry {(τ_4 = 0.94 for Al_2(**4**)Me_2, τ_4 = 0.90 for **III**}, which is exemplified by the bond angles for N(1)-Al(1)-C(1) having bond angles slightly larger than the idea of 109°, with 112.99(9)° and 111.08(3) for **III**. Significant distortion is observed in both examples for the N(1)-Al(1)-O(1) angles, which are 93.38(8)° for Al_2(**4**)Me_2 and 93.66(8)° for **III**. This appears to be a result of the rigidity of the ligand effecting the steric environment. The bond lengths are in close agreement between the two structures. This, along with the close τ_4 values, allows us to assume these two complexes have aluminium centres in approximately identical steric and electronic environments. Any difference in polymerisation control should therefore be a result of the proximity of the aluminium centres, allowing for investigation into potential cooperative enhancement.

Recently, a bimetallic aluminium complex bearing a *syn*-anthracene backbone was reported, along with its *anti*- counterpart (Figure 3.18).[37] The authors in this study report the complexes as being active for the ROP of *rac*-LA but do not give any indication of tacticities of polymer products. However, they describe the immortal polymerisation observed with the *syn*- complex but not the *anti*- as arising from the close distance possible between aluminium centres (measured by X-ray crystallography as 6.665 Å), which is not possible in the *anti*- complex.

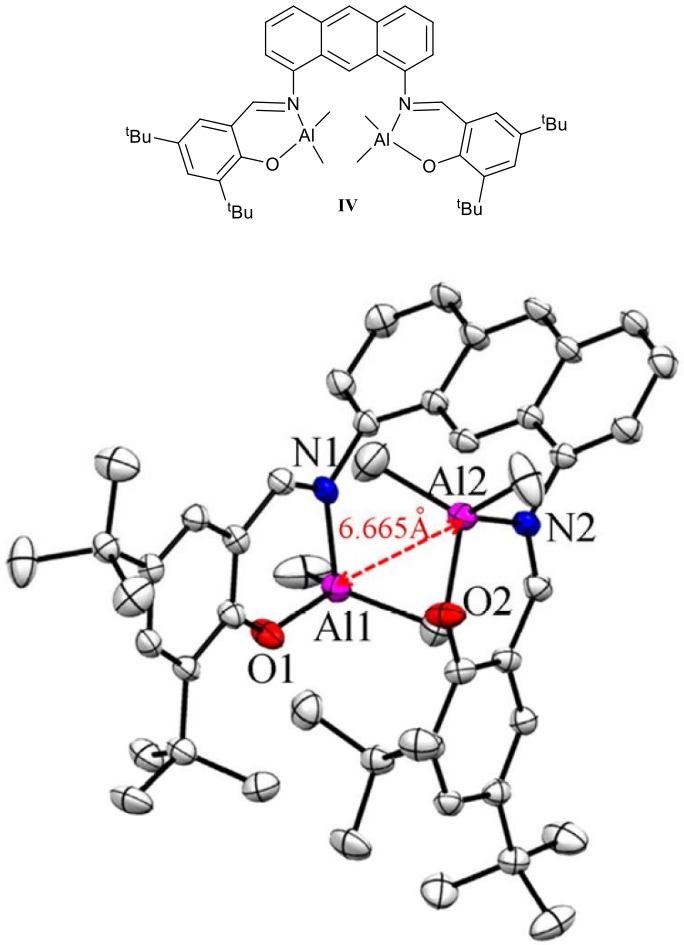

Figure 3.18. Dialuminium complex reported with a *syn*-anthracene backbone (**IV**). Solid-state structure has ellipsoids shown at 50% probability level. Hydrogen atoms omitted for clarity. Reproduced from Shi *et al.* with permission, Springer Nature (2018).[37]

Table 3.4. Selected bond angles (°) and lengths (Å) for Al_2(**4**)Me_2 and literature compounds **III** and **IV** for comparison

	Al_2(**4**)Me_2	**III**	**IV**
Al(1)-O(1)	1.773(15)	1.774(2)	1.768(2)
Al(1)-N(1)	1.975(2)	1.960(3)	1.970(3)
Al(1)-C(1)	1.962(2)	1.952(3)	1.944(4)
Al(1)-C(2)	1.962(2)	1.955(3)	1.768(2)
N(1)-Al(1)-O(1)	93.38(8)	93.66(8)	93.94(10)
N(1)-Al(1)-C(1)	112.99(9)	111.08(11)	110.88(16)
O(1)-Al(1)-C(1)	115.07(9)	110.63(11)	107.96(15)
O(1)-Al(1)-C(2)	112.18(10)	113.37(11)	112.66(18)
Al(1)···Al(2)	5.358	8.968	6.665
τ_4	0.94	0.90	0.97

The solid-state structure is retained in solution, as evidenced by the ^{1}H NMR spectrum of Al_2(**4**)Me_2 (Figure 3.19). There are two discrete Al-Me resonances at -0.32 ppm and -0.37 ppm, each with an integration of 6 protons, showing the chemical inequivalence of the Al-Me bonds. The complex was also characterised by elemental analysis, with the resulting compositional values in close agreement with calculated values.

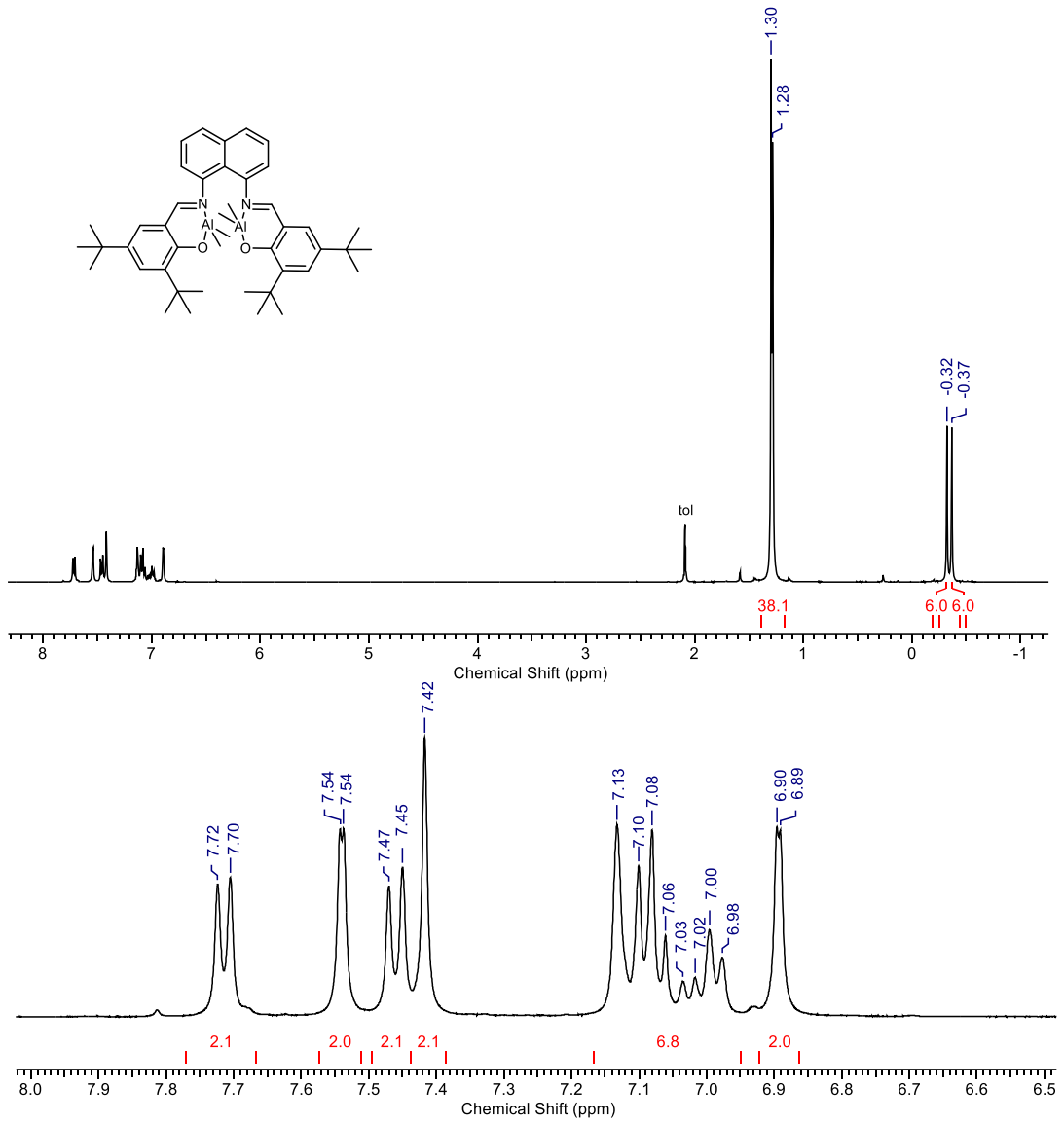

Figure 3.19. NMR spectrum of Al_2(**4**)Me_2 ($C_6D_5CD_3$, 400 MHz) with expansion of aromatic region (below)

It is interesting to note that a dinuclear complex was always isolated with this ligand, regardless of stoichiometry or conditions of complexation. A mononuclear aluminium complex of this ligand has been previously reported by Gibson *et al.* (Figure 3.20) in a study of substituent effect in aluminium salen complexes for ROP of lactide.[11] They too were also only able to synthesise the ^{t}Bu ligand. The complex they reported was moderately isoselective for ROP of *rac*-LA, producing PLA with P_m = 0.72 and $Đ$ = 1.14. In a kinetic study, they reported a modest k_{app} value of 7.84 x 10^{-4} s^{-1} at 70 °C in toluene.

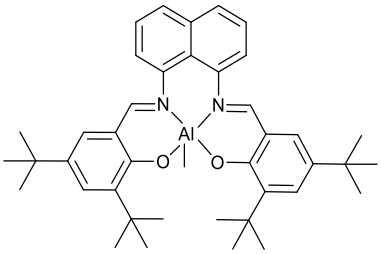

Figure 3.20. Monomeric aluminium complex reported by Gibson *et al.*[11]

For **III** the Al(1)···Al(2) distance is *ca.* 8.968 Å, far above the reported threshold for cooperativity of *ca.* 3.0 Å.[15] DFT calculations performed for Al_2(**4**)Me_2 in collaboration with Dr. Antoine Buchard indicated that if free rotation about the N_{imine}-C-C_{naphth} sp^3 hybridised bond then this distance could possibly reduce to around 7.0 Å. However, for the 1,8-naphthalene complex the same rotation calculations reduce the Al···Al distance to *ca.* 3.5 Å, much closer to reported distances for cooperativity. However, DFT calculations show that they are unlikely to get closer in proximity than 4.0 Å under the polymerisation conditions. A graph of the energy cost for rotation to bring the aluminium centres closer together is shown in Figure 3.21. This distance is significantly shorter than the distance seen in the 1,5 system and should determine if an Al···Al cooperative effect is possible with this system.

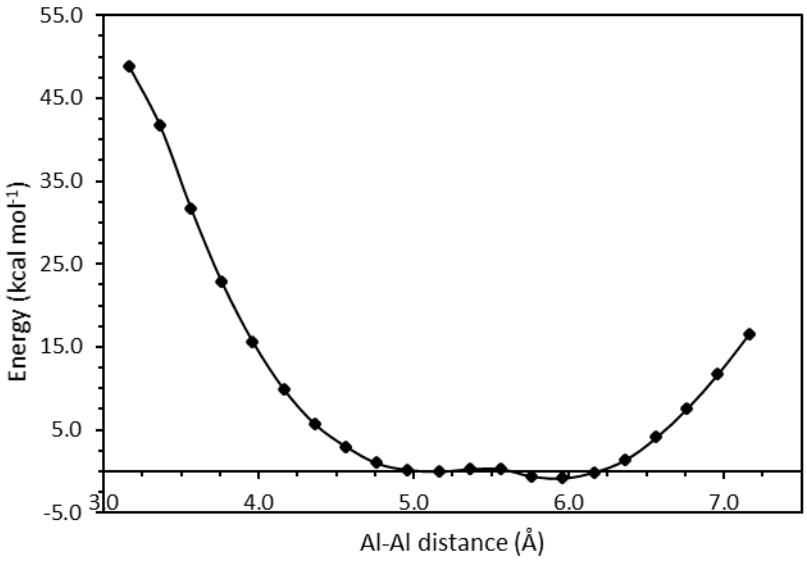

Figure 3.21. DFT calculated energy associated with rotation to reduce the Al···Al distance. DFT calculations performed by Dr. Antoine Buchard at the M06/6-31+g(d)/toluene/298K level of theory

Complexation with two equivalents of dimethylzinc was also attempted in toluene endeavouring to prepare a dinuclear zinc complex analogous to Al_2(**4**)Me_2. Over half an hour the yellow turbid solution gradually became clear and deep orange in colour. This was

stirred for a further hour and a half at room temperature before removing solvent and recrystallisation from hexane/toluene. Crystals suitable for X-ray crystallography were grown, and the solid-state structure obtained is shown in Figure 3.22, and selected bond lengths (Å) and angles (°) are given in Table 3.5. The complex was found to be a dimer, $Zn_2(\mathbf{4})_2$, and isolated in 65 % yield.

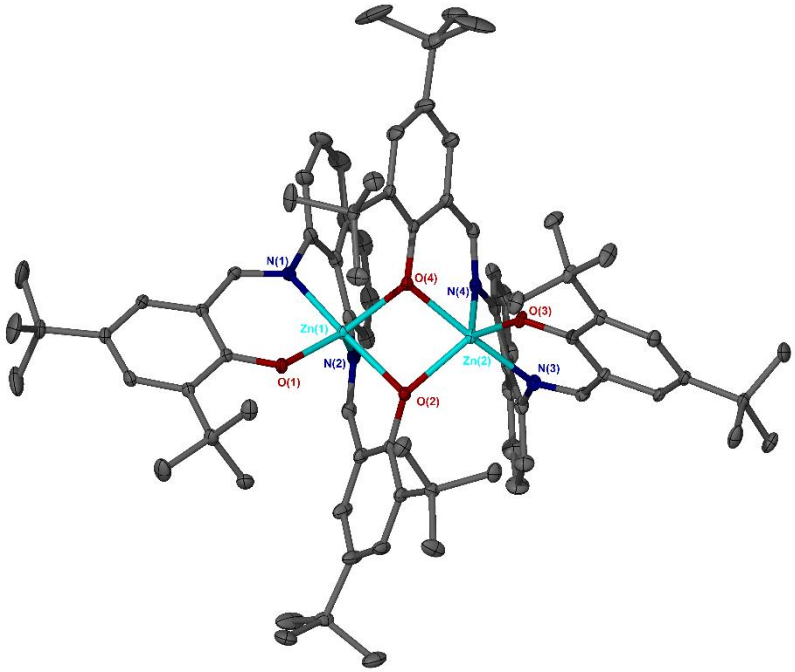

Figure 3.22. Solid-state structure of $Zn_2(\mathbf{4})_2$. Ellipsoids are shown at the 30% probability level and all hydrogen atoms and disordered solvent (toluene/hexane) have been removed for clarity.

The zinc dimer, $Zn_2(\mathbf{4})_2$, was found to crystallise in the triclinic space group *P*-1, and both zinc centres are 5-coordinate. One phenoxy moiety from each ligand bridges between the two zinc centres, forming a Zn-O-Zn linkage. Both zinc centres are coordinated to three oxygen atoms and two nitrogen atoms. This gives a fully coordinated complex with no classical initiating group for polymerisation, somewhat reminiscent of the Mg structures discussed in the previous chapter. Zinc salophen complexes have been reported with similar structures, although not applied for ROP of lactide (Figure 3.23).[38]

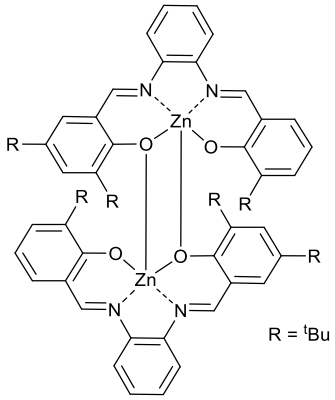

V

Figure 3.23. Structure of dinuclear Zn(salophen) complex, **V**[38]

In this complex, the zinc centres have τ_5 = 0.66, which is significantly distorted away from the ideal trigonal bipyramidal value of τ_5 = 1.0, as evidenced from the bond angles seen in Table 3.5. where all angles are distorted to an extent from the ideal 90/120/180°. The angle between O(2)-Zn(1)-N(1) in the axial positions is 165.33(8)°, more acute than the ideal 180°, as is the angle between axial and equatorial positioned nitrogen atoms N(1)-Zn(1)-N(2), at 82.39(9)°. The angle between equatorial positions are roughly 120° - 120.58(8)°, 125.59(7)° - although the angle between N(2)-Zn(1)-O(4) is again more acute at 113.25(8)°. The coordination about Zn(II) is similar, with the exception of O(1)-Zn(1)-N(2), which is more acute in Zn_2(**4**)$_2$ (120.58(8)° *vs* 133.34(5)°) and O(1)-Zn(1)-O(4), which is more acute in **V** (125.59(7)° *vs* 113.01(5)°). This structure has a degree of trigonality, τ_5 = 0.83, closer to a trigonal bipyramidal environment than Zn_2(**4**)$_2$. Presumably this distortion in Zn_2(**4**)$_2$ arises from the extreme rigidity of the naphthalene backbone.

Table 3.5. Selected bond angles (°) and lengths (Å) for $Zn_2(\mathbf{4})_2$ and Zn(salphen) complex, **V** [38]

	$Zn_2(\mathbf{4})_2$	**V**
Zn(1)-O(1)	1.9428(17)	1.9246(11)
Zn(1)-O(2)	2.0600(17)	2.0412(11)
Zn(1)-O(4)	2.0084(17)	1.9953(12)
Zn(1)-N(1)	2.029(2)	2.0499(12)
Zn(1)-N(2)	2.138(2)	2.0735(12)
Zn(1)-Zn(2)	2.9969(10)	3.0292(3)
O(1)-Zn(1)-N(1)	91.97(8)	90.97(5)
O(1)-Zn(1)-N(2)	120.58(8)	133.34(5)
O(1)-Zn(1)-O(2)	98.60(7)	97.75(5)
O(1)-Zn(1)-O(4)	125.59(7)	113.01(5)
O(2)-Zn(1)-O(4)	79.46(7)	82.75(5)
O(2)-Zn(1)-N(2)	83.48(8)	85.29(5
N(1)-Zn(1)-O(2)	165.33(8)	163.84(5)
N(1)-Zn(1)-O(4)	102.60(8)	106.38(5)
N(2)-Zn(1)-O(4)	113.25(8)	113.56(5)
N(1)-Zn(1)-N(2)	82.39(9)	78.85(5)
τ_4	0.49	0.46

The ^{1}H NMR spectrum for this complex in C_6D_6 is shown in Figure 3.24. The solid-state structure is confirmed in solution, with no dissociation is observed. Due to the coordination geometry of the ligand having one bridging phenoxide and one non-bridging, a lack of symmetry is now observed in the spectrum compared to that of the free ligand. There are now four resonances for the ^{t}Bu groups, which are all inequivalent, rather than two seen in the uncoordinated ligand. The aryl protons also now appear as two sets of doublets. Addition of BnOH made no difference to the ^{1}H NMR spectrum, indicating the structure does not dissociate in solution.

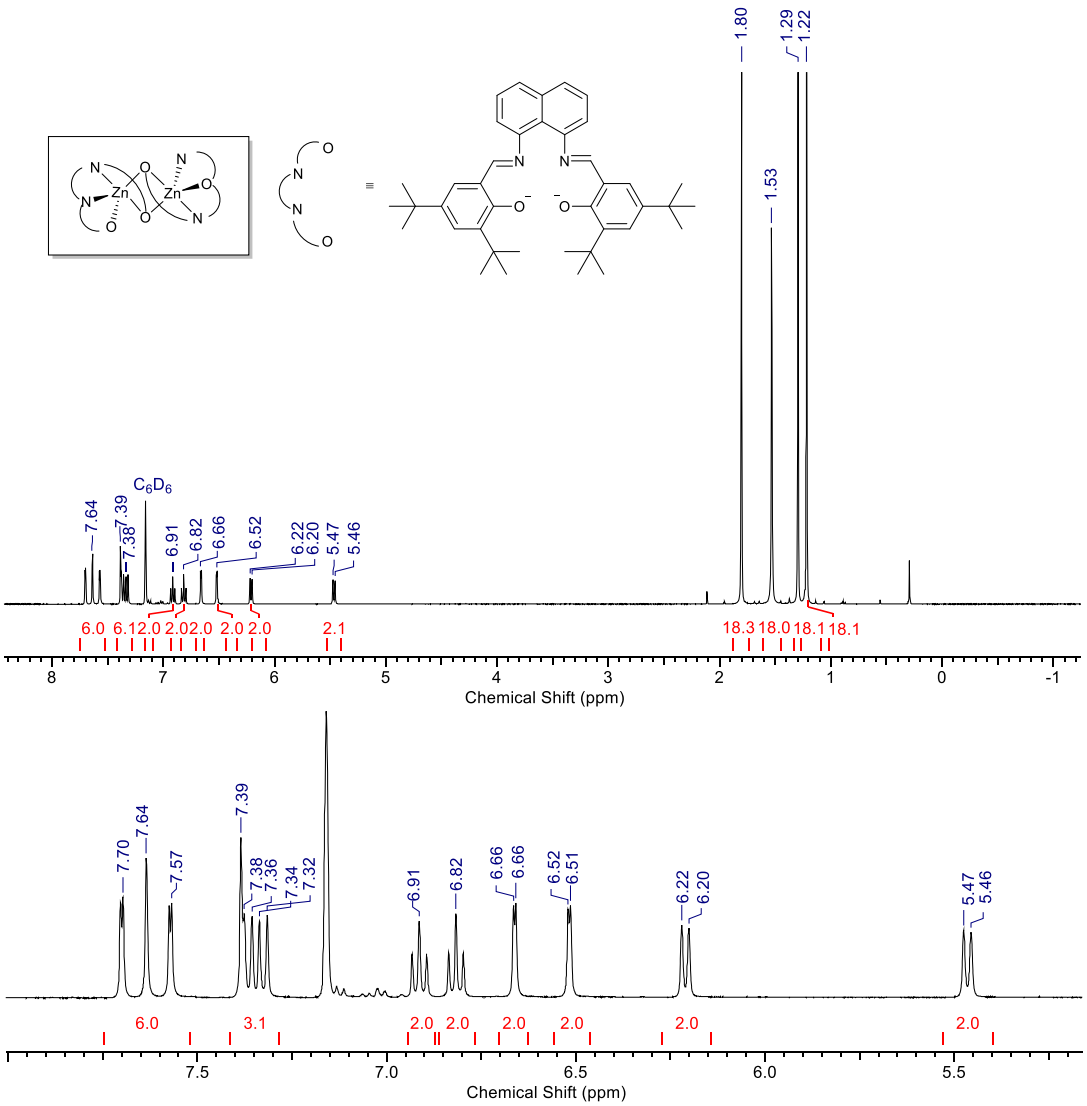

Figure 3.24. ^{1}H NMR spectrum for Zn_2(**4**)$_2$ (400 MHz, C_6D_6,), expanded aromatic section is shown below

3.3.1 Polymerisation results

Data for the solution polymerisation of *rac*-LA with the 1,8-naphthalene complexes Al_2(**4**)Me_2 and Zn_2(**4**)$_2$ is given in Table 3.6, at a [LA]:[I]:[BnOH] loading of 100:1:2 (one equivalent of BnOH per metal centre).

Table 3.6. Polymerisation data for *rac*-LA with 1,8 naphthalene bis(phenolates) Al_2(**4**)Me_2 and Zn_2(**4**)$_2$ in toluene. And data from literature for **II**, **III**[33,] and **IV**[38]. All [LA]:[I]:[BnOH] = 100:1:2 except entry 7.

Entry	Initiator	Temp (°C)	Time (h)	Conv. (%)[a]	$M_{n\ theo}$ (gmol^{-1})	M_n (gmol^{-1})[b]	$Đ$[b]	P_r[c]
1	Al_2(**4**)Me_2	80	2	97	7100	5200	1.16	0.75
2	**II**	80	24	92	13350	16800	1.48	0.56
3	**III**	80	18	91	6650	6550	1.20	0.50
4	**IV**	70	24	94	7000	12000	1.14	-
5	Zn_2(**4**)$_2$	80	2	29*	2200	-	-	-
6	Zn_2(**4**)$_2$	25	24	0	-	-	-	-
7[d]	Zn_2(**4**)$_2$	130	2	0	-	-	-	-

[a]As determined *via* ^{1}H NMR, [b]Determined from GPC (in THF) referenced to polystyrene standards. It is noted that a Mark-Houwink correction not applied as analysis was performed by triple detection. [c]P_r is the probability of heterotactic enchainment, determined via homonuclear decoupled ^{1}H NMR spectroscopy. [d]Solvent free, no BnOH added. Theoretical molecular weight calculated from conversion {100 × (Conv. × 144.13) + 108.14} (rounded to the nearest 50). *Polymer product showed transesterification in NMR.

The polymerisation with Al_2(**4**)Me_2 was initially trialled at 80 °C but stopped after 2 hours when the solution became very viscous, at which time conversion was determined to be 97% by NMR spectroscopy. For the mono-aluminium analogue, **II**, and 1,5-dinuclearcomplex, **III**, reaction times were reported to be much longer for high conversion (18 h and 24 h respectively).[32] Similarly, Shi reported polymerisation times of 24 h for 94% conversion for the *syn*-anthracene complex **IV**.[37]

Zn_2(**4**)$_2$ was not a good initiator for lactide polymerisation. 29% conversion was observed after 2 hours at 80 °C (Table 3.6 entry 5), but the ^{1}H NMR spectrum suggested degradation of the polymer product. No conversion was observed on trialling under melt conditions (Table 3.6, entry 7), and at lower temperatures no conversion was observed at all, so this complex was not pursued.

Polymerisation data for *rac*-LA with the Al_2(**4**)Me_2 initiator at varying temperatures is given in Table 3.7. The complex is active for ROP of lactide even at room temperature, which is somewhat rare for aluminium Schiff base complexes. Excellent control over molecular weight was observed, with narrow dispersities ($Đ$ = 1.16-1.01). The polymer produced at room temperature (Table 3.7, entry 3) was determined *via* HND NMR to have a P_m of 0.82, having a high degree of isotacticity (Figure 3.25). Analysis of the microstructure of the PLA by HND ^{1}H NMR also showed a small contribution from the *sis* tetrad and the *sii*, *iis* and *isi* are approximately 1:1:1, indicating that a chain end control mechanism is operative, which would lead to a stereoblock structure to the PLA.[39] Although a high degree of isotacticity

was observed by NMR, a sample analysed by DSC showed no thermal event, indicating that the stereoselectivity is not significant to produce crystalline domains in the polymer. It is unusual for a L-AlMe$_2$ system to impart tacticity on the polymer product, with most examples in the literature affording PLA of a mostly atactic nature.[15,24,40–42]

Complex Al$_2$(**4**)Me$_2$ was also trialled for the ROP of ε-caprolactone at [ε-CL]:[I]:[BnOH] = 100:1:2 at 80 °C in toluene. High conversion was seen in 20 min, achieving high conversion (99%), although the dispersity was broader than observed with LA (M_n = 11 000, $Đ$ = 1.64).

Table 3.7. Polymerisation data for *rac*-LA with Al$_2$(**4**)Me$_2$ at different temperatures. [LA]:[I]:[BnOH] = 100:1:2

Entry	Temperature	Time (h)	Conv. (%)[a]	$M_{n\ \text{theo}}$ (gmol^{-1})	M_n (gmo^{l-1})[b]	$Đ$[b]	P_m[c]
1	80	2	97	7100	5200	1.16	0.75
2	40	18	99	7250	10450	1.02	0.78
3	25	24	86	7300	7000	1.01	0.82

[a] As determined *via* ^{1}H NMR, [b] Determined from GPC (in THF) referenced to polystyrene standards. It is noted that a Mark-Houwink correction is not applied as analysis was performed by triple detection. [c]*D*etermined *via* homonuclear decoupled ^{1}H NMR spectroscopy. The calculated molecular weights were determined by the following (144 x conversion) + 108 {where 108 is the mass of the end groups (H/OCH$_2$Ph)}

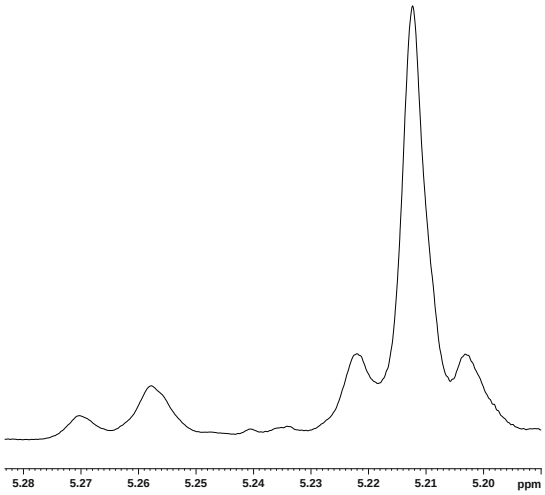

Figure 3.25. ^{1}H homonuclear decoupled NMR (400 MHz, CDCl$_3$) of the methine region of PLA prepared using Al$_2$(**4**)Me$_2$, Table 1.7, Entry 3.

The complex was also trialled with different loadings of *rac*-LA to investigate immortal behaviour (Table 3.8). Generally, molecular weights increased proportionally with [LA], while the dispersity remained reasonably narrow, showing the process to be well controlled with this initiator. When the amount of BnOH added was doubled (Table 3.8, entry 5), a broader dispersity was observed ($Đ$ = 1.45). MALDI-ToF analysis of the polymer produced from this entry is shown in Figure 3.26, where two species are clearly present. Both have spacings between major peaks of 144.1 m/z, as expected for PLA with no transesterification. Series A corresponds to polylactide containing ~8 lactide units, while B

contains ~32 lactide units. The excess benzyl alcohol may be acting as a chain transfer agent in this case.

Table 3.8. Polymerisation data with varying loadings of *rac*-LA. Room temperature, 2 h.

Entry	[LA]:[I]:[BnOH]	Conv. (%)[a]	$M_{n\ theo}$ (gmol^{-1})	M_n (gmo^{l-1})[b]	$Đ$ [b]	P_r [c]
1	50:1:2	91	3400	3300	1.30	0.75
2	100:1:2	97	7100	5200	1.16	0.75
3	200:1:2	92	13350	10450	1.18	0.73
4	400:1:2	96	26650	21650	1.21	0.71
5	100:1:4	98	3650	4550	1.45	0.65

[a] As determined *via* ^{1}H NMR, [b] Determined from GPC (in THF) referenced to polystyrene standards. It is noted that a Mark-Houwink correction is not applied as analysis was performed by triple detection. [c] *D*etermined *via* homonuclear decoupled ^{1}H NMR spectroscopy. The calculated molecular weights were determined by the following (144 x conversion) + 108 {where 108 is the mass of the end groups (H/OCH$_2$Ph)}

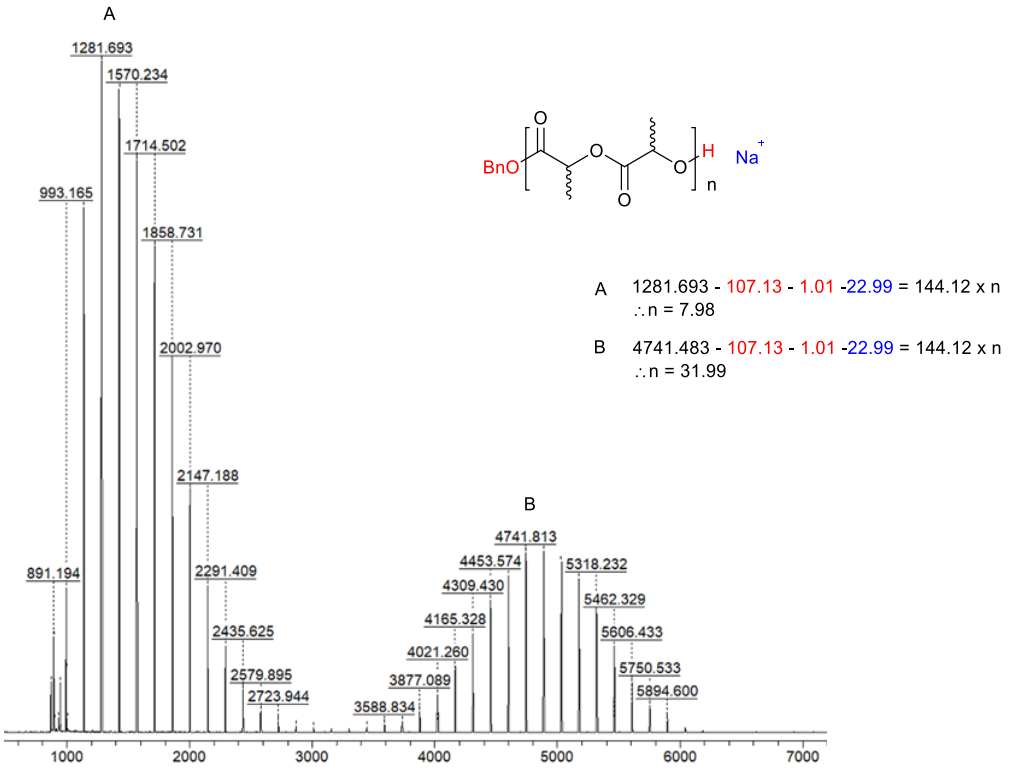

Figure 3.26. MALDI-ToF spectrum of polylactide produced using Al_2(**4**)Me_2. Conditions: [LA]:[I]:[BnOH] = 100:1:4, toluene, 25 °C, 2 h. Table 1.8, entry 5.

The MALDI-ToF spectrum of the polymer from Table 3.8, entry 3 is given in Figure 3.27. There is a single, symmetrical series with a repeat unit of 144.1 m/z. No transesterification of the polymer is apparent. The residual mass is in good agreement with a polylactide sample containing 42 repeat units and end groups of -H and -OBn, indicating that the polymerisation occurred following a coordination-insertion mechanism.

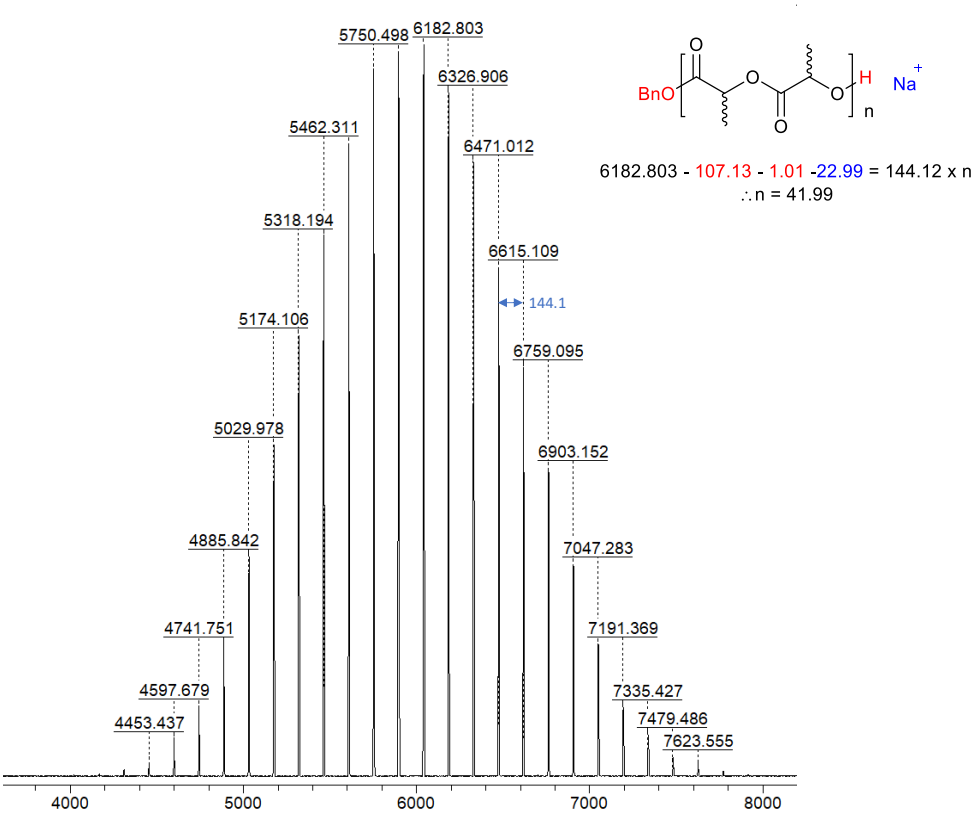

Figure 3.27. MALDI-ToF spectrum of polylactide produced using Al_2(**4**)Me_2 at 200:1:2 Conditions: [LA]:[I]:[BnOH] = 200:1:2, toluene, 25 °C, 2 h. Table 1.8, entry 3.

3.3.2 Polymerisation kinetics

The activity of the dialuminium initiator was evaluated using NMR spectroscopic kinetic studies, performed at 358 K inside a 400 MHz NMR spectrometer to allow for comparison with analogous species **II** and **III**. A graph showing the first order rate plot for *rac*-lactide in solution in toluene-d^8 at a 100:1:2 loading of [LA]:[I]:[BnOH] is given in Figure 3.28. The data was analysed by fitting with a pseudo-first order rate kinetic plot (Figure 3.28). The polymerisation with this complex was observed to be significantly more active than complex **III**, based on the 1,5-naphthalene backbone, having a pseudo first order rate constant, k_{app}, an order of magnitude larger: 33.0 x 10^{-3} min^{-1} *vs* 4.1 x 10^{-3} for **II** and 1.0 x 10^{-3} min^{-1} for **III** at a monomer loading of 100:1:2 (Table 3.9). The kinetics of the *syn*-anthracene complex were not reported.[37]

The kinetics were studied at a fixed concentration of *rac*-LA of 0.58 $moldm^{-3}$. As expected as the concentration of catalyst and co-initiator reduce the apparent first order rate constant reduces, although the slowest rate was observed with the lowest loading of [LA]. This would have the lowest concentration of monomers in solution, so could be diffusion hindered.

The rate constant is determined from the gradient of the slope, which should pass through 0,0 (i.e. no conversion at *t = 0*). The nature of the experiment using an NMR spectrometer requires time increase the temperature gradually to and shim the sample, meaning that some conversion had already occurred in the time taken from preparing the sample to taking the first data point.

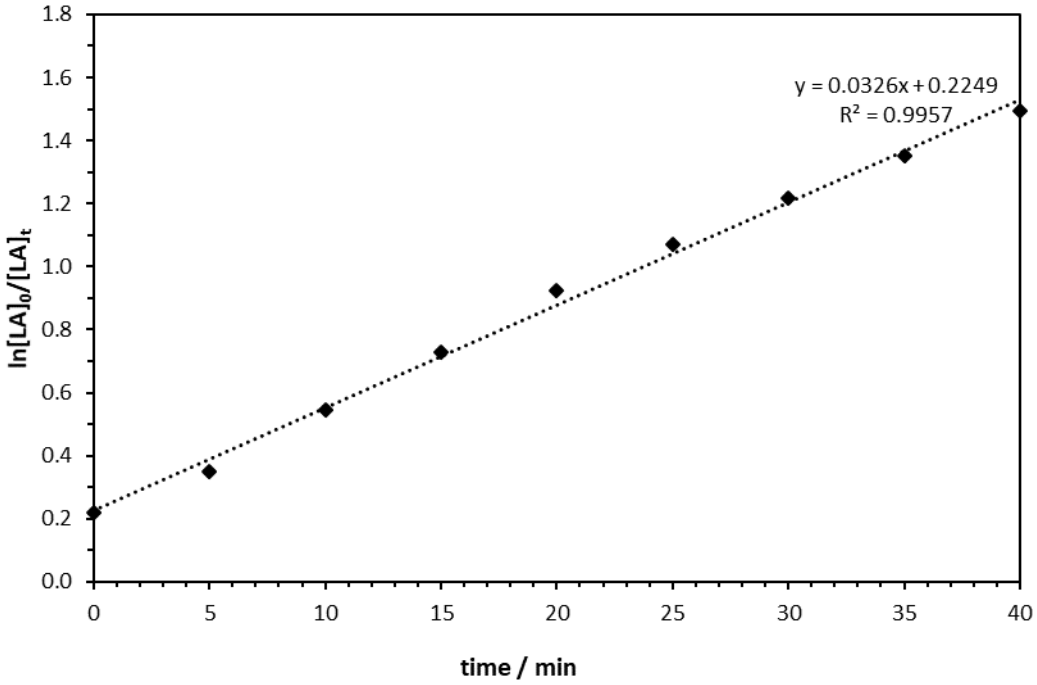

Figure 3.28. Pseudo first-order rate kinetic plot for 100:1:2 (toluene-d^8) at 353 K.

Table 3.9. k_{app} values with different [LA] loadings

Entry	[LA]:[I]:[BnOH]	k_{app} (x 10^{-3} min^{-1})		
		Al_2(**4**)Me_2	**II**	**III**
1	50:1:2	12.7	-	-
2	100:1:2	33.0	4.1	1.0
3	200:1:2	29.1	-	-
4	400:1:2	14.9	-	-

The order with respect to metal centres can be evaluated by taking natural logarithms of both k_{app} and [Al]. When the order with respect to Al_2(**4**)Me_4 was investigated at 100 (200 or 400):1:2 (at constant [LA]) the order was observed to be less than 1 (0.58) with respect to initiator (Figure 3.29). Such non-integer orders are unusual but not uncommon, particularly in dinuclear systems.[43–45]

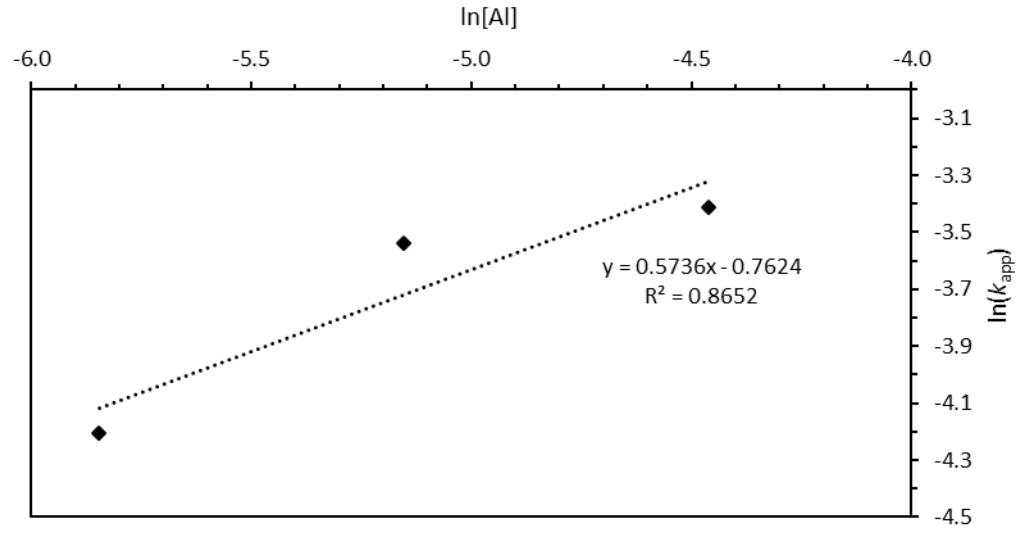

Figure 3.29. Plot of ln(k_{app}) *vs* ln[Al] for Al_2(**4**)Me_4 at 353 K in d^8 toluene with [LA] = 100,200,400.

This system shows much promise in producing isotactic PLA from *rac*-LA under mild conditions. Further investigations into ligand substitution and kinetic behaviour would be beneficial in the future.

3.4 Other ligands and further work

3.4.1 Synthesis of imidazolidine ligands

The success of salen ligands has been partially attributed to their rigidity, which can be difficult to achieve in salan systems. Additionally, different coordination modes have been observed depending on the metal centres and bis(phenolate) ligand backbone employed, leading to different catalytic performances. Attempts were made to further modify some of the ligands discussed in this chapter by reduction to the salan followed by condensation with an aldehyde to form a rigidified imidazolidine ligand, following the scheme shown in Scheme 3.3. Judicial choice of the aldehyde or ketone would allow for investigations into different substituents at this position – for example the use of acetone would give an imidazolidine ring with two methyl groups on the N-C-N carbon atom. Carbene ligands have been extensively investigated in PLA research before as ligands and organocatalysts but neutral ligands are somewhat rarer.[46–49]

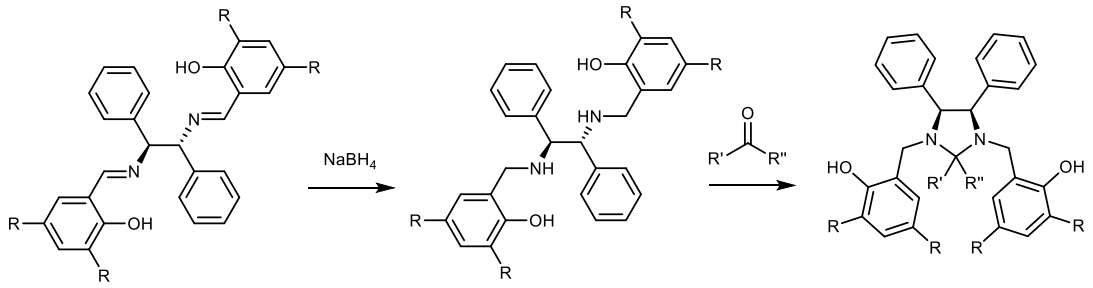

Scheme 3.3. Proposed synthesis of imidazolidine ligands

This process was initially attempted with **3**H_2, firstly by reduction of the Schiff base using sodium borohydride followed by reflux with formaldehyde. A white powder was isolated but was found not to be the desired product. Instead, ^{1}H NMR spectroscopy confirmed this to instead be a benzoxazine-type structure, **5** (Figure 3.30). Analysis by MS showed a peak at *m/z* = 661.4879, which corresponds to an asymmetrical structure where only one benzoxazime is present (*m/z* calc. for $[C_{45}H_{61}N_2O_2]^+$ = 661.4728). It is possible that fragmentation occurred during the MS process, as the ^{1}H NMR spectrum supposrts a symmetrical species. The benzoxazine formation is shown by the presence of four diasterotopic doublets, corresponding to the methylene and benzoxazine protons. Imidazolidine formation has been reported under these conditions for the synthesis of chiral bis(ferrocenyl) ligands, which do not bear phenolic moieties.[50] With these present the formation of a six-membered heterocycle is favoured.

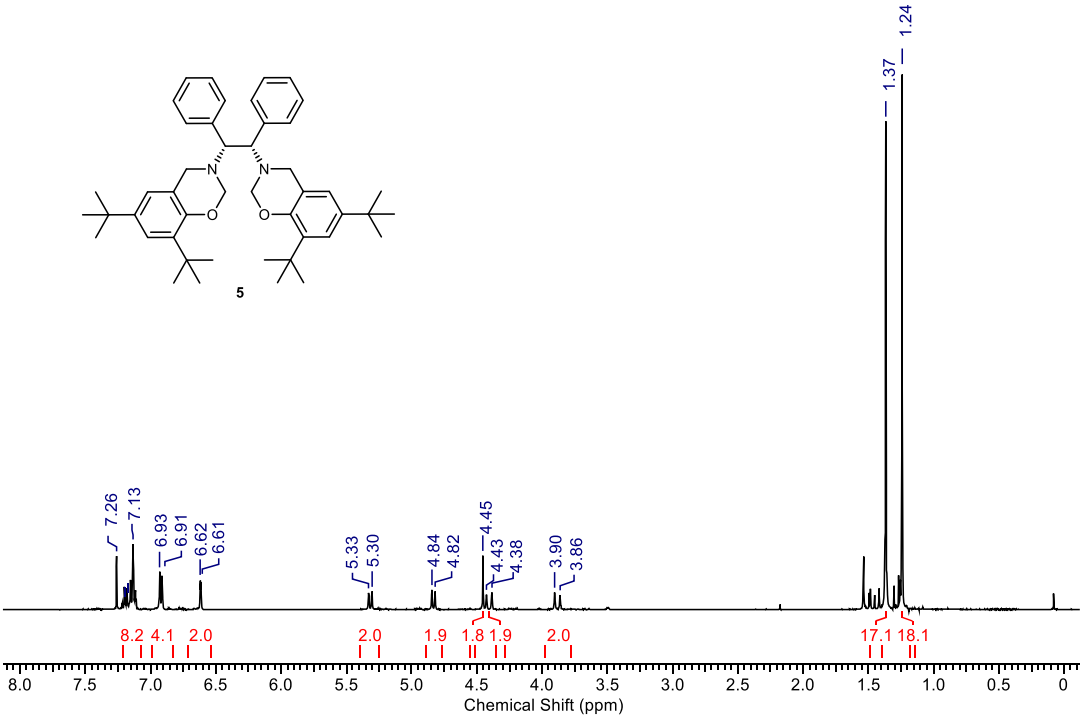

Figure 3.30. ^{1}H NMR spectrum (400 MHz, $CDCl_3$) of benzoxazime **5**

Benzoxazine structures of this type are well-known in the literature and are used in the production of polymers.[51,52] These benzoxazines have also been utilised as a stable surrogate for the putative iminium intermediate of the Mannich condensation. The benzoxazine rings and can be cleaved to form a methylated dimethyltetrahydrosalan ligand as shown in Scheme 3.4. Benzoxazine formation and reduction may be done in a two-step, one-pot process from the Schiff Base, and this method has been utilised previously in work by Jones *et al.* for the preparation of methylated salalen ligands.[24]

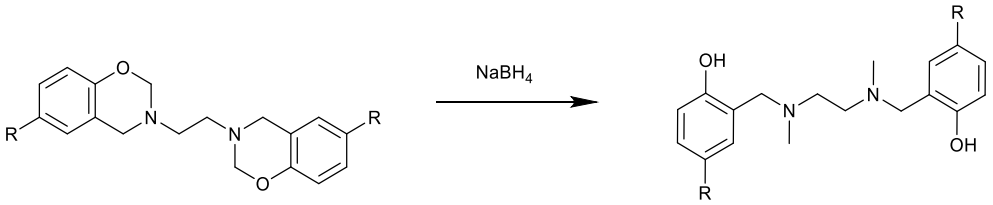

Scheme 3.4. Reduction of benzoxazine to produce *N,N'*-dimethyltetrahydrosalen ligands. Reproduced from Rivera *et al.*[53]

Attempts to form an imidazolidine ligand by refluxing **3**H_2 in acetone were also unsuccessful. This could possibly be due to the scaffold being too sterically demanding to form the imidazolidine heterocycle. Thus, it was decided to investigate more simple ligand backbones with different aldehydes or ketones. For this purpose, a series of Schiff base ligands with simple ethylenediamine backbones were prepared *via* established literature methods,[54] then reduced to the corresponding salan compounds with $NaBH_4$. Refluxing in acetone gave dimethyl compound **6**H_2 in 65% yield, which crystallised from acetone on cooling. A series of phenyl substituted imidazolidine compounds were prepared by condensation with a slight excess (1.2 eq.) of benzaldehyde in EtOH at 50 °C, forming bis(phenolate) imidazolidine ligands **7**-**9**H_2, or salicylaldehyde to yield a tris(phenolate) compound, **10**H_3. In all cases the yield was high (>80%) and products were easily isolated through precipitation from EtOH on cooling, filtration, and washing with copious cold EtOH to remove unreacted aldehyde.

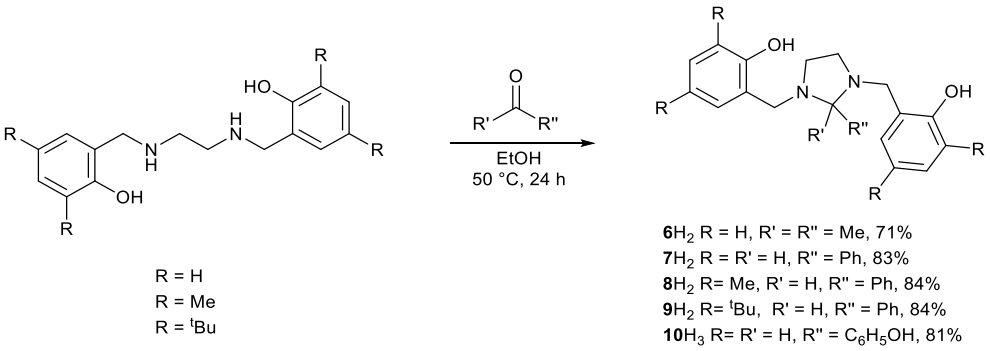

Scheme 3.5. Synthesis of imidazolidine ligands **6**-**10**$H_{2/3}$

These imidazolidine compounds were characterised by NMR spectroscopy and mass spectrometry. Several example spectra are given in Figure 3.31 and Figure 3.32.

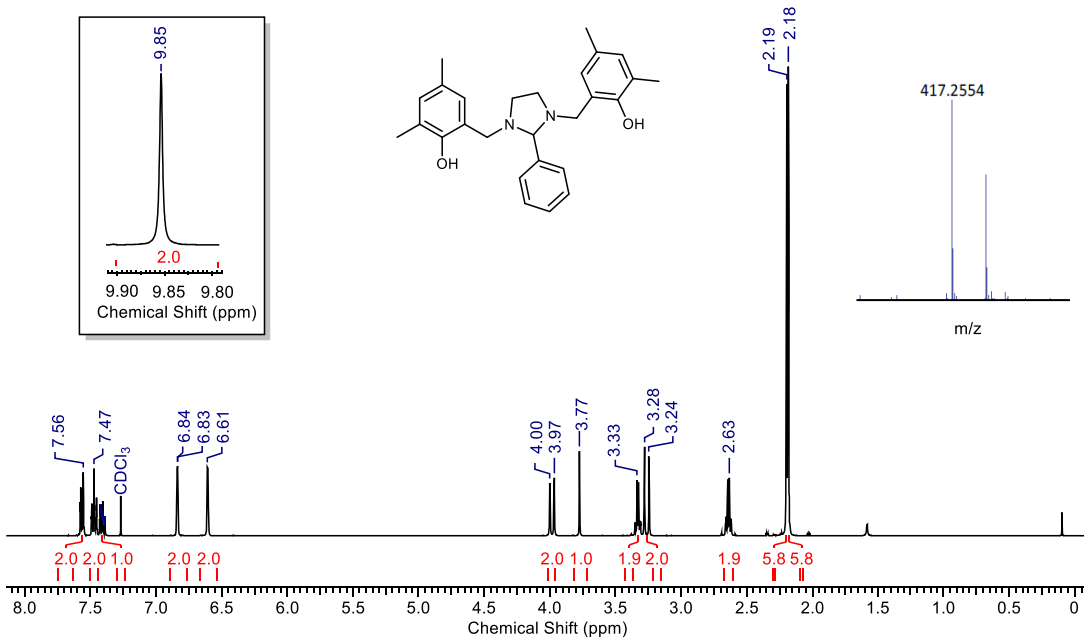

Figure 3.31. ^{1}H NMR spectrum (400 MHz, $CDCl_3$) and mass spectrum of **8**H_2. The labelled peak in the mass spectrum is the protonated compound, smaller peak is the sodiated peak.

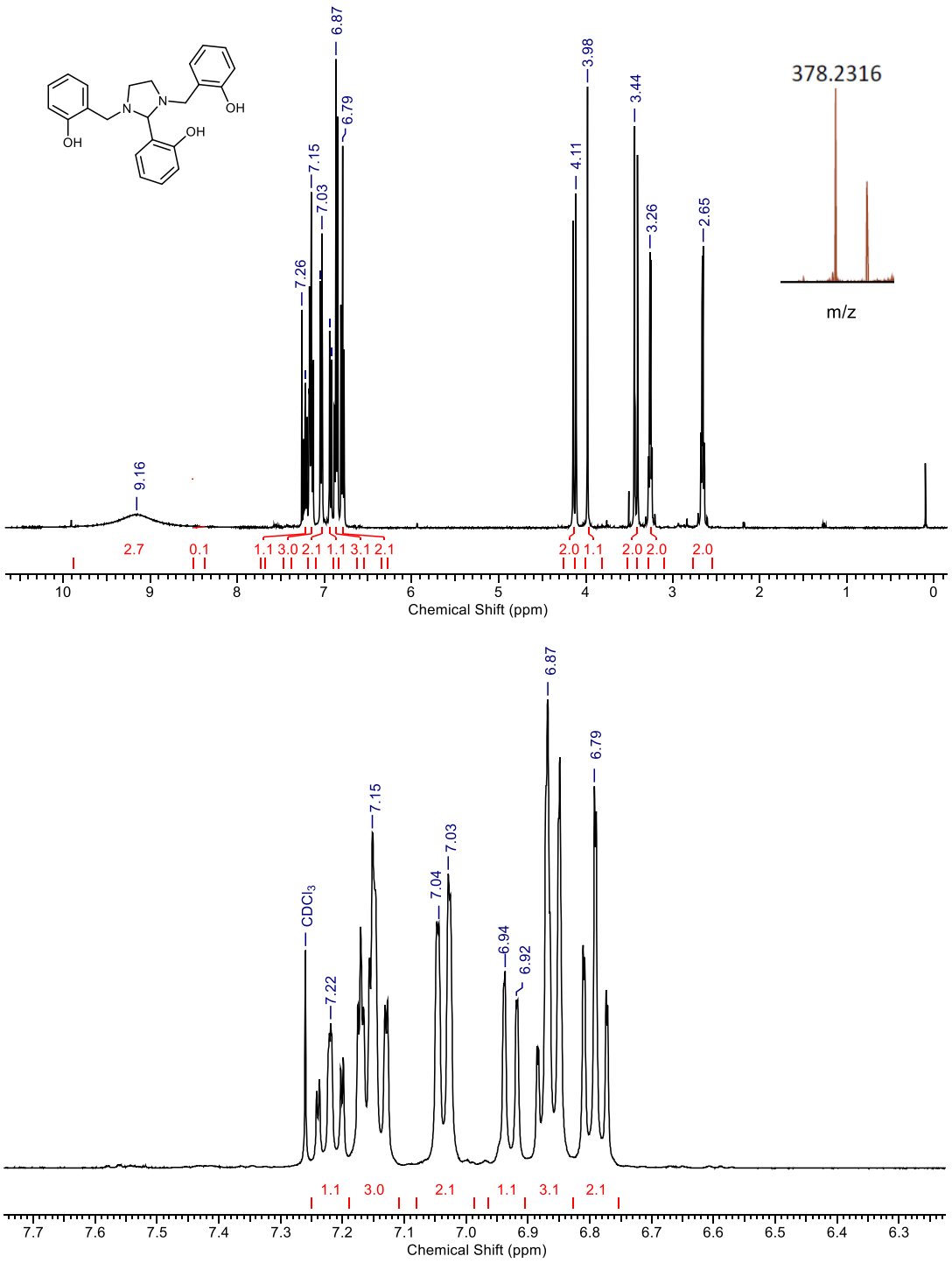

Figure 3.32. ^{1}H NMR spectrum (400 MHz, $CDCl_3$) and mass spectrum (inset) of tris(phenolate) compound **10**H_3. A zoomed in spectrum of the aromatic region is included for clarity. The major peak in the MS is the protonated compound. smaller peak is the sodiated peak

In both spectra, a singlet resonance is observed for the imidazolidine CH proton, at 3.77 ppm and 3.98 ppm for **8**H_2 and **10**H_3 respectively. The rigidity of the imidazolidine "bridged" compound is seen in both cases, with the methylene protons seen as diastereotopic doublets as they are fixed in place, presumably due to hydrogen bonding.

Interestingly, in both cases the ethylenediamine protons are also split into two resonances. In the salen and salan compounds these are observed as a sharp singlet.

The condensation reaction with the salan precursor with a dialdehyde was also performed, refluxing with 0.5 equivalents of terephthaldehyde to yield tetra(phenolate) compounds in high yields (Scheme 3.6). Formation of tetra(phenolate) compounds was confirmed by mass spectrometry and NMR spectroscopy, where a singlet resonance is observed for the terephthalic linker of compound **12**H_4 at 9.76 ppm, and the same locking in position is observed for the methylene protons as in previous examples (Figure 3.33).

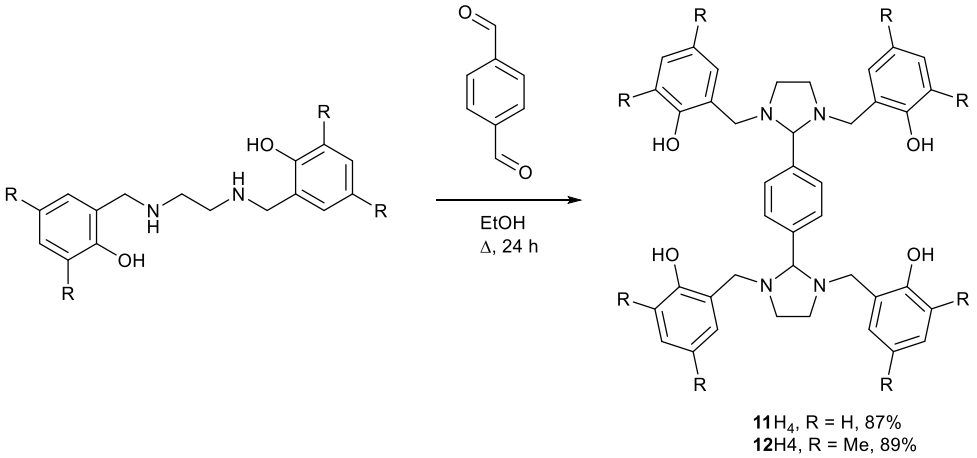

Scheme 3.6 Synthesis of tetra(phenolate) compounds **11**/**12**H_4.

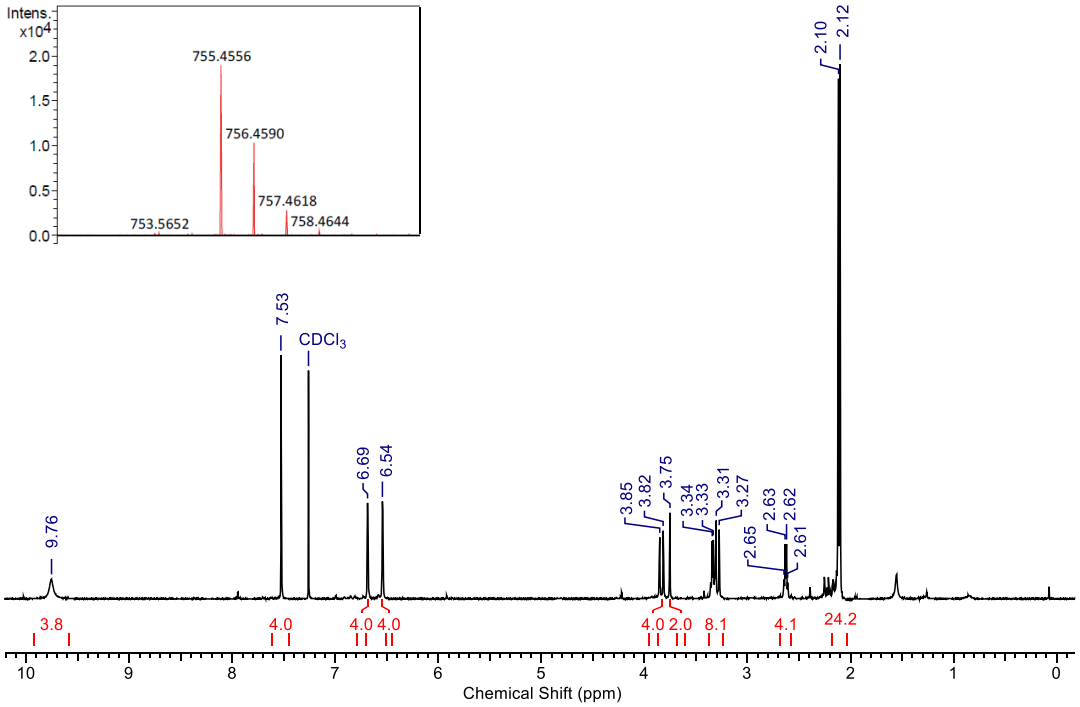

Figure 3.33. ^{1}H NMR (400 MHz, $CDCl_3$) of comound **12**H_4. Mass spectrum given as insert, major peak is the protonated ion.

3.4.2 Complexation of ligands

Due to time constraints, limited complexes of these ligands were prepared and trialled for ROP of *rac*-LA. While the synthesis and purification of the ligands was very simple, the complexation appeared to be somewhat more complicated, with several attempts yielding no isolatable complexes. On complexation of ligand **7**H_2 stoichiometrically with trimethylaluminium in toluene at room temperature, a yellow solution rapidly formed. On removal of solvent a precipitate formed which was heated gently back into solution and left to crystallise overnight at room temperature to afford crystals suitable for X-ray analysis. These were not the expected monomeric structure proposed in Scheme 3.7, whereby the tetradentate ligand would be deprotonated by one equivalent of trimethaluminium to yield an -ONNO- bound structure. Instead an interesting structure formed comprising two ligands and two aluminium centres.

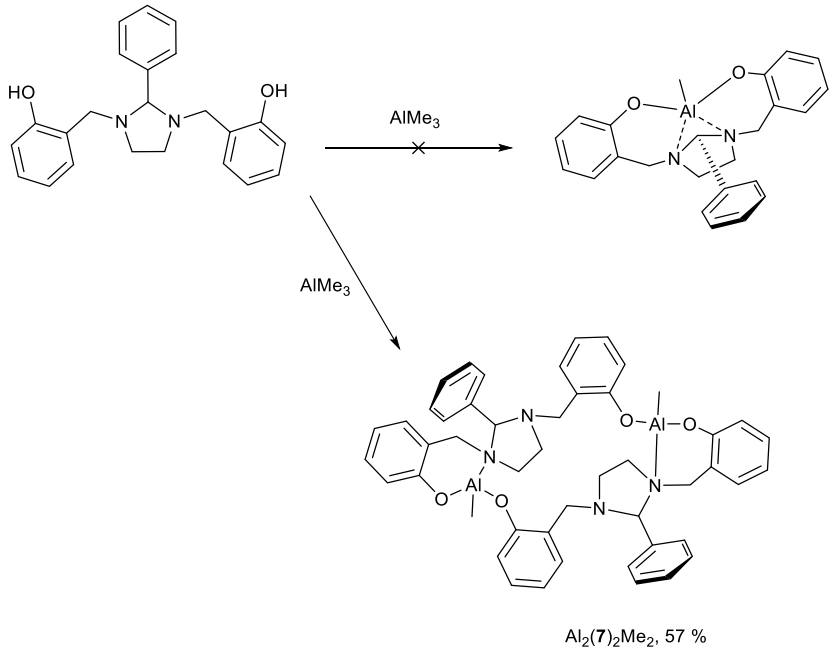

Scheme 3.7. Expected and actual structures on complexation of **7**H_2 to trimethylaluminium in toluene at room temperature.

The solid-state structure of Al_2(**7**)$_2Me_2$ is given in Figure 3.34. Selected bond lengths and angles can be found in Table 3.10. The structure determined from X-ray crystallography was found to be a 2:2 structure, where each ligand is coordinated to two aluminium centres through the phenoxide oxygen. Each aluminium centre is 4-coordinate, have retained one methyl ligand per centre, with slightly distorted tetrahedral geometry around Al (τ_4 = 0.93). There is a plane of symmetry through the molecule, with it crystallising in the orthorhombic space group *Fdd*2. Interestingly, the aluminium centres coordinate with only

one nitrogen atom from each imidazolidine ring, while one remains oriented away in space. The overall effect is an unusual 24-membered metallacycle. Presumably the imidazolidine ring in too inflexible to allow the second nitrogen atom to approach the aluminium centre to coordinate, coupled steric interactions from the pendant phenyl ring.

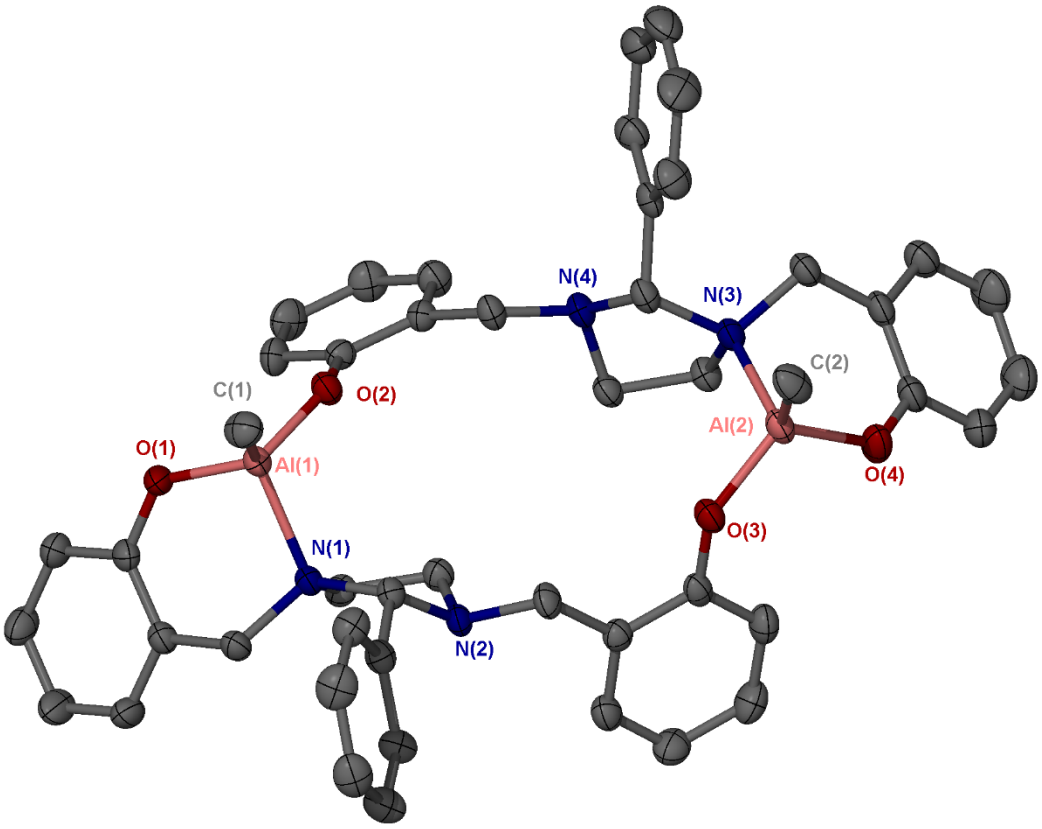

Figure 3.34. Solid-state crystal structure of Al_2(**7**)$_2Me_2$. Ellipsoids are shown at the 30 % probability level. Hydrogen atoms and solvent of recrystallization have been removed for clarity.

A similar metallacycle was reported by Zhang *et al*., who reported an aluminium complex with a zwitterionic carbene ligand, and its activity for ROP of ε-CL (Scheme 3.8).[55] However, in this complex the nitrogen atoms can play no part in the binding mode of the ligand, resulting in a macrocycle where both Al centres coordinate a methyl ligand and chloride ligand from the ligand salt. The solid-state structure of this metallacycle is shown in Figure 3.35 and bond lengths and angles are included in Table 3.10 for comparison.

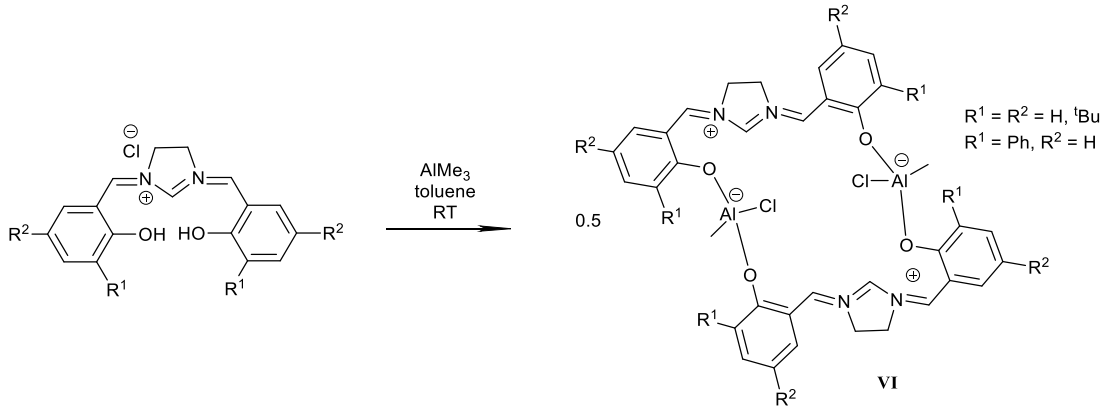

Scheme 3.8. Preparation of aluminium complex, **VI**, described by Zhang *et al*.[55]

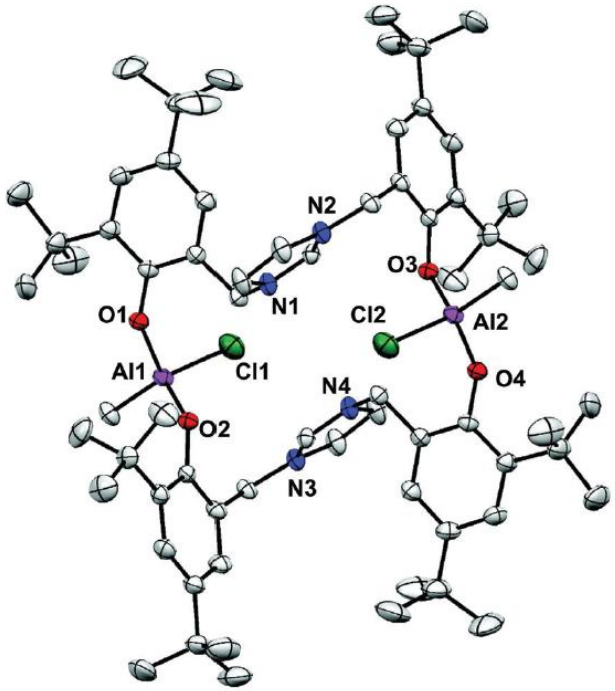

Figure 3.35. Solid-state structure of zwitterionic Al complex, **VI**. Reproduced from Zhang *et al.*, with permission, Royal Society of Chemistry (2017).[55] ellipsoids at 50% probability, hydrogen atoms and CH_2Cl_2 molecule not shown for clarity.

Table 3.10. Selected bond lengths (Å) and angles (°) for $Al_2(\mathbf{7})_2Me_2$ and literature complex, **VI**.[55]

	$Al_2(\mathbf{7})_2Me_2$	**VI**
Al(1)-O(1)	1.737(3)	1.7356(15)
Al(1)-O(2)	1.731(3)	1.7651(15)
Al(1)-N(1)/Cl(1)	1.993(3)	2.1712(9)
Al(1)-C(1)	1.934(4)	1.959(2)
O(1)-Al(1)-O(2)	114.22(14)	105.97(7)
O(2)-Al(1)-C(1)	110.96(15)	110.60(9)
O(1)-Al(1)-C(1)	114.02(16)	113.90(9)
O(2)-Al(1)-N(1)/Cl(1)	105.69(12)	108.44(5)
O(1)-Al(1)-N(1)/Cl(1)	96.74(12)	104.19(6)
C(1)-Al(1)-N(1)/Cl(1)	114.26(15)	113.25(7)
τ_4	0.93	0.94

A ^{1}H NMR spectrum was obtained in toluene for this complex (Figure 3.36). The solution behaviour is clearly more complex than the solid state, as there appears to be more than one species in solution. This is evident from the two distinct Al-Me resonances at -0.52 ppm and -0.33 ppm, in addition to multiple diastereotopic doublets for methylene protons and two resonances for the CH of the imidazolidine at 5.20 ppm and 5.34 ppm, which have shifted downfield on complexation. This could either be an impurity or dissociation of the cycle in solution. Initially it was thought that the additional resonances could be due to diastereoiseomers arising from different orientation of the ligands, however DOSY NMR (Figure 3.37) confirmed that the resonances belonged to several different species with different diffusion coefficients, confirming they are different species. The signals moving with diffusion coefficient, D = 5.5 x 10-^{10} m^2s^{-1} correspond to the resonances for $Al_2(\mathbf{7})_2Me_2$ in the ^{1}H NMR spectrum, and can be correlated to a species with volume, V = 3020 Å^3 and slightly overestimated molecular weight, M_n = 1126.1 $gmol^{-1}$ (M_n = 800.95 g mol^{-1}). The species with D = 8.0 x 10^{-10} m^2s^{-1} gives an estimated molecular weight of 489 $gmol^{-1}$, which could be the monomeric species, Al(**7**)Me.

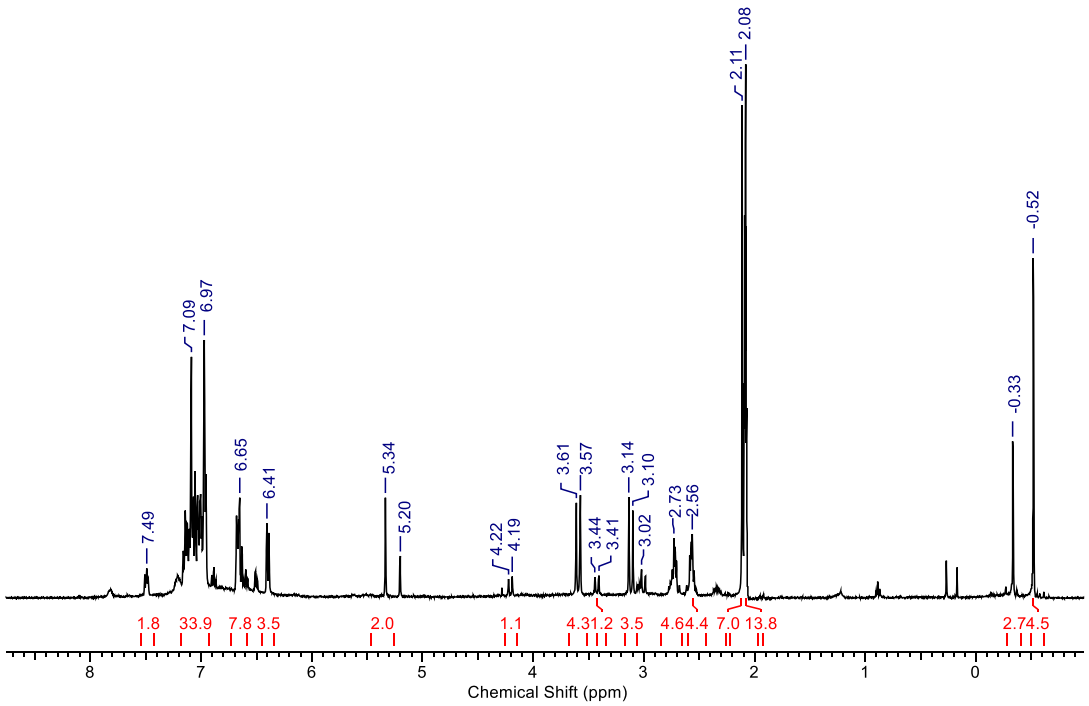

Figure 3.36. NMR spectrum (400 MHz, toluene-d^8) for complex $Al_2(\mathbf{7})_2Me_2$

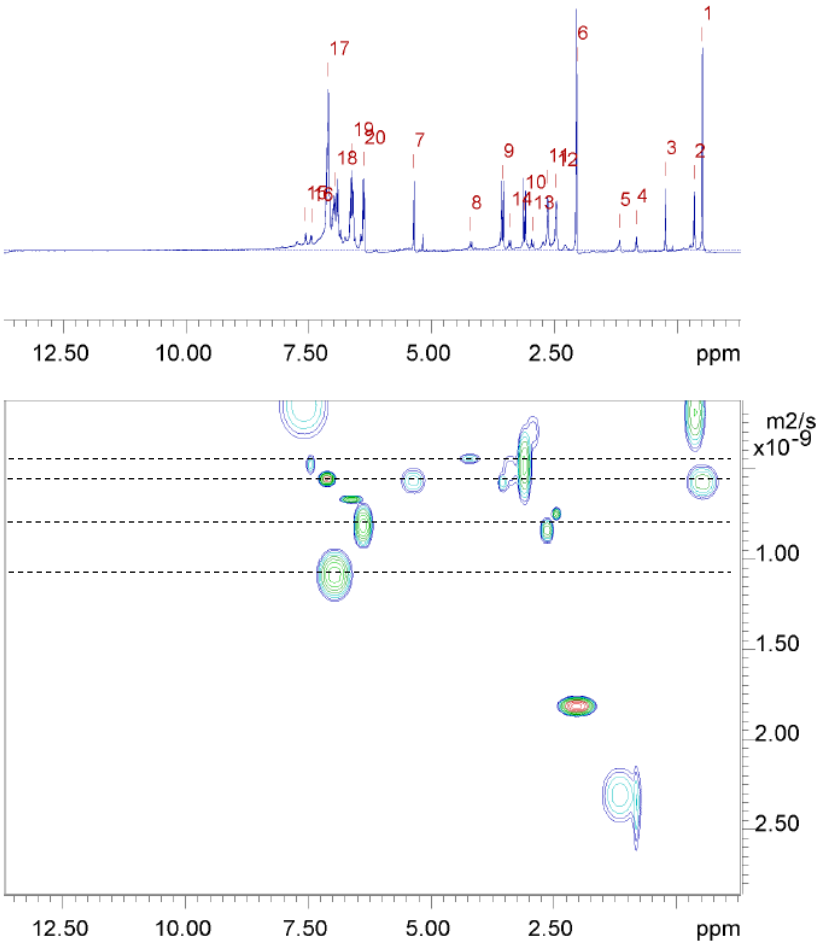

Figure 3.37. ^{1}H DOSY NMR for $Al_2(\mathbf{7})_2Me_2$ (400 MHz, toluene-d^8) showing different species with different diffusion coefficients.

Attempts to coordinate the methyl substituted imidazolidine ligand **8**H_2 with trimethylaluminium with different stoichiometries has at present yielded no isolatable products. However, on reacting with 2 equivalents of ^{n}BuLi in THF at -78 °C a lithium complex comprising a Li_4O_4 core was isolated in high yield (62%), similar to the structures discussed in Chapter 2.

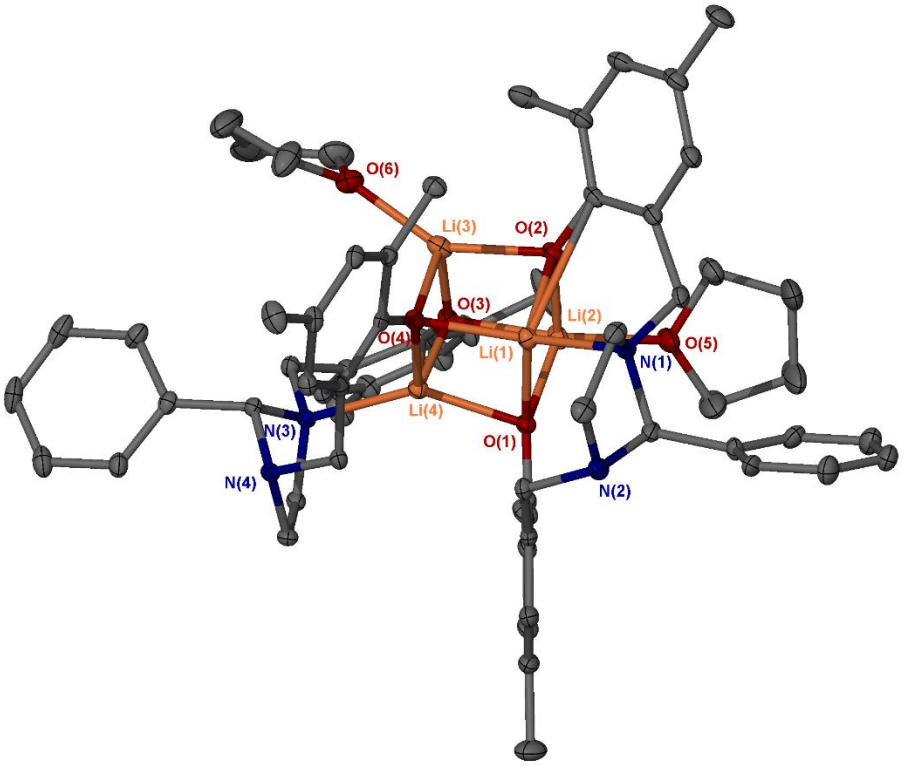

Figure 3.38. Solid-state structure of Li_4(**8**)$_2$(THF)$_3$. Ellipsoids are shown at the 30% probability level. One molecule of toluene (65:35), a further toluene (80%) and pentane (20%) have been removed for clarity. Two Li_4O_4 units are present in the lattice.

As with the aluminium complex Al_2(**7**)$_2Me_2$, only one of the imidazolidine nitrogen atoms coordinates to the metal centres, possibly because of the rigidity of the ligand restricting its ability to wrap around the metals. The ^{1}H NMR spectrum of Li_4(**8**)$_2$(THF)$_3$ is shown in Figure 3.39, which confirms the structure is retained in solution. The CH proton is again shifted downfield relative to the free ligand (5.82 ppm).

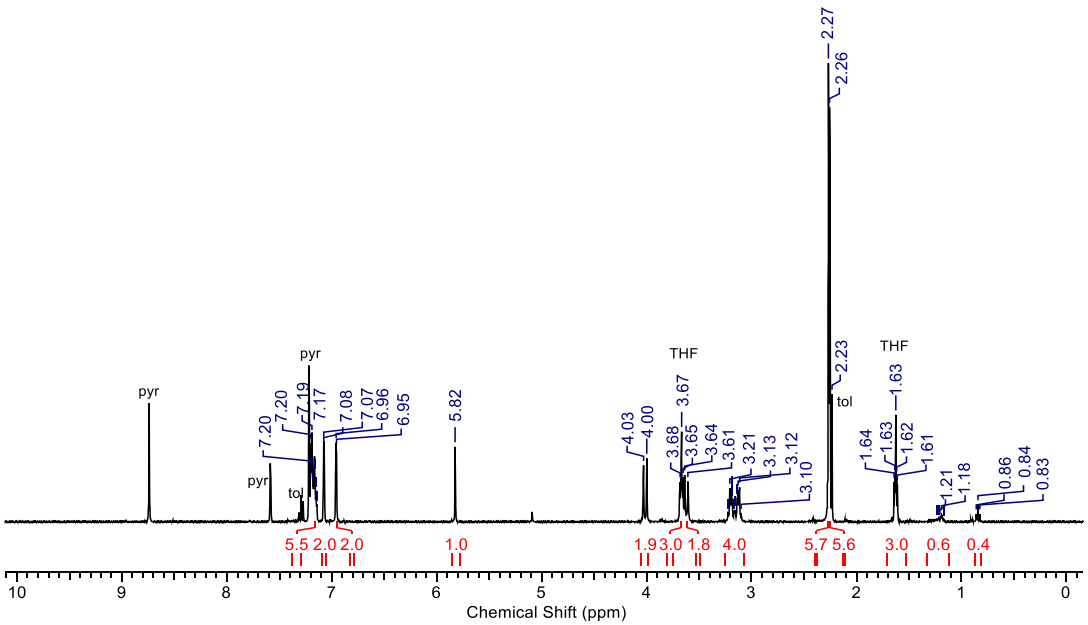

Figure 3.39. ^{1}H NMR spectrum (400 MHz, pyridine-d^{5}) of Li_4(**8**)$_2$(THF)$_3$.

Finally, tetra(phenolate) ligand **12**H_4 was reacted with 2 equivalents of trimethylaluminium in toluene, intending to form a dinuclear species. The solution rapidly turned yellow and a yellow precipitate formed almost instantly which would not dissolve in hot toluene. No crystals were obtained suitable for X-ray crystallography but the solid was isolated *via* cannula filtration, washed with hexane and characterised by ^{1}H and ^{13}C{^{1}H} NMR spectrum. The ^{1}H NMR spectrum for the product in benzene-d^{6} is shown in Figure 3.40, along with the proposed structure. From the NMR spectrum there is clearly a high level of symmetry in the complex, evidenced by the single Al-Me resonance at -0.37 ppm, a single resonance for the CH of the two imidazolidine rings at 5.44 ppm and two diastereotopic doublets with a large coupling constant of 14.5 Hz for the methylene protons as the molecule is “locked” in position. From this information, we can determine that there are two aluminium centres bound in the scaffold, each with a single methyl ligand. The ligands must be coordinating in an -ONNO- fashion in each binding “pocket” to allow for the symmetry seen in the spectrum. The aromatic protons for the terephthaldehyde linker are not evident in this spectrum as they fall beneath the C_6D_6 peak, although they can be seen in 2D experiments, or alternatively a different NMR solvent could be used. No other complexes of these ligands were successfully isolated within the timeframe of the project.

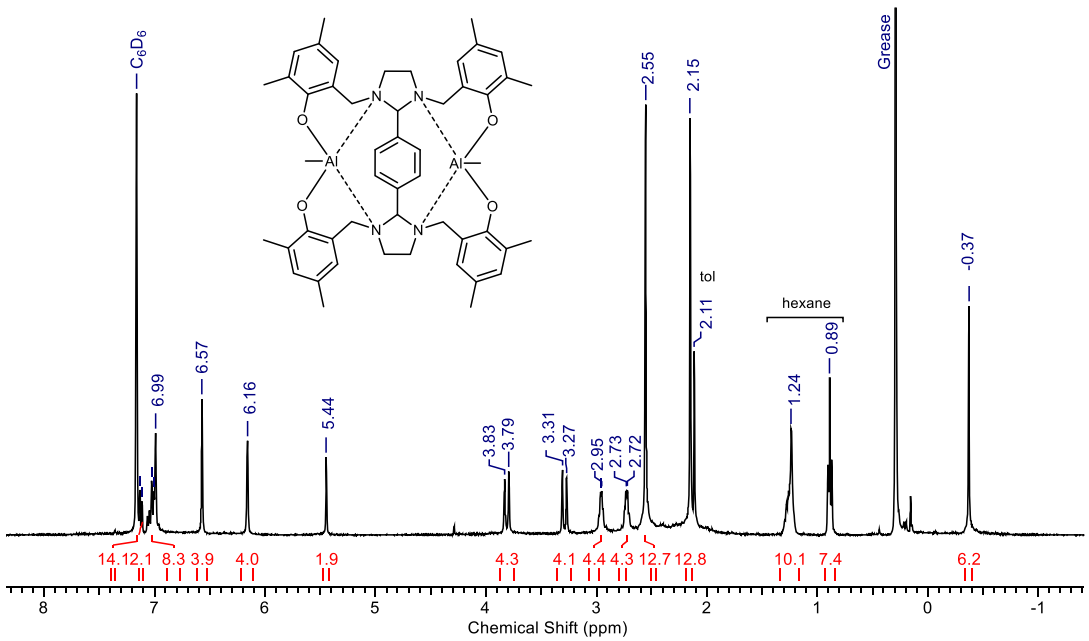

Figure 3.40. ^{1}H NMR spectrum (400 MHz, C_6D_6) for Al_2(**12**)Me_2

Preliminary polymerisation studies were performed with these isolated complexes, as summarised in Table 3.11.

Table 3.11. Preliminary polymerisation data for ROP of *rac*-LA with imidazolidine complexes at loading [LA]:[I]:[BnOH]= 100:1:2 in toluene

Entry	Initiator	Temp (°C)	Time (h)	Conv. (%)[a]	$M_{n\ theo}$ (gmol^{-1})	M_n (gmol^{-1})[b]	$Đ$ [b]	P_r [c]
1	Al_2(**7**)$_2Me_2$	80	24	91	6650	2700	1.89	0.50
2	Al_2(**7**)$_2Me_2$	80	2	92	7150	6650	1.22	0.50
3*	Al_2(**7**)$_2Me_2$	25	24	9	750	-	-	-
4[$]	Li_4(**8**)$_2$THF	80	2	98	14420	950	4.66	0.46
5[$]	Li_4(**8**)$_2$THF	25	0.75	99	14350	12250	1.67	0.44
6	Al_2(**12**)Me_2	80	2	37	2750	-	-	-
7	Al_2(**12**)Me_2	80	24	45	3350	-	-	-

[a] As determined *via* ^{1}H NMR, [b] Determined from GPC (in THF) referenced to PS standards. It is noted that a Mark-Houwink correction is not applied as triple detection was used; [c] P_r is the probability of heterotactic enchainment, determined *via* homonuclear decoupled ^{1}H NMR. Theoretical molecular weight calculated from conversion {[M]:[I]} × (Conv. × 144.13) + 108.14 (rounded to the nearest 50). [$]100:1:1 *Performed in CH_2Cl_2.

Al_2(**7**)$_2Me_2$ is reasonably active in toluene at 80 °C, with 92% conversion in 2 h. The polymer produced was in good agreement with predicted molecular weight and had a narrow dispersity, $Đ$ = 1.22. However, no stereoselectivity was attained with this complex. The complex is sparingly soluble in hot toluene, but lower temperature polymerisations in this solvent were not possible. A room temperature polymerisation in CH_2Cl_2 was attempted

but poor conversion was seen over 24 h. Polymerisation was found to be first order with respect to LA, and a modest value for k_{app} (7.9 x 10^{-3} min^{-1}) was obtained *via* an NMR-scale kinetic experiment at 80 °C (Figure 3.41). The lithium complex is active at room temperature, producing PLA of broad dispersity in 45 minutes. At elevated temperatures, near quantitative conversion of lactide is observed, but analysis by GPC suggested only very disperse oligomers. It is possible that the initiator is also active for depolymerisation of polylactide as observed in Chapter 2. For entries 6 and 7, no polymeric material was observed in GPC analysis, although analysis by ^{1}H NMR spectroscopy showed some conversion of monomer. It is possible that depolymerisation occurred on addition of MeOH with this complex, which could be investigated in future experiments.

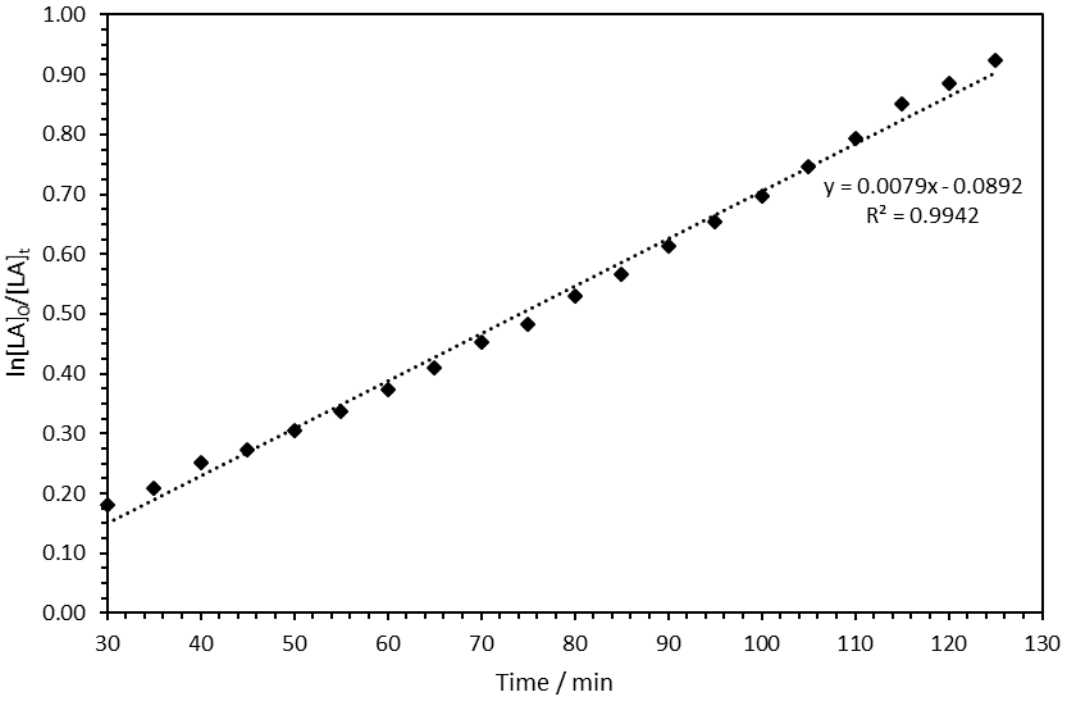

Figure 3.41. Pseudo first-order rate kinetic plot for ROP of *rac*-LA with Al_2(**7**)$_2Me_2$. Conditions: [LA]:[I]:[BnOH] = 100:1:2, toluene-d^8, 353 K.

The synthesis of neutral imidazolidine ligands have been discussed and three examples of complexation to Al(III) and Li(I) investigated, with some interesting coordination observed in resulting complexes. Complexes did not impart any stereoselectivity on ROP of *rac*-LA, but only preliminary investigations have been undertaken, and further experiments should be done in the future.

3.4.3 Conclusions and future work

In this chapter, a series of salen ligands with a *meso*-diphenylethylene backbone were prepared and complexed with one or two equivalents of trimethylaluminium to yield

mononuclear or dinuclear complexes. Al(**1**)Me was determined to be mononuclear by ^{1}H NMR spectroscopy. Al(**2**)Me and Al(**3**)Me were identified to be mononuclear by X-ray crystallography, which was confirmed in solution for Al(**2**)Me. However, the ^{t}Bu analogue was observed to exist as a dinuclear species in solution by ^{1}H NMR spectroscopy. Both Al(**1**)Me and Al(**2**)Me produced atactic PLA in a poorly controlled manner. Al_2(**3**)Me_2 showed more control, producing atactic PLA with predictable molecular weight and narrow dispersity. Little evidence of cooperative behaviour was observed in the dinuclear complex. MALDI-ToF analysis confirmed ROP *via* a coordination-insertion mechanism.

A salen ligand with a 1,8-naphthalene backbone was also complexed to aluminium. The complex was identified as a dinuclear species, Al_2(**4**)Me_2, by X-ray crystallography and this was confirmed in solution by ^{1}H NMR spectroscopy. Al_2(**4**)Me_2 was found to show high activity for producing isotactic PLA (P_m = 0.82) from *rac*-LA even at room temperature, which is highly unusual for a species with L-AlMe_2. At 80 °C, the polymerisation was an order of magnitude faster than the analogous monomeric species (k_{app} = 3.3 x 10^{-3} min^{-1} compared with 0.6 x 10^{-3} min^{-1})[32] and well controlled, although an investigation into order with respect to [Al] gave a non-integer value which should be further probed. DFT calculations showed that under polymerisation conditions it is possible for the Al···Al distance to approach close enough to allow for cooperativity.

The substitution of the phenyl rings or synthesis of asymmetrical ligands could be investigated to attempt to increase the isoselectivity of the initiator (Figure 3.42). Complexation to other metals could also be investigated. Attempts to prepare a Zr(IV) were unsuccessful, but this may be possible with smaller Ti(IV) as well as Li(I) and Mg(II). Lithium complexes bearing NNO-tridentate Schiff base ligands have recently been shown to be highly active for ROP of LA.[54]

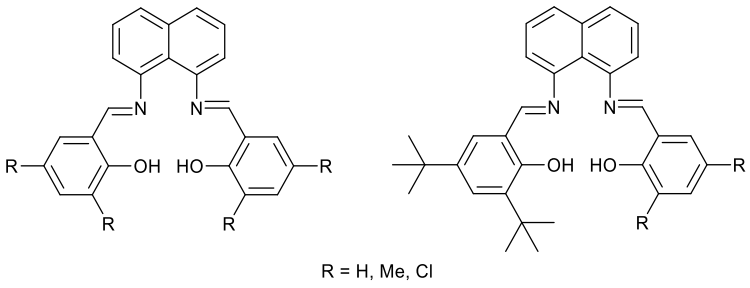

Figure 3.42. Potential ligands with 1,8-naphthalene backbone for future experiments

A series of neutral imidazolidine ligands have also been prepared by simple methods. Complexation of a bis(phenolate) ligand **7**H_2 with one equivalent of aluminium yielded an

interesting metallocycle, which was identified by X-ray crystallography, although its behaviour in solution appeared more complex. DOSY NMR suggested more than one species was present in solution, which should be further probed in future experiments. It is not clear whether there is an equilibrium between 1:1 and 2:2 species in solution or if both species are present. This complex was not stereoselective when utilised for ROP of *rac*-LA. Preparation of metallocycles with substitution of the phenyl rings could be investigated with other ligands to see if this imparts any selectivity. It would also be interesting to attempt the complexation with two equivalents of aluminium to attempt to prepare a dinuclear species such as the structure in Figure 3.43, and investigate any potential cooperativity between metal centres.

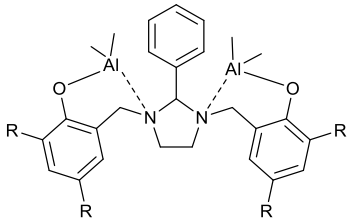

Figure 3.43. Proposed structure of dinuclear aluminium complex with imidazolidine ligand.

On complexation to Li(I), a tetrametallic complex with a central Li_4O_4 core was observed, as seen in Chapter 2, with the activity of this complex for ROP being comparable to similar structures. For dinuclear tetra(phenolate) complex, Al_2(**12**)Me_2, no polymer was observed on analysis by GPC, which could suggest depolymerisation of the polymer on work-up. The rigidity of this ligand is such that no cooperative effect would be possible between aluminium centres. However, utilising different dialdehydes could give complexes with more flexible linkers between imidazolidine moieties, allowing for more flexibility in the complex. Alternatively, introducing a longer rigid linker such as a biphenyl moiety might allow for coordination of more aluminium centres. Structural variation of these imidazolidine ligands is easily achieved by condensation of a salan precursor with an aldehyde or ketone, and many other structures can be envisaged with different coordination sites. Furthermore, other metals should be investigated, such as Mg(II), Zn(II) and Zr(IV). Attempts to prepare a Zr(IV) or Ti(IV) complex were unsuccessful with tris(phenolate) ligand **10**H_3, but this could be pursued further in different solvents, or with gentle heating.

3.5 Chapter 3 References

1 P. Das and W. Linert, *Coord. Chem. Rev.*, 2016, 311, 1–23.
2 T. P. Yoon and E. N. Jacobsen, *Science*, 2003, **299**, 1691–1693.
3 D. J. Darensbourg, *Chem. Rev.*, 2007, 107, 2388–2410.
4 K. C. Gupta and A. K. Sutar, *Coord. Chem. Rev.*, 2008, 252, 1420–1450.
5 P. G. Cozzi, *Chem. Soc. Rev.*, 2004, **33**, 410–421.
6 N. Spassky, M. Wisniewski, C. Pluta and A. Le Borgne, *Macromol. Chem. Phys.*, 1996, **197**, 2627–2637.
7 Z. Zhong, P. J. Dijkstra and J. Feijen, *Angew. Chem. Int. ed*, 2002, **41**, 4510–4513.
8 N. Maudoux, T. Roisnel, V. Dorcet, J.-F. Carpentier and Y. Sarazin, *Chem. Eur. J.*, 2014, **20**, 6131–6147.
9 N. Nomura, R. Ishii, Y. Yamamoto and T. Kondo, *Chem. Eur. J.*, 2007, **13**, 4433–4451.
10 H.-L. Chen, S. Dutta, P.-Y. Huang and C.-C. Lin, *Organometallics*, 2012, **31**, 2016–2025.
11 P. Hormnirun, E. L. Marshall, V. C. Gibson, R. I. Pugh and A. J. P. White, *Proc. Natl. Acad. Sci.*, 2006, **103**, 15343–15348.
12 D. J. Darensbourg, O. Karroonnirun and S. J. Wilson, *Inorg. Chem.*, 2011, **50**, 6775–6787.
13 E. D. Cross, L. E. N. Allan, A. Decken and M. P. Shaver, *J. Polym. Sci. Part A Polym. Chem.*, 2013, **51**, 1137–1146.
14 S. J. Wezenberg and A. W. Kleij, *Angew. Chem. Int. Ed.*, 2008, **47**, 2354–2364.
15 M. Normand, T. Roisnel, J.-F. Carpentier and E. Kirillov, *Chem. Commun.*, 2013, **49**, 11692-11694.
16 L. Chen, W. Li, D. Yuan, Y. Zhang, Q. Shen and Y. Yao, *Inorg. Chem.*, 2015, **54**, 4699–4708.
17 H.-C. Huang, B. Wang, Y.-P. Zhang, Y.-S. Li, Y. S. Li, Q. Shen, B. A. Messerle and M. Michalake, *Polym. Chem.*, 2016, **7**, 5819–5827.
18 X.-F. Yu and Z.-X. Wang, *Dalt. Trans.*, 2013, **42**, 3860-3868.
19 F. Isnard, M. Lamberti, L. Lettieri, I. D'auria, K. Press, R. Troiano, M. Mazzeo, X. Chen and M. Lamberti, *Dalt. Trans.*, 2016, **45**, 16001–16010.
20 P. D. Knight, P. N. O'Shaughnessy, I. J. Munslow, B. S. Kimberley and P. Scott, *J. Organomet. Chem.*, 2003, **683**, 103–113.
21 A. Alaaeddine, T. Roisnel, C. M. Thomas and J.-F. Carpentier, *Adv. Synth. Catal.*, 2008, **350**, 731–740.
22 M. D. Jones, S. L. Hancock, P. McKeown, P. M. Schäfer, A. Buchard, L. H. Thomas, M. F. Mahon and J. P. Lowe, *Chem. Commun.*, 2014, **50**, 15967–15970.
23 A. W. Addison, T. N. Rao, J. Reedijk, J. van Rijn and G. C. Verschoor, *J. Chem. Soc., Dalt. Trans.*, 1984, **0**, 1349–1356.
24 S. L. Hancock, M. F. Mahon and M. D. Jones, *Dalt. Trans.*, 2013, **42**, 9279–9285.
25 D. Myers, A. J. P. White, C. M. Forsyth, M. Bown and C. K. Williams, *Angew. Chem. Int. Ed.*, 2017, **56**, 5277–5282.
26 Y. Zhu, C. Romain and C. K. Williams, *Nature*, 2016, **540**, 354–362.
27 J.-C. Buffet and J. Okuda, *Chem. Commun.*, 2011, **47**, 4796–4798.
28 R. H. Platel, L. M. Hodgson and C. K. Williams, *Polym. Rev.*, 2008, **48**, 11–63.
29 P. McKeown, M. G. Davidson, G. Kociok-Köhn and M. D. Jones, *Chem. Commun.*, 2016, **52**, 10431–10434.
30 P. Hormnirun, E. L. Marshall, V. C. Gibson, A. J. P. White and D. J. Williams, *J. Am. Chem. Soc.*, 2004, **126**, 2688–2689.
31 E. L. Whitelaw, G. Loraine, M. F. Mahon and M. D. Jones, *Dalt. Trans.*, 2011, **40**, 11469-11473.

32 S. M. Kirk, H. C. Quilter, A. Buchard, L. H. Thomas, G. Kociok-Kohn and M. D. Jones, *Dalt. Trans.*, 2016, **4**, 835–864.

33 G. J. Clarkson, V. C. Gibson, P. K. Y. Goh, M. L. Hammond, P. D. Knight, P. Scott, T. M. Smit, A. J. P. White and D. J. Williams, *Dalton Trans.*, 2006, **7**, 5484–5491.

34 M. R. Ganjali, M. Hosseini, A. Karimi, H. Haji-Hashemi, M. Salavati-Niasari and P. Norouzi, *Spectrochim. Acta Part A Mol. Biomol. Spectrosc.*, 2014, **121**, 224–229.

35 S. Kirk, PhD Thesis, 2017.

36 L. Yang, D. R. Powell, R. P. Houser, F. Mohr, M. Laguna, S. Alvarez, P. L. Holland and H. -k. Fun, *Dalt. Trans.*, 2007, **96**, 955–964.

37 T. Shi, Q. De Zheng, W. W. Zuo, S. F. Liu and Z. B. Li, *Chinese J. Polym. Sci. (English Ed.*, 2018, **36**, 149–156.

38 M. M. Belmonte, S. J. Wezenberg, R. M. Haak, D. Anselmo, E. C. Escudero-Adán, J. Benet-Buchholz and A. W. Kleij, *Dalt. Trans.*, 2010, **39**, 4541.

39 T. M. Ovitt and G. W. Coates, *J. Am. Chem. Soc.*, 2002, **124**, 1316–1326.

40 C. Kan, J. Ge and H. Ma, *Dalt. Trans.*, 2016, **45**, 6682–6695.

41 S. Bian, S. Abbina, Z. Lu, E. Kolodka and G. Du, *Organometallics*, 2014, **33**, 2489–2495.

42 T. R. Forder and M. D. Jones, *New J. Chem.*, 2015, **39**, 1974–1978.

43 B. J. O'Keefe, L. E. Breyfogle, M. A. Hillmyer and W. B. Tolman, *J. Am. Chem. Soc.*, 2002, **124**, 4384–4393.

44 B. M. Chamberlain, M. Cheng, D. R. Moore, T. M. Ovitt, E. B. Lobkovsky and G. W. Coates, *J. Am. Chem. Soc.*, 2001, **123**, 3229–3238.

45 C. K. Williams, L. E. Breyfogle, S. K. Choi, W. Nam, V. G. Young, M. A. Hillmyer and W. B. Tolman, *J. Am. Chem. Soc.*, 2003, **125**, 11350–11359.

46 M. J. Stanford and A. P. Dove, *Chem. Soc. Rev.*, 2010, **39**, 486–494.

47 P. J. Dijkstra, H. Du and J. Feijen, *Polym. Chem.*, 2011, **2**, 520–527.

48 C. Romain, B. Heinrich, S. B. Laponnaz and S. Dagorne, *Chem. Commun.*, 2012, **48**, 2213-2215.

49 T. R. Jensen, L. E. Breyfogle, M. A. Hillmyer and W. B. Tolman, *Chem. Commun.*, 2004, **135**, 2504–2505.

50 O. B. Sutcliffe, M. R. Bryce and A. S. Batsanov, *J. Organomet. Chem.*, 2002, **656**, 211–216.

51 C. S. Higham, D. P. Dowling, J. L. Shaw, A. Cetin, C. J. Ziegler and J. R. Farrell, *Multidentate aminophenol ligands prepared with Mannich condensations*, 2006, vol. 47.

52 D. J. Allen and H. Ishida, *Polymer (Guildf).*, 2009, **50**, 613–626.

53 A. Rivera, J. J. Rojas, J. Salazar-Barrios, M. Maldonado and J. Ríos-Motta, *Molecules*, 2010, **15**, 4102–4110.

54 N. Nomura, R. Ishii, M. Akakura and K. Aoi, *J. Am. Chem. Soc.*, 2002, **124**, 5938–5939.

55 J. Zhang, S. Liu, W. Zuo, H. Ye and Z. Li, *New J. Chem.*, 2017, **41**, 2358–2363.

4 Chapter 4. Synthesis of terpene-derived monomers

4.1 Preamble

A prominent source of renewable hydrocarbon molecules are terpenes and related oxygenated terpenoids.[1–3] These naturally occurring molecules find widespread use in the flavourings and fragrance industries and are the principle component of essential oils in many plants.[4] Some of the most commonly occurring terpenes, and therefore most widely researched as potential monomers, are the monoterpenes α- and β-pinene (from turpentine) and *D*-limonene (from citrus waste), as well as the most simple terpene: isoprene. The abundance of alkene bonds in terpenes can be utilised for cationic and radical polymerisation, as well as epoxidation as a route to oxygenated polymers, as reported for limonene oxide[5–7] and α-pinene oxide.[8]

Few examples of terpenoid monomers for ROP are currently available, but recently there has been great interest in deriving new, functional monomers for the preparation of sustainable polymers from terpenes. Hillmyer and Tolman have reported the ROP of lactones derived from oxidised menthol[9] and carvone[10] to produce high-performing thermoplastic elastomers *via* block copolymerisation with LA. For menthone, the elastomers have properties comparable to commercial styrene-based triblock copolymers, and retained properties under physiological conditions for significant periods, highlighting their potential for biomedical applications.[11] The carvone-derived block copolymers could be modified by post-polymerisation modification (PPM) to yield networks with shape-memory properties.[10]

While *L*-menthol has shown some potential in this area, its annual production of around 19000 tonnes[12] is somewhat limiting for development of commodity materials. The production of turpentine, however, is estimated at some 350000 tonnes per annum, of which up to almost 33% may be β-pinene.[13]

Recently, Winnacker and co-workers reported lactams derived from both isomers of nopinone, produced from β-pinene,[14,15] in addition to lactams derived from *L*-menthone[16–18] to provide chiral polyamide materials with excellent thermal properties, which highlights the potential for making future high-performance polymers from turpentine feedstocks. However, both isomers of the nopinone lactam are made in the process and must be separated to prepare the desired monomers for enantiopure polymers.[14]

The work reported in this chapter aims to widen the library of available terpene-derived monomers for ROP by reporting synthetic routes to convert an abundant, naturally occurring terpene feedstock (β-pinene) into substituted lactones and lactams. Routes to unsaturated lactones which could be further modified after polymerisation are also described.

4.2 Synthesis of saturated monomers from β-pinene

The synthesis of 4-isopropylcaprolactone (4^{i}PrCL, **4**) was achieved in four, high-yielding steps from naturally occurring β-pinene, following the reaction sequence shown in Scheme 4.1. 4^{i}PrCL has been previously reported as a product in enantioselective Baeyer-Villiger oxidation (BVO) reactions,[19,20] but had not been reported as a monomer for ROP before publication of the work in this chapter.[21]

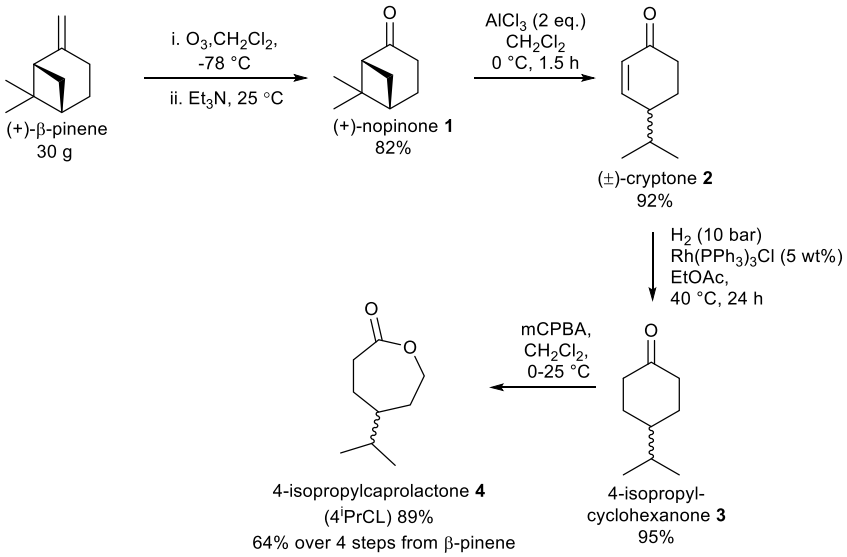

Scheme 4.1. Preparation of 4-isopropylcaprolactone, **4,** from β-pinene in four high-yielding steps (64% overall).

Firstly, ozonolysis of β-pinene in CH_2Cl_2 or MeOH afforded the bicyclic ketone, (+)-nopinone (**1**) in 82% yield on a 30 g scale. (+)-Nopinone is a naturally occurring terpenoid but is found in much smaller quantities in nature than β-pinene. Typically, triethylamine was added to quench the ozonide intermediate, followed by thorough washing with 1M HCl to remove the by-products. It is also possible to perform an oxidative ozonolysis with NaOH. Indeed, research at Bath as part of the wider *Terpene-Based Manufacturing* group has shown that if turpentine was used as the starting material rather than β-pinene, facile separation of nopinone and aqueous-soluble ozonolysis products is possible, as shown in Scheme 4.2.[22] The aqueous-soluble products could be further reduced to hydroxy acids, which are potentially useful synthetic intermediates. Additionally, the sulphurous content of crude

sulphated turpentine (CST), a by-product of the Kraft pulping process, would also be oxidised in this process, and readily removed without the need for difficult desulphurisation. The utilisation of a cheap, readily available, waste feedstock makes the notion of using β-pinene for the preparation of commodity polymers particularly attractive.

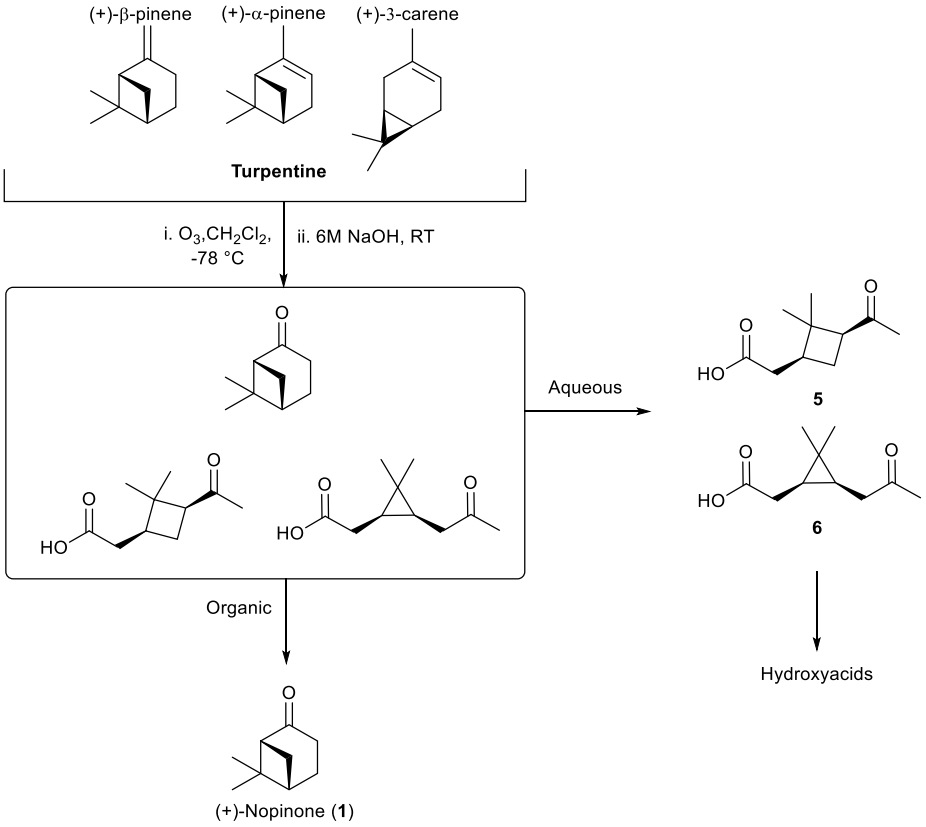

Scheme 4.2. Oxidative ozonolysis of common components of crude sulphate turpentine (CST)[22]

Lewis acid promoted isomerisation of **1**, following a procedure by Mori,[23] was found to cleave the strained cis-cyclobutane ring to produce exclusively the monocyclic product (±)-cryptone (**2**) in high yield, 92% (Scheme 4.3). No isomeric by-products were observed on a 10 g scale, evidenced by the absence of unconjugated alkene resonances in the ^{1}H NMR spectrum (shown in Figure 4.1). Mori also reported the synthesis of enantiopure (+)-cryptone as an intermediate in pheromone synthesis from another, less abundant terpenoid: perillyl alcohol. In this study, Mori investigated the rearrangement of (+)-nopinone to (±)-cryptone but observed purity of 80-85%, with an isomeric product observed in the alkene region of the ^{1}H NMR spectrum.

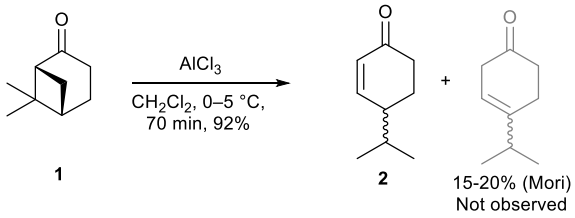

Scheme 4.3. Isomerisation of (+)-nopinone (**1**) to (±)-cryptone (**2**) and by-product reported by Mori[23]

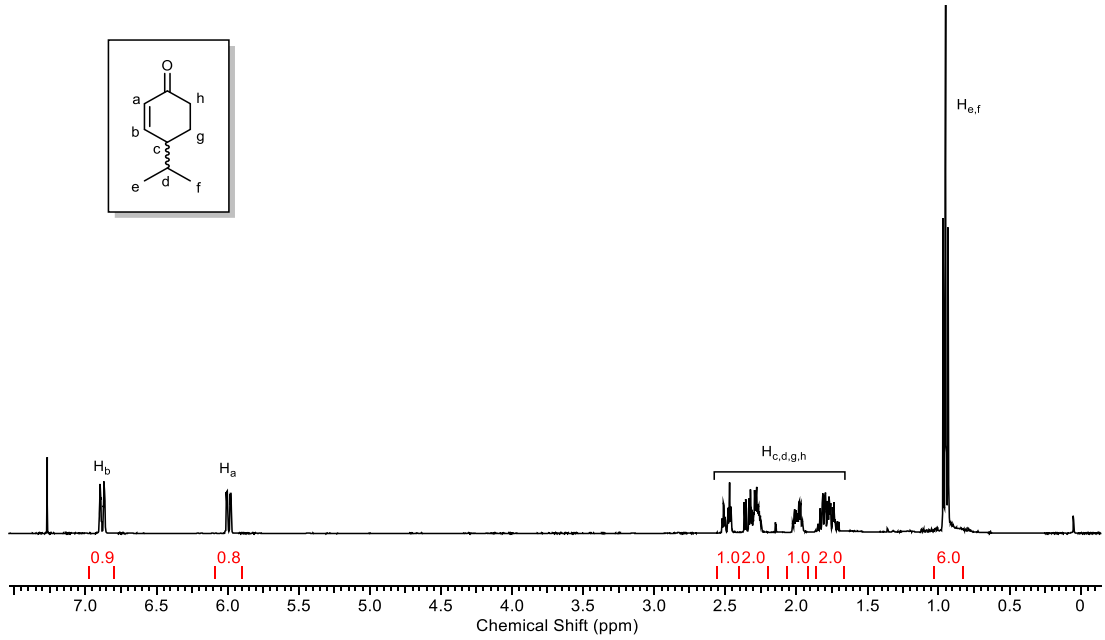

Figure 4.1. ^{1}H NMR (400 MHz, $CDCl_3$) spectrum of (±)-cryptone (**2**).

Quantitative hydrogenation of the α,β-unsaturated ketone **2** to 4-isoproylcyclohexanone (**3**) was afforded with Wilkinson's catalyst and H_2 (10 bar) in EtOAc at 40 °C. No alcohol by-products were observed under these conditions, which shows the benefit of using Wilkinson's catalyst over other systems which might allow further hydrogenation to occur. The saturated ketone **3** was isolated by column chromatography on silica or vacuum distillation and its ^{1}H NMR spectrum was identical to a sample of the same compound purchased from Flourochem. Finally, Baeyer-Villiger oxidation with *meta*-chloroperoxybenzoic acid (mCPBA) afforded the desired lactone **4** in good yields (89%) after purification *via* column chromatography on silica, and was characterised by ^{1}H and $^{13}C\{^{1}H\}$ NMR, GC-MS and ESI-MS. This was further purified before polymerisation by distillation over CaH_2 and stored in a glove box under argon prior to use.

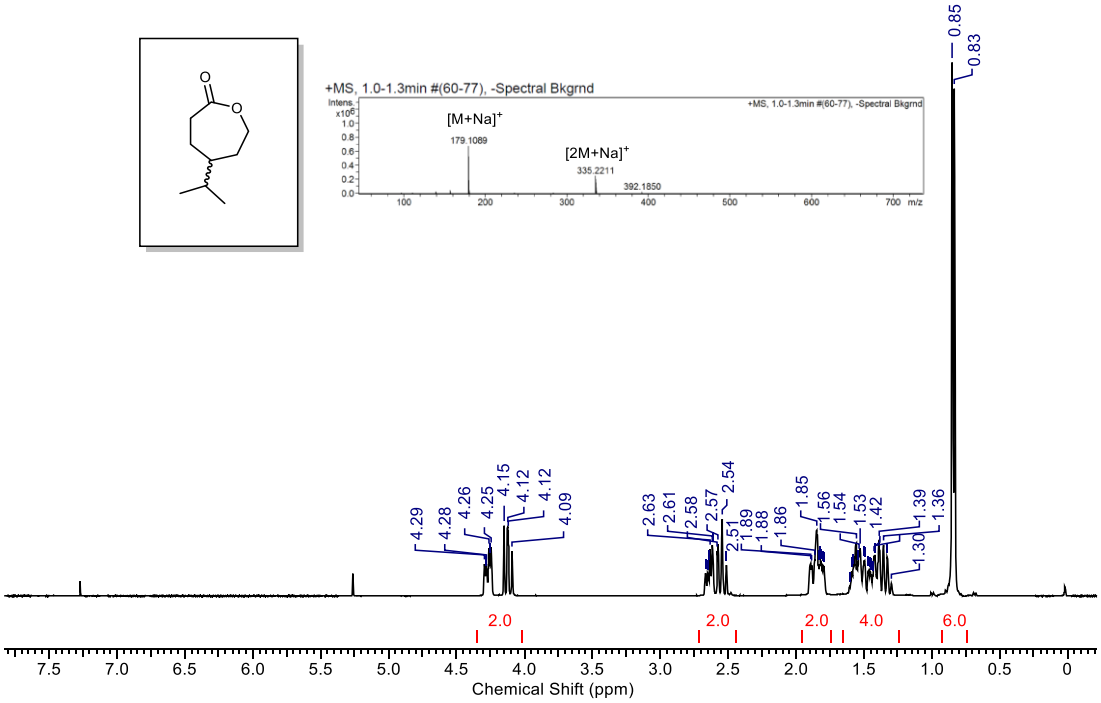

Figure 4.2. ^{1}H NMR spectrum (400 MHz, $CDCl_3$) and ESI-MS spectrum (inset) of 4-isopropylcaprolactone (**4**). The major peak is the sodium adduct, while a dimeric ion is also observed.

This route represents a laboratory scale proof of principle to establish the feasibility of utilising abundant, naturally occurring terpenes for polyester synthesis. It is important to note that the process at current has not been fully optimised, employing chlorinated solvents, stoichiometric oxidants, and cryogenic temperatures during ozonolysis. However, solvent-free[24] and flow[25] methods for the ozonolysis of β-pinene have been reported. "Green" Baeyer-Villiger oxidations have also been widely reported, such as catalytic oxidations with H_2O_2 or molecular oxygen,[26] or enzymatic transformations.[27] Indeed, this could offer a route to an enantiomerically pure lactone but would significantly lower the yields of products by utilising a single enantiomer. It is encouraging that all four steps to achieve monomer **4** are common transformations that are amenable to scale-up through standard process development methodologies. Recent advances in preparation of **4** (after publication of this work) include continuous flow production with a Sn-β/H_2O_2 BVO process.[28]

An intermediate in the process, 4-isoproylcyclohexanone, **3**, was also converted to a lactam (**8**) *via* a Beckmann rearrangement of the *N*-oxime (**7**) to prepare a bio-based monomer for functionalised polyamides similar to Nylon (Figure 4.3). Structural confirmation of **8** was obtained by NMR (Figure 4.4) spectroscopy, electrospray ionisation mass spectrometry (ESI-MS) and single-crystal X-ray diffraction of crystals obtained *via* sublimation (Figure 4.5).

Lactam **8** was originally obtained as a brown solid. Recrystallisation from hexane yielded a "sand"-coloured solid which was further purified *via* sublimation to yield fluffy, white crystals in a 77% yield from commercially available 4-isopropylcyclohexanone, or 55% from β-pinene directly.

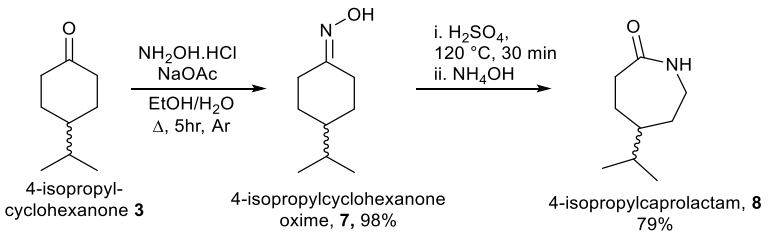

Figure 4.3. Syntheses of 4-isopropylcaprolactam, **8**, from β-pinene (scheme shown from intermediate **3**)

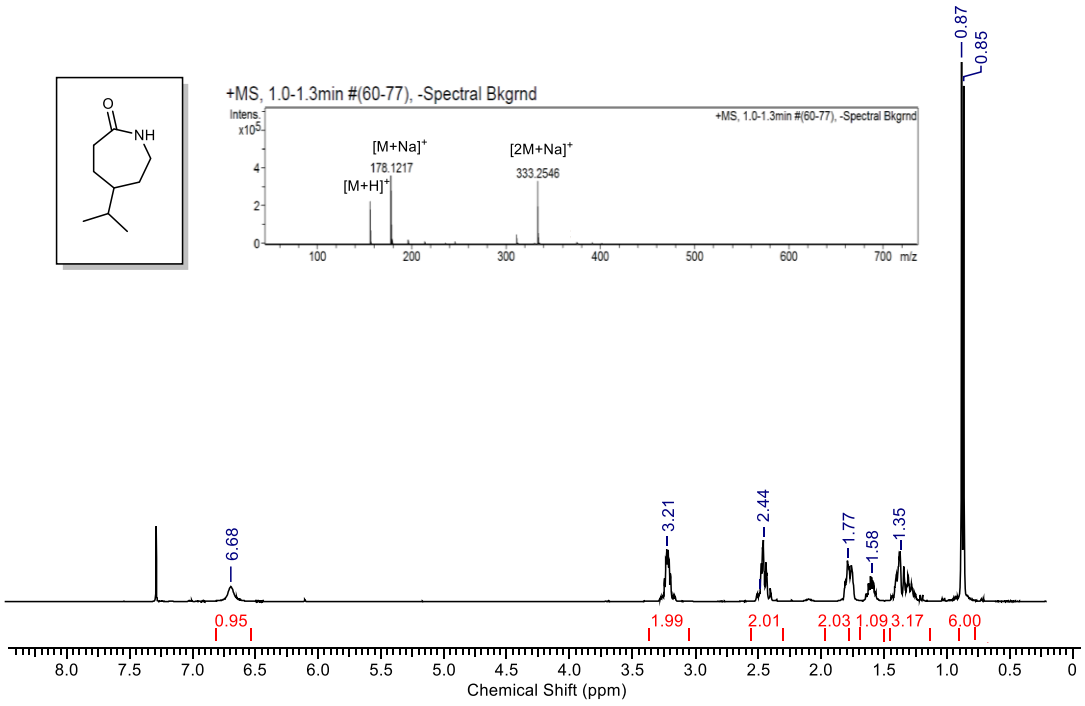

Figure 4.4. ^{1}H NMR spectrum (400 MHz, $CDCl_3$) of **8** with ESI-MS spectrum inset. Peaks shown are the sodium and protonated adducts, and a dimeric ion.

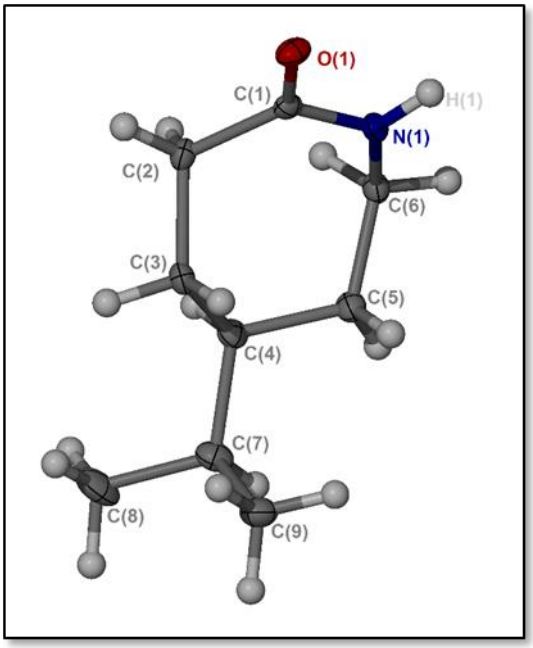

Figure 4.5. Solid-state structure of lactam **8**. Ellipsoids are shown at the 30% probability level. Selected bond lengths (Å) and angles (°): O(1)-C(1) 1.223(3), N(1)-C(1) 1.343(4), N(1)-C(6) 1.448(4), C(1)-N(1)-C(6) 125.4(2), O(1)-C(1)-N(1) 121.3(3), O(1)-C(1)-C(2) 121.8(3), N(1)-C(1)-C(2) 116.8(2), N(1)-C(6)-C(5) 114.0(2).

Unfortunately, polymerisation attempts with this monomer have been mostly unsuccessful under a range of established literature procedures for the anionic and cationic polymerisation of ε-caprolactam, and conditions reported for the ROP of terpene-derived substituted lactams.[14,15] Some polymerisation attempts are summarised in Table 4.1. Discolouration of **8** was also observed above the melting temperature (mp = 78 °C), with the resulting molten lactam being a dark brown liquid. This discolouration was not observed upon attempting the polymerisation process with commercial ε-caprolactam. It is probable that an impurity remains in the monomer despite purification by sublimation. Many reports conditions for the ROP of caprolactam use high temperatures (150-250 °C), which proved difficult in this case as the monomer sublimed at these higher temperatures.

Table 4.1. Attempted conditions for the polymerisation of **8**.

Entry	Initiator	Co-initiator	M:I	Time / h	Temp. / °C	Con.[a] / %
1	H^+ (1 drop HCl)	-	100:1	4	150	Quantitative
2	KOtBu	-	100:1	24	100	0
3	KOtBu	-	100:1	4	150 (vac)	0
4	KOtBu	Benzoyl chloride	100:1:1	5	150	0
5	KOtBu	Benzoyl chloride	100:1:1	5	150 (vac)	Quantitative.

[a]Determined from the ^{1}H NMR spectrum.

Under most conditions trialled, no conversion of monomer was observed. For entry 1, a brown solid was obtained which was poorly soluble in most solvents. The ^{1}H NMR spectrum

(Figure 4.6) showed no monomer remained in the product but no polymeric material was observed by GPC in THF or chloroform. For entry 5, no monomer was observed in the ^{1}H NMR spetrum, but the mass was greatly reduced: possibly residual monomer was lost as a light vacuum was applied.

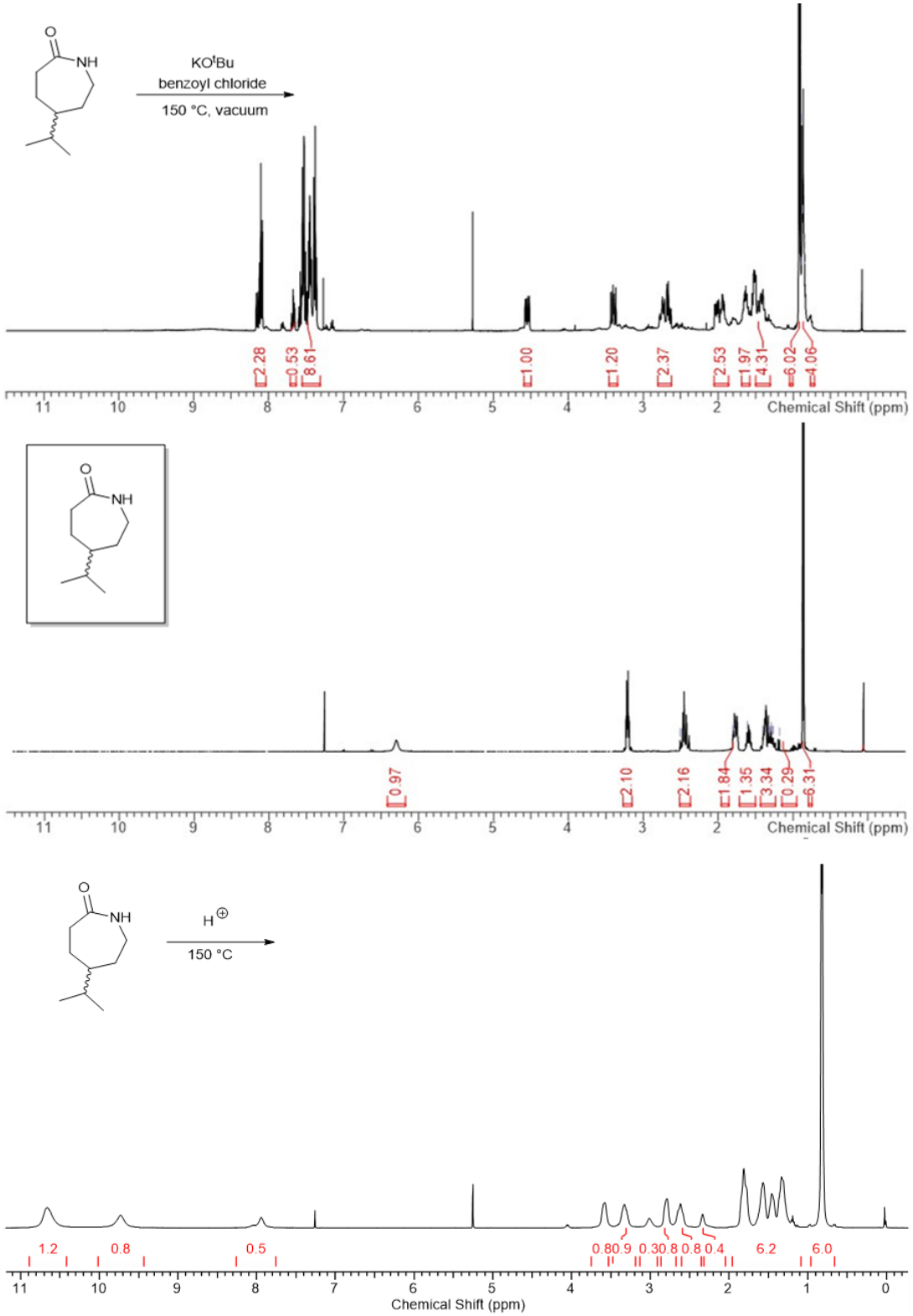

Figure 4.6. ^{1}H NMR spectra (400 MHz, $CDCl_3$) of crude polymerisation mixtures attempted with lactam **8** – Table 4.1, entry 1 (top) and entry 5 (bottom) with monomer spectrum for comparison.

Polymerisation of substituted lactams is reportedly complex, depending on enthalpic and entropic effects, in addition to gauche interactions within the heterocycle.[29] In this project, the polymerisation of this monomer was not further pursued, although research is on-going in the Jones group into its polymerisation.

4.3 Polymerisation of 4-isopropylcaprolactone

4.3.1 Homopolymerisation of 4-isopropylcaprolactone

4.3.1.1 Initiator screening, kinetics and controlled "living" polymerisation

The ROP of 4^{i}PrCL affords a linear aliphatic polyester with evenly spaced pendant isopropyl groups. **4** was also prepared from commercially available **3** to allow for polymerisation studies to be carried out simultaneously with the synthesis of the new monomer from β-pinene. Efforts have been made here to highlight when commercial **3** was used to prepare the monomer.

A range of coordinative insertion polymerisation initiators were investigated for the homopolymerisation of **4** (Table 4.2). $Sn(Oct)_2$ and diethylzinc/benzyl alcohol systems, favoured by Hillmyer in similar studies,[9,10] were investigated for their industrial relevance. Two zirconium complexes (Figure 4.7), which have previously been shown to be stereoselective in the ROP of *rac*-LA, were chosen to as they are easily prepared and are relatively robust: a zirconium amine tris(phenolate) complex, {Zr(tris)(O^{i}Pr)}, which shows heterotactic bias with *rac*-LA,[30] and a zirconium bipyrollidine-based salan complex, {Zr(bis)(O^{i}Pr)$_2$}, which exhibits an isotactic bias with *rac*-LA.[31] Since publication of this work, the organocatalytic polymerisation of this monomer with 1,8-Diazabicyclo(5.4.0)undec-7-ene (DBU) has also been reported.[28]

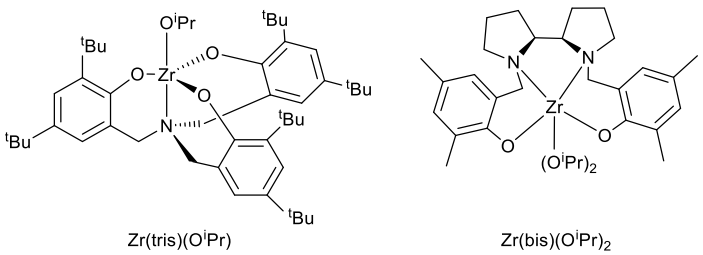

Zr(tris)(O^{i}Pr) Zr(bis)(O^{i}Pr)$_2$

Figure 4.7. Structures of zirconium initiators used in this study.

Generally, polymerisations were performed solvent free at 100 °C or in toluene at 80 °C, with a monomer [M] to initiator [I] ratio of 100:1. Benzyl alcohol was added as co-initiator if required to generate the necessary metal alkoxide for ROP *via* a coordination-insertion mechanism. Polymers were found to be thick, colourless gels with low glass transition

temperatures (T_g = *ca.* −50 °C), although discolouration was observed for Table 4.2, Entry 1, where a higher temperature of 130 °C was employed during polymerisation. By comparison, unsubstituted ε-CL is a crystalline polymer with T_g = -60 °C. Polyesters derived from menthone and carvone were reported to have T_g values between -20 and -27 °C.[9,10] These polyesters have less flexible structures due to the presence of chiral methyl substituents. The lack of crystallinity in poly(**4**) is likely a consequence of the presence of the bulky, mixed configuration isopropyl substituents, as observed for polymenthide.[9]

Table 4.2. Initiator screen for the ROP of monomer **4**.

Entry	Initiator	Time / h	Temp. / °C	Con.[a] / %	$M_{n\ pred.}$	M_n [b]	$Đ$[b]
1	$Sn(Oct)_2$/BnOH	2	130	99	15500	3350	1.69
2	$Sn(Oct)_2$/BnOH	4	100	74	11650	32000	1.55
3	$Sn(Oct)_2$/BnOH	4	80	7	1200	-	-
4	$ZnEt_2$/BnOH	2	100	91	14300	22500	1.34
5	$ZnEt_2$/BnOH	24	80	44	6950	16700	1.19
6	$ZnEt_2$/BnOH	24	40	14	2350	16300	1.35
7	Zr(bis)(O^iPr)$_2$	2	100	99	15500	11500	1.46
8	Zr(bis)(O^iPr)$_2$	24	80	88	13800	5700	1.18
9	Zr(tris)(O^iPr)	24	100	96	15000	11400	1.42
10	Zr(tris)(O^iPr)	24	80	66	10350	3200	1.29
11[c]	$ZnEt_2$/BnOH	2	100	95	14900	4900	1.54
12[c]	Zr(bis)(O^iPr)$_2$	2	100	95	14900	4900	1.52
13[c]	Zr(tris)(O^iPr)	24	100	96	15100	3400	1.57

All polymerisations performed solvent free except entries 3, 5, 9 & 11, which were conducted in toluene. For all entries [M]:[I] = 100. Where BnOH is added as co-initiator, [M]:[I]:[BnOH] = 100:1:1. [a]Determined by ^{1}H NMR spectroscopy. [b]Determined by GPC (THF), using polystyrene standards, RI detection. [c]Monomer produced from β-pinene. The predicted molecular weight can be calculated by the following equation: (156 × M_{eq} × conversion)/I_{eq} + end group.

The ROP of **4** (prepared with commercial **3**) with $ZnEt_2$/BnOH was found to proceed rapidly at 100 °C, with quantitative conversion to polymer within 2 hours. $Sn(Oct)_2$ afforded a conversion of 94% after 2 hours at 130 °C or 74% conversion after 4 hours at 100 °C. At higher temperature (Table 4.2, entry 1) the molecular weight was lower than predicted, with a broad $Đ$ and discolouration of the polymer product. For entry 2, a broad $Đ$ and exaggerated M_n could be indicative of transesterification.

Monomer conversion with $Sn(Oct)_2$ at 130 °C with BnOH as a co-initiator was monitored as a function of time by ^{1}H NMR spectroscopy of polymerisation samples run for set time intervals. The polymerisation proceeded rapidly, with near-complete conversion (94%) in 2

hours for [M]:[I]:[BnOH] = 100:1:1 (Figure 4.8a). A k_{app} value of 4.9 x 10^{-2} min^{-1} was determined from a linear plot of $ln([M]_0/[M]_t)$ against time (Figure 4.8b).

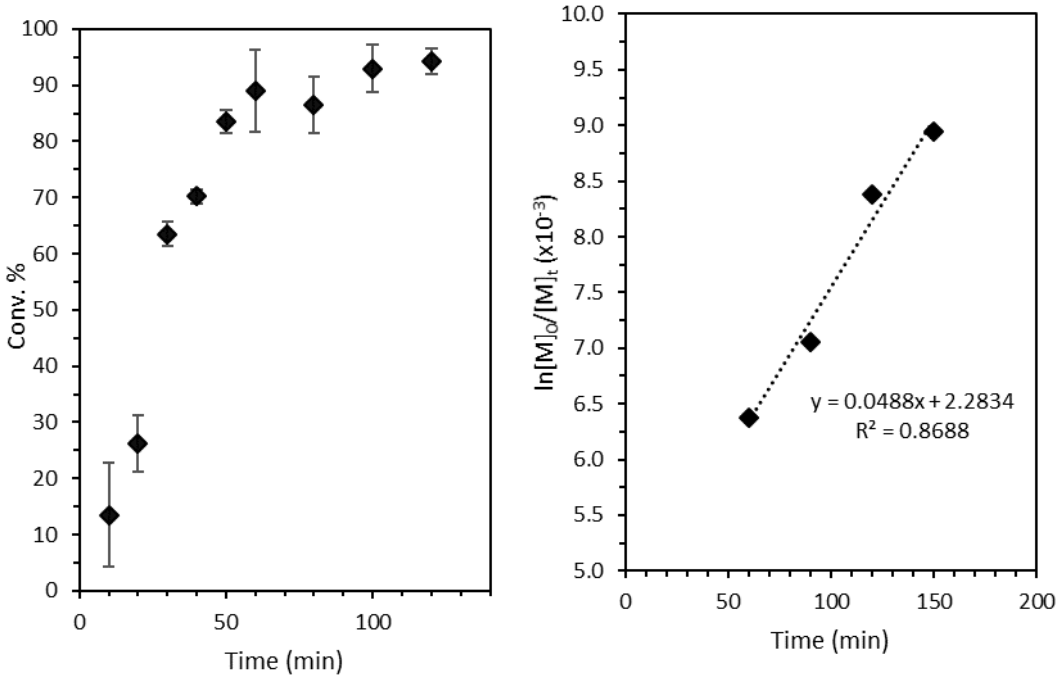

Figure 4.8. a) Monomer conversion as a function time for a ROP of **4** carried out with 100:1:1 [**4**]:[Sn]:[BnOH] at 130 °C. Conversion determined by relative integration of the methylene proton environments of the monomer (4.24 ppm) to the polymer (4.07 ppm) in the ^{1}H NMR spectra (400 MHz, $CDCl_3$) of polymerisations run for specific time intervals. Error bars represent standard deviation. b) Semi-logarithmic plot showing pseudo-first order kinetics in concentration of monomer [M] as a function of time.

Changes in chemical environments were observed in the ^{1}H NMR spectrum of the polymer compared to the monomer, indicative of polyester formation and relief of ring strain (Figure 4.9). Generally, the polymers prepared from β-pinene-derived **4** exhibited lowed molecular weights and broader dispersities than those prepared from the commercially available intermediate under analogous conditions despite best efforts to remove any impurities at each step.

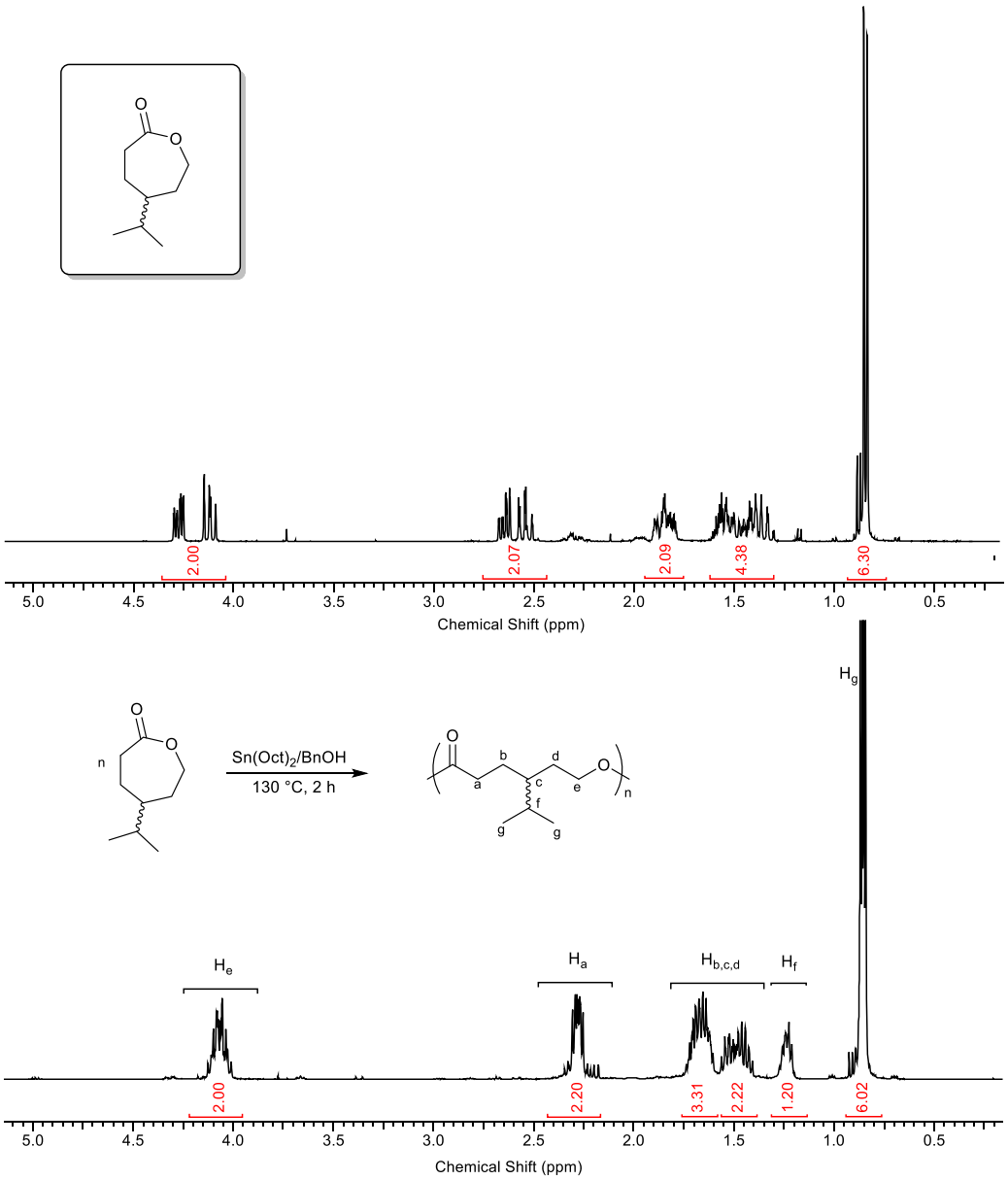

Figure 4.9. ^{1}H NMR spectra (400 MHz, $CDCl_3$) of **4** and poly(**4**)

The kinetics of polymerisation with $Sn(Oct)_2$/BnOH were also investigated by running parallel polymerisation reactions at a set [M]:[Sn]:[BnOH] = 100:1:1, quenching at regular time intervals and calculating conversion of monomer by NMR. A linear plot of $\ln([M]_0/[M]_t)$ against time at $[M]_0$:$[Sn]_0$:$[BnOH]_0$ of 100:1:1 fitted pseudo first-order kinetics, typical of ROP (Figure 4.10). From these, a value of k_{app} of 2.6 x 10^{-2} min^{-1} was determined.

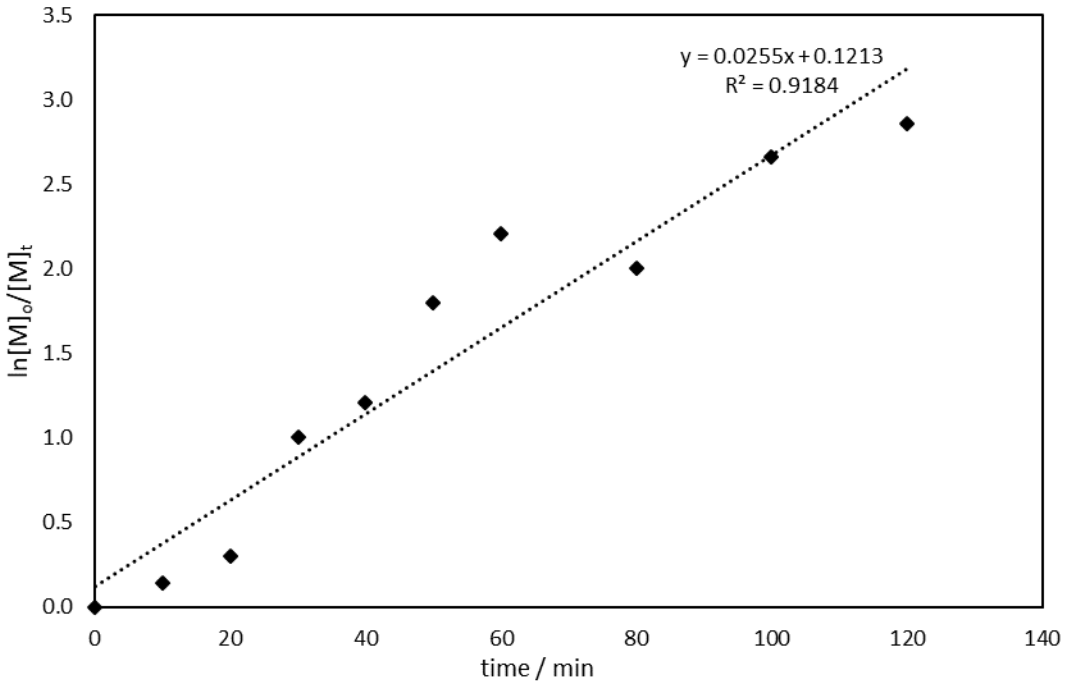

Figure 4.10. Semi-logarithmic plot - kinetics for homopolymerisation of **4** with $Sn(Oct)_2$/BnOH at [**4**]:[Sn]:[BnOH] = 100:1:1, 100 °C, solvent free.

Kinetics with $ZnEt_2$/BnOH were also investigated at 100 °C by varying the time intervals for polymerisation, giving a first order rate constant, $k_{app} = 1.7 \times 10^{-2}$ min^{-1}. The polymerisation was poorly controlled in terms of molecular weight and polydispersity.

The zirconium systems were observed to be superior in terms of predictability of molecular weight and polydispersity and were therefore taken forward for further studies. While the bipyrrolidine system appeared to be the superior system, the tris(phenolate) complex was investigated due to its ease of preparation. Near quantitative conversion (96%) was observed after 24 h with [M]:[I] = 100, with rate constant, $k_{app} = 2.4 \times 10^{-3}$ min^{-1}. Solution-state kinetics were also investigated on an NMR scale at 80 °C in toluene-d^8, giving a rate constant $k_{app} = 2.0 \times 10^{-4}$ min^{-1}, an order of magnitude slower. The rate of polymerisation with {Zr(bis)($O^iPr)_2$} was also determined in toluene-d^8 at 60 °C (Figure 4.11) and found to proceed with $k_{app} = 2.96 \times 10^{-5}$ min (polymer from commercial **3**). The polymerisation of ε-CL under the same conditions proceeds much more rapidly. Indeed, even at room temperature the rate of polymerisation is far quicker for ε-CL ($k_{app} = 7.61 \times 10^{-3}$ min^{-1}) than 4^iPrCL at elevated temperatures.

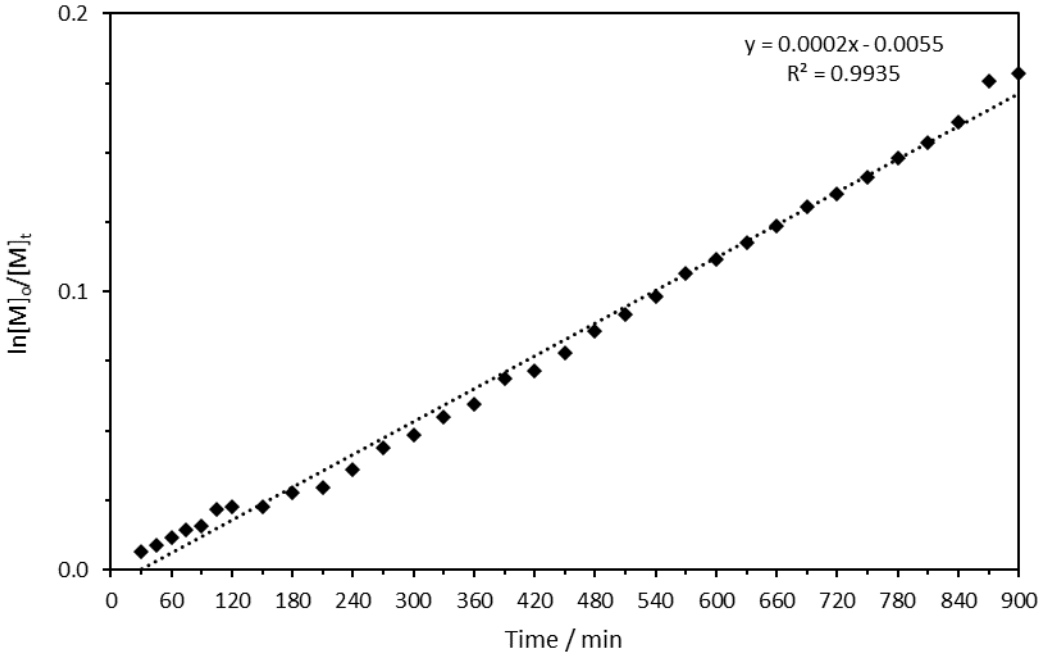

Figure 4.11. Semi-logarithmic plot - solution kinetics for homopolymerisation of **4** with {Zr(tris)(O^{i}Pr)} on NMR scale in toluene-d^{8} at 80 °C.

With {Zr(tris)(O^{i}Pr)} as initiator, and at a fixed monomer-to-initiator ratio, the molecular weight was observed to increase relative to the conversion of monomer while the polydispersity of polymer products remained reasonably constant (*Đ* = 1.17-1.24), indicative of a well-controlled, living polymerisation (Figure 4.12). Prolonged reaction times led to a broadening of Đ to 1.42, potentially due to intramolecular transesterification reactions. Polymer molecular weights and molecular weight distributions were estimated by GPC *vs* polystyrene standards in THF eluent using RI detector. The gradient of the graph is 112 gmol^{-1}, slightly smaller than the molecular weight of one monomer. A gradient of 156 gmol^{-1} would be indicative of one chain growing per metal centre.

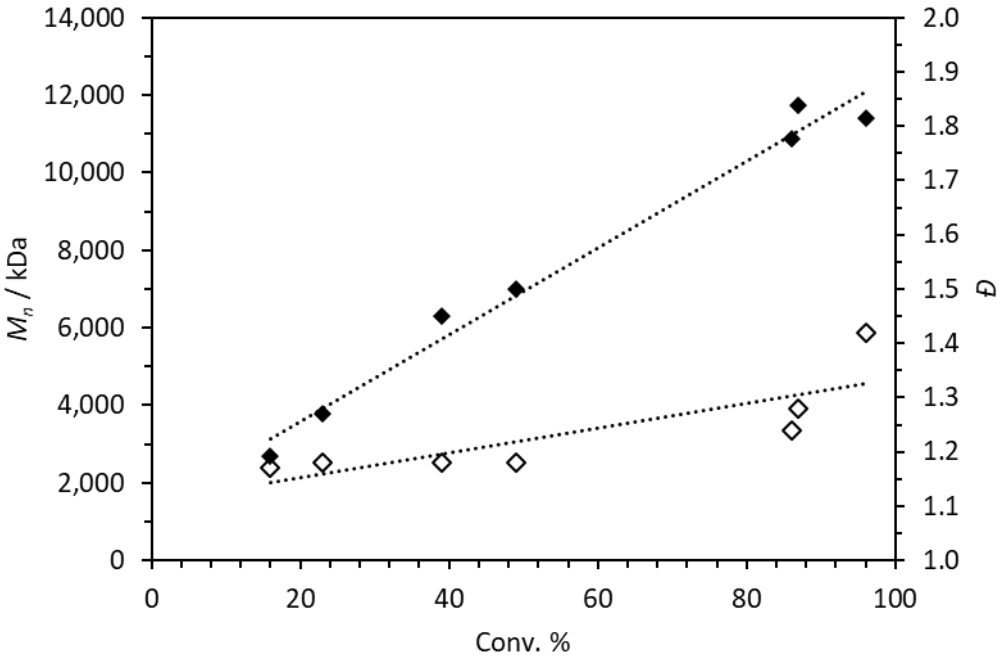

Figure 4.12. Graph showing the relationship between conversion and M_n (◆, left axis) and $Đ$ (◇, right axis) determined by GPC (RI) relative to polystyrene standards with THF eluent. Conditions = [**4**]:[{Zr(tris)(O^{i}Pr)}] = 100, 100 °C, solvent-free, 0–24 h. Using **4** derived from commercial **3**.

Experiments were carried out over a range of catalyst and [M]:[I] loadings. At lower initiator loadings, the polymerisation did not reach completion even after longer reaction times of up to 72 hours, and good correlation was not observed between the predicated and observed molecular weights (Table 4.3). It is possible that impurities that have been carried through the synthesis despite purification processes are significant enough to act as chain transfer agents, reducing M_n.

Table 4.3. ROP of **4** with {Zr(tris)O^{i}Pr} at various [M]:[I] loadings.

Entry	[M]:[I]	t	Conv. %[a]	$M_{n\ calc}$[b]	M_n[c]	$Đ$[c]	T_g / °C[d]
1	50	24	94	7392	10100	1.58	-50.1
2	100	24	96	15036	11400	1.42	-50.9
3	200	24	79	24708	13500	1.18	-52.6
4	300	24	54	25332	9800	1.14	-
5	400	24	37	23148	7100	1.14	-
6	300	72	87	40776	14100	1.47	-51.6
7	400	72	55	34380	9200	1.30	-47.5

All polymerisations performed solvent free at 100 °C. [a]Determined by ^{1}H NMR spectroscopy. [b]The predicted molecular weight can be calculated by the following equation: (156 × M_{eq} × conversion)/I_{eq} + end group. [c]Determined by GPC (THF), using polystyrene standards, [d]Determined by DSC.

4.3.1.2 End-group determination by MALDI-ToF mass spectrometry

MALDI-ToF mass spectrometry of a low molecular weight polymer sample (M_n = 5700, $Đ$ = 1.18) confirmed the polymer to be consistent to the expected polyester from the ROP of **4**,

having the correct repeat unit ($\Delta m/z$ = 156.20 Da). In this example, two series were observed (Figure 4.13). One series was seen having *m/z* values consistent with the sodium adduct of a linear polymer capped by -O^{i}Pr and -H groups, whereby the isopropoxide group has been transferred from the initiator to the polymer chain, confirming ROP *via* a coordination-insertion mechanism. A second series was also evident (M_n = 2054 Da), having no end groups, corresponding to cyclic oligomers – the product of intramolecular transesterification (or "backbiting"), a common competing side-reaction in ROP. This is evidence of backbiting of the polymer chain, causing the smaller molecular weights and broad polydispersity observed during polymerisation.

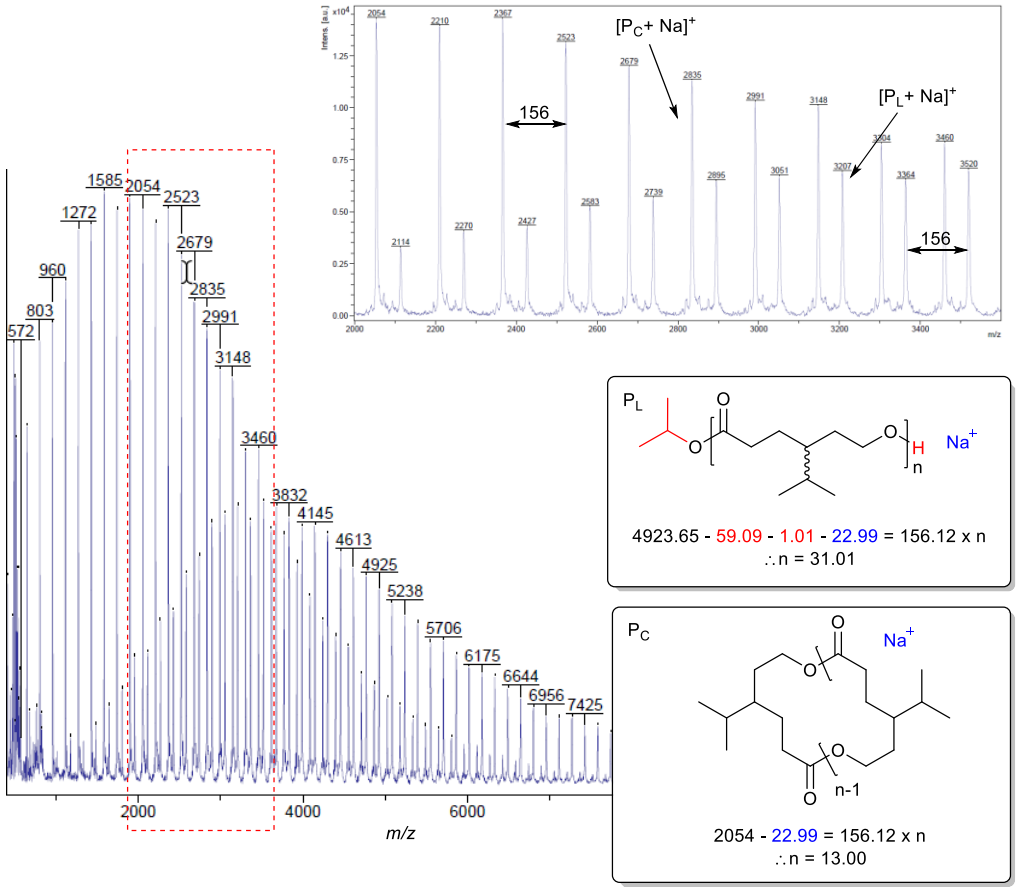

Figure 4.13. MALDI-ToF MS of poly(**4**) ($M_{n,\ GPC}$ = 5700, $Đ$ = 1.18). The less intense series is assigned to the sodium adduct of the linear polymer (shown) with -O^{i}Pr and -H end groups. The smaller series is a cyclic polymeric species with no end groups, arising from backbiting of the growing polymer chain.

A polymer sample prepared with {Zr(tris)O^{i}Pr} was also analysed by MALDI-ToF, shown in Figure 4.14. The series is seen having *m/z* values consistent with the sodium adduct of a linear polymer capped by -OH and -H groups rather than the expected -O^{i}Pr and -H moieties arising from the expected coordination-insertion mechanism. It is likely that the

isopropoxide functionality was cleaved by hydrolysis during polymer work-up, replacing an isopropoxide group with -OH.

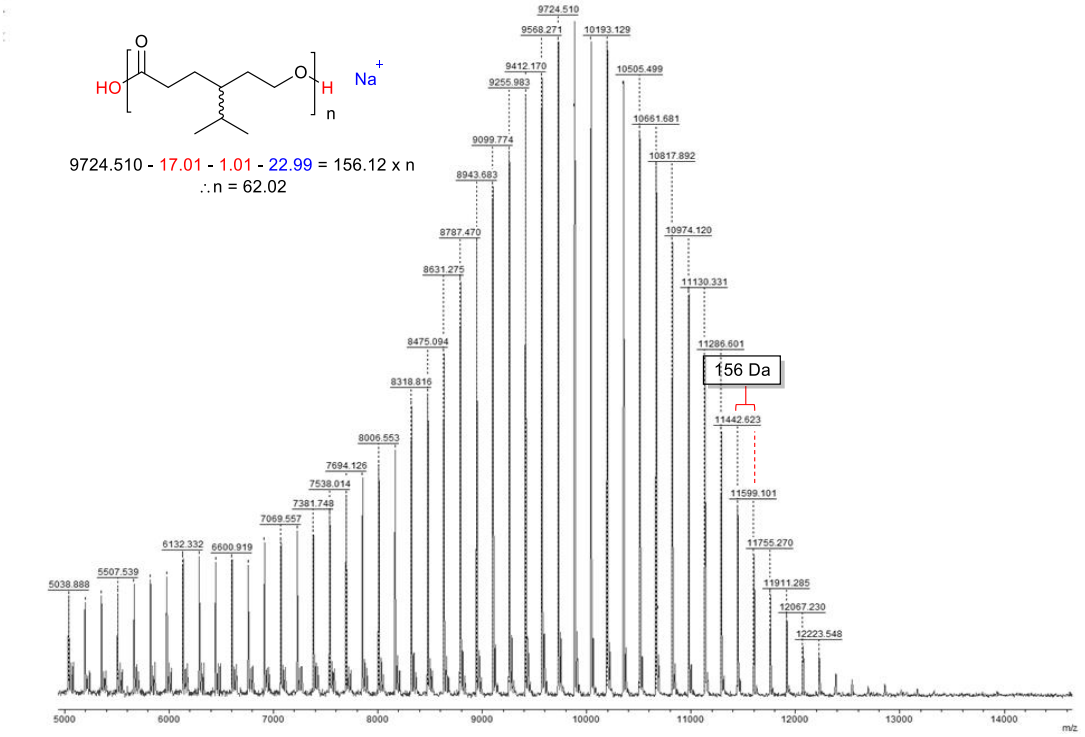

Figure 4.14 . MALDI-ToF MS of poly(**4**) (M_n, $_{GPC}$ = 9680, $Đ$ = 1.17). The major series is assigned to the sodium adduct of the linear polymer (shown) with -OH and -H end groups.

4.3.1.3 Other polyester characterisation

FTIR spectroscopic analysis of the polymer showed a characteristic strong absorption due to the C=O stretch of the polyester linkages at *ca*. 1756 cm^{-1}.

Analysis of the polymer by differential scanning calorimetry (DSC) showed a glass transition temperature (T_g) of *ca.* -50 °C (Figure 4.15). DSC analysis of these polymer products showed very slight variation in the T_g with the molecular weight of the polymer.

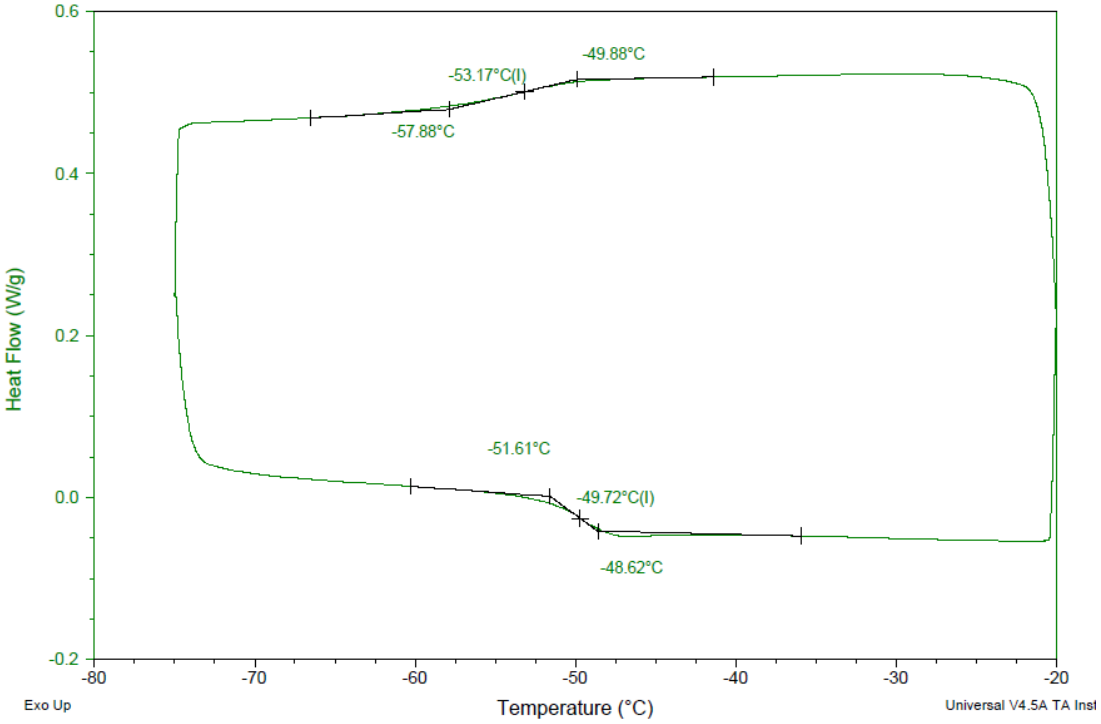

Figure 4.15. DSC trace of poly(**4**), showing a glass transition temperature, T_g = -49.7 °C.

4.3.2 Copolymerisation of 4-isopropylcaprolactone with LA

The synthesis of lactide co-monomers from bio-renewable resources is an attractive route for the preparation of fully renewable copolymers. Copolymerisation studies of *L*- and *rac*-LA with 4^{i}PrCL (**4**) were conducted, with the aim of preparing copolymers with different ratios of each monomer *via* "one-pot" or sequential addition respectively (Table 4.4). Investigations were initially conducted with *L*-LA to produce purely isotactic LA regions in polymer products. In all cases the conversion of *L*-LA was higher than for **4**, particularly for entries with higher [LA]:[**4**], indicating that the relative rate of enchainment for lactide monomers is much faster than for the substituted caprolactone. Copolymer products were generally found to be low molecular weight. Random, "one-pot" copolymerisations were then attempted with {Zr(bis)(O^{i}Pr)$_2$}– both solvent-free and in solution (Table 4.4, entries 5-10) with 4^{i}PrCL derived from β-pinene. In all cases a high conversion of both LA and **4** was observed.

Table 4.4. Selected copolymerisation data for **4** with LA.

Entry	Initiator	LA	[LA]:[**4**]	Time / h	Temp. / °C	Con. [a] / % LA	Con. [a] / % **4**	M_n [b]	$Đ$ [b]
1	Zr(tris)(O^{i}Pr)	*L*-LA	25:75	48	100	99	90	4540	1.42
2	Zr(tris)(O^{i}Pr)	*L*-LA	50:50	48	100	99	90	3800	1.46
3	Zr(tris)(O^{i}Pr)	*L*-LA	75:25	48	100	85	45	4570	1.23
4	Zr(tris)(O^{i}Pr)	*L*-LA	85:15	48	100	85	44	6870	1.32
5[$]	Zr(bis)(O^{i}Pr)$_2$	*L*-LA	50:50	2	100	96	89	4900	2.00
6[$]	Zr(bis)(O^{i}Pr)$_2$	*L*-LA	25:75	2	100	98	91	4600	1.79
7[$]	Zr(bis)(O^{i}Pr)$_2$	*L*-LA	75:25	2	100	98	87	7500	1.67
8[$]	Zr(bis)(O^{i}Pr)$_2$	*L*-LA	50:50	6	80	96	84	4600	1.42
9[$]	Zr(bis)(O^{i}Pr)$_2$	*L*-LA	25:75	6	80	96	89	3350	1.51
10[$]	Zr(bis)(O^{i}Pr)$_2$	*L*-LA	75:25	6	80	96	80	6860	1.39
11[d]	Zr(tris)(O^{i}Pr)	*L*-LA	50:50	24+24	80	99	31	7900	1.15
12[e]	Zr(tris)(O^{i}Pr)	*L*-LA	50:50	24+24	80	22	37	2020	2.32
13[d]	Zr(bis)(O^{i}Pr)$_2$	*rac*-LA	50:50	24+4	80	93	91	6220	1.19
14	Zr(bis)(O^{i}Pr)$_2$	*rac*-LA	50:50	24	80	92	74	9160	1.72

All polymerisations performed neat except entries 8, 9 and 10 which were conducted in toluene. [a]Determined from analysis by ^{1}H NMR spectroscopy. [b]Determined by GPC (THF), using polystyrene standards. [c]Determined from DSC analysis. [d]LA added first, addition of 4^{i}PrCL after 24 h. [e]4^{i}PrCL added first. [$]4^{i}PrCL monomer prepared from β-pinene.

Attempts were made to prepare block copolymers with **4** and *rac*-LA with both zirconium-based initiators (entries 11 - 13 in Table 4.4) v*ia* sequential addition of monomers. Again, higher conversion of both monomers was observed with {Zr(bis)(O^{i}Pr)$_2$}. Interestingly, when monomer **4** was added first followed by the addition of LA after 24 h (Entry 12), very low conversion of both monomers was observed. DSC analysis (Table 4.4, entries 11 & 13) were found to have T_m = 137.9 °C and 139.3 °C respectively, slightly lower than expected for pure PLLA.

However, diffusion-ordered spectroscopy (DOSY) analysis of entry 13 (Figure 4.16) showed the polymer product to be an independent mixture of poly(**4**) and polylactide, with resonances for the polylactide and poly(**4**) corresponding to signals which are aligned on different horizontal lines, thus indicating there are two distinct macromolecules with diffusion coefficients (D = 2.0 x 10^{-10} m^2s^{-1} and D = 6.0 x 10^{-10} m^2s^{-1} respectively). This constitutes proof of the presence of at least two species with different hydrodynamic radii instead of the desired block copolymer. For a poly(**4**-*co*-LA) block copolymer, the signals would all exist on the same horizontal line, *i.e.* a single species with one diffusion coefficient.[32,33] Some residual monomer **4** is also observed in the polymer.

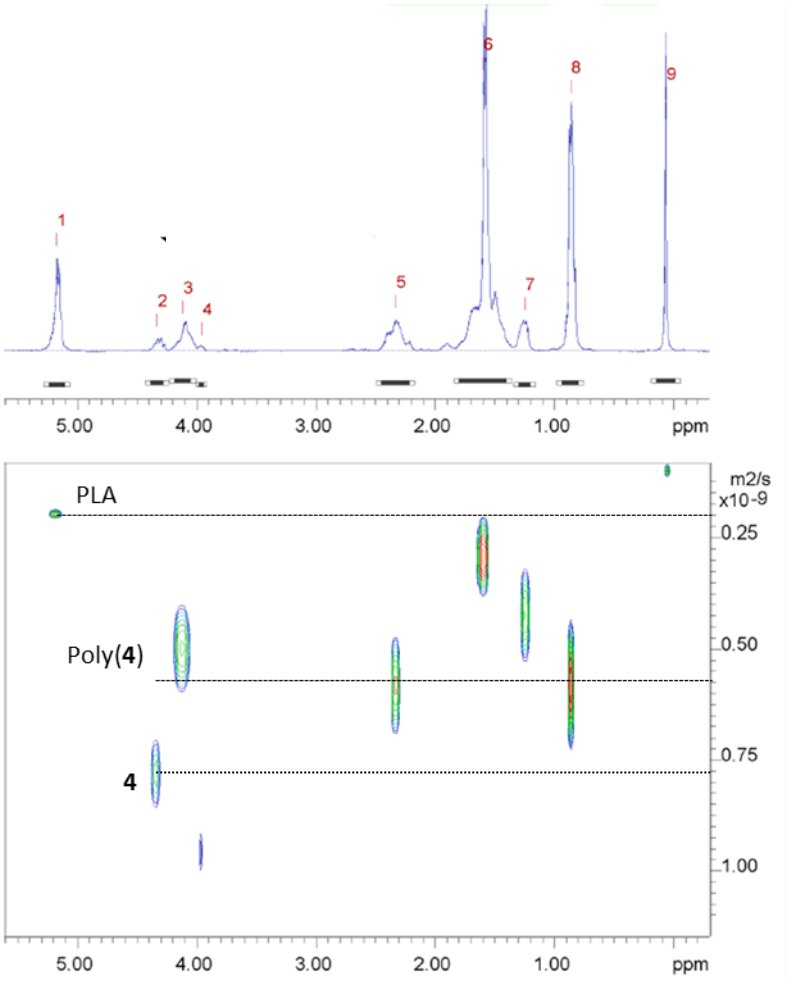

Figure 4.16. DOSY NMR spectrum of attempted block copolymer (Table 4.4, entry 13), showing homopolymer formation only.

To enable block polymer formation, it would be beneficial to first polymerise 4^{i}PrCL, and isolate this as a hydroxy-functionalised polymer which could be used as a macroinitiator for the lactide polymerisation, as has been well reported in the literature in the preparation of functional triblock polymers.[34,35] However, attempts to successfully synthesise block copolymers *via* this method have been unsuccessful thus far.

DOSY analysis of a random ("one-pot") copolymer (Table 4.4, entry 14) was consistent with copolymer formation, where all resonances of the proton spectrum are seen to belong to one species, with a diffusion coefficient, D = 0.65 x 10^{-10} m^2s^{-1} (Figure 4.17). This DOSY spectrum is very different from the previous example, as all resonances correspond to a single diffusion coefficient rather than several being present. The faster the molecules move, the faster their intensity decreases. Larger molecules move more slowly, and therefore have a smaller diffusion coefficient. DOSY has been reported as a useful tool in

prediction of polymer molecular weights for several polymers including PLLA[36] and more recently PEF,[37] but this requires a calibration curve to be produced with polymers of known molecular weights to give accurate results.[38]

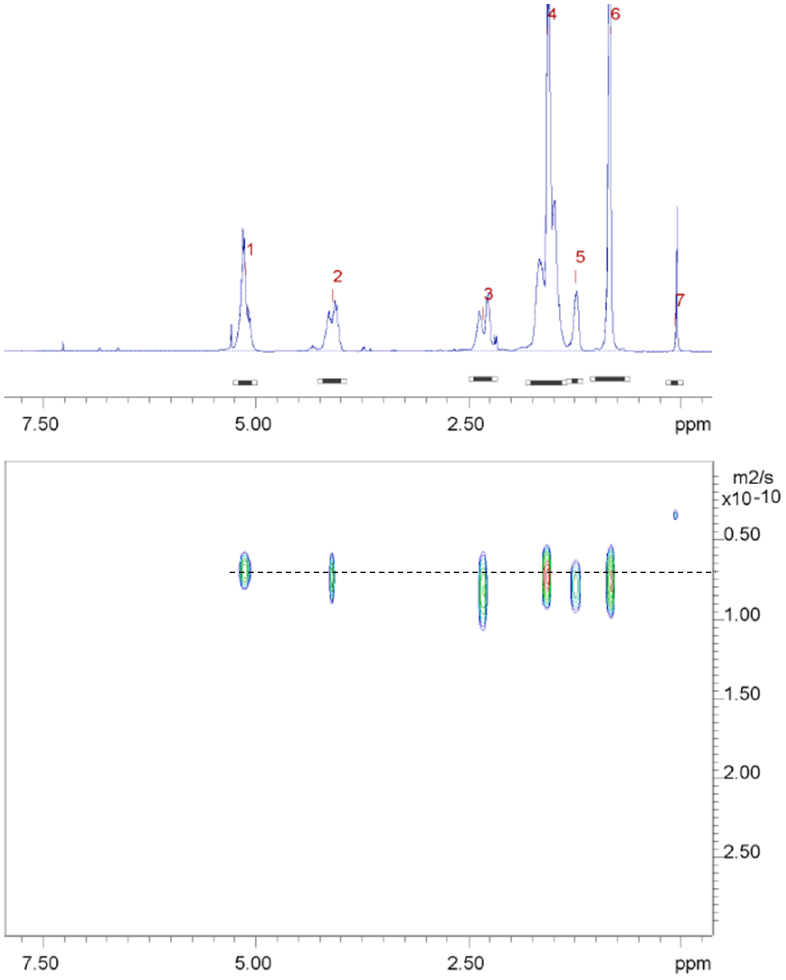

Figure 4.17. DOSY NMR spectrum of poly(**4**-*co*-LA) (Table 4.4, entry 14)

While initial copolymerisation studies have been performed, there is much scope here for synthesising testing the properties of new, fully renewable copolymer materials. It would be interesting to prepare triblock elastomers having **4** as the "rubbery" midblock, for example, as reported by Hillmyer and co-workers for similar monomers.[34,35]

4.4 Synthesis of unsaturated monomers from β-pinene

An attractive attribute of terpenes as monomers is their inherent functionality. The incorporation of alkene moieties in polymeric materials can provide a handle for post-polymerisation modification *via* common synthetic strategies such as epoxidation or thiol-ene click chemistry. Unsaturated lactone molecules could afford polyesters with regularly

spaced alkene moieties either incorporated into the backbone (increasing rigidity) or as periodic pendant groups throughout the polymer architecture.

Treatment of intermediate **2** with 3 equivalents of mCPBA in CH_2Cl_2 gave the normal lactone-epoxide, **9**, in 53% yield after purification *via* crystallisation from hexanes (Scheme 4.4). The ^1H NMR spectrum of this epoxide-lactone is shown in Figure 4.18. The presence of a doublet resonance at 5.18 ppm is indicative of this regioisomer being isolated rather than the abnormal lactone, whereby oxygen insertion would occur on the other side of the carbonyl moiety. If the abnormal lactone were the product, one would expect to see a multiplet integrating to 2 protons, corresponding to the methylene adjacent to the oxygen atom of the ester moiety, and a doublet corresponding to the CH between the carbonyl and epoxide. The methyl groups of the isopropyl moiety are observed as two doublets but with somewhat different chemical shifts, arising from the rigid confinement of the molecule. A peak at *m/z* = 193.0836 was observed in the ESI-MS spectrum, corresponding to the sodiated ion of the expected molecule (*m/z* calc. for $[C_9H_{14}O_3+Na]^+$ = 193.0841).

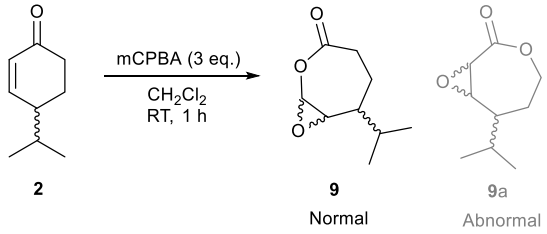

Scheme 4.4. BVO of **2**, with the structures of possible normal and abnormal lactone products **9**/**9**a.

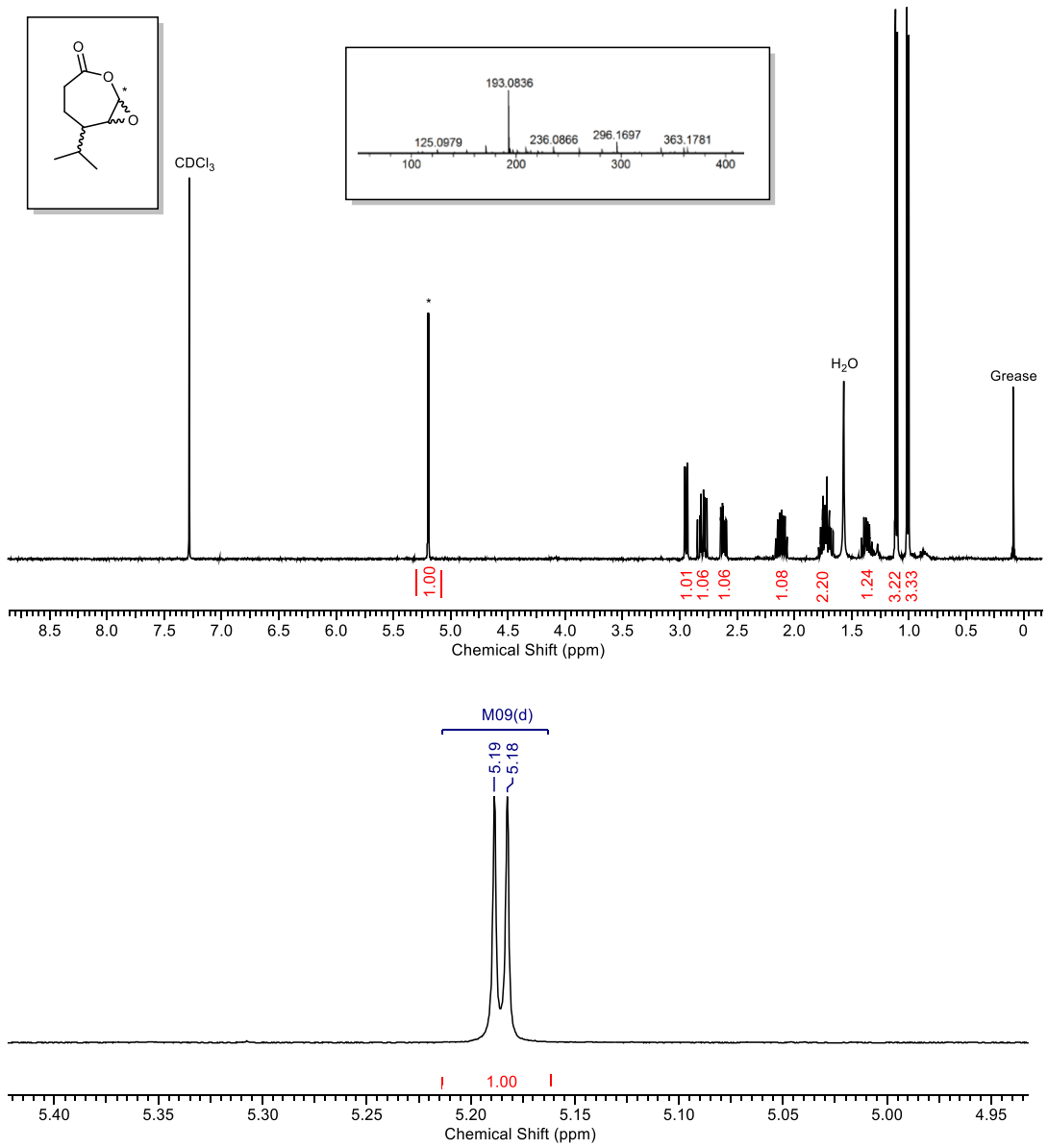

Figure 4.18. ^{1}H NMR spectrum of lactone-epoxide **9** derived from (±)-cryptone, **2**, with zoomed in region showing the doublet at 5.18 ppm. ESI-MS spectrum of **9**, major peak is the sodiated ion.

The solid-state structure of **9** is shown in Figure 4.19. Four molecules were observed per unit cell, which is relatively unusual but arises from the presence of three chiral centres in the molecule giving different diastereoisomers in the solid state.

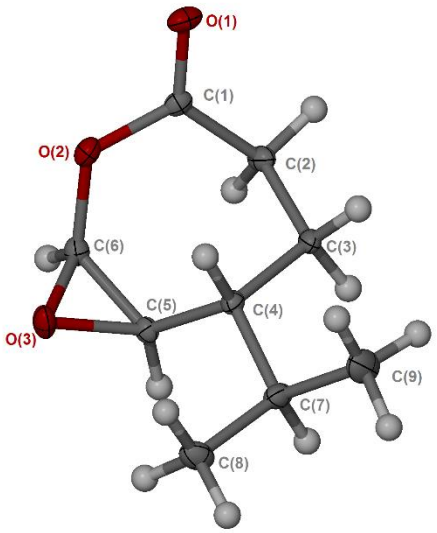

Figure 4.19. Solid-state structure for lactone-epoxide **9**. Ellipsoids are shown at the 30% probability level. Four molecules are present in the asymmetric unit (chiral centres are at C4, C5, C6) form shown is *R,R,S*. Selected bond lengths (Å) and angles (°): O(1)-C(1) 1.2021(14), C(1)-O(2) 1.3688(15), C(1)-C(2) 1.5013(16), O(2)-C(6) 1.4124(15), C(2)-C(3) 1.5394(16), O(3)-C(6) 1.4132(14), O(3)-C(5) 1.4616(13), C(3)-C(4) 1.5370(15), O(1)-C(1)-O(2) 116.91(11), O(1)-C(1)-C(2) 125.20(12), O(2)-C(1)-C(2) 117.89(10), C(1)-O(2)-C(6) 119.07(9), C(6)-O(3)-C(5) 60.86(7), C(5)-C(4)-C(7) 111.96(9), C(6)-C(5)-O(3) 57.93(7), C(6)-C(5)-C(4) 119.39(10), O(3)-C(5)-C(4) 117.36(9), O(2)-C(6)-O(3) 113.27(10), O(2)-C(6)-C(5) 119.34(10), O(3)-C(6)-C(5) 61.21(7).

Polymerisation of **9** was originally attempted with $Sn(Oct)_2$/BnOH with [**9**]:[Sn]:[BnOH] = 50:1:1 in toluene at 80 °C and solvent-free at 100 °C. No conversion was observed in solution, and at 100 °C sublimation of the monomer in the Young's tube was observed. A final attempt was made at 60 °C (mp = 56-58 °C), solvent-free. After 18 h a thick, yellow oil was obtained. Analysis of the crude reaction mixture using ^{1}H NMR spectroscopy (Figure 4.20) showed little difference from the lactone-epoxide to the crude reaction mixture although a smaller amount of a new species was observed (*ca.* 11%), with a singlet resonance at 9.85 ppm, which could be a hydrolysis product. No polymeric material was observed by GPC (THF).

With $ZnEt_2$/BnOH, it was possible to prepare polymeric material in 2 hours at 100 °C. The polymerisation was poorly controlled and bimodal, with two broad peaks observed in the GPC trace, corresponding to M_n = 29400, $Đ$ = 2.52 and M_n = 560, $Đ$ = 1.76. $ZnEt_2$/BnOH exhibits no selectivity for lactone ROP over epoxide ROP, so both groups will react under these conditions. No polymerisation was observed in solution at 80 °C or at lower temperatures.

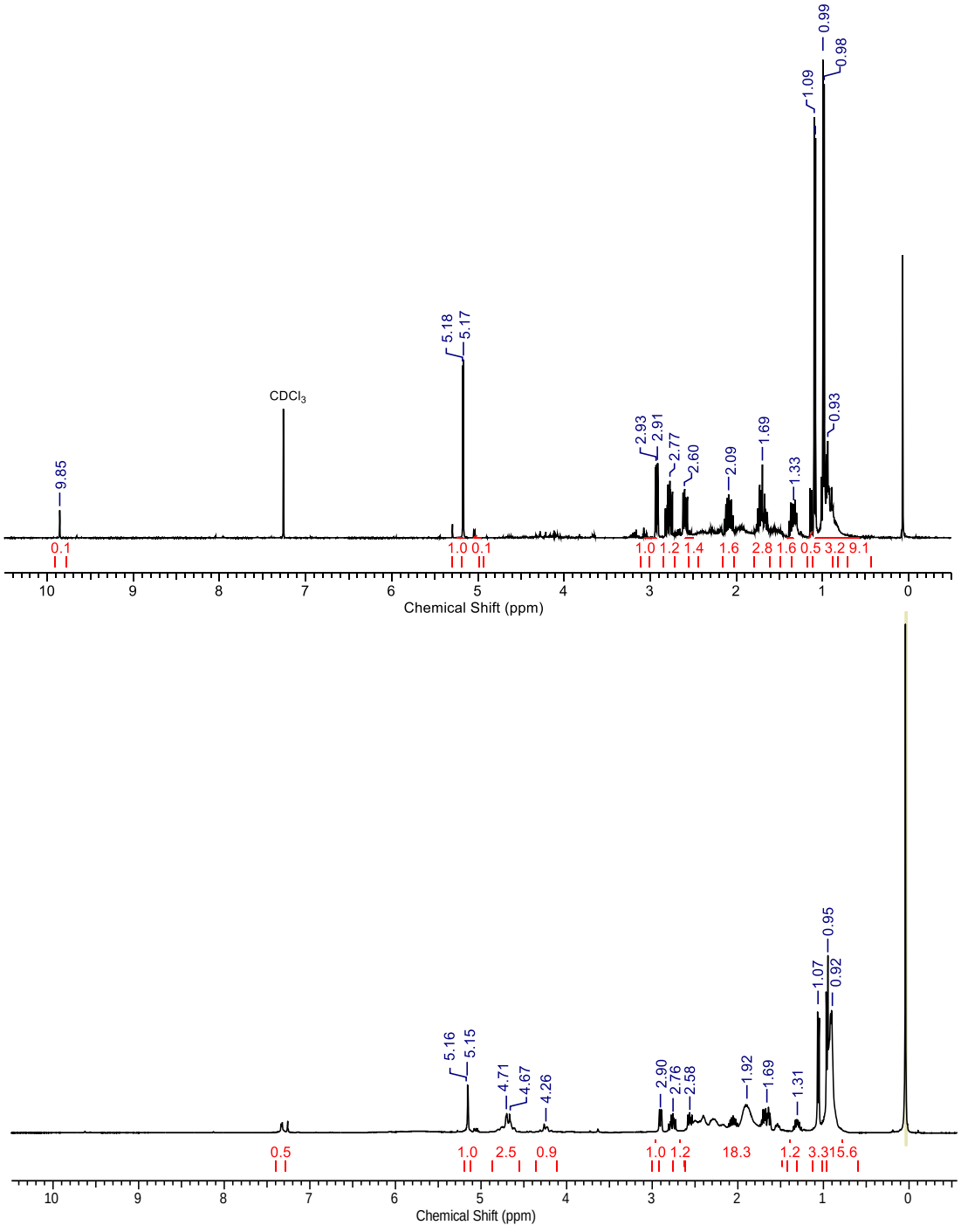

Figure 4.20. ^{1}H NMR spectra of the crude reaction mixtures obtained from ROP attempts of **9** with a) $Sn(Oct)_2$/BnOH (conditions: [**9**]:[Sn]:[BnOH] = 50:1:1, solvent-free, 60 °C, 18 h) and b) $ZnEt_2$/BnOH (conditions: [**9**]:[Zn]:[BnOH] = 50:1:1, solvent-free, 100 °C, 2 h).

As little success was found with the lactone-epoxide, **9**, an alternate approach whereby the unsaturated lactone could be prepared *via* a chemoselective BVO using conditions developed for the synthesis of vinyl esters by Lawrence[39] was utilised to provide a route to

the unsaturated lactone **10** in 40% yield after purification by flash column chromatography (Scheme 4.5). This was performed in collaboration with Dr. Robert Chapman. The chemoselectivity arises from the addition of 4-(dimethylamino)pyridine (DMAP) into the reaction mixture, which is oxidised *in situ* to a catalytically active *N*-oxide species, which promotes ester formation over epoxidation of the alkene.

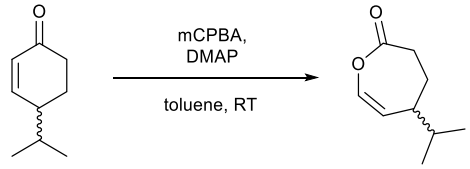

2 **10**

40%

Scheme 4.5. Selective Baeyer-Villiger Oxidation under chemoselective conditions

Only one isomer was observed to form by TLC analysis. A change in conjugation from **2** is evident in the ^{1}H NMR spectrum (Figure 4.21), where the resonances of the alkene protons are shifted upfield compared to the spectrum for the cyclic ketone. It is evident that the product of the chemoselective BVO is the normal lactone where the oxygen insertion has occurred between the carbonyl and alkene moieties. No resonance is observed for a methylene -CH_2- adjacent to an ester, which would be expected around 4-4.5 ppm if the other isomer had formed. The ethylene protons are observed as a doublet of doublets at 6.38 ppm (J = 6.5, 2.0 Hz), and a pseudo triplet at 5.24 ppm.

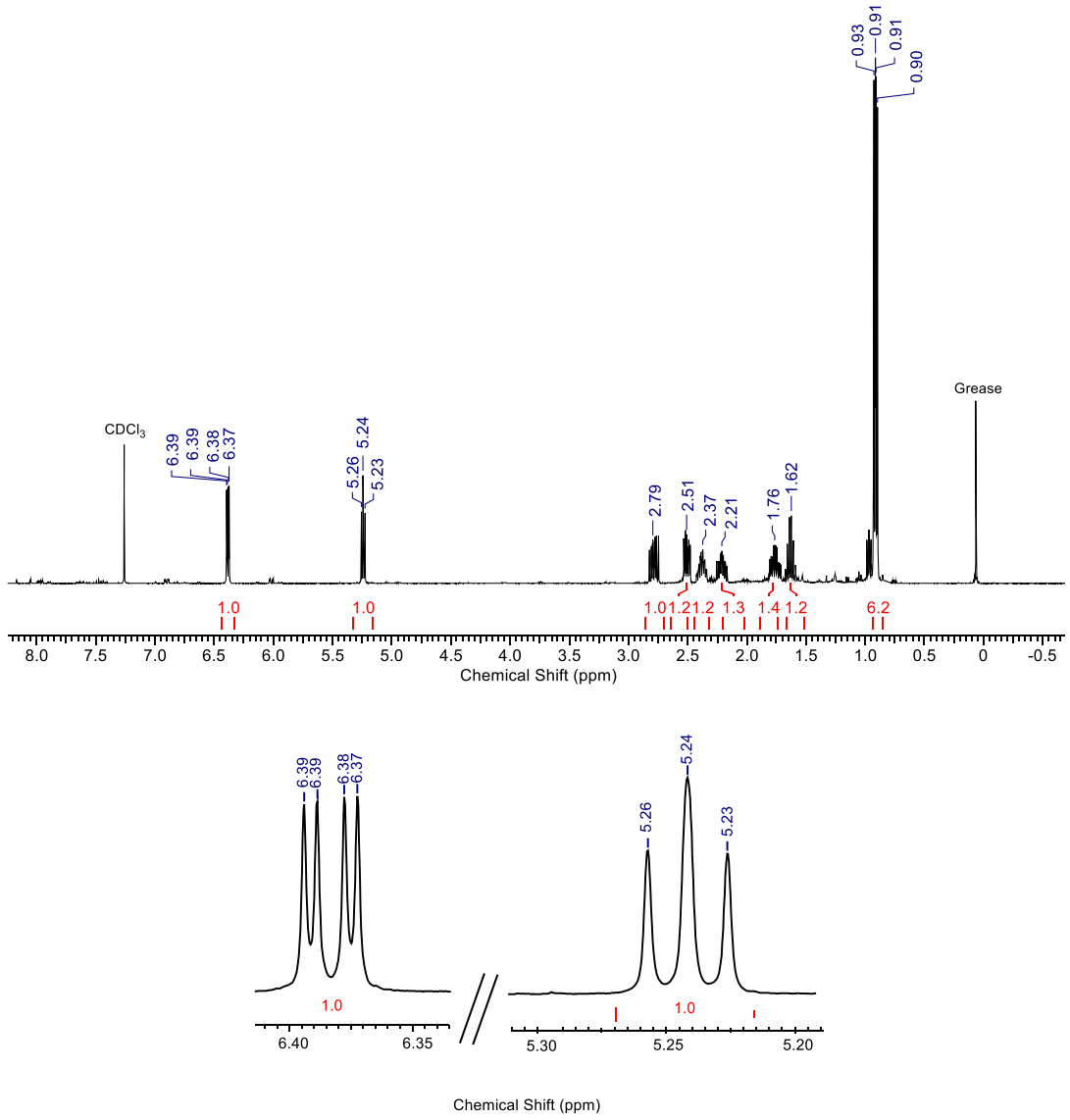

Figure 4.21. ^{1}H NMR ($CDCl_3$, 400 MHz) of molecule **10** with expanded regions for the alkene protons

The ROP of this molecule would theoretically yield polyesters with alkene moieties built into the backbone of the polymer, which could have a marked effect on the thermal properties and provide a handle for post-polymerisation modification (PPM). Unsaturated polyesters such as this have been reported *via* ROP of the unsaturated caprolactone[40] or modification of polymers with cleavable functional groups.[41]

No polymer was obtained under solvent-free conditions with $Sn(Oct)_2$ as the catalyst and BnOH as co-initiator ([**10**]:[Sn]:[BnOH] = 50:1:1, solvent-free, 130 °C, 2 h). It is possible that further purification was required to achieve polymerisation, which was not possible within time constraints, but would warrant investigation in the future.

Routes from β-pinene to other unsaturated cyclohexanone molecules were also investigated, which could provide a route to unsaturated lactones *via* chemoselective BVO, while preserving some inherent terpene functionality and removing the alkene hydrogenation steps required to make monomer **4**. Few examples of unsaturated caprolactones as monomers with the potential for PPM exist in the literature, while routes to 6-membered compounds *via* Diels-Alder cycloadditions are more common.[42,43]

A synthetic route to unsaturated cyclohexanones found to be of interest was the acid catalysed isomerisation of (+)-nopinone with trimethyl orthoformate, as reported in a 1971 US patent (Scheme 4.6).[44] Upon repeating this reaction on a laboratory scale, GC-MS analysis of the crude product mixture showed 50% conversion to 4-isopropenylcyclohexanone, **11**, and *ca.* 25% to both the tetra-substituted alkene, **12**, and methoxy analogue, **13**. Although the stringent conditions for the separation of these three molecules were reported *via* vacuum distillation, attempts to do this on a laboratory scale proved unsuccessful, and column chromatography only allowed for the separation of **13**, with the two alkene substrates being inseparable on silica. Research by Cunningham as part of a project on catalytic modification of terpenes[45] showed that it was possible to exploit the higher reactivity of the tetra-substituted alkene to epoxidation by treatment with 0.3 equivalents of mCPBA to yield epoxide **14**, as shown in Scheme 4.6. 4-Isopropenylcyclohexanone (**11**) could then be separated easily from **13** and **14** by column chromatography on silica (95:5 hexane/EtOAc, R_f **11** = 0.3) in *ca*. 50% yield over two steps (44% isolated after column chromatography).

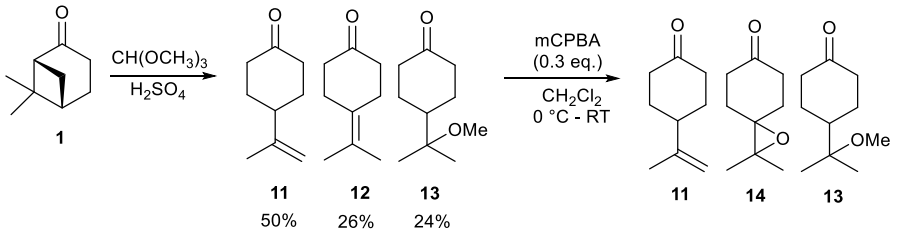

Scheme 4.6. Acid-catalysed isomerisation of nopinone to substituted cyclohexanone products and selective epoxidation of tetra-substituted alkene **12**.

The ^{1}H NMR spectrum of compound **11** is shown in Figure 4.22. A characteristic resonance for the alkene protons is observed at 4.73 ppm, similar to reported values for compounds bearing this isopropenyl moiety.[44]

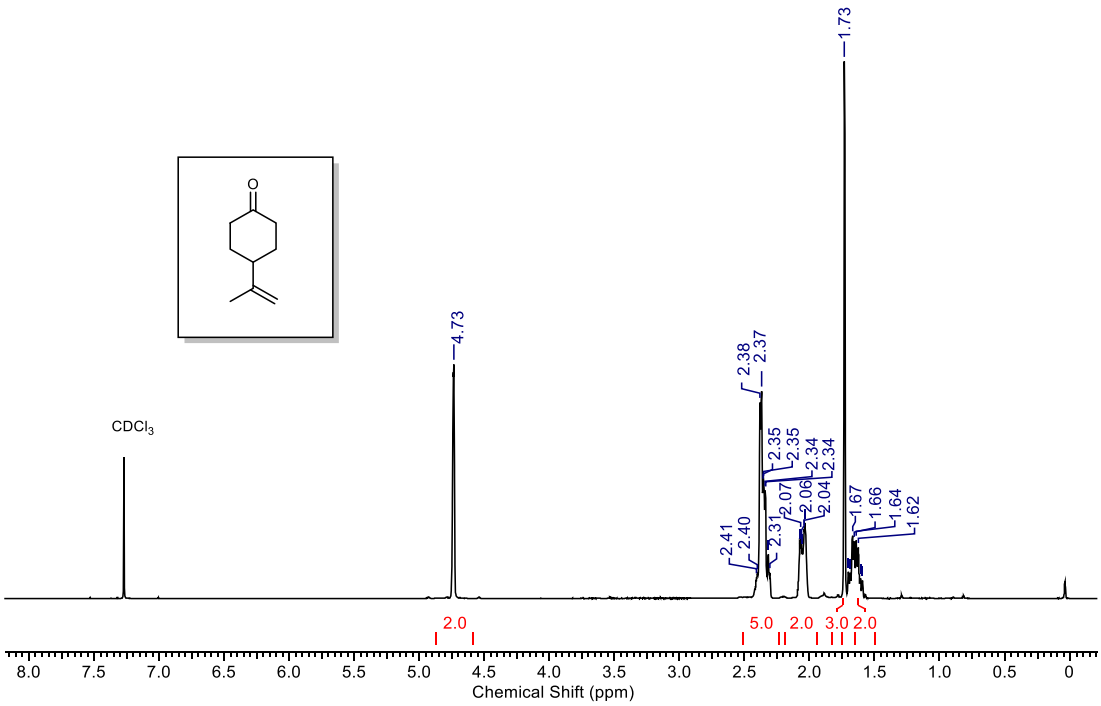

Figure 4.22. ^{1}H NMR spectrum (400 MHz, $CDCl_3$) of **11**.

The BVO of **11** was initially attempted with mCPBA to form the lactone with an epoxide in the pendant position. Two equivalents of oxidant are required for both lactone and epoxidation formation while using sub-stoichiometric quantities of mCPBA affords a mixture of oxidised products (Scheme 4.7).

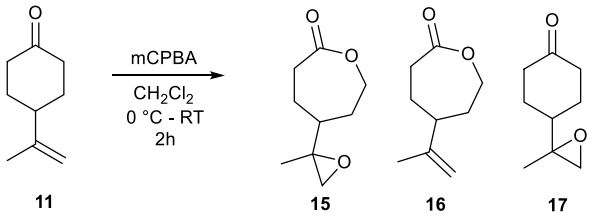

Scheme 4.7 Oxidation of **11** with mCPBA

The polymerisation of lactones such as **15** is complex as there are competing functional groups amenable to ring-opening reactions present, as observed for the polymerisation of **9**. Indeed, attempts to polymerise **15** with $Sn(Oct)_2$/BnOH at 100 °C (100:1:1) gave an orange, oligomeric gel material (M_n = 1420, $Đ$ = 1.78) which was difficult to characterise by ^{1}H NMR spectroscopy. This material had a T_g of -26.6 °C, significantly higher than the T_g of poly(**4**) (*ca.* -50 °C). It was decided to investigate methodologies for lactone formation which would leave the alkene moiety intact, allowing for a range of post-polymerisation modification methodologies, including epoxidation, to be investigated.

The conditions employed for the chemoselective Baeyer-Villiger oxidation of cryptone were also successful here in forming the desired lactone but leaving the alkene >98% "intact". At higher conversion (62% lactone), the formation of small amounts of epoxide was observed in the ^{1}H NMR spectrum of the crude reaction mixture, but this could be easily separated from the desired product by column chromatography on silica with EtOAc (1 -10%)/hexane as eluent. The unsaturated lactone **16** was prepared from **1** in 31% yield over four steps.

Corma *et al.* described a method to chemoselectively produce lactones in substrates with alkene moieties such as terpenoid dihydrocarvone, using a β-Sn doped zeolite and aqueous H_2O_2 as oxidant.[46] This proceeds *via* initial selective activation of the carbonyl group through coordination to a Sn(IV) site, followed by reaction with non-activated H_2O_2. Recently advances in this process have included simple, scalable catalyst preparation[47] and investigations into the BVO of saturated cyclohexanones in flow systems.[48] Very recently, this system was reported for the continuous production of bio-renewable polymer grade lactone monomers, including the production of 4^{i}PrCL.[28] Interestingly, the authors discussed the enhanced rate of BVO of 4-substituted over 2-subsituted cyclohexanones. It was proposed that this system could allow for selective BVO of cyclohexanone **11** to lactone **16** under analogous conditions to those reported by Yakabe *et al.* (Scheme 4.8).[48]

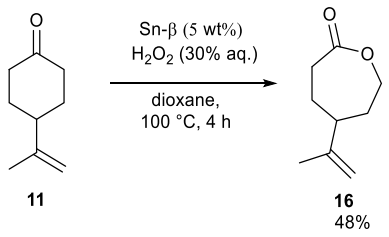

Scheme 4.8. Chemoselective BVO of **11** using Sn-β catalyst and H_2O_2

The process was monitored by sampling of the reaction mixture at regular time intervals and analysis by GC-MS. Conversion to the desired lactone alone was observed for the first 3 hours, after which time two other products began to form, presumably products of further oxidation of the lactone. The integrated data from the GC-MS is shown in Table 4.5 and graphically in Figure 4.23.

Table 4.5. BVO of 4-isopropenylcyclohexanone **11** to lactone **16** using 5 wt% Sn -β catalyst and aq. H_2O_2 as oxidant in 1,4-dioxane at 100 °C. Samples taken at regular intervals and monitored by GC-MS. Comparison to an internal standard.

Time (min)	Ketone	Lactone	Unknown A	Unknown B
0	100.0	0.0	0.0	0.0
15	94.8	5.2	0.0	0.0
30	88.5	11.5	0.0	0.0
45	84.6	15.4	0.0	0.0
60	80.9	19.1	0.0	0.0
75	76.9	23.1	0.0	0.0
90	73.8	26.2	0.0	0.0
180	56.0	42.4	1.6	0.0
240	48.9	48.0	2.1	0.9
300	41.6	54.0	2.5	1.9
360	38.4	56.7	2.8	2.1

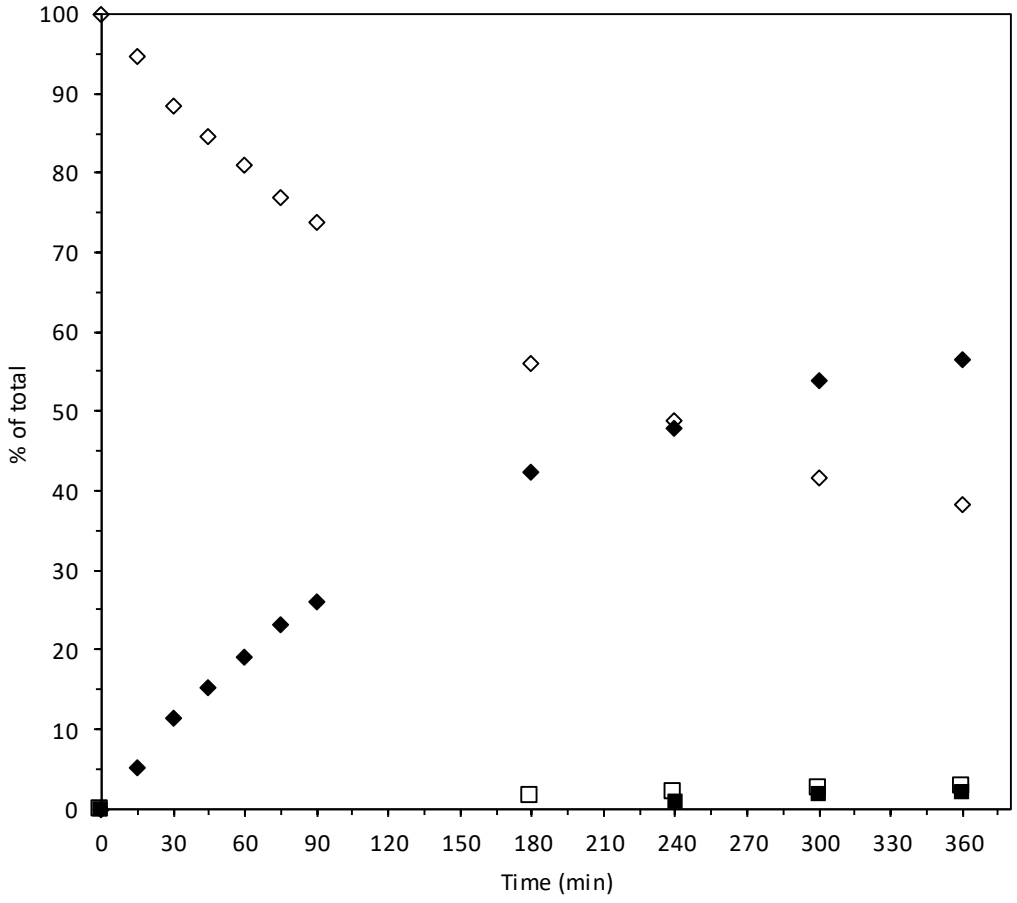

Figure 4.23. Catalytic activity of Sn-β for the BVO of 4-isopropenylcyclohexanone (◇) to 4-isopropenylcaprolactone (◆) and further oxidised by-products A (□) and B (■), monitored by GC-MS.

The side products are observed only after initial formation of the lactone and can be rationalised as further ring-opened oxidation products (Scheme 4.9), as reported in the case of the oxidation of cyclohexanone.[48] These products were not isolated in this investigation. To avoid production of these by-products, short reaction times were utilised (< 3 h) and unreacted **4** was recycled in further experiments.

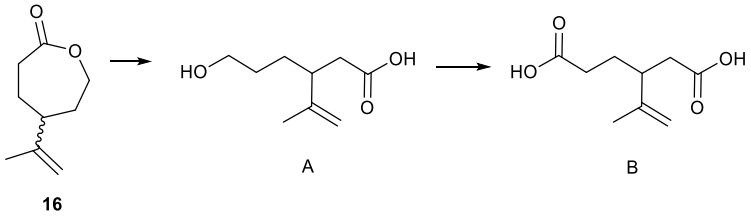

Scheme 4.9. Proposed further oxidation products, A and B, as seen in Figure 4.23

Lactone **16** was isolated as a colourless oil in 48% yield after chromatography on silica. The ^{1}H NMR spectrum is shown in Figure 4.24, featuring resonances for alkenyl protons at *ca.* 4.7 ppm. It was not possible to remove the impurities *via* column chromatography (10% EtOAc/hexane), where it was found to elute with the same R_f as the desired lactone in all solvent systems investigated. Thus, the monomer was taken forward for initial polymerisation studies without further purification. However, this may suggest that the first synthetic route described is the better choice here as it affords a purer monomer product (Figure 4.24b).

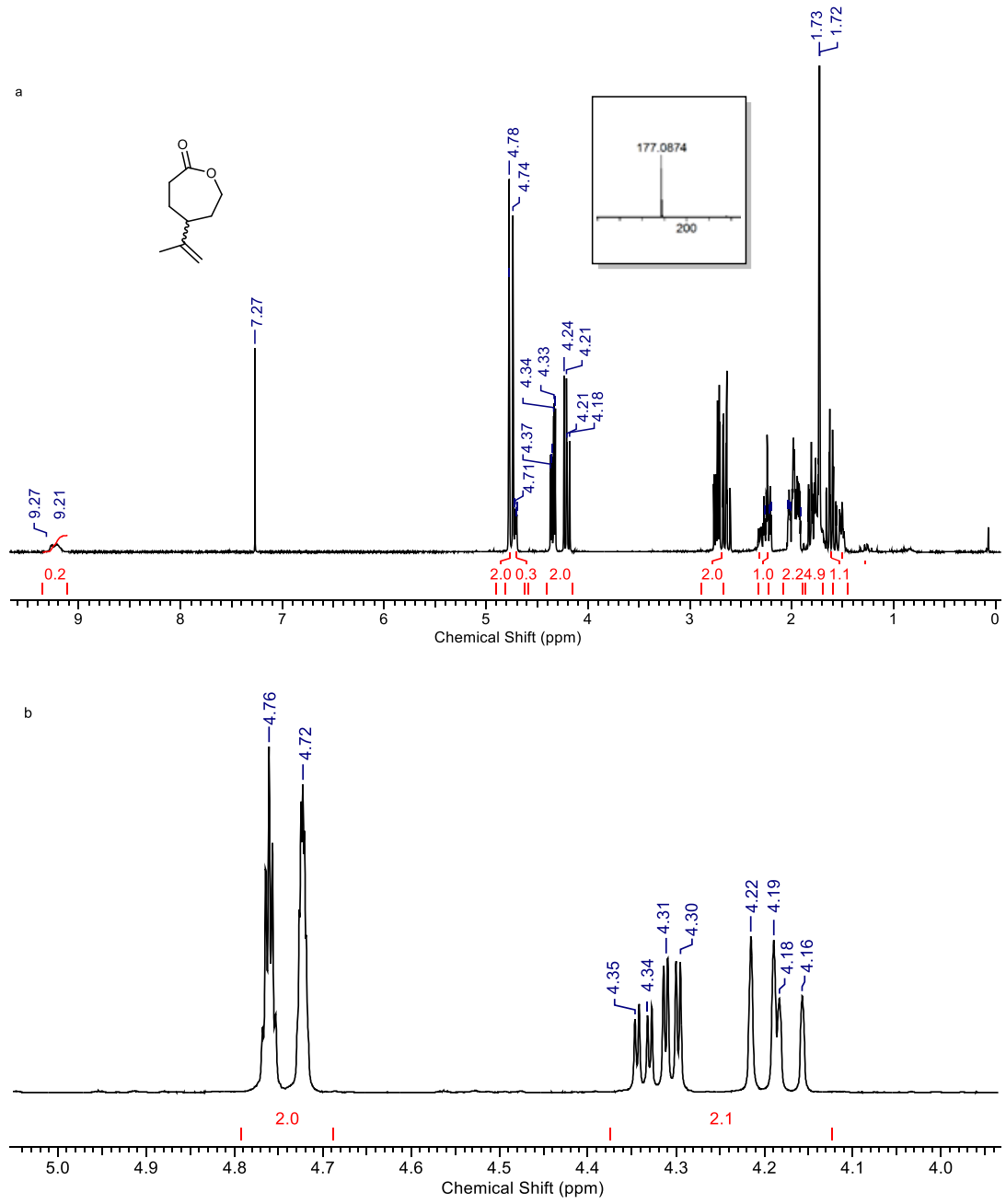

Figure 4.24. a. ^{1}H NMR (400 MHz, $CDCl_3$) of lactone **16** prepared *via* BVO with Sn-β and H_2O_2. b. ^{1}H NMR between 4.0-5.0 ppm showing resonances for the alkenyl protons with no ring-opened by-product obtained by BVO with mCPBA and DMAP. Mass spectrum is given in inset. Peak shown is the sodium adduct, $[M+Na]^+$.

4.5 Polymerisation of 4-isopropenylcaprolactone

Initial polymerisation attempts with monomer **16** were trialled solvent-free with $Sn(Oct)_2$ with BnOH as co-initiator at 100 and 130 °C (Table 4.6). Only $Sn(Oct)_2$ has been trialled so far as only small quantities of the monomer have been isolated, and there was seen to be some impurity which was difficult to remove. $Sn(Oct)_2$ is more robust than the Zr systems trialled in 4.3.1, and thus more able to tolerate impurities and the presence of water in the

polymerisation, which are likely as this monomer was not dried under the same vigorous conditions as was possible with monomer **4**.

Table 4.6. Initial polymerisation tests for monomer **16** with $Sn(Oct)_2$/BnOH

Entry	Initiator	[M]:[I]:[BnOH]	T / °C	t / h	Conv. %[a]	M_n[b]	$Đ$[b]
1	$Sn(Oct)_2$	50:1:1	100	4	74	1450	1.42
2	$Sn(Oct)_2$	100:1:1	100	24	85	2000	1.74
3	$Sn(Oct)_2$	100:1:1	130	2	72	4760	2.20

All polymerisations performed solvent-free. [a]Determined by ^{1}H NMR spectroscopy. [b]As determined by GPC (THF), using PS standards.

The oligomeric products with low molecular weight and had broad dispersities ($Đ$ = 1.42 – 2.20). This is somewhat unsurprising with the presence of impurities which could act as chain transfer agents. However, these experiments proved that the monomer could be ring-opened to the desired, novel linear polyester. Further testing of polymerisation kinetics and living character with fully purified monomer dried *via* distillation over CaH_2 should be undertaken in the future. The ^{1}H NMR spectrum of poly(**16**) prepared with $Sn(Oct)_2$/BnOH at 130 °C (Table 4.6, entry 3) is shown in Figure 4.25. The alkene functionality is preserved and is seen at 4.81 and 4.71 ppm. Conversion can be calculated by comparing the normalised integrals of the residual monomer (4.25, 4.65 ppm) with the integration of the methylene resonances (3.96, 2.19 ppm).

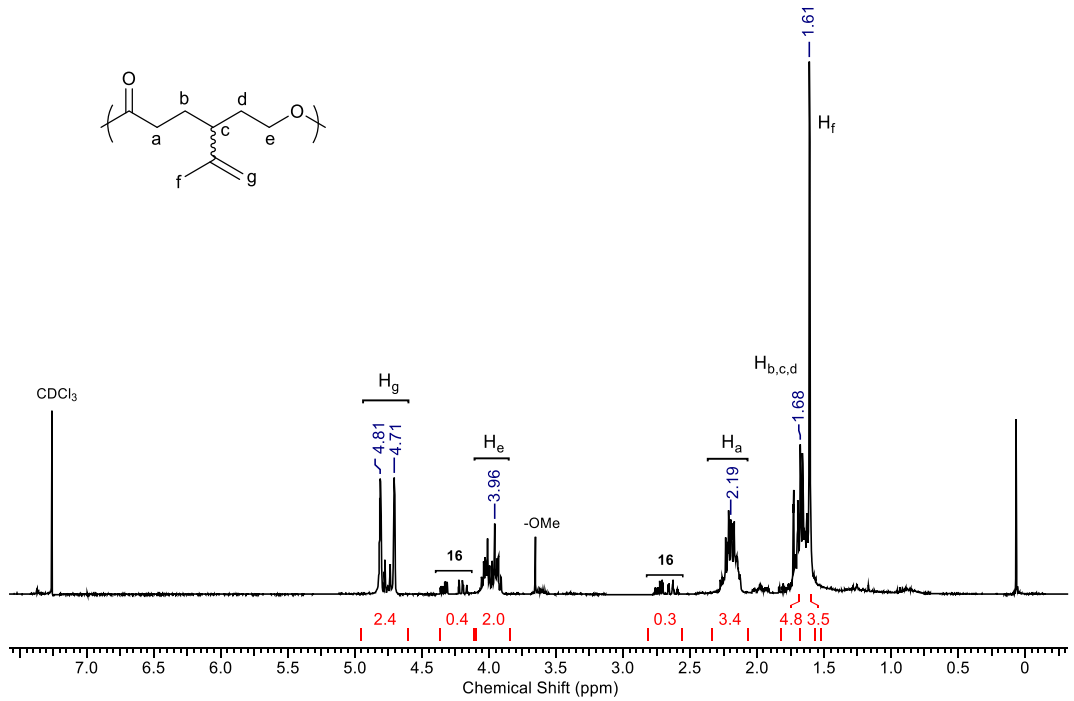

Figure 4.25. 1H NMR (400 MHz, CDCl3) of poly(**16**) prepared with $Sn(Oct)_2$/BnOH, Table 4.6, entry 3. Conditions: [16]:[Sn]:[BnOH] = 100:1:1, solvent-free, 130 °C, 2 h.

MALDI-ToF analysis of the sample from Table 4.6, entry 1 showed the polymer structure to agree with the polymer formed by ROP of the monomer, having repeat units of 154.1 Da (Figure 4.26). The end group here is -OMe, where the methoxy group has likely replaced a -OBn moiety. The methoxy group was also seen in the ^{1}H NMR spectrum (Figure 4.25), which could indicate an impurity present in the monomer which has not been thoroughly dried. This could be acting as a chain transfer agent, resulting in smaller, disperse polymers. A smaller, cyclic series is also observed.

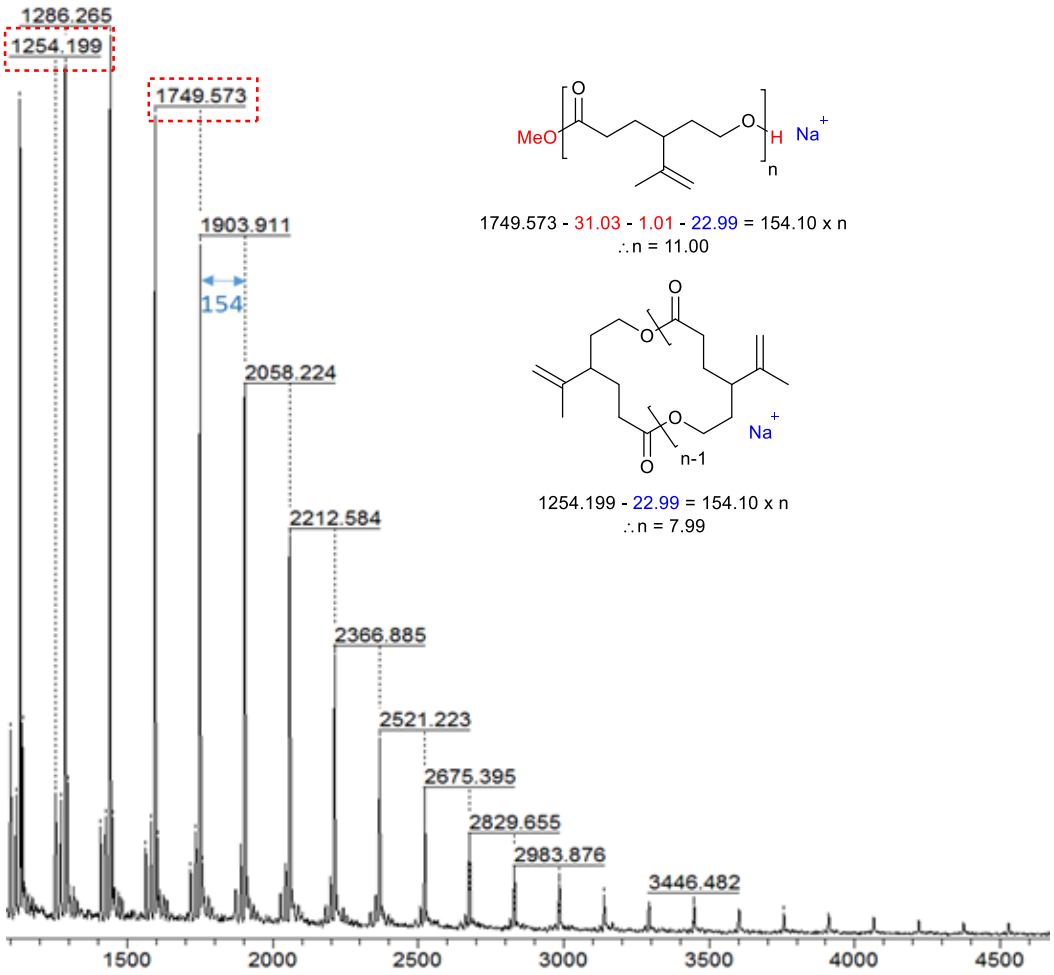

Figure 4.26. MALDI-ToF MS of polymer ($M_{n,\ GPC}$ = 1450, $Đ$ = 1.42). The major series is assigned to the sodium adduct of the linear polymer (shown) with -OMe and -H end groups. There is also a small amount of cyclic polymeric species present.

The T_g of the polymer was determined by DSC to be *ca*. -30 °C (Figure 4.27). This is somewhat higher than for poly(**4**) (T_g = -50 °C), possibly due to increased rigidity of the isopropenyl moieties.

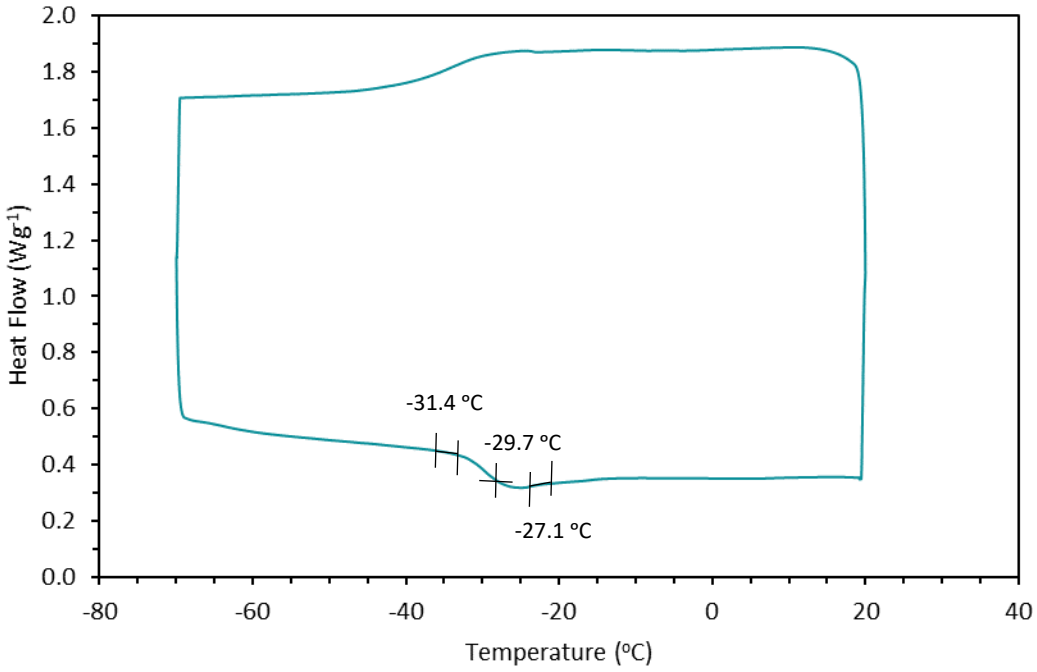

Figure 4.27. DSC trace of poly(**16**) showing a glass transition temperature of *ca*. -30 °C.

Attempts to prepare random copolymers with *rac*-LA or ε-CL yielded only homopolymers of PLA or PCL respectively, with no incorporation of **16**. As the rate of polymerisation of **4** with $Sn(Oct)_2$/BnOH is somewhat slower than for LA or ε-CL, it was decided to attempt a copolymerisation with this monomer instead, expecting that ROP would proceed more slowly and allow for incorporation of **16**. It was possible to prepare a sample of poly(**4**-*co*-**16**) containing 25% unsaturated monomer (determined by ^{1}H NMR spectroscopy) *via* "random" copolymerisation with $Sn(Oct)_2$/BnOH at 100 °C. Copolymer formation was confirmed *via* ^{1}H DOSY NMR (Figure 4.28), with all the signals from the polymer corresponding to a species with the one diffusion coefficient, D = 2.1 x 10^{-10} m^2s^{-1} (M_n = 3150, $Đ$ = 1.48).

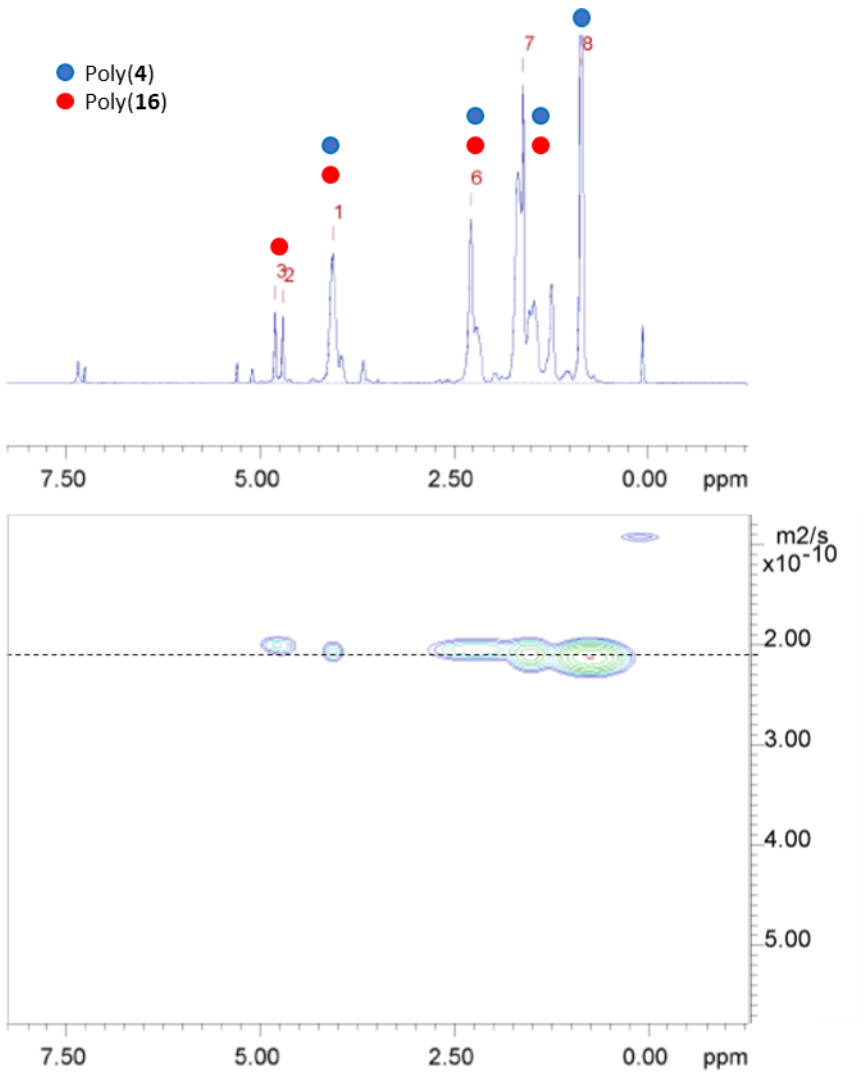

Figure 4.28. ^{1}H DOSY NMR (400 MHz, $CDCl_3$) of poly(**4**$_{75}$-co-**12**$_{25}$)

The T_g of this copolymer was more comparable to poly(**4**), with a single T_g observed at -50.8 °C (M_n = 3150, $Đ$ = 1.48), showing that more incorporation of the unsaturated monomer would be needed to increase the T_g of the copolymer.

While the alkene moiety of this monomer should allow for crosslinking by methods such as thiol-ene chemistry, the few small-scale experiments attempted here following literature precedent for similar systems[10] were unsuccessful, with the ^{1}H NMR spectra being identical to the unmodified polymer. More success was found *via* epoxidation of poly(**4**$_{75}$-co-**16**$_{25}$) with mCPBA, with the ^{1}H NMR spectrum showing full conversion of the alkene moiety to the epoxide in 2 hours in CH_2Cl_2 at RT (Figure 4.29). The M_n of the epoxidised polymer is reduced from the original copolymer (from 3150 to 2680), and the dispersity somewhat broader (1.48 to 1.65), possibly due to the acidic nature of mCPBA causing degradation of the polymer. This could be overcome by buffering the solution in future experiments.

The resonances arising from the alkenyl protons are seen as two indistinct multiplets at 4.70 and 4.80 ppm. Upon treatment with mCPBA these resonances are no longer observed in the spectrum, suggesting full conversion of the alkene bond to the epoxide moieties. A new multiplet is observed at 2.51 ppm, which presumably corresponds to the -CH_2- of the new epoxide.

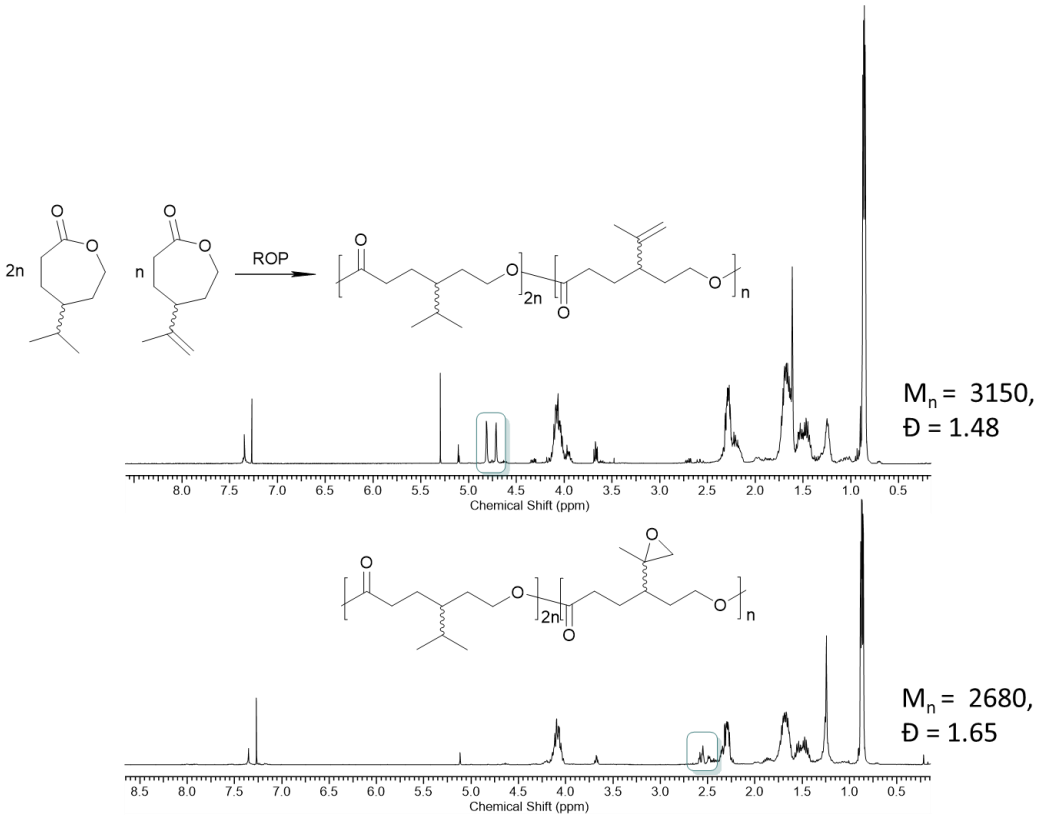

Figure 4.29. ^{1}H NMR spectra (400 MHz, $CDCl_3$) before and after post-polymerisation modification of a copolymer with 25% unsaturated monomer by epoxidation with mCPBA.

Further modifications of the epoxidised polymer would be possible *via* nucleophilic substitutions with a range of substrates. To attempt some of this chemistry on larger scales which might allow for more rigorous purification to be performed, a model cyclohexanone compound, **18**, was prepared on a 2 g scale (76%) from cheap, commercially available cyclohexen-2-one following a literature method, having the pendant isopropenyl moiety in the 2-position rather than 3 (Scheme 4.10).[49] It was hoped it would be possible to selectively prepare the lactone using the same chemoselective BVO as for compound **16**. However, the chemoselective BVO did not proceed by either method as for compound **16**. This presumably relates to the phenomenon reported by Yakabe *et al*., where 3-substituted cyclohexanones were observed to undergo selective BVO more readily than 2-

substituted.[28] Therefore, further studies into the post-polymerisation modification of these unsaturated polyesters was not possible.

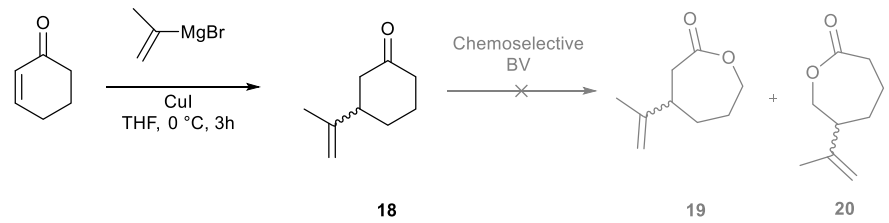

Scheme 4.10. Synthesis of 3-isopropenylcyclohexanone (**18**) and expected chemoselective BVO products (not observed).

4.6 Looking forward: other lactones from terpenes

In this chapter, routes to two substituted lactones have been discussed, but looking forward there is scope to broaden the range of bio-derived lactones from terpene feedstocks such as β-pinene. Some initial work here will be discussed in this section, which could be built on in the future.

Firstly, attempts were made to selectively prepare the tetra-substituted cyclohexanone **12** from the process described in section 4.4. This can be selectively prepared from nopinone by isomerisation, as described previously, or from commercially available 1,4-cyclohexanedione monoethylene acetal (Scheme 4.11). An attempted synthesis of lactone **22** under chemoselective conditions used for **16** were not successful.

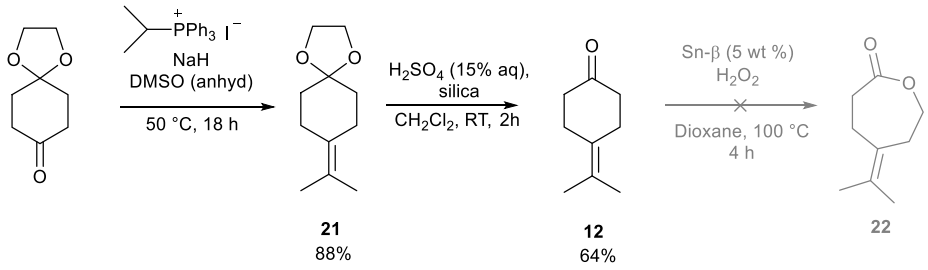

Scheme 4.11. Proposed synthesis of unsaturated lactone **22.**

The methoxy-substituted cyclohexanone (**13**) produced in the acid-catalysed isomerisation of **1** can also be selectively prepared *via* acid promoted ring-opening of nopinone in an excess of MeOH to yield exclusively the methoxy substituted cyclohexanone in 63% in 5 h at RT, which was easily separated from unreacted **1** by flash chromatography (pet ether/EtOAc 10%, dry loaded, R_f = 0.13). This yield was not optimised, and longer reaction times or recycling of (+)-nopinone would lead to higher yields. **13** was oxidised with mCPBA to attain methoxy-lactone **23** in good yield (83%). Initial polymerisation attempts with

$Sn(Oct)_2$ were unsuccessful, possibly due to coordination competition between the ester and ether moieties. However, routes to prepare different lactones from all three components of the nopinone isomerisation mixture using trimethyl orthoformate can be envisaged. It would also be possible to prepare molecules with different substituents the products by judicial choice of alcohol in the ring-opening isomerisation of (+)-nopinone, allowing for an investigation of the effect of different chain lengths or possibly preparing difunctional monomers by linking two cyclohexanone units together with a diol such as ethylene glycol. The ^{1}H NMR spectrum of the methoxy substituted lactone, **23**, is given in Figure 4.30, where a characteristic singlet at 3.18 ppm is observed, corresponding to the three protons of the methoxy moiety.

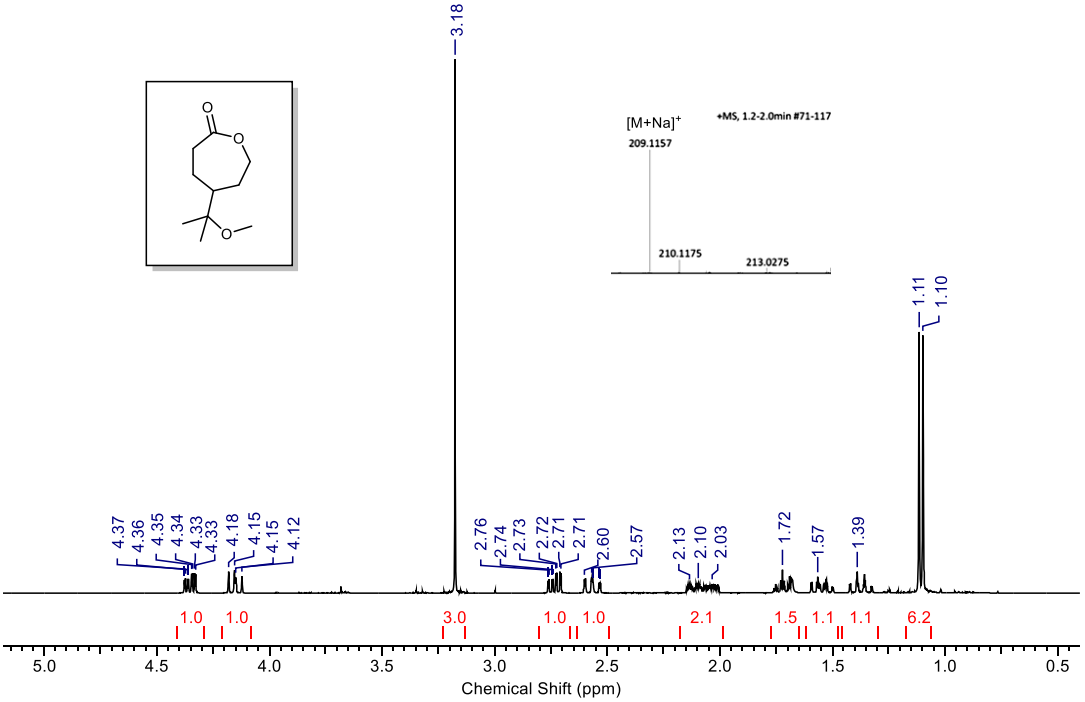

Figure 4.30. ^{1}H NMR spectrum (400 MHz, $CDCl_3$) of **23** produced from β-pinene, ESI-MS showing peaks for the sodiated ions.

Furthermore, the hydroxy-substituted molecule **24** can be accessed by introduction of water rather than alcohol in the isomerisation process, and this can be further functionalised to prepare an acetylated lactone (Figure 4.31a). During this project it was possible to prepare the hydroxy-substituted cyclohexanone (**24**), but acetylation by refluxing in acetic anhydride was unsuccessful. Further work would be needed to prepare the acetylated compound **25**. The BVO of **25** would yield an acetylated lactone, **26**, similar to molecules reported by Vaida, who reported the polymerisation of various γ-acyloxy-ε-

caprolactones but also observed competing rearrangement reactions to yield γ-acyloxyethyl-γ-butyrolactones (Figure 4.31b).[50]

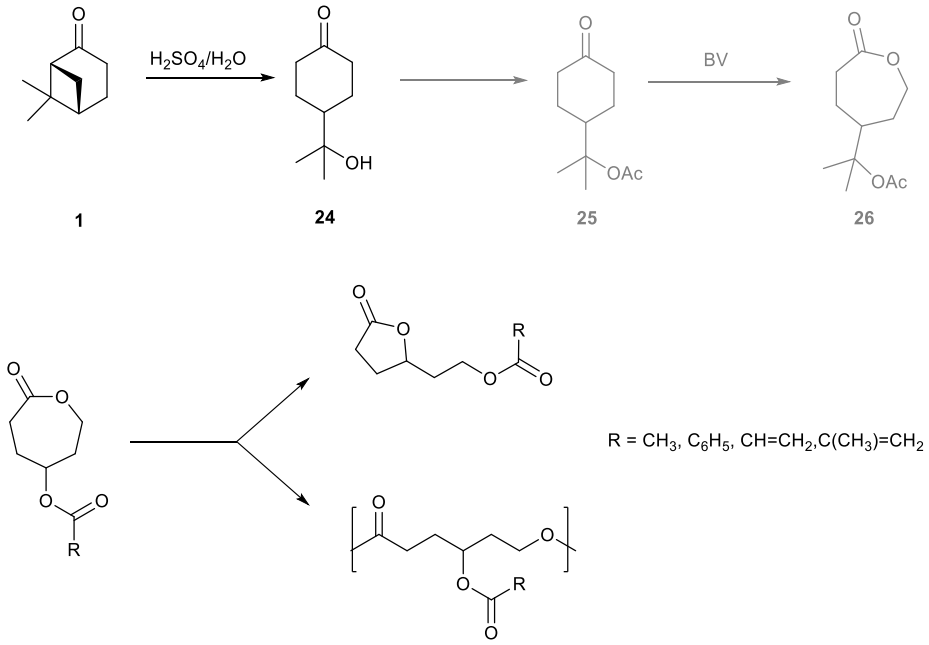

Figure 4.31. Preparation of (a) acetoxy lactone **26**, (b) competing polymerisation and rearrangement reactions reported by Vaida *et al.* [50]

The preparation of lactones from α-pinene and 3-carene would also be attractive as a method of preparing polyesters from all the major components of crude sulphate turpentine (CST). As discussed in section 4.2, the oxidative ozonolysis of CST can be used as a simple way to separate (+)-nopinone from the hydroxyacid products obtained from oxidative cleavage of the endocyclic double bonds in terpenes such as α-pinene and 3-carene. These hydroxyacids can be further reduced by addition of $NaBH_4$ to produce the corresponding diol. Doi *et al.* reported a methodology to prepare a chiral lactone (**28**) from the diol produced in this manner from 3-carene, although its polymerisation remains unreported.[44] The ROP of chiral lactones such as this would yield chiral polyesters. Following literature methodologies (Scheme 4.12a), the oxidative ozonolysis of 3-carene was performed and lactonization proceeded as reported, with spectral values matching literature values.[51] The lactone was easily separated from the diol by flash chromatography on silica (pet ether/EtOAc 20%, R_f = 0.13), yielding **28** as a colourless oil in 56% yield. Only a small quantity of this lactone was isolated, and initial polymerisation attempts were unsuccessful. The lactonization was also attempted for the diol prepared from α-pinene (Scheme 4.12b), but under these conditions lactone **30** was not formed, possibly due to the increased steric demand imposed by the cyclobutene ring.

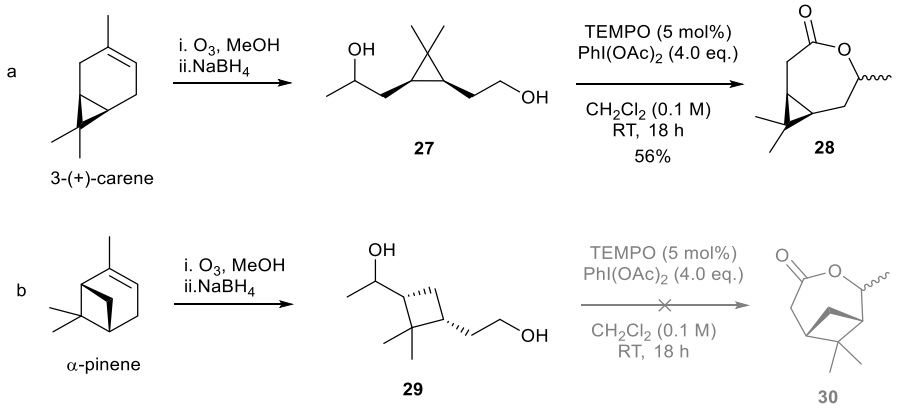

Scheme 4.12. Preparation of chiral lactone prepared from 3-carene[51] and proposed lactone preparation from α-pinene.

4.7 Conclusions & future work

This chapter has described the synthesis of saturated and unsaturated lactones from β-pinene and their ROP to aliphatic polyesters. Currently attempts to prepare copolymers of 4^{i}PrCL (**4**) with lactide have been limited to random copolymers prepared in a "one-pot" fashion. It would be beneficial to further probe the scope of materials which could be made *via* the copolymerisation of this monomer with lactide and other related cyclic esters, including the successful preparation of fully bio-based block polymers.

The synthesis of these monomers at present has not been optimised, and there is scope to improve the synthetic routes from biomass to monomers. The crosslinking of the unsaturated polymer *via* well-established thiol-ene chemistry was not achieved in this work, but this would be an interesting direction to follow, as similar terpene-derived polymers have been shown to have shape-memory properties when cross-linked in this fashion.[10] The non-trivial preparation of the unsaturated lactone was found to be prohibitive in performing full investigations of this monomer, although looking forward it could be possible to incorporate small amounts of it in copolymer blends. Finding optimised routes to scale up the synthesis of this molecule to allow for thorough investigations of polymer kinetics and to prepare polymers on reasonable scales for PPM would be highly beneficial. Other chemoselective BVO methods could also be investigated to retain valuable terpene functionality, such as enzymatic processes. Indeed, this could also provide a route to prepare enantiopure monomers, and it would be interesting to see how this affects the properties of the polymer products.

Further testing of polymer properties should be performed for poly(**4**). A useful study would be a degradation profile to determine if these polymers would be suitable for

applications where degradation of the polymer is key, such as more sustainable food packaging or biomedical applications. In-depth investigations of the polymerisation of lactam **8** and determination of polymer properties are also on-going.

The facile separation of (+)-nopinone from a waste product (CST) *via* oxidative ozonolysis makes the synthesis of aliphatic polyesters such as poly(**4**) from terpene feedstocks an attractive process. Finding uses for the hydroxyacid products as monomers in polymer synthesis *via* lactonisation, direct polycondensation or possibly conversion to amines for the preparation of polyamides would be beneficial in this process.

4.8 Chapter 4 References

1 M. Winnacker and B. Rieger, *ChemSusChem*, 2015, **8**, 2455–2471.
2 P. A. Wilbon, F. Chu and C. Tang, *Macromol. Rapid Commun.*, 2013, **34**, 8–37.
3 M. Golets, S. Ajaikumar and J.-P. Mikkola, *Chem. Rev.*, 2015, **115**, 3141–3169.
4 A. Corma, S. Iborra and A. Velty, *Chem. Rev.*, 2007, **107**, 2411–2502.
5 C. M. Byrne, S. D. Allen, E. B. Lobkovsky and G. W. Coates, *J. Am. Chem. Soc.*, 2004, **126**, 11404–11405.
6 F. Auriemma, C. De Rosa, M. R. Di Caprio, R. Di Girolamo and G. W. Coates, *Macromolecules*, 2015, **48**, 2534–2550.
7 F. Auriemma, C. De Rosa, M. R. Di Caprio, R. Di Girolamo, W. C. Ellis and G. W. Coates, *Angew. Chem. Int. Ed.*, 2015, **54**, 1215–1218.
8 C. Robert, F. De Montigny and C. M. Thomas, *Nat. Commun.*, 2011, **2**, 586.
9 D. Zhang, M. A. Hillmyer and W. B. Tolman, *Biomacromolecules*, 2005, **6**, 2091–2095.
10 J. R. Lowe, M. T. Martello, W. B. Tolman and M. A. Hillmyer, *Polym. Chem.*, 2011, **2**, 702–708.
11 M. A. Hillmyer and W. B. Tolman, *Acc. Chem. Res.*, 2014, **47**, 2390–2396.
12 J.-G. Yin, G.-C. Xu, G.-W. Zheng and J.-H. Xu, *Appl. Biochem. Biotechnol.*, 2015, **176**, 1102–1113.
13 A. Gandini and T. M. Lacerda, *Prog. Polym. Sci.*, 2015, **48**, 1–39.
14 M. Winnacker, J. Sag, A. Tischner and B. Rieger, *Macromol. Rapid Commun.*, 2017, **38**, 1600787-1600794.
15 M. Winnacker and J. Sag, *Chem. Commun.*, 2018, **54**, 841–844.
16 M. Winnacker, M. Neumeier, X. Zhang, C. M. Papadakis and B. Rieger, *Macromol. Rapid Commun.*, 2016, **37**, 851–857.
17 M. Winnacker, S. Vagin, V. Auer and B. Rieger, *Macromol. Chem. Phys.*, 2014, **215**, 1654–1660.
18 M. Winnacker, A. Tischner, M. Neumeier and B. Rieger, *RSC Adv.*, 2015, **5**, 77699–77705.
19 L. Zhou, X. Liu, J. Ji, Y. Zhang, X. Hu, L. Lin and X. Feng, *J. Am. Chem. Soc.*, 2012, **134**, 17023–17026.
20 B. G. Kyte, P. Rouvière, Q. Cheng and J. D. Stewart, *J. Org. Chem.*, 2004, **69**, 12–17.
21 H. C. Quilter, M. Hutchby, M. G. Davidson and M. D. Jones, *Polym. Chem.*, 2017, **8**, 833–837.
22 M. Hutchby, *Unpubl. results*.

23 K. Mori, *Tetrahedron: Asymmetry*, 2006, **17**, 2133–2142.
24 T. Szuppa, A. Stolle, B. Ondruschka and W. Hopfe, *ChemSusChem*, 2010, **3**, 1181–1191.
25 M. Irfan, T. N. Glasnov and C. O. Kappe, *Org. Lett.*, 2011, **13**, 984–987.
26 G.-J. ten Brink, I. W. C. E. Arends and R. A. Sheldon, *Chem. Rev.*, 2004, **104**, 4105–4124.
27 H. L. Messiha, S. T. Ahmed, V. Karuppiah, R. Suardíaz, G. A. Ascue Avalos, N. Fey, S. Yeates, H. S. Toogood, A. J. Mulholland and N. S. Scrutton, *Biochemistry*, 2018, **57**, 1997–2008.
28 K. Yakabi, T. Mathieux, K. Milne, E. M. López-Vidal, A. Buchard and C. Hammond, *ChemSusChem*, 2017, **10**, 3652–3659.
29 R. C. P. Cubbon, *Die Makromol. Chemie*, 1964, **80**, 44–53.
30 A. J. Chmura, M. G. Davidson, C. J. Frankis, M. D. Jones and M. D. Lunn, *Chem. Commun.*, 2008, 1293–1295.
31 M. D. Jones, S. L. Hancock, P. McKeown, P. M. Schäfer, A. Buchard, L. H. Thomas, M. F. Mahon and J. P. Lowe, *Chem. Commun.*, 2014, **50**, 15967–15970.
32 T. S. Jiménez-Martínez, S. Romero-Manig, N. Esturau-Escofet and M. Briseño-Terán, *Chem. Soc*, 2011, **55**, 101–104.
33 P. Groves, *Polym. Chem.*, 2017, **8**, 6700–6708.
34 C. L. Wanamaker, L. E. O'Leary, N. A. Lynd, M. A. Hillmeyer and W. B. Tolman, *Biomacromolecules*, 2007, **8**, 3634–3640.
35 A. Watts, N. Kurokawa and M. A. Hillmyer, *Biomacromolecules*, 2017, **18**, 1845–1854.
36 P. Lewinski, S. Sosnowski, S. Kazmierski and S. Penczek, *Polym. Chem.*, 2015, **6**, 4353–4357.
37 J. G. Rosenboom, J. De Roo, G. Storti and M. Morbidelli, *Macromol. Chem. Phys.*, 2017, **218**, 1600436-1600446.
38 W. Li, H. Chung, C. Daeffler, J. A. Johnson and R. H. Grubbs, *Macromolecules*, 2012, **45**, 9595–9603.
39 R. Lawrence, University of Bath, 2016.
40 X. Lou, C. Detrembleur, P. Lecomte and R. Jérôme, *J. Polym. Sci. Part A Polym. Chem.*, 2002, **40**, 2286–2297.
41 C. Detrembleur, M. Mazza, X. Lou, O. Halleux, P. Lecomte, D. Mecerreyes, J. L. Hedrick and R. Jérôme, *Macromolecules*, 2000, **33**, 7751–7760.
42 V. Boucard, G. Broustal and J. M. Campagne, *European J. Org. Chem.*, 2007, **2007**, 225–236.
43 M. Kumar, A. Kumar, M. Rizvi, M. Mane, K. Vanka, S. C. Taneja and B. A. Shah, *European J. Org. Chem.*, 2014, **2014**, 5247–5255.
44 Bozzato, G. and Pesaro, M., *US Pat.US3816537A*.
45 W. Cunningham, University of Bath, 2018.
46 A. Corma, L. T. Nemeth, M. Renz and S. Valencia, *Nature*, 2001, **412**, 423–425.
47 C. Hammond, S. Conrad and I. Hermans, *Angew. Chem. Int. Ed.*, 2012, **51**, 11736–11739.
48 K. Yakabi, K. Milne, A. Buchard and C. Hammond, *ChemCatChem*, 2016, **8**, 3490–3498.
49 E. J. Horn, J. S. Silverston and C. D. Vanderwal, *J. Org. Chem.*, 2016, **81**, 1819–1838.
50 C. Vaida, M. Takwa, M. Martinelle, K. Hult, H. Keul and M. Möller, *Macromol. Symp.*, 2008, **272**, 28–38.
51 R. Doi, M. Shibuya, T. Murayama, Y. Yamamoto and Y. Iwabuchi, *J. Org. Chem.*, 2015, **80**, 401–413.

5 Concluding remarks

The derivation of bio-based polymers, which are competitive with current petrochemical plastics in terms of properties and cost to produce, is a crucial challenge in developing a more sustainable society. To realise the potential for biopolymers, different approaches are necessary, including improving existing processes, and development of new monomers from biomass to replace existing monomers or widen the library of available materials from bio-based sources. The work in this thesis significantly contributes to the larger puzzle.

In Chapter 2, the preparation and characterisation of a series of multinuclear Zr(IV), Li(I), Mg(II) and Zn(II) complexes based on simple amine bis(phenolate) ligands were reported. These metals are desirable in catalyst design in the synthesis of biocompatible PLA, particularly coordinated to simple ligands. The complexes in this chapter were applied for ROP of *rac*-LA, achieving good control and predictable molecular weights with the addition of BnOH as co-initiator. The complexes reported here widen the library of available initiators for ROP comprising abundant, non-toxic metals, and cheap bis(phenolate) ligands, although little influence in stereoselectivity was achieved. Atactic PLA or mild heterotacticity was observed in most cases. For one Li(I) complex, Li_3(**3**)$_2$(THF), the addition of MeOH during work-up of the polymerisation was shown to promote chain scission. This complex should be further investigated as a depolymerisation catalyst for PLA. This would be very attractive as depolymerisation has been suggested as a promising end-of-life route for PLA, allowing for recovery of raw materials. An unusual mixed Li(I)/Mg(II) species was also prepared and identified in the solid-state to comprise a previously unprecedented central Li_3MgO_4 cubic core. This is evidence that such structures are attainable and the synthesis of other mixed-metal species of this type could be further pursued with simple amine bis(phenolate) ligands.

Dinuclear Mg(II) species prepared in this chapter were also subjected to preliminary studies as initiators for ROCOP of epoxides and anhydrides. The results were promising, with exclusively polyester formation observed from propylene oxide and succinic anhydride for one Mg(II) species, with no competing ether formation. This type of polymerisation is a fast-developing area of research which has the potential to greatly increase the library of polymeric materials available from renewable sources through development of bio-based epoxides and anhydrides, in addition to terpolymerisation with CO_2 or lactones. Derivation of simple catalysts which are active for this process would be very desirable, and further

experiments with these Mg(II) complexes should be performed, with emphasis on screening potential monomers for the process.

The synthesis and characterisation of Al(III) complexes with Schiff base ligands was investigated in Chapter 3, with the aim to prepare highly active and selective dinuclear initiators. While Al(III) salen complexes have been widely reported for the stereoselective ROP of *rac*-LA in the scientific literature, recent trends have included the design of dinuclear aluminium complexes which show enhanced kinetic activity for ROP. Previously, limited examples of dinuclear complexes imparting stereoselectivity had been reported. The dinuclear complex described in Chapter 3, comprising a 1,8-naphthalene backbone, is a rare example of a L-$AlMe_2$ complex imparting stereoselectivity over the ROP process. Polymerisation was achieved in 2 hours at 80 °C or 24 h at RT with the addition of 1 eq. of BnOH per aluminium centre, yielding isotactically enriched PLA (P_m < 0.82) in a highly controlled manner. Monomer-to-initiator loadings up to 800:1:1 were successfully investigated and this could be expanded to include industrial catalytic loadings ([LA]:[I]:[BnOH] = 10000:1:10) in the future. A dramatic increase in polymerisation rate was observed compared to an analogous monomeric counterpart. DFT calculations and comparison with literature complexes having Al centres in effectively identical steric and electronic environments supported the theory of cooperativity between Al centres. Further developing this initiator by modifying ligand substitution may lead to enhanced selectivity, and this merits further investigation.

In Chapter 4, significant progress in the synthesis of monomers for bio-based materials from terpene feedstocks was reported. Terpenes and terpenoids are a vastly underutilised, abundant resource, which are prime candidates as a source of renewable monomers. In this work, the synthesis of a substituted caprolactone monomer was described in four high-yielding steps (65% overall process yield) from β-pinene. The polymerisation of this with a range of initiators was achieved, and potential for preparing copolymers with LA was also described. The scalability of the monomer synthesis is an important consideration in the design of new monomers. The synthetic strategy outlined in the preparation of 4-isopropylcaprolactone, while not yet optimised in line with green chemistry principles, comprises common transformations that are amenable to scale-up through standard process development methodologies. Furthermore, β-pinene can be readily accessed from an industrial waste product (CST), demonstrating the feasibility of utilising terpenes for polyester synthesis. Valorisation of other components of CST (α-pinene, carene) should also

be attempted; finding routes to high-value chemicals would be financially beneficial to the process.

An attractive trait of terpenes for manufacturing is their inherent functionality, including chirality and abundance of unsaturated moiety. To this end, chemoselective routes to prepare lactones from β-pinene which would leave alkene moieties untouched were investigated in Chapter 4. Two lactones with alkene moieties were successfully prepared *via* different chemoselective methods. The lactone prepared from cryptone was previously unreported in the scientific literature. While 4-isopropenylcaprolactone had been previously reported, the polymerisation of this molecule to prepare a polyester with pendant isopropenyl groups had not been reported. The ROP of these unsaturated monomers could also lead to new polymeric materials or networks *via* post-polymerisation modification, but at present the preparation of these materials has been limited by scalability of the monomer synthesis. Full studies into the polymerisation of these monomers should be performed in future experiments, and further testing of polymer properties. Additionally, a range of PPM methodologies could be investigated, including epoxidation and thiol-ene chemistry, both of which were attempted in this thesis.

The synthesis of a β-pinene derived lactam has also been demonstrated in this work. This is a significant result as only very few lactam monomers are currently available which are derived from renewable resources, and polyamides represent a large group of commercial polymers. Although polymerisation of this lactam has not been realised at present, this is a highly promising step forward in the realisation of bio-based monomers for polyamide production and should be investigated thoroughly in the future.

There is great potential for the derivation of further monomers for ROP and ROCOP from terpenes. Retaining chirality in monomers may lead to polymeric materials with interesting optical and thermal properties for new applications. Future studies should aim to prepare chiral analogues of the monomers described here, while the racemic monomers reported in this thesis have potential as alternatives for the preparation of low T_g polymers currently derived from petrochemical feedstocks. Focus should reside on the preparation of monomers from the components of CST, an underutilised waste resource. If this approach is combined with others, such as metabolic engineering to increase future production, terpenes offer a very attractive source of monomers for future sustainable plastic production.

6 Chapter 6. Experimental

6.1 General experimental

The preparation and characterisation of all metal complexes was carried out under inert argon atmosphere using standard Schlenk or glovebox techniques. Dry solvents for the handling and preparation of metal complexes were collected from an MBraun solvent purification system (SPS) and stored over molecular sieves prior to use. Solvents and reagents for synthesis and characterisation were purchased from Sigma Aldrich, Acros, Fluorochem or Fisher Scientific and used without further purification unless otherwise stated. Lactide was twice recrystallised from dry toluene. CHO and PO were dried by distillation over CaH_2 and stored in a glove box prior to use. 2,2'-bipyrrolidine starting materials were purchased from Orbiter. Methyl 2-formylbenzoate,[1] 2-hydroxy-3,5-dimethylbenzaldehyde,[2] 3,5-di-tert-butyl-2-hydroxybenzylbromide[3] and zirconium complexes in Chapter 4[4,5] were prepared following published methods. Ligand **6**H_2 was provided by James Beament.

^{1}H and ^{13}C{^{1}H} NMR spectra were recorded on a Bruker 400 or 500 MHz instrument and referenced to residual solvent peaks. ^{7}Li spectra were recorded on a Bruker 400 or 500 MHz instrument and referenced to an external 1M LiCl solution in D_2O. Chemical shifts are quoted in ppm and coupling values, *J*, are quoted in Hz to the nearest 0.5. For analysis of metal complexes, $CDCl_3$ was dried by distillation over CaH_2. Toluene-d^8, benzene-d^6 and pyridine-d^5 were degassed and stored over molecular sieves prior to use. Diffusional ordered spectroscopy (DOSY) NMR experiments were run on a Bruker 400 MHz spectrometer using the standard Bruker pulse sequence ledbpgp2s, with d1 of 5 seconds, 64k data points and 16 scans per gradient level. Ten gradient strengths were used between 2 and 95 %. Data was processed to estimate molecular weights using published methods.[6]

All crystallographic data was collected on a Nonnius Kappa or Bruker SuperNova EOS detector diffractometer using Mo-Kα radiation (λ = 0.71073 Å) or Cu-Kα (1.54056 Å) at 150 K by Dr. Matthew Jones, with assistance from Dr. Mary Mahon and Dr. Gabriele Kociok-Köhn. All structures were solved by direct methods and refined on all F^2 data using the SHELXL-97 or 2014 suite of programs. All hydrogen atoms were included in idealised positions and refined using the riding model.

Electrospray mass spectra (ES-MS) were recorded using an electrospray Time-of-Flight MicroTOF mass spectrometer. Samples were prepared in HPLC grade methanol or acetonitrile at approximately 1 μgmL^{-1} concentration. Masses were recorded in positive loop injection mode and are reported as mass to charge ratios (*m/z*) in Daltons.

GC-MS were recorded using an Agilent Technologies GC-MS system (GC: 7890B, MS: 5977A, column: capillary nitroterephthalic acid-modified polyethylene glycol column of high polarity DB-FFAP 30 m x 0.250 mm x 0.25 µm equipped with a flame ionisation detector (FID) and an Agilent 5975C Mass Spec. Method initial temperature: 40 °C, held for 2 min, heated to 250 °C at a ramp rate of 20 $°Cmin^{-1}$, then held isothermally at that final temperature for 5.5 minutes.

Air-sensitive CHN elemental microanalysis (carbon, hydrogen, nitrogen) were recorded by Mr Stephen Boyer at London Metropolitan University.

IR spectra were recorded on a Perkin-Elmer 1600 FT IR spectrometer, with only selected peaks, $\nu_{max,}$ recorded in wavenumbers (cm^{-1}).

Capillary melting point (mp) determinations were carried out on a variable temperature Griffen melting point apparatus.

Analytical thin layer chromatography (TLC) was carried out using commercially available polyethylene backed plates coated with Merck Kieselgel 60 GF254. Plates were visualised under UV light (at 254 nm) or by staining with phosphomolybdic acid followed by heating. Flash chromatography was performed using Merck 60 H silica gel (35-75 µm). Samples were loaded as saturated solutions in an appropriate solvent unless otherwise stated.

6.2 General polymerisation procedures

6.2.1 Solution polymerisations

General procedure: inside a glove box, metal initiator, monomer and co-initiator (BnOH, if required (typically 5.6 µL, 1 equivalent at 100:1 loading, 0.72 g LA, 0.5 mmol) were charged into a Young's ampule with a stirrer bar and dissolved in toluene (10 mL). The ampule was removed from the glove box and placed in an oil bath preheated to 80 °C and stirred for the desired length of time. The reaction was quenched *via* exposure to air and addition of a few drops of MeOH. The solvent was removed, and a sample taken to run a ^{1}H NMR sample to determine monomer conversion. The polymer was isolated by washing with MeOH to remove unreacted monomer and drying *in vacuo*.

6.2.2 Melt/solvent-free polymerisations

General procedure: inside a glove box, metal initiator and monomer were charged into a Youngs ampule with a stirrer bar. The tube was placed in a preheated oil bath set to the desired temperature (130 °C for *rac*-lactide) and stirred for the required length of time. The reaction was quenched via exposure to air. CH_2Cl_2 and a second stirrer bar were added, and the mixture stirred until the polymer was fully dissolved. The CH_2Cl_2 was then removed, conversion NMR sample obtained, and the polymer washed with MeOH and dried in vacuo as before.

6.2.3 Melt copolymerisation of lactide and 4-isopropylcaprolactone

An ampoule was charged with appropriate quantities of each monomer and initiator and typically heated to 100 °C. Once complete, the ampule was exposed to air and methanol (1-2 drops) was added to quench the reaction. The polymer was dissolved in CH_2Cl_2 and transferred to a round-bottomed flask was removed *in vacuo* and a crude sample was taken to determine conversion of each monomer *via* ^{1}H NMR spectroscopy. The polymer was then washed with methanol (3 x 10 mL) to remove any residual monomer and dried under high vacuum before analysis *via* NMR spectroscopy and GPC.

6.2.4 Solution copolymerisation of lactide and 4-isopropylcaprolactone

An ampoule was charged with appropriate amounts of each monomer and initiator. Benzyl alcohol was added as required and the mixture dissolved in toluene (10 mL) and heated to 80 °C. Once complete, methanol (1-2 drops) was added to quench the reaction. The solvent was removed *in vacuo* and a sample was taken to determine conversion of each monomer *via* ^{1}H NMR spectroscopy. The polymer was then washed with methanol (3 x 10 mL) to remove any remaining monomer and dried under high vacuum before analysis *via* NMR spectroscopy and GPC.

6.2.5 Kinetic study of polymerisations

A Young's NMR tube was charged with 50 mg of *rac*-lactide or 54 mg 4^{i}PrCLand dissolved in 0.5 mL toluene-d^8 or $CDCl_3$. A stock solution of initiator dissolved in NMR solvent (and benzyl alcohol, if required) was prepared. Typically, this would be the required mass of initiator multiplied by 10 and dissolved in 1 mL solvent. 0.1 mL of the stock solution was added to the NMR tube, giving an overall volume of 0.6 mL. The concentration of lactide/4^{i}PrCL in the sample was 0.58 M. The sample was heated to the desired temperature inside a Bruker 400 MHz NMR instrument. ^{1}H NMR spectra were taken at

minute-scale intervals and conversion with time determined by relative integration of monomer and polymer methine resonances.

6.2.6 Polymer characterisation

The average polymer molecular weight and molecular weight distribution of purified polymers were determined by gel permeation chromatography (GPC) analysis using a Polymer Laboratories PL-GPC 50 integrated system with a PL_{gel} 5 µm MIXED-D 300 x 7.5 mm column at 35 °C and a flow rate of 1 mL/min. Samples were prepared in THF as 2 $mgmL^{-1}$ solutions and filtered through a PTFE 0.2 µm filter prior to auto sampler injection. The GPC M_n values quoted here are relative to 11 narrow polystyrene standards with detection via refractive index response, giving a calibrated molecular weight range of 615-568000 Da. In some cases a correction value has been applied to the GPC values for PLA according to the Mark-Houwink equation: [M_n(obsd) = 0.58 x Mn(GPC)]. *Đ* was calculated automatically from M_w/M_n (M_w = weight average molecular weight, M_n = number average molecular weight).

The tacticity of PLA samples were analysed by ^{1}H homonuclear decoupled (HND) NMR spectroscopy to probe the methine region of the polymer and determine a P_r value by Bernoullian statistics described by Coates *et al*..[7]

MALDI-ToF mass spectra were determined by the EPSRC National Mass Spectrometry Service Centre in Swansea, or on a Bruker Autoflex speed instrument using DCTB (trans-2-[3-(4-tert-Butylphenyl)-2-methyl-2-propenylidene]malononitrile) as the matrix and ionized using NaTFA.

DSC analysis was recorded on a TA Instruments DSC Q20. For homopolymers the sample was held at -70 °C for 1 minute, heated to 0 °C at 5 °Cmin^{-1} held at this temperature for 1 minute, cooled to -70 °C at 5 °Cmin^{-1} held at this temperature for 1 minute and finally heated to 25 °C at 5 °Cmin^{-1}. For copolymers the range was -70 °C – 220 °C and rate was 10 °Cmin^{-1}. T_g and T_m values are quoted for the second heating cycle.

6.3 Chapter 2 experimental

6.3.1 Synthesis of ligands

General Modified Mannich Procedure

General procedure is as follows: diamine (1 eq.) was dissolved in methanol (40 mL), to which was added 2,4-dimethylphenol or 2,4-di-*tert*-butylphenol (2.4 eq) and

paraformaldehyde (10 eq.). The resulting solution was heated to reflux for 4-6 hours. A white precipitate was observed upon cooling which was collected by vacuum filtration, washed with cold methanol and dried in vacuo. Ligand was recrystallised from MeOH if further purification was required.

1H_2[8]

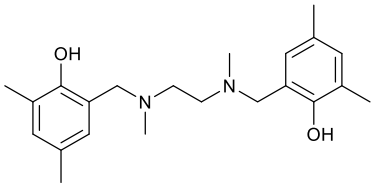

Diamine = *N,N'*-dimethylethylenediamine (1.64 g, 1.4 mL, 19.0 mmol). Product isolated as a white powder (5.64 g, 15.8 mmol, 83 %,).

^{1}H NMR ($CDCl_3$, 400 MHz): δ 10.60 (br. s., 2 H, OH), 6.87 (s, 2 H, Ar-H), 6.61 (s, 2 H, Ar-H), 3.64 (s, 4 H, N-CH_2-Ar), 2.66 (s, 4 H (CH_2), 2.27 (s, 6 H, N-CH_3), 2.22 (s, 6 H, CH_3), 2.20 (s, 6 H, CH_3). $^{13}C\{^1H\}$ NMR ($CDCl_3$, 101 MHz): δ 153.1 (Ar-OH), 130.3 (Ar-CH_3), 127.3 (Ar-H), 126.3 (Ar-CH_3), 124.3 (Ar-H), 120.3 (Ar-CH_2), 61.5 (N-CH_2CH_2), 53.8 (N-CH_2-Ar), 41.3 (N-CH_3), 20.1 (Ar-CH_3), 15.3 (Ar-CH_3).

2H_2[9]

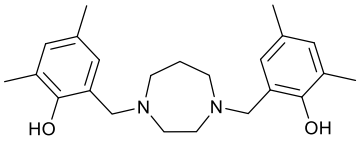

Diamine = homopiperazine (1.00 g, 10.0 mmol). Product isolated as a cream powder (1.55 g, 4.21 mmol, 42 %).

^{1}H NMR ($CDCl_3$, 400 MHz): δ 10.87 (br. S, 2H, OH), 6.87 (s, 2H, Ar), 6.62 (s, 2H, Ar), 3.74 (s, 4H, N-CH2-Ar), 2.79 - 2.93 (m, 4 H, CH2), 2.78 (s, 4 H, CH2), 2.21 (s, 12 H, CH3), 1.91 ppm (s, 2H, CH2); $^{13}C\{^1H\}$ NMR ($CDCl_3$, 101 MHz): δ 153.6 (Ar-O), 130.6, 127.6, 126.6, 124.6, 120.7 (Ar), 61.8 (Ar-CH_2-N), 54.5 (N-CH_2), 53.4 (CH_2), 26.6 (CH_2), 20.3 (Ar-CH_3), 15.6 (Ar-CH_3).

3H_2[5]

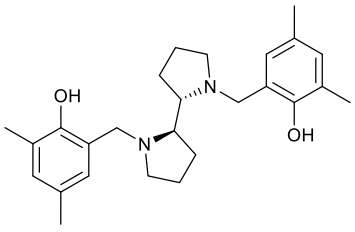

Diamine = *meso*-2,2'-bipyrrolidine (1.00 g, 7.1 mmol). Product isolated as a fine white powder (1.31 g, 3.2 mmol, 45 %).

^{1}H NMR ($CDCl_3$, 400 MHz): δ 10.68 (br. s., 2 H, OH), 6.87 (s, 2 H, Ar-H), 6.65 (s, 2 H, Ar-H), 4.35 (d, *J* = 13.5 Hz, 2 H, N-CH_2), 3.40 (d, *J* = 13.5 Hz, 2 H, N-CH_2), 2.95 - 3.05 (m, 2 H, CH_2), 2.80 - 2.91 (m, 2 H, CH_2), 2.31 - 2.43 (m, 2 H CH_2), 2.23 (s, 6 H, CH_3), 2.21 (s, 6 H, CH_3), 2.04 - 2.17 (m, 2 H CH_2), 1.75 - 1.97 (m, 6 H CH_2 + CH). $^{13}C\{^1H\}$ NMR ($CDCl_3$,101 MHz): δ 153.3 (Ar-OH), 130.4 (Ar-H), 127.5 (Ar-CH_3), 126.3 (Ar-H), 124.5 (Ar-CH_3), 121.5 (Ar-C), 68.2 (CH), 60.4 (Ar-CH_2-N), 54.3 (CH_2),

28.5 (CH_2), 23.0 (CH_2), 20.4(CH_3), 15.6 (CH_3). ESI-MS (MeOH): *m/z* calc. for $[C_{26}H_{37}N_2O_2]^+$ = 409.2850, found *m/z* = 409.3006.

4H_2[5]

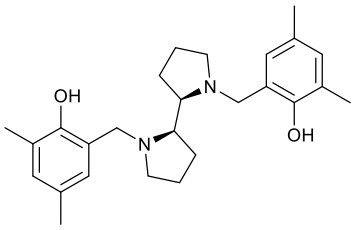

Diamine = (2*R*,2'*R*)-2,2'-bipyrrolidine (1.00 g, 7.1 mmol). Product isolated as fine white needles (2.09 g, 5.1 mmol, 72 %).

^{1}H NMR (400 MHz, $CDCl_3$) δ 10.69 (s, br, 2H, OH), 6.86 (m, 2H, Ar-H), 6.64 (m, 2H, Ar- H), 4.25 (d, *J* = 13.5 Hz, 2 H, CH_2), 3.29 (d *J* = 13.5 Hz, 2H, CH_2), 3.07 (m, 2H, CH_2) 2.95 (m, 2H, CH_2) 2.22 (s, 6H, CH_3), 2.20 (s, 6H, CH_3), 2.06 (m, 2H, CH_2), 1.83 (m, 6H, CH_2 + CH), 1.60 (m, 2H, CH_2).^{13}C{^{1}H} NMR ($CDCl_3$,101 MHz) δ 153.1 (Ar-O), 130.4 (Ar-H), 127.6 (Ar) 126.0 (Ar-H) 124.3 (Ar), 121.4 (Ar), 64.8 (CH), 58.1 (CH_2), 54.8 (CH_2), 25.4 (CH_2), 23.6 (CH_2), 20.4 (CH_3), 15.7 (CH_3). ESI-MS (MeOH): *m/z* calc. for $[C_{26}H_{36}N_2O_2Na]^+$ = 431.2674, found *m/z* = 431.2688.

5H_2[5]

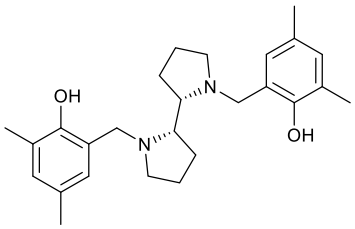

Diamine = (2*S*,2'*S*)-2,2'-bipyrrolidine (1.20 g, 8.6 mmol). White solid (2.00 g, 4.9 mmol, 57 %).

^{1}H NMR (400 MHz, $CDCl_3$) δ 10.66 (s, 2H, OH), 6.86 (d, *J* = 2.2 Hz, 2H, Ar), 6.64 (d, *J* = 2.1 Hz, 2H, Ar), 4.23 (d, *J* = 13.5 Hz, 2H, N-CH_2), 3.29 (d, *J* = 13.5 Hz, 2H, N-CH_2), 3.06 (m, 2H, CH_2), 2.99 – 2.88 (m, 2H, CH_2), 2.22 (s, 6H, CH_3), 2.20 (s, 6H, CH_3), 2.15 – 1.99 (m, 2H, CH_2), 1.93 – 1.69 (m, 6H, CH_2 + CH). ^{13}C{^{1}H} NMR (400 MHz, $CDCl_3$) δ 153.5 (Ar-OH), 130.0 (Ar-H), 127.5 (Ar-CH_3), 126.0 (Ar-H), 124.0 (Ar-CH_3), 121.5 (Ar-CH_2), 64.5 (-N-CH_2), 58.0 (CH_2), 54.5 (CH), 25.3 (CH_2), 23.9 (CH_2), 20.5 (CH_3), 15.5 (CH_3). ESI-MS (MeOH): *m/z* calc. for $[C_{26}H_{36}N_2O_2 + Na]^+$: 431.2674, found *m/z* = 431.2678.

7H_2

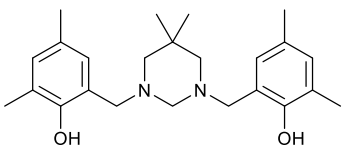

Diamine = 2,2-dimethylpropane-1,3-diamine (1.0 g, 1.18 mL, 10.0 mmol). Product isolated as a white powder (1.26 g, 3.30 mmol, 33 %).

^{1}H NMR (400 MHz, $CDCl_3$) δ 10.04 (2H, s, OH), 6.88 (2H, d, *J* = 1.0 Hz, Ar-H), 6.61 (2H, d, *J* = 1.0 Hz, Ar-H), 3.58 (4H, s, N-CH_2-Ar), 3.17 (2H, br. S, N-CH_2-N), 2.22 (18H, m, CH_3 + CH_2), 1.04 (6H, s, CH_3). ^{13}C NMR (101 MHz, $CDCl_3$) δ 153.3 (Ar-OH), 130.8 (Ar-H), 127.6 (Ar-CH_3) ,

126.7 (Ar-H), 124.92 (Ar-CH_3), 119.5 (Ar-H), 75.0 (Ar-CH_2-N), 63.9 (N-CH_2-N), 58.9 (CH_2), 31.0 ($C(CH_3)_2$), 25.6 (CH_3), 20.4 (CH_3), 15.7 (CH_3). ESI-MS (MeOH): *m/z* calc. for $[C_{24}H_{35}N_2O_2]^+$ = 383.2693, found *m/z* = 383.2764.

6.3.2 Synthesis of zirconium complexes

Zr(**1**)(O^iPr)$_2$

Following literature method, ligand **1**H_2 (0.50 g, 1.4 mmol) and $Zr(O^iPr)_4(OH^iPr)$ (0.51 g, 1.4 mol, 1 mol eq.) were dissolved in toluene (10 mL) and stirred at room temperature for 3 h. The solvent was removed *in vacuo* and the residue recrystallised in hexane. The white crystals were filtered *via* cannula and thoroughly dried to give the 1:1 complex as a white powder (0.27 g, 0.48 mmol, 32%).

^{1}H NMR ($CDCl_3$, 400 MHz): δ 6.93 (s, 2 H, Ar), 6.62 (s, 2 H, Ar), 4.61 (d, *J* = 13.0 Hz, 2 H, N-CH_2), 4.47 (sept., 2 H, *J* = 6.0 Hz, C**H**(CH_3)$_2$), 3.04 (2H, d, *J* = 13.0 Hz), 2.98 (2H, d, *J* = 10.0 Hz), 2.46 (s, 6 H, N(CH_3)$_2$), 2.23 (s, 12 H, CH_3), 1.74 (d, *J* = 9.5 Hz, 2 H, N-CH_2), 1.26 (dd, *J* = 12.0, 6.0 Hz, 12 H, CH(C**H**$_3$)$_2$). ^{13}C{^{1}H} NMR ($CDCl_3$, 101 MHz): δ 162.0 (Ar-O), 131.5, 127.3, 126.1, 124.5, 121.9 (Ar), 70.9 (C**H**(CH_3)$_2$) 68.2 (Ar-CH_2-N), 55.4 (N-CH_2), 26.2 (CH(**C**H_3)$_2$), 25.1 (CH_3), 20.1 (CH_3), 16.3 (CH_3).

Zr(**2**)(O^iPr)$_2$

Ligand **2**H_2 (0.50 g, 1.4 mmol) and $Zr(O^iPr)_4(^iPrOH)$ (0.51 g, 1.4 mol 1 mol eq.) were dissolved in toluene (10 mL) and stirred at room temperature for 3 h. The solvent was removed in vacuo and the residue recrystallised in hexane/toluene. The white crystals were filtered *via* cannula and thoroughly dried to give the 1:1 complex as a white solid (0.27 g, 0.47 mmol, 33%).

^{1}H NMR ($CDCl_3$, 400 MHz, 233 K): δ = 6.91 (br. s., 2H, Ar), 6.67 (br. s., 2H, Ar), 4.50 (sept, *J* = 6.0 Hz, 1H, (C**H**(CH_3)$_2$), 4.38 (d, *J* = 11.5 Hz, 2H, N-CH_2-Ar), 3.56 (d, *J* = 6.5 Hz, 2H, CH_2), 3.22 - 3.40 (m, 3H, CH_2), 3.08 (d, *J* = 11.5 Hz, 2H, CH_2), 2.90 (d, *J* = 6.5 Hz, 2H, CH_2), 2.14 - 2.31 (m, 12H, CH_3), 2.10 (br. s., 2H, CH_2), 1.68 (d, *J* = 14.5 Hz, 1H, CH_2), 1.32 (d, *J* = 6.5 Hz, 1H, CH_2), 1.24 (d, *J* = 6.0 Hz, 6H, CH(C**H**$_3$)$_2$), 0.27 ppm (d, *J* =6.0 Hz, 6 H, CH(C**H**$_3$)$_2$). ^{13}C{^{1}H} NMR ($CDCl_3$, 101 MHz, 233 K): δ = 160.0 (Ar-O), 132.1, 128.0, 126.5, 124.9, 122.6 (Ar), 69.4, 67.7, 63.4, 56.2, 54.4, 27.4, 26.6, 20.8, 17.3 ppm

$Zr(\mathbf{1})_2$

^{1}H NMR (400 MHz, $CDCl_3$) δ 6.90 (s, 4H, Ar), 6.48 (s, 4H, Ar), 4.37 (d, *J* = 13.5 Hz, 4H N-CH_2-Ar), 3.03 (d, *J* = 9.0 Hz, 4H, CH_2), 2.69 (d, *J* = 13.5 Hz, 4H N-CH_2-Ar), 2.60 (s, 12H, N-CH_3), 2.40 (s, 12H, Ar-CH_3), 2.17 (s, 12H, Ar-CH_3), 1.55 (d, *J* = 9.0 Hz, CH_2). ^{13}C{^{1}H} NMR (400 MHz, $CDCl_3$) δ 157.12 (Ar-O), 131.14 (Ar), 128.67 (Ar), 125.83 (Ar), 125.40 (Ar), 125.03 (Ar), 63.60 (N-CH_2-Ar), 51.78 (CH_2), 46.88 (N-CH_3), 20.49 (Ar-CH_3), 17.65 (Ar-CH_3).

{(Zr(**1**)(O^iPr)$_2$)$_2$μ-O}

Zr(**1**)(O^iPr)$_2$ (0.15 g, 0.27 mmol) was taken up in CH_2Cl_2 (10 mL) and stirred at RT for 1 h under an Ar atmosphere. The flask was then opened to atmosphere and left to stand overnight. The solvent was removed *in vacuo and* the white residue was recrystallised in minimum hexane. The white crystals that formed were isolated by cannula filter and dried *in vacuo* to give {(Zr(**1**)(O^iPr)$_2$)$_2$μ -O} as a white solid (85 mg, 0.08 mmol, 61 %).

^{1}H NMR ($CDCl_3$, 400 MHz): δ = 6.88 (br. s., 4H, Ar), 6.57 (br. s., 4H, Ar), 5.11 (d, *J* = 13.4 Hz, 2H, NCH_2Ar), 4.51 (d, *J* = 12.5 Hz, 2H, NCH_2Ar), 4.29 (spt, *J* = 1.0 Hz, 2H, O^iPr), 2.79 - 3.09 (m, 8H, CH_2), 2.38 (s, 6H, NCH_3), 2.41 (s, 6H, NCH_3), 2.12 - 2.27 (m, 18H, Ar-CH_3), 2.09 (s, 3H, Ar-CH_3), 1.11 ppm (dd, *J* = 13.5, 6.0 Hz, 12H, O^iPr). Calc. (%) for $C_{50}H_{74}N_4O_7Zr_2$: C 58.56, H 7.27, N 5.46. Found (%) 53.06, 7.03, 4.43.

{(Zr(**2**)(O^iPr)$_2$)$_2$μ-O}

Zr(**2**)(O^iPr)$_2$ (0.15 g, 0.27 mmol) was taken up in CH_2Cl_2 (10 mL) and stirred at RT for 1 h under an Ar atmosphere. The flask was then opened to atmosphere and left to stand overnight. The solvent was removed *in vacuo and* the white residue was recrystallised in hexane and toluene. {(Zr(**2**)(O^iPr)$_2$) $_2$μ-O} was isolated as a white solid (30 mg, 0.03 mmol, 21%).

^{1}H NMR ($CDCl_3$, 400 MHz, 233 K): δ = 6.85 (s, 2H,A r), 6.70 (s, 2H, Ar), 6.58 (s, 2H, Ar), 6.51 (s, 2H, Ar), 4.90 (d, *J* = 11.0 Hz, 2H, N-CH_2-Ar), 4.10 (d, *J* = 11.0 Hz, 2H, N-CH_2-Ar), 3.75 (sept, *J* = 6.0 Hz, 2H, (C**H**(CH_3)$_2$), 3.26 - 3.52 (m, 6H, CH_2), 2.98 - 3.12 (m, 2H, CH_2), 2.96 - 3.09 (d, 2H, *J* = 11.5 Hz, N-CH_2-Ar), 2.94 (d, *J* = 11.5 Hz, 2H, N-CH_2-Ar), 2.76 - 2.83 (m, 2H, CH_2), 2.53 (s, 6H, CH_3), 2.59 - 2.68 (m, 2H, CH_2), 2.18 - 2.30 (m, 2H, CH_2), 2.16 (s, 6H, CH_3), 2.10 (s, 6H, CH_3), 1.65 - 1.74 (m, 2H, CH_2), 1.25 (s, 6H, CH_3), 1.22 (d, *J* = 6.0 Hz, 2H, CH_2), 0.48 (d, *J* = 6.0 Hz, 6H, CH(C**H**$_3$)$_2$), 0.30 (d, *J* = 6.0 Hz, 6 H, CH_3, CH(C**H**$_3$)$_2$). ^{13}C{^{1}H} NMR ($CDCl_3$,101 MHz) δ

159.8 (Ar-O), 131.7, 127.6, 126.7, 124.7, 122.1 (Ar), 68.4, 55.7, 55.3, 26.4, 25.3, 23.2, 20.4, 16.5. Calc. (%) for $C_{52}H_{76}N_4O_7Zr_2$: C 59.50, H 7.11, N 5.34. Found (%) 57.76, 7.03, 4.69.

6.3.3 Synthesis of lithium complexes

$Li_4(\mathbf{1})_2(THF)_2$

1H_2, (0.50 g, 1.4 mmol) was dissolved in THF (10 mL) and cooled to -78 °C. ^{n}BuLi (2.5 M in hexane, 1.12 mL, 2.8 mmol, 2 eq.) was added dropwise and after complete addition the solution was warmed to RT with stirring over 1 hr, after which the solvent was removed in vacuo and the crude product was recrystallised from hexane. Product was washed with hexane and isolated as a white powder (0.42 g, 0.5 mmol, 71 %).

^{1}H NMR (400 MHz, pyridine-d^5) δ 7.03 (br. s., 2H, Ar), 6.91 (br. s., H, Ar), 3.60 - 3.70 (m, 3H, THF), 2.32 (br. s., 6H, CH_3), 2.20 (s, 6H, CH_3), 2.07 (br. s., 6H, CH_3), 1.50 - 1.66 (m, 3 H, THF). ^{13}C{^{1}H} NMR (101 MHz, pyridine-d^5) δ 167.2 (Ar-O), 146.7 (Ar), 133.4 (Ar-H), 132.3 (Ar-H), 128.1 (Ar), 120.2 (Ar), 69.8 (THF), 63.5 (Ar-CH_2-N), 44.1 (CH_2), 27.8 (THF), 22.8 (Ar-CH_3), 20.7 (Ar-CH_3). ^{7}Li NMR (THF-d^8) δ 1.22, 0.84. Calc (%) for $C_{52}H_{76}N_4O_6Li_4$: C 70.09, H 8.70, N 6.36, found (%) C 70.57, H 8.92, N 6.12.

$Li_4(\mathbf{3})_2(THF)$

As $Li_4(\mathbf{1})_2(THF)_2$. Ligand **3**$H_2$ (0.40 g, 1.0 mmol). Product isolated as white crystals (0.27 g, 0.30 mmol, 59 %).

^{1}H NMR (400 MHz, pyridine-d^5) δ 7.06 (d, *J* = 2.5 Hz, 2 H, Ar), 6.94 (d, *J* = 2.5 Hz, 2H, Ar), 4.60 (d, *J* = 10.5 Hz, 2H, N-CH_2), 3.64 - 3.70 (m, 2 H, THF), 2.97 (d, *J* = 10.5 Hz, 2 H, N-CH_2), 2.62 - 2.84 (m, 6 H, CH_2 + CH), 2.37 (s, 6 H, 2 x CH_3), 2.09 (s, 6 H, 2 x CH_3), 1.81 (m, 2 H, CH_2), 1.63 (m, 2 H, THF), 1.51 - 1.61 (m, 2 H, CH_2), 1.35 - 1.47 (m, 2 H, CH_2), 1.14 - 1.34 (m, 2 H, CH_2). ^{13}C{^{1}H} NMR (101 MHz, pyridine-d^5) δ 166.3 (Ar-O), 131.7, 130.6, 126.3, 126.2, 117.8 (Ar), 68.3 (C), 61.0 (Ar-CH_2-N), 53.3 (N-CH_2), 27.5 (CH_2), 26.3 (CH_2), 22.1 (CH_2), 21.3 (CH_3), 19.5 (CH_3). ^{7}Li NMR (THF-d^8) δ 1.19, 0.55. Calc (%) for $C_{56}H_{76}N_4O_5Li_4$: C 73.67, H 8.39, N 6.14, found (%) C 71.30, H 8.00, N 5.93.

$Li_4(\mathbf{7})_2(THF)_4$

As $Li_4(\mathbf{1})_2(THF)_2$. Ligand **7**$H_2$ (0.50 g, 1.3 mmol). Product isolated as white crystals (0.51 g, 0.47 mmol, 72%).

^{1}H NMR (400 MHz, pyridine-d^5) δ 7.04 (s, 4H, Ar), 6.78 (s, 4H, Ar), 4.66 (d, *J* = 10.0 Hz, 2H, N-CH_2-N) 4.37 (d, *J* = 11.0 Hz, 4H, N-CH_2-Ar), 3.83 (m, 8H, N-CH_2-C), 3.65 (m, 8H, THF), 3.57

(d, *J* = 11.0 Hz, 4H, N-CH_2-Ar), 3.05 (d, *J* = 10.0 Hz, 2H, N-CH_2-N), 2.54 (s, 12H, Ar-CH_3), 2.37 (s, 12H, Ar-CH_3), 2.34 (m, 24H, CH_3), 1.62 (m, 8H, THF).

Li_3(**1**)Mg(^{n}Bu)$(THF)_2(OCH{=}CH_2)_2$

1H_2, (0.5 g, 1.4 mmol) was dissolved in THF (10 mL) and cooled to -78 °C. ^{n}BuLi (2.5 M in hexane, 1.12 ml, 2.8 mmol, 2 eq.) was added dropwise and after complete addition the solution was warmed to RT with stirring over 1 hr. $^n Bu_2Mg$ (1 M in heptane, 0.56 mL, 0.56 mmol) was then added, and the yellow solution stirred for a further 2 hours, over which time the yellow colour faded. The solvent was removed *in vacuo*, and the off-white residue was recrystallised from hexane (15 mL). After a period of two weeks, a few small crystals were obtained and analysed by X-ray crystallography.

^{1}H NMR (400 MHz, toluene-d^8) δ 7.49 (dd, *J* = 5.0 Hz, 13.5 Hz, 1H, LiOCH), 6.66 (s, 2H, Ar), 6.65 (s, 2H, Ar), 4.36 (d, *J* = 12.0 Hz, 2H, N-CH_2-Ar), 4.04 (d, *J* = 13.5 Hz, 1H, LiOCH=C**H**$_2$), 3.91 (d, *J* = 5.0 Hz, 1H, LiOCH=C**H**$_2$), 3.49 (16H, THF) 2.76 (d, *J* = 12.0 Hz, 2H, Ar-CH_2-N), 2.49 (d, *J* = 9.0 Hz, 2H, CH_2), 2.18 (s, 6H, N-CH_3), 1.91 (s, 6H, Ar-CH_3), 1.83 (s, 6H, Ar-CH_3), 1.71 (m, *J* = 7.5 Hz, 5H), 1.37 (16H, THF) 1.23 (m, 2H, hexane), 1.18 (m, 4H, butyl), 1.11 (d, *J* = 9.0 Hz, 2H, CH_2), 0.86 (t, *J* = 7.0 Hz, hexane), 0.13 (t, *J* = 8.50 Hz, CH_2, butyl).

6.3.4 Synthesis of dinuclear magnesium complexes

Mg_2(**1**)$_2$

1H_2, (0.3 g, 0.84 mmol) was dissolved in toluene (10 mL) with stirring. $^n Bu_2Mg$ (1 M in heptane, 0.84 mL, 0.84 mmol) was added dropwise and after complete addition the solution was stirred at RT for 3 hr, after which the solvent was removed *in vacuo* and the crude product recrystallised from hexane. Product isolated as a white powder (0.25 g, 0.33 mmol, 79%).

^{1}H NMR (400 MHz, $CDCl_3$) δ 6.92 (d, *J* = 2.0 Hz, 2H, Ar), 6.78 (d, *J* = 2.0 Hz, 2H, Ar), 6.58 (d, *J* = 2.0 Hz, 2H, Ar), 6.46 (d, *J* = 2.0 Hz, 2H, Ar), 4.04 (d, *J* = 11.0 Hz, 2H, CH_2), 3.88 (d, *J* = 12.5 Hz, 2H, CH_2), 2.98 (m, 2H, CH_2), 2.93 (d, *J* = 11.0 Hz, 2H, CH_2), 2.67 (d, *J* = 12.5 Hz, 2H, CH_2), 2.51 (s, 6H, N-CH_3), 2.37 (s, 6H, N-CH_3), 2.21 (s, 6H, CH_3), 1.92 (s, 6H, CH_3), 1.87 (s, 6H, CH_3), 1.74 (m, 2H), 1.42 (s, 6H, CH_3). $^{13}C\{^1H\}$ NMR (101 MHz (101 MHz, $CDCl_3$) δ 162.7 (Ar-O), 157.1 (Ar-O), 132.5 (Ar-H), 131.0 (Ar-H), 129.5 (Ar), 129.1 (Ar-H), 128.3 (Ar), 128.0 (Ar-H), 126.0 (Ar), 124.6 (Ar), 120.6 (Ar), 119.8 (Ar), 63.7 (N-CH_2), 56.2 (CH_2), 51.1 (CH_2), 44.1 (CH_3),

39.5 (CH_3), 20.5 (CH_3), 20.3 (CH_3), 17.4 (CH_3), 16.5 (CH_3). Elemental Analysis: % Calculated for $C_{50}H_{74}Mg_2N_4O_4$ (inc. hexane) C, 71.17; H, 8.84; N, 6.64, found: C, 71.92; H 8.17; N, 6.50.

Mg_2(**4**)$_2$

As Mg_2(**1**)$_2$. Ligand **4**H_2 (0.30 g, 0.73 mmol). Product isolated as a crystalline, white powder (0.19 g, 0.22 mmol, 60%).

^{1}H NMR (400 MHz, $CDCl_3$) δ 6.92 (d, *J* = 1.5 Hz, 2 H, Ar), 6.77 (d, *J* = 1.5 Hz, 2 H, Ar), 6.55 (d, *J* = 1.5 Hz, 2 H, Ar), 6.35 (d, *J* = 1.5 Hz, 2 H, Ar), 3.75 (appt. t, *J* = 11.5 Hz, 4 H, 2 x N-CH_2), 3.07 (d, *J* = 11.5 Hz, 2 H N-CH_2), 2.71 (d, *J* = 12.5 Hz, 2 H, N-CH_2), 2.56 - 2.80 (m, 6 H, 4 x CH & CH_2), 2.54 (s, 6 H, 2 x CH_3), 2.24 - 2.31 (m, 2 H, CH_2), 2.22 (s, 6 H, 2 x CH_3), 2.11 (s, 6 H, 2 x CH_3), 1.93 - 2.02 (m, 4 H, CH_2), 1.91 (s, 6 H, 2 x CH_3), 1.76 - 1.89 (m, 6 H, CH_2), 1.54 - 1.73 (m, 4 H, CH_2), 1.25 - 1.45 (m, 6 H, CH_2). ^{13}C{^{1}H} NMR (101 MHz, $CDCl_3$) δ 162.9 (Ar-O), 157.4 (Ar-O), 132.4 (Ar-H), 130.9 (Ar-H), 129.7 (Ar), 128.7 (Ar-H), 128.1 (Ar), 127.7 (Ar-H), 125.5 (Ar), 125.0 (Ar), 121.1 (Ar), 119.3 (Ar), 67.8 (CH), 62.0 (CH), 58.4 (N-CH_2), 57.4 (N-CH_2), 51.2 (CH_2), 45.4 (CH_2), 24.6 (CH_2), 24.6 (CH_2), 21.6 (CH_2), 20.5 (CH_3), 20.4 (CH_3), 19.6 (CH_2), 17.6 (CH_3), 16.5 (CH_3). Elemental Analysis: predicted for $C_{52}H_{68}Mg_2N_4O_4$: C 72.48; H 7.95; N, 6.50, found: C, 72.63; H, 8.05; N, 6.40.

Mg_2(**5**)$_2$

As Mg_2(**1**)$_2$. Ligand **5**H_2 (0.3 g, 7.0 mmol). Product isolated as white crystals (84 mg, 0.1 mmol, 28 %).

^{1}H NMR (400 MHz, $CDCl_3$) δ 6.92 (d, *J* = 1.0 Hz, 2H, Ar), 6.77 (d, *J* = 1.5 Hz, 2H, Ar), 6.55 (d, *J* = 1.0 Hz, 2H, Ar), 6.35 (d, *J* = 1.0 Hz, 2H, Ar), 3.75 (appt. t, *J* = 11.0 Hz, 4H, 2 x N-CH_2), 3.07 (d, *J* = 11.0 Hz, 2H, CH_2), 2.71 (d, *J* = 12.5 Hz, 2H, CH_2), 2.57 - 2.81 (m, 6H, CH + CH_2), 2.54 (s, 6H, 2 x CH_3), 2.25 - 2.28 (m, 2H, CH_2), 2.22 (s, 6H, CH_3), 2.11 (s, 6H, CH_3), 1.89 (s, 6H, 2 x CH_3), 1.76 - 2.03 (m, 6H, CH_2), 1.62 (m, 4H, CH_2). ^{13}C{^{1}H} NMR (101 MHz, $CDCl_3$) δ 162.8 (Ar-O), 157.4 (Ar-O), 132.4 (Ar-H), 130.9 (Ar-H), 129.6 (Ar), 128.7 (Ar-H), 128.1 (Ar), 127.7 (Ar-H), 125.5 (Ar), 125.0 (Ar), 121.1 (Ar), 119.3 (Ar), 67.8 (CH), 62.0 (CH), 58.4 (N-CH_2), 57.4 (N-CH_2), 51.2 (CH_2), 45.4 (CH_2), 24.6 (CH_2), 24.6 (CH_2), 21.6 (CH_2), 20.5 (CH_3), 20.4 (CH_3), 19.6 (CH_2), 17.6 (CH_3), 16.6 (CH_3).

6.3.5 Synthesis of zinc complexes

Zn_3(**1**)$_2$(Me)$_2$

Ligand **1**H_2 (0.5 g, 1.4 mmol) was dissolved in toluene, and the solution was cooled with a dry ice/acetone bath before adding $ZnMe_2$ (1 M solution in heptane, 2.1 mL, 2.1 mmol, 1.5 mol eq.) was added quickly with vigorous stirring. The solution was warmed to room temperature and stirred for 2 h. The solvent was removed in vacuo, and the white residue was recrystallised from hexane/toluene (30 mL: 5 mL). Product was isolated as a white powder (85 mg, 24%).

^{1}H NMR (400 MHz, C_6D_6) δ 6.76 (s, 1 H), 6.70 (s, 1 H), 6.49 (m, 1 H), 4.20 (d, *J* = 11.80 Hz, 1 H), 3.95 (d, *J* = 11.5 Hz, 1 H), 2.55 (br. s., 5 H), 2.43 - 2.51 (m, 6 H), 2.41 (br. s., 6 H), 2.21 - 2.33 (m, 13 H), 2.17 (s, 1 H), 2.11 (s, 11 H, toluene), 2.02 (br. s., 2 H), 1.94 (br. s., 2 H), 1.84 (s, 2 H), 1.71 (s, 3 H), 1.63 (s, 3 H), 1.56 (br. s., 3 H), 0.29 (s, 1 H), -0.14 (s, 1 H), -0.18 (s, 1 H), -0.19 (s, 1 H), -0.82 (s, 1 H), -0.96 (s, 1 H). Elemental Analysis: Calc (%) for $C_{46}H_{66}N_4O_4Zn_3.C_6H_5CH_3$: C 62.31, H 7.30, N 5.48, found (%) C 63.74, H 7.83, N 5.76.

Zn_4(**3**)$_2$(Me)$_2$(OMe)$_2$

Ligand **3**H_2 (0.25 g, 0.61 mmol) was dissolved in toluene (10 mL) with a little gentle heating. The solution was cooled with a dry ice/acetone bath and $ZnMe_2$ (1.22 mL, 1.2 mmol, 2 eq., 1M solution in heptane) was added quickly with vigorous stirring. The solution was warmed to room temperature and stirred for 2 h. The turbid solution was heated until all precipitate dissolved and left to crystallise. Product isolated as white crystals (110 mg, 0.10 mmol, 33%).

^{1}H NMR (400 MHz, C_6D_6) δ 6.77 (br. s., 2 H, Ar), 6.64 (br. s., 2 H, Ar), 4.62 (d, *J* = 11.0 Hz, 2 H, N-CH_2), 4.15 (d, *J* = 11.5 Hz, 3H, N-CH_2), 3.87 - 4.02 (m, 3 H, O-CH_3), 3.84 (s, 2 H, O-CH_3), 2.79 (d, *J* = 11.0 Hz, 2H, CH_2), 2.60 (s, 3 H), 2.63 (s, 5 H), 2.39 (s, 9 H, CH_3), 2.43 (s, 6H, CH_3), 2.16 - 2.37 (m, 16 H, CH_3), 1.49 (br. s., 3 H), 1.15 - 1.44 (m, 15 H), 0.29 (grease), -0.31 (s, 1 H, Zn-CH_3), -0.37 (s, 2 H, Zn-CH_3), -0.43 - -0.57 (m, 3 H, Zn-CH_3). Elemental Analysis: Calc (%) for $C_{56}H_{80}N_4O_6Zn_4$: C 57.65, H 6.91, N 4.80, found (%) C 57.71, H 6.98, N 4.62.

6.3.6 Attempted synthesis of bi-isoindolene ligands

8[10]

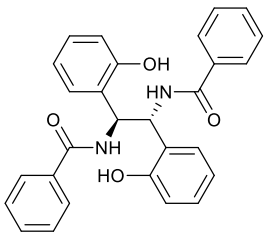

Benzil (26.3 g, 0.125 mol) and salicylaldehyde (26.7 mL, 0.25 mol, 2 eq.) were dissolved in EtOH (185 mL) and heated to 60 °C. Ammonia (35 % aq., 10 eq.) was added in portions with stirring over 3 h, during which time a yellow precipitate formed. The reaction mixture was cooled to room temperature, filtered and the precipitate washed thoroughly with cold ethanol and dried *in vacuo* to yield a fine yellow powder (43 g, 0.10 mol, 76%).

^{1}H NMR (DMSO-d^6, 400 MHz) δ 9.94 (s, 2H, OH), 8.44 - 8.73 (m, 2H, NH), 7.59 - 7.68 (m, 4H, Ar), 7.35 - 7.53 (m, 8H, Ar), 6.96 - 7.06 (m, 2H, Ar), 6.70 - 6.82 (m, 4H, Ar), 5.88 (br. s., 2H, CH). ^{13}C{^{1}H} NMR (DMSO-d_6 ,101 MHz) δ 165.08 (C=O), 155.0 (Ar-O), 134.6, 131.1, 128.9 128.3, 128.0, 127.6, 126.9, 118.8, 115.2 (Ar), 52.4 (CH). ESI-MS (MeOH): *m/z* calc. for $[C_{28}H_{24}N_2O_4Na]^+$ = 475.4992, found *m/z* = 475.1727.

9[10]

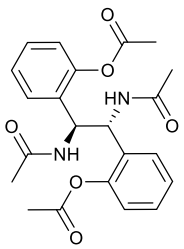

A suspension of **8** (40.0 g, 88 mmol) in acetic anhydride (125 mL) was heated to reflux (150 °C) for 18 h, resulting in a dark brown solution. This was slowly cooled to room temperature, after which a precipitate gradually formed which was collected by vacuum filtration, washed with acetic anhydride until no brown colouration remained and dried *in vacuo* to yield **9** as a white solid (24.2 g, 58.7 mmol, 67 %).

^{1}H NMR (DMSO-d_6, 400 MHz): δ 8.01 (d, *J* = 8.0 Hz, 2H, NH), 7.51 (dd, *J* = 8.0, 1.5 Hz, 2H, Ar), 7.14 - 7.32 (m, 4H, Ar), 7.04 (dd, *J* = 8.0, 1.5 Hz, 2H, Ar), 5.55 - 5.76 (m, 2H, CH), 2.28 (s, 6H, CH_3), 1.54 ppm (s, 6 H, CH_3). ^{13}C{^{1}H} NMR (DMSO-d_6 ,101 MHz) δ 169.1 (C=O), 167.8 (C=O), 148.6 (Ar-O), 131.9 (Ar), 128.4 (Ar), 127.8 (Ar), 125.3 (Ar), 122.6 (Ar), 47.8 (CH), 22.4 (CH_3), 20.9 (CH_3). ESI-MS (MeOH): *m/z* calc. for $[C_{22}H_{25}N_2O_6]^+$ = 413.1713, found *m/z* = 413.1724.

11[10]

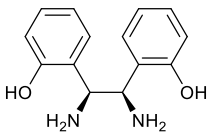

A solution of **9** (15.0 g, 36 mmol) in a 1:1 mixture of AcOH/HBr (42 %, aq.) (70 mL) was heated to reflux for 4 h. Upon cooling to room temperature, a pale brown precipitate formed, which was collected by filtration. This was dissolved in hot water (100 mL) and neutralised with 20 % NaOH,

resulting in a flocculent white precipitate in an orange solution. This was collected by vacuum filtration and recrystallised from MeCN to yield **11** as a white solid (3.14 g, 12.9 mmol, 36 %).

^{1}H NMR (DMSO-d_6, 400 MHz): δ 7.05 (td, *J* = 7.7, 1.6 Hz, 2H, Ar), 6.97 (dd, *J* = 7.5, 1.5 Hz, 2H, Ar), 6.54 - 6.81 (m, 4H, Ar), 5.39 (br. s., 4H, NH_2), 4.19 ppm (s, 2H, CH). ^{13}C{^{1}H} NMR (DMSO-d_6, 101 MHz): δ = 156.8 (Ar), 129.0 (Ar), 127.9(Ar), 127.0 (Ar), 118.2 (Ar), 116.1 (Ar), 57.9 (CH). ESI-MS (MeOH): *m/z* calc. for $[C_{14}H_{17}N_2O_2]^+$ = 245.1290, found *m/z* =245.1271.

12[11]

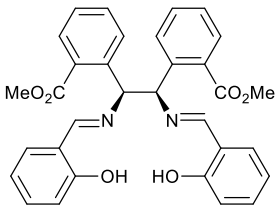

Method slightly modified from that of Zhu *et. al.*[10] *Meso*-1,2-bis(2-hydroxylphenyl)-1,2-diaminoethane (**11**) (3.14 g, 12.9 mmol) and methyl-2-formylbenzoate (5.0 g, mmol, 2.4 eq) were suspended in EtOH (40 mL). The resulting mixture was heated to reflux for 18 h. The now yellow suspension was cooled to room temperature. The precipitate was collected by vacuum filtration, washed several times with cold EtOH and dried *in vacuo* to obtain **12** as a fine yellow powder (6.57 g, 12.2 mmol, 95%);

^{1}H NMR (DMSO-d^6, 400 MHz): δ 12.93 (s, 2H, 2 x OH), 8.39 (s, 2H, 2 x N=CH), 7.72 (d, 2H, Ar-H), 7.73-7.54 (m, 4H, Ar-H), 7.38-7.29 (m, 6H, Ar-H), 6.86-6.82 (m, 4H, Ar-H), 6.07 (s, 2H, 2 x CH), 3.78 (s, 6H, 2 x CH_3). ^{13}C{^{1}H} NMR (DMSO-d^6, 101 MHz): δ = 167.2 (C=O), 166.7 (C=N), 160.1 (Ar-OH), 140.3 (Ar), 132.8 (Ar), 132.2 (Ar), 132.0 (Ar), 129.9 (Ar), 129.7 (Ar), 128.7 (Ar), 127.5 (Ar), 118.8 (Ar), 118.6 (Ar), 116.3 (Ar), 73.1 (CH), 52.1 (OCH_3). ESI-MS (MeOH): *m/z* calc. for $[C_{32}H_{28}N_2O_6Na]^+$ = 559.1845, found *m/z* = 559.1850.

13[11]

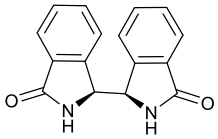

12 (1.0 g, 1.86 mmol) was dissolved in 1:1 ^{t}BuOH/H_2O (25 mL). CF_3COOH (0.3 mL, 2 eq.) was added, and the resulting solution stirred at 70 °C for 2 h. The solvent was removed under vacuum and the residue suspended in EtOAc (15 mL). The precipitate was collected by filtration and washed with EtOAc to give **13** as a fine white powder (0.33 g, 1.25 mmol, 67 %).

^{1}H NMR (DMSO-d^6, 400 MHz): δ = 8.80 (s, 2H, NH), 7.64 (d, *J* = 6.7 Hz, 2H, Ar-H), 7.37 - 7.56 (m, 4H, Ar-H), 6.82 (d, *J* = 7.0 Hz, 2H, Ar-H), 5.24 ppm (s, 2H, CH). ^{13}C{^{1}H} NMR (DMSO-d^6 ,101 MHz): δ = 169.1 (C=O), 142.9 (Ar), 133.6 (Ar), 131.2 (Ar), 128.6 (Ar), 123.0 (Ar), 122.8

(Ar), 58.0 (CH). ESI-MS (MeOH): *m/z* calc. for $[C_{16}H_{13}N_2O_2]^+$ = 265.0977, found *m/*z = 265.0969.

14[11]

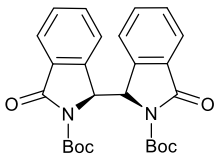

To a solution of **13** (1.28 g, 4.84 mmol) in CH_2Cl_2 (50 mL) at 0 °C were added triethylamine (0.98 g, 9.7 mmol), di-*tert*-butyl dicarbonate (4.20 g, 19.2 mmol) and DMAP (4.19 g, 9.7 mmol) in CH_2Cl_2 (20 mL) over 30 minutes. The solution was warmed to room temperature and stirred for 8 h under an argon atmosphere. Reaction was quenched by addition of water. The organic phase was separated, and the volatiles were removed *in vacuo*. The residue was purified by recrystallisation from MeOH to afford the desired di-Boc protected lactam **14** as a white solid (1.94 g, 4.18 mmol, 87%).

^{1}H NMR ($CDCl_3$, 400 MHz) δ 7.86 (2H, t, *J* = 4.5 Hz, Ar-H), 7.52 (4H, q, *J* = 2.5 Hz, Ar-H), 6.87 (2H, s, br., Ar-H), 5.92 (2H, s, 2 x CH), 1.56 (18H, s, 2 x $C(CH_3)_3$).^{13}C{^{1}H} NMR ($CDCl_3$, 101 MHz) δ = 165.6 (C=O), 150.5 (**C**$OOCH_3$), 140.7 (Ar), 133.8 (Ar), 1.6 (Ar), 129.7 (Ar), 125.2(Ar), 122.9(Ar), 83.8 ($\mathbf{C}(CH_3)_3$), 61.8 (CH), 28.0 ($C(\mathbf{C}H_3)_3$). ESI-MS (MeOH): *m/z* calc. for $[C_{26}H_{28}N_2O_6Na]^+$ = 487.1840, found *m/*z =487.1952.

16

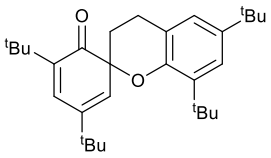

13 (0.30 g, 1.1 mmol), 2-(bromomethyl)-4,6-di-tert-butylphenol (0.68 g, 2.2 mmol, 2 eq.) and trimethylamine (0.32 mL, 2 eq.) were refluxed in THF for 24 h. The solution became bright yellow and a white precipitate was formed which was isolated by filtration on cooling. Solvent was removed, and the yellow residue recrystallised from MeOH to yield **16** as yellow crystalline needles (0.30 g, 0.7 mmol, 64%). X-ray crystallography was required to elucidate the structure.

^{1}H NMR (400 MHz, $CDCl_3$) δ 7.20 (d, *J* = 2.5 Hz, 1 H, Ar-H), 6.87 (d, *J* = 2.5 Hz, 1 H, Ar-H), 6.78 (d, *J* = 2.5 Hz, 1 H, Ar-H), 6.06 (d, *J* = 2.5 Hz, 1 H, Ar-H), 2.60 - 2.80 (m, 2 H, CH_2), 1.94 - 2.12 (m, 2 H, CH_2), 1.43 (s, 9 H, $C(CH_3)_3$), 1.30 (s, 9 H, $C(CH_3)_3$), 1.26 (s, 9 H, $C(CH_3)_3$), 1.14 (s, 9 H, $C(CH_3)_3$). ^{13}C{^{1}H} NMR (101 MHz $CDCl_3$) δ 202.4 (C=O), 149.8 (Ar-H), 144.0 (Ar-H),, 141.9 (Ar-H), 141.0 (Ar-H), 136.0 (Ar-H), 132.9 (Ar-H), 130.0 (Ar-H), 123.6 (Ar-H), 121.8 (Ar-H), 118.8 (Ar-H), 82.0 (C_{spiro}), 34.7 ($\mathbf{C}(CH_3)_3$), 34.1 ($\mathbf{C}(CH_3)_3$), 33.9 ($\mathbf{C}(CH_3)_3$), 33.8 ($\mathbf{C}(CH_3)_3$), 31.3 ($C(\mathbf{C}H_3)_3$), 29.6 ($C(\mathbf{C}H_3)_3$), 29.2 ($C(\mathbf{C}H_3)_3$), 28.9 (CH_2) 28.4 ($C(\mathbf{C}H_3)_3$), 22.5 (CH_2). ESI-MS (MeOH): *m/z* calc. for $[C_{30}H_{45}O_2]^+$ = 459.6698, found *m/*z = 459.3225.

6.4 Chapter 3 experimental

6.4.1 Preparation of Schiff base ligands and complexes

1H_2

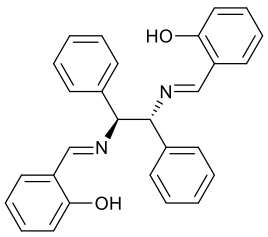

A solution of *meso*-1,2-diphenylethylenediamine (0.5 g, 2.4 mmol) and salicylaldehyde (0.69 g, 5.7 mmol, 2.4 eq.) in MeOH (10mL) was refluxed overnight. Upon cooling, the pale-yellow precipitate was separated via filtration and washed with cold methanol. The solid was taken up in $CHCl_3$, dried over $MgSO_4$ and concentrated to give **1**H_2 as a pale-yellow powder (0.92 g, 2.2 mmol, 91%).

^{1}H NMR (400 MHz, $CDCl_3$) δ 13.12 (s, 2 H, OH), 8.10 (s, 2 H, HC=N), 7.23 - 7.34 (m, 14 H, Ar), 7.08 (dd, *J* = 7.5, 1.5 Hz, 2 H, Ar), 6.94 (dd, *J* = 8.5, 0.5 Hz, 2 H, Ar), 6.82 (td, *J* = 7.5, 1.0 Hz, 2 H, Ar), 4.77 (s, 2 H, CH). ^{13}C{^{1}H} NMR ($CDCl_3$, 101 MHz): δ 165.8 (HC=N), 160.8 (Ar-OH), 139.6 (Ar), 132.6 (Ar), 131.7 (Ar), 128.6 (Ar), 128.0 (Ar), 127.9 (Ar), 118.7 (Ar), 116.9 (Ar), 80.0 (CH). ESI-MS (MeOH): *m/z* calc. for $[C_{28}H_{25}N_2O_2]$+ = 421.5195. Found *m/z* = 421.5190.

2H_2

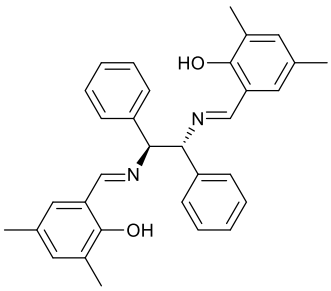

Meso-1,2-diphenylethylenediamine (0.69 g, 3.3 mmol) and 2-hydroxy-3,5-dimethylbenzaldehyde (1.18 g, 7.8 mmol, 2.4 eq.) were refluxed in MeOH (40 mL) for 18 h. A fine yellow precipitate formed, which was collected by vacuum filtration after cooling to RT and washed with cold MeOH. The solid was taken up in $CHCl_3$, dried over $MgSO_4$ and concentrated to give **2**H_2 as a pale-yellow powder (1.43 g, 3.0 mmol, 91%).

^{1}H NMR ($CDCl_3$, 400 MHz): δ = 13.12 (s, 2H, OH), 8.00 (s, 2H, N=CH), 7.35-7.29 (m, 10H, Ar-H), 6.97 (d, *J* = 2.5, 2H, phenolic Ar-H) 6.70 (d, *J* = 2.5, 2H, phenolic Ar-H), 6.71 (s, 2H, CH), 2.25 (s, 6H, CH_3), 2.19 (s, 6H, CH_3). ^{13}C{^{1}H} NMR ($CDCl_3$, 101 MHz): δ 166.9 (HC=N), 159.9 (Ar-OH), 140.3 (Ar), 133.2 (Ar), 131.3 (Ar), 129.9 (Ar), 128.5 (Ar), 127.9 (Ar), 118.7 (Ar), 116.8 (Ar), 80.0 (CH), 15.6 (CH_3). ESI-MS (MeOH): *m/z* calc. for $[C_{32}H_{33}N_2O_2]^+$ = 477.6275. Found *m/z* = 477.6250.

3H_2

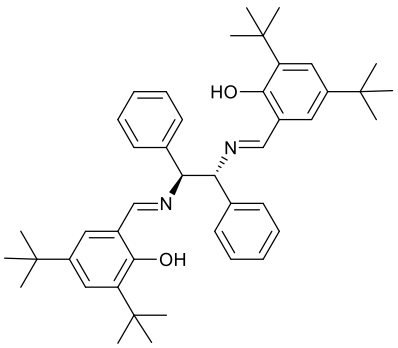

Meso-1,2-diphenylethylenediamine (0.50 g, 2.4 mmol) and 3,5-di-tert-butyl-2-hydroxybenzaldehyde (1.34 g, 5.7 mmol, 2.4 eq.) were dissolved in EtOH (30 mL) and heated to reflux for 18 h. A yellow solid formed, which was isolated by vacuum filtration. The solid was taken up in $CHCl_3$, dried over $MgSO_4$ and dried *in vacuo* to yield **3**H_2 as a shiny bright yellow solid (1.41 g, 2.1 mmol, 90%)

^{1}H NMR (400 MHz, $CDCl_3$): δ = 13.48 (s, 2 H, OH), 8.24 (s, 2 H, HC=N), 7.36 (d, *J* = 2.5 Hz, 2 H, Ar), 7.19 - 7.31 (m, 10 H, Ar), 6.96 (d, *J* = 2.5 Hz, 2 H, Ar), 4.79 (s, 2 H, CH), 1.46 (s, 18 H, $C(CH_3)_3$), 1.27 (s, 18 H, $C(CH_3)_3$). $^{13}C\{^1H\}$ NMR ($CDCl_3$, 101 MHz): δ 167.6 (HC=N), 160.1 (Ar-OH), 140.3 (Ar), 133.2 (Ar), 131.6 (Ar), 130.3 (Ar), 128.5 (Ar), 128.1 (Ar), 118.7 (Ar), 116.8 (Ar), 80.3 (CH), 35.9 (**C**$(CH_3)_3$), 34.4 (**C**$(CH_3)_3$), 31.8 (C(**C**$H_3)_3$), 29.9 (C(**C**$H_3)_3$). ESI-MS (MeOH): *m/z* calc. for $[C_{44}H_{57}N_2O_2]^+$ = 645.4415. Found *m/z* = 655.4420.

Al(**1**)Me

Ligand **1**H_2 (0.5 g, 1.2 mmol) was dissolved in toluene (10 mL). $AlMe_3$ (0.6 mL, 2 M in hexane, 1 eq.) was added and the resulting yellow solution was stirred at RT for 2 hours. The solvent was then removed, and the yellow residue was recrystallised from hot hexane/toluene to yield a yellow powder (0.21 g, 0.46 mmol, 38 %).

^{1}H NMR (400 MHz, C_6D_6) δ 7.71 (s, 2 H N= CH), 7.34 (d, *J* = 8.0 Hz, 2H, Ar–H), 7.30 (d, *J* = 8.0 Hz, 2H, Ar–H) 6.97 - 7.08 (m, 6 H), 6.79 - 6.93 (m, 6 H, Ar-H), 6.08 - 6.21 (m, 2 H), 4.94 (s, 2 H, CH), -0.11 (s, 3 H, Al-CH_3). $^{13}C\{^1H\}$ NMR (101 MHz, C_6D_6) δ 172.2 (Ar-O), 165.5 (N=CH), 140.2, 139.6, 131.8, 131.2, 130.7, 130.3, 129.3, 126.7, 124.5, 119.2, 72.2 (2 x CH) [Al-CH_3 not observed].

Al(**2**)Me

As Al(**1**)Me. Ligand **2**H_2 (0.32 g, 0.68 mmol) Yellow crystals (0.13 g, 0.25 mmol, 37 %).

^{1}H NMR (400 MHz, C_6D_6) δ 7.75 (s, 2 H N= CH), 6.97 - 7.08 (m, 6 H, Ar), 6.79 - 6.93 (m, 6 H, Ar), 6.08 - 6.21 (m, 2 H, Ar), 4.94 (s, 2 H, CH), 2.67 (s, 6 H, Ar-CH_3), 2.01 (s, 6 H, Ar-CH_3), -0.12 (s, 3 H, Al-CH_3). ^{13}C NMR (101 MHz, C_6D_6) δ 171.6 (Ar-O), 164.5 (N=CH), 139.7, 138.6,

131.2, 130.8, 130.4, 129.7, 128.9, 126.0, 124.5, 118.8, 72.2 (2 x CH), 20.6 (Ar-CH_3), 16.9 (Ar-CH_3) [Al-CH_3 not observed].

Al_2(**3**)Me_2

Ligand **3**H_2 (0.5 g, 0.77 mmol) was dissolved in toluene (10 mL). $AlMe_3$ (1.54 mL, 2 M in hexane, 2 eq.) was added and the resulting yellow solution was stirred at RT for 2 hours. The solvent was then removed, and the yellow residue was recrystallised from hot toluene to yield a bright yellow powder (0.42 g, 0.55 mmol, 72 %).

^{1}H NMR (400 MHz, C_6D_6) δ 7.61 (d, 2H, *J* = 2.5 Hz, Ar-H), 7.43 (s, 2H, CH=N) 7.27 (m, 4H, Ar-H), 6.88 (m, 6H, Ar), 6.68 (d, *J* = 2.5 Hz, 2H, Ar-H), 5.27 (s, 2H, CH), 1.49 (s, 18H, C(CH_3)$_3$), 1.26 (s, 18H, C(CH_3)$_3$), -0.38 (s, 3H, Al-CH_3), -0.61 (s, 3H, Al-CH_3). ^{13}C NMR (101 MHz, C_6D_6) δ 172.6 (N=CH), 163.0 (Ar-O), 141.6 (Ar), 139.4 (Ar), 135.0 (Ar), 133.1 (Ar-H), 129.7 (Ar-H), 129.2 (Ar-H), 128.9 (Ar), 128.8 (Ar), 118.9 (Ar-CH=N), 72.4 (CH), 35.9 (**C**(CH_3)$_3$), 34.4 (**C**(CH_3)$_3$), 31.7 (C(**C**H_3)$_3$), 29.8 (C(**C**H_3)$_3$), -7.3 (Al-CH_3), -9.4 (Al-CH_3). Elemental Analysis: Calc (%) for $C_{48}H_{66}Al_2N_2O_2$: C 76.16% H 8.79% N 3.70% Found: C 75.99% H 8.85% N 3.65%.

4H_2[12]

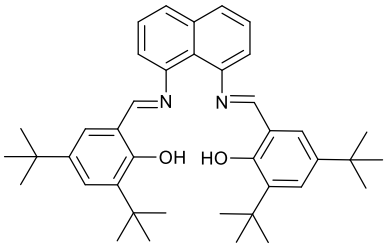

A solution of 1,8-diaminonaphthalene (1.08 g, 6.85 mmol), 3,5-di-tert-butyl-2-hydroxybenzaldehyde (3.85 g, 2.4 eq.) and formic acid (5 drops) in EtOH was heated to reflux for 48 h. On cooling to RT a yellow precipitate formed which was isolated by vacuum filtration and washed with cold EtOH. The product was taken up in $CHCl_3$, dried over $MgSO_4$ to remove traces of H_2O and dried *in vacuo* to yield **4**H_2 as a deep yellow powder, 1.46 g, 2.47 mmol, 36%).

^{1}H NMR ($CDCl_3$, 400 MHz): δ = 13.25 (s, 2H, OH), 8.66 (s, 2H, N=CH), 7.77 (dd, *J* = 8.5 Hz, 1.0 Hz, 2H, Ar), 7.51 (dd, *J* = 8.0, 7.5 Hz, 2H, Ar), 7.29 (s, 4H, Ar), 6.98 (dd, *J* = 7.5, 1.0 Hz, 2H, Ar), 1.32 (s, 18H, C(CH_3)$_3$), 1.01 ppm (s, 18H, C(CH_3)$_3$). ^{13}C {^{1}H} NMR ($CDCl_3$, 101 MHz): δ = 161.7 (CH=N), 158.6 (Ar-OH), 147.0, 140.1, 136.4, 127.9, 126.8, 126.7, 126.5, 119.0, 117.2 (Ar), 34.7 (**C**(CH_3)$_3$), 34.1 (**C**(CH_3)$_3$), 31.5 (C(**C**H_3)$_3$), 29.1 (C(**C**H_3)$_3$). ESI-MS (MeOH): *m/z* calc. for $[C_{40}H_{51}N_2O_2]^+$: 591.9651, found *m/*z = 591.3950.

Al_2(**4**)Me_2

Ligand **4**H_2 (0.50 g, 0.85 mmol) was dissolved in toluene (20 mL) with a little gentle heating. Once cooled to room temperature, $AlMe_3$ (2M in hexanes, 0.85 mL, 1.7 mmol, 2 mol eq.) was added in one portion and the dark yellow solution was stirred at RT for 1 h. The solution became cloudy but the precipitate dissolved on gentle heating. The crystals which formed after 7 days in the freezer were isolated by cannula filter and dried under vacuum (heated to 60 °C to remove toluene), giving Al_2(**4**)Me_2 as a bright yellow crystalline solid (0.27 g, 0.38 mmol, 45%).

^{1}H NMR (C_6D_6, 400 MHz): δ 7.74 (d, *J* = 7.5 Hz, 2H, Ar–H), 7.57 (d, *J* = 2.0 Hz, 2H, Ar–H), 7.49 (d, *J* = 8.0 Hz, 2H, Ar–H), 7.44 (s, 2H, CH=N), 7.03–7.11 (m, 2H, Ar–H), 6.92 (d, *J* = 2.5 Hz, 2H, Ar–H), 1.32 (s, 18H, $(C(CH_3)_3)$), 1.31 (br. s., 18H, $(C(CH_3)_3)$), −0.29 (s, 6H, Al–CH_3), −0.34 ppm (s, 6 H, Al–CH_3). $^{13}C\{^1H\}$ NMR (C_6D_6, 101 MHz): δ 175.4 (CH=N), 163.6 (Ar–O), 142.0, 140.8, 139.5, 134.5, 131.2, 129.7, 128.9, 126.5, 126.0, 124.9, 119.7, 35.6 (**C**$(CH_3)_3$), 34.7 (**C**$(CH_3)_3$), 31.9 (C(**C**$H_3)_3$), 30.2 (C(**C**$H_3)_3$), −6.9 (Al–CH_3), −9.2 ppm (Al–CH_3). Elemental Analysis: Calc (%) for $C_{44}H_{60}Al_2N_2O_2$: C 75.18% H 8.60% N 3.99% Found: C 74.78% H 8.49% N 3.65%.

Zn_2(**4**)$_2$

Ligand **4**H_2 (0.45 gm 0.76 mmol) was suspended in toluene (15 mL). Dimethylzinc (1.5 mL, 1M solution, 1.5 mmol, 2 eq.) was added in one portion and the suspension was stirred for 30 minutes, after which time the solution became clear. The solution was stirred for a further 1.5 h, then the solvent was removed *in vacuo* and the yellow residue was recrystallised from hexane/toluene (30:3 mL). Product isolated as a bright yellow powder (0.33 g, 0.25 mmol, 65%)

^{1}H NMR (C_6D_6, 400 MHz): δ 1.22 (s, 18 H), 1.29 (s, 18 H), 1.53 (s, 18 H), 1.80 (s, 18 H), 5.46 (d, *J* = 7.5 Hz, 2 H), 6.21 (d, *J* = 7.0 Hz, 2 H), 6.52 (d, *J* = 2.5 Hz, 2 H), 6.66 (d, *J* = 2.5 Hz, 2 H), 6.82 (t, *J* = 8.0 Hz, 2 H), 6.91 (t, *J* = 8.0 Hz, 2 H), 7.28 - 7.41 (m, 6 H), 7.55 - 7.72 (m, 6 H). $^{13}C\{^1H\}$ NMR (C_6D_6, 101 MHz): δ 171.8 (CH=N), 171.4 (Ar–O), 166.5, 164.7, 151.4, 145.6, 142.7, 142.7, 139.2, 135.8, 135.0, 132.1, 131.5, 130.5, 130.3, 129.7, 127.7, 127.0, 125.5, 123.8, 123.6, 118.8, 118.2, 115.6, 36.5, 36.4, 34.4, 34.2, 33.0, 32.0, 31.9, 30.4.

6.4.2 Preparation of imidazolidine ligands

5H_2

*Step 1: reduction of **3**H_2*

3H_2 (0.90 g, 1.40 mmol) was dissolved in MeOH/THF (1:1) 40 mL. Sodium borohydride (0.13 g, 3.3 mmol, 2.4 eq.) was added with stirring and the resulting yellow solution stirred at RT for 6 h, until the solution became colourless. H_2O was added (10 mL) and the volatile solvent removed, resulting in the formation of a white precipitate which was collected by vacuum filtration and thoroughly dried, yielding the desired product as a white powder (0.56 g, 1.34 mmol, 96%).

^{1}H NMR ($CDCl_3$, 400 MHz) δ 9.86 (br. s., 2 H, OH), 7.29 - 7.43 (m, 6 H, Ar-H), 7.26 (d, *J* = 8.0 Hz, 4 H, Ar-H), 7.14 (d, *J* = 2.5 Hz, 2 H, Ar-H), 6.59 (d, *J* = 2.5 Hz, 2 H, Ar-H), 3.87 (s, 2 H, CH), 3.69 (d, *J* = 13.5 Hz, 2 H, CH_2), 3.46 (d, *J* = 13.5 Hz, 2 H, CH_2), 1.36 (s, 18 H, $C(CH_3)_3$), 1.20 ppm (s, 18 H, $C(CH_3)_3$). ^{13}C {^{1}H} NMR ($CDCl_3$, 101 MHz): δ 154.1 (Ar-OH), 149.1, 146.1, 140.4, 138.7, 135.8, 129.0, 128.3, 127.9, 123.2, 122.9, 121.7 (Ar), 67.7 (**C**H), 51.1 (**C**H_2), 34.8 (**C**$(CH_3)_3$), 34.0 (**C**$(CH_3)_3$), 31.5(C(**C**$H_3)_3$), 29.5 ppm (C(**C**$H_3)_3$).

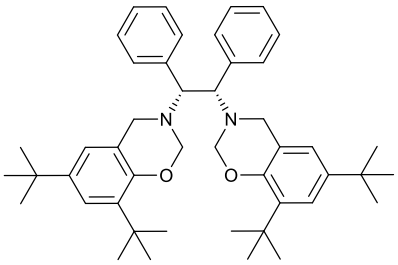

Step 2

*P*roduct from previous step (0.54 g, 0.85 mmol) was dissolved in $CHCl_3$ (25 mL). To this was added paraformaldehyde (0.038 g, 1.3 mmol), $MgSO_4$ (0.5 g) and K_2CO_3 (0.5 g). The solution was stirred at RT for 18 hours, filtered and reduced *in vacuo*. The white residue was recrystallised from MeOH to yield benzoxazime **5** as a cream, crystalline solid (0.4 g, 0.60 mmol, 70%)

^{1}H NMR ($CDCl_3$, 400 MHz) δ ppm 7.11 - 7.23 (m, 8 H, Ar), 6.93 (m, 4 H, Ar), 6.63 (d, *J* = 2.3 Hz, 2 H, Ar), 5.32 (d, *J* = 10.0 Hz, 2 H, CH_2), 4.84 (d, *J* = 10.0 Hz, 2H, CH_2), 4.46 (s, 2H, CH), 4.41 (d, *J* = 17.0 Hz, 2H, CH_2), 3.89 (d, *J* = 17.0Hz, 2H, CH_2), 1.38 (s, 18 H, $C(CH_3)_3$), 1.25 (s, 18 H, $C(CH_3)_3$). ^{13}C NMR (101 MHz, $CDCl_3$) δ ppm 150.82 (Ar-O), 142.00, 138.51, 136.28, 130.29 (Ar-H), 127.36(Ar-H), 127.23 (Ar-H), 121.90 (Ar-H), 121.68 (Ar-H), 119.51 (Ar), 80.60 (CH_2), 65.75 (CH), 50.28 (CH_2), 34.81 (C(**C**$H_3)_3$), 34.20 (**C**$(CH_3)_3$), 31.54 (C(**C**$H_3)_3$), 29.68 (C(**C**$H_3)_3$).

Imidazolidine general procedure:

Step 1: Schiff Base formation

Ethylenediamine (1.0 g, 16.6 mmol) and desired 2,4-substituted salicylaldehyde (2.1 mol eq.) were refluxed in MeOH overnight. The resulting yellow precipitate was isolated by filtration and washed with cold MeOH.

Step 2: Reduction

Schiff base ligand was dissolved in MeOH/THF (1:1, 40 mL). Sodium borohydride (2.4 eq.) was added with stirring and the resulting yellow solution stirred at RT for 6 h, until the colour faded. H_2O was added (10 mL) and the volatile solvent removed, resulting in the formation of a white precipitate which was collected by vacuum filtration and thoroughly dried, yielding the desired salan product.

Step 3: Condensation with aldehyde

Salan from step 2 was suspended in EtOH (20 mL). The desired aldehyde (1.1 eq.) was added, and the mixture heated to 50 °C (all reagents dissolved) with stirring overnight. On cooling, a white precipitate formed. The precipitate was filtered from solution, and the solid was recrystallised from MeOH to yield the desired product.

6H_2

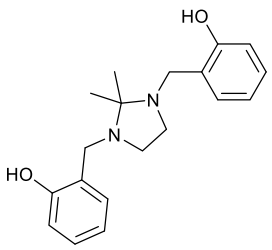

As general procedure for steps 1 and 2. In step 3 the salan was refluxed in acetone (20 mL).

Unsubstituted salan used (0.43 g, 1.67 mmol). Product isolated as a white powder (0.37 g, 1.18 mmol, 71 %).

^{1}H NMR (400 MHz, $CDCl_3$) δ ppm 10.66 (br s, 2 H, OH), 7.19 (td, *J* = 7.5, 1.5 Hz, 2 H, Ar), 7.02 (d, *J* = 7.0 Hz, 2 H, Ar), 6.84 (dd, *J* = 8.0, 1.0 Hz, 2 H, Ar), 6.80 (td, *J* = 7.5, 1.0 Hz, 2 H, Ar), 3.89 (s, 4 H, CH_2), 2.86 (s, 4 H, CH_2), 1.37 (s, 6 H, CH_3). $^{13}C\{^1H\}$ NMR ($CDCl_3$, 101 MHz) δ ppm 157.73 (Ar-OH), 128.92 (Ar-H), 128.28 (Ar-H), 121.18 (Ar-CH_2), 119.21 (Ar-H), 116.11 (Ar-H), 78.85 (C), 52.82 (CH_2), 47.91 (CH_2), 19.60 (CH_3)

7H_2

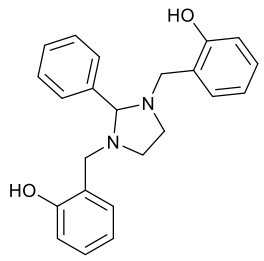

Unsubstituted salan used (0.5 g, 1.84 mmol), benzaldehyde (0.21 g, 0.21 mL, 2.02 mmol, 1.1 eq.) Product isolated as a white powder (0.54 g, 1.50 mmol, 83%).

^{1}H NMR (400 MHz, $CDCl_3$) δ 10.04 (br. s., 2 H, 2 X OH), 7.50 - 7.58 (m, 2 H, Ar), 7.37 - 7.50 (m, 3 H, Ar), 7.09 - 7.20 (m, 2 H, Ar), 6.95 (d, *J* = 7.5 Hz, 2 H, Ar), 6.67 - 6.86 (m, 4 H, Ar), 4.04 (d, *J* = 13.5 Hz, 2 H, N-CH_2-Ar), 3.82 (s, 1 H, CH), 3.25 - 3.47 (m, 4 H, CH_2, N-CH_2-Ar), 2.58 - 2.79 (m, 2 H, CH_2). ^{13}C{^{1}H} NMR (101 MHz, $CDCl_3$) δ ppm 157.14 (Ar-OH), 136.85 (Ar), 130.04 (Ar-H), 129.34 (Ar-H), 129.00 (Ar-H), 128.54 (Ar-H), 128.30 (Ar-H), 121.13 (Ar), 119.24 (Ar-H), 116.00 (Ar-H), 89.39 (CH), 55.83 (CH_2), 50.26 (CH_2). ESI-MS (MeOH): *m/z* calc. for $[C_{23}H_{25}N_2O_2]^+$ = 361.1911, found *m/z* = 361.1962.

8H_2

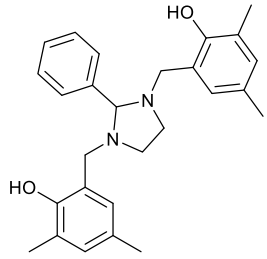

2,4-Dimethyl substituted salan used (1.5 g, 4.6 mmol), benzaldehyde (0.53 g, 0.51 mL, 5.1 mmol, 1.1 eq.). Product isolated as a white powder. (1.60 g, 3.84 mmol, 84 %).

^{1}H NMR (400 MHz, $CDCl_3$) δ 9.85 (s, 2 H, 2 x OH), 7.56 (dt, *J* = 8.0, 2.0 Hz, 2 H, Ar), 7.44 - 7.50 (m, 2 H, Ar), 7.38 - 7.44 (m, 1 H, Ar), 6.77 - 6.89 (m, 2 H Ar), 6.54 - 6.66 (m, 2 H, Ar), 3.98 (d, *J* = 13.0 Hz, 2 H, N-CH_2-Ar), 3.77 (s, 1 H, CH), 3.30 - 3.36 (m, 2 H, CH_2-CH_2), 3.26 (d, *J* = 13.5 Hz, 2 H, N-CH_2-Ar), 2.61 - 2.67 (m, 2 H. CH_2-CH_2), 2.19 (s, 6 H, 2 x CH_3), 2.18 (s, 6 H, 2 x CH_3). ^{13}C{^{1}H} NMR (101 MHz, $CDCl_3$) δ 152.8 (Ar-OH), 137.0 (Ar), 130.7 (Ar-H), 129.9 (Ar-H), 129.3 (Ar-H), 128.6 (Ar-H), 127.7 (Ar), 126.4 (Ar-H), 124.5, 120.2, 89.5 (CH), 55.9 (CH_2), 50.1 (CH_2), 20.4 (CH_3), 15.6 (CH_3). ESI-MS (MeOH): *m/z* calc. for $[C_{27}H_{33}N_2O_2]^+$ = 417.2537, found *m/z* = 417.2554.

9H_2

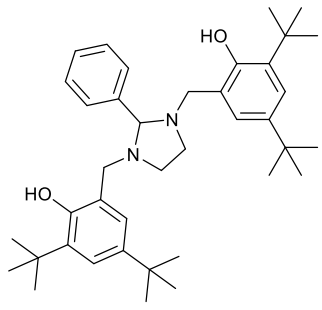

2,4-Di-*tert*-butyl substituted salan used (1.40 g, 2.82 mmol), benzaldehyde (0.33 g, 0.32 mL, 3.1 mmol, 1.1 eq.). Product isolated as a cream solid (1.38 g, 2.35 mmol, 84%)

^{1}H NMR (400 MHz, $CDCl_3$) δ 10.01 (br s, 2 H, OH), 7.48 (d, *J* = 7.5 Hz, 2 H), 7.28 - 7.40 (m, 3 H, Ar), 7.16 (d, *J* = 2.5 Hz, 2 H, Ar), 6.77 (d, *J* = 2.5 Hz, 2 H, Ar), 3.99 (d, *J* = 13.5 Hz, 2 H, Ar-CH_2-N), 3.81 (s, 1 H, CH), 3.32 - 3.42 (m, 4 H, CH_2, Ar-CH_2-N), 2.72 (q, *J* = 5.0 Hz, 2 H, CH_2),

1.39 (s, 18 H, C(CH$_3$)$_3$), 1.25 (s, 18 H, C(CH$_3$)$_3$). ^{13}C{^{1}H} NMR (101 MHz, CDCl$_3$) δ ppm 153.6 (Ar-OH), 140.5, 135.4, 129.5, 129.5, 128.9, 128.8, 123.1, 123.0, 120.5, 89.8 (Ar), 76.8 (CH), 56.9 (CH$_2$), 50.3 (CH$_2$), 34.8 (**C**(CH$_3$)$_3$), 34.1 (**C**(CH$_3$)$_3$), 31.6 (C(**C**H$_3$)$_3$), 29.5 (C(**C**H$_3$)$_3$). ESI-MS (MeOH): *m/z* calc. for [C$_{39}$H$_{57}$N$_2$O$_2$]$^+$ = 585.4415, found *m/z* = 585.4437.

10H$_3$

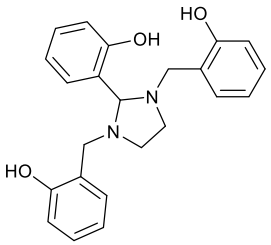

Unsubstituted salan used (0.5 g, 1.84 mmol), salicylaldehyde (0.23 g, 0.19 mL, 2.02 mmol, 1.1 eq.). Product isolated as a very pale yellow powder (0.62 g, 1.64 mmol, 81%).

^{1}H NMR (400 MHz, CDCl$_3$) δ 9.16 (br. s., 3 H, 3 x OH), 7.26 (m, 7.20 - 1 H, Ar), 7.11 - 7.20 (m, 3 H, Ar), 7.02 - 7.07 (m, 2 H, Ar), 6.92 - 6.97 (m, 1 H, Ar), 6.84 - 6.91 (m, 3 H, Ar), 6.76 - 6.84 (m, 2 H, Ar), 4.14 (d, *J* = 13.0 Hz, 2 H, N-CH$_2$-Ar), 3.99 (s, 1 H, CH), 3.43 (d, *J* = 13.0 Hz, 2 H, N-CH$_2$-Ar), 3.18 - 3.36 (m, 2 H, CH$_2$-CH$_2$), 2.56 - 2.77 (m, 2 H, CH$_2$-CH$_2$). ^{13}C{^{1}H} NMR (101 MHz, CDCl$_3$) δ 156.9 (Ar-OH) 156.2 (Ar-OH), 131.3, 130.9, 129.3, 129.0, 121.8, 120.5, 119.6, 119.5, 117.4, 116.2 (Ar), 88.3 (CH), 54.2 (N-CH$_2$-Ar), 49.5 (CH$_2$-CH$_2$). ESI-MS (MeOH): *m/z* calc. for [C$_{23}$H$_{25}$N$_2$O$_3$]$^+$ = 377.1860, found *m/z* = 377.1909.

11H$_4$

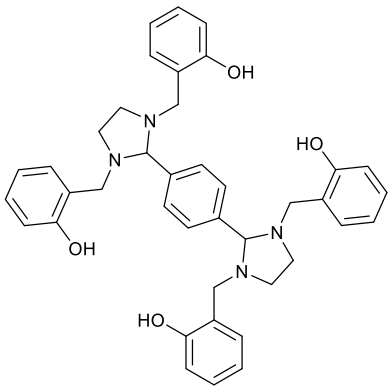

Unsubstituted salan (1.15 g, 4.23 mmol) and terephthaldehyde (0.28 g, 2.11 mmol, 0.5 eq.) were refluxed in EtOH for 25 h. A precipitate formed on heating above 70 °C, which was collected by filtration on cooling to give **11**H$_4$ as a white solid (1.18 g, 1.84 mmol, 87%).

^{1}H NMR (400 MHz, CDCl$_3$) δ 9.92 (br s, 4 H, OH), 7.52 (s, 4 H, Ar), 6.95 - 7.10 (m, 4H, Ar-H), 6.90 (d, *J* =7.5 Hz, 4H, Ar-H), 6.65 - 6.78 (m, 8 H, Ar), 3.92 (d, *J* = 13.5 Hz, 4 H, Ar-CH$_2$-N), 3.81 (s, 2 H, CH), 3.33 - 3.46 (m, 8 H, CH$_2$ + Ar-CH$_2$-N), 2.70 (q, *J* = 5.0 Hz, 4 H, CH$_2$). ^{13}C{^{1}H} NMR (101 MHz, CDCl$_3$) δ ppm 157.0 (Ar-OH), 138.7 (Ar), 129.4 (Ar-H), 128.9 (Ar-H), 128.3 (Ar-H), 121.0 (Ar), 119.3 (Ar-H), 115.9 (Ar-H), 89.3 (CH), 56.1 (CH$_2$), 50.5 (CH$_2$). ESI-MS (MeOH): *m/z* calc. for [C$_{40}$H$_{43}$N$_4$O$_4$]$^+$ = 643.3279, found *m/z* = 643.3305.

12H_4

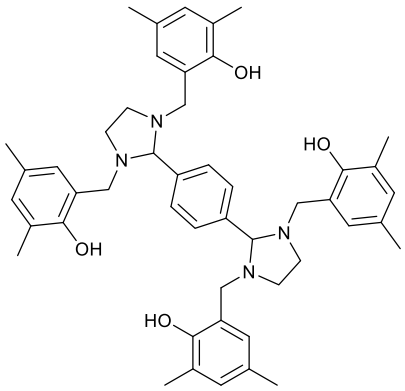

2,4-Dimethyl substituted salan (0.85 g, 2.6 mmol) and terephthaldehyde (0.17 g, 1.30 mmol, 0.5 eq.) were refluxed in EtOH for 24 h. A pink precipitate formed which was isolated by filtration on cooling, and recrystallised from MeOH to yield **12**H_4 as a fluffy, white powder, (0.87 g, 1.16 mmol, 89%).

^{1}H NMR (400 MHz, $CDCl_3$) δ ppm 9.77 (br s, 4 H, OH), 7.54 (s, 4 H, Ar), 6.70 (s, 4 H, Ar), 6.55 (s, 4 H Ar), 3.85 (d, *J* = 13.5 Hz, 4H, Ar-CH_2-N), 3.76 (s, 2 H, CH), 3.26 - 3.43 (m, 8H, Ar-CH_2-N), 2.64 (q, *J* = 5.0 Hz, 5 H, CH_2), 2.13 (s, 12 H, CH_3), 2.11 (s, 12 H, CH_3). ^{13}C{1H} NMR (101 MHz, $CDCl_3$) δ ppm 152.7 (Ar-OH), 138.5 (Ar), 130.7 (Ar-H), 129.3 (Ar-H), 127.7 (Ar), 126.4 (Ar-H), 124.3 (Ar), 120.1 (Ar), 89.4 (CH), 56.1 (CH_2), 50.3 (CH_2), 20.3 (CH_3), 15.5 (CH_3). ESI-MS (MeOH): *m/z* calc. for $[C_{48}H_{59}N_4O_4]$+ = 755.4531, found *m/z* = 755.4556.

Al_2(**7**)$_2Me_2$

Ligand **7**H_2 (0.5 g, 1.4 mmol) was dissolved in toluene (10 mL) with a little gentle heating. Once cooled to RT, $AlMe_3$ was added in one potion (2M in hexanes, 0.7 mL, 1.4 mmol, 1 mol eq.). The solution was stirred at RT for 2 hours. The volume of solvent was reduced by roughly half, at which point a solid precipitated from solution. The suspension was gently heated until fully dissolved and left to crystallise. Product was isolated as pale yellow crystals (0.32 g, 0.4 mmol, 57%).

^{1}H NMR (400 MHz, C_6D_6) δ 7.14 (10H, Ar) 7.01 (m, 4H, Ar), 6.69 (m, 8H, Ar), 6.44 (d, *J* = 7.0 Hz, 4H, Ar), 5.42 (s,2 H, CH), 3.62 (d, *J* = 15.0 Hz, 4H, N-CH_2-Ar), 3.17 (d, *J* = 15.0 Hz, 4H, N-CH_2-Ar), 2.70 (q, *J* = 5.5 Hz, 4H, CH_2), 2.52 (q, *J* = 5.5 Hz, 4H, CH_2), -0.46 (s, 6H, Al-CH_3). ^{13}C{^{1}H} NMR (101 MHz, C_6D_6) δ 159.34 (Ar-O), 137.39 (Ar), 130.87 (Ar), 130.70 (Ar), 130.33 (Ar), 129.07 (Ar), 125.64 (Ar), 123.31 (Ar), 120.72 (Ar), 118.47 (Ar), 85.59 (CH), 55.10 (N-CH_2-Ar), 48.76 (CH_2).

Li_4(**9**)$_{2(}$THF)$_3$

9H_2, (0.5 g, 1.2 mmol) was dissolved in THF (10 mL) and cooled to -78 °C. ^{n}BuLi (2.5 M in hexanes, 0.96 ml, 2.4 mmol, 2 eq.) was added dropwise and after complete addition the solution was warmed to RT with stirring over 1 hr, after which the solvent was removed *in*

vacuo. The crude product was recrystallised from hexane/toluene. The crystals were isolated via cannula filtration, washed with hexane and dried to yield the product as a white powder (0.4 g, 0.37 mmol, 62%).

^{1}H NMR (400 MHz, pyridine-d^{5}) δ 7.12 - 7.20 (m, 5H, Ar), 7.08 (d, *J* = 2.0 Hz, 2H, Ar), 6.96 (d, *J* = 2.0 Hz, 2H, Ar), 5.82 (s, 1H, CH), 4.01 (d, *J* = 11.5 Hz, 2H, N-CH_2-Ar), 3.67 (dt, *J* = 6.5, 3.0 Hz, 3H, THF), 3.62 (d, *J* = 11.5 Hz, 2H, N-CH_2-Ar), 3.08 - 3.26 (m, 4H, 2 x CH_2), 2.27 (s, 6H, 2 x CH_3), 2.25 (s, 6H, 2 x CH_3), 1.63 (dt, *J* = 6.5, 3.0 Hz, 3H, THF). ^{13}C{^{1}H} NMR (101 MHz, pyridine-d^{5}) δ 167.6 (Ar-O), 133.3 (Ar), 132.3 (Ar-H), 131.4 (Ar-H), 131.1 (Ar), 130.6 (Ar), 129.8 (Ar), 129.1 (Ar), 128.7 (Ar), 127.7 (Ar), 127.6 (Ar), 121.0 (Ar), 85.3 (CH), 69.8 (THF), 59.2 (CH_2), 53.3 (CH_2CH_2), 27.8 (THF), 22.7 (CH_3), 20.7(CH_3).

Al_2(**12**)Me_2

Ligand **12**H_4 (0.5 g, 0.66 mmol) was dissolved in toluene (15 mL) and $AlMe_3$ (0.66 mL, 2 M solution, 1.32 mmol, 2 eq.) was added in one portion. The solution turned yellow and a precipitate formed which would not be heated back into solution. This was isolated *via* cannula filtration, and the yellow solid was washed with copious hexane. Product isolated as a bright yellow solid (0.34 g, 0.41 mmol, 62%).

^{1}H NMR (400 MHz, C_6D_6) δ 6.57 (s, 4H, Ar), 6.16 (s, 4H, Ar), 5.44 (s, 2H, CH), 3.81 (d, *J* = 14.5 Hz, 4H, Ar-CH_2-N), 3.29 (d, *J* = 14.5 Hz, 4H, Ar-CH_2-N), 2.88 - 3.04 (m, 4H, CH_2), 2.66 - 2.79 (m, *J* = 4.39 Hz, 4H, CH_2), 2.55 (s, 12H, Ar-CH_3), 2.15 (s, 12H, Ar-CH_3), -0.37 (s, 6H, Al-CH_3). ^{13}C{^{1}H} NMR (101 MHz, C_6D_6) δ 155.4 (Ar-O), 138.5 (Ar), 132.2 (Ar-H), 129.9 (Ar-H), 129.2 (Ar), 126.5 (Ar), 125.7 (Ar), 122.0 (Ar-CH_2), 84.1 (CH), 55.7 (CH_2), 49.8 (CH_2), 20.7 (CH_3), 17.1 (CH_3).

6.5 Chapter 4 experimental

6.5.1 Preparation of saturated monomers from β-pinene

(+)-Nopinone (**1**).

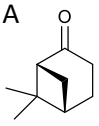

A solution of β-pinene (30 g, 0.22 mol) in CH_2Cl_2 (or MeOH) (300 mL) was treated with a gentle flow of ozone at -78 °C until a characteristic blue colour was observed (typically 6 h). The ozone treatment was stopped, and nitrogen was bubbled through the solution to remove excess ozone (typically 5 min, until blue colour dissipates). The ozonide intermediate was quenched *via* dropwise addition of triethylamine (2 eq.) with stirring while gradually warming to room temperature. The resulting solution

was stirred for 18 hr at RT before washing with 1M HCl (5 x 200 mL). The organic layer was dried over $MgSO_4$ and concentrated *in vacuo* to afford pale yellow-green oil which was purified by vacuum distillation (85 °C, 0.45 torr) to yield **1** as a pale yellow-green oil (26.27 g, 0.18 mol, 82%).

^{1}H NMR (400 MHz, $CDCl_3$) δ 2.52 (m, 3H, CH_2 + CH), 2.32 (m, 1H, CH), 2.22 (m, 1H, CH), 1.98 (m, 1H, CH), 1.56 (d, *J* = 10.0 Hz, 1H, CH), 1.31 (s, 3H, CH_3), 0.84 (s, 3H, CH_3). ^{13}C{1H} NMR (101 MHz, $CDCl_3$) δ 214.8 (C=O), 58.0, 41.2, 40.4, 32.7, 25.9, 25.2, 22.1, 21.4. GC-MS retention time = 6.2 min.

(±)-Cryptone (**2**)[13]

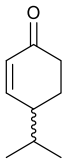

1 (6.0 g, 43.4 mmol) was dissolved in CH_2Cl_2 (150 mL) under Ar and cooled to 0 °C. $AlCl_3$ (11.6 g, 2 eq.) was added slowly with stirring, and the resulting mixture stirred for 1.5 h. During this time the solution became dark brown. The reaction was quenched by pouring the solution slowly into ice and water (100 mL), and an instant colour change to yellow was observed. The phases were separated, and the organic layer washed with saturated solutions of sodium bicarbonate (100 mL) and brine (100 mL), dried over $MgSO_4$ and concentrated *in vacuo* to give a brown oil. This was purified by column chromatography on silica (pet ether/Et_2O 95:5) to yield the product as a pale yellow oil (5.53 g, 40.0 mmol, 92%).

^{1}H NMR (400 MHz, $CDCl_3$) δ 6.88 (dt, *J* = 10.5, 1.5 Hz, 1H, **H**C=CHC(O)), 5.99 (dt, *J* = 10.5, 1.5 Hz, 1H, HC=C**H**C(O)), 2.49 (dt, *J* = 1.0 Hz, 1H, CH), 2.14 - 2.38 (m, 2H, CH_2), 1.91 - 2.12 (m, 1H, CH), 1.61 - 1.87 (m, 2H, CH_2), 0.95 (td, *J* = 1.0 Hz, 6H, CH_3). ^{13}C{^{1}H} NMR (101 MHz, $CDCl_3$) δ 200.0 (C=O), 154.2 (C=C), 129.6 (C=C), 42.4 (CH), 37.3 (CH_2), 31.4 (CH), 25.2 (CH_2), 19.5 (CH_3), 19.4 (CH_3). GC-MS retention time = 6.8 min.

4-Isopropylcyclohexhanone (**3**)

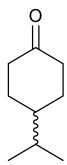

A Parr 5500 high pressure reactor was charged with cryptone (**2**) (1.0 g, 7.24 mmol), $Rh(PPh_3)_3Cl$ (Wilkinson's catalyst, 5 wt%, 50 mg) and EtOAc (20 mL). The reactor was flushed with hydrogen (10 bar) before sealing and heating at 40 °C for 24 h with stirring. After this time the rector was vented, allowed to cool and the solution was passed over Celite before removing the solvent, giving a brown oil. Purified by vacuum distillation to yield **3** as a colourless oil (0.96 g, 6.88 mmol, 95 %).

^{1}H NMR (400 MHz, $CDCl_3$) δ 2.31 (m, 4H, CH_2-C(O)), 1.98 (m, 2H, CH), 1.49 (m, 4H, CH_2), 0.90 (d, *J* = 6.5 Hz, 6H, CH_3). $^{13}C\{^{1}H\}$ NMR (101 MHz, $CDCl_3$) δ 211.6 (C=O), 41.5 (CH), 40.0 (CH_2), 30.8 (CH), 28.6 (CH_2), 18.9 (CH_3). GC-MS retention time = 6.1 min.

4-isopropylcaprolactone (4^{i}PrCL) (**4**)

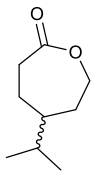

To a stirred solution of 4-isopropylcyclohexanone (Fluorochem, 10.0 g, 70 mmol, or **3**) in CH_2Cl_2 (150 mL) under Ar at 0 °C was added mCPBA in portions (14.8 g, 84 mmol, 1.2 eq.). On warming to RT a white precipitate formed, and the suspension was stirred for 48 h. The precipitate was removed by vacuum filtration and the solution was washed with Na_2SO_3 (10% aq., 200 mL), and saturated solutions of sodium bicarbonate (200 mL) and brine (200 mL). The organic fraction was dried over $MgSO_4$ and concentrated to a yellow oil (10.32 g). This was purified *via* column chromatography on silica (hexane/EtOAc 6:1) and dried by vacuum distillation over CaH_2 (bp = 239 °C, 1 atm, 95 °C, 0.45 torr) to yield **3** as a colourless oil (9.7 g, 62 mmol, 89%).

FTIR: ν (cm^{-1}) 1732 (C=O). ^{1}H NMR ($CDCl_3$, 400 MHz) δ 4.20 (m, 2H, C(O)CH_2), 2.59 (m, 2H, CH_2), 1.85 (m, 2H, CH_2), 1.46 (m, 4H, CH, CH_2), 0.85 (dd, *J* = 2.5 Hz, 6H, CH_3). $^{13}C\{^{1}H\}$ NMR (101 MHz, $CDCl_3$) δ 176.0 (C=O), 68.4 (CH_2-O), 46.4 (CH), 33.3 (CH_2), 32.4 (CH), 31.9 (CH_2), 25.6 (CH_2), 19.2 (CH_3), 19.1 (CH_3). ESI-MS (MeOH): *m/z* calc. for $[C_9H_{16}O_2Na]^+$ = 179.1048, found *m/z* = 179.1083. GC-MS retention time = 9.4 min.

Poly(**4**)

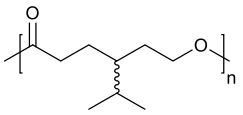

Thick, colourless gel.

FTIR: ν (cm^{-1}) 1756 (C=O). ^{1}H NMR (400 MHz, $CDCl_3$) δ 3.99 - 4.15 (m, 2H, CH_2), 2.17 - 2.37 (m, 2H, CH_2), 1.59 - 1.76 (m, 3H, CH + CH_2), 1.40 - 1.59 (m, 2H, CH_2), 1.18 - 1.31 (m, 1H, CH), 0.87 (dd, *J* = 7.0, 3.5 Hz, 6H, CH_3). $^{13}C\{^{1}H\}$ NMR (101 MHz, $CDCl_3$) δ 173.6 (C=O), 63.3 (CH_2-O), 40.3 (CH), 32.5(CH_2), 29.2 (CH), 29.1 (CH_2), 25.9 (CH_2), 19.1 (CH_3), 18.6 (CH_3).

4-isopropylcyclohexanone oxime (**7**)

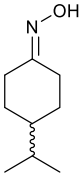

4-isopropropylcyclohexanone (**3**) (1.0 g, 7.2 mmol) was mixed with hydroxylamine hydrochloride ($NH_2OH.HCl$, 0.75 g, 10.8 mmol, 1.5 eq.) and sodium acetate (NaOAc, 1.1 g, 13 mmol, 1.8 eq.) in a mixture of ethanol (10 mL) and water (7 mL). The mixture was refluxed for 5 h under Ar before cooling to room temperature and stirring overnight. The solvent was removed in vacuo and the residue was taken up in

EtOAc (25 mL), washed with water (25 mL) and brine (sat., 25 mL). The organic phase was dried over Na_2SO_4 and the solvent removed to yield the product (**7**) as a thick, yellow oil (1.0 g, 0.70 mmol, 98%).

^{1}H NMR (400 MHz, $CDCl_3$) δ 8.96 (br. s., 1H, OH), 3.25 - 3.38 (m, 1H, CH_2), 2.37 - 2.47 (m, 1H, CH_2), 2.08 (dt, *J* = 13.5, Hz, 1H, CH_2), 1.81 - 1.93 (m, 2H, CH_2), 1.68 - 1.81 (m, 1H, CH_2), 1.43 - 1.56 (m, 1H, CH), 1.11 - 1.37 (m, 3H, CH_2 + CH), 0.88 (d, *J* = 7.0 Hz, 6 H, CH_3). ^{13}C{^{1}H} NMR (101 MHz, $CDCl_3$) δ 160.9 (C=N), 43.3 (CH), 32.1 (CH), 31.6 (CH_2), 29.6 (CH_2), 28.4 (CH_2), 19.8 (CH_3), 19.8 (CH_3). ESI-MS (MeOH): *m/z* calc. for $[C_9H_{18}NO]^+$ = 156.1388, found *m/z* = 156.1397.

4-isopropylcaprolactam (**8**)

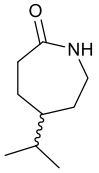

4-isopropylcycohexanone oxime, **7** (1.0 g, 0.70 mmol) was dissolved in 80% H_2SO_4 (10 mL) and heated to 120 °C. The mixture was refluxed for 30 minutes before cooling to room temperature. Water was added (20 mL) to dilute the solution, and then NH_4OH was added to dropwise to bring the mixture to pH 6. The product was extracted with CH_2Cl_2 (3 x 20 mL), and the combined organic phases washed with brine (sat., 50 mL), dried over Na_2SO_4 and concentrated in vacuo to yield **8** as a pale brown solid (0.86 g, 5.5 mol, 79%).

mp = 78 °C. FTIR: ν (cm^{-1}) 2959 (NH) 1651 (C=O). ^{1}H NMR (400 MHz, $CDCl_3$) δ 6.68 (br. s., 1H, NH), 3.09 - 3.38 (m, 2H, CH_2), 2.31 - 2.57 (m, 2H, CH_2), 1.68 - 1.87 (m, 2H, CH_2), 1.49 - 1.68 (m, 1H, CH), 1.16 - 1.46 (m, 3H, CH_2 + CH), 0.86 (d, *J* = 7.0 Hz, 6H, CH_3). ^{13}C{^{1}H} NMR (101 MHz, $CDCl_3$) δ 179.0 (C=O), 48.0 (CH), 42.0 (CH_2), 35.6 (CH_2), 33.1 (CH), 32.4 (CH_2), 25.9 (CH_2), 19.3 (CH_3), 19.2 (CH_3). ESI-MS (MeOH): *m/z* calc. for $[C_9H_{17}NONa]^+$ = 178.1208, found *m/z* = 178.1217.

6.5.1 Preparation of unsaturated monomers from β-pinene

9

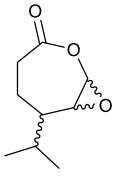

2 (1.0 g, 7.2 mmol) was dissolved in CH_2Cl_2 (30 mL) under Ar and cooled to 0 °C. mCPBA (3 eq.) was added in portions over 30 mins with stirring. The resulting solution was warmed to RT and left to stir for 24 h, after which time a white precipitate had formed. The solution was filtered to remove the precipitate, washed with 10% aq. Na_2SO_3 (50 mL), sat. bicarbonate (50 mL) and brine (50 mL) before drying over $MgSO_4$, filtering and concentrating to an off-white sludgy solid. This was

recrystallised from hexane to yield the product as fine white needles (0.65 g, 3.82 mmol, 53%).

mp = 56-58 °C. ^{1}H NMR (400 MHz, $CDCl_3$) δ 5.19 (d, *J* = 2.5 Hz, 1H (OCHO)), 2.93 (dd, *J* = 8.0, 2.0 Hz, 1H, CCH(O)), 2.73 - 2.86 (m, 1H, $CH_2C(O)$), 2.61 (ddd, *J* = 12.5, 7.0, 1.0 Hz, 1H, $CH_2C(O)$), 2.10 (ddt, *J* = 14.0, 12.0, 7.0 Hz, 1H, CH), 1.63 - 1.80 (m, 2H, CH_2), 1.28 - 1.43 (m, 1H, CH), 1.10 (d, *J* = 7.0 Hz, 3H, CH_3), 1.00 (d, *J* = 6.5 Hz, 3H, CH_3). $^{13}C\{^{1}H\}$ NMR (101 MHz, $CDCl_3$) δ 170.0 (C=O), 76.2 (CH), 56.7 (CH), 43.9 (CH), 32.2 (CH_2), 32.1 (CH), 23.7 (CH_2), 20.3 (CH_3), 20.0 (CH_3). ESI-MS (MeOH): *m/z* calc. for $[C_9H_{15}O_3]^+$ = 171.1021, found *m/z* = 171.1030.

10

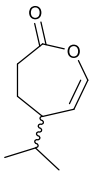

To a vigorously stirring suspension of mCPBA (0.81 g, 3.6 mmol, 1.8 equiv.) in toluene (7 mL) was added cryptone (2 mmol) and DMAP (0.13 g, 1.0 mmol, 50 mol%). The resulting mixture was stirred at room temperature (monitored by NMR), after which the standard work-up procedure was then applied to remove mCPBA/mCBA. The crude product was purified by flash column chromatography, (20% EtOAc/pet ether, product R_f = 0.18), to afford the desired lactone as a pale yellow oil (0.12 g, 0.8 mmol, 40 %).

FTIR ν (cm^{-1}): 1750 (C=O), 904, 727 (C=C). ^{1}H NMR (400 MHz, $CDCl_3$) δ 6.39 (dd, *J* = 6.5, 2.0 Hz, 1H, CHC(O)), 5.25 (t, *J* = 6.0 Hz, 1H, C**H**=CHC(O)), 2.80 (ddd, *J* = 12.5, 10.5, 7.0 Hz, 1H, CH_2), 2.18 - 2.44 (m, 2H, CH + CH_2), 1.72 - 1.87 (m, 1H, CH_2), 1.57 - 1.71 (m, 1H, CH), 0.92 (dd, *J* = 6.5, 4.5 Hz, 6H, CH_3). $^{13}C\{^{1}H\}$ NMR (101 MHz, $CDCl_3$) δ 172.7 (C=O), 139.7 (**C**HC(O)), 117.6 (**C**H=CHC(O)), 41.3 (CH), 32.3 (CH_2), 31.4 (CH), 29.3 (CH_2), 19.9 (CH_3), 19.8 (CH_3). ESI-MS (MeOH): *m/z* calc. for $[C_9H_{15}O_2]^+$ = 155.1067, found *m/z* = 155.1070.

4-Isopropenylcyclohexanone (**11**)

Step 1[14]

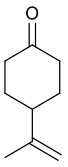

1 (17.6 g, 0.13 mol) was mixed with trimethylorthorformate (14.2 mL (0.14 mol, 1.1 eq.) and cooled over an ice bath. H_2SO_4 was added, and the mixture turned instantly very dark brown. The mixture was warmed to room temperature and stirred for 2 hours, after which TLC analysis showed full consumption of **1**. Acetone (80 mL), water (200 mL) and H_2SO_4 (2N, 2 mL) was added and the solution stirred for a further 2 hours. The volatiles were removed *in vacuo* until a biphasic mixture was observed. The

product mixture was extracted with EtOAc, washed with brine and dried over $MgSO_4$ and concentrated to yield a mixture of 3 ketone products which were quantified by GCMS: **11** (50%), **12** (26%) and **13** (24%).

Step 2

The mixture of products from step 1 (**11**-**13**, 4.64 g, 0.033 mol) were diluted with CH_2Cl_2 (100 mL) and the solution cooled to 0 °C. mCPBA (1.74 g, 0.01 mol, 0.3 eq) was added in one portion and the mixture was stirred for 30 mins at 0 °C, then 30 minutes at RT. Reaction was monitored by GCMS, and stopped when full consumption of the tetrasubstituted alkene was observed. Aqueous sodium bicarbonate (sat. 100 mL) was added and the mixture stirred for an hour before separating the organic layer, washing with saturated brine and drying over $MgSO_4$. The crude mixture was purified by column chromatography on silica (95:5 hexane/EtOAc) as a pale yellow oil (1.99 g, 0.014 mol, 44% from **1**).

^{1}H NMR (400 MHz, $CDCl_3$) δ 4.58 - 4.87 (m, 2H, C=CH_2), 2.24 - 2.51 (m, 5H, CH + C(O)CH_2), 1.95 - 2.18 (m, 2H, CH_2), 1.73 (s, 3H, CH_3), 1.65 (qd, *J* = 12.0, 6.0 Hz, 2H, CH_2). ^{13}C{^{1}H} NMR (101 MHz, $CDCl_3$) δ 211.2 (C=O), 147.9 (**C**=CH_2), 109.6 (C=**CH**$_2$), 43.4 (CH), 40.9 (CH_2), 31.3 (CH_2), 20.8 (CH_3). ESI-MS (MeOH): *m/z* calc. for $[C_9H_{14}NaO]^+$ = 161.0937, found *m/z* = 161.0937. GC-MS retention time = 6.42 min.

12

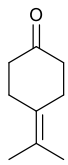

^{1}H NMR (400 MHz, $CDCl_3$) δ 2.51 (br t, *J* = 7.0 Hz, 4H, CH_2), 2.37 (t, *J* = 7.0 Hz, 4H, CH_2), 1.70 (s, 6H, CH_3). ^{13}C{^{1}H} NMR (101 MHz, $CDCl_3$) δ 213.1 (C=O), 126.5 (C=C), 125.1 (C=C), 40.6 (CH_2), 27.2 (CH_2), 20.5 (CH_3). GC-MS retention time = 7.09 min.

13

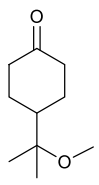

^{1}H NMR (400 MHz, $CDCl_3$) δ 4.35 (ddd, *J* = 13.0, 6.0, 2.0 Hz, 1H, CH_2-O), 4.15 (dd, *J* = 13.0, 10.5 Hz, 1H, CH_2-O), 3.18 (s, 3H, O-CH_3), 2.73 (ddd, *J* = 14.0, 7.5, 1.5 Hz, 1H, CH_2C(O)), 2.57 (ddd, *J* = 14.0, 12.5, 2.0 Hz, 1H, CH_2C(O)), 1.98 - 2.18 (m, 2H), 1.65 - 1.79 (m, 1H), 1.47 - 1.62 (m, 1H), 1.29 - 1.45 (m, 1H), 1.11 (d, *J* = 7.03 Hz, 6H, CH_3). ESI-MS (MeOH): *m/z* calc. for $[C_{10}H_{17}O_2]^+$ = 155.1067, found *m/z* = 155.1070. GC-MS retention time = 8.12 min.

15

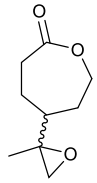

11 (1.99 g, 14.0 mol) was diluted with CH_2Cl_2 (50 mL) and cooled to 0 °C in an ice bath. mCPBA (7.47 g, 43.0 mmol, 3 eq.) was added in portions over 30 mins and the resulting mixture was warmed to room temperature. After 2 h a white precipitate had formed, and TLC analysis no longer showed the presence of starting material. The solution was filtered to remove the precipitate, washed with sodium bisulphite (10 %, aq., 100 mL), and saturated solutions of sodium bicarbonate (100 mL) and brine (100 mL). The organic layer was dried over $MgSO_4$ and concentrated *in vacuo* to yield **11** as a viscous oil (mixture of epoxide isomers) (1.62 g, 9.5 mmol, 68 %).

^{1}H NMR (400 MHz, $CDCl_3$) δ 4.21 - 4.44 (m, 2H, CH_2-O), 3.99 - 4.21 (m, 2H, CH_2-O), 2.63 - 2.79 (m, 1H, CH), 2.49 - 2.63 (m, 3H, CH_2 + CH), 1.87 - 2.16 (m, 2H, CH_2), 1.51 - 1.75 (m, 1H, CH_2), 1.36 - 1.49 (m, 2H, CH_2), 1.22 (d, *J* = 4.5 Hz, 3H, CH_3). ^{13}C {^{1}H} NMR (101 MHz, $CDCl_3$) δ 175.2 (C=O), 175.2 (C=O), 67.7 (CH_2), 67.5 (CH_2), 58.6 (C-CH_3), 53.8 (CH_2), 53.5 (CH_2), 47.5 (CH), 47.3 (CH), 32.9 (CH_2), 32.8 (CH_2), 31.5 (CH_2), 31.0 (CH_2), 25.1 (CH_2), 24.5 (CH_2), 17.4 (CH_3), 17.2 (CH_3). ESI-MS (MeOH): *m/z* calc. for $[C_9H_{14}O_3Na]^+$ = 193.0841, found *m/z* = 193.0825. GC-MS retention time: 11.32 & 11.38 min (cis/trans isomers of epoxide, ratio 56:44).

4-Isopropenylcaprolactone (**16**)

Method 1

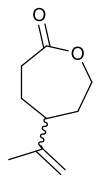

Methodology adapted from Yakabi *et al.*[15] A 50 mL round-bottomed flask fitted with a reflux condenser was charged with a solution of **11** (0.46 g, 3.3 mmol) in 1,4-dioxane (total volume = 10 mL, 0.33 M). The catalyst, Sn-β 2% (46 mg, 10 wt%) and H_2O_2 (30% aq., ~1 mL, 2 eq.) were added, and the mixture was heated to 100 °C in a silicone oil bath for 6 hours. Aliquots were taken at regular time intervals for GC-MS analysis. After 6 hours the reaction mixture was cooled to room temperature despite TLC analysis showing starting material, to avoid hydrolysis of the product, and filtered over Celite to remove the catalyst. Water (20 mL) and CH_2Cl_2 were added and the organic layer was separated, washed with a further 2 portions of H_2O (2 x 20 mL) and brine (1 x 20 mL), dried over $MgSO_4$ and concentrated in vacuo to yield a colourless oil which was shown by GC-MS to contain 57% product. This was purified by flash column chromatography on silica (20% EtOAc/pet ether, column dry loaded, product R_f = 0.21) to

yield the product as a colourless oil (0.24 g, 1.58 mmol, 48%). 0.080 g of starting material also recovered (R_f = 0.61).

^{1}H NMR (400 MHz, $CDCl_3$) δ 4.72 - 4.81 (m, 2H, C=CH), 4.18 - 4.37 (m, 2H, CH_2-O), 2.58 - 2.80 (m, 2H, CH_2-C(O)), 2.24 (tt, *J* = 12.0, 3.5 Hz, 1H), 1.90 - 2.09 (m, 2H, CH_2), 1.74 - 1.87 (m, 1H), 1.73 (s, 3H, CH_3), 1.61 (dtd, *J* = 14.0, 12.0, 2.0 Hz, 1H, CH). ^{13}C {^{1}H} NMR (101 MHz, $CDCl_3$) δ 176.2 (C=O), 148.0 (**C**=CH_2), 110.4 (C=**C**H_2), 68.2 (O-CH_2) 47.9 (CH), 34.2 (CH_2), 33.3 (CH_2), 27.7 (CH_2), 20.5 (CH_3). ESI-MS (MeOH): *m/z* calc. for $[C_9H_{14}O_2Na]^+$ = 177.0886, found *m/z* = 177.0874. GC-MS retention time: 9.56 min.

Method 2

To a vigorously stirring suspension of mCPBA (0.81 g, 3.6 mmol, 1.8 eq.) in toluene (7 mL) was added DMAP (0.13 g, 1.0 mmol, 50 mol%) and **11** (2 mmol). The resulting mixture was stirred at room temperature for the specified period of time (monitored by NMR), after which the standard work-up procedure was then applied to remove mCPBA/mCBA. The crude product was purified by flash column chromatography, (20% EtOAc/pet ether, product R_f = 0.21), to afford the desired lactone as a colourless oil (0.19 g 1.24 mmol, 62%).

Poly(**16**)

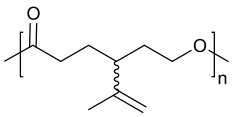

Thick, yellow gel.

FTIR ν (cm^{-1}): 1729 (C=O), 1159 (C=C). ^{1}H NMR (400 MHz, $CDCl_3$) δ 4.79 (s, br, 1H, C=CH_2), 4.65 (s, br, 1H, C=CH_2), 3.93 (m, 2H, CH_2), 2.13 (m, 3H, CH_2 + CH), 1.63 (m, 4H, CH_2), 1.56 (s, CH_3). ^{13}C{^{1}H} NMR (101 MHz, $CDCl_3$) δ 178.2 (C=O), 149.2 (**C**=CH_2), 107.5 (C=**C**H_2), 65.2 (O-CH_2), 45.2 (CH), 32.2 (CH_2), 27.3 (CH_2), 24.4 (CH_2), 18.3 (CH_3).

3-isopropenylcyclohexanone **18**[16]

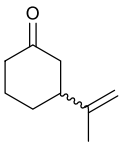

To a suspension of copper iodide (1.18 g, 6.24 mmol) in THF (40 mL) was added a 0.5 M solution of isopropenyl magnesium bromide in THF (183 ml, 41.6 mmol) at 0 °C. After stirring for 10 min, a solution of 2-cyclohexene-1-one (2.0 ml, 20.8 mmol) in THF (8 mL) was added slowly over 30 minutes. After stirring at 0 °C for 3 hours a solution of 10 % 4 N NaOH in saturated ammonium chloride was added (400 mL). The organic layer was separated and washed with 2 x 200 mL H_2O, 100 mL brine and dried over $MgSO_4$. The solvent was evaporated *in vacuo* to yield a light brown oil that was purified by column chromatography (10 % EtOAc/pet ether, dry loaded column, R_f = 0.63)

to provide (±)-**17** (2.25 g, 18.3 mmol, 76 %) as a slightly yellow, volatile oil. Spectral data were in agreement with previously reported values.

^{1}H NMR ($CDCl_3$, 400 MHz) δ 4.75 (2H, dt, *J* = 7.0 Hz, C=CH_2), 2.34 (5H, m, 2 x C(O)CH_2 + CH), 2.07 (1H, m, CH_2), 1.93 (1H, m, CH_2), 1.74 (2H, s, CH_2), 1.63 (3H, s, CH_3). ESI-MS (MeOH): *m/z* calc. for $[C_9H_{15}O]^+$ = 139.1117, found *m/z* = 139.1117.

21[17]

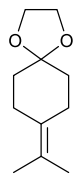

Slightly modified from literature method. [17] Isopropyltriphenylphosphonium iodide (13.8 g, 32.0 mmol) was added to NaH (60% in mineral oil, 0.93 g, 38.5 mmol) in dry DMSO (40 mL) at RT. The reaction mixture was warmed to 50°C with stirring until the appearance of a blood red colour; then, a solution of commercial 1,4-cyclohexanedione mono-ethylene ketal (5,08 g, 32.1 mmol) in dry DMSO (40 mL) was added. After stirring for 16 h at 50°C the reaction mixture was cooled to RT and water (20 mL) was added dropwise. After ether extraction, the triphenylphosphine oxide was removed by filtration after precipitation from hexane and filtration over Celite. Silica was added (10 g) and the suspension was stirred for 1 hr before filtering. The solvent was removed *in vacuo* to yield **21** as a colourless oil (5.14 g, 28.2 mmol, 88 %).

^{1}H NMR ($CDCl_3$, 400 MHz) δ 3.94 (4H, s, O-CH_2-CH_2-O), 2.28 (4H, t, *J* = 6.5 Hz, CH_2), 1.66 (6H, s, CH_3), 1.62 (4H, t, *J* = 6.5 Hz, CH_2). $^{13}C\{^1H\}$ NMR (101 MHz, $CDCl_3$) δ 129.3 (C=C), 121.8 (C=C), 109.0 (O-C-O), 64.2 (O-CH_2-CH_2-O), 35.7 (CH_2), 26.7 (CH_2), 20.0 (CH_3). GC-MS retention time = 8.39 min.

12[17]

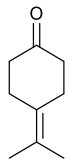

H_2SO_4 (15% aq., 1.8 mL) was added to a mixture of silica gel (10.6 g) and CH_2Cl_2, (32 mL) and stirred at room temperature. After 2 minutes, **21** (5.0 g, 27.5 mmol) was added, and the resulting mixture was stirred vigorously for a further 2 hours. After filtration to remove the silica gel, the organic layer was washed with water (25 mL), sat. bicarbonate (25 mL) and brine (25 mL) before drying over $MgSO_4$ and removal of solvent in vacuo to yield **12** as a light yellow oil (2.42 g, 17.6 mmol, 64%).

^{1}H NMR (400 MHz, $CDCl_3$) δ 2.51 (br t, *J* = 7.0 Hz, 4H, CH_2), 2.37 (t, *J* = 7.0 Hz, 4H, CH_2), 1.70 (s, 6H, CH_3). $^{13}C\{^1H\}$ NMR (101 MHz, $CDCl_3$) δ ppm 213.1 (C=O), 126.5 (C=C), 125.1 (C=C), 40.6 (CH_2), 27.2 (CH_2), 20.5 (CH_3). GC-MS retention time = 7.09 min.

13[14]

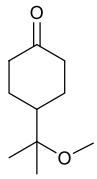

(+)-Nopinone, **1**, (5.0 g, 36.0 mmol) was mixed with MeOH (80 mL) and cooled to 0 °C. Conc. H_2SO_4 was added (20 mL), and the mixture turned instantly very dark brown. The mixture was warmed to room temperature and stirred for 5 hours, after which TLC analysis showed full consumption of **1**. The mixture was poured into a mixture of water (100 mL) and ice (10 g), saturated with NaCl and extracted with $CHCl_3$ (4 x 100 mL). The combined organic layers were washed with brine and dried over $MgSO_4$ and concentrated *in vacuo* to a dark orange oil. This was purified by flash chromatography on silica (10% EtOAc/pet ether, R_f = 0.13) to yield **13** as an orange oil (3.84 g, 22.6 mmol, 63%).

^{1}H NMR (400 MHz, $CDCl_3$) δ 4.35 (ddd, *J* = 13.0, 6.0, 2.0 Hz, 1H, CH_2-O), 4.15 (dd, *J* = 13.0, 10.5 Hz, 1H, CH_2-O), 3.18 (s, 3H, O-CH_3), 2.73 (ddd, *J* = 14.0, 7.5, 1.5 Hz, 1 H, $CH_2C(O)$), 2.57 (ddd, *J* = 14.0, 12.5, 2.0 Hz, 1H, $CH_2C(O)$), 1.98 - 2.18 (m, 2H), 1.65 - 1.79 (m, 1H), 1.47 - 1.62 (m,1H), 1.29 - 1.45 (m, 1H), 1.11 (d, *J* = 7.0 Hz, 6H, CH_3). ESI-MS (MeOH): *m/z* calc. for $[C_{10}H_{17}O_2]^+$ = 155.1067, found *m/z* = 155.1070. GCMS Retention time = 8.12 min.

4-Methoxycaprolactone, **23**

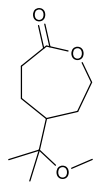

To a stirred solution of **13** (3.84 g, 20 mmol) in CH_2Cl_2 (100 mL) under Ar at 0 °C was added mCPBA in portions (5.85 g, 0.03 mol, 1.5 mol eq.). On warming to RT, a white precipitate formed, and the suspension was stirred for 24 h. The precipitate was removed by vacuum filtration and the solution was washed with Na_2SO_3 (10% aq., 200 mL), and saturated solutions of sodium bicarbonate (200 mL) and brine (200 mL). The organic fraction was dried over $MgSO_4$ and concentrated to a yellow oil (10.32 g). This was purified *via* column chromatography on silica (hexane/EtOAc 4:1) to yield **23** as a pale yellow oil (3.10 g, 16.5 mmol, 2 mmol, 83%).

^{1}H NMR (400 MHz, $CDCl_3$) δ 4.35 (ddd, *J* = 13.0, 6.0, 2.0 Hz, 1 H, CH_2-O), 4.15 (dd, *J* = 13.0, 10.5 Hz, 1H, CH_2-O), 3.18 (s, 3 H, O-CH_3), 2.73 (ddd, *J* = 14.0, 7.5, 1.5 Hz, 1H, $CH_2C(O)$), 2.57 (ddd, *J* = 14.0, 12.5, 2.0 Hz, 1 H, $CH_2C(O)$), 1.98 - 2.18 (m, 2H), 1.65 - 1.79 (m, 1H), 1.47 - 1.62 (m, 1H), 1.29 - 1.45 (m, 1H), 1.11 (d, *J* = 7.0 Hz, 6H, CH_3).^{13}C{^{1}H} NMR (101 MHz, $CDCl_3$) δ 175.9 (C=O)), 76.2 (**C**OCH_3)), 68.5 (O-CH_2), 49.3 (CH), 48.7 (OCH_3), 33.4 (CH_2), 30.2 (CH_2), 23.6 (CH_2), 22.0 (CH_3), 21.8 (CH_3). ESI-MS (MeOH): *m/z* calc. for $[C_{10}H_{18}O_3Na]^+$ = 209.1148, found *m/z* = 209.1157. GCMS Retention time = 12.46 min.

24

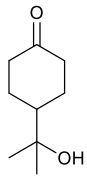

(+)-Nopinone, **1**, (5.0 g, 36 mmol) was mixed with H_2O (50 mL) and cooled to 0 °C. Conc. H_2SO_4 was added (20 mL), and the slowly turned dark yellow. The mixture was warmed to room temperature and stirred for 3 hours, then poured into a mixture of water (100 mL) and ice (10 g), saturated with NaCl and extracted with $CHCl_3$ (4 x 100 mL). The combined organic layers were washed with brine and dried over $MgSO_4$ and concentrated *in vacuo* to a yellow oil, which solidified on standing to yield **24** as a waxy, pale yellow solid (4.26 g, 27 mmol, 75%).

^{1}H NMR (400 MHz, $CDCl_3$) δ 2.30 - 2.47 (m, 4H, CH_2), 2.13 - 2.22 (m, 2H, CH), 1.45 - 1.60 (m, 4H, CH_2), 1.24 (s, 6H, CH_3) $^{13}C\{^1H\}$ NMR (101 MHz, $CDCl_3$) δ ppm 211.9 (C=O), 72.4 (C), 47.4 (CH), 40.9 (CH_2), 27.4 (CH_2), 27.3 (CH_3). ESI-MS (MeOH): *m/z* calc. for $[C_9H_{17}O_2]^+$ = 157.223, found *m/z* = 157.0177.

6.6 References

1 Y. He, C. Cheng, B. Chen, K. Duan, Y. Zhuang, B. Yuan, M. Zhang, Y. Zhou, Z. Zhou, Y.-J. Su, R. Cao and L. Qiu, *Org. Lett.*, 2014, **16**, 6366–6369.

2 P. D. Knight, P. N. O'Shaughnessy, I. J. Munslow, B. S. Kimberley and P. Scott, *J. Organomet. Chem.*, 2003, **683**, 103–113.

3 A. Sokolowski, J. Müller, T. Weyhermüller, R. Schnepf, P. Hildebrandt, K. Hildenbrand, E. Bothe and K. Wieghardt, *J. Am. Chem. Soc.*, 1997, **119**, 8889–8900.

4 A. J. Chmura, M. G. Davidson, C. J. Frankis, M. D. Jones and M. D. Lunn, *Chem. Commun.*, 2008, **0**, 1293–1295.

5 M. D. Jones, S. L. Hancock, P. McKeown, P. M. Schäfer, A. Buchard, L. H. Thomas, M. F. Mahon and J. P. Lowe, *Chem. Commun.*, 2014, **50**, 15967–15970.

6 R. Evans, Z. Deng, A. K. Rogerson, A. S. McLachlan, J. J. Richards, M. Nilsson and G. A. Morris, *Angew. Chem. Int. Ed.*, 2013, **52**, 3199–3202.

7 T. M. Ovitt, G. W. Coates, T. M. O. and and G. W. Coates, *J. Am. Chem. Soc.*, 2002, **124**, 1316–1326.

8 W. Clegg, M. G. Davidson, D. V. Graham, G. Griffen, M. D. Jones, A. R. Kennedy, C. T. O'Hara, L. Russo and C. M. Thomson, *Dalt. Trans.*, 2008, **10**, 1295.

9 S. L. Hancock, M. F. Mahon, G. Kociok-Kőhn and M. D. Jones, *Eur. J. Inorg. Chem.*, 2011, **2011**, 4596–4602.

10 F. Vögtle and E. Goldschmitt, *Chem. Ber.*, 1976, **109**, 1–40.

11 Q. Zhu, H. Huang, D. Shi, Z. Shen and C. Xia, *Org. Lett.*, 2009, **11**, 4536–4539.

12 G. J. Clarkson, V. C. Gibson, P. K. Y. Goh, M. L. Hammond, P. D. Knight, P. Scott, T. M. Smit, A. J. P. White and D. J. Williams, *Dalton Trans.*, 2006, **7**, 5484–5491.

13 K. Mori, *Tetrahedron: Asymmetry*, 2006, **17**, 2133–2142.

14 Bozzato, G. and Pesaro, M., *US Pat.US3816537A,*.

15 K. Yakabi, K. Milne, A. Buchard and C. Hammond, *ChemCatChem*, 2016, **8**, 3490–3498.

16 E. J. Horn, J. S. Silverston and C. D. Vanderwal, *J. Org. Chem.*, 2016, **81**, 1819–1838.

17 G. Revial, I. Jabin and M. Pfau, *Tetrahedron: Asymmetry*, 2000, **11**, 4975–4983.

7 Appendix

7.1 X-ray diffraction data

7.1.1 Chapter 2 complexes and molecules

$Zr(\mathbf{1})_2$

Empirical formula	$C_{45}H_{62}Cl_2N_4O_4Zr$	
Formula weight	885.11	
Temperature	150(2) K	
Wavelength	1.54184 Å	
Crystal system	Monoclinic	
Space group	$P2_1/n$	
Unit cell dimensions	a = 12.99240(10) Å	α= 90°.
	b = 18.13990(10) Å	β= 95.3950(10)°.
	c = 18.96860(10) Å	γ = 90°.
Volume	4450.73(5) $Å^3$	
Z	4	
Density (calculated)	1.321 Mg/m^3	
Absorption coefficient	3.485 mm^{-1}	
F(000)	1864	
Crystal size	0.30 x 0.20 x 0.20 mm^3	
Theta range for data collection	4.32 to 71.92°.	
Index ranges	-15≤h≤16, -22≤k≤22, -21≤l≤23	
Reflections collected	65098	
Independent reflections	8724 [R(int) = 0.0532]	
Completeness to theta = 71.92°	99.9 %	
Max. and min. transmission	0.5424 and 0.4212	
Refinement method	Full-matrix least-squares on F^2	
Data / restraints / parameters	8724 / 0 / 517	
Goodness-of-fit on F^2	1.057	
Final R indices [I>2σ(I)]	R1 = 0.0501, wR2 = 0.1370	
R indices (all data)	R1 = 0.0513, wR2 = 0.1384	
Largest diff. peak and hole	1.145 and -1.485 e.$Å^{-3}$	

{(Zr(**2**)O^{i}Pr)$_2$-O}

Empirical formula	$C_{55}H_{80}Cl_6N_4O_7Zr_2$	
Formula weight	1304.37	
Temperature	150(2) K	
Wavelength	0.71073 Å	
Crystal system	Monoclinic	
Space group	*C*2/*c*	
Unit cell dimensions	a = 21.8517(6) Å	α = 90°.
	b = 15.3090(4) Å	β = 96.038(5)°.
	c = 18.1317(14) Å	γ = 90°.
Volume	6031.9(5) Å^3	
Z	4	
Density (calculated)	1.436 Mg/m^3	
Absorption coefficient	0.663 mm^{-1}	
F(000)	2704	
Crystal size	0.20 x 0.10 x 0.10 mm^3	
Theta range for data collection	3.38 to 25.03°.	
Index ranges	-25≤h≤26, -17≤k≤18, -20≤l≤21	
Reflections collected	27276	
Independent reflections	5310 [R(int) = 0.0376]	
Completeness to theta = 25.03°	99.7 %	
Max. and min. transmission	0.9367 and 0.8788	
Refinement method	Full-matrix least-squares on F^2	
Data / restraints / parameters	5310 / 0 / 346	
Goodness-of-fit on F^2	1.054	
Final R indices [I>2σ(I)]	R1 = 0.0398, wR2 = 0.1042	
R indices (all data)	R1 = 0.0518, wR2 = 0.1107	
Largest diff. peak and hole	1.084 and -0.959 e.Å^{-3}	

$Li_4(\mathbf{1})_2(THF)_2$

Empirical formula	$C_{55}H_{83}Li_4N_4O_6$	
Formula weight	924.01	
Temperature	150(2) K	
Wavelength	1.54184 Å	
Crystal system	Triclinic	
Space group	*P* -1	
Unit cell dimensions	a = 11.1628(3) Å	α = 100.479(2)°.
	b = 11.4527(4) Å	β = 98.220(2)°.
	c = 22.0321(6) Å	γ = 91.455(2)°.
Volume	2737.42(14) $Å^3$	
Z	2	
Density (calculated)	1.121 Mg/m^3	
Absorption coefficient	0.551 mm^{-1}	
F(000)	1002	
Crystal size	0.100 x 0.050 x 0.050 mm^3	
Theta range for data collection	3.931 to 70.060°.	
Index ranges	-13≤h≤12, -12≤k≤13, -26≤l≤21	
Reflections collected	21174	
Independent reflections	10316 [R(int) = 0.0285]	
Completeness to theta = 67.684°	99.7 %	
Absorption correction	Semi-empirical from equivalents	
Max. and min. transmission	1.00000 and 0.90764	
Refinement method	Full-matrix least-squares on F^2	
Data / restraints / parameters	10316 / 0 / 608	
Goodness-of-fit on F^2	1.036	
Final R indices [I>2σ(I)]	R1 = 0.0656, wR2 = 0.1763	
R indices (all data)	R1 = 0.0783, wR2 = 0.1861	
Extinction coefficient	n/a	
Largest diff. peak and hole	0.912 and -0.336 e.$Å^{-3}$	

Li_4(**3**)$_2$(THF)

Empirical formula	$C_{65}H_{97}Li_4N_4O_5$	
Formula weight	1042.23	
Temperature	150(2) K	
Wavelength	0.71073 Å	
Crystal system	Triclinic	
Space group	*P*-1	
Unit cell dimensions	a = 14.6562(6) Å	α = 71.311(5)°.
	b = 14.8626(8) Å	β = 83.665(4)°.
	c = 15.7941(8) Å	γ = 67.674(4)°.
Volume	3014.5(3) Å^3	
Z	2	
Density (calculated)	1.148 Mg/m^3	
Absorption coefficient	0.070 mm^{-1}	
F(000)	1134	
Crystal size	0.30 x 0.20 x 0.20 mm^3	
Theta range for data collection	3.32 to 25.02°.	
Index ranges	-17≤h≤15, -17≤k≤17, -17≤l≤18	
Reflections collected	23426	
Independent reflections	10630 [R(int) = 0.0348]	
Completeness to theta = 25.02°	99.7 %	
Max. and min. transmission	0.9861 and 0.9792	
Refinement method	Full-matrix least-squares on F^2	
Data / restraints / parameters	10630 / 24 / 714	
Goodness-of-fit on F^2	1.059	
Final R indices [I>2σ(I)]	R1 = 0.0674, wR2 = 0.1708	
R indices (all data)	R1 = 0.1001, wR2 = 0.1919	
Largest diff. peak and hole	0.437 and -0.405 e.Å^{-3}	

Li_2(**7**)$_2$(THF)$_4$

Empirical formula	$C_{68}H_{104}Li_4N_4O_9$	
Formula weight	1149.31	
Temperature	150.01(10) K	
Wavelength	1.54184 Å	
Crystal system	Monoclinic	
Space group	*I*2/a	
Unit cell dimensions	a = 18.8690(5) Å	α = 90°.
	b = 18.1831(3) Å	β = 110.294(3)°.
	c = 21.0874(5) Å	γ = 90°.
Volume	6785.9(3) Å^3	
Z	4	
Density (calculated)	1.125 Mg/m^3	
Absorption coefficient	0.568 mm^{-1}	
F(000)	2496	
Crystal size	0.100 x 0.080 x 0.060 mm^3	
Theta range for data collection	3.302 to 73.066°.	
Index ranges	-23≤h≤22, -22≤k≤20, -26≤l≤26	
Reflections collected	22248	
Independent reflections	6624 [R(int) = 0.0271]	
Completeness to theta = 67.684°	98.5 %	
Absorption correction	Semi-empirical from equivalents	
Max. and min. transmission	1.00000 and 0.91222	
Refinement method	Full-matrix least-squares on F^2	
Data / restraints / parameters	6624 / 4 / 477	
Goodness-of-fit on F^2	1.032	
Final R indices [I>2σ(I)]	R1 = 0.0504, wR2 = 0.1392	
R indices (all data)	R1 = 0.0607, wR2 = 0.1498	
Extinction coefficient	n/a	
Largest diff. peak and hole	0.342 and -0.292 e.Å^{-3}	

Li_3(**1**)Mg(^{n}Bu)$(THF)_2(OCH{=}CH_2)_2$

Empirical formula	$C_{37.50}H_{58}Li_3MgN_2O_6$	
Formula weight	677.99	
Temperature	150(2) K	
Wavelength	1.5418 Å	
Crystal system	Monoclinic	
Space group	*$P2_1/m$*	
Unit cell dimensions	a = 9.0453(3) Å	α = 90°.
	b = 17.2098(5) Å	β = 108.963(4)°.
	c = 13.7284(6) Å	γ = 90°.
Volume	2021.09(13) Å^3	
Z	2	
Density (calculated)	1.114 Mg/m^3	
Absorption coefficient	0.713 mm^{-1}	
F(000)	732	
Crystal size	0.200 x 0.200 x 0.100 mm^3	
Theta range for data collection	3.404 to 70.065°.	
Index ranges	-11≤h≤10, -20≤k≤15, -16≤l≤16	
Reflections collected	14768	
Independent reflections	3960 [R(int) = 0.0260]	
Completeness to theta = 67.684°	100%	
Absorption correction	0.713 mm^{-1}	
Refinement method	Full-matrix least-squares on F^2	
Data / restraints / parameters	3960 / 82 / 343	
Goodness-of-fit on F^2	1.074	
Final R indices [I>2σ(I)]	R1 = 0.0698, wR2 = 0.2313	
R indices (all data)	R1 = 0.0825, wR2 = 0.2281	
Extinction coefficient	n/a	
Largest diff. peak and hole	0.689 and -0.415 e.Å^{-3}	

Mg_2(**1**)$_2$

Empirical formula	$C_{102}H_{136}Mg_4N_8O_8$	
Formula weight	1699.43	
Temperature	150(2) K	
Wavelength	1.54184 Å	
Crystal system	Monoclinic	
Space group	$P2_1/c$	
Unit cell dimensions	a = 19.2211(2) Å	α = 90°.
	b = 23.7287(3) Å	β = 91.5300(10)°.
	c = 21.0682(3) Å	γ = 90°.
Volume	9605.6(2) Å^3	
Z	4	
Density (calculated)	1.175 Mg/m^3	
Absorption coefficient	0.813 mm^{-1}	
F(000)	3664	
Crystal size	0.05 x 0.05 x 0.05 mm^3	
Theta range for data collection	4.20 to 66.60°.	
Index ranges	-13≤h≤22, -28≤k≤28, -25≤l≤24	
Reflections collected	40455	
Independent reflections	16922 [R(int) = 0.0476]	
Completeness to theta = 66.60°	99.7 %	
Max. and min. transmission	0.9605 and 0.9605	
Refinement method	Full-matrix least-squares on F^2	
Data / restraints / parameters	16922 / 0 / 1124	
Goodness-of-fit on F^2	0.998	
Final R indices [I>2σ(I)]	R1 = 0.0452, wR2 = 0.1030	
R indices (all data)	R1 = 0.0779, wR2 = 0.1162	
Largest diff. peak and hole	0.403 and -0.243 e.Å^{-3}	

Mg_2(**2**)$_2$

Empirical formula	$C_{58.20}H_{73.80}Mg_2N_4O_4$	
Formula weight	942.03	
Temperature	150(2) K	
Wavelength	1.54184 Å	
Crystal system	Tetragonal	
Space group	*R*-3	
Unit cell dimensions	a = 32.4900(4) Å	α = 90°
	b = 32.4900(4) Å	β = 90°
	c = 13.3612(2) Å	γ = 120°
Volume	12214.5(3) Å^3	
Z	9	
Density (calculated)	1.153 Mg/m^3	
Absorption coefficient	0.767 mm^{-1}	
F(000)	4563	
Crystal size	0.20 x 0.20 x 0.10 mm^3	
Theta range for data collection	3.66 to 72.03°.	
Index ranges	-39≤h≤39, -39≤k≤39, -16≤l≤12	
Reflections collected	41517	
Independent reflections	5306 [R(int) = 0.0296]	
Completeness to theta = 72.03°	99.5 %	
Max. and min. transmission	0.9272 and 0.8617	
Refinement method	Full-matrix least-squares on F^2	
Data / restraints / parameters	5306 / 127 / 419	
Goodness-of-fit on F^2	1.088	
Final R indices [I>2σ(I)]	R1 = 0.0677, wR2 = 0.1860	
R indices (all data)	R1 = 0.0719, wR2 = 0.1897	
Largest diff. peak and hole	0.789 and -0.299 e.Å^{-3}	

Mg_2(**4**)$_2$

Empirical formula	$C_{58}H_{82}Mg_2N_4O_4$	
Formula weight	947.90	
Temperature	150(2) K	
Wavelength	0.71073 Å	
Crystal system	Orthorhombic	
Space group	$P2_12_12_1$	
Unit cell dimensions	a = 10.2791(5) Å	α = 90°.
	b = 12.5213(5) Å	β = 90°.
	c = 41.718(3) Å	γ = 90°.
Volume	5369.5(5) $Å^3$	
Z	4	
Density (calculated)	1.173 Mg/m^3	
Absorption coefficient	0.094 mm^{-1}	
F(000)	2056	
Crystal size	0.20 x 0.15 x 0.02 mm^3	
Theta range for data collection	3.35 to 26.37°.	
Index ranges	-8≤h≤12, -15≤k≤15, -46≤l≤52	
Reflections collected	20750	
Independent reflections	10480 [R(int) = 0.0655]	
Completeness to theta = 26.37°	99.7 %	
Max. and min. transmission	0.9981 and 0.9815	
Refinement method	Full-matrix least-squares on F^2	
Data / restraints / parameters	10480 / 0 / 623	
Goodness-of-fit on F^2	1.017	
Final R indices [I>2σ(I)]	R1 = 0.0727, wR2 = 0.1136	
R indices (all data)	R1 = 0.1370, wR2 = 0.1345	
Absolute structure parameter	0.0(3)	
Largest diff. peak and hole	0.454 and -0.288 e.$Å^{-3}$	

Mg_2(**5**)$_2$

Empirical formula	$C_{58}H_{82}Mg_2N_4O_4$	
Formula weight	947.90	
Temperature	150(2) K	
Wavelength	1.54184 Å	
Crystal system	Orthorhombic	
Space group	$P2_12_12_1$	
Unit cell dimensions	a = 10.26780(10) Å	α = 90°.
	b = 41.6560(6) Å	β = 90°.
	c = 12.50510(10) Å	γ = 90°.
Volume	5348.63(10) Å^3	
Z	4	
Density (calculated)	1.177 Mg/m^3	
Absorption coefficient	0.777 mm^{-1}	
F(000)	2056	
Crystal size	0.20 x 0.20 x 0.05 mm^3	
Theta range for data collection	4.12 to 71.99°.	
Index ranges	-12≤h≤11, -51≤k≤51, -14≤l≤15	
Reflections collected	80246	
Independent reflections	10489 [R(int) = 0.0753]	
Completeness to theta = 71.99°	99.9 %	
Max. and min. transmission	0.9622 and 0.8600	
Refinement method	Full-matrix least-squares on F^2	
Data / restraints / parameters	10489 / 0 / 623	
Goodness-of-fit on F^2	1.082	
Final R indices [I>2σ(I)]	R1 = 0.0577, wR2 = 0.1393	
R indices (all data)	R1 = 0.0608, wR2 = 0.1408	
Absolute structure parameter	0.05(5)	
Largest diff. peak and hole	0.680 and -0.251 e.Å^{-3}	

Mg_2(**6**)$_2$

Empirical formula	$C_{89}H_{132}Mg_2N_4O_4$	
Formula weight	1370.60	
Temperature	150.00(10) K	
Wavelength	0.71073 Å	
Crystal system	Monoclinic	
Space group	$P2_1$	
Unit cell dimensions	a = 14.6277(4) Å	α = 90°.
	b = 19.1736(4) Å	β = 93.345(2)°.
	c = 14.8820(3) Å	γ = 90°.
Volume	4166.78(17) Å^3	
Z	2	
Density (calculated)	1.092 Mg/m^3	
Absorption coefficient	0.079 mm^{-1}	
F(000)	1500	
Crystal size	0.350 x 0.250 x 0.250 mm^3	
Theta range for data collection	3.470 to 29.558°.	
Index ranges	-12≤h≤19, -26≤k≤26, -20≤l≤20	
Reflections collected	37362	
Independent reflections	19066 [R(int) = 0.0255]	
Completeness to theta = 25.242°	99.7 %	
Absorption correction	Semi-empirical from equivalents	
Max. and min. transmission	1.00000 and 0.95107	
Refinement method	Full-matrix least-squares on F^2	
Data / restraints / parameters	19066 / 49 / 1072	
Goodness-of-fit on F^2	1.010	
Final R indices [I>2σ(I)]	R1 = 0.0456, wR2 = 0.0915	
R indices (all data)	R1 = 0.0639, wR2 = 0.0991	
Absolute structure parameter	0.04(7)	
Extinction coefficient	n/a	
Largest diff. peak and hole	0.252 and -0.221 e.Å^{-3}	

$Zn_3(\mathbf{1})_2(Me)_2$

Empirical formula	$C_{247}H_{336}N_{16}O_{16}Zn_{12}$	
Formula weight	4569.74	
Temperature	150(2) K	
Wavelength	0.71073 Å	
Crystal system	Monoclinic	
Space group	*I*2/*a*	
Unit cell dimensions	a = 22.2121(5) Å	α = 90°.
	b = 11.7241(4) Å	β = 97.823(2)°.
	c = 47.0060(11) Å	γ = 90°.
Volume	12127.2(6) $Å^3$	
Z	2	
Density (calculated)	1.251 Mg/m^3	
Absorption coefficient	1.224 mm^{-1}	
F(000)	4836	
Crystal size	0.500 x 0.300 x 0.200 mm^3	
Theta range for data collection	3.381 to 30.392°.	
Index ranges	-26≤h≤31, -15≤k≤16, -61≤l≤64	
Reflections collected	59644	
Independent reflections	16117 [R(int) = 0.0292]	
Completeness to theta = 25.242°	99.7 %	
Absorption correction	Semi-empirical from equivalents	
Max. and min. transmission	1.00000 and 0.90758	
Refinement method	Full-matrix least-squares on F^2	
Data / restraints / parameters	16117 / 87 / 749	
Goodness-of-fit on F^2	1.041	
Final R indices [I>2σ(I)]	R1 = 0.0362, wR2 = 0.0825	
R indices (all data)	R1 = 0.0566, wR2 = 0.0928	
Extinction coefficient	n/a	
Largest diff. peak and hole	0.599 and -0.424 e.$Å^{-3}$	

$Zn_4(\mathbf{2})_2(Me)_2(OMe)$

Empirical formula	$C_{63}H_{88}N_4O_6Zn_4$	
Formula weight	1258.85	
Temperature	150(2) K	
Wavelength	1.54184 Å	
Crystal system	Monoclinic	
Space group	$P2_1/n$	
Unit cell dimensions	a = 18.0242(3) Å	α = 90°.
	b = 16.8036(3) Å	β = 114.160(2)°.
	c = 21.2570(3) Å	γ = 90°.
Volume	5874.19(17) $Å^3$	
Z	4	
Density (calculated)	1.423 Mg/m^3	
Absorption coefficient	2.274 mm^{-1}	
F(000)	2648	
Crystal size	0.10 x 0.10 x 0.10 mm^3	
Theta range for data collection	4.18 to 72.07°.hqh	
Index ranges	-21≤h≤22, -20≤k≤19, -25≤l≤26	
Reflections collected	49098	
Independent reflections	11516 [R(int) = 0.0303]	
Completeness to theta = 72.07°	99.5 %	
Max. and min. transmission	0.8045 and 0.8045	
Refinement method	Full-matrix least-squares on F^2	
Data / restraints / parameters	11516 / 0 / 707	
Goodness-of-fit on F^2	1.034	
Final R indices [I>2σ(I)]	R1 = 0.0305, wR2 = 0.0788	
R indices (all data)	R1 = 0.0363, wR2 = 0.0823	
Largest diff. peak and hole	0.432 and -0.574 e.$Å^{-3}$	

10

Empirical formula	$C_{40}H_2D_{50}N_2O_{10}S_4$	
Formula weight	899.38	
Temperature	150(2) K	
Wavelength	0.71073 Å	
Crystal system	Triclinic	
Space group	*P*-1	
Unit cell dimensions	a = 9.7549(6) Å	α = 113.588(5)°.
	b = 10.9269(5) Å	β = 101.373(5)°.
	c = 11.7236(8) Å	γ = 101.699(5)°.
Volume	1066.12(11) $Å^3$	
Z	1	
Density (calculated)	1.401 Mg/m^3	
Absorption coefficient	0.280 mm^{-1}	
F(000)	450	
Crystal size	0.30 x 0.20 x 0.10 mm^3	
Theta range for data collection	3.42 to 27.48°.	
Index ranges	-9≤h≤12, -14≤k≤10, -15≤l≤14	
Reflections collected	8881	
Independent reflections	4837 [R(int) = 0.0156]	
Completeness to theta = 27.48°	99.0 %	
Max. and min. transmission	0.9725 and 0.9207	
Refinement method	Full-matrix least-squares on F^2	
Data / restraints / parameters	4837 / 0 / 306	
Goodness-of-fit on F^2	1.042	
Final R indices [I>2σ(I)]	R1 = 0.0337, wR2 = 0.0843	
R indices (all data)	R1 = 0.0410, wR2 = 0.0894	
Largest diff. peak and hole	0.393 and -0.305 e.$Å^{-3}$	

16

Empirical formula	$C_{30}H_{44}O_2$	
Formula weight	436.65	
Temperature	150(2) K	
Wavelength	1.54184 Å	
Crystal system	Orthorhombic	
Space group	*P*bca	
Unit cell dimensions	a = 10.9805(3) Å	α = 90°.
	b = 9.9191(3) Å	β = 90°.
	c = 48.9685(14) Å	γ = 90°.
Volume	5333.5(3) $Å^3$	
Z	8	
Density (calculated)	1.088 Mg/m^3	
Absorption coefficient	0.500 mm^{-1}	
F(000)	1920	
Crystal size	0.40 x 0.30 x 0.20 mm^3	
Theta range for data collection	3.61 to 74.96°.	
Index ranges	-13≤h≤13, -12≤k≤12, -60≤l≤60	
Reflections collected	73511	
Independent reflections	5391 [R(int) = 0.0598]	
Completeness to theta = 74.96°	98.1 %	
Max. and min. transmission	0.9066 and 0.8250	
Refinement method	Full-matrix least-squares on F^2	
Data / restraints / parameters	5391 / 6 / 326	
Goodness-of-fit on F^2	1.106	
Final R indices [I>2σ(I)]	R1 = 0.1110, wR2 = 0.2651	
R indices (all data)	R1 = 0.1121, wR2 = 0.2658	
Largest diff. peak and hole	1.011 and -0.751 e.$Å^{-3}$	

7.1.2 Chapter 3 ligands and complexes

3H_2

Empirical formula	$C_{22}H_{28}NO$	
Formula weight	322.45	
Temperature	150(2) K	
Wavelength	1.54184 Å	
Crystal system	Monoclinic	
Space group	$P2_1/c$	
Unit cell dimensions	a = 17.2730(10) Å	□= 90°.
	b = 11.1428(6) Å	□= 104.391(7)°.
	c = 10.4484(7) Å	□ = 90°.
Volume	1947.9(2) $Å^3$	
Z	4	
Density (calculated)	1.100 Mg/m^3	
Absorption coefficient	0.508 mm^{-1}	
F(000)	700	
Crystal size	0.30 x 0.30 x 0.05 mm^3	
Theta range for data collection	4.77 to 70.07°.	
Index ranges	-21≤h≤21, -13≤k≤12, -12≤l≤12	
Reflections collected	27782	
Independent reflections	3703 [R(int) = 0.0773]	
Completeness to theta = 70.07°	100.0 %	
Max. and min. transmission	0.9751 and 0.8626	
Refinement method	Full-matrix least-squares on F^2	
Data / restraints / parameters	3703 / 0 / 224	
Goodness-of-fit on F^2	1.042	
Final R indices [I>2σ(I)]	R1 = 0.0659, wR2 = 0.1757	
R indices (all data)	R1 = 0.0816, wR2 = 0.1893	
Largest diff. peak and hole	0.301 and -0.184 e.$Å^{-3}$	

Al(**2**)Me

Empirical formula	$C_{36.50}H_{37}AlN_2O_2$	
Formula weight	562.66	
Temperature	150(2) K	
Wavelength	0.71073 Å	
Crystal system	Monoclinic	
Space group	$P2_1/n$	
Unit cell dimensions	a = 12.1270(2) Å	α = 90°.
	b = 16.2347(4) Å	β = 96.493(2)°.
	c = 15.8489(3) Å	γ = 90°.
Volume	3100.29(11) $Å^3$	
Z	4	
Density (calculated)	1.205 Mg/m^3	
Absorption coefficient	0.100 mm^{-1}	
F(000)	1196	
Crystal size	0.20 x 0.20 x 0.15 mm^3	
Theta range for data collection	3.37 to 25.68°.	
Index ranges	-13≤h≤14, -19≤k≤19, -19≤l≤19	
Reflections collected	17997	
Independent reflections	5877 [R(int) = 0.0333]	
Completeness to theta = 25.68°	99.7 %	
Max. and min. transmission	0.9851 and 0.9803	
Refinement method	Full-matrix least-squares on F^2	
Data / restraints / parameters	5877 / 45 / 400	
Goodness-of-fit on F^2	1.016	
Final R indices [I>2σ(I)]	R1 = 0.0473, wR2 = 0.1183	
R indices (all data)	R1 = 0.0711, wR2 = 0.1323	
Largest diff. peak and hole	0.437 and -0.296 e.$Å^{-3}$	

Al(**2**)Me		
Empirical formula	$C_{45}H_{57}AlN_2O_2$	
Formula weight	684.90	
Temperature	150(2) K	
Wavelength	1.54184 Å	
Crystal system	Triclinic	
Space group	*P* -1	
Unit cell dimensions	a = 11.7072(8) Å	α = 74.665(4)°.
	b = 12.7980(6) Å	β = 77.586(5)°.
	c = 13.9427(6) Å	γ = 83.929(5)°.
Volume	1964.88(19) $Å^3$	
Z	2	
Density (calculated)	1.158 Mg/m^3	
Absorption coefficient	0.739 mm^{-1}	
F(000)	740	
Crystal size	0.200 x 0.150 x 0.100 mm^3	
Theta range for data collection	3.351 to 66.594°.	
Index ranges	-13≤h≤12, -15≤k≤15, -16≤l≤16	
Reflections collected	11979	
Independent reflections	11979 [R(int) = 0.0]	
Completeness to theta = 66.594°	100.0 %	
Refinement method	Full-matrix least-squares on F^2	
Data / restraints / parameters	11979 / 0 / 465	
Goodness-of-fit on F^2	0.986	
Final R indices [I>2σ(I)]	R1 = 0.0456, wR2 = 0.1327	
R indices (all data)	R1 = 0.0575, wR2 = 0.1390	
Extinction coefficient	n/a	
Largest diff. peak and hole	0.541 and -0.331 e.$Å^{-3}$	

4H_2		
Empirical formula	$C_{54}H_{66}N_2O_2$	
Formula weight	775.08	
Temperature	150(2) K	
Wavelength	0.71073 Å	
Crystal system	Triclinic	
Space group	*P*-1	
Unit cell dimensions	a = 10.9943(6) Å	α = 74.210(4)°.
	b = 14.0152(6) Å	β = 87.748(4)°.
	c = 15.5968(7) Å	γ = 78.386(4)°.
Volume	2264.93(19) $Å^3$	
Z	2	
Density (calculated)	1.137 Mg/m^3	
Absorption coefficient	0.068 mm^{-1}	
F(000)	840	
Crystal size	0.300 x 0.050 x 0.050 mm^3	
Theta range for data collection	3.465 to 29.333°.	
Index ranges	-14≤h≤14, -18≤k≤18, -20≤l≤21	
Reflections collected	20192	
Independent reflections	10409 [R(int) = 0.0291]	
Completeness to theta = 25.242°	99.7 %	
Refinement method	Full-matrix least-squares on F^2	
Data / restraints / parameters	10409 / 14 / 617	
Goodness-of-fit on F^2	1.010	
Final R indices [I>2σ(I)]	R1 = 0.0575, wR2 = 0.1140	
R indices (all data)	R1 = 0.1037, wR2 = 0.1343	
Extinction coefficient	n/a	
Largest diff. peak and hole	0.238 and -0.233 e.$Å^{-3}$	

Al_2(**4**)Me_2

Empirical formula	$C_{51}H_{68}Al_2N_2O_2$	
Formula weight	795.03	
Temperature	150(2) K	
Wavelength	1.54184 Å	
Crystal system	Triclinic	
Space group	*P*-1	
Unit cell dimensions	a = 12.6028(6) Å	α = 109.990(4)°.
	b = 12.7588(6) Å	β = 107.578(4)°.
	c = 16.5415(5) Å	γ = 90.572(4)°.
Volume	2363.75(17) $Å^3$	
Z	2	
Density (calculated)	1.117 Mg/m^3	
Absorption coefficient	0.848 mm^{-1}	
F(000)	860	
Crystal size	0.20 x 0.10 x 0.10 mm^3	
Theta range for data collection	3.71 to 67.11°.	
Index ranges	-15≤h≤15, -15≤k≤15, -19≤l≤19	
Reflections collected	16144	
Independent reflections	16144 [R(int) = 0.0000]	
Completeness to theta = 67.11°	99.2 %	
Max. and min. transmission	0.9200 and 0.8487	
Refinement method	Full-matrix least-squares on F^2	
Data / restraints / parameters	16144 / 0 / 532	
Goodness-of-fit on F^2	1.010	
Final R indices [I>2σ(I)]	R1 = 0.0543, wR2 = 0.1705	
R indices (all data)	R1 = 0.0723, wR2 = 0.1896	
Largest diff. peak and hole	0.469 and -0.347 e.$Å^{-3}$	

Zn_2(**4**)$_2$

Empirical formula	$C_{91}H_{111}N_4O_4Zn_2$	
Formula weight	1455.57	
Temperature	150(2) K	
Wavelength	0.71073 Å	
Crystal system	Triclinic	
Space group	*P* -1	
Unit cell dimensions	a = 16.074(5) Å	α = 83.21(3)°.
	b = 16.509(5) Å	β = 73.13(3)°.
	c = 17.840(6) Å	γ = 66.90(3)°.
Volume	4167(2) Å^3	
Z	2	
Density (calculated)	1.160 Mg/m^3	
Absorption coefficient	0.626 mm^{-1}	
F(000)	1554	
Crystal size	0.200 x 0.200 x 0.200 mm^3	
Theta range for data collection	3.217 to 29.519°.	
Index ranges	-21≤h≤21, -21≤k≤19, -22≤l≤24	
Reflections collected	35710	
Independent reflections	20394 [R(int) = 0.0270]	
Completeness to theta = 25.242°	99.8 %	
Absorption correction	Semi-empirical from equivalents	
Max. and min. transmission	1.00000 and 0.93803	
Refinement method	Full-matrix least-squares on F^2	
Data / restraints / parameters	20394 / 93 / 1075	
Goodness-of-fit on F^2	1.032	
Final R indices [I>2σ(I)]	R1 = 0.0506, wR2 = 0.1311	
R indices (all data)	R1 = 0.0744, wR2 = 0.1462	
Extinction coefficient	n/a	
Largest diff. peak and hole	1.285 and -0.687 e.Å^{-3}	

$Al_2(\mathbf{7})_2Me_2$

Empirical formula	$C_{62}H_{66}Al_2N_4O_4$	
Formula weight	985.14	
Temperature	150(2) K	
Wavelength	1.54184 Å	
Crystal system	Orthorhombic	
Space group	*F d d* 2	
Unit cell dimensions	a = 58.081(2) Å	α = 90°.
	b = 25.7596(8) Å	β = 90°.
	c = 14.2949(3) Å	γ = 90°.
Volume	21387.1(11) $Å^3$	
Z	16	
Density (calculated)	1.224 Mg/m^3	
Absorption coefficient	0.895 mm^{-1}	
F(000)	8384	
Crystal size	0.100 x 0.100 x 0.050 mm^3	
Theta range for data collection	3.043 to 73.302°.	
Index ranges	-66≤h≤72, -31≤k≤30, -17≤l≤13	
Reflections collected	57192	
Independent reflections	9255 [R(int) = 0.0694]	
Completeness to theta = 67.684°	100.0 %	
Absorption correction	Semi-empirical from equivalents	
Max. and min. transmission	1.00000 and 0.85060	
Refinement method	Full-matrix least-squares on F^2	
Data / restraints / parameters	9255 / 1 / 653	
Goodness-of-fit on F^2	1.031	
Final R indices [I>2σ(I)]	R1 = 0.0472, wR2 = 0.1144	
R indices (all data)	R1 = 0.0571, wR2 = 0.1206	
Absolute structure parameter	-0.03(2)	
Extinction coefficient	n/a	
Largest diff. peak and hole	0.307 and -0.310 e.$Å^{-3}$	

Li_4(**8**)$_2$(THF)$_3$

Empirical formula	$C_{68.80}H_{84.40}Li_4N_4O_6$	
Formula weight	1091.16	
Temperature	150.01(10) K	
Wavelength	1.54184 Å	
Crystal system	Triclinic	
Space group	*P*-1	
Unit cell dimensions	a = 14.4046(10) Å	α = 109.750(6)°.
	b = 20.0215(16) Å	β = 105.732(5)°.
	c = 24.2582(14) Å	γ = 96.674(6)°.
Volume	6168.8(8) Å^3	
Z	4	
Density (calculated)	1.175 Mg/m^3	
Absorption coefficient	0.569 mm^{-1}	
F(000)	2341	
Crystal size	0.250 x 0.020 x 0.020 mm^3	
Theta range for data collection	3.236 to 70.539°.	
Index ranges	-17≤h≤17, -24≤k≤24, -29≤l≤25	
Reflections collected	49708	
Independent reflections	23474 [R(int) = 0.0772]	
Completeness to theta = 67.684°	99.9 %	
Absorption correction	Semi-empirical from equivalents	
Max. and min. transmission	1.00000 and 0.87869	
Refinement method	Full-matrix least-squares on F^2	
Data / restraints / parameters	23474 / 198 / 1639	
Goodness-of-fit on F^2	0.990	
Final R indices [I>2σ(I)]	R1 = 0.0663, wR2 = 0.1249	
R indices (all data)	R1 = 0.1293, wR2 = 0.1533	
Extinction coefficient	n/a	
Largest diff. peak and hole	0.330 and -0.245 e.Å^{-3}	

7.1.3 Chapter 4 monomers

8

Empirical formula	$C_9H_{17}NO$	
Formula weight	155.23	
Temperature	150(2) K	
Wavelength	1.54184 Å	
Crystal system	Monoclinic	
Space group	$P2_1/c$	
Unit cell dimensions	a = 15.978(3) Å	α = 90°.
	b = 5.9817(11) Å	β = 98.627(15)°.
	c = 9.6332(14) Å	γ = 90°.
Volume	910.3(3) $Å^3$	
Z	4	
Density (calculated)	1.133 Mg/m^3	
Absorption coefficient	0.570 mm^{-1}	
F(000)	344	
Crystal size	0.200 x 0.200 x 0.020 mm^3	
Theta range for data collection	2.797 to 68.216°.	
Index ranges	-19≤h≤19, -7≤k≤6, -11≤l≤10	
Reflections collected	2998	
Independent reflections	1646 [R(int) = 0.0423]	
Completeness to theta = 67.684°	98.9 %	
Refinement method	Full-matrix least-squares on F^2	
Data / restraints / parameters	1646 / 0 / 106	
Goodness-of-fit on F^2	1.064	
Final R indices [I>2σ(I)]	R1 = 0.0735, wR2 = 0.1888	
R indices (all data)	R1 = 0.0941, wR2 = 0.2045	
Extinction coefficient	n/a	
Largest diff. peak and hole	0.310 and -0.205 $e.Å^{-3}$	

9

Empirical formula	$C_{36}H_{56}O_{12}$	
Formula weight	680.80	
Temperature	150(2) K	
Wavelength	1.54184 Å	
Crystal system	Monoclinic	
Space group	$P2_1/c$	
Unit cell dimensions	a = 9.7396(2) Å	α = 90°.
	b = 15.7803(3) Å	β = 89.411(2)°.
	c = 23.2892(5) Å	γ = 90°.
Volume	3579.22(13) $Å^3$	
Z	4	
Density (calculated)	1.263 Mg/m^3	
Absorption coefficient	0.773 mm^{-1}	
F(000)	1472	
Crystal size	0.200 x 0.200 x 0.050 mm^3	
Theta range for data collection	3.383 to 73.398°.	
Index ranges	-11≤h≤12, -19≤k≤19, -28≤l≤24	
Reflections collected	33081	
Independent reflections	7142 [R(int) = 0.0301]	
Completeness to theta = 67.684°	100.0 %	
Refinement method	Full-matrix least-squares on F^2	
Data / restraints / parameters	7142 / 0 / 441	
Goodness-of-fit on F^2	1.021	
Final R indices [I>2σ(I)]	R1 = 0.0373, wR2 = 0.1014	
R indices (all data)	R1 = 0.0447, wR2 = 0.1068	
Extinction coefficient	n/a	
Largest diff. peak and hole	0.268 and -0.182 $e.Å^{-3}$	

7.2 DFT calculations

Comparison X-day structure/ DFT calculated

model: M06

6-311+g(d)[N,O,Al]/6-31+g(d) [C,H]

scrf(cpcm,solvent=toluene)

T=298.15K

Distances (Å), angles (°)	X-ray	DFT Calculated
Al(1)-Al(2)	5.358	5.16118
Al(1)-N(1)	1.972	1.98704
Al(1)-O(1)	1.774	1.80542
Al(1)-C(1)	1.962	1.96913
Al(1)-C(2)	1.958	1.96626
Al(2)-N(2)	1.974	1.98745
Al(2)-O(2)	1.775	1.80558
Al(2)-C(3)	1.960	1.96592
Al(2)-C(4)	1.963	1.96937
N(1)-C(20)-C(26)-N(2)	12.64	19.29533
C(20)-C(19)-N(1)-Al(1)	158.38	156.38442
C(26)-C(30)-N(2)-Al(2)	157.35	155.55865
C(26)-C(20)-N(1)-C(19)	-101.50	-113.42292
C(20)-C(26)-N(2)-C(30)	-102.11	-113.75044

Energy versus Al-Al distance

model: M06 6-31+g(d)

scrf(cpcm,solvent=toluene)

T=298.15K

Al(1)-Al(2) distance (Å)	Energy (Hartree)	Energy (kcal mol^{-1})
7.161176	-2456.364622	16.6
6.961176	-2456.372181	11.8
6.761176	-2456.378939	7.6
6.561176	-2456.384568	4.1
6.361176	-2456.388717	1.4
6.161176	-2456.391248	-0.1
5.961176	-2456.392241	-0.8
5.761176	-2456.391986	-0.6
5.561176	-2456.390472	0.3
5.361176	-2456.390559	0.3
5.161176	-2456.391027	0.0
4.961176	-2456.390746	0.2
4.761176	-2456.389441	1.0
4.561176	-2456.386300	3.0
4.361177	-2456.381934	5.7
4.161176	-2456.375290	9.9
3.961177	-2456.366087	15.6
3.761177	-2456.354699	22.8
3.561177	-2456.340551	31.7
3.361177	-2456.324596	41.7
3.161177	-2456.313104	48.9